Covalent Cysteine Protease Inhibitors in Disease: How to Optimize their Pharmacokinetic Properties and Selectivity Profiles

Doctoral Thesis

submitted in fulfilling the regulations to attain the degree of

“Doktor der Naturwissenschaften (Dr. rer. nat.)“

in Pharmaceutical and Medicinal Chemistry

at the faculty of Chemistry, Pharmacy, Geography and

Geosciences at the Johannes Gutenberg University of Mainz

Natalie Sabrina Fuchs

born in Mainz

Mainz, 2023

Submitted at the Faculty of Chemistry, Pharmacy, Geography and Geosciences:

Dean: Prof. Dr. [redacted]

Name of 1st reviewer: Prof. Dr. [redacted]

Name of 2nd reviewer: Prof. Dr. [redacted]

Date of doctoral examination: 11.05.2023

Authorship Declaration

I, Natalie Sabrina Fuchs, declare that this thesis titled, “Covalent Cysteine Protease Inhibitors in Disease: How to Optimize their Pharmacokinetic Properties and Selectivity Profiles” and the work presented in it are my own. I hereby confirm that:

- I did this work completely while in candidature for a research degree at this university.
- I have clearly stated which parts of this thesis have already been submitted for another degree or qualification at this university or other institutions.
- I always attributed clearly where I have consulted the published work of others.
- I always gave the source when I have quoted from other works. Excluding those quotations, this thesis is entirely my own work.
- I have acknowledged all main help sources.
- I have made clear exactly what was done by others and what I have contributed myself.

Signature: __[redacted]__

Date: 29.03.2023

“Words are, in my not so humble opinion,
our most inexhaustible source of magic […]”

– Albus Dumbledore from J. K. Rowling’s “Harry Potter” –

List of Contents

Abstract

Cysteine proteases have become promising targets for drug development, particularly in light of recent advancements in treating COVID-19 with nirmatrelvir, a covalent reversible inhibitor of the SARS-CoV-2 main protease (M^{pro}). Given the wide range of cysteine proteases found in various organisms, the potential applications of covalent cysteine protease inhibitors to address parasitic, viral, cancerous, and autoimmune diseases are numerous. However, achieving effective drug delivery to target sites and minimizing off-target effects requires the development of selective scaffolds with optimal physicochemical properties.

In this dissertation, I present the development of selective (F-)vinylsulfon(at)e-based cysteine protease inhibitors with beneficial pharmacokinetic properties, focusing on three target proteases from the cathepsin family as examples: *Trypanosoma brucei* cathepsin L (*Tb*CatL, rhodesain), *Schistosoma mansoni* cathepsin B1 (*Sm*CB1), and human cathepsin S (CatS).

Molecular docking studies combined with enzyme and phenotypic assays were crucial for the inhibitor design and evaluation. The results of these studies have been essential in guiding the development of inhibitors with enhanced efficacy and selectivity. Moreover, valuable insights into the biodistribution and metabolism of several compounds have been obtained through *in vivo* studies as well as *in vitro* metabolism studies. To further improve efficacy, targeted drug delivery strategies were explored in one of the projects.

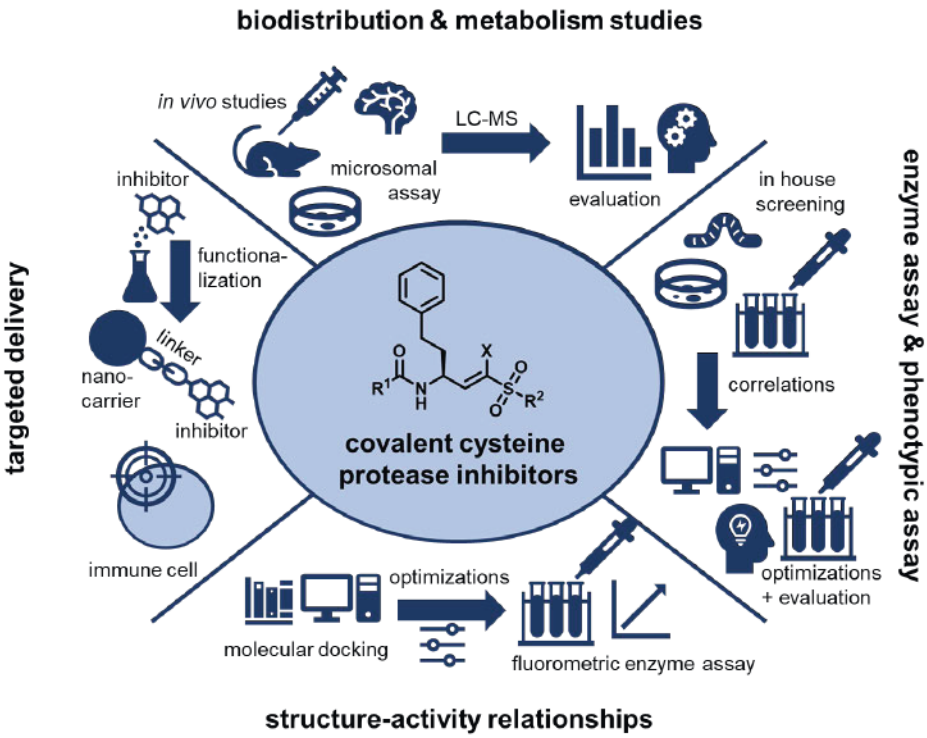

Kurzdarstellung

Cysteinproteasen sind zu vielversprechenden Zielstrukturen für die Arzneimittelentwicklung geworden, insbesondere angesichts der jüngsten Fortschritte bei der Behandlung von COVID-19 mit Nirmatrelvir, einem kovalent-reversiblen Inhibitor der SARS-CoV-2 Main Protease (M^{pro}). Angesichts des breiten Spektrums an Cysteinproteasen, die in verschiedenen Organismen vorkommen, gibt es zahlreiche potenzielle Anwendungsmöglichkeiten für kovalente Cysteinprotease-Inhibitoren zur Behandlung von parasitären, viralen, cancerogenen und Autoimmunkrankheiten. Um jedoch einen effektiven Wirkstofftransport an die Zielorte zu erreichen und Off-Target-Effekte zu minimieren, ist die Entwicklung selektiver Strukturen mit optimalen physikochemischen Eigenschaften erforderlich.

In dieser Dissertation wird die Entwicklung selektiver auf (F-)Vinylsulfon(at)en basierender Cysteinprotease-Inhibitoren mit vorteilhaften pharmakokinetischen Eigenschaften präsentiert, mit Fokus auf drei Zielproteasen aus der Cathepsin-Familie: *Trypanosoma brucei* cathepsin L (*Tb*CatL, rhodesain), *Schistosoma mansoni* cathepsin B1 (*Sm*CB1) und das humane Cathepsin S (CatS).

Molekulare Docking-Studien in Verbindung mit Enzymassays und phänotypischen Tests waren entscheidend für die Entwicklung und Bewertung der Inhibitoren. Die Ergebnisse dieser Studien waren ausschlaggebend für die Entwicklung von Inhibitoren mit verbesserter Wirksamkeit und Selektivität. Darüber hinaus wurden durch *In-vivo*-Studien und *In-vitro*-Metabolismus-Studien wertvolle Erkenntnisse über die biologische Verteilung und den Metabolismus einiger Substanzen gewonnen. Um die Wirksamkeit weiter zu verbessern, wurden in einem der Projekte Strategien zur gezielten Verabreichung („targeted delivery“) verfolgt.

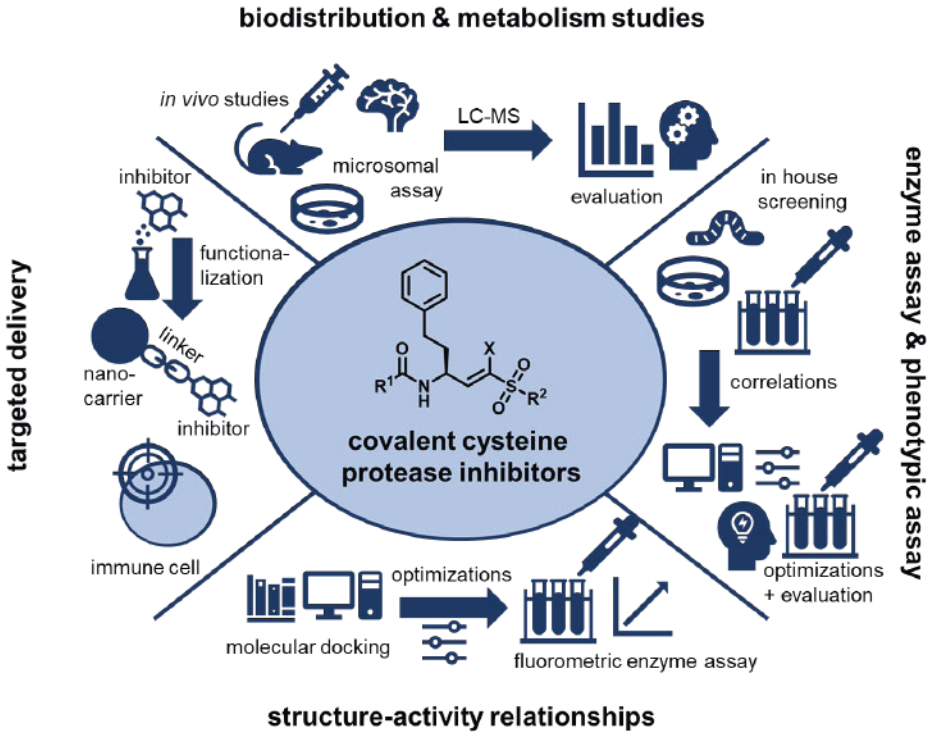

Abbreviations

ACE	angiotensin-converting enzyme
ADME	absorption, distribution, metabolism, excretion
AI	artificial intelligence
AMC	7-amino-4-methylcoumarin
ATP	adenosine triphosphate
BBB	blood-brain barrier
Cat	cathepsin
CDS	chemical drug delivery system
CH	cyclohexane
CMT	carrier-mediated transport
COVID	coronavirus disease
CSF	cerebrospinal fluid
cyAla	cyclohexylalanine
CYP	cytochrome P450
DCM	dichloromethane
DECP	diethyl chlorophosphate
DIPEA	*N*,*N*-diisopropylethylamine
DMF	dimethyl formamide
EA	ethyl acetate
EC	endothelial cell
ECM	extracellular matrix
GSH	glutathione
GST	glutathione-*S*-transferase
HATU	*O*-(7-azabenzotriazol-1-yl)-*N*,*N*,*N*′,*N*′-tetramethyluronium hexafluorophosphate
HBA	hydrogen bond acceptor
HBD	hydrogen bond donor
HOBt	1-hydroxybenzotriazole
hPhe	homophenylalanine
HPLC	high pressure liquid chromatography
LDL	low density lipoprotein
MDSC	myeloid-derived suppressor cell
MHC	major histocompatibility complex
MOE	Molecular Operating Environment
M^{pro}	(SARS-CoV-2) main protease

MS	mass spectrometry
NMR	nuclear magnetic resonance
NTS	newly transformed schistosomula
NVU	neurovascular unit
PAMPA	parallel artificial membrane permeability assay
P-gp	P-glycoprotein
PPB	plasma protein binding
ppm	parts per million
PSA	polar surface area
PZQ	praziquantel
Rho	rhodesain
RMSD	root mean square deviation
RMT	receptor-mediated transport
S1P	sphingosine-1-phosphate
SARS	severe acute respiratory syndrome
*Sm*CB1	*Schistosoma mansoni* cathepsin B1
SULT	sulfonyltransferase
TAM	tumor-associated macrophage
*Tb*CatL	*Trypanosoma brucei* cathepsin L
TBTU	(*O*-(benzotriazole-1-yl)-*N,N,N',N'*-tetramethyluronium tetrafluoroborate)
TCI	targeted covalent inhibition
THF	tetrahydrofuran
TLC	thin-layer chromatography
TME	tumor microenvironment
Treg	regulatory T cells
UGT	UDP glucuronosyltransferase

Introduction

1 Relevance of Physicochemical Properties and ADME Parameters in Drug Design

Imagine a world where every medication you take is specifically designed to target the cause of your disease. This is the reality of modern drug design, where we use a variety of tools and techniques to develop targeted treatments. In this process, one of the most important aspects is to consider the physicochemical properties of potential drugs. These parameters, such as lipophilicity, solubility, and molecular weight, can greatly impact a drug's effectiveness and safety, and must be carefully evaluated to develop successful treatments. Here, I will discuss the effect of physicochemical parameters on pharmacokinetic properties and how structural modifications of covalent cysteine protease inhibitors can affect their selectivity profiles and efficacy.

1.1 Rule of Five

Optimizing lead structures with high biological activity towards drug candidates in drug development requires the consideration of physicochemical parameters. The concept of “less is more” is embodied in the widely used LIPINSKI rule of five in drug design.[1,2] This guideline states that a drug candidate should not violate certain physicochemical parameters, including molecular weight, lipophilicity, often represented by the logP value, and hydrogen bond donors (HBD) and acceptors (HBA). By following these criteria, drugs have the potential to be orally bioavailable and effectively penetrate cell membranes to interact with target proteins, leading to enhanced efficacy.[1,2]

MOLECULAR WEIGHT

The LIPINSKI rule of five states that the molecular weight of a drug candidate should not exceed 500 Dalton. This restriction on molecular weight is based on the idea that larger molecules are more likely to have decreased solubility and increased permeability, which can lead to reduced efficacy and increased toxicity.[2] Large lipophilic compounds can accumulate in membranes or various tissues and cause adverse effects. On the other hand, some large molecules might have reduced permeability and therefore rely on active transport.[3]

PARTITION COEFFICIENT

The logP value, or partition coefficient, serves as a metric for a molecule's lipophilicity. It is calculated as the logarithmic ratio of a molecule's concentration in *n*-octanol to its concentration in water. This fundamental parameter in drug development is used to predict a drug's solubility, permeability, and (oral) bioavailability. A higher logP value indicates elevated lipophilicity, which affects a drug's capacity to pass across cell membranes and interact with target structures. It is a valuable tool to improve the pharmacokinetic and pharmacodynamic properties of a drug and, thus, plays a critical role in evaluating a molecule's suitability as a drug candidate.[4,5] In LIPINSKI's rule of five, the logP value should not exceed five.[1,2] Nevertheless, it should also be considered that compounds with low logP values, thus hydrophilic or even charged, are also not likely to be permeable.[6]

HYDROGEN BONDS

The rule of five also states that a drug candidate should have no more than five hydrogen bond donors and no more than ten acceptors.[1,2] In drug design, it's important to consider the number of HBD and HBA, since these functional groups can affect a drug's solubility, stability, and bioavailability.[7] If a drug has too many HBD and HBA, it may be more likely to form unwanted H-bonds with other molecules in the body, reducing efficacy and increasing toxicity.[8] Still, hydrogen bonds can improve solubility and stabilize conformations.[7]

EXTENDED RULE OF FIVE

The extended rule of five, also known as the VEBER rule, is a modification of the LIPINSKI rule of five that includes additional parameters for drug-like properties.[6] In addition to the modified original parameters of molecular weight (500–700 Da), lipophilicity (logP $\leq$ 7.5), and HBA/HBD (10/5), the extended rule of five adds constraints on a molecule's rotatable bonds ($\leq$ 15) and polar surface area (PSA, $\leq$ 140 Å²).[9] These additional parameters contribute to a more comprehensive evaluation of a molecule's potential as a drug candidate. The idea behind the extended rule of five is that drugs with too many rotatable bonds or a too large polar surface area tend to have lower stability and bioavailability.[10] Increased rotational degrees of freedom may lead to a larger diffusional cross section, influencing permeability. A large polar surface can also reduce passive diffusion. Adhering to this rule can improve the chances of success for drug candidates. However, it should be noted that these guidelines are not absolute and a molecule that violates one or more of these parameters may still have therapeutic potential (e.g., antiviral agents like ritonavir).[9]

Three examples for drugs within or beyond the rule of five, that are orally bioavailable after all, are shown in **Figure 1**.

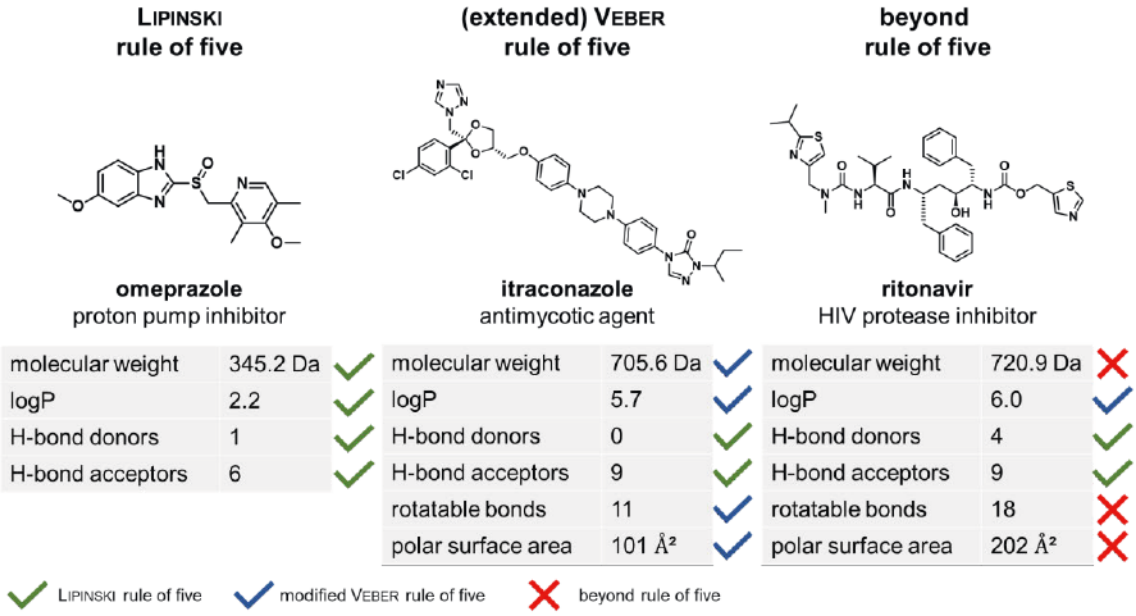

Figure 1. Examples for drugs that are within the scope of LIPINSKI's rule of five (omeprazole, left),[11] the extended rule of five (itraconazole, middle)[6] or beyond the rule of five (ritonavir, right).[9] Physicochemical parameters retrieved from the NATIONAL CENTER FOR BIOTECHNOLOGY INFORMATION (PubChem, 2023).[12]

1.2 ADME Parameters

Pharmacokinetics, often referred to as "what the body does to the drug", is the study of how a drug is absorbed (A), distributed (D), metabolized (M), and eliminated (E) from the body, in short: ADME (**Figure 2**).[13–15] This field of study is critical in determining the dosing and administration route of a drug, as well as understanding the factors that can impact its efficacy and safety. By carefully analyzing the pharmacokinetic properties of a drug, we can optimize its therapeutic effect and minimize unwanted side effects. The study of pharmacokinetics is an essential part of drug design and development, allowing us to better understand the dynamic relationship between a drug and the body.[16,17] The ADME parameters are highly dependent on the drug's physicochemical parameters.[18]

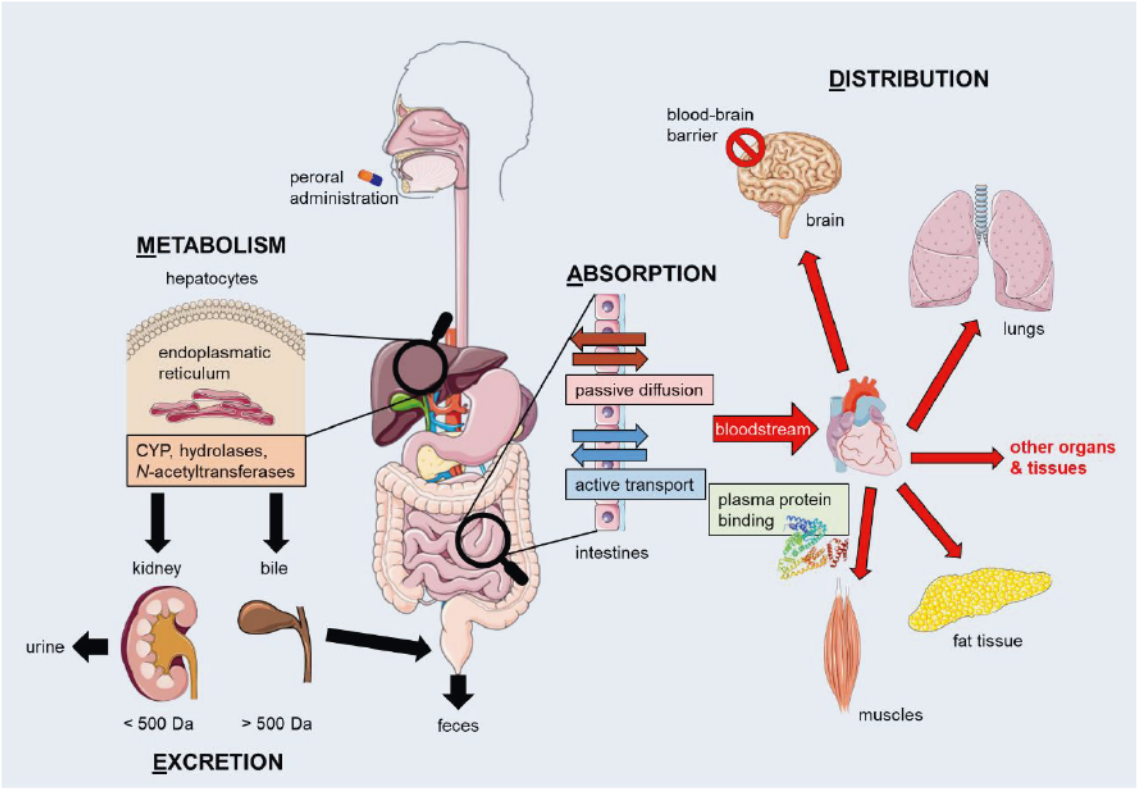

Figure 2. ADME exemplified for peroral administration – schematic overview of some important aspects. The figure was partly generated using SERVIER MEDICAL ART, provided by SERVIER, licensed under a Creative Commons Attribution 3.0 open license.

ABSORPTION (A)

As described above, the LIPINSKI rule of five plays an important role in a drug's absorption in the intestines. Oral bioavailability refers to the fraction of a drug that enters the bloodstream after peroral administration and can reach its target site in the body.[19,20] It is influenced by several factors, including the drug's solubility, stability, and metabolism in the intestine and liver. Cell permeability, especially via passive diffusion, remains crucial for oral bioavailability.[21,22]

DISTRIBUTION (D)

Several factors affect the distribution, depending on the tissue. Firstly, the cell permeability that is determined by physicochemical properties, such as logP and PSA.[21,22] Usually, passive diffusion across membranes is critical, but in some cell types or tissues, active transport is key.[23] In others, efflux from cells is involved, limiting distribution in some tissues, e.g., by P-glycoprotein (P-gp) in brain tissue (see chapter **1.2.1**).[24–27] Another factor influencing the biodistribution is plasma protein binding (PPB).[28–30] Lipophilic drugs like phenytoin adsorb to plasma proteins, such as serum albumin, which immensely improves their plasma solubility.[31] PPB generally prolongs a drug's plasma half-life, since only the free drug amount is essential for the

effect as well as metabolism and excretion. Adsorption to serum albumin is a steady state between the bound and unbound fraction.[32] When the unbound drug is metabolized and excreted, new drug is released from plasma protein binding. This prolongs the half-life compared to drugs that are completely unbound and thus, metabolized and excreted more rapidly.[33,34] The distribution volume is a fundamental concept in pharmacokinetics that helps to characterize drug distribution in the body. Defined as the theoretical volume of fluid required to account for the total amount of drug in the body, this parameter takes into consideration the dynamic interplay between drug concentration and the various physiological compartments.[35,36] The physicochemical parameters of a drug can greatly influence its distribution volume.[37] For example, drugs with high lipophilicity tend to have a larger distribution volume, as they can more easily penetrate cell membranes and distribute to lipid-rich tissues. On the other hand, drugs with high hydrophilicity tend to have a smaller distribution volume, as they are more restricted to the extracellular fluid compartment. Other physicochemical factors such as molecular weight, protein binding, and ionization can also impact the distribution volume of a drug.[37] Understanding these parameters and their effects on drug distribution is crucial for predicting drug efficacy and toxicity.[38]

METABOLISM (M)

A drug's lipophilicity also has a major effect on its metabolization.[39,40] The more lipophilic, the higher the metabolism rate in hepatocytes since this usually requires phase I and phase II reactions to enable excretion (see chapter **1.2.2**). Higher metabolization rates lead to a potentially higher first-pass effect which reduces a drug's half-life.[41,42] The first-pass effect refers to the phenomenon where a drug, upon oral administration, is absorbed into the bloodstream through the intestinal wall, transported directly to and then metabolized by the liver before reaching the systemic circulation. This metabolic process can result in a significant decrease in the drug's bioavailability, as a portion of the dose may be metabolized or eliminated before reaching its intended target site. The extent of the first-pass effect varies depending on the drug and individual factors, such as liver function and blood flow to the liver.[41–43]

EXCRETION (E)

Drugs can be excreted from the body in various ways. Most commonly, they are excreted by the bile or kidneys, but also via sweat, the mammary or salivary glands, and the lungs.[44,45] Again, passive diffusion is crucial. Nevertheless, depending on the substance, there may be additional active transport processes.[46] Biliary excretion

includes lipophilic drugs and their metabolites.[47] In the enterohepatic circulation, the drug is secreted into the intestinal lumen via the bile where it can be reabsorbed, prolonging its half-life.[48,49] The enterohepatic circulation is critical for drugs like digitoxin or steroids as well as endogenous hormones.[50] Here, the drugs are eventually excreted in the feces. Renal excretion is highly regulated.[44,47,51] There are three main processes: glomerular filtration, active secretion, and passive reabsorption. Kidneys can excrete substances with a molecular weight up to 5 kDa, retaining most proteins. Generally, renal excretion includes more hydrophilic drugs, often with molecular weights $\leq$ 500 Da.[52] Understanding the relative contribution of renal and biliary excretion to drug elimination is important for optimizing drug dosing and reducing the risk of toxicity.

1.2.1 Blood-Brain Barrier

The blood-brain barrier (BBB) is a selectively permeable membrane that separates the blood circulating in the body from the central nervous system (CNS). It is one of three barrier structures in the CNS – BBB, blood-CSF barrier, and arachnoid epithelium.[53] Composed of specialized cells, such as astrocytes and endothelial cells, the BBB helps to protect the delicate neural tissue of the brain and spinal cord from harmful substances and pathogens that may be present in the bloodstream. Its structure is unique, with tight junctions between cells that prevent large molecules and most toxins from passing through. While this serves a vital protective function, it can also hinder drug delivery to the brain.[54–56]

ANATOMY

The BBB is a cellular and biochemical structure consisting of five major parts, the neurovascular unit (NVU): endothelial cells (EC), pericytes, astrocytes, immune cells, and basement membrane.[57] The area between the basement membrane and the neurons is called VIRCHOW-ROBIN space and contains interstitial fluid with residing microglia.

EC are bound together by tight junctions to prevent transport through the paracellular space.[58,59] Too large or too polar molecules (e.g., glucose) can enter the CNS via transport proteins.[60]

Pericytes cover the EC layer and regulate the blood flow in the CNS with their long membrane extensions, and maintain the BBB permeability.[61,62]

Astrocytes are glial cells known primarily for their maintenance functions within the BBB microenvironment, such as innate immune regulation, electrochemical activity monitoring, and parenchymal water balance.[63,64]

Immune cells that are usually present in the CNS include perivascular macrophages and microglia. The macrophages mainly phagocytose cell debris, waste products, and pathogens.[65] Microglia are accountable for innate immunity, antigen presentation, and neuronal development.[66]

The basement membrane is a highly intricate matrix of biomolecules that envelops the vascular tube and pericytes. It is part of the extracellular matrix (ECM), and comes into direct contact with the astrocyte endfeet. Additionally, it contains many structural support molecules (collagen IV, laminins, heparine sulfate proteoglycans, and fibronectin). Consisting of two layers comprising different laminins, it serves as both physical barrier and scaffold for chemical signals.[67,68]

Figure 3 shows a schematic overview of the BBB.

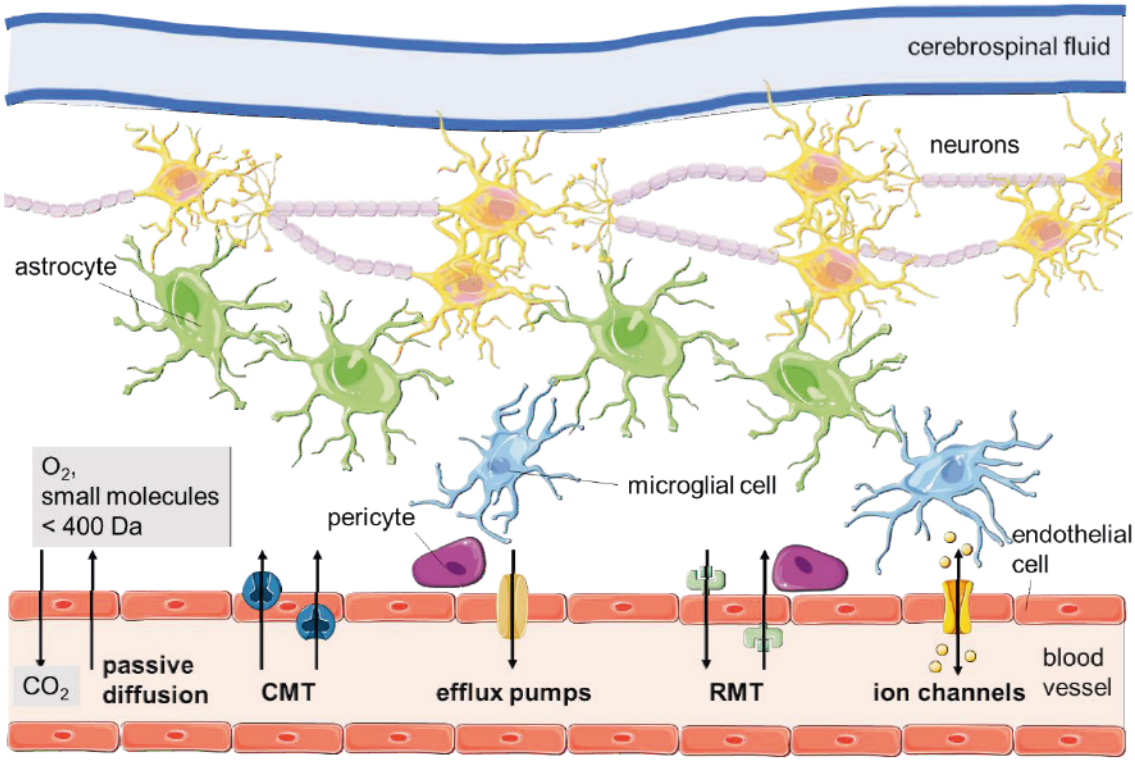

Figure 3. Overview of cells and transport mechanisms of the blood-brain barrier. Adapted from SHARIF ET AL. (2018) and XIAO ET AL. (2020).[69,70] CMT, carrier-mediated transport; RMT, receptor-mediated transport. The figure was partly generated using SERVIER MEDICAL ART, provided by SERVIER, licensed under a Creative Commons Attribution 3.0 open license.

PHYSIOLOGY

The BBB endothelial cells contain two transporter types – nutrient and efflux transporters.[71,72] For example, GLUT1 supplies brain cells with vital glucose, and GLUT1 levels are higher in the brain than in peripheral tissues.[73] Additionally, receptor-mediated transport (RMT) systems provide iron, amyloid proteins, or low-density lipoprotein (LDL) that carries cholesterol and lipids. Foreign, potentially toxic, materials must be eliminated from the CNS as well as metabolic waste products. Therefore, efflux pumps hydrolyze adenosine triphosphate (ATP) in order to generate energy to move compounds against their concentration gradients. A prominent example is P-glycoprotein (Mdr1, P-gp) that transports small lipophilic molecules from brain cells into the vascular lumen.[71,74–76]

In addition to physical barriers and transport mechanisms, the NVU has other ways to regulate the BBB. Pericyte-mediated regulation involves glutamate, which triggers the release of nitric oxide and prostaglandin E2, relaxing pericyte extensions.[77,78] These cells also contain receptors for platelet-derived growth factor (PDGF), crucial for barrier formation and integrity, which has been demonstrated using knock-out and knock-down mutants in rodent models.[79–81] Pericytes direct astrocyte foot projections and reduce levels of leukocyte adhesion molecules. Still, their impact on other transport molecules is limited, implying their main role is to limit paracellular influx of substances to the CNS. Astrocyte-mediated regulation contributes to the BBB integrity by secreting ang1 to upregulate the tight junction expression.[82] Additionally, astrocytes reduce vascular permeability by secreting TGF-β to stimulate the expression of P-gp.[82] They secrete angiotensin converting enzyme-1 (ACE-1) to increase angiotensin II and induce vasoconstriction, limiting the blood flow.[83] Astrocytes also regulate BBB permeability by secreting apolipoprotein E, which regulates tight junction integrity via Lrp1.[84] Moreover, astrocytes regulate the production of aquaporin-4, which is necessary for water transport into the CNS.[85,86]

OVERCOMING THE BLOOD-BRAIN BARRIER

Again, several physicochemical parameters influence the extent to which substances can passively cross the BBB. Small lipophilic molecules (< 500 Da) are more likely to cross the barrier via passive diffusion.[87,88] Charged molecules have more difficulty but positively charged ones (amine groups, etc.) penetrate the BBB more easily than negatively charged ones (carboxyl acids, etc.).[55,56] The negative charge is repelled by the negatively charged endothelial cells.

Some compounds can actively cross the BBB by binding to specific transporters that are expressed on the BBB's endothelial cells. For instance, amino acids and glucose are known to utilize specific transporters to facilitate BBB crossing.[56,73,89] The unique capillaries in the BBB possess extra mechanisms to regulate transport, in- and efflux to the brain. Small gases (N_2, O_2) can penetrate the BBB whereas bivalent cations (Ca^{2+}, Mg^{2+}) rarely pass.[57] An important regulator is P-gp, an active efflux pump.[75,76,90] Many lipophilic molecules are substrates of P-gp (digoxine, loperamide, etc.).[90–92] Therefore, even if they can pass the BBB in the first place, they do not remain in brain tissue.

Other drugs can be metabolized into more lipophilic forms that more likely cross the BBB. A prime example is fingolimod, an immunomodulatory agent used in the treatment of Multiple Sclerosis. Fingolimod is a prodrug of a sphingosine 1-phosphate (S1P) receptor agonist that can traverse the BBB and is subsequently metabolized in brain tissue. It is phosphorylated by sphingosine kinase, generating its active form, fingolimod phosphate. Notably, fingolimod phosphate, due to its negative charge, would not have been able to penetrate the BBB on its own.[93,94]

In summary, a drug's ability to cross the blood-brain barrier is dependent on its molecular size, lipophilicity, charge, binding to transporters, and metabolism. These factors should be considered when designing drugs that target the central nervous system.

1.2.2 Metabolism

Drug metabolism refers to the biochemical transformation of drugs and other xenobiotics in the body, involving a series of enzymatic reactions that modify the chemical structure and properties of these compounds.[95] This process is essential for the elimination of drugs from the body, as well as for the activation or inactivation of their pharmacological effects. Drug metabolism occurs mainly in the liver and other organs, where several enzymes, including cytochrome P450s (CYP), flavin-containing monooxygenases, and UDP glucuronosyltransferases, catalyze a variety of reactions, such as oxidation, reduction, hydrolysis, and conjugations.[39,40,96,97] The inter-individual variability in drug metabolism, due to genetic, environmental, and lifestyle factors, can have significant implications for drug efficacy and safety, as well as for drug interactions and personalized medicine.[98] Understanding the mechanisms and regulation of drug metabolism is thus crucial for developing and optimizing effective and safe therapies.[18] The biotransformation of drugs typically involves two phases: phase I and phase II metabolism.[96]

PHASE I BIOTRANSFORMATION

Phase I is the initial step, involving the conversion of the parent compound into one or more metabolites through oxidation, reduction, or hydrolysis reactions, among others. The enzymes primarily participating in phase I metabolism are the cytochrome P450 (CYP) enzymes, which are found mainly in the liver but also in other tissues such as the intestine and brain.[39,40,97,99,100] These enzymes play a critical role in determining a drug's pharmacokinetics, efficacy, and potential for toxicity. Other important phase I enzymes are hydrolases (e.g., esterases) or *N*-acetyltransferases.[101,102] Phase I metabolism can increase the hydrophilicity of a drug, making it more readily excreted by the body. However, it can also generate toxic intermediates (e.g., metabolism of acetaminophen) that require further metabolism by phase II enzymes to prevent harm (**Figure 4**).[103,104]

PHASE II BIOTRANSFORMATION

Phase II drug metabolism usually follows phase I metabolism and involves the conjugation of the parent compound or its phase I metabolites with endogenous compounds, such as glucuronic acid, sulfate, or amino acids. This process, known as conjugation, highly increases the hydrophilicity of the drug or its metabolites, facilitating their excretion through the urine or feces.[105,106] The major enzymes involved in phase II are UDP glucuronosyltransferases (UGTs), sulfotransferases (SULTs), and glutathione S-transferases (GSTs), among others.[107–113] Unlike phase I metabolism, phase II biotransformation does not involve creating new chemical groups on the drug but rather adding pre-existing functional groups. By detoxifying and eliminating toxic and potentially hazardous metabolites arising from phase I reactions, phase II metabolism plays a crucial role in safeguarding the body (**Figure 4**).[111,113]

Figure 4 illustrates the biotransformation of acetaminophen, a prime example. The majority of acetaminophen is rapidly glucuronidated, skipping phase I metabolism.[104,114,115] Nonetheless, phase I reactions like deacetylation or oxidation via CYP2E1 can occur. The oxidation results in the hepatotoxic metabolite NAPQI, a Michael acceptor that can react with all sorts of proteins to form adducts (biotoxification).[103,115] To detoxify, GST has to attach a glutathione residue to NAPQI, which can be transformed to the mercapturic acid derivative.[104,116]

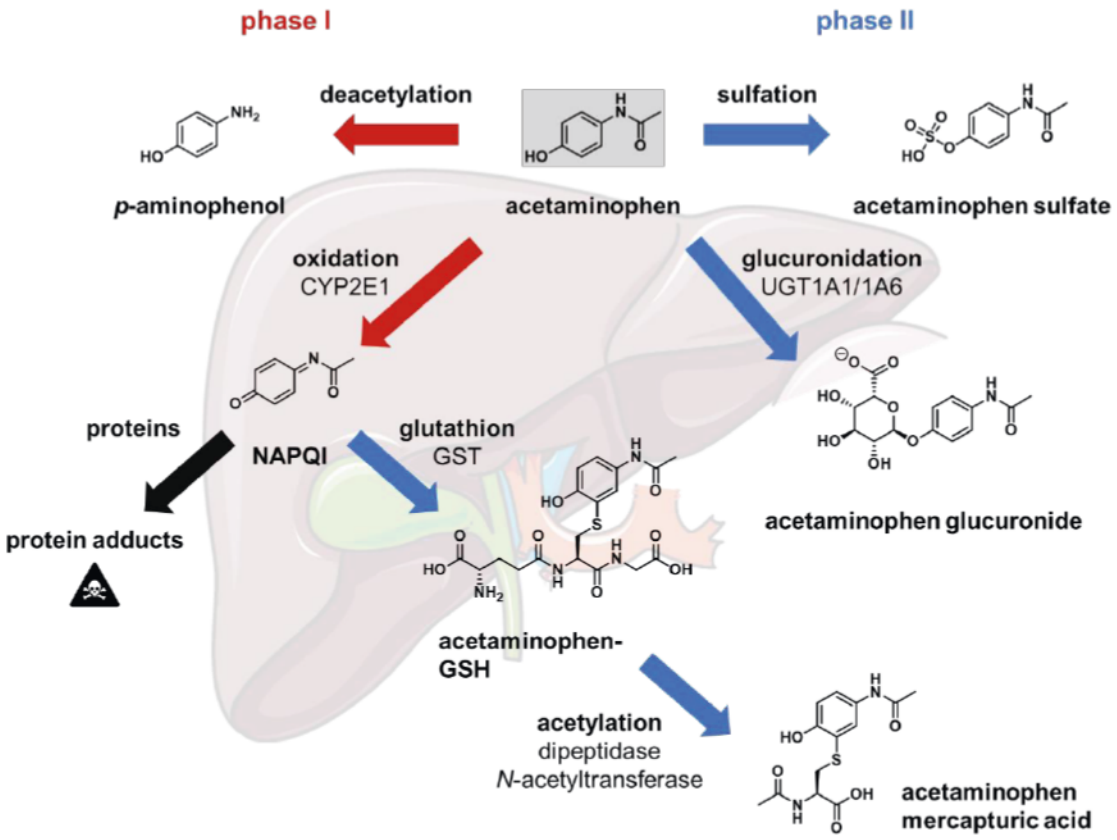

Figure 4. Biotransformation of acetaminophen, phase I and phase II metabolism including biotoxification. The figure was partly generated using SERVIER MEDICAL ART, provided by SERVIER, licensed under a Creative Commons Attribution 3.0 open license.

Some drugs and metabolites may also be transported out of cells and into the blood or urine by efflux transporters, such as P-gp, which is often referred to as "phase III metabolism". However, this process is not considered a distinct phase of drug metabolism, but rather a part of the excretion process.[117]

2 Proteases

Proteases, also known as peptidases or proteinases, are enzymes that catalyze the hydrolysis of peptide bonds in proteins, thereby breaking down large protein molecules into smaller peptides and amino acids. Once considered nonspecific degrading enzymes, they have emerged as key players in mediating signaling pathways and specific cleavage processes in all living organisms.[118,119] Approximately 600 proteases have been identified in the human genome.[120,121] These enzymes are substantial for numerous physiological processes, such as protein digestion, blood coagulation, immune response, apoptosis, and cellular signaling.[122] They also play essential roles in regulating protein turnover, folding, and degradation. Protein turnover is crucial for all cellular processes and thus highly regulated, maintaining cellular homeostasis and responding to changes in the environment or disease states.[123–125] Proteases are highly diverse in structure, function, and substrate specificity, making them attractive targets for drug discovery.

Dysregulation of protease function is associated with various diseases, such as osteoporosis, cardiovascular diseases, neurodegenerative disorders, inflammation, and cancer, where uncontrolled and increased proteolytic activity is a common feature.[121,126,127] Not to be missed are exogenous proteases from parasites, viruses, or bacteria, which can be essential in infectious diseases.[128–131] Consequently, protease inhibitors have emerged as promising therapeutic agents to combat protease-associated diseases (see chapter **4**).

2.1 Classification and Nomenclature

Proteases are classified according to the Enzyme Commission (EC) system. They are hydrolases (EC 3), more precisely peptidases (EC 3.4).[132] There are two main sorts, endo- and exopeptidases. Endopeptidases cleave peptide bonds within a peptide chain, while exopeptidases cleave at the N- or C-terminus (amino- or carboxypeptidases).[118,119] Another way to classify proteases is related to their active site residue mainly responsible for catalysis (MEROPS system).[133] It comprises five protease classes: aspartate, cysteine, metallo-, serine, and threonine proteases.[134] Based on their evolutionary origin and tertiary structure, these protease classes are further divided into superfamilies (clans) and families. [133,134] **Figure 5** shows the protease classification after EC and MEROPS with focus on relevant cysteine proteases.

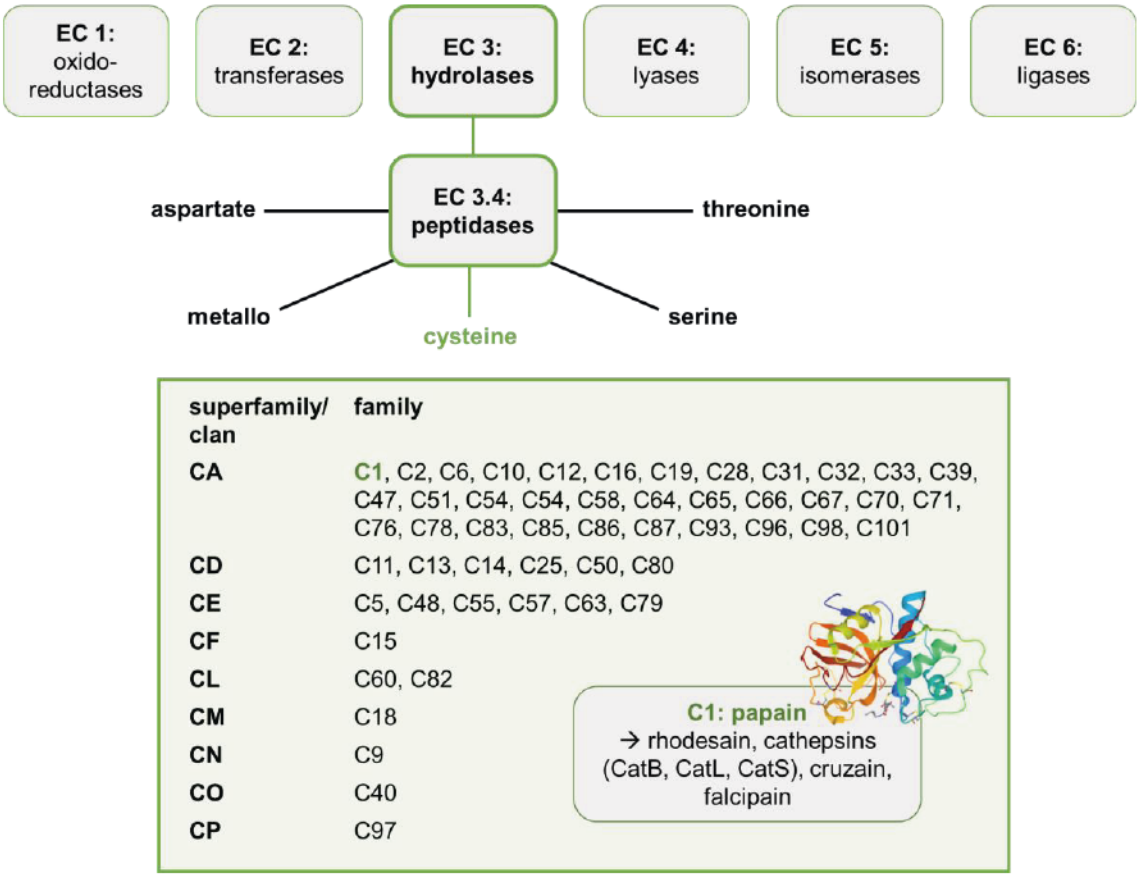

Figure 5. Classification of (cysteine) proteases according to EC and MEROPS, Papain structure: pdb 1ppp.[133–136]

A protease's binding pocket can be characterized according to a nomenclature by SCHECHTER and BERGER (**Figure 6**).[137] Here, the active site is divided into subsites, each occupied by the substrate's amino acid side chains. Beginning at the cleavage site, residues towards the substrate's N-terminus (non-primed site) are labeled P1 – Pn whereas residues towards the C-terminus (primed site) are labeled P1' – Pn'. Accordingly, the respective binding pockets/subsites are labeled S1 – Sn and S1' – Sn'.

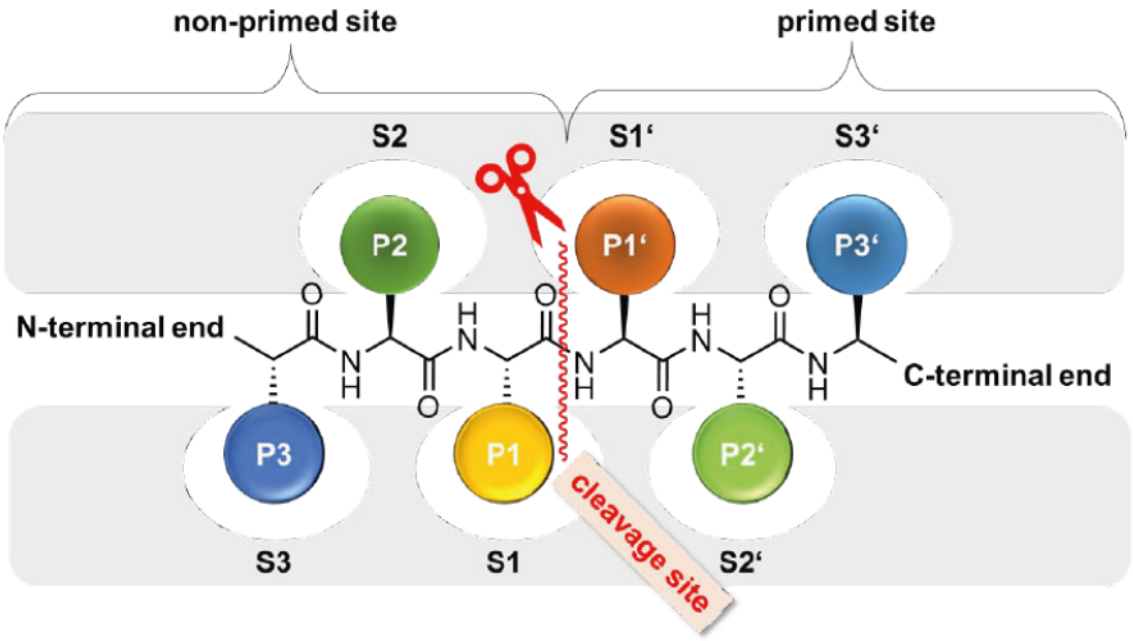

Figure 6. SCHECHTER and BERGER nomenclature of protein active site and substrate side chains. Cleavage site indicated in red.[137]

2.2 Cysteine Proteases

Cysteine proteases are ubiquitous enzymes. They are found in a variety of organisms, including viruses, bacteria, fungi, parasites, plants, and mammals.[128] As already discussed in chapter **2.1**, they are classified into nine clans and 69 families according to their tertiary structure and evolutionary origin (**Figure 5**).

Each clan incorporates the characteristic catalytic triad (or dyad), but different protein folds, indicating a convergent evolution of the catalytic mechanism (**Scheme 1**).[138]

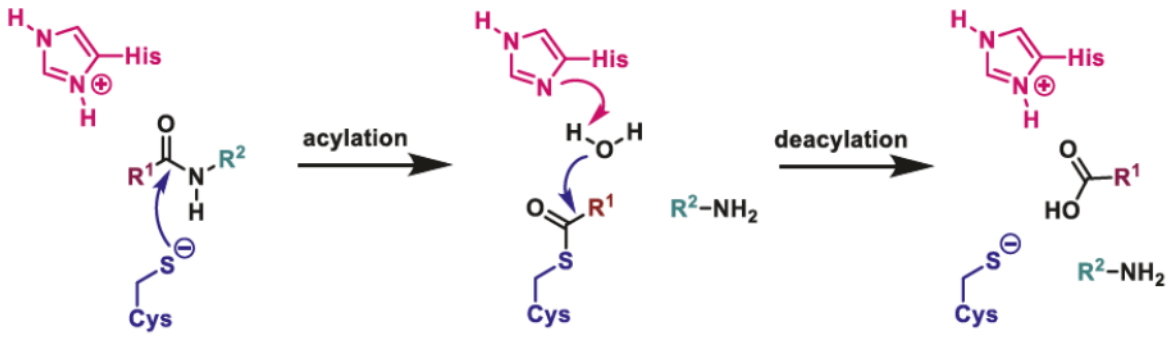

Scheme 1. Catalytic steps for peptide bond hydrolysis by cysteine proteases (catalytic dyad). Catalytic cysteine in blue, histidine in magenta.

The ion pair mechanism is widely accepted and supported by experimental and computational evidence for clan CA cysteine proteases.[139–142] The active site cysteine's nucleophilicity is amplified through the enzymatic environment, which

involves a basic histidine residue serving as a proton acceptor (catalytic dyad). This leads to the formation of a highly nucleophilic thiolate/imidazolium pair pre-catalytically.[143] This is experimentally confirmed by potentiometric ionization state determination and QM/MM studies, with evidence suggesting strong preference for the ionic state within the enzyme's environment.[141,144] For most clan CA proteases, the proper orientation of the histidine is facilitated through hydrogen bonding of an asparagine or aspartate residue (catalytic triad), an essential factor to preserve the ion pair ground state.[140] Additional factors include a dipole moment arising from a nearby α-helix and a complex hydrogen bond network in the active site environment.[139,145,146] From a mechanistic point of view, peptide bond hydrolysis in cysteine proteases occurs in two main steps: acylation and deacylation (**Scheme 1**). In the acylation stage, the nucleophilic cysteine thiolate attacks the peptide bond's carbonyl carbon, producing an acyl-enzyme intermediate. The following deacylation occurs via base catalysis. The imidazole nitrogen of the active site histidine deprotonates a water molecule, which then attacks the thioester intermediate's carbonyl-C, resulting in the final cleavage products.

Within a clan, cysteine proteases are classified into families, based mainly on their sequence and tertiary structure similarities. The largest family is C1, incorporating papain-like proteases.[147] It features parasitic cysteine proteases (*Trypanosoma brucei* cathepsin L, *Schistosoma mansoni* cathepsin B1, etc.) as well as human cathepsins (e.g., cathepsins B, K, L, S). These are further discussed in the following chapter.

3 Cysteine Cathepsins as Drug Targets

Cysteine cathepsins are found in humans and various other organisms and exhibit high sequence and structural similarity among themselves. Due to this similarity, off-target effects must be considered.

3.1 Disease Relevant Cathepsins

Cathepsins are relevant in many physiological and pathological processes. **Table 1** shows several disease relevant cathepsin-like proteases and their functions.

Cathepsins are primarily endopeptidases that operate within endolysosomal compartments, with some being expressed constitutively in all tissues while others are regulated and occur mainly in specific cell types.[148,149] Cathepsin K (CatK), for example, is specifically expressed in osteoclasts and plays a crucial role in bone remodeling.[150] On the other hand, cathepsin S (CatS) is predominantly expressed in immune cells and is essential for antigen presentation.[151–154] While cathepsins are mainly located in lysosomal compartments, recent research has also shown that some of them have extracellular roles. For instance, CatS is secreted and plays a role in degrading the extracellular matrix (ECM).[155] In addition, the upregulation of certain cathepsins is associated with several invasive and degenerative diseases, such as osteoporosis, rheumatoid arthritis, and cancer.[156–159] Cysteine cathepsins, in particular, have been found to play critical roles in tumor progression and migration by promoting extracellular matrix degradation and angiogenesis.[148,159,160] While small molecule cysteine protease inhibitors have demonstrated a reduction in tumor invasion *in vitro*, the question remains as to whether both the extracellular and intracellular enzyme pools need to be targeted for effective treatment.[148,161] Despite the challenges, inhibiting cathepsins still represents a promising approach to mitigate tumor progression.[162–164]

Table 1. Disease relevant cysteine cathepsins (C1 family) and their functions.

enzyme	organism	functions	disease
T. brucei cathepsin L / rhodesain	*Trypanosoma brucei*	host protein degradation, BBB crossing, immune evasion	Human African Trypanosomiasis
T. brucei cathepsin B		host protein and transferrin degradation	
T. cruzi cathepsin L / cruzain	*Trypanosoma cruzi*	tissue invasion, immune evasion, parasite development	Chagas disease
S. mansoni cathepsin B1	*Schistosoma mansoni*	host protein degradation, parasite development	schistosomiasis
falcipains	*Plasmodium falciparum*	hemoglobin degradation	malaria
cathepsin B	human	lysosomal protein degradation, apoptosis	cancer, pancreatitis
cathepsin K		bone resorption/modeling	osteoporosis
cathepsin L		lysosomal protein degradation, antigen processing	cancer, hyperplasia
cathepsin S		ECM turnover, antigen presentation and processing, macrophage polarization	auto-immune diseases, cancer

ECM = extracellular matrix.

3.2 Cathepsin S in Tumor Microenvironment

Parts of this chapter have been published in a review in 2020.[165] Cysteine cathepsins are a group of 11 proteases, out of which five (cathepsins B, H, K, L, and S) have been repeatedly implicated in the progression of solid cancers.[166] They are a group of lysosomal proteases that mainly function in intracellular protein catabolism. However, certain cathepsins, such as CatB, CatH, CatK, CatL, and CatS, are also expressed on the cell surface and can degrade ECM proteins. CatS, in particular, can break down various collagens, elastin, laminin-5, cell surface receptors such as protease-activated receptor-2, and cell adhesion molecules like E-cadherin and junctional

adhesion molecule B (JAM-B).[166] This proteolytic activity is key in tissue remodeling, cancer cell growth, and metastasis.

The expression and activity of cysteine cathepsins are upregulated in chronic inflammation and cancer, with CatB and CatS being overexpressed in various cancers, including follicular lymphoma, gastric, colon, brain, breast, and pancreatic cancer.[164,167,168] These cathepsin-mediated mechanisms can enhance ECM turnover and angiogenesis, promoting tumor expansion and securing cancer nutrient supply. They can also suppress the T-cell-mediated anti-cancer immune response located in the tumor microenvironment (TME).

Cancer cells have developed several mechanisms to escape immune surveillance, including limited tumor antigen presentation, secreting factors that polarize non-tumor antigen-presenting cells (APC) towards an M2-type, and inhibiting the activation of tumor-destroying CD8+ T cells. M2-type APCs induce tumor tolerogenic regulatory CD4+ T cells (Treg) while suppressing the cytotoxic CD8+ T cells responsible for eliminating tumor cells.[167,169,170] CatB and CatS have a particularly devastating effect on anti-tumor immune responses by polarizing myeloid APCs towards an M2-phenotype, favoring the expansion of myeloid-derived suppressor cells (MDSCs) and tumor-associated macrophages (TAMs), and decreasing cytotoxic CD8+ T cells while promoting Treg cells.[166,171]

CatS is also involved in antigen processing and presentation, enhancing the expression of major histocompatibility complex class II (MHC-II) and antigen loading on myeloid cells, including cancer epithelia.[151–153,172] However, while antigen presentation via MHC class I (MHC-I) activates cytotoxic CD8+ T cells, MHC-II presentation in the TME usually activates CD4+ Treg cells. This can actively suppress the immune response towards cancer cells.[169,170,173] A mouse model has suggested that inhibiting CatS activity decreases overall T cell immunity under physiological conditions but increases CD8+ T cell immunity when cancer cells are present.[174]

Overall, inhibiting cysteine cathepsins, such as CatS, appears to be a promising approach to restrain tumor growth and enhance the immune response against tumors.[151–153,167]

3.3 Cathepsin Structure

Discovering the crystal structure of numerous cathepsin-like proteases has led to a deeper understanding of their molecular composition.[175,176] Despite differences in their specific functions, the tertiary structure of these proteases remains remarkably

conserved across the family. These proteases are produced in an inactive form, pre-pro-cathepsins, consisting of a signal domain (pre-peptide), an N-terminal pro-domain (pro-peptide), and a catalytic domain, with the pro-domain serving multiple crucial purposes.[177–179] Not only does it ensure correct folding and trafficking, but it also acts as a reversible inhibitor, preventing premature proteolytic activity.[180–182] An example for this would be *T. brucei* cathepsin L (*Tb*CatL, rhodesain).[183] The N-terminal signal peptide directs the protease into the lumen of the endoplasmatic reticulum where it is cleaved off by a signal peptidase, generating the inactive pro-cathepsin.[179] The N-terminal pro-domain occupies the active site cleft of the catalytic domain in rhodesain, preventing substrate binding as shown by the superposition of the crystal structures in **Figure 7**. The proteolytic activity is only activated after autocatalytic cleavage (*cis* activation) or cleavage by other proteases (*trans* activation) in the lysosome, allowing the proteases to perform their functions effectively in their designated compartments.[184–186]

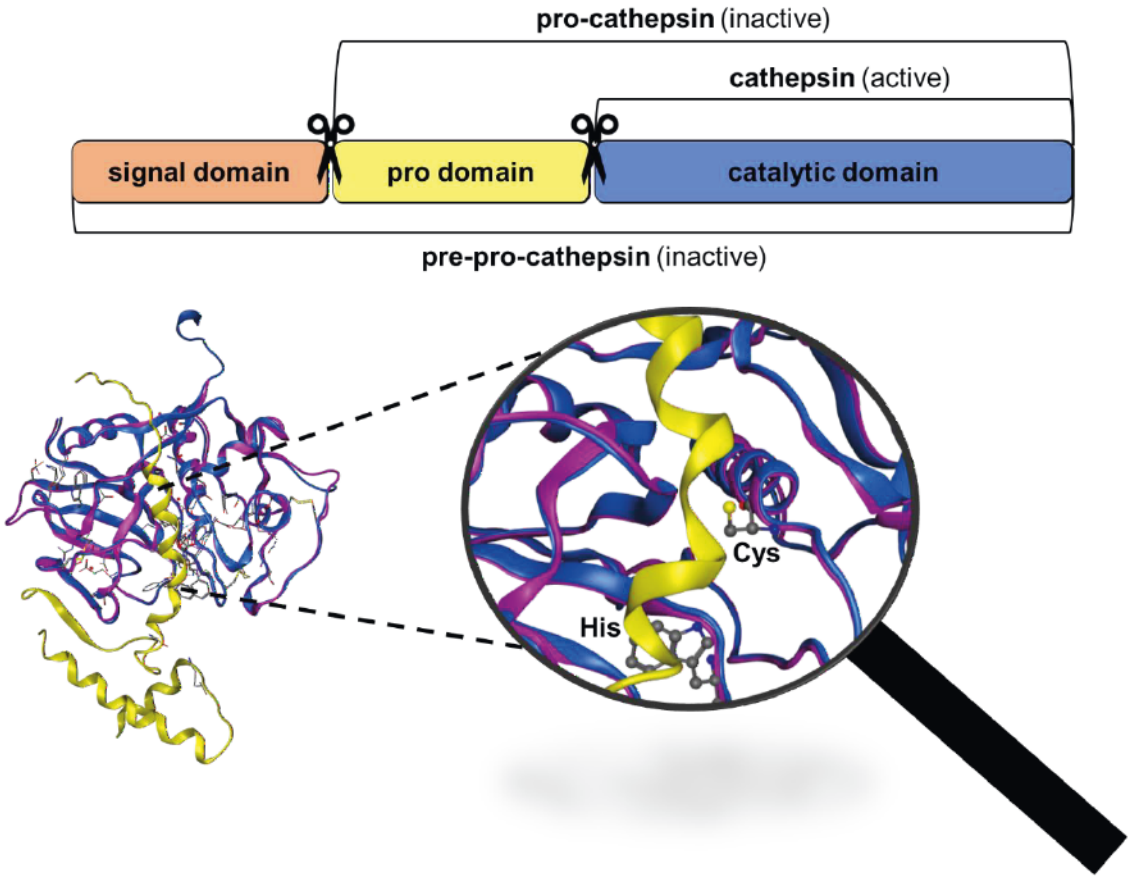

Figure 7. Schematic overview of the protease domains. The inactive precursor (pre-pro-cathepsin) is converted into the active form after cleavage of the signal peptide and pro-domain. Crystal structure overlay of active rhodesain (pdb 2p7u, purple) and pro-rhodesain (pdb 7avm blue) with the highlighted pro-peptide (yellow). The pro-peptide blocks the active site residues and thus, hinders substrate cleavage.[176,183]

The structural resemblance can be confirmed by superposition of crystal structures. **Figure 8** reveals that rhodesain (*Tb*CatL) shares a high sequence identity (45%) and structural similarity (59%) with human CatL, which is underlined by the root mean square deviation (RMSD) of 1.34 Å.[187] RMSD is a measure of the distance between two sets of coordinates in three-dimensional space, often used to quantify the structural similarity between two molecules or protein structures. It measures the average deviation of the atoms between two structures after optimal alignment, providing an overall measure of the differences in their spatial arrangement.[188,189]

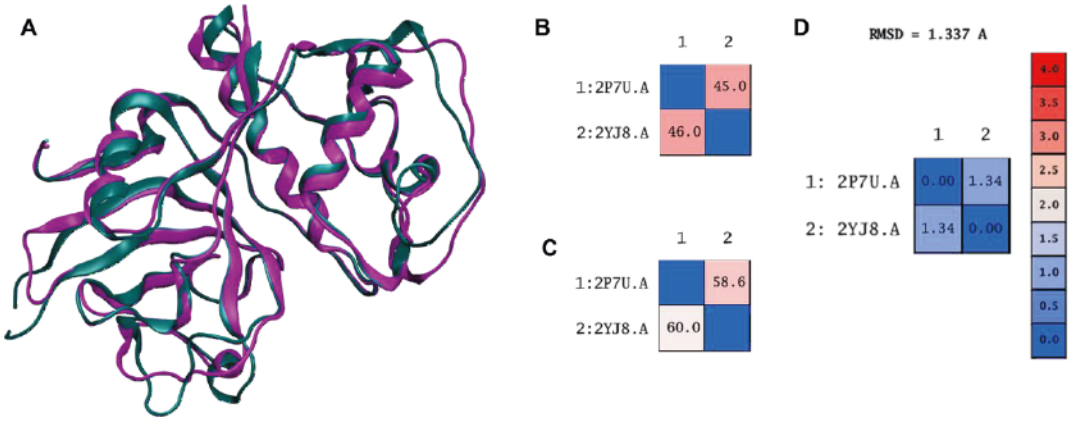

Figure 8. (**A**) Crystal structure overlay of rhodesain (pdb 2p7u, purple) and human cathepsin L (pdb 2yj8, deepteal).[190,191] Superposition performed with MOE.[187] (**B**) Calculated identity. (**C**) Calculated similarity. (**D**) Calculated RMSD.

The remarkable structural resemblance between interspecies cathepsins becomes even more apparent when comparing *Schistosoma mansoni* cathepsin B1 (*Sm*CB1) with its human equivalent, cathepsin B (CatB). CatB-like proteases possess a unique feature in the form of an occluding loop, a flexible region absent in CatL-like proteases. Under acidic conditions (pH <5.5), the occluding loop structure is responsible for the enhanced carboxypeptidase activity of CatB since it blocks part of the active site cleft.[192] This allows for two histidine residues located within the occluding loop (**Figure 9**, yellow), which are partly protonated under acidic conditions, to form ionic interactions and specifically target the C-terminal carboxyl group of a substrate peptide at the P2' position, giving preference to the cleavage of a C-terminal dipeptide.[193] Conversely, at pH values above 5.5, the normal endopeptidase activity of cathepsin B is favored.[194] This unique feature of cathepsin B highlights its versatile activity and emphasizes its importance in various biological processes.

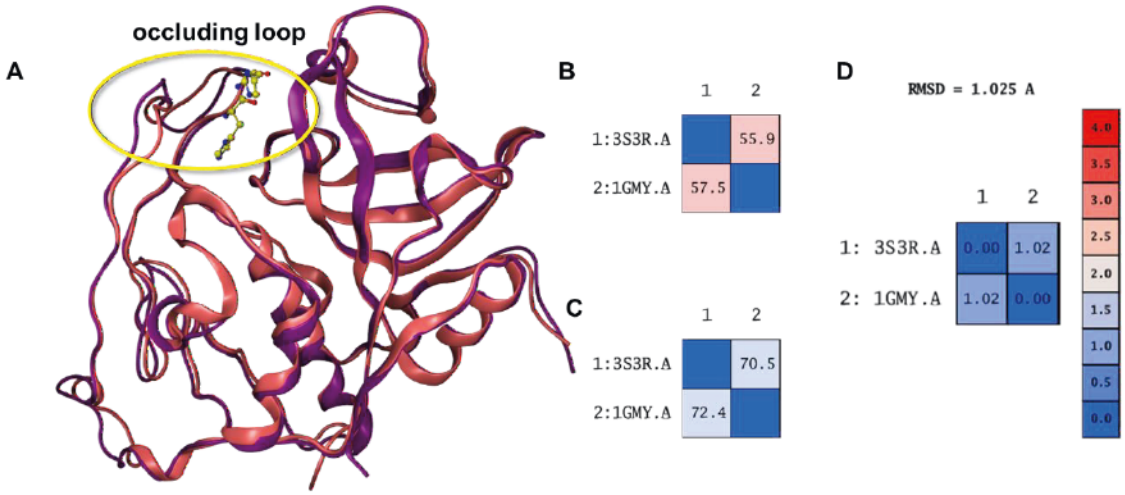

Figure 9. (**A**) Crystal structure overlay of *Sm*CB1 (pdb 3s3r, deep purple) and human cathepsin B (pdb 1gmy, salmon), occluding loop histidines in yellow.[195,196] Superposition performed with MOE.[187] (**B**) Calculated identity. (**C**) Calculated similarity. (**D**) Calculated RMSD.

As illustrated in **Figure 9**, the sequence identity between parasitic *Sm*CB1 and human CatB is 56%, while their structural similarity is 71%, resulting in an RMSD of 1.02 Å.[187]

This high degree of similarity highlights the evolutionary conservation of cathepsin structure and function across species, despite their diverse biological roles. It also suggests the potential for cross-species inhibition of cathepsins, which could be leveraged for the development of broad-spectrum therapeutics targeting cathepsin activity.

However, there are still remarkable differences between cathepsins of the same species, e.g., cathepsins B and L (**Figure 10**). They only share about 25–30% sequence identity and 38–45% structural similarity with an RMSD of 2.21 Å after alignment in MOE.[187] This is due to the fact that some cathepsins have special features, such as the occluding loop in CatB-like proteases mentioned earlier. Other important differences arise from the active site which is discussed in the following chapter **3.4**. These distinctions are crucial to develop selective inhibitors.

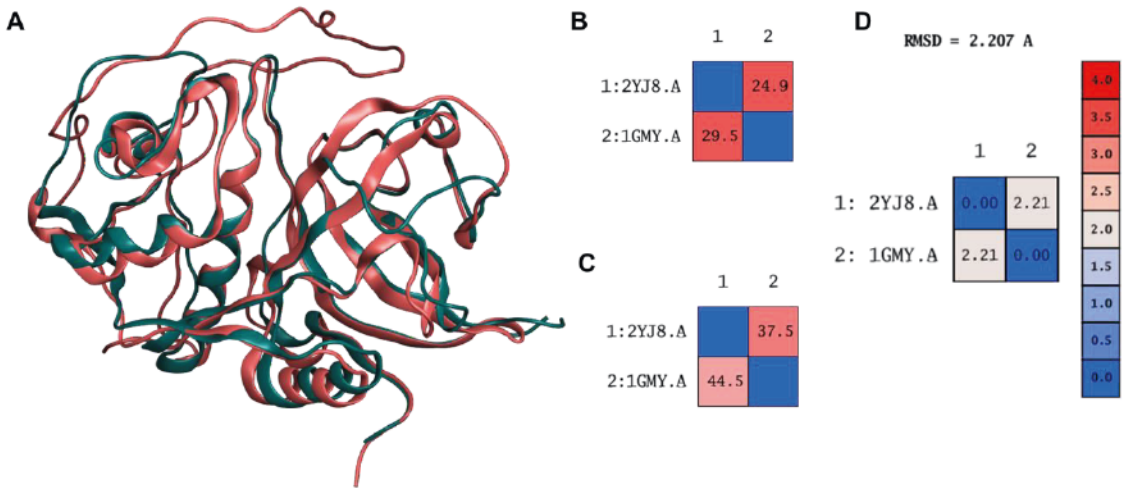

Figure 10. (**A**) Crystal structure overlay of human CatL (pdb 2yj8, deepteal) and human CatB (pdb 1gmy, salmon).[191,196] Superposition performed with MOE.[187] (**B**) Calculated identity. (**C**) Calculated similarity. (**D**) Calculated RMSD.

3.4 Active Site

The structure of C1 cysteine proteases such as cathepsins, represented by cathepsin S (CatS) complexed with the vinylsulfone morpholino-Leu-hPhe-Ψ(CH=CH−SO_2−Ph) in **Figure 11**, reveals a conserved active site in the protease family, with slight variations among different cathepsin-like proteases.[197,198]

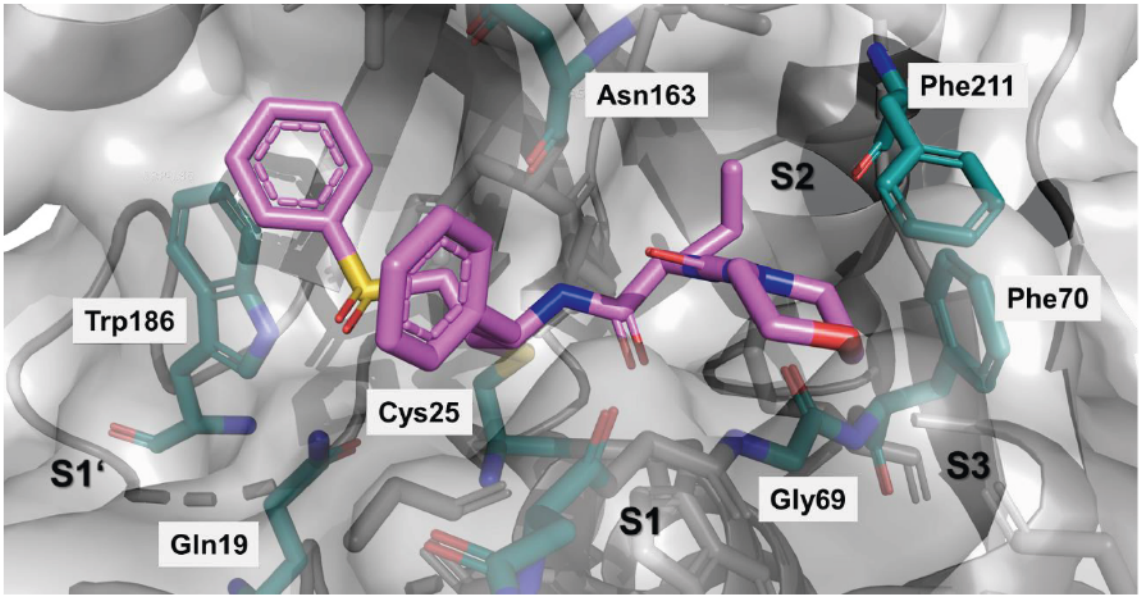

Figure 11. CatS active site (pdb 1npz) with vinylsulfone ligand morpholino-Leu-hPhe-Ψ(CH=CH−SO_2−Ph) in violet.[197] Important residues in deepteal.

The inhibitor interacts with four different regions around the active site, including three non-primed (S1–S3) and one primed site (S1'). The substrate specificity is

predominantly influenced by the S2 pocket, which favors large hydrophobic side chains such as L-phenylalanine, L-leucine or even larger residues like cyclohexylalanine, especially due to Phe211 between S2 and S3.[190,197] It can flip, therefore allowing bulkier residues in S2 compared to other cathepsins, such as CatB or CatL.[197] Although L-arginine is preferred in the S1 pocket, L-homophenylalanine is also tolerated. This is advantageous with regards to physicochemical properties since the charged L-arginine residue can decrease permeability compared to L-homophenylalanine. Both the S3 and S1' pockets are relatively unstructured and lack specificity for particular side chains.[197,198] These observations highlight the potential for rational drug design against cathepsin-like cysteine proteases by exploiting the subtle differences in the active site.

4 Covalent Protease Inhibitors

Covalent drugs have been known since the 19th century, even though their covalent mechanism of action often remained elusive until they were clinically tested or even until after they were approved. Prominent examples are aspirin, penicillin antibiotics, acetaminophen or clopidogrel.[199–202] Nevertheless, many medicinal chemists have been hesitant to introduce chemically reactive electrophilic groups into the structure of potential drugs to avoid toxicity or selectivity problems.[199] Hepatotoxicity in particular is of relevance, since electrophilic Michael acceptors can bind covalently to liver proteins, as has been shown for acetaminophen.[203] Here, metabolism to the highly reactive intermediate is essential for toxicity (see chapter **1.2.2**). These concerns have limited the development of covalent drugs for a long time.

However, covalent drugs have reemerged (**Figure 12**).[204–207] Since the beginning of the 21st century, scientists have begun to introduce mildly reactive electrophilic groups into drug candidates to address nucleophilic residues in target proteins, a process known as targeted covalent inhibition (TCI).[208,209] In contrast to the coincidental development of covalent drugs without knowing their mode of action ("serendipity"), this method relies on a structure-guided approach. Fine-tuning the chemical reactivity and selectivity of covalent drug candidates is possible due to advanced computational methods.[208,210] Designing a targeted covalent ligand can improve its inhibition properties compared to non-covalent drugs.[209,210]

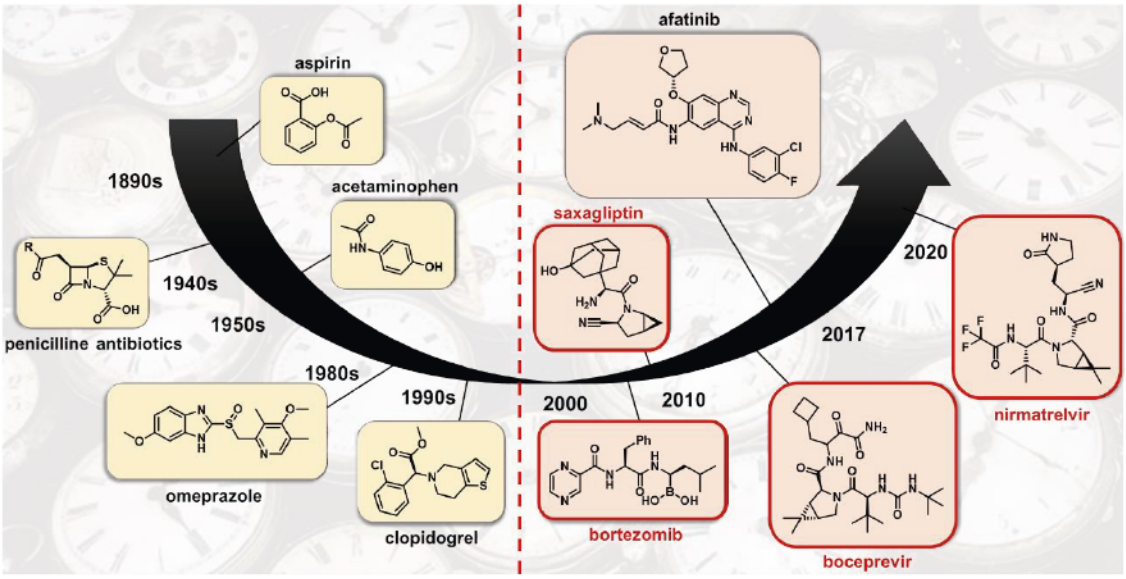

Figure 12. Covalent drug development – a timeline. Coincidental covalent drugs are highlighted in yellow, targeted covalent inhibitors are highlighted in light red. Protease inhibitors are framed in red.

One of the first approved targeted covalent protease inhibitors is the proteasome inhibitor bortezomib to treat multiple myeloma.[211] Many other protease inhibitors targeting viral proteases (e.g., boceprevir for hepatitis C virus, nirmatrelvir for severe acute respiratory syndrome coronavirus 2 (SARS-CoV-2)) have been approved as well as anti-diabetic drugs targeting dipeptidyl peptidase IV (e.g., saxagliptin).[212–215] Apart from covalent protease inhibitors, several covalent kinase inhibitors have been developed for cancer treatment (e.g., afatinib).[216,217]

Still, there are some limitations to the electrophilic groups ("warheads"). Depending on the active site residue (cysteine, serine, etc.), warheads can be more or less suitable. Appropriate warheads for cysteine proteases are discussed in chapter **4.1**.

4.1 Cysteine Protease Inhibitors

Cysteine protease inhibitors usually consist of a peptidomimetic recognition unit that is required for non-covalent interactions in the active site. These interactions bring the warhead into position, i.e., at the right angle and distance from the nucleophilic cysteine. After the warhead is in the correct position, the covalent reaction with the nucleophilic residue can occur, reversibly or irreversibly modifying the active site cysteine (see chapter **4.2**). There are few existing examples of non-covalent cysteine protease inhibitors.[218–220]

The electrophilic moiety has to be well chosen since highly reactive groups lead to selectivity issues. Nitriles are widely used due to their mild electrophilicity and reversibility, resulting in fewer off-target effects (see chapter **4.2.2**).[221,222] A prominent example is nirmatrelvir (Paxlovid®), a covalent inhibitor of the SARS-CoV-2 main protease (M^{pro}), that has been on the market since 2021 (**Figure 12**), the first oral treatment for COVID-19.[214,223] It marks a milestone not only in the COVID-19 treatment, but also in drug development since it is the first approved targeted covalent cysteine protease inhibitor with a high impact. It is used in combination with ritonavir, which acts as a "booster" to reduce the rapid metabolism of nirmatrelvir by CYP3A.[214,224] However, nitriles can also react with serine residues, which again limits their selectivity.[225,226] Saxagliptin (Onglyza®) inhibits the serine protease dipeptidyl peptidase IV and was first approved by the FDA in 2009 for the treatment of type 2 diabetes mellitus (**Figure 12**).[227]

A frequently used warhead that almost exclusively reacts with cysteines is the vinylsulfone moiety.[228–231] Contrary to nitriles, unsubstituted vinylsulfones react irreversibly with the active site cysteine but still exhibit no activity towards endogenous

thiol-containing nucleophiles.[232] Their mechanism of action and possible modifications are described in chapter **4.3**.

4.2 Covalent-Reversible vs. Covalent-Irreversible Inhibition

Different electrophilic groups result in different modes of inhibition. Acrylamides bind irreversibly to their target whereas nitriles can dissociate again.[233–235] Therefore, we distinguish covalent-irreversible from covalent-reversible inhibitors. They differ in their covalent inhibition course (chapter **4.2.1**), leading to different advantages and disadvantages (chapter **4.2.2**).

4.2.1 Covalent Inhibition Course

The reaction of a covalent inhibitor with its target protein is more complex than that of non-covalent compounds and consists of at least two steps.[236] **Figure 13** illustrates the simplest two-step mechanism.

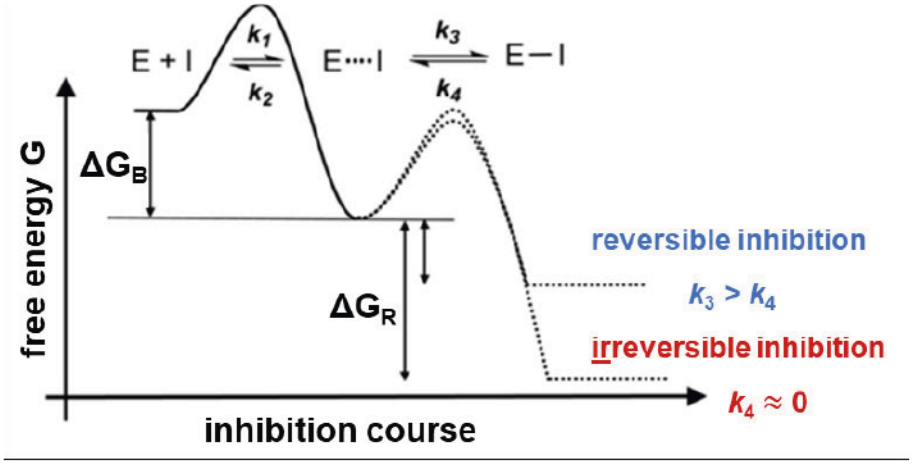

Figure 13. Energy diagram for the inhibition mechanism of a covalently reacting ligand. Figure modified after SCHIRMEISTER et al.[237]

In the first step, the ligand's recognition unit brings the molecule in position, forming a non-covalent enzyme-inhibitor complex (E····I). This reaction features non-covalent interactions of the ligand with the active site residues. It is reversible but can lead to conformational changes that enable "slow-tight binding". The IC_{50} value can be used to describe this first step. It is the inhibitor concentration that leads to 50% inhibition.[238] However, it is still dependent on the substrate concentration [S] and the MICHAELIS-MENTEN constant K_m, which is a measure for the substrate's affinity.[239] Therefore, the K_i value ($K_i = k_2/k_1$) is more suitable, also to compare different compounds. It describes the non-covalent complex as a measure for the ligand's affinity to the target protein

with non-covalent interactions.[236] IC_{50} values can be converted into K_i values with the CHENG-PRUSOFF equation for competitive inhibitors:[238]

$$K_i = \frac{IC_{50}}{(1 + \frac{[S]}{K_m})}$$

When the reactive electrophilic moiety is in the correct position, hence sufficiently close and in the right angle, it can undergo a covalent reaction with a nucleophilic residue (cysteine, serine, threonine, etc.). This is described in step two, resulting in the covalent complex (E–I). Depending on product stability, the reaction can be reversible or irreversible. If $k_4 >> 0$, the reaction can be reversible, but if $k_4 \approx 0$, the reaction is irreversible. If $k_4 << k_3$, the reaction is slowly reversible, whereas inhibitors with $k_3 \cong k_4$ often show a one-step mechanism like non-covalent reversible binders.[236,240]

For irreversible inhibition, the reaction is highly exothermic, so reversing the covalent reaction would require a too high large activation energy. The reaction course can be described as follows:[236]

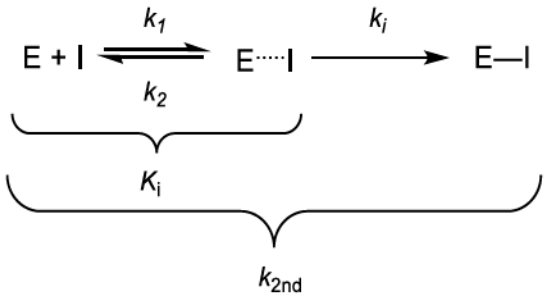

Here, the first-order rate constant describing step two, the covalent reaction's velocity, k_i (or k_{inact}) is equal to k_3 in **Figure 13**. In addition to K_i and k_i, the second-order rate constant k_{2nd} can be determined for irreversible inhibitors:[241]

$$k_{2nd} = \frac{k_i}{K_i}$$

It combines the formation and decomposition of the non-covalent complex as well as the complete irreversible inhibition process. A well-known warhead that undergoes a covalent-irreversible Michael addition with active site cysteines is the vinylsulfone moiety.[231,232]

Covalent reversible inhibitors form a weaker covalent bond than irreversible ligands. They can be subdivided into time-independent and time-dependent inhibitors based on their progress curves in enzyme assays. Depending on k_3 and k_4, they can react

in a one-step or two-step mechanism (see above). Reversible time-dependent inhibitors often react in a slowly reversible manner (k_3 >> k_4), thus imitating progress curves from irreversible inhibitors ("two-step mechanism", see **Figure 14**). **Figure 14A** and **14C** both display biphasic progress curves that indicate a two-step mechanism and are difficult to distinguish. To differentiate, further experiments have to be conducted (e.g., dilution assays).

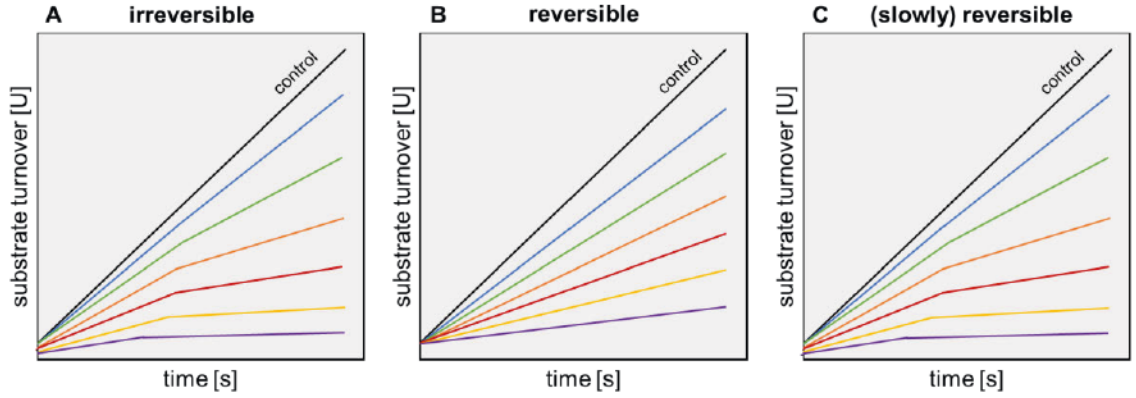

Figure 14. Schematic progress curves for different inhibitors at different concentrations. Control without added inhibitor in black. (**A**) Progress curves for irreversible inhibitors. Biphasic progress curves indicate time-dependency. (**B**) Progress curves for reversible, non-time-dependent inhibitors. Linear progress curves indicate time-independency. (**C**) Progress curves for reversible, time-dependent inhibitors. Biphasic progress curves indicate time-dependency.

Time-independent inhibitors have linear progress curves ("one-step" mechanism, $k_3 \cong k_4$) that allow the calculation of an IC_{50} value that can further be transformed into the K_i value using the CHENG-PRUSOFF equation.[238] The progress curves for time-dependent inhibitors, such as irreversible or slowly reversible inhibitors, are biphasic (**Figure 14**). Forming the non-covalent complex (E···I) is reflected in the higher slope in the beginning. After positioning the warhead in the active site, the covalent bond is forming (E–I), resulting in a slope flattening in case of time-dependent inhibitors. Those inhibitors do not react or react very slowly back to the non-covalent complex, thus blocking the binding pocket for prolonged periods of time. This results in a slower substrate turnover, hence the flattening of the slope.

For slowly reversible inhibitors, the overall reaction with the target protein can be described as follows:[236,240]

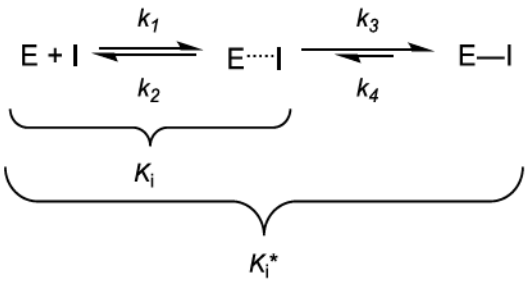

The inhibition constants can be determined using the slow-binding equation:[236]

$$[\mathrm{P}] = \mathrm{v_s} \cdot \mathrm{t} + \frac{\mathrm{v_i} - \mathrm{v_s}}{k_{\mathrm{obs}}} \cdot [1 - \exp(-k_{\mathrm{obs}} \cdot \mathrm{t})] + \mathrm{off}$$

Plotting the k_{obs} values against the inhibitor concentrations [I] results in the following equation from which K_i^{app} can be derived:[236]

$$k_{\mathrm{obs}} = k_4 + \left(\frac{k_3 \cdot [\mathrm{I}]}{K_{\mathrm{i}}^{\mathrm{app}} + [\mathrm{I}]}\right)$$

K_i^{app}, the apparent K_i, is equivalent to the IC_{50} for time-independent inhibitors. It can be used in the CHENG-PRUSOFF equation to calculate K_i.[236,238] The rate constants k_3 and k_4 can often be determined since $k_4 << k_3$ for slowly reversible tight binders.[236] Additional to K_i, which describes the non-covalent complex, the global dissociation constant K_i^* for the total covalent inhibition can be derived using the following equation:

$$K_{\mathrm{i}}^{*} = \frac{K_{\mathrm{i}}}{\left(1 + \frac{k_3}{k_4}\right)}$$

Reversible, slow-tight binders can be differentiated from irreversible inhibitors with various methods, such as dilution assays. In this method, the target enzyme is pre-incubated with the inhibitors and the mixture is then diluted with assay buffer (approximately 100-fold), followed by substrate addition. If the inhibition is reversible, the enzymatic activity will recover.[237,242]

4.2.2 Pros and Cons

Historically, covalent inhibitors have been avoided as drug candidates since they are associated with several disadvantages (**Figure 15**). As mentioned in chapter **4**, they or their metabolites can react covalently with off-target proteins, such as liver proteins. These off-target modifications are problematic for irreversible inhibitors. They can result in (hepato-)toxicity or other adverse events.[243,244] Additionally, irreversibly bound ligands remain bound even after the target protein is degraded, leading to haptenization, and thus triggering an immune response.[245] Nevertheless, covalent

inhibitors have some advantages. Due to the covalent reaction, the residence time at the target site is usually prolonged, which can improve efficiency and allow dosage reduction.[233,246] Another advantage is reduced sensitivity to pharmacokinetic effects and resistance.[245]

Modifying the ligands to be covalently reversible is an elegant way to minimize the disadvantages while preserving the advantages of covalent inhibition, as shown in **Figure 15**.[247]

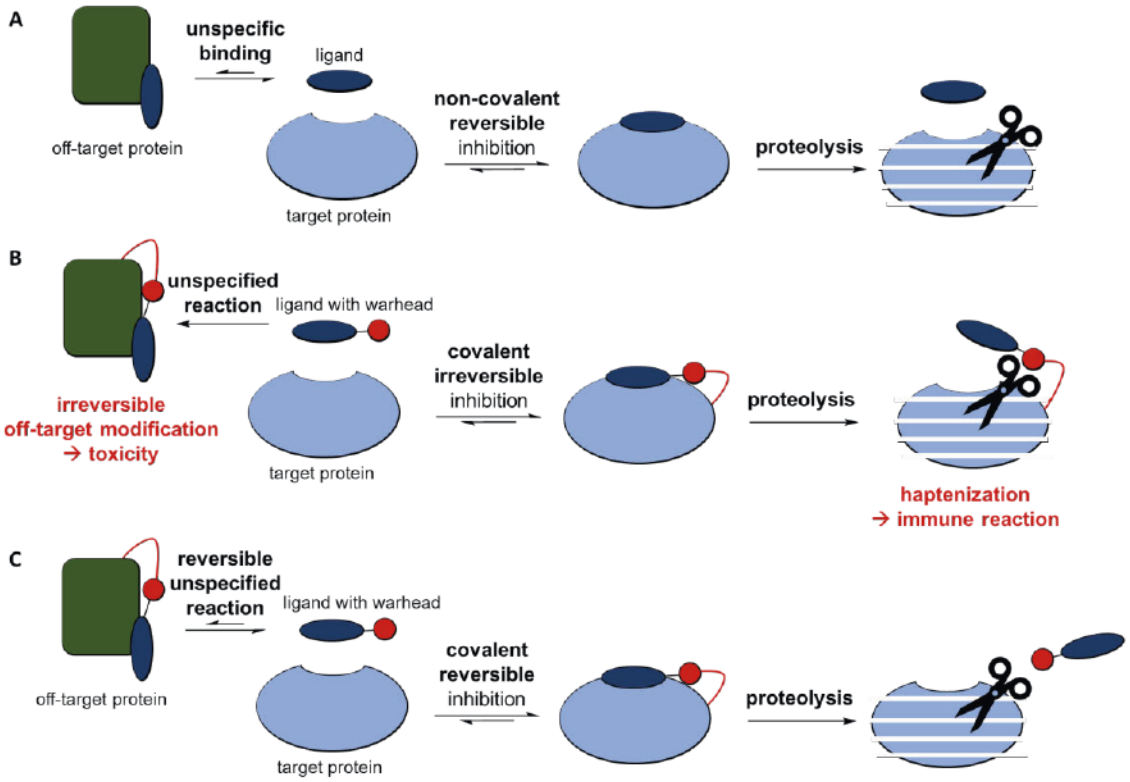

Figure 15. Inhibitor mode of action and potential side effects. Ligand in dark blue, warhead in red, target protein in light blue and off-target protein in green. (**A**) Non-covalent reversible inhibitor. Unspecific binding as well as binding to the target protein is reversible. (**B**) Covalent-irreversible inhibitor. Unspecified reactions with off-target proteins can lead to toxicity. Proteolysis results in haptenization potentially triggering immune-related side effects. (**C**) Covalent-reversible inhibitor. Improved residence time through covalent binding without risk of haptenization or irreversible off-target modifications.

4.3 Vinylsulfones and -sulfonates as Cysteine Protease Inhibitors

Vinylsulfones are known to be covalent-irreversible cysteine protease inhibitors (see **4.1**).[176,231,232] A prominent example is pan-cathepsin inhibitor **K11777** that has already entered clinical trials for Chagas disease in the past (**Figure 16**).[248–250] Apart from that, many other cathepsin-like proteases are targets for **K11777**. There are studies regarding parasitic diseases like Human African Trypanosomiasis (HAT), schistosomiasis or leishmaniasis. Other irreversible vinylsulfone-based inhibitors to

treat parasitic diseases, such as schistosomiasis, include **WRR-286** and **WRR-391**, that were both based on the **K11777** scaffold and found to be highly active against the parasite's major cysteine protease *Sm*CB1 with subnanomolar affinity.[251]

Inhibiting human cathepsins like CatB can decrease the cell entry of coronaviruses or filoviruses. More recently, a study revealed that inhibiting human CatL with **K11777** reduces the processing of the SARS-CoV-2 spike protein, blocking the infection in human and monkey cells.[252]

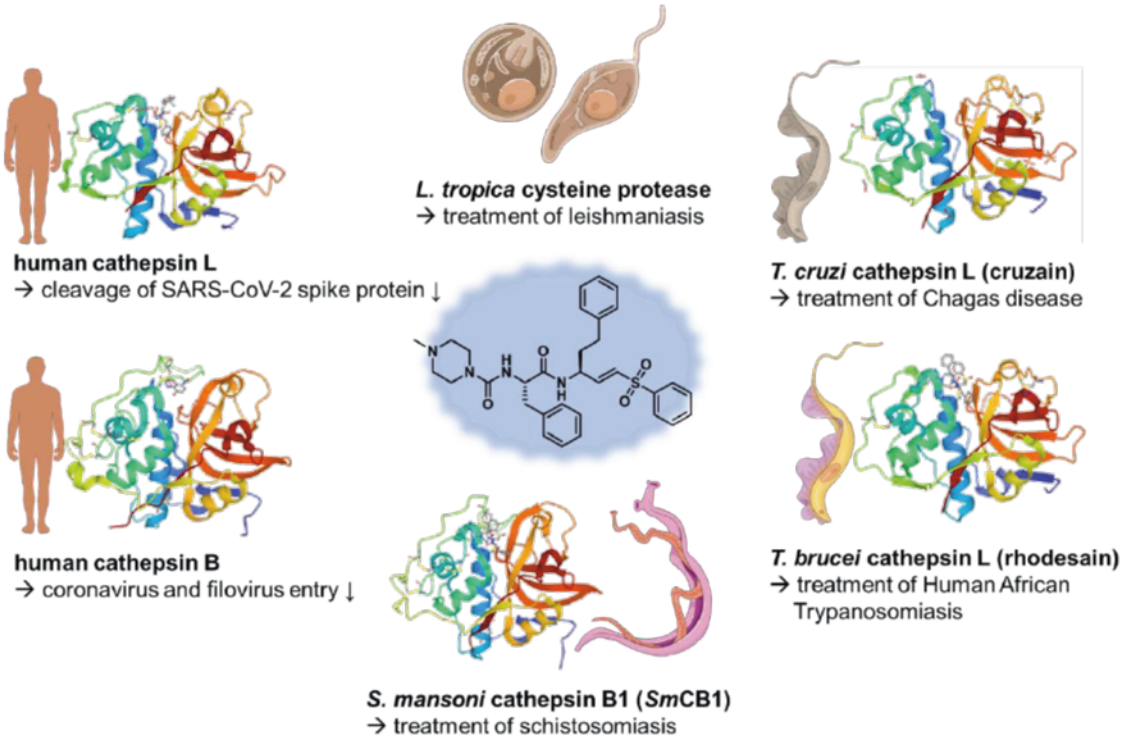

Figure 16. Structure and targets of **K11777** and the resulting effects upon its inhibition. **K11777** is a potential drug for the treatment of various diseases by targeting cathepsin-like proteases in humans (CatL, CatB) and parasites (trypanosomes, schistosomes, *Leishmania* parasites). The figure was partly generated using SERVIER MEDICAL ART, provided by SERVIER, licensed under a Creative Commons Attribution 3.0 unported license.

In preclinical investigations, **K11777** was found to have an acceptable pharmacokinetic profile, was orally bioavailable, safe in various animals, and non-mutagenic.[176,231,250,253,254] To further improve the **K11777** scaffold and warhead reactivity, [redacted] and [redacted] have conducted several studies on the parasitic cysteine protease rhodesain.[255,256]

Based on their work, I performed further optimizations in terms of pharmacokinetic properties and selectivity profile for rhodesain and other cathepsin targets. I have worked with irreversible as well as reversible inhibitors. Introducing a fluorine in the α-position of the vinylsulfone double bond results in covalent-reversible inhibitors.[237]

Scheme 2 shows the schematic reaction mechanisms of irreversible vs. reversible vinylsulfone-based inhibitors.

Both inhibitor types undergo a Michael-type addition with the nucleophilic cysteine residue in the active site.[232] The arising carbanion is then protonated, leading to a covalent enzyme-inhibitor complex. Depending on its stability (see chapter **4.2.1**), the reaction can be reversed.

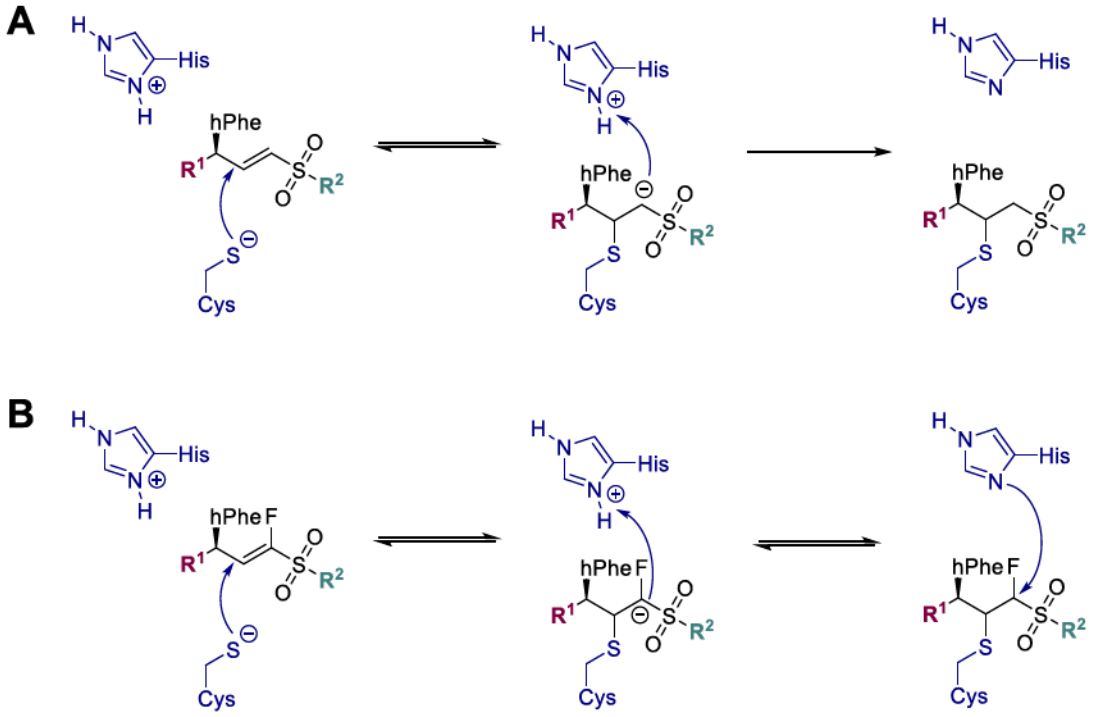

Scheme 2. Inhibition mechanism of irreversible and reversible vinylsulfone derivatives. R^1 = peptidomimetic recognition unit, R^2 = Ph for vinylsulfones or OPh for vinylsulfonates. (**A**) Irreversible vinylsulfon(at)es. After Michael addition to the active site cysteine, the formed covalent bond is stable, and the enzyme is blocked irreversibly. (**B**) Reversible fluorinated vinylsulfon(at)es. The resulting covalent bond is not as stable and can be cleaved to reverse the reaction.

The projects in this thesis focus on reversible and irreversible vinylsulfon(at)e-based inhibitors for several cathepsin-like proteases, namely the parasitic proteases *Trypanosoma brucei* cathepsin L (TbCatL, rhodesain), *Schistosoma mansoni* cathepsin B1 (SmCB1), and human cathepsin S (CatS). The inhibitors were designed with regard to selectivity towards off-target cathepsins and optimized physicochemical properties.

Projects and Objectives

The results presented in this dissertation belong to the four following projects, with three already published or in manuscript form to be submitted for publication.

Project 1: Investigating the Pharmacokinetic Properties of Rhodesain Inhibitors

The background and results of this project have already been published in the *Journal of Medicinal Chemistry* in 2021: "Fluorovinylsulfones and -Sulfonates as Potent Covalent Reversible Inhibitors of the Trypanosomal Cysteine Protease Rhodesain: Structure–Activity Relationship, Inhibition Mechanism, Metabolism, and In Vivo Studies." *J. Med. Chem.* **2021**, *64*, *16*, 12322 – 12358 (see chapter **1**).

Project 2: Optimizing the Physicochemical Properties of New *Schistosoma mansoni* Cathepsin B1 Inhibitors

This project was part of an Open Lab Initiative with [redacted]. The background and results of this project are presented in the manuscript "Dual Strategy to Design New Agents Targeting *Schistosoma mansoni*: Advancing Phenotypic and *Sm*CB1 Inhibitors for Improved Efficacy" to be submitted to *ACS Infectious Diseases* (see chapter **2**).

Project 3: Designing Potent and Selective Covalent Reversible Cathepsin S Inhibitors as Potential Immunomodulators in Cancer Therapy

This project was part of the CRC1066 (Q5 subproject). The background and results of this project are discussed in the manuscript "New subnanomolar cathepsin S inhibitors with high selectivity: Optimizing covalent-reversible α-fluorovinylsulfones and -sulfonates as potential immunomodulators in cancer" that has been submitted to *ChemMedChem* in March 2023 (see chapter **3**).

Project 4: Improving the Efficiency of Cathepsin S Inhibitors by Nanocarrier-Mediated Delivery

This project was part of the CRC1066 (Q5 subproject), continuing project 3. The background and results are presented in chapter **4**.

Publications and Manuscripts

1 Publications

1.1 Research Articles

In this dissertation:

S. Jung,* N. Fuchs,* P. Johe, A. Wagner, E. Diehl, T. Yuliani, C. Zimmer, F. Barthels, R. A. Zimmermann, P. Klein, W. Waigel, J. Meyr, T. Opatz, S. Tenzer, U. Distler, H.-J. Räder, C. Kersten, B. Engels, U. A. Hellmich, J. Klein, and T. Schirmeister. "Fluorovinylsulfones and -Sulfonates as Potent Covalent Reversible Inhibitors of the Trypanosomal Cysteine Protease Rhodesain: Structure–Activity Relationship, Inhibition Mechanism, Metabolism, and In Vivo Studies." *J. Med. Chem.* **2021**, *64*, *16*, 12322 – 12358.

Not included:

S. Jung, N. Fuchs, C. Grathwol, U. A. Hellmich, A. Wagner, E. Diehl, T. Willmes, C. Sotriffer, and T. Schirmeister. "New peptidomimetic rhodesain inhibitors with improved selectivity towards human cathepsins" *Eur. J. Med. Chem.* **2022**, *238*, 114460.

S. Brinkmann,* S. Semmler,* C. Kersten, M. A. Patras, M. Kurz, N. Fuchs, S. J. Hammerschmidt, J. Legac, P. E. Hammann, A. Vilcinskas, P. J. Rosenthal, T. Schirmeister, A. Bauer, and T. F. Schäberle. "Identification, Characterization, and Synthesis of Natural Parasitic Cysteine Protease Inhibitors: Pentacitidins Are More Potent Falcitidin Analogues" *ACS Chem. Biol.* **2022**, *17*, *3*, 576 – 589.

W. Soerjawinata, K. Schlegel, N. Fuchs, A. Schüffler, T. Schirmeister, R. Ulber, and P. Kampeis. "Applicability of a single-use bioreactor compared to a glass bioreactor for the fermentation of filamentous fungi and evaluation of the reproducibility of growth in pellet form" *Eng. Life Sci.* **2021**, *21*, *5*, 324 – 339.

1.2 Reviews

Not included:

N. Fuchs,* M. Meta,* D. Schuppan, L. Nuhn, and T. Schirmeister. "Novel Opportunities for Cathepsin S Inhibitors in Cancer Immunotherapy by Nanocarrier-Mediated Delivery" *Cells* **2020**, *9*, *9*, 2021.

*shared first authorship

2 Manuscripts

In this dissertation:

N. Fuchs,* M. Meta,* B. Lantzberg, M. Bros, S. L. Kuan, T. Weil, and T. Schirmeister. "New subnanomolar cathepsin S inhibitors with high selectivity: Optimizing covalent-reversible α-fluorovinylsulfones and -sulfonates as potential immunomodulators in cancer", submitted to *ChemMedChem*.

N. Fuchs,* R. A. Zimmermann,* M. Schwickert,* A. Gunkel, C. Zimmer, M. Meta, K. Schwickert, J. Keiser, W. Kiefer, and T. Schirmeister. "Dual Strategy to Design New Agents Targeting *Schistosoma mansoni*: Advancing Phenotypic and *Sm*CB1 Inhibitors for Improved Efficacy", to be submitted to *ACS Infectious Diseases*.

*shared first authorship

Results and Discussion

1 Fluorovinylsulfones and -Sulfonates as Potent Covalent Reversible Inhibitors of the Trypanosomal Cysteine Protease Rhodesain: Structure-Activity Relationship, Inhibition Mechanism, Metabolism, and *In Vivo* Studies

4.1 Summary and Own Contribution

Human African Trypanosomiasis (HAT, African sleeping sickness) is a severe parasitic disease classified as a neglected tropical disease (NTD).[257] The causative protozoan parasites are trypanosomes (*Trypanosoma brucei, T. b.*), transmitted to humans via tsetse flies.[258] The pathophysiology of HAT is shown in **Figure 17**.

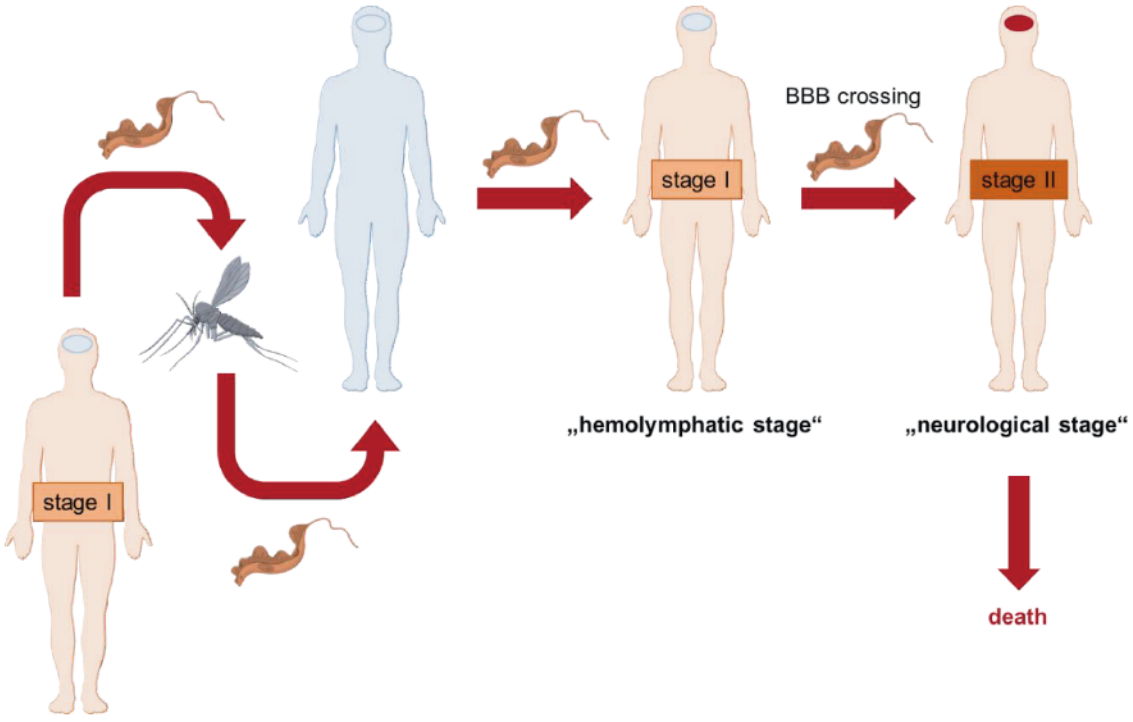

Figure 17. Pathophysiology of Human African Trypanosomiasis. Trypanosomes are transmitted from infected to healthy humans via tsetse flies. Firstly, the patients develop a hemolymphatic stage of the trypanosomal infection with unspecific symptoms. After crossing the blood-brain barrier (BBB), the trypanosomes infect brain tissue resulting in more severe symptoms and, eventually, death.

The parasitic infection starts with the hemolymphatic stage (stage I) with rather unspecific symptoms (e.g., headache, fever, pruritus).[259] During disease progression, the trypanosomes cross the blood-brain barrier (BBB), proceeding to the neurological stage (stage II). Stage II is characterized by sleep disturbances, leading to coma and

death if left untreated.[259] However, most available drugs (e.g., melarsoprol, suramin) show severe toxicity, poor bioavailability, and need long-time administration due to their lack of efficiency, resulting in an urgent need to develop new therapies against HAT.[260]

Parasite development and disease progression rely on rhodesain (*Tb*CatL), a major trypanosomal cysteine protease (**Figure 18**). Rhodesain is a cathepsin L-like protease from the papain family involved in degrading host immunoglobulins, iron acquisition, turning over variant surface glycoproteins, and crossing the BBB.[176,183,259,261] Rhodesain is considered a promising target for drug development against HAT.[262]

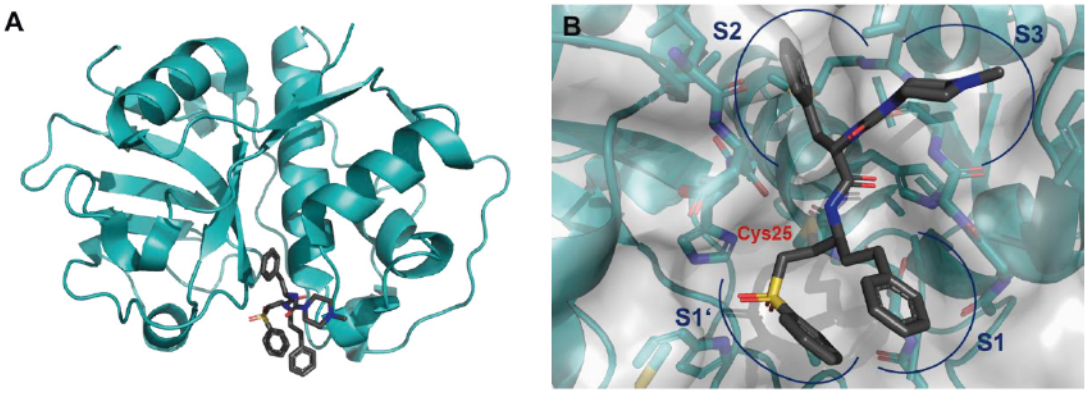

Figure 18. Crystal structure of rhodesain (PDB: 2p7u) with **K11777** bound in the active site.[176] (**A**) Structural overview. (**B**) **K1177** (dark grey) in the active site bound covalently to Cys25 (red label).

Here, we designed, synthesized, and evaluated a series of fluorinated vinylsulfones and -sulfonates based on the **K11777** scaffold, resulting in covalent reversible rhodesain inhibitors with a high affinity, low cytotoxicity, and improved antitrypanosomal activity and selectivity towards human cathepsins. Furthermore, we investigated their biodistribution, especially their ability to cross the BBB. Our findings suggest that compound **2d-(H)** crosses the BBB and accumulates in brain tissue, making it a potential candidate for further optimizations to develop new drugs against HAT.

The resulting article was published in the *Journal of Medicinal Chemistry* titled "Fluorovinylsulfones and -sulfonates as potent covalent reversible inhibitors of the trypanosomal cysteine protease rhodesain: structure-activity relationship, inhibition mechanism, metabolism, and *in vivo* studies".[242]

My contribution to the publication is shown in **Figure 19** and consisted of re-synthesizing vinysulfone-based inhibitors (**1**, **2d-(H)**) that were previously designed

by [redacted] and [redacted] to investigate their pharmacokinetic properties.[255,256]

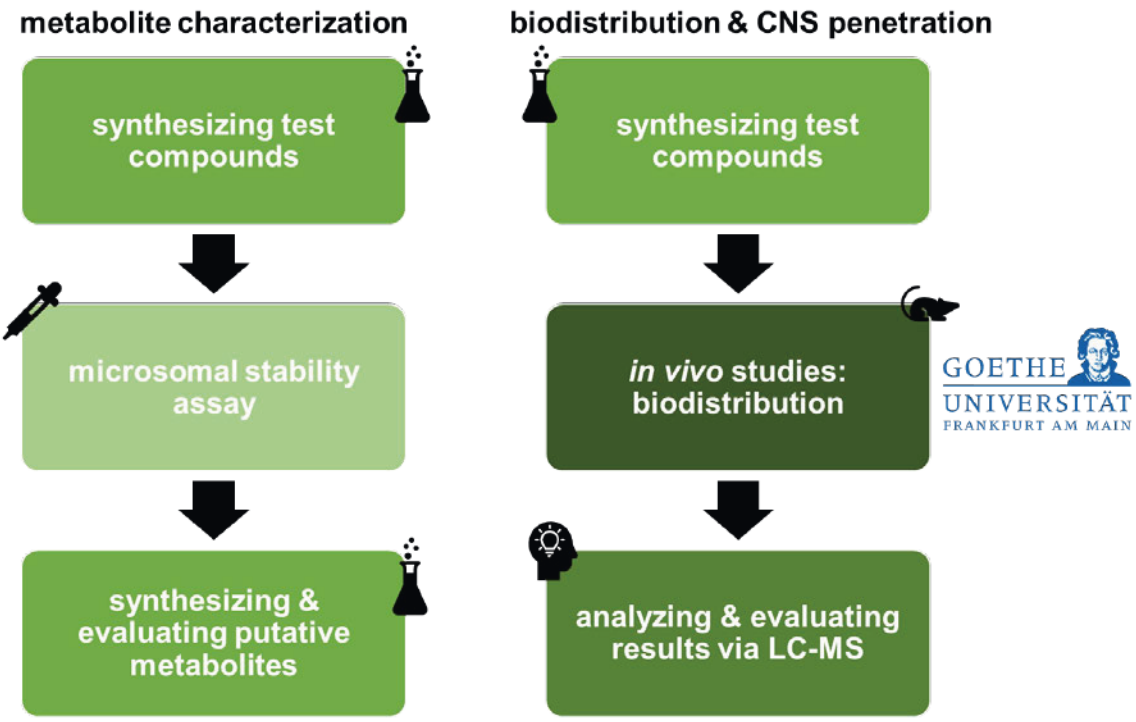

Figure 19. Workflow for project 1.

Own contribution: (re-)synthesis of **1, 2d-(H),** synthesis of their putative metabolites (**1a**, **1b**, **2l**), microsomal stability assays, HPLC-MS assays for metabolite characterization, fluorometric enzyme assays for metabolites and **2d-(H)**, biodistribution studies in collaboration with [redacted] from PROF. DR. [redacted]'s group, sample preparations from tissues, HPLC-MS method for tissue-derived samples, writing parts of the article and the supporting information, preparing figures (18, 19), schemes (4–6), and tables (7, 8).

Contribution from others: original design of the compounds (**1–4l**), molecular docking experiments, synthesis of compounds **1–4l**, fluorometric enzyme assay for compounds **1–4l,** ESI-MS and MALDI-MS experiments, MTT assay, QM/MM calculations, rhodesain expression and purification, anti-trypanosomal activity assay, writing of the original draft.

Supporting Information is available at the following link: *https://pubs.acs.org/doi/10.1021/acs.jmedchem.1c01002?goto=supporting-info*

1.2 Publication

Journal of Medicinal Chemistry

pubs.acs.org/jmc Article

Fluorovinylsulfones and -Sulfonates as Potent Covalent Reversible Inhibitors of the Trypanosomal Cysteine Protease Rhodesain: Structure−Activity Relationship, Inhibition Mechanism, Metabolism, and In Vivo Studies

Sascha Jung,[‡‡] Natalie Fuchs,[‡‡] Patrick Johe, Annika Wagner, Erika Diehl, Tri Yuliani, Collin Zimmer, Fabian Barthels, Robert A. Zimmermann, Philipp Klein, Waldemar Waigel, Jessica Meyr, Till Opatz, Stefan Tenzer, Ute Distler, Hans Joachim Räder, Christian Kersten, Bernd Engels, Ute A. Hellmich, Jochen Klein, and Tanja Schirmeister*

Cite This: J. Med. Chem. 2021, 64, 12322 12358 Read Online

ACCESS | Metrics & More | Article Recommendations | Supporting Information

ABSTRACT: Rhodesain is a major cysteine protease of *Trypanosoma brucei rhodesiense*, a pathogen causing Human African Trypanosomiasis, and a validated drug target. Recently, we reported the development of α-halovinylsulfones as a new class of covalent reversible cysteine protease inhibitors. Here, α-fluorovinylsulfones/-sulfonates were optimized for rhodesain based on molecular modeling approaches. **2d**, the most potent and selective inhibitor in the series, shows a single-digit nanomolar affinity and high selectivity toward mammalian cathepsins B and L. Enzymatic dilution assays and MS experiments indicate that **2d** is a slow-tight binder (K_i = 3 nM). Furthermore, the nonfluorinated **2d-(H)** shows favorable metabolism and biodistribution by accumulation in mice brain tissue after intraperitoneal and oral administration. The highest antitrypanosomal activity was observed for inhibitors with an N-terminal 2,3-dihydrobenzo[*b*][1,4]dioxine group and a 4-Me-Phe residue in P2 (**2e/4e**) with nanomolar EC_{50} values (0.14/0.80 μM). The different mechanisms of reversible and irreversible inhibitors were explained using QM/MM calculations and MD simulations.

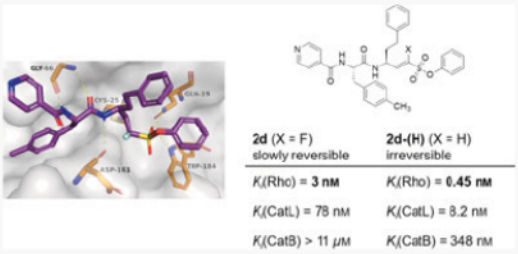

INTRODUCTION

Human African Trypanosomiasis (HAT, sleeping sickness) is a severe disease classified as a neglected tropical disease (NTD).[1] HAT is caused by the protozoan parasite *Trypanosoma brucei* (*T. brucei*), which is transmitted to humans via the bite of the Tsetse fly.[2] Sleeping sickness is fatal if left untreated. Pentamidine and suramin are used to treat the early, hemolymphatic stage of the disease, while eflornithine and melarsoprol and the combination therapy nifurtimox-eflornithine target the late, neurological stage of the disease.[3] Recently, the nitroimidazole fexinidazole was introduced as the first oral treatment of both, stage-1 and stage-2 *T. b. gambiense* HAT.[4] However, most available drugs show severe toxicity, poor bioavailability, and need long-time administration due to their lack of efficiency.[5] Therefore, there is an urgent need to develop new therapies against this disease and, in addition, *T. brucei* can serve as a valuable model organism for other pathogenic kinetoplastid diseases. The cysteine protease rhodesain (*Tb*CatL) is essential for the development of the parasite and for the progression of the disease.[6,7] Inhibition of the parasitic cysteine protease activity has been validated as a drug target in vitro and in vivo.[8] Consequently, rhodesain represents a promising target for the development of safer drugs against HAT.

Rhodesain belongs to the papain family of cysteine proteases and shares high structural similarity with the human cathepsins, especially cathepsin L (CatL; sequence identity 44.7%, similarity 59.1%, C_α-RMSD 1.35 Å).[9,10] A prominent inhibitor of papain-family cysteine proteases is K11777, a peptide-based vinylsulfone that mimics the autoinhibition of prorhodesain and that reacts in a Michael-type addition with the active-site cysteine (Figure 1).[10,11] The arising carbanion is protonated, resulting in the irreversible formation of the covalent enzyme inhibitor complex. Substitution of the hydrogen at the α-position of the

Received: June 3, 2021
Published: August 11, 2021

https://doi.org/10.1021/acs.jmedchem.1c01002
J. Med. Chem. 2021, 64, 12322 12358

Journal of Medicinal Chemistry pubs.acs.org/jmc Article

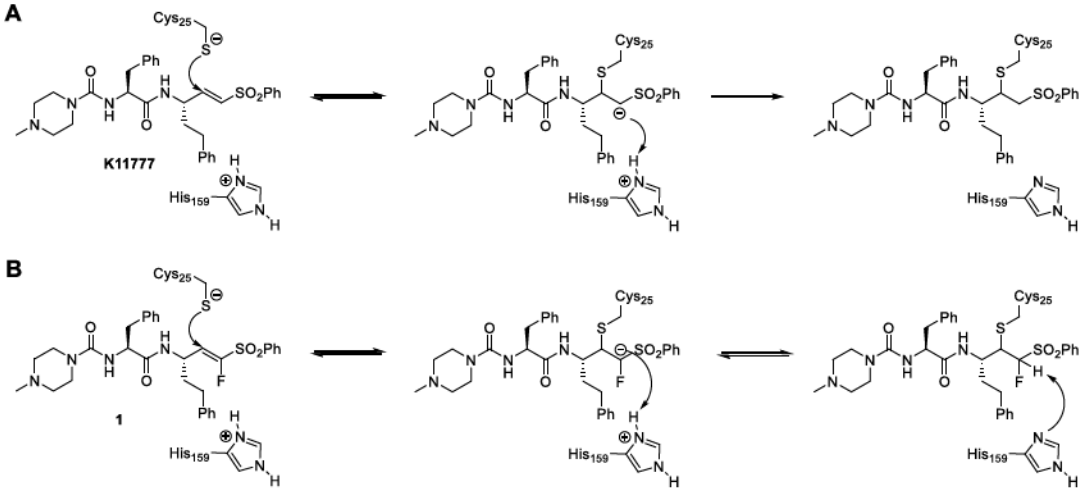

Figure 1. Structures and inhibition mechanisms of irreversible (**K11777**; A) and covalent reversible (**1**; B) peptide-based vinylsulfones.

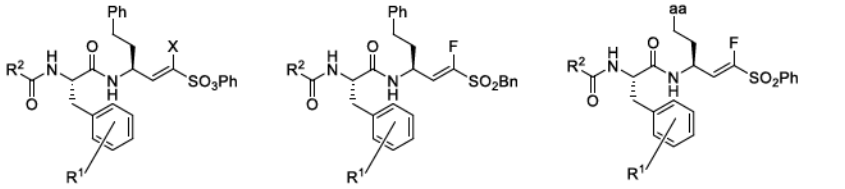

2a	R^1 = H, R^2 = 4-Pyr, X = F	**3a**	R^1 = H, R^2 = 4-Pyr	**4a**	R^1 = H, R^2 = 4-Pyr, aa = hPhe
2a-(*Z*)	R^1 = H, R^2 = 4-Pyr, X = F	**3b**	R^1 = H, R^2 = DHBD	**4b**	R^1 = H, R^2 = DHBD, aa = hPhe
2b	R^1 = H, R^2 = DHBD, X = F	**3c**	R^1 = H, R^2 = 3,5-DiFPh	**4c**	R^1 = H, R^2 = 3,5-DiFPh, aa = hPhe
2d	R^1 = 4-Me, R^2 = 4-Pyr, X = F	**3d**	R^1 = 4-Me, R^2 = 4-Pyr	**4d**	R^1 = 4-Me, R^2 = 4-Pyr, aa = hPhe
2d-(H)	R^1 = 4-Me, R^2 = 4-Pyr, X = H	**3e**	R^1 = 4-Me, R^2 = DHBD	**4e**	R^1 = 4-Me, R^2 = DHBD, aa = hPhe
2e	R^1 = 4-Me, R^2 = DHBD, X = F	**3f**	R^1 = 4-Me, R^2 = 3,5-DiFPh	**4f**	R^1 = 4-Me, R^2 = 3,5-DiFPh, aa = hPhe
2f	R^1 = 4-Me, R^2 = 3,5-DiFPh, X = F	**3g**	R^1 = 3-Me, R^2 = 4-Pyr	**4g**	R^1 = 3-Me, R^2 = 4-Pyr, aa = hPhe
2g	R^1 = 3-Me, R^2 = 4-Pyr, X = F	**3h**	R^1 = 3-Me, R^2 = DHBD	**4h**	R^1 = 3-Me, R^2 = DHBD, aa = hPhe
2h	R^1 = 3-Me, R^2 = DHBD, X = F	**3i**	R^1 = 3-Me, R^2 = 3,5-DiFPh	**4i**	R^1 = 3-Me, R^2 = 3,5-DiFPh, aa = hPhe
2i	R^1 = 3-Me, R^2 = 3,5-DiFPh, X = F			**4j**	R^1 = H, R^2 = *N*-MePip, aa = Met
2j	R^1 = H, R^2 = OBn, X = F			**4k**	R^1 = H, R^2 = 4-Pyr, aa = Met
2k	R^1 = H, R^2 = *N*-MePip, X = F			**4l**	R^1 = H, R^2 = *N*-MePip, aa = Cys(Bn)

Figure 2. Structures of compounds **2a**–**4l**.

double bond by fluorine (compound **1**) generates an α-fluorovinylsulfone, which can undergo a reversible Michael-type addition with thiols (Figure 1).[12]

The development of covalent inhibitors has seen a resurgence in academia as well as in the industry during the past decade.[13] There is much debate on the advantages and disadvantages of covalent inhibition, especially concerning reversible covalent inhibition mechanisms.[14] On the one hand, covalent reversible inhibitors alleviate some of the concerns arising from covalent irreversible protein modifications, such as toxicity emerging from off-target effects,[15] idiosyncratic toxicity,[16] and haptenization,[17] but maintain benefits such as enhanced potency and prolonged residence times.[18,19] In recent studies with reversible fluorinated vinylsulfones and their irreversible counterparts, it was shown that the electrophilic group, the so-called warhead, and not the binding of the peptidic recognition unit limits the kinetics of inhibition of the protease and that the fluorinated vinylsulfone warhead reduces the rate constant of binding.[20,21]

https://doi.org/10.1021/acs.jmedchem.1c01002
J. Med. Chem. 2021, 64, 12322 12358

Scheme 1. Synthesis of Building Blocks 13 17[a]

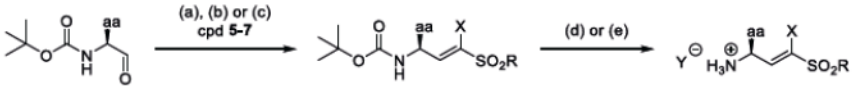

VI aa = hPhe
VII aa = Met
VIII aa = Cys(Bn)

(a) 8 R = Ph, X = F, aa = hPhe
9 R = OPh, X = F, aa = Met
(Z)-9 R = OPh, X = F, aa = Cys(Bn)
(b) 10 R = Bn, X = F, aa = hPhe
(c) 9-(H) R = OPh, X = H, aa = hPhe
11 R = Ph, X = F, aa = Met
12 R = Ph, X = F, aa = Cys(Bn)

(d) 13 Y = Cl, R = Ph, X = F, aa = hPhe
14 Y = Cl, R = OPh, X = F, aa = hPhe
(Z)-14 Y = Cl, R = OPh, X = F, aa = hPhe
14-(H) Y = Cl, R = OPh, X = H, aa = hPhe
15 Y = Cl, R = Bn, X = F, aa = hPhe
(e) 16 Y = TFA, R = Ph, X = F, aa = Met
17 Y = TFA, R = Ph, X = F, aa = Cys(Bn)

[a]Reagents and conditions: aa = amino acid side chain; (a) NaH, THF, 0 °C, 1 h, 22 43%; (b) KHMDS, THF, 78 °C for 20 min, 1 h at rt, 47%; (c) LHMDS, THF, 78 °C for 30 min, 12 h at rt, 54 75%; (d) 4 M HCl in dioxane, rt, 30 min, quant.; and (e) TFA, DCM, 0 °C, 1 h, quant.

Scheme 2. Preparation of Phosphonates 5 7[a]

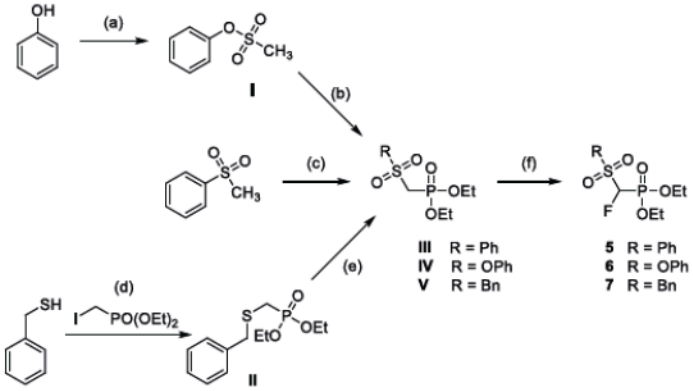

[a]Reagents and conditions: (a) Ms-Cl, TEA, EtOAc, 0 °C to rt, 30 min, 92%; (b) diethyl chlorophosphite (DECP), KHMDS, THF, 78 to 60 °C, 1 h, 74%; (c) DECP, *n*-BuLi, THF, 0 °C, 1 h, 52%; (d) NaH, THF, 0 °C to rt, 4 h, 84%; (e) *m*CPBA, DCM, 0 °C to rt, 12 h, 99%; and (f) Selectfluor, KHMDS, THF/DMF, 78 °C to rt, 3 h, 48 62%.

Based on the previously reported structure of the covalent reversible inhibitor 1,[12] in the present study we performed structure activity relationship (SAR) studies to optimize inhibition potency for rhodesain and selectivity against human cathepsins B and L using molecular docking approaches. Additionally, quantum chemical-based computations were performed to get further information about the differences in the inhibition mechanisms of K11777 and its fluorinated counterpart 1. These studies were performed because in our previous study, the computed reaction energies for X = F and X = H in the α-position of the warhead (Figure 1) did not differ significantly. Thus, the transition from irreversible to reversible inhibition by exchange of hydrogen by fluorine could not be explained conclusively. The covalent behavior of the compounds was experimentally evaluated with MS studies, and reversibility was demonstrated with enzymatic dilution and dialysis assays.

Furthermore, the ADME parameters of compound 1 and the optimized inhibitor **2d-(H)** were investigated via in vitro metabolism studies and in vivo mouse studies in order to determine their organ distribution and their accumulation in brain tissue, thus evaluating their potential as candidates for the treatment of stage-2 HAT.

RESULTS AND DISCUSSION

Design of Inhibitors. Structural variations of the fluorinated vinylsulfone 1 (Figure 1B) were inspired by peptide-based inhibitors of rhodesain, which contain structural elements at the P3, P2, and P1′ positions[21] that are known to either enhance potency against rhodesain and/or increase selectivity against CatL and CatB.[22−25] For the P3 position, introduction of aromatic and heteroaromatic systems was reported to favor inhibition of rhodesain over CatL and CatB.[22−24] Introduction of an additional methyl group to the 3- or 4-position of the phenylalanine aromatic ring at the P2 position can improve potency and selectivity for rhodesain.[22] Additionally, the extension of the phenyl ring at the warhead into the S1′ pocket via linker atoms increases potency for rhodesain.[25] Based on these observations, a virtual library of 511 modified compounds was generated. These compounds were docked at rhodesain (crystal structure of rhodesain bound to K11777, protein databank (PDB) 2p7u[11]) using FlexX[26] and DOCKTITE,[27] as reported previously (Table S1).[12] The noncovalent enzyme inhibitor complex was generated with FlexX, and the scores reflect whether the designed compounds have an improved noncovalent affinity compared to the starting vinylsulfone 1. Only compounds with a comparable or higher score were selected for synthesis. In addition, the covalent complex was modeled with DOCKTITE.[27] In this case, the scores (Table S1)

https://doi.org/10.1021/acs.jmedchem.1c01002
J. Med. Chem. 2021, 64, 12322 12358

Scheme 3. Synthesis of Compounds 2a 4l from Building Blocks 13 17[a]

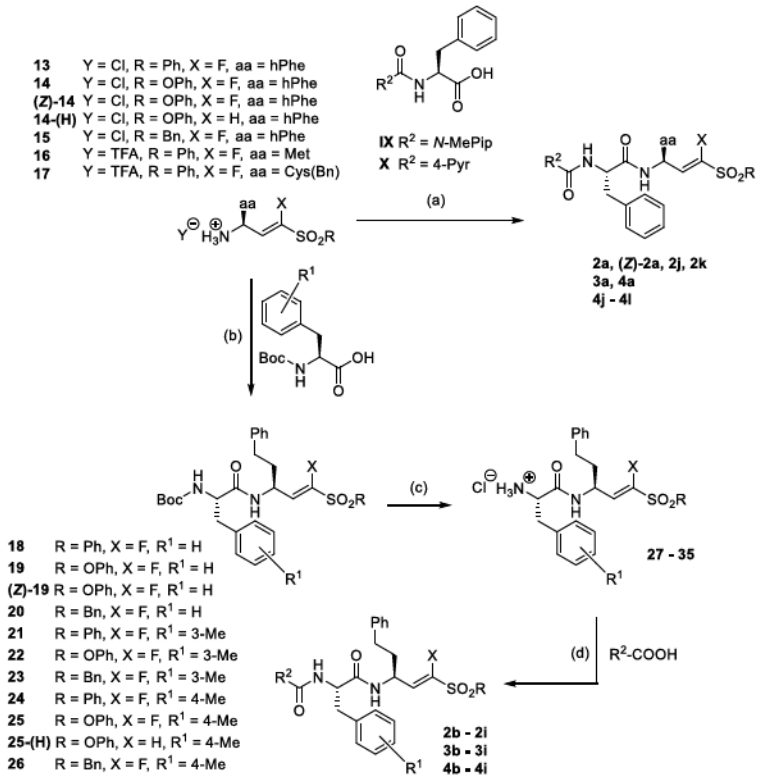

[a]Reagents and conditions: (a) TBTU, HOBt, DIEA, DMF, 0 °C to rt, 12 h, 59 81%; (b) TBTU, HOBt, DIEA, DCM, 0 °C to rt, 12 h, 69 83%; (c) 4 M HCl in dioxane, rt, 30 min, quant.; and (d) TBTU, DIEA, DCM, 0 °C to rt, 12 h, 62 84%.

may be interpreted in terms of stability of the protein-bound state.

Based on the results obtained from docking, a series of compounds (2a 4i) were selected for synthesis and subsequent evaluation of SAR (Figure 2). For all selected compounds, scores obtained from both docking approaches were generally higher when compared to starting compound 1 (Table S1). Depending on the substitution pattern of the warhead at the P1′ position, compounds can be subdivided into aromatic fluorovinylsulfones (phenyl substituent at P1′, cpds 4a 4i), aliphatic fluorovinylsulfones (benzyl group at P1′, cpds 3a 3i), and fluorovinylsulfonates (phenol ester at P1′, cpds 2a 2k).

Based on noncovalent docking (Table S1), compounds (4j 4l) with methionine and *S*-benzylcysteine at P1 were suggested to show a comparable (yet slightly lower) affinity to the respective molecules with a homophenylalanine residue. Therefore, these compounds were included in the present study and investigated for their potency.

Chemistry. Compounds 2a 4l (Figure 2) were synthesized using Horner Wadsworth Emmons (HWE) chemistry as the key step (Scheme 1). The required boc-protected aminoaldehydes (VI VIII) were prepared using Weinreb chemistry. The appropriate phosphonates (5 7) were synthesized in three different ways (Scheme 2). The preparation of phosphonate 5 has been published previously.[12] Phosphonates 6 and 7 were obtained by fluorination of the respective nonhalogenated precursors (IV, V) with Selectfluor in the presence of KHMDS. The nonhalogenated precursors (III V) were synthesized according to literature procedures.[28]

HWE olefination of the aldehydes (VI VII) with the respective phosphonates (5 7) provided the corresponding boc-protected vinylsulfones (8 12) as mixtures of (*E*)/(*Z*)-isomers (Scheme 1), whereby the (*E*)-isomer was generally favored under the employed conditions. Overall yields ranged from 59 to 75%. The (*E*)-isomers were isolated by column chromatography in acceptable yields (41 63%) and used for the next steps. In the case of vinylsulfonate 9, the (*Z*)-isomer was also isolated ((*Z*)-9, yield 22%). In the next step, the boc-group was removed using standard protocols, either 4 M HCl in dioxane or TFA in DCM, giving the amine building blocks 13 17 in quantitative yields (Scheme 2). These building blocks were subjected to peptide chemistry based on the boc strategy with TBTU/HOBt as the coupling reagent (Scheme 3). The desired compounds (2a 4l) were obtained after one or two coupling and deprotection steps.

The metabolites of compounds 1 and 2d-(H), namely 1a, 1b, and 2l, were synthesized using similar procedures to that described above. For the *N*-demethylated metabolite 1a (Scheme 4), vinylsulfone 13 was coupled with XIII. After removal of the boc group, 1a was obtained with a yield of 93%.

https://doi.org/10.1021/acs.jmedchem.1c01002
J. Med. Chem. 2021, 64, 12322 12358

Scheme 4. Synthesis of the *N*-Demethylated Metabolite 1a[a]

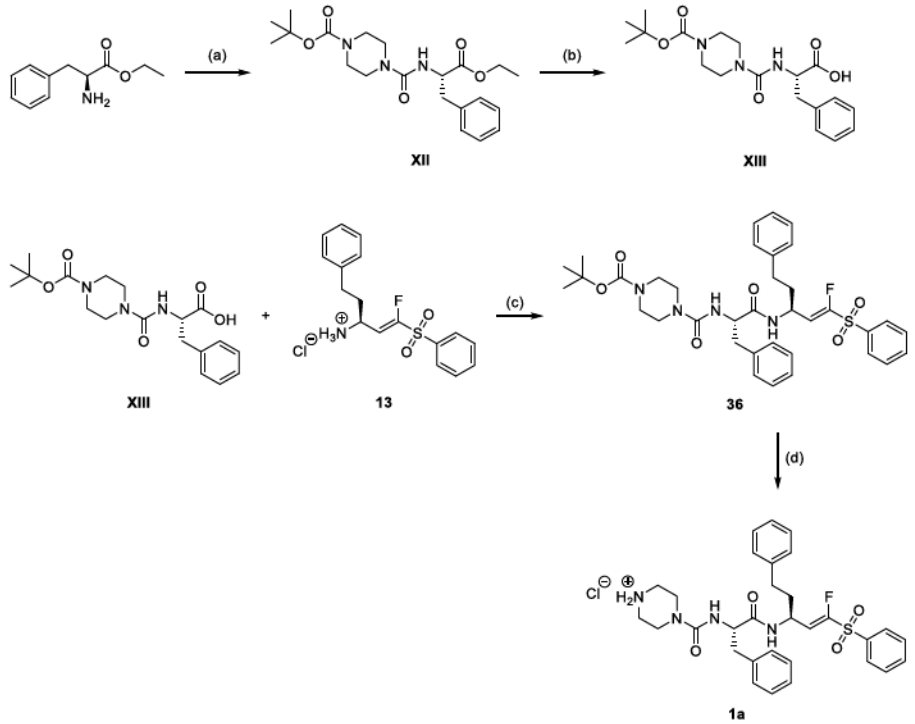

[a]Reagents and conditions: (a) (1) triphosgene, DCM, 0 °C, 1 h, 85%. (2) 1-Boc piperazine, THF, rt, 18 h, 50%, (b) LiOH, THF, 0 °C to rt, 3 h, 74%, (c) HOBt, TBTU, DIEA, DCM, 0 °C to rt, 12 h, 45%, and (d) 4 M HCl in dioxane, rt, 1 h, 93%.

Scheme 5. Synthesis of the *N*-Oxidized Metabolite 1b[a]

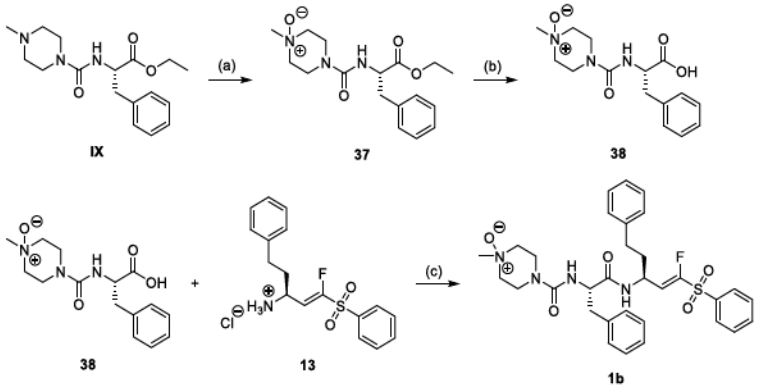

[a]Reagents and conditions: (a) *m*CPBA, DCM, 0 °C, 16 h, 52%; (b) LiOH, THF, 0 °C to rt, 3 h, 53%; and (c) HOBt, TBTU, DIEA, DCM/DMF, 0 °C to rt, 24 h, 23%.

In Scheme 5, the preparation of the metabolite **1b**, the *N*-oxide of compound **1**, is described. The synthesis started with compound **IX**, which was oxidized with *m*CPBA,[29] resulting in ester **37**, which was hydrolyzed with LiOH. Compound **38** was then coupled with vinylsulfone **13**, yielding compound **1b**.

The *N*-oxidized metabolite **2l** of compound **2d-(H)** was prepared as shown in Scheme 6. Isonicotinic acid was esterified and then oxidized with *m*CPBA.[29] The resulting compound **40** was hydrolyzed to **41** and then coupled with **34-(H)**, yielding the *N*-oxide **2l**.

https://doi.org/10.1021/acs.jmedchem.1c01002
J. Med. Chem. 2021, 64, 12322 12358

Scheme 6. Synthesis of the N-Oxidized Metabolite 2l of Compound 2d-(H)[a]

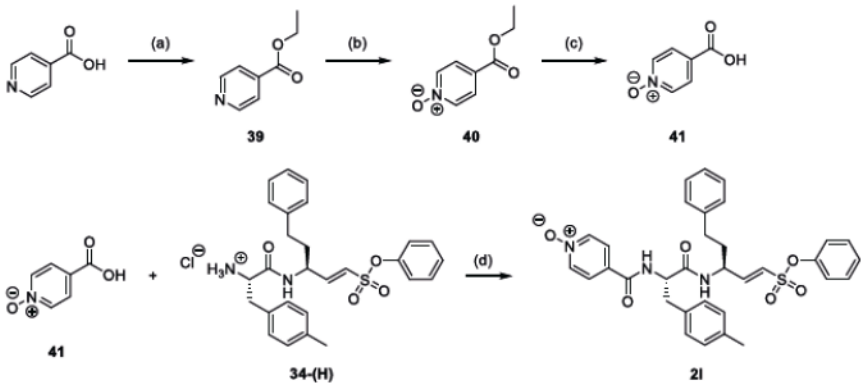

[a]Reagents and conditions: (a) ethanol, H_2SO_4, reflux, 24 h, 73%; (b) *m*CPBA, DCM, 0 °C, 16 h, 29%; (c) LiOH, THF, 0 °C to rt, 3 h, 90%; and (d) HOBt, TBTU, DIEA, DCM, 0 °C to rt, 24 h, 13%.

Table 1. Inhibition Data for Compounds 2a 2k[a]

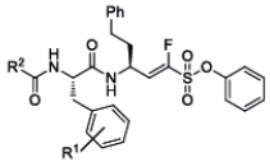

	substitution		rhodesain		CatL			CatB
Cpd	R^1	R^2	K_i/μM[b]	K_i^*/μM[b]	K_i/μM[c]	K_i^*/μM[c]	SI[d]	K_i/μM
2a	H	4-Pyr	0.098[g]	0.015[g]	0.258[g]	0.060[g]	4	1.7
(Z)-2a	H	4-Pyr	0.525[e,g]		n.d.		n.d.	n.d.
2b	H	DHBD	0.045[g]	0.009[g]	n.d.	n.d.	n.d.	n.d.
2d	4-Me	4-Pyr	0.024[g]	0.003[g]	0.313[g]	0.078[g]	26	38%[f]
2e	4-Me	DHBD	0.098[g]	0.007[g]	0.348[g]	0.039[g]	6	14%[f]
2f	4-Me	3,5-F_2Ph	0.034[g]	0.005[g]	n.d.	n.d.	n.d.	n.d.
2g	3-Me	4-Pyr	0.094[g]	0.007[g]	0.266[g]	0.030[g]	4	50%[f]
2h	3-Me	DHBD	0.059[g]	0.010[g]	n.d.	n.d.	n.d.	n.d.
2i	3-Me	3,5-F_2Ph	0.152[g]	0.021[g]	n.d.	n.d.	n.d.	n.d.
2j	H	OBn	0.158[e,g]		n.d.		n.d.	n.d.
2k	H	*N*-MePip	0.108[e]		n.d.		n.d.	n.d.

[a]K_i^* denotes the dissociation constant of the high-affinity complex in the case of biphasic, time-dependent inhibition. [b]Calculated with method 1 (see the text). [c]Calculated with method 2 (Dixon equation).[31] [d]K_i^*(CatL)/K_i^*(rhodesain). [e]Calculated from IC_{50} value with the Cheng Prusoff equation.[32] [f]% inhibition at 11 μM inhibitor concentration (single measurement). [g]Mean value of three independent assays; standard deviations less than 10%.

Enzyme Assays. Inhibition of rhodesain was tested with the fluorogenic substrate Cbz-Phe-Arg-AMC as described previously.[12,30] For the three series of compounds, the results from the fluorometric enzyme assays with rhodesain and the related mammalian enzymes cathepsin L and B are summarized in Tables 1 3.

For benzyl and phenyl fluorovinylsulfones (cpds 3a 3i, 4a 4l), the progress curves for inhibition of rhodesain were found to be linear in all cases, indicating a fast reversible inhibition (exemplarily shown for compound **3d** in Figure 3A and for **4a** in Figure 3B). In order to confirm the competitive behavior of these compounds, IC_{50} values were measured at seven different substrate concentrations. IC_{50} values were found to increase linearly with ascending substrate concentration, showing competitive inhibition (Figure 3C,D). This was assumed to be the case for all compounds of the series. Consequently, IC_{50} values were converted to K_i values using the Cheng Prusoff relationship (Tables 2 and 3).[32]

Reversibility was confirmed by dilution assays, that is, the enzyme was incubated with an excess of inhibitor (10-fold the IC_{50} concentration) to ensure full inhibition. Then, the mixture was diluted 100-fold to yield an inhibitor concentration of 0.1-fold the IC_{50} concentration. In the case of reversible inhibition, the enzyme activity should recover, whereas in the case of irreversible inhibition, it should not. For both compounds (**3d**, **4a**), enzyme activity recovers after dilution, whereas for the irreversible inhibitor K11777 used as a control, enzyme activity does not recover (Figure 4A).

For vinylsulfonates (**2a** **2k**), the progress curves for inhibition of rhodesain were not linear for most of the

https://doi.org/10.1021/acs.jmedchem.1c01002
J. Med. Chem. 2021, 64, 12322 12358

Table 2. Inhibition Data for Compounds 3a 3i

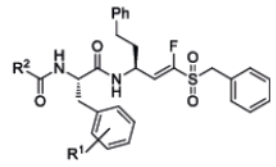

	substitution		rhodesain	CatL		CatB
cpd	R^1	R^2	K_i/μM	K_i/μM	SI[a]	K_i/μM
3a	H	4-Pyr	0.053[d]	0.226[d]	4	44%[b]
3b	H	DHBD	0.046[d]	n.d.	n.d.	n.d.
3c	H	3,5-F_2Ph	0.124[d]	n.d.	n.d.	n.d.
3d	4-Me	4-Pyr	0.015[d]	0.181[d]	12	35%[b]
3e	4-Me	DHBD	0.014[d]	0.076[d]	6	8%[b]
3f	4-Me	3,5-F_2Ph	0.029[d]	n.d.	n.d.	n.d.
3g	3-Me	4-Pyr	0.061[d]	0.122[d]	2	1.7[c]
3h	3-Me	DHBD	0.092[d]	n.d.	n.d.	n.d.
3i	3-Me	3,5-F_2Ph	0.380[d]	n.d.	n.d.	n.d.

[a] K_i(CatL)/K_i(rhodesain). [b] % inhibition at 11 μM (single measurement). [c] Single measurement. [d] Mean value of three independent assays; standard deviations less than 10%.

compounds (2a 2i), but showed time-dependency (exemplified for 2d in Figure 5A). Inhibition by all vinylsulfonates was found to be competitive with respect to the substrate (Figure 5B). Time-dependent inhibition is typical for irreversible inhibitors but may also be observed for covalent reversible inhibition. In the case of irreversible inhibition, the progress curves reach a plateau value with the terminal enzyme activity, that is, the steady-state velocity of substrate turnover in the presence of the inhibitor, $v_s = 0$. For covalent reversible inhibition, time-dependent progress curves reflect a biphasic behavior with the terminal enzyme activity in the presence of the inhibitor $v_s \neq 0$, but with $v_s < v_i$ (v_i = the initial enzyme activity in the presence of the inhibitor). To distinguish between these two scenarios, dilution assays were performed (see above), exemplarily shown for inhibitor 2d (Figure 4A). The results clearly indicate that vinylsulfonate 2d is a reversible inhibitor, but dissociates significantly slower compared to compounds 4a and 3d, indicating a tight covalent reversible inhibition according to the following inhibition mechanism, with $K_i = k_2/k_1$ as the dissociation constant of the initial noncovalent enzyme inhibitor (E I) complex and K_i^* as the dissociation constant of the final covalent, high-affinity complex (E I)[33]

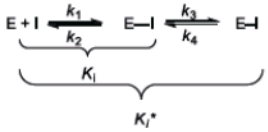

For these inhibitors, the initial (v_i) and steady-state (v_s) velocities in the presence of the inhibitor as well as the pseudo-first order rate constants k_{obs} were determined for the different inhibitor concentrations by fitting the progress curves (shown for cpd 2d in Figure 5A) to the slow-binding equation (off = offset)[33]

$$[P] = v_s \times t + \frac{v_i - v_s}{k_{obs}}[1 - \exp(-k_{obs} \times t)] + \text{off}$$

The k_{obs} values were replotted against the inhibitor concentrations [I] (Figure 5C) with the equation[33]

$$k_{obs} = k_4 + \left(\frac{k_3 \times [I]}{K_i^{app} + [I]}\right)$$

to yield the apparent dissociation constant K_i^{app} of the initial enzyme inhibitor complex, as well as the rate constants k_3 and k_4 of the second inhibition step (Method 1). Because the compounds display competitive inhibition with respect to the substrate (Figure 5B), the K_i^{app} value was converted to K_i for the

Table 3. Inhibition Data for Compounds 4a 4l

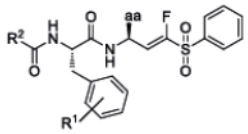

	substitution			rhodesain	CatL		CatB
cpd	R^1	R^2	aa	K_i/μM	K_i/μM	SI[a]	K_i/μM
1	H	*N*-MePip	hPhe	0.190[c,e]	0.023[e]	0.1	0.47[d]
4a	H	4-Pyr	hPhe	0.032[c,e]	0.110[e]	3	3.13[d]
4b	H	DHBD	hPhe	0.012[e]	0.033[e]	3	4.81[d]
4c	H	3,5-F_2Ph	hPhe	0.035[e]	n.d.	n.d.	n.d.
4d	4-Me	4-Pyr	hPhe	0.008[e]	0.115[e]	14	2.08[d]
4e	4-Me	DHBD	hPhe	0.005[e]	0.023[e]	5	34%[b]
4f	4-Me	3,5-F_2Ph	hPhe	0.010[e]	n.d.	n.d.	n.d.
4g	3-Me	4-Pyr	hPhe	0.025[e]	0.049[e]	2	0.35[d]
4h	3-Me	DHBD	hPhe	0.035[e]	n.d.	n.d.	n.d.
4i	3-Me	3,5-F_2Ph	hPhe	0.329[e]	n.d.	n.d.	n.d.
4j	H	*N*-MePip	Met	0.360[e]	0.173[e]	0.5	1.20[d]
4k	H	4-Pyr	Met	0.056[e]	0.577[e]	10	6.17[d]
4l	H	*N*-MePip	Cys(Bn)	0.630[e]	0.628[e]	1	8.62[d]

[a] K_i(CatL)/K_i(rhodesain). [b] % inhibition at 11 μM. [c] Ref 12 ; n.d.: not determined. [d] Single measurement. [e] Mean value of three independent assays; standard deviations less than 10%.

https://doi.org/10.1021/acs.jmedchem.1c01002
J. Med. Chem. 2021, 64, 12322 12358

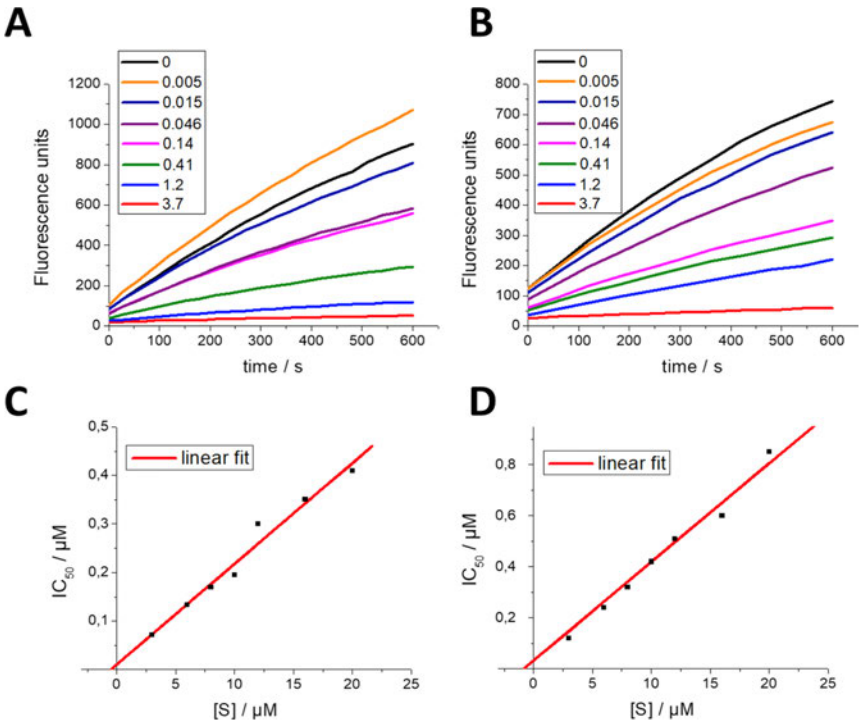

Figure 3. (A) Example for progress curves for inhibition of rhodesain by compound **3d**. Inhibitor concentrations in μM. (B) Example for progress curves for inhibition of rhodesain by compound **4a**. Inhibitor concentrations in μM. (C) Dependence of inhibition potency (IC_{50} values) on substrate concentration for inhibition of rhodesain by compound **3d**. Increasing IC_{50} values at ascending substrate concentrations show competitive inhibition. The K_i value is obtained as the intercept of the regression line with the y-axis (K_i = 25 nM). (D) Dependence of inhibition potency (IC_{50} values) on the substrate concentration for inhibition of rhodesain by compound **4a**. Increasing IC_{50} values at ascending substrate concentrations prove competitive inhibition. The K_i value is obtained as the intercept of the regression line with the y-axis (K_i = 47 nM).

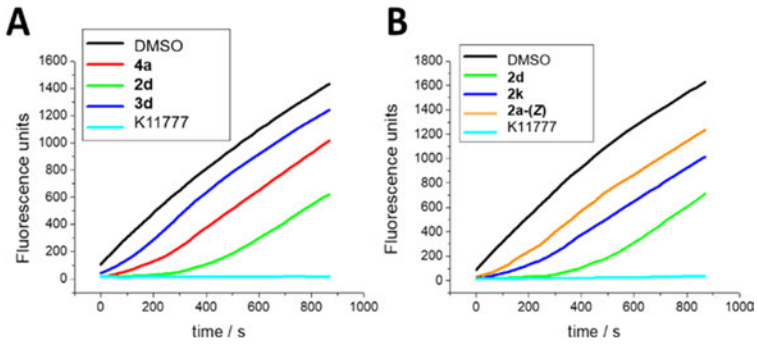

Figure 4. (A) Dilution assays show reversible inhibition of rhodesain (see the text). For all compounds, enzyme activity did recover after dilution, except for the irreversible vinylsulfone **K11777** (control). Compound **3d** showed faster reversibility than compound **4a**. Vinylsulfonate **2d** can be considered a tight-binding, slowly reversible inhibitor. (B) Dilution assays of several compounds of the series of vinylsulfonates. In the case of compound **2d**, which showed two-step inhibition in the enzyme assay, enzymatic activity recovers slower compared to vinylsulfonates **2k** and **2a**-(*Z*), which did not show biphasic behavior. The irreversible inhibitor **K11777** was used as a control.

initial inhibitor complex with the Cheng Prusoff equation.[32]

$$K_i^* = \frac{K_i}{1 + \left(\frac{k_3}{k_4}\right)}$$

The K_i^* value as the dissociation constant of the final complex was calculated from

https://doi.org/10.1021/acs.jmedchem.1c01002
J. Med. Chem. 2021, 64, 12322 12358

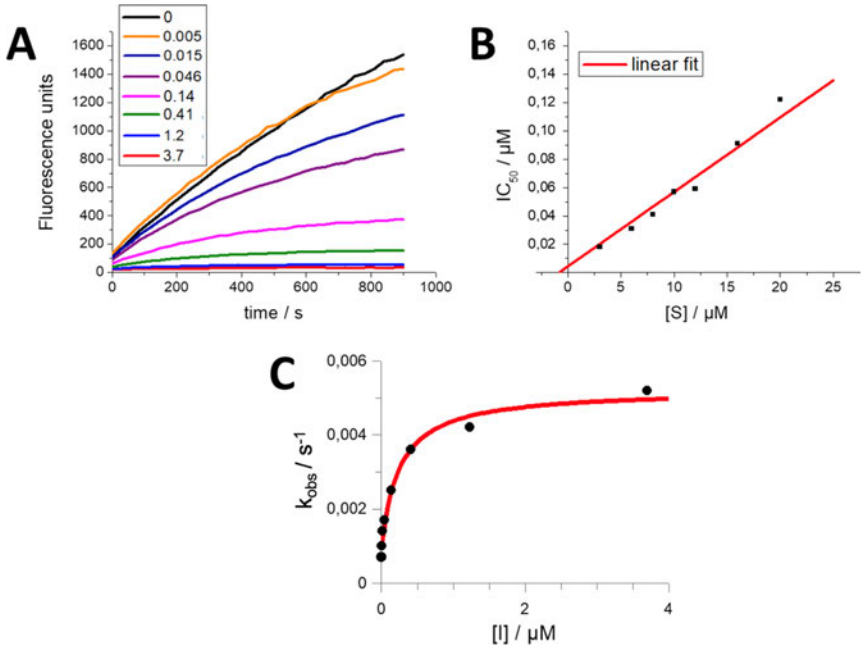

Figure 5. (A) Example for progress curves for inhibition of rhodesain by compound **2d**. Curve shape indicates time-dependent inhibition. Inhibitor concentrations in μM. (B) Dependence of inhibition potency (IC_{50} values) from the substrate concentration for inhibition of rhodesain by compound **2d**. Increasing IC_{50} values at ascending substrate concentrations show competitive inhibition. The K_i value is obtained as the intercept of the regression line with the *y*-axis (K_i = 19 nM). (C) Plot of the rate constants k_{obs} for the progress curves of compound **2d** from Figure 5A as a function of the inhibitor concentration. k_4 is obtained from the intercept of the regression curve with the *y*-axis. The maximum value of k_{obs} at infinite inhibitor concentration provides the sum of k_3 and k_4. The concentration of inhibitor yielding a half-maximal value of k_{obs} is equal to K_i^{app}.

Both dissociation constants, K_i and K_i^*, were also calculated by fitting the initial (v_i) and steady-state (v_s) velocities, respectively, against the inhibitor concentrations using the Dixon equation (Method 2)[31]

$$\frac{v_{i,s}}{v_0} = \frac{[I]}{1 + \left(\frac{[I]}{K_i^{(*)app}}\right)}$$

K_i^{app} was obtained from fitting v_i against [I] and $K_i^{(*)app}$ from fitting v_s against [I] (v_0 is the substrate turnover velocity in the absence of the inhibitor), and both constants were converted into K_i and K_i^* with the Cheng Prusoff equation.[32]

A comparison of the dissociation constants for inhibition of rhodesain by inhibitors **2a** **2i** obtained by both methods is shown in Table 4.

The data show that both methods yield similar dissociation constants for the initial low-affinity as well as for the final high-affinity complex proving that both methods are reliable. For all compounds, the rate constant of dissociation of the final complex (k_4) was found to be slower than the rate constant of association (k_3), indicating tight binding of these inhibitors. Interestingly, vinylsulfonates (*Z*)-**2a**, **2k**, and **2j** did not show time dependency of inhibition, but linear progress curves similar to the benzyl and phenyl vinylsulfones. Dilution assays for these three vinylsulfonates [(*Z*)-**2a**, **2k**, and **2j**] indicated a significantly faster recovery of the enzyme activity compared to the time-dependent inhibitor **2d** [shown for compound (*Z*)-**2a** and **2k** in Figure 4B].

Table 4. Inhibition Data and Kinetic Parameters k_3 and k_4 for Time-Dependent Inhibition of Rhodesain by Compounds 2a 2i

	method 1 (slow-binding equation)[a]				method 2 (Dixon equation)[b]	
Cpd	K_i/μM	K_i^*/μM	k_3/s^{-1}	k_4/s^{-1}	K_i/μM	K_i^*/μM
2a	0.098	0.015	0.055	0.010	0.110	0.008
2b	0.045	0.009	0.045	0.011	0.060	0.005
2d	0.024	0.003	0.075	0.010	0.022	0.002
2e	0.098	0.007	0.065	0.005	0.124	0.002
2f	0.034	0.005	0.049	0.009	0.052	0.004
2g	0.094	0.007	0.062	0.005	0.089	0.004
2h	0.059	0.010	0.074	0.015	0.068	0.006
2i	0.152	0.021	0.055	0.010	0.155	0.024

[a]Calculated with slow-binding equation (see the text). [b]Calculated with the Dixon equation (see the text).[31] Mean values of three independent assays, standard deviations less than 10%.

To further quantify the degree of reversibility for the different warheads, compounds **2d**, **3d**, and **4d** with identical recognition units were subjected to a dialysis experiment.[12] Here, rhodesain was incubated with an excess of inhibitor (10-fold the IC_{50} concentration) to ensure full inhibition. Then, the mixture was dialyzed against a continuous flow of enzyme buffer using a 3.5 kDa cut-off dialysis tubing.[34] Samples were taken after 10, 30, 60, and 120 min and analyzed for their residual enzyme activity with the standard fluorometric assay. The results are presented as the

https://doi.org/10.1021/acs.jmedchem.1c01002
J. Med. Chem. 2021, 64, 12322 12358

fractional activity of uninhibited rhodesain, which was subjected to dialysis in the same experiment (Figure 6). Compound **3d** showed the fastest reversibility (89% recovery after 1 h), which is in accordance with findings from the dilution assay. Compound **4d** dissociated significantly slower (47% recovery after 1 h). Vinylsulfonate **2d** displayed the slowest reversibility (29% after 1 h), which supports the tight-binding nature of the inhibition with the formation of a very stable high-affinity complex. **K11777** was used as an irreversible control, showing no recovery of the enzymatic activity.

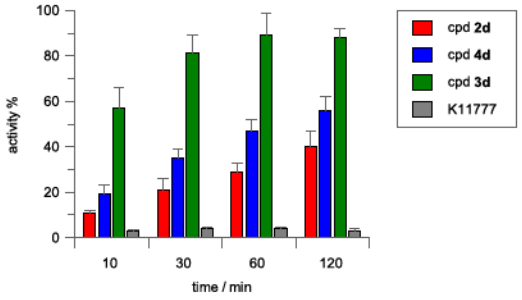

Figure 6. Dialysis experiment for compounds **2d**, **3d**, **4d**, and **K11777**. Rhodesain was incubated with the inhibitors at a concentration of 10-fold the respective IC_{50} value. The mixture was dialyzed against a continuous flow of buffer. Samples were taken after 10, 30, 60, and 120 min and the substrate was added to measure the residual enzyme activity. **K11777** was used as an irreversible control.

The most potent compounds of each series were also tested against the human enzymes CatL and CatB. For the tested vinylsulfonates (**2a**, **2d**, **2e**, and **2g**), a biphasic behavior was also observed for inhibition of CatL. In these cases, K_i and K_i^* values were calculated with the Dixon equation (Table 2).[31] For inhibition of CatB, no biphasic behavior was observed for these compounds (**2a**, **2d**, **2e**, and **2g**). This can be explained with the low affinity of the compounds for CatB. Notably, compounds **2d**, **2e**, and **2g** showed only very weak inhibition at concentrations of up to 11 μM.

Discussion of SAR. Comparison of the K_i values for rhodesain of the starting compound **1** (K_i = 190 nM) with the P3-modified analogues **4a**–**4c** demonstrates that the exchange of *N*-methyl piperazine against aromatic residues with no or only limited basicity significantly enhances inhibition potency (e.g., cpd **4b** with K_i = 12 nM). This is also reflected by the scores obtained from docking for these compounds, for example, for **4b** noncovalent affinity as well as the stability of the covalent complex are predicted to be higher (Table S1). Additionally, compounds **4a**–**4c** show improved selectivity for rhodesain over the human cathepsins. Lead compound **1** shows a higher affinity for human CatL (K_i = 23 nM) than for rhodesain (K_i = 190 nM), while P3-modified compounds **4a** and **4b** slightly favor inhibition of rhodesain (3-fold). Furthermore, selectivity for rhodesain over CatB is dramatically enhanced by these structural variations. This is a remarkable improvement (2-fold) compared to the weak selectivity of starting compound **1**. A further increase in potency for rhodesain is observed for compounds with an additional 4-methyl substituent at the phenylalanine aromatic ring (**4d**–**4f**), with compound **4e** (K_i = 5 nM) being the most potent inhibitor in the series of phenyl vinylsulfones. As suggested from noncovalent docking, this increase in potency may be directly attributed to additional hydrophobic interactions of the 4-methyl group with lipophilic residues lining the S2 pocket (Ala208, Leu160, Figure 7), which is also reflected in higher scores compared to compounds **4a**–**4c** (Table S1). Additionally, introduction of the 4-methyl substituent further increases selectivity against CatL (14-fold for **4d**). In contrast, incorporation of a 3-methyl substituent (**4g**–**4i**) does reduce potency and selectivity compared to compounds **4a**–**4c**. In particular, the combination of the 3-methyl substituent and the 3,5-difluorophenyl moiety (**4i**) is not advantageous: compound **4i** displayed significantly reduced potency (K_i = 329 nM). The considerable difference compared to compound **4e** with a 4-methyl substituent (K_i = 10 nM) cannot be explained exclusively with the slightly reduced docking scores (Table S1).

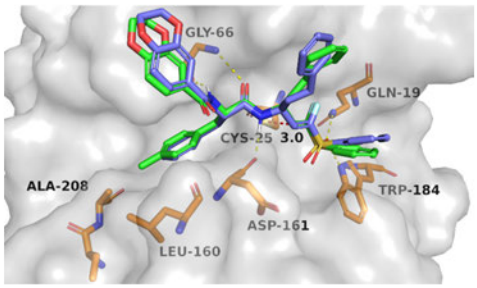

Figure 7. Noncovalent binding mode of compound **4b** (light blue, FlexX score: −31.2, Hyde score: −10.0 kcal mol^{-1}) and **4e** (green, FlexX score: −32.5, Hyde score: −11.7 kcal mol^{-1}) as predicted by FlexX. The electrophilic β-carbon of the fluorovinylsulfone warhead comes in close proximity to the nucleophilic sulfur of Cys25 (3.0 Å). The sulfone group forms hydrogen bonds with Gln19 and Trp184. The recognition unit forms hydrogen bonds to Gly66 and Asp161. The additional 4-methyl group of **4e** at the phenylalanine aromatic ring points into a hydrophobic cavity between Ala208 and Leu160, resulting in additional lipophilic interactions compared to compound **4b**.

Within the set of benzyl vinylsulfones (**3a**–**3i**), the SAR relationships are very similar compared to phenyl vinylsulfones (**4a**–**4i**). Consequently, compounds **3d** and **3e** with a 4-methyl substituent and a 4-pyridyl or DHBD moiety, respectively, are the most potent and most selective inhibitors (**3d**: K_i = 15 nM, 12-fold selectivity over CatL). Remarkably, compound **3d** showed even lower activity against CatB (35% inhibition at 11 μM) compared with its counterpart **4d**. Again, compound **3i** with a 3-methyl substituent and 3,5-difluorophenyl residue shows noticeably lower potency (K_i = 380 nM). Comparison of inhibitory potency for benzyl and phenyl vinylsulfones with the same recognition unit (e.g., **3a** vs **4a**) reveals that the benzyl substituent at the warhead has a negative influence on inhibition potency. In general, benzyl vinylsulfones have slightly increased K_i values compared to their phenyl counterparts.

These findings cannot be correlated with scores from docking, which generally predicted a higher affinity for compounds with a benzyl group at P1′. Computational conclusions to explain these differences between theory and experiment would be desirable, but are difficult because the differences in K_i values result from an increase in binding energy of less than 1 kcal mol^{-1} (e.g., **3d** K_i = 0.015 μM, i.e., ΔG = −11.10 kcal mol^{-1} vs **4d** K_i = 0.008 μM, i.e., ΔG = −11.49 kcal mol^{-1}), which is out of the scope of even high-level quantum chemical computations. Possibly, entropic

https://doi.org/10.1021/acs.jmedchem.1c01002
J. Med. Chem. 2021, 64, 12322−12358

effects due to the higher flexibility of the benzyl group in the noncovalent enzyme inhibitor complex may contribute.

The results from dilution and dialysis assays revealed that benzyl vinylsulfones are faster reversible than their phenyl counterparts, which may be explained with a lower reaction energy for the covalent bond-forming step, resulting in a weaker covalent bond.

Comparison of the K_i values of starting compound **1** (K_i = 190 nM) and the corresponding vinylsulfonate **2k** (K_i = 108 nM) demonstrates a nearly 2-fold improvement in affinity for rhodesain. The increase in potency may be partly attributed to the enlarged substituent at P1′. The results from noncovalent docking suggest that the vinylsulfonate moiety extends further into the S1′ pocket and forms nonpolar interactions with Trp184 (Figure 8), which is also reflected by the slightly

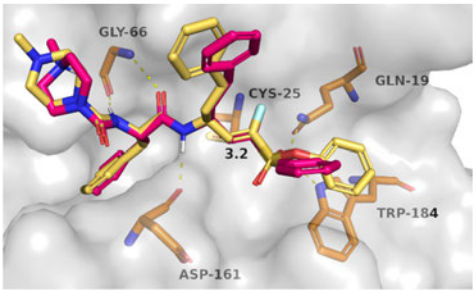

Figure 8. Overlay of noncovalent docking poses of compound **1** (magenta, FlexX score: 27.9, Hyde score: 6.2 kcal mol $^{-1}$) and compound **2k** (gold, FlexX score: 28.4, Hyde score: 8.8 kcal mol $^{-1}$). The enlarged vinylsulfonate moiety of compound **2k** extends further into the S1′ pocket and the aromatic ring can form additional hydrophobic interactions with Trp184 (π π-stacking interactions).

enhanced scores. Again, substitution of the *N*-methyl piperazine against aromatic residues (cpds **2a** **2i**) further improves affinity for rhodesain. Additionally, and in contrast to compound **2k**, compounds **2a** **2i** show a biphasic, time-dependent inhibition mechanism.

Dilution and dialysis experiments demonstrated reversibility for compound **2d** (Figures 4 and 6), which is, however, significantly slower compared to vinylsulfonate **2k**, which supports the tight-binding properties of **2d**. The related vinylsufones (**3d** and **4d**) do not show two-step inhibition, indicating that a combination of the properties of the fluorovinylsulfonate warhead with appropriate noncovalent interactions is required for tight binding. This is further supported by vinylsulfonate **2j** with a Cbz group at P3, which also does not show time-dependent inhibition. Among the tight-binding compounds, **2d** shows the highest potency for rhodesain with a dissociation constant of the initial encounter complex K_i = 24 nM, and with a high-affinity complex formed in the second step (K_i^* = 3 nM). Especially, the covalent complex is predicted to be very stable (Figure 9B). This is in excellent accordance with the high scores obtained from both docking approaches for compound **2d** (Table S1). Notably, compound **2d** showed good selectivity over the human cathepsins, with 26-fold selectivity against CatL and virtually no activity against CatB (38% at 11 μM), which is a significant improvement compared to the starting compound **1**.

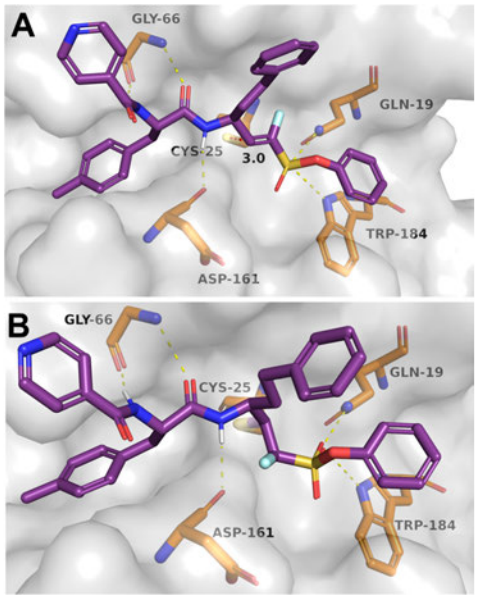

Figure 9. (A) Non-covalent docking pose of compound **2d** predicted with FlexX (FlexX score: 34.3, Hyde score: 38). (B) Geometry of the covalent complex between rhodesain and compound **2d** as predicted with DOCKTITE [score (affinity ΔG, kcal mol $^{-1}$): 6.2, DSX score: 195.5]. The combination of the vinylsulfonate aromatic ring extending further into the S1′ pocket and forming lipophilic interactions with Trp184, additional hydrophobic interactions of the 4-methyl group at phenylalanine aromatic ring with the S2 pocket and the preferred 4-pyridyl group at P3 results in a high affinity of compound **2d** for the binding site. This is reflected from higher scores obtained from both docking approaches compared to its analogues (Table S1).

Assuming that inhibitor binding to CatL and CatB is similar to rhodesain binding and that the binding mode is not largely altered for the compounds presented herein compared to K11777, which is also suggested by the docking (Figures 7 9), the underlying molecular mechanisms for selectivity can be explained by analysis of the known X-ray structures. Rhodesain shares an overall sequence identity of 44.7% and similarity of 59.1% with CatL and 27.9% identity and 47.4% similarity with CatB, as well as a highly similar fold with an C_α-RMSD of 1.35 and 2.15 Å, respectively, known from crystal structures available in the PDB[35] (entries, rhodesain: 2p7u,[11] CatL: 2xu1,[36] and CatB: 3ai8).[37] For residues forming the binding site (defined as all amino acids within 6 Å of reference ligand K11777) identity/similarity even increase to 59.1%/70.2% for CatL and 40.4%/49.1% for CatB. Nevertheless, slight structural differences of residues forming the S1 S3 sites can be observed, explaining the selectivity profile of the compounds under investigation. Additionally, CatB, divergent from CatL and rhodesain, contains a so-called occluding loop (residues 104 124), which is crucial for this enzyme's exopeptidase activity.[38] This loop structure closes upon the S′ sites. Neither phenyl- nor benzylfluorovinylsulfone nor fluorovinylsulfonate moieties of the compounds within this study reach far enough toward this sites to form interactions, but in contrast may even cause clashes with the residues of CatB (Figure 10A). Further focusing on the S1 site reveals one residue of the CatB occluding loop, which provides

https://doi.org/10.1021/acs.jmedchem.1c01002
J. Med. Chem. 2021, 64, 12322 12358

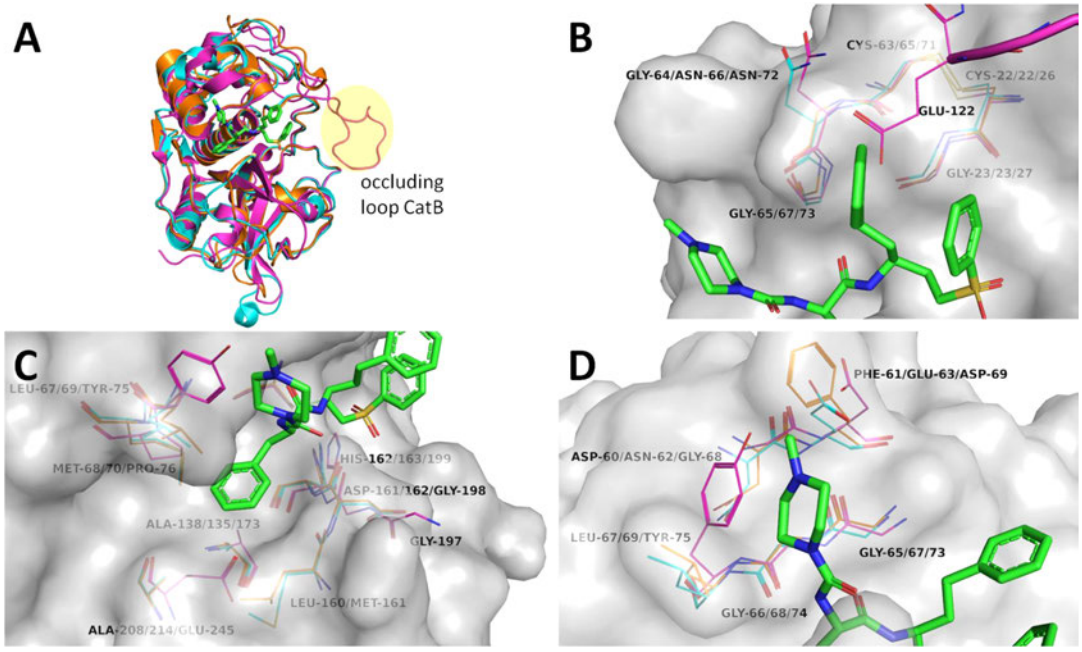

Figure 10. Structure comparison of rhodesain (orange carbon atoms, pdb entry 2p7u), CatL (cyan carbon atoms, pdb entry 2xu1), and CatB (magenta carbon atoms, pdb entry 3ai8) with inhibitor **K11777** shown with green carbon atoms. Residue enumeration is rhodesain/CatL/CatB. For (B D), the rhodesain surface is shown in gray for orientation. (A) Whole protease structures depicted as cartoons with the CatB occluding loop highlighted. (B) Close view of S1 site residues. CatB-unique occluding loop shown in the upper right with Glu122 as a selectivity determining feature over CatB. (C) Close view of S2 site residues. (D) Close view of S3 site residues reveals acidic Glu63 and Asp69 in cathepsins to form ionic interactions with the basic center of compound **K11777**, which is absent in compounds with more favorable selectivity profiles.

an explanation for selectivity (Figure 10B). Glu122 reaches toward the S1 pocket, not only making this site more polar, but also narrower, clashing with the homophenylalanine moiety of the inhibitors and thereby causing selectivity over CatB. Within the S2 pocket, the largest differences were found for CatB as well (Figure 10C). CatB Gly197 shows a different orientation than the corresponding residues Leu160 in rhodesain and Met161 in CatL. Additionally, Ala208/214 (enumeration is rhodesain/CatL) is exchanged to Glu246, Met69/70 to Pro76, and Leu67/69 to Tyr75. These differences all together result in a more open and polar pocket within CatB, which leads to a higher affinity for rhodesain and CatL for inhibitors carrying (3- or 4-methyl)-phenylalanine moieties. Additionally, the selectivity for rhodesain over CatL introduced by the 4-methyl substitution (compounds **2d**, **3d**, and **4d**) is likely to be caused by non-polar interactions with Leu160 being more favorable compared to the CatL Met161, which is slightly more distant and potentially impaired in its flexibility upon binding. The most significant improvement in selectivity was the displacement of *N*-methyl piperazine by 4-pyridine or less pronounced by DHDB (compounds **2d**, **2e**, **3d**, **3e**, **4d**, and **4e**). Within the S3 site, acidic amino acids Glu63 and Asp69 are found in CatL and CatB, respectively, while in rhodesain Phe61 sits at the corresponding position (Figure 1D). By the removal of the positively charged *N*-methyl piperazine, the loss of potential ionic interactions only with the off-target cathepsins is, therefore, likely to improve the selectivity profile of these compounds. Additionally, the Tyr75 residue in CatB compared to Leu in rhodesain and CatL results in a smaller S3 pocket and an enhanced selectivity over CatB, too.

In contrast to all other compounds in this study, the geometry of the double bond of compound (*Z*)-**2a** has a (*Z*)-configuration. Because (*Z*)-isomers are obtained as side products from HWE olefination, it was obvious to explore the influence of the geometry of the double bond on inhibitory potency. Compared to the (*E*)-isomer **2a** (K_i^* = 15 nM), compound (*Z*)-**2a** (K_i = 525 nM) shows markedly reduced potency and forms no high-affinity complex, indicating that the (*Z*)-configuration of the double bond is not favorable.

Compounds with a modified P1 residue (**4j** **4l**) showed reduced potency for rhodesain compared to the counterparts with homophenylalanine, which was already anticipated from non-covalent docking scores. Nevertheless, compound **4k**, with methionine at P1 and the 4-pyridyl moiety at P3, is still a potent inhibitor of rhodesain (K_i = 56 nM).

MS Analysis. Covalent protein ligand interactions were verified by ESI MS for compounds **2a**, (*Z*)-**2a**, and **2j** and MALDI-TOF MS for **K11777**, **1**, **2a**, **2j**, and **2k**.

In all three cases (**2a**, (*Z*)-**2a**, and **2j**), the protein ligand adduct resulting from Michael addition was detected in the ESI mass spectra. The observed mass shift corresponds to the mass of the inhibitor [exemplified for compound **2a** in Figure 11; for compounds (*Z*)-**2a** and **2j**, see Figure S2], which shows covalent bond formation.

To further elucidate possible differences in binding mode related to compound variability, especially to confirm the

https://doi.org/10.1021/acs.jmedchem.1c01002
J. Med. Chem. 2021, 64, 12322 12358

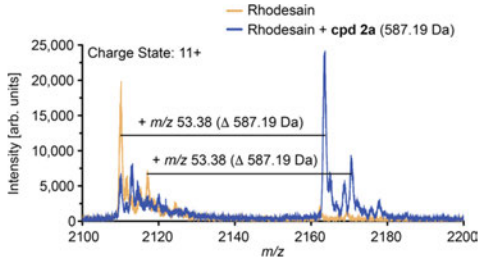

Figure 11. Intact protein ligand adducts obtained by mass spectrometry for compound **2a**. The observed shift corresponds to the mass of the inhibitor considering the charge state of the protein ($m/z = 11^+$).

covalent inhibition, a representative subset of compounds covering the majority of synthesized modifications was selected and analyzed by MALDI-TOF MS. The aim here was to analyze whether these modifications impede covalent bond formation between the catalytic thiolate and the vinyl moiety. ESI MS is a softer method in terms of transition to the gas phase, where non-covalent adducts can be found as well as covalent adducts. Depending on the matrix, MALDI-TOF MS can discriminate between covalent and non-covalent binding: the formation of non-covalent adducts can be suppressed by using an acidic matrix, which was attributed to the disruption of salt bridges and the subsequent destabilization of the non-covalent protein ligand complex.[39−41] Therefore, MALDI-TOF MS was applied to further investigate the binding mode.[40,42,43]

In terms of warhead modification, vinyl sulfone **K11777**, α-fluorovinylsulfone **1**, and α-fluorovinylsulfonates **2a**, **2j**, and **2k** were evaluated. Furthermore, the selected subset differed in their substituents in the P3 position, namely isonicotinyl amide (**2a**), benzylcarbamate (**2j**), and 4-methylpiperazine-1-carboxamide (**K11777**, **1**, and **2k**), while sharing the preceding PhehPhe motif in P2 and P1, respectively. **K11777** was used as a known, structurally equivalent control compound for its analogous, though covalent irreversible binding mode. A non-covalent inhibitor of rhodesain (**42**) carrying a fluorodinitrobenzene moiety as an aromatic electrophile was chosen as a control substance for its different inhibition mode (Figure 12) compared to the vinylsulfones. The compound forms a tight π-complex with the catalytic thiolate, the adduct mass of which was detectable in ESI MS experiments with rhodesain.[44]

For all evaluated α-fluorovinyl analogues (**1**, **2a**, **2j**, and **2k**), covalent adducts with rhodesain were observed by MALDI-TOF MS. The resulting spectra consisted of a broad peak corresponding to the protein (ca. 23.3 kDa),[45−47] and a second peak corresponding to the covalent protein inhibitor adduct (ca. 23.8 kDa) that shows a mass shift corresponding to the mass of the respective compound (Figure 12). The observed multiplicity of the peaks was attributed to additions of matrix molecules [m(sinapinic acid) = 224 Da] to rhodesain, as similar phenomena are described in the literature.[47] The four fluorovinyl derivatives (**1**, **2a**, **2j**, and **2k**) behaved like the irreversible control substance **K11777**, while the non-covalent inhibitor (**42**) did not show any detectable adduct signals under the evaluated conditions. Apart from that, an adduct of **42** was found with ESI MS as published previously.[39,40,44] The identical behavior of **K11777** and the α-fluorovinylsulfones/-sulfonates in the MALDI-TOF MS experiments could be observed using two different matrices, sinapinic acid and a mixture of α-cyano-4-hydroxycinnamic acid and 2,5-dihydroxybenzoic acid,[43] respectively, the latter data are shown in the Figure S1. These findings, combined with the results from ESI MS and the dialysis

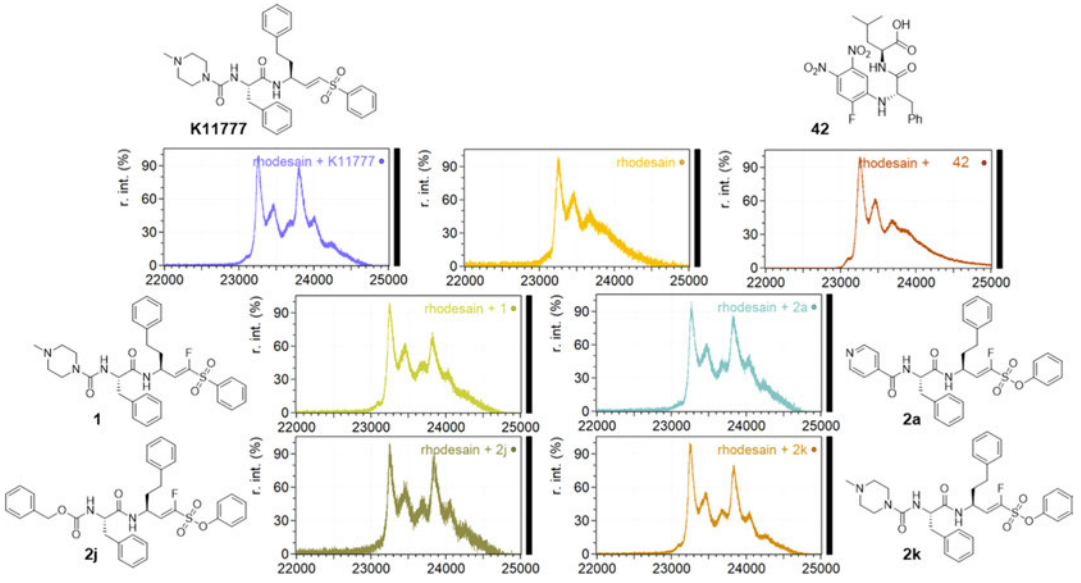

Figure 12. MALDI-TOF mass spectra of rhodesain (ca. 23 kDa) in the presence of different inhibitors (10-fold molar excess of inhibitor to protein). Sinapinic acid was used as the matrix substance. The figures show the relevant range of the spectrum to display $[M + H]^+$, which were baseline corrected.

https://doi.org/10.1021/acs.jmedchem.1c01002
J. Med. Chem. 2021, 64, 12322 12358

and dilution assays, clearly show that the α-fluorovinylsulfones and -sulfonates are indeed covalent reversible inhibitors of rhodesain.

Comparison of the Inhibition Mechanisms of K11777 and 1 by QM/MM Modeling. In our previous study,[12] the computed reaction energies of **K11777** and **1** differed only marginally so that the computational results could hardly explain the transition from irreversible to reversible inhibition. In that study, both reaction pathways had been calculated starting from the X-ray structure of the covalent enzyme inhibitor complex of K1177 with rhodesain (PDB: 2p7u) going backwards from the covalent toward the non-covalent complex. To generate the reaction path for **1**, the hydrogen atom had been substituted for fluorine in the X-ray structure. It had been necessary to start the computations from the X-ray structure of the covalent complex because no experimental information on the non-covalent complex was available. Moreover, such procedures had been very successful to explain the stereo- and regioselectivity of various epoxide- and aziridine-based inhibitors and to predict improved inhibitors.[48−50] However, such approaches can be error-prone in cases when the geometries of the covalent and non-covalent enzyme inhibitor complexes differ largely, especially when substitution leads to large differences in the non-covalent complex.

To obtain more reliable insights into possible differences between the non-covalent enzyme-inhibitor complexes of **K11777** and **1**, at first, non-covalent structures starting from the X-ray structure of **K11777** with rhodesain (PDB: 2p7u) were calculated. For **1**, the hydrogen atom in the α-position was substituted by fluorine. These structures then were used as starting points for MD simulations (10 times 10 ns sequences for each compound). Exemplarily, Figure 13 presents the

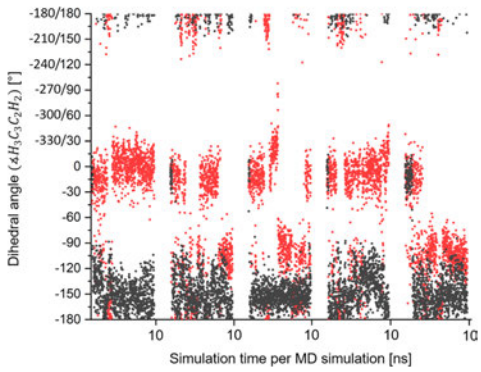

Figure 13. Variation of the dihedral angle $\angle H^3C^3C^2H^2$ along the MD simulations (sequences of 10.0 ns, respectively) for **K11777** with X = H (in red) and the fluorinated vinylsulfone with X = F (in black). Figure 13 defines the dihedral angle and gives the corresponding orientation of the warhead in the active site. Please note that $\angle H^3C^3C^2H^2 = 150°$ is equal to $\angle H^3C^3C^2H^2 = -210°$.

fluctuations in the dihedral angle $\angle H^3C^3C^2H^2$ (see Figure 14 for definition) for five different MD samplings. A variation of $\angle H^3C^3C^2H^2$ from 0 to ±180° describes the rotation of the inhibitor around the C^3C^2 single bond, adjacent to the double bond. Due to this rotation, the C^1X bond (X = H1, F) moves from the Gly23-oriented side to the opposite side (Figure 14). For **K11777**, mainly values between −40 and 40° (≈ 320°) were found for the $\angle H^3C^3C^2H^2$ angle. In the following, we denominate alignments with $-40° < \angle H^3C^3C^2H^2 < 40°$ (Figure 14) as "H-orientation". For **1**, $\angle H^3C^3C^2H^2$ adopted values between 120 and 190° (−170°), that is, the warhead of the compound oscillates around a position, where the F-atom is oriented toward the backbone NH groups of Cys25, Ser24, and the side-chain NH_2 group of Gln19 (Figure 14b), but mainly adopts positions with $\angle H^3C^3C^2H^2 > 180°$. In the following, geometries with $190° < \angle H^3C^3C^2H^2 < 120°$ are denominated "F-orientation".

During the MD simulation, **K11777** populated both H- (≈80%) and F-orientation (≈20%) indicating that both alignments are energetically quite similar. In contrast, **1** predominantly adopted the F-orientation due to attractive interactions with the NH backbone group of Cys25, the side chain NH_2 group of Gln19 (known as the oxyanion hole of rhodesain), and the NH backbone group of Ser24. Similar variations in the structures upon fluorination were reported in the literature).[51,52]

While the orientation of the recognition unit (in Figure 14 given in purple) remained fixed in the torsional motion around $\angle H^3C^3C^2H^2$, the relative positions between the attacked double bond of the inhibitor and the involved side chains of Cys25 and His162 changed drastically as shown in Figure 15. In both cases, a syn-addition takes place because the thiolate group of Cys25 and the protonated imidazole ring of His162 are found to be on the same side of the double bond (Figure 15), but for the H-orientation, the CS bond of the Cys25 side chain is orthogonally oriented with respect to the C^1C^2 double bond while it is oriented in parallel for the F-orientation. The position of the protonated imidazole ring of His162 also changed accordingly.

To calculate the influence of the different orientation of the warhead of **K11777** and **1** on the inhibition mechanism (Figure 1), the corresponding reaction paths were computed. However, due to the large number of local minima for the non-covalent complex (the reactant) and the covalent complex (the product) in combination with the roughness of the underlying potential energy surface (PES), the appropriate picture of the inhibition reaction is not that of a single reaction path with one starting point, one transition state, and one product, but that of a very rough PES with various energetically similar pathways starting from and ending at slightly different reactants and products. To achieve representative pathways, we performed geometry optimizations starting from two selected snapshots of the MD simulation for each inhibitor and computed the reaction paths starting from the obtained minima. The geometrical parameters of the respective minima are given in Table S2.

To characterize the reaction mechanism, we first computed two-dimensional scans using the distances $R(S_{cys}\ C_2)$ and $R(H_{His}\ C_1)$ as main reaction parameters (Figure 14). The resulting transition states served as starting points for subsequent IRC (intrinsic reaction paths) simulations,[53] the course of which generally gives good insights into the reaction mechanism (reaction barrier, reaction energy, and structural changes in the course of the reaction). More details are given in the Experimental Section. In Figure 15, representative IRCs for **K11777** starting from the H-orientation and **1** starting from the F-orientation are compared. Figure 16 also sketches the geometry variations along the IRCs. Further information on the geometries is given in Table S3. Additional paths starting from other reactant minima showing similar shapes can also be found in the Supporting Information (Figures S4 and S7).

https://doi.org/10.1021/acs.jmedchem.1c01002
J. Med. Chem. 2021, 64, 12322 12358

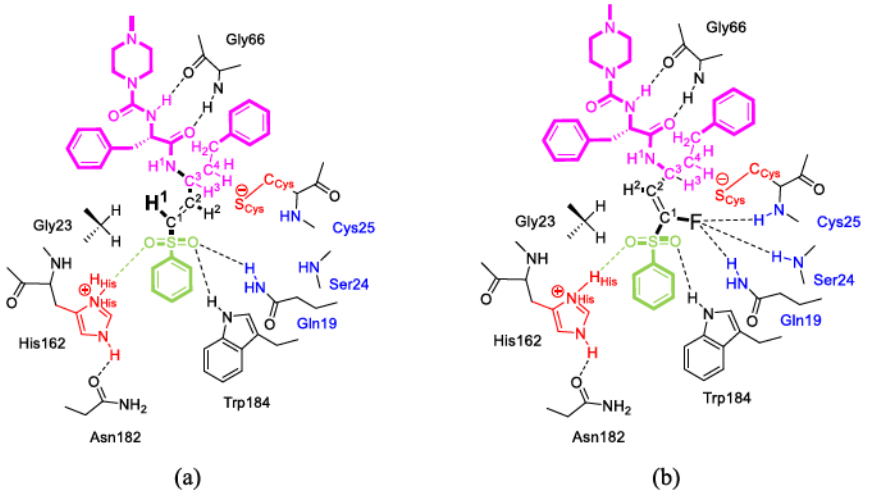

Figure 14. Sketch of the predominant orientation of the warheads (bold) in the active site during the MD simulations given in Figure 13. (a) H-orientation: predominant conformations of **K11777** (X = H) with $40° \leq \angle H^3C^3C^2H^2 \leq 40°$ (b) F-orientation: predominant conformations for the fluorinated vinylsulfone **1**, with $190° \leq \angle H^3C^3C^2H^2 \leq 120°$. For more information, see the text.

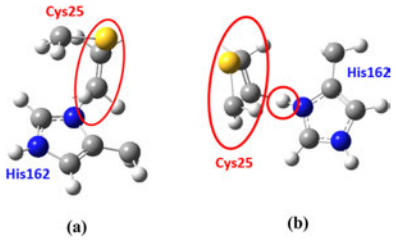

Figure 15. Relative orientation of Cys25 and His162 moieties with respect to the double bond of the vinylsulfone group attacked by Cys25, (a) for **K11777** (X = H) in the H-orientation, and (b) for the fluorinated vinylsulfone (X = F) in the F-orientation.

Figure 16 shows considerable differences in the IRCs of both compounds. While the reaction pathway for the inhibition of rhodesain by **K11777** passes over a barrier of about 12 kcal mol^{-1} and has an exothermic reaction energy of about 20 kcal mol^{-1}, we predict a thermoneutral reaction for the inhibition reaction of **1** with a very high barrier of 25 kcal mol^{-1}. The small reaction barrier and the strong exothermicity nicely explain why **K11777** is an efficient irreversible inhibitor.

The different shapes of the reaction pathways presented in Figure 16 may result from the different orientation of the olefin in the active site or from changes in the electronic structure due to the fluorine substitution in **1**. To obtain more insights, the reaction of **K11777** from the F-orientation was computed. For this purpose, we first computed the energy profile of the torsional motion of the C^1C^2 double bond around the dihedral angle $\angle H^3C^3C^2H^2$ (Figure S3). As expected from the MD simulations, for **K11777**, the energy difference between the H- and the F-orientation was found to be small (1 2 kcal mol^{-1}) so that the reaction could take place from both orientations. However, the two-dimensional scan starting from the F-orientation predicted barriers of about 33 kcal mol^{-1} and nearly isothermal reactions (ΔE_{reac} = 3 kcal mol^{-1}). This indicates that the different starting orientations are leading forces for the observed differences. Attempts to generate IRCs failed, possibly because the paths energetically lie above the path given in Figure 15a.

This finding could also indicate that a reaction of **1** starting from the H-orientation is more favorable. To answer this question, we calculated a two-step mechanism for inhibitor **1**. In the first step, **1** was found to twist from the F- into the H-orientation (variation of $\angle H^3C^3C^2H^2$). Starting from the obtained local minimum, we then calculated the course of inhibition by compound **1** starting from the H-orientation as the second step of the overall inhibition reaction. The result of this two-step inhibition reaction is shown in Figure 17.

Figure 17 indicates that the shape of the reaction path of **1**, if it starts from the H-orientation, resembles the path found for **K11777** (Figure 16). Starting from the H-orientation (Figure 17, structure 3), the reaction proceeds over a barrier of about 18 kcal mol^{-1} and has a reaction energy of about 12 kcal mol^{-1}. However, the exothermicity of the whole reaction drops to only 4 kcal mol^{-1}, due to the previously necessary transition from the F- to the H-orientation. Other reaction courses given in the Supporting Information provide a similar picture (Figures S8 S10).

Our investigation revealed that the differences between **K11777** and **1** are mainly due to the interaction between the fluorine atom and the oxyanion hole of rhodesain, which induces a flip of the olefin group of the warhead within the active site. This change in the orientation significantly complicates the further course of the inhibition reaction. As a result, for inhibitor **1**, a two-step mechanism becomes more favorable, which contains a torsional movement from the F- to the H-orientation before the actual covalent Michael-type reaction can take place leading to a considerably reduced exothermicity. These differences nicely explain the switch from the irreversible (**K11777**) to the reversible (**1**) inhibition mode and are in line with all experimental data, which indicate a covalent, but reversible bond formation for various fluorinated inhibitors.

https://doi.org/10.1021/acs.jmedchem.1c01002
J. Med. Chem. 2021, 64, 12322 12358

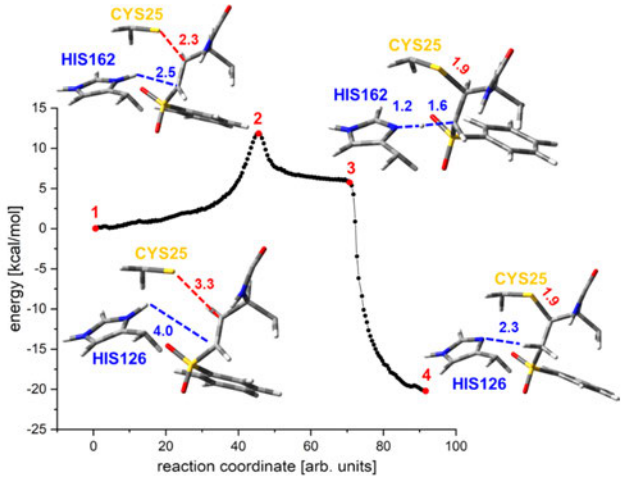

(a)

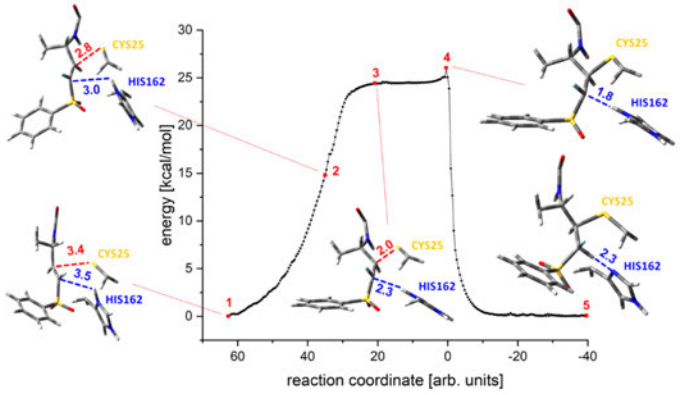

(b)

Figure 16. Representative intrinsic reaction coordinate (IRC) simulation of the inhibition reaction of **K11777** (a) and **1** (b). Selected geometrical parameters of the indicated structures are summarized in Table S3.

Antitrypanosomal Activity and Toxicity. Selected compounds were tested for antitrypanosomal activity and cytotoxicity (Table 5). Trypanocidal activity was measured against *T. brucei brucei* TC211[54,55] or *T. brucei brucei* BS449, as described previously.[56,57] Cytotoxicity was measured for selected compounds in the macrophage cell line J774.1 and in HeLa cells as described before.[12,55] Most inhibitors tested showed significantly improved antitrypanosomal activity compared to starting compound **1**. This correlates very well with the higher inhibitory potency of the compounds for rhodesain. The compounds also displayed an improved safety profile by showing no relevant cytotoxicity in HeLa cells or in the J774.1 macrophage cell line. Most interestingly, from the hPhe series, the compounds with N-terminal DHBD group and 4-Me-Phe residue at the P2 position (**2e**, **4e**) exhibited highest antitrypanosomal potency with the sulfonate **2e** being the most potent compound (EC_{50} = 0.14 μM), similarly active to the irreversible **K11777**. Also, within the 4-Pyr series, the compounds with 4-Me-Phe residue (**2d**, **3d**, and **4d**) are more potent than those with Phe at P2 position (**2a**, **4a**). Probably, the higher lipophilicity and thus better membrane permeability of these compounds contribute to their better antitrypanosomal activity. No differences are observed between the various warheads (phenyl vinylsulfonate **2d**, benzyl vinylsulfone **3d**, and phenyl vinylsulfone **4d**). Within the *N* Me-Pip series (**1**, **4j**, and **4l**), the compound with Cys(Bn) in the P1 position (**4l**) is most active (3.0 μM) despite being a much less-potent inhibitor of rhodesain. This observation may be explained with the relatively high toxicity of the compound, which seems to be also

https://doi.org/10.1021/acs.jmedchem.1c01002
J. Med. Chem. 2021, 64, 12322 12358

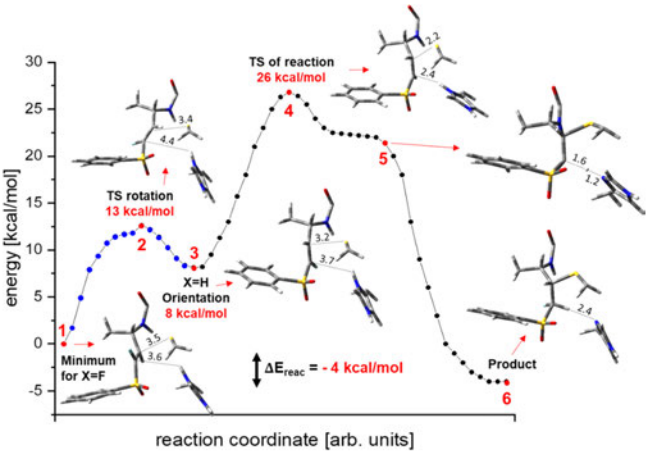

Figure 17. Reaction profile of the two-step inhibition reaction of **1**. The rotation about ∠$H^3C^3C^2H^2$ is given in blue. Please note that the reaction path is put together from several IRCs. Selected geometrical parameters of the indicated structures are summarized in Table S3. See also Figure S6.

Table 5. Antitrypanosomal Activity and Cytotoxicity of Selected Compounds[a]

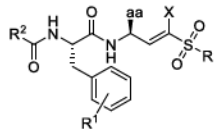

	substitution					*T. b. b.* EC_{50}/μM	cytotoxicity CC_{50}/μM	
cpd	R	R^1	R^2	aa	X	48 h	J774.1	HeLa
K11777	Ph	H	*N*-MePip	hPhe	H	0.18 ± 0.03[b,c]	41[b]	>10[d]
1	Ph	H	*N*-MePip	hPhe	F	12.5 ± 0.4[c]	38	10 ± 2
2a	OPh	H	4-Pyr	hPhe	F	4.8 ± 0.9[c]	n.d.	>100
2d	OPh	4-Me	4-Pyr	hPhe	F	1.9 ± 1.8[e]	n.d.	>100
2e	OPh	4-Me	DHBD	hPhe	F	0.14 ± 0.05[e]	n.d.	>100
3d	Bn	4-Me	4-Pyr	hPhe	F	1.4 ± 0.9[e]	n.d.	>100
4a	Ph	H	4-Pyr	hPhe	F	3.0 ± 0.4[c]	>100	>100
4d	Ph	4-Me	4-Pyr	hPhe	F	1.9 ± 1.2[e]	n.d.	>100
4e	Ph	4-Me	DHBD	hPhe	F	0.80 ± 0.5[e]	n.d.	>100
4j	Ph	H	*N*-MePip	Met	F	14.1 ± 0.6[c]	43	77 ± 8
4l	Ph	H	*N*-MePip	Cys(Bn)	F	3.0 ± 0.1[c]	8.7	8 ± 0.4

[a]n.d. not determined. [b]See ref 12. [c]*T. brucei brucei* TC211. [d]See ref 58. [e]*T. brucei brucei* BS449.

connected to the *N*-Me-Pip moiety (compounds **K11777**, **1**, **4j**, and **4l**).

Selectivity over Serine and Threonine Proteases. For selected compounds, inhibitory potency against other proteases (the threonine protease 20S proteasome and the serine protease NS2B/NS3 of the Dengue virus) was tested (Table 6). The activity of the compounds against the different catalytically active subunits of the proteasome (trypsin-like, caspase-like, and α-chymotrypsin-like) was tested separately by the use of specific fluorogenic substrates (see Experimental Section). Most compounds showed no relevant inhibition (less than 50%) at concentrations of 11 μM. Highest percentage inhibition was observed in the case of the caspase-like activity for compounds **2d** (44%) and **4a** (41%). Inhibitor **4l** was the only compound that showed relevant inhibition of the α-chymotrypsin-like activity of the proteasome (71% at 11 μM).

In Vitro Metabolism. The metabolism of compounds **1** and **2d-(H)** was investigated using rat liver microsomes and an NADPH-generating system. The covalent cysteine protease inhibitor **K11777** was used as a control. Previous in vitro metabolism studies by Jacobsen and co-workers revealed three metabolites of **K11777** depicted in Figure 18.[59]

Compound **1** (fluorinated **K11777**) also showed N-demethylation (**1a**) and N-oxidation (**1b**) as shown in Figure S13. The metabolites were analyzed via LC MS fragmentation. Additionally, the potential metabolites were synthesized as described in the Chemistry section, and their fragments and retention times were compared to those found in the metabolism studies to ensure the identity of the metabolites. In contrast to the reported metabolism of **K11777**, the β-hydroxy homophenylalanine derivative[32] did not occur, neither in the experiments with compound **1** nor in those with **K11777**.

https://doi.org/10.1021/acs.jmedchem.1c01002
J. Med. Chem. 2021, 64, 12322 12358

Table 6. Inhibition Data for 20S Proteasome and Dengue NS2B/NS3 Protease for Selected Compounds

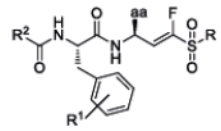

	substitution				human 20S proteasome/%[a]			dengue
cpd	R	R^1	R^2	aa	trypsin	caspase	α-chymotrps.	NS2B/NS3%[a]
1	Ph	H	*N*-MePip	hPhe	n.i.	16	13	n.i.
2a	OPh	H	4-Pyr	hPhe	n.i.	22	11	n.i.
2d	OPh	4-Me	4-Pyr	hPhe	10	44	20	n.i.
2e	OPh	4-Me	DHBD	hPhe	n.i.	31	22	11
3d	Bn	4-Me	4-Pyr	hPhe	n.i.	n.i.	n.i.	n.i.
4a	Ph	H	4-Pyr	hPhe	n.i.	41	10	n.i.
4b	Ph	H	DHBD	hPhe	n.i.	26	n.i.	n.d.
4d	Ph	4-Me	4-Pyr	hPhe	12	28	13	n.d.
4j	Ph	H	*N*-MePip	Met	n.i.	18	n.i.	n.d.
4l	Ph	H	*N*-MePip	Cys(Bn)	14	n.i.	71	13

[a]% inhibition at inhibitor concentrations of 11 μM; n.i. = <10% inhibition at 11 μM; and n.d. = not determined.

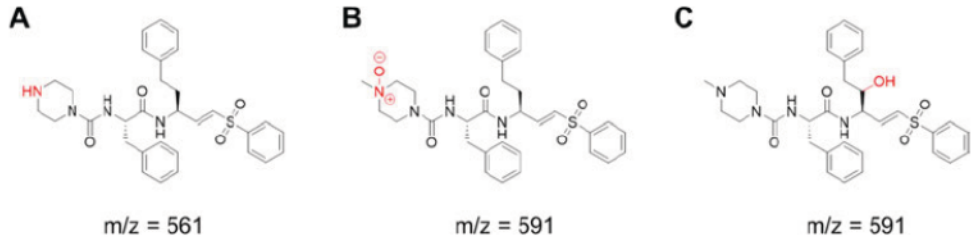

Figure 18. Metabolites of **K11777** as published by Jacobsen and co-workers.[59] N-Demethylation at the *N*-methyl piperazine moiety (A) and N-oxidation (B) are the major metabolic reactions. Additionally, a β-hydroxy homophenylalanine metabolite was found (C).

Table 7. Assay Results of the Metabolites

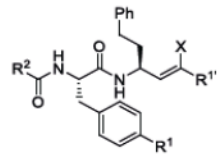

	substitution				rhodesain		
cpd	R^1	R^2	$R^{1'}$	X	K_i/nm	k_i/s^{-1}	k_{2nd}/M^{-1} s^{-1}
1	H	*N*-MePip	SO_2Ph	F	190[a,b]	n.a.	n.a.
1a	H	Pip	SO_2Ph	F	192 ± 40[b]	n.a.	n.a.
2d-(H)	Me	4-Pyr	SO_2Ph	H	0.45 ± 0.06	0.020	46×10^6
2l	Me	4-Pyr-*N*-oxide	SO_2Ph	H	1.50 ± 0.46	0.018	12×10^6

[a]See ref 12. [b]K_i calculated from the Cheng–Prusoff equation;[32] n.a. not applicable.

The metabolism studies of **2d-(H)** only resulted in a single metabolite, the N-oxidized derivative **2l** as shown in Figure S14. In order to verify the structure, the metabolite was synthesized as described in the Chemistry section and retention times and fragments were compared as described above.

The synthesized metabolites were also tested in the fluorometric enzyme assay in order to determine their K_i values. The assays were performed as described in the Enzyme assays section and the results are shown in Table 7.

The demethylation of compound **1** to its metabolite **1a** does not decrease its inhibitory activity significantly. Both, compound **2d-(H)** and its metabolite **2l**, show a good inhibition of rhodesain in the low nanomolar range. Therefore, it can be concluded that the metabolites retain most of the inhibitory potency of the parent drug.

In Vivo Distribution. Compound **1** as an example for a covalent reversible and compound **2d-(H)** as an example for a covalent irreversible inhibitor were tested for their biodistribution in vivo in wild type CD1 mice. Their biodistribution after oral (p.o.) or intraperitoneal (i.p.) application was investigated by LC–MS analysis of plasma samples and brain tissues to determine the ability of the compounds to cross the blood

https://doi.org/10.1021/acs.jmedchem.1c01002
J. Med. Chem. 2021, 64, 12322−12358

brain barrier. The compounds were chosen for the in vivo assays based on their differences in the mode of inhibition (covalent reversible vs irreversible) and based on their physicochemical properties (Table 8), which are similar for compound **2d-(H)** and its fluorinated counterpart **2d**.

Table 8. Comparison of 1, 2d, and 2d-(H) in Terms of Physicochemical Properties and the Mechanism of Inhibition

cpd	inhibition mode	SlogP (calc.)[a]	TPSA [Å^2] (calc.)[a]
1	covalent reversible	3.96	98.82
2d	covalent reversible	5.07	114.46
2d-(H)	covalent irreversible	4.77	114.46

[a]Calculated using MOE.[60]

Compound **1** was found in plasma samples but not in the brain homogenate, whereas compound **2d-(H)** could be found in both, plasma and brain tissue after i.p. and p.o. administration, respectively (Figures 19, S15, and S16). Therefore, it can be concluded that **2d-(H)** is able to cross the blood brain barrier due to its higher lipophilicity. An accumulation of this compound was also suggested because of a higher AUC after multiple oral administration compared to a single dose i.p. administration, thus making it a possible candidate for the treatment of stage-2 HAT.

Furthermore, the distribution of the compounds in the brain extracellular space was also investigated via microdialysis. Only compound **2d-(H)** could be found in the dialysate with recovery rates from the plasma concentration between 0.8 and 6% of plasma values after i.p. injection. This indicates that the lipophilic compound **2d-(H)** reaches higher concentrations intracellularly than in the extracellular fluid.

Notably, the mice treated with the compounds did not show any signs of toxification.

It can be concluded that the optimization of compound **1** through SAR studies not only enhanced the inhibitory potency against rhodesain and the selectivity over CatB and CatL but also resulted in a potential drug candidate for stage-2 HAT with a higher lipophilicity (calc. *S* log *P* = 4.77 compared to 3.96 for **1**) that is able to cross the blood brain barrier and accumulate in brain tissue.

CONCLUSIONS

In this study, compound **1** (K_i = 190 nM, EC_{50} (*T. brucei*) = 12.5 μM), which was recently identified as a covalent reversible cysteine protease inhibitor by the application of a quantum-chemical-based design protocol,[12] was optimized in terms of inhibitory potency and selectivity for rhodesain. Based on the results obtained from molecular docking and MD simulations, a series of compounds with a modified recognition unit and an altered substitution pattern of the warhead were synthesized. Introduction of aromatic residues at P3 significantly enhanced the potency for rhodesain (**4b**: K_i = 12 nM) and increased the trypanocidal activity against *T. brucei* [**4a**: EC_{50} (*T. brucei*) = 3.0 μM]. Incorporation of a 4-methyl substituent at the phenylalanine aromatic ring additionally improved selectivity against human cathepsins (**4d**: K_i = 8 nM, 12-fold selectivity over CatL, more than 200-fold selectivity over CatB). By alteration of the substitution pattern of the warhead, two new classes of covalent reversible cysteine protease inhibitors with distinct properties were obtained. The compounds from the series of benzyl fluorovinylsulfones (cpds **3a**–**3i**) showed a similar potency compared to the respective analogues with phenyl substituents (**4a**–**4i**) but were significantly more rapidly reversible in dilution and dialysis assays. Several compounds in the series of fluorovinylsulfonates (**2a**–**2i**) showed a biphasic inhibition mechanism, with the formation of a single digit nanomolar, high-affinity complex in the second step (**2d**: K_i^* = 3 nM). This complex was shown to dissociate markedly slower in dialysis experiments for compound **2d**. Therefore, compound **2d** represents a potent, tight binding, and slowly reversible inhibitor of rhodesain. Furthermore, compound **2d** shows selectivity over CatL (26-fold) and is only a weak inhibitor of CatB (38% at 11 μM). In addition, no relevant off-target activity against threonine and serine proteases was observed and the cytotoxicity profile improved considerably. Compounds with a DHBD moiety at the N-terminus and 4-Me-Phe in the P2 position (**2e**, **4e**) are not only nanomolar inhibitors of rhodesain, but are most promising with regard to their the antitrypanosomal activity and cytotoxicity profile, with EC_{50} values comparable to those of the irreversible inhibitor **K11777** (EC_{50} = 0.14 – 0.80 μM) and no cytotoxic effects against HeLa cells (EC_{50} > 100 μM).

Microsomal stability assays revealed N-oxidation of the 4-Pyr substituent in the P3 position of **2d-(H)**. However, this does not seem to reduce the inhibitory potency. Moreover, the

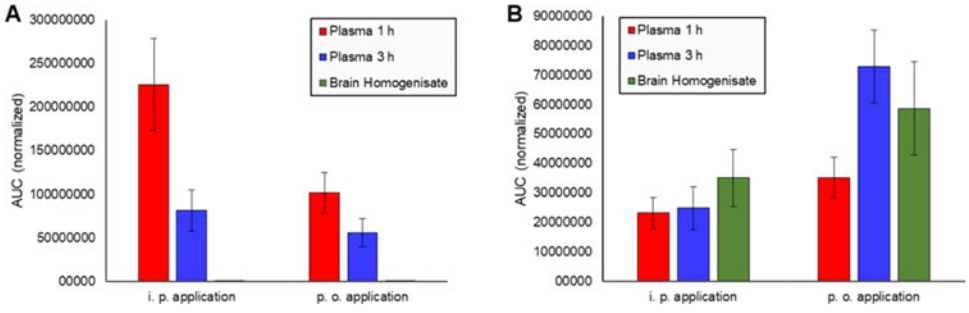

Figure 19. (A) Compound **1** was found in mouse plasma after 1 and 3 h, but not in the brain homogenate after i.p. and p.o. administration, respectively. (B) Compound **2d-(H)** showed plasma levels and distribution in brain tissue after both i.p. and p.o. administration. Both diagrams show the average AUC values of all tested mice (five for each compound and route of administration).

https://doi.org/10.1021/acs.jmedchem.1c01002
J. Med. Chem. 2021, 64, 12322 12358

accumulation of **2d**-(**H**) in mouse brain tissue, which did not occur with **1**, indicates a correlation of CNS permeation with the physicochemical properties of the tested inhibitors, such as SlogP values. These findings confirm that the optimized covalent reversible fluorovinylsulfonates should be further investigated as possible candidates for the treatment of both stage-1 and -2 HAT.

Based on these features, the high-affinity, lipophilic, and selective reversible α-fluorovinylsulfones and sulfonates as inhibitors of rhodesain may serve as a basis for the future development of effective and non-toxic drugs for the treatment of HAT.

In addition, we used mass spectrometry to demonstrate the formation of a covalent bond. Using QM/MM and MD computations, we could attribute the differences in inhibition mechanisms between **K11777** (irreversible) and **1** (reversible) to the interaction between the fluorine atom and the oxyanion hole of rhodesain. Due to this interaction, the olefin group of the warhead flips in the active site significantly complicating the further course of the inhibition reaction and leading to a considerably reduced exothermicity and thus a reversible inhibition.

EXPERIMENTAL SECTION

Syntheses. *General.* All reagents and solvents were of analytical grade quality and purchased from Sigma-Aldrich, Alfa Aesar, Acros, or TCI. Chemicals were used without further purification. Solvents were purified by distillation and desiccated by standard methods if necessary. ^{1}H and ^{13}C spectra were recorded on a Bruker Fourier 300 using DMSO-d_6, $CDCl_3$, or CD_2Cl_2 as a solvent. Chemical shifts δ are given in parts per million (ppm) using residual proton peaks of the solvent as the internal standard (^{1}H/^{13}C: DMSO: 2.50/39.52 ppm, $CHCl_3$: 7.26/77.16 ppm, CH_2Cl_2: 5.32/54.00 ppm). The purity of the compounds was determined via HPLC-MS (δ = 254 nm). All compounds are >95% pure according to HPLC analysis. High-resolution mass spectra were obtained on a Waters Q-TOF-Ultima 3-instrument. Alternatively, the mass spectra were obtained from an LC MS system consisting of a 1100 series HPLC system from Agilent with an Agilent Poroshell 120 EC-C_{18} 150 × 2.10 mm, 4 μm column. The mobile phase was 80% acetonitrile, 10% H_2O, and 10% of a 0.1% solution of formic acid in water. Detection wavelength was 254 nm. The molecular mass was detected using an Agilent 1100 series LC/MSD Trap with electron spray ionization (ESI) in positive mode. Purification with a preparative HPLC system was performed with a Varian PrepStar system (model 218) with an Agilent Zorbax XDB-C18 21.2 × 150 mm, 5 μm column. Column chromatography was performed with silica gel (0.06 0.02 mm or 0.040 0.063 mm) obtained from Carl Roth. All reactions were monitored by thin-layer chromatography using Macherey-Nagel ALUGRAM Xtra SIL G/UV254 silica gel 60 plates for detection at 254 nm. Melting points were determined in open capillaries using a Stuart SMP10-instrument. Optical rotation $[\alpha]_D^{22}$ was measured on an P3000 polarimeter from Kruss at 22 °C and is reported in cm^3 g^{-1} dm^{-1}.

Synthesis of Starting Materials. Phenyl Methanesulfonate[61] *(I).* Phenol (2.35 g, 1.0 equiv) was dissolved in EtOAc and cooled to 0 °C. TEA (6.93 mL, 2.0 equiv) and methanesulfonyl chloride (2.52 mL, 1.3 equiv) were added successively and the mixture was allowed to warm to rt. After stirring for 30 min, the solution was washed with water (3×) and brine (1×) and was dried with Na_2SO_4. Evaporation of the solvent yielded phenyl methanesulfonate (**I**) as a colorless powder (3.95 g, 92%). Spectral data matched those reported in the literature.[28]

Diethyl((benzylthio)methyl)phosphonate[28] *(II).* Benzyl mercaptan (0.84 mL, 1.0 equiv) was dissolved in THF and cooled to 0 °C. NaH (60% in mineral oil, 0.32 g, 1.0 equiv) was added in portions and the mixture was stirred for 15 min. Diethyl iodomethylphosphonate (1.24 mL, 1.0 equiv) was added dropwise and the mixture was stirred for 3.5 h at rt. THF was removed in vacuo and EtOAc was added. The organic phase was washed with water (2×) and brine (1×) and dried with Na_2SO_4. After evaporation of the solvent, the residue was purified by column chromatography (petroleum ether/EtOAc 1:1), yielding the title compound as a colorless liquid. Yield: 1.66 g (84%). ^{1}H NMR (300 MHz, $CDCl_3$): δ 7.43 7.21 (m, 5H), 4.25 4.08 (m, 4H), 3.90 (s, 2H), 2.54 (d, $J_{H\ P}$ = 12.9 Hz, 2H), 1.34 (t, J = 7.1 Hz, 6H). ^{13}C NMR (75 MHz, $CDCl_3$): δ 137.3, 129.4, 128.7, 127.4, 62.7 (d, $J_{C\ P}$ = 6.7 Hz), 37.0 ($J_{C\ P}$ = 2.9 Hz), 23.8 ($J_{C\ P}$ = 150 Hz), 16.6 ($J_{C\ P}$ = 6.0 Hz). ^{1}H NMR data are consistent with the literature.[12]

Diethyl((phenylsulfonyl)methyl)phosphonate[12] *(III).* To a solution of methyl phenyl sulfone (3.81 g, 24 mmol) in dry THF, *n*-BuLi (2.5 M in hexane, 21.5 mL, 60 mmol) was added at 0 °C with stirring. After 30 min, diethyl chlorophosphate was added dropwise and the reaction mixture was stirred at 0 °C for 1 h. 25 mL of a saturated solution of ammonium chloride was added and the volatiles were evaporated. The residue was extracted with DCM and the combined extracts were washed with brine, dried with sodium sulfate, concentrated under reduced pressure, and purified by column chromatography (light petroleum/EtOAc 1:5) to afford the title compound as a colorless oil, which solidified upon standing (4.11 g, 52%). NMR data were consistent with the literature.[28,62]

Phenyl(diethoxyphosphoryl)methanesulfonate (IV). Phenyl methanesulfonate (I, 2.5 g, 1.0 equiv) was dissolved in THF and cooled to 78 °C. KHMDS (1.0 M in THF, 15 mL. 1.1 equiv) was added dropwise and the mixture was stirred for an additional 15 min. Diethyl chlorophosphate (1.5 mL, 0.7 equiv) was added slowly and stirred for 1 h at 60 °C. The reaction was quenched by addition of glacial AcOH (1 mL) and then allowed to warm to rt. THF was removed in vacuo and EtOAc was added to the residue. The solution was washed with water (2×) and brine (1×) and then dried with Na_2SO_4. Evaporation of the solvent gave a crude product, which was purified by column chromatography (petroleum ether/EtOAc 1:1 to 1:3), yielding the title compound as a colorless liquid (3.3 g, 74%). ^{1}H NMR (300 MHz, $CDCl_3$): δ 7.52 7.29 (m, 5H), 4.36 4.20 (m, 4H), 3.81 (d, $J_{H\ P}$ = 17 Hz, 2H), 1.44 1.31 (m, 6H). ^{13}C NMR (75 MHz, $CDCl_3$): δ 149.4, 130.2, 127.8, 122.3, 64.2 (d, $J_{C\ P}$ = 6.5 Hz), 47.3 (d, $J_{C\ P}$ = 139 Hz), 16.4 (d, $J_{C\ P}$ = 6.3 Hz).

Diethyl((benzylsulfonyl)methyl)phosphonate[28] *(V).* Compound **II** (2.55 g, 1.0 equiv) was dissolved in DCM and cooled to 0 °C. Subsequently, *m*CPBA (77%, 5.8 g, 3.0 equiv) was added in portions and the mixture was stirred for 12 h at rt. Then, the solution was filtered and washed with 1 M NaOH (4×), water (1×), and brine (1×) and dried with Na_2SO_4. After evaporation of the solvent, the title compound was obtained as a colorless oil. Yield: 2.82 g (99%). ^{1}H NMR (300 MHz, $CDCl_3$): δ 7.57 7.47 (m, 2H), 7.44 7.34 (m, 3H), 4.60 (s, 2H), 4.24 (dq, J = 8.1, 7.1 Hz, 4H), 3.36 (d, J = 16 Hz, 2H), 1.37 (dt, J = 7.1, 0.4 Hz, 6H). ^{13}C NMR (75 MHz, $CDCl_3$): δ 131.2, 129.3, 129.2, 128.2, 63.9 (d, $J_{C\ P}$ = 6.5 Hz), 60.4, 48.0 (d, $J_{C\ P}$ = 140 Hz), 16.50 (d, $J_{C\ P}$ = 6.4 Hz). Spectral data are consistent with the literature.[12,63]

(S) tert Butyl(1 oxo 4 phenylbutan 2 yl)carbamate (VI). L-Homophenylalanine (5.0 g, 28 mmol) was dissolved in THF (15 mL) and a solution of Na_2CO_3 (3 g, 28 mmol) in 100 mL of water was added followed by di-*tert*-butyl dicarbonate (31 mmol) in 75 mL THF. The mixture was stirred overnight, diluted with water (100 mL), and extracted with CH_2Cl_2. The aqueous layer was acidified with $KHSO_4$ to pH 3 and extracted with CH_2Cl_2. The combined organic extracts were dried with sodium sulfate and concentrated under reduced pressure to give crude boc-L-homophenylalanine (7.0 g, 89%). This crude material (4.91 g, 18 mmol) was dissolved in DCM (100 mL) and cooled to 0 °C. EDC HCl (4.05 g, 21 mmol), HOBt (3.23 g, 21 mmol), and DIEA (13.5 mL, 78 mmol) were added and the mixture was stirred for 15 min before *N*,*O*-dimethylhydroxylamine hydrochloride (2.06 g, 21 mmol) was added. The mixture was allowed to warm to rt and was stirred for 18 h. DCM was removed under reduced pressure, water (60 mL) was added, and the suspension was extracted with EtOAc. The combined organic extracts were washed with saturated aq $NaHCO_3$ (5×) and brine, dried with sodium sulfate, and concentrated under reduced pressure to give *tert*-butyl (*S*)-(1-(methoxy(methyl)amino)-1-oxo-4-phenylbutan-2-yl)carbamate as a crude yellow oil (5.64 g, 99%), which was used in the next step without further purification. ^{1}H NMR (300 MHz, DMSO-d_6): δ 7.46 7.18 (m, 5H), 5.28 (d, J = 9.3 Hz, 1H), 4.73

https://doi.org/10.1021/acs.jmedchem.1c01002
J. Med. Chem. 2021, 64, 12322 12358

(s, 1H), 3.67 (s, 3H), 3.21 (s, 3H), 2.88 2.61 (m, 2H), 2.18 1.79 (m, 2H), 1.52 (s, 9H). The crude oil (4.05 g, 12.5 mmol) was dissolved in dry diethyl ether (130 mL) and cooled to 0 °C. $LiAlH_4$ (0.59 g, 15.7 mmol) was added portion wise. The mixture was stirred for 30 min and subsequently quenched by addition of aqueous $KHSO_4$ (0.33 M, 65 mL). The organic phase was separated, and the aqueous phase was extracted with diethyl ether. The combined organic extracts were washed with 3 M HCl, saturated aq $NaHCO_3$, and brine, dried with sodium sulfate, concentrated under reduced pressure, and purified by column chromatography (light petroleum/EtOAc 3:1), yielding the title compound as a colorless solid (2.44 g, 74%). ^{1}H NMR (300 MHz, $CDCl_3$): δ 9.55 (s, 1H), 7.40 7.13 (m, 5H), 5.08 (d, J = 4.1 Hz, 1H), 4.26 (q, J = 5.9 Hz, 1H), 2.87 2.63 (m, 2H), 2.35 2.06 (m, 1H), 2.02 1.77 (m, 2H), 1.47 (s, 9H). ^{13}C NMR (75 MHz, $CDCl_3$): δ 199.6, 155.6, 140.7, 128.8, 128.7, 126.5, 80.4, 59.7, 31.6, 31.2, 28.4. NMR data are consistent with the literature.[64]

(S) tert Butyl(4 (methylthio) 1 oxobutan 2 yl)carbamate (VII). Boc-L-Met-OH (2.43 g, 1.0 equiv) was dissolved in DCM and cooled to 0 °C. HOBt (1.49 g, 1.0 equiv) and DIEA (5.0 mL, 3.0 equiv) were added successively, and the mixture was stirred until all materials were solubilized. To this mixture, TBTU (3.12 g, 1.0 equiv) was added in one portion and then stirred for 15 min at 0 °C. *N,O*-Dimethylhydroxylamine hydrochloride (1.0 g, 1.1 equiv) was added in one portion and the mixture was stirred for 12 h at rt. DCM was removed in vacuo, and the residue was diluted with EtOAc. The organic layer was washed with water (5×), conc. $NaHCO_3$ (2×), and 1 M aq HCl (2×) and dried with Na_2SO_4. After evaporation of the solvent, the residue was purified by column chromatography (petroleum ether/EtOAc 2:1), yielding *tert*-butyl (*S*)-(1-methoxy(methyl)amino)-4-(methylthio)-1-oxobutan-2-yl)carbamate as a colorless oil (2.42 g, 85%). ^{1}H NMR (300 MHz, $CDCl_3$): δ 5.23 (d, J = 7.7 Hz, 1H), 4.78 (s, 1H), 3.77 (s, 3H), 3.20 (s, 3H), 2.68 2.42 (m, 2H), 2.08 (s, 3H), 2.05 1.92 (m, 1H), 1.89 1.71 (m, 1H), 1.42 (s, 9H). ^{13}C NMR (75 MHz, $CDCl_3$): δ 172.7, 155.7, 79.9, 61.8, 50.0, 32.6, 32.3, 30.3, 28.5, 15.6. This material (2.42 g, 1.0 equiv) was dissolved in THF and cooled to 0 °C. $LiAlH_4$ (0.41 g, 1.3 equiv) was added in portions and stirred for 30 min. The mixture was diluted with 50 mL diethyl ether and then 1 M $KHSO_4$ (50 mL) was added carefully. The layers were separated, and the aqueous phase was extracted twice with diethyl ether. The combined organic layers were washed with 1 M HCl (2×), saturated aq $NaHCO_3$, and brine, and then dried with Na_2SO_4. After evaporation of the solvent, the residue was purified by column chromatography (petroleum ether/EtOAc 2:1) to give the title compound as a colorless solid (1.49 g, 77%). ^{1}H NMR (300 MHz, $CDCl_3$): δ 9.63 (s, 1H), 5.21 (s, 1H), 4.39 4.11 (m, 1H), 2.56 (t, J = 7.2 Hz, 2H), 2.34 2.13 (m, 1H), 2.07 (s, 3H), 1.99 1.83 (m, 1H), 1.44 (s, 9H). ^{13}C NMR (75 MHz, $CDCl_3$): δ 199.2, 155.6, 80.4, 59.1, 29.9, 28.8, 28.4, 15.5. NMR data are consistent with the literature.[65]

(R) tert Butyl(1 (benzylthio) 3 oxopropan 2 yl)carbamate (VIII). L-Cysteine hydrochloride (5.20 g, 1.0 equiv) was dissolved in 60 mL 2 M NaOH and 150 mL EtOH. To the mixture, 5.64 g (3.92 mL, 1.0 equiv) benzyl bromide is added dropwise. After stirring for 1 h, the mixture is neutralized by addition of conc. HCl. The precipitate is collected by filtration and washed with water, diethyl ether, and ethanol. *S*-Benzyl L-cysteine is obtained as a colorless solid and directly used for the next step (6.4 g, 91%). ^{1}H NMR (300 MHz, D_2O): δ 7.50 7.24 (m, 5H), 4.17 (q, J = 6.5 Hz, 1H), 3.88 3.71 (s, 2H), 3.09 2.87 (m, 2H). ^{13}C NMR (75 MHz, D_2O): δ 171.7, 138.2, 129.3, 129.1, 127.8, 51.8, 35.5, 30.7. *S*-Benzyl L-cysteine (3.0 g, 1.0 equiv) was dissolved in THF (50 mL), and K_2CO_3 (2.94 g, 1.5 equiv) and water (50 mL) were added. Di-*tert*-butyl-dicarbonate (3.25 g, 1.05 equiv) dissolved in 50 mL THF was added dropwise and stirred for 12 h at rt. THF was removed in vacuo and the residue was extracted twice with DCM. The aqueous layer was acidified to pH 3 by addition of 1 M $KHSO_4$ and extracted with DCM (3×). The combined organic layers were washed with brine (2×), dried with Na_2SO_4, and evaporated under reduced pressure to give crude boc-*S*-benzyl L-cysteine as a colorless oil (3.05 g, 69%). ^{1}H NMR (300 MHz, DMSO-d_6): δ 7.38 7.03 (m, 5H), 4.14 4.02 (m, 1H), 3.71 (s, 2H), 2.67 (m, 2H), 1.35 (s, 9H). ^{13}C NMR (75 MHz, DMSO-d_6): δ 172.6, 155.4, 138.3, 128.9, 128.4, 126.9, 78.3, 53.2, 39.5, 35.2, 32.4, 28.2. This material (3.05 g, 1.0 equiv) was dissolved in DCM and cooled to 0 °C. HOBt (1.49 g, 1.0 equiv) and DIEA (5.0 mL, 3.0 equiv) were added successively, and the mixture was stirred until all materials were solubilized. To this mixture, TBTU (3.40 g, 1.0 equiv) was added in one portion and then stirred for 15 min at 0 °C. *N,O*-Dimethylhydroxylamine hydrochloride (1.0 g, 1.1 equiv) was added in one portion and the mixture was stirred for 12 h at rt. DCM was removed in vacuo, and the residue was diluted with EtOAc. The organic layer was washed with water (5×), conc. $NaHCO_3$ (2×), and 1 M aq HCl (2×) and dried with Na_2SO_4. After evaporation of the solvent, the residue was purified by column chromatography (petroleum ether/EtOAc 2:1), yielding (*R*)-*tert*-butyl (3-(benzylthio)-1-(methoxy-(methyl)amino)-1-oxopropan-2-yl)carbamate as a colorless oil (3.25 g, 95%). ^{1}H NMR (300 MHz, $CDCl_3$): δ 7.42 7.15 (m, 5H), 5.28 (d, J = 8.6 Hz, 1H), 4.84 4.59 (m, 1H), 3.67 (s, 3H), 3.21 (s, 3H), 2.83 2.54 (m, 2H), 2.15 1.77 (m, 2H), 1.50 (s, 9H). ^{13}C NMR (75 MHz, $CDCl_3$): δ 173.2, 155.7, 141.3, 128.7, 128.5, 126.1, 61.6, 50.2, 38.8, 34.7, 31.8, 28.5. The above compound (3.0 g, 1.0 equiv) was dissolved in diethyl ether and cooled to 0 °C. $LiAlH_4$ (0.42 g, 1.3 equiv) was added in portions and stirred for 30 min. The mixture was diluted with 50 mL diethyl ether and then 1 M $KHSO_4$ (50 mL) was added carefully. The layers were separated, and the aqueous phase was extracted twice with diethyl ether. The combined organic layers were washed with 1 M HCl (2×), saturated aq $NaHCO_3$, and brine, and then dried with Na_2SO_4. After evaporation of the solvent, the residue was purified by column chromatography (petroleum ether/EtOAc 2:1) to give the title compound as a colorless solid (1.70 g, 68%). ^{1}H NMR (300 MHz, $CDCl_3$): δ 9.46 (s, 2H), 7.32 7.21 (m, 13H), 5.29 (d, J = 21.5 Hz, 2H), 4.32 4.16 (m, 2H), 3.67 (s, 5H), 2.86 2.70 (m, 5H), 1.39 (s, 24H). ^{13}C NMR (75 MHz, $CDCl_3$): δ 198.8, 137.7, 129.1, 128.8, 127.3, 80.6, 77.2, 59.3, 37.1, 30.8, 28.4. NMR data are consistent with the literature.[12]

(S) 2 (4 Methylpiperazin 1 ium 1 carboxamido) 3 phenylpropanoate[12] (IX). L-Phenylalanine methyl ester hydrochloride (2.0 g, 1.0 equiv) was suspended in CH_2Cl_2 and 25 mL of a saturated aqueous solution of $NaHCO_3$ was added. At 0 °C, triphosgene (0.92 g, 0.3 equiv) was added and the mixture was allowed to stir for 30 min at this temperature. Subsequently, the organic phase was separated, and the aqueous phase was extracted with three portions of DCM. The combined organic extracts were washed with brine, dried with Na_2SO_4, and concentrated under reduced pressure. The residue was dissolved in THF and cooled to 0 °C. *N*-Methyl piperazine (0.93 g, 1.03 mL, 1.0 equiv) was added dropwise. After stirring for 1 h, THF was removed under reduced pressure and the residue was diluted with EtOAc. Aqueous work-up was performed with water (1×), saturated aq $NaHCO_3$ (1×), and brine (1×). The organic layer was dried with Na_2SO_4 and evaporated. The crude product was purified by column chromatography (CH_2Cl_2/MeOH 9:1), giving methyl (4-methylpiperazine-1-carbonyl)-L-phenylalaninate as a colorless oil. Yield: ^{1}H NMR (300 MHz, $CDCl_2$): δ 7.30 7.10 (m, 3H), 7.04 (d, J = 7.3 Hz, 2H), 4.77 (d, J = 7.3 Hz, 1H), 4.61 (m, 1H), 3.61 (s, 3H), 3.29 3.11 (m, 4H), 3.00 (m, 2H), 2.22 (t, J = 5.0 Hz, 4H), 2.16 (s, 3H). This material (3.0 g, 9.4 mmol) was dissolved in THF (20 mL) and LiOH (1.4 g, 33.4 mmol) in 10 mL water was added. The mixture was stirred for 18 h at rt and the volatiles were removed under reduced pressure. Water was added to the residue and the pH was adjusted to 2 with 1 M aq HCl. The title compound was crystallized at 4 °C along with some LiCl and collected by filtration. Recrystallization from methanol gave the pure compound as a colorless powder. ^{1}H NMR (300 MHz, DMSO-d_6): δ 7.33 7.05 (m, 5H), 6.68 (d, J = 7.9 Hz, 1H), 4.28 4.09 (m, 1H), 3.50 3.16 (m, 4H), 2.98 (m, 2H), 2.46 2.30 (m, 4H), 2.25 (s, 3H). ^{13}C NMR (75 MHz, DMSO-d_6): δ 174.6, 157.1, 139.0, 129.4, 128.0, 126.1, 56.0, 53.1, 44.8, 42.7, 39.5, 36.9.

Isonicotinoyl L phenylalanine[66] (X). To a solution of L-phenylalanine ethyl ester hydrochloride (2.50 g, 10.88 mmol) and TEA (4.5 mL, 32.65 mmol) in DCM, isonicotinoyl chloride hydrochloride (1.93 g, 10.88 mmol) was added in small portions. The mixture was stirred for 3 h, washed with a saturated solution of $NaHCO_3$, and dried with Na_2SO_4, and concentrated under reduced pressure. Ethyl isonicotinoyl-L-phenylalaninate (2.84 g, yield 87%) was obtained as a yellowish oil,

https://doi.org/10.1021/acs.jmedchem.1c01002
J. Med. Chem. 2021, 64, 12322 12358

which crystallized upon standing and was used in the next step without further purification. ^{1}H NMR (300 MHz, DMSO-d_6): δ 9.18 (d, J = 7.7 Hz, 1H), 8.73 (d, J = 5.2 Hz, 2H), 7.69 (d, J = 5.2 Hz, 2H), 7.37 7.12 (m, 5H), 4.75 4.57 (m, 1H), 4.10 (q, J = 7.1 Hz, 2H), 3.05 3.21 (m, 2H), 1.14 (t, J = 7.1 Hz, 3H). ^{13}C NMR (75 MHz, DMSO-d_6): δ 171.3, 165.0, 150.3, 140.6, 137.4, 129.1, 128.3, 126.6, 121.3, 60.7, 54.4, 45.7, 39.5, 36.2, 14.0. The above compound (2.84 g, 9.53 mmol) was dissolved in water (30 mL) and THF (30 mL), then LiOH (1.20 g, 28.6 mmol) was added. The mixture was stirred for 2 h before the organic solvent was removed under reduced pressure and the aqueous residue was neutralized with 1 M aq HCl. The title compound was crystallized at 4 °C along with LiCl. Recrystallization from methanol gave the pure product as a colorless powder (1.59 g, 62%). ^{1}H NMR (300 MHz, DMSO-d_6): δ 8.76 8.57 (m, 2H), 8.22 (d, J = 7.3 Hz, 1H), 7.71 7.57 (m, 2H), 7.25 6.99 (m, 5H), 4.26 (td, J = 7.4, 4.6 Hz, 1H), 3.27 2.95 (m, 3H). ^{13}C NMR (75 MHz, DMSO-d_6): δ 171.9, 163.4, 150.2, 142.1, 139.5, 129.4, 127.7, 125.6, 121.0, 56.1, 37.2.

11 (Tritylthio)undecanoic Acid (XI). Triphenylmethyl chloride (0.63 g, 1.0 equiv) was dissolved in DCM (5 mL). Thereto, a solution of 11-mercaptoundecanoic acid (MUA) (0.5 g, 1.0 equiv) in DCM (15 mL) was added dropwise. The mixture was stirred for 2 h at rt. DCM was removed by distillation, and the residue was purified by column chromatography (petroleum ether/EtOAc 2:1). ^{1}H NMR (300 MHz, $CDCl_3$): δ 7.40 (d, J = 7.6 Hz, 6H), 7.31 7.09 (m, 9H), 2.32 (t, J = 7.1 Hz, 2H), 2.11 (t, J = 7.3 Hz, 2H), 1.60 (q, J = 7.4 Hz, 2H), 1.46 0.95 (m, 14H). ^{13}C NMR (75 MHz, $CDCl_3$): δ 179.7, 145.2, 129.8, 127.9, 126.6, 66.5, 34.1, 32.2, 29.5, 29.32, 29.27, 29.16, 29.12, 28.7, 24.8. NMR data are consistent with the literature.[12]

tert Butyl (S) 4 ((1 Ethoxy 1 oxo 3 phenylpropan 2 yl) carbamoyl)piperazine 1 carboxylate (XII). To a stirred solution of 0.798 g 1-boc piperazine in THF, a suspension of 0.860 g (*S*)-ethyl-2-isocyanate-3-phenylpropanoate in THF was added dropwise. The mixture was stirred for 18 h and the solvent was removed under reduced pressure. The residue was extracted with EtOAc and the combined extracts were washed with a saturated solution of $NaHCO_3$ and brine, dried with Na_2SO_4, and concentrated under reduced pressure, resulting in a colorless oil (0.81 g, 50%). ^{1}H NMR (300 MHz, $CDCl_3$): δ 7.49 7.33 (m, 3H), 7.29 7.18 (m, 2H), 5.10 4.83 (m, 1H), 4.28 (dq, J = 15.5, 7.2 Hz, 2H), 3.70 3.57 (m, 1H), 3.57 3.48 (m, 4H), 3.48 3.35 (m, 4H), 3.29 3.22 (m, 2H), 1.60 (s, 9H), 1.39 (td, J = 7.1, 3.3 Hz, 3H). ^{13}C NMR (75 MHz, $CDCl_3$): δ 172.6, 156.5, 154.6, 136.3, 129.3, 128.5, 127.0, 80.2, 61.4, 60.4, 54.37, 43.9, 38.4, 28.4, 21.1, 14.2.

(4 (tert Butoxycarbonyl)piperazine 1 carbonyl) L phenylalanine (XIII). 0.81 g of compound **XII** was dissolved in THF and cooled to 0 °C. A solution of 0.29 g LiOH in water was added dropwise and the mixture was stirred for 3 h at room temperature. The solvent was removed under reduced pressure and the pH of the residue was adjusted to 2 with 1 M HCl. The residue was extracted with ethyl acetate and the combined extracts were washed with brine, dried with Na_2SO_4, and concentrated under reduced pressure. The crude product was dissolved in diethyl ether, *n*-pentane was added, and the product was crystallized at 4 °C, giving a colorless solid (0.56 g, 74%). ^{1}H NMR (300 MHz, $CDCl_3$): δ 9.39 (s, 1H), 7.25 7.14 (m, 3H), 7.14 7.04 (m, 2H), 5.05 (d, J = 7.1 Hz, NH), 4.61 (q, J = 6.2 Hz, 1H), 3.30 (dd, J = 7.9, 4.0 Hz, 4H), 3.24 3.09 (m, 4H), 3.04 (dd, J = 14.0, 6.8 Hz, 2H), 1.39 (s, 9H). ^{13}C NMR (75 MHz, $CDCl_3$): δ 174.7, 157.5, 154.8, 136.4, 129.5, 128.7, 127.2, 80.6, 54.9, 43.7, 37.5, 28.5.

Preparation of Phosphonates 5 7. Diethyl(fluoro (phenylsulfonyl)methyl)phosphonate[12,67] (5). To a stirred solution of phosphonate **III** (1.54 g, 1.0 equiv) in THF, KHMDS (1 M in THF, 6.59 mL, 1.25 equiv) was added dropwise at 80 °C. After 30 min at this temperature, Selectfluor (2.80 g, 1.5 equiv) in 10 mL DMF was added and the reaction mixture was stirred for 3 h, slowly warming to 0 °C. 15 mL of a saturated solution of ammonium chloride was added and the volatiles were evaporated. The residue was extracted with DCM and the combined extracts were washed with a saturated solution of $NaHCO_3$ and brine, dried with Na_2SO_4, concentrated under reduced pressure, and purified by column chromatography (light petroleum/EtOAc 1:6) to afford the title compound as a colorless solid. Yield: 1.0 g (62%). ^{1}H NMR (300 MHz, $CDCl_3$): δ 8.01 (d, J = 7.5 Hz, 2H), 7.74 (t, J = 7.4 Hz, 1H), 7.61 (t, J = 7.7 Hz, 2H), 5.38 (dd, $J_{H\ F}$ = 45.5 Hz, $J_{H\ F}$ = 6.6 Hz, 1H), 4.40 4.18 (m, 4H), 1.35 (t, J = 7.1 Hz, 6H). NMR data were consistent with the literature.[12]

Phenyl(diethoxyphosphoryl)fluoromethanesulfonate (6). Phosphonate **IV** (1.73 g, 1.0 equiv) was dissolved in THF (15 mL) and cooled to 78 °C. KHMDS (1 M in THF, 7.0 mL, 1.25 equiv) was added dropwise and the mixture was stirred for an additional 30 min. Selectfluor (3.0 g, 1.5 equiv) was added in one portion and the mixture was stirred for 5 min. Then, DMF (12 mL) was added in one portion and the mixture was allowed to warm to 0 °C. After stirring for 3 h, the reaction was quenched with conc. aq NH_4Cl (5 mL) and THF was removed in vacuo. EtOAc was added and the organic phase was washed with water (3×) and brine (2×) and dried with Na_2SO_4. The solvent was removed under reduced pressure and the residue was purified by column chromatography (petroleum ether/EtOAc 1:1), yielding the title compound as a colorless oil (0.95 g, 52%). ^{1}H NMR (300 MHz, $CDCl_3$): δ 7.50 7.39 (m, 2H), 7.39 7.28 (m, 3H), 5.63 (dd, $J_{H\ F}$ = 45 Hz, $J_{H\ P}$ = 7.2 Hz, 1H), 4.45 4.25 (m, 4H), 1.39 (tdd, J = 7.1, 2.0, 0.7 Hz, 6H). ^{13}C NMR (75 MHz, $CDCl_3$): δ 149.6, 130.3, 128.0, 122.2, 93.4 (dd, $J_{C\ F}$ = 232 Hz, $J_{C\ P}$ = 162 Hz), 65.7 (dd, $J_{C\ P}$ = 10.7 Hz, $J_{C\ F}$ = 6.7 Hz), 16.44 (d, $J_{C\ P}$ = 5.8 Hz).

Diethyl((benzylsulfonyl)fluoromethyl)phosphonate (7). Phosphonate **V** (3.77 g, 1.0 equiv) was dissolved in THF (40 mL) and cooled to 78 °C. KHMDS (1 M in THF, 15.4 mL, 1.25 equiv) was added dropwise and the mixture was stirred for an additional 30 min. Selectfluor (6.55 g, 1.5 equiv) was added in one portion and the mixture was stirred for 5 min. Then, DMF (24 mL) was added in one portion and the mixture was allowed to warm to 0 °C. After stirring for 3 h, the reaction was quenched with conc. NH_4Cl (5 mL) and THF was removed in vacuo. EtOAc was added and the organic phase was washed with water (3×) and brine (2×) and dried with Na_2SO_4. The solvent was removed under reduced pressure and the residue was purified by column chromatography (DCM/EtOAc 9:1), yielding the title compound as a colorless oil (1.92 g, 48%). ^{1}H NMR (300 MHz, $CDCl_3$): δ 7.51 7.32 (m, 5H), 5.28 (dd, $J_{H\ F}$ = 45 Hz, $J_{H\ P}$ = 7.1 Hz, 1H), 4.67 4.49 (m, 2H), 4.42 4.21 (m, 4H), 1.39 (td, J = 7.1, 0.7 Hz, 6H). ^{13}C NMR (75 MHz, $CDCl_3$): δ 131.4, 129.5, 129.2, 125.8, 95.2 (dd, $J_{C\ F}$ = 228 Hz, $J_{C\ P}$ = 161 Hz), 65.4 (dd, $J_{C\ F}$ = 6.3 Hz, $J_{C\ P}$ = 6.2 Hz), 57.5, 16.5 (d, $J_{C\ P}$ = 5.8 Hz).

HWE Olefination (Compounds 8 12). Procedure A. The specified phosphonate (1.0 equiv) was dissolved in THF and cooled to 0 °C. NaH (60% in mineral oil, 1.1 equiv) was added in portions and the mixture was stirred for 15 min. The corresponding boc-protected aminoaldehyde (1.0 equiv) was added in one portion, and the mixture was allowed to warm to rt. After stirring for 1 h, EtOAc was added and the organic phase was extracted with water, saturated aq $NaHCO_3$, and brine and finally dried with Na_2SO_4. Evaporation of the solvent under reduced pressure provided the boc-protected vinylsulfones as a crude mixture of *E*/*Z* isomers. Purification and separation of the isomers were achieved by column chromatography. The products were obtained as colorless solids.

Procedure B. The specified phosphonate (1.0 equiv) was dissolved in THF and cooled to 78 °C. KHMDS (1 M in THF, 1.0 equiv) or LHMDS (1 M in THF, 1.0 equiv) was added dropwise and it was stirred for additional 20 min. The respective aldehyde (1.0 equiv) was added in one portion and the mixture was allowed to warm to rt over a period of 1 h. After stirring for an additional hour at rt, EtOAc was added and the organic phase was extracted with water (2×) and brine (1×). Evaporation of the solvent under reduced pressure gave the crude product as *E*/*Z* isomers. Purification by column chromatography allowed the isolation of the desired (*E*)-isomers. The products were obtained as colorless solids.

tert Butyl (S,E) (1 Fluoro 5 phenyl 1 (phenylsulfonyl)pent 1 en 3 yl)carbamate[12] (8). Prepared following procedure A using 0.35 g of phosphonate **5**, 0.3 g boc-homophenylalaninal or boc-homophenylalanine aldehyde or boc-hPhe-H (**VI**), and 0.05 g NaH in 6 mL THF. Column chromatography: petroleum ether/EtOAc 3:1. (*E*)-isomer: Yield 0.20 g (41%). ^{1}H NMR (300 MHz, $CDCl_3$): δ 7.95 (d, J = 7.6 Hz, 2H), 7.70 (t, J = 7.4 Hz, 1H), 7.58 (t, J = 7.6 Hz, 2H), 7.36 7.16 (m, 3H), 7.12 (d, J = 7.1 Hz, 2H), 6.19 (dd, $J_{H\ F}$ = 32.3 Hz, $J_{H\ H}$ = 7.1 Hz,

https://doi.org/10.1021/acs.jmedchem.1c01002
J. Med. Chem. 2021, 64, 12322 12358

1H), 4.61 (s, 1H), 4.46 (s, 1H), 2.74 2.52 (m, 2H), 2.00 1.77 (m, 2H), 1.39 (s, 9H). ^{13}C NMR (75 MHz, $CDCl_3$): δ 154.9, 154.7 (d, $J_{C\ F}$ = 300 Hz), 140.5, 137.2, 134.7, 129.61, 128.8, 128.7, 128.4, 126.4, 118.4 (d, $J_{C\ F}$ = 4.6 Hz), 80.3, 46.4 (d, $J_{C\ F}$ = 2.7 Hz), 36.2, 32.0, 28.3. (*Z*)-isomer: Yield 0.10 g (21%). ^{1}H NMR (300 MHz, $CDCl_3$): δ 8.09 (d, J = 4.2 Hz, 2H), 7.69 (t, J = 7.4 Hz, 1H), 7.57 (t, J = 7.7 Hz, 2H), 7.37 7.12 (m, 5H), 5.81 (dd, $J_{H\ F}$ = 21 Hz, $J_{H\ H}$ = 10 Hz, 1H), 5.35 5.18 (m, 1H), 4.70 (s, 1H), 2.89 2.62 (m, 2H), 2.14 1.86 (m, 2H), 1.46 (s, 9H). ^{13}C NMR (75 MHz, $CDCl_3$): δ 155.0, 152.7 (d, $J_{C\ F}$ = 293 Hz), 141.0, 137.7, 134.7, 129.5, 129.1, 128.7, 128.5, 126.3, 121.4 (d, $J_{C\ F}$ = 11 Hz), 80.0, 46.6 (d, $J_{C\ F}$ = 5 Hz), 37.3, 32.3, 28.5.

*Phenyl (S,E) 3 ((tert Butoxycarbonyl)amino) 1 fluoro 5 phenyl pent 1 ene 1 sulfonate (**9**).* Prepared following procedure A using 0.66 g of phosphonate **6**, 0.53 g boc-homophenylalaninal or boc-homophenylalanine aldehyde or boc-hPhe-H (**VI**), and 0.09 g NaH in 12 mL THF. Column chromatography: petroleum ether/EtOAc 5:1. (*E*)-isomer: Yield 0.38 g (43%). ^{1}H NMR (300 MHz, $CDCl_3$): δ 7.46 7.32 (m, 2H), 7.32 7.15 (m, 6H), 7.10 (d, J = 7.0 Hz, 2H), 5.91 (dd, $J_{H\ F}$ = 31.3 Hz, $J_{H\ H}$ = 8.6 Hz, 1H), 4.68 4.27 (m, 2H), 2.66 2.43 (m, 2H), 1.97 1.66 (m, 2H), 1.43 (s, 9H). ^{13}C NMR (75 MHz, $CDCl_3$): δ 154.8, 150.8, 148.9 (d, $J_{C\ F}$ = 296 Hz), 140.2, 130.2, 128.8, 128.4, 128.0, 126.5, 122.4 (d, $J_{C\ F}$ = 4.1 Hz), 122.3, 80.4, 46.3 (d, $J_{C\ F}$ = 2.1 Hz), 35.9, 31.9, 28.4. (*Z*)-isomer: yield 0.22 g (22%). ^{1}H NMR (300 MHz, $CDCl_3$): δ 7.44 7.32 (m, 2H), 7.32 7.13 (m, 6H), 7.04 (d, J = 7.2 Hz, 2H), 6.14 (br, 1H), 4.88 4.44 (br, 2H), 2.59 2.46 (m, 1H), 2.46 2.29 (m, 1H), 1.84 (br, 1H), 1.42 (br, 1H), 1.43 (s, 9H). ^{13}C NMR (75 MHz, $CDCl_3$): δ 154.8, 149.3, 147.5 (d, $J_{C\ F}$ = 296 Hz), 140.7, 130.1, 128.5, 128.4, 128.1, 126.3, 124.1 (d, $J_{C\ F}$ = 9.9 Hz), 122.4, 80.4, 47.1 (d, $J_{C\ F}$ = 3.6 Hz), 36.3, 32.0, 28.4.

*Phenyl (S,E) 3 ((tert Butoxycarbonyl)amino) 5 phenylpent 1 ene 1 sulfonate (**9 (H)**).* Prepared following procedure B using 1.45 g of phosphonate **IV**, 1.24 g boc-homophenylalaninal or boc-homophenylalanine aldehyde or boc-hPhe-H (**VI**), and 6.0 mL 1 M LHMDS in 25 mL THF. Column chromatography: cyclohexane/EtOAc 5:1. (*E*)-isomer: Yield 0.80 g (41%). ^{1}H NMR (300 MHz, $CDCl_3$): δ 7.43 7.35 (m, 2H), 7.35 7.27 (m, 3H), 7.27 7.20 (m, 3H), 7.18 7.10 (m, 2H), 6.76 (dd, J = 15.1, 5.1 Hz, 1H), 6.48 (dd, J = 15.1, 1.5 Hz, 1H), 4.58 (d, J = 8.2 Hz, 1H), 4.33 (s, 1H), 2.77 2.52 (m, 2H), 1.98 1.72 (m, 2H), 1.49 (s, 9H). ^{13}C NMR (75 MHz, $CDCl_3$): δ 154.9, 150.4, 149.6, 140.2, 130.0, 128.8, 128.4, 127.4, 126.6, 124.4, 122.6, 80.5, 51.0, 35.6, 32.0, 28.4.

*tert Butyl (S,E) (1 (Benzylsulfonyl) 1 fluoro 5 phenylpent 1 en 3 yl)carbamate (**10**).* Synthesized following procedure B using 0.92 g phosphonate **7**, 0.74 g boc-homophenylalaninal or boc-homophenylalanine aldehyde or boc-hPhe-H (**VI**), and 2.8 mL KHMDS (1 M in THF) in 14 mL THF. Column chromatography: DCM/EtOAc 100:1. (*E*)-isomer: yield: 0.57 g (47%). ^{1}H NMR (300 MHz, $CDCl_3$): δ 7.39 7.16 (m, 8H), 7.10 (d, J = 7.0 Hz, 2H), 5.76 (dd, $J_{H\ F}$ = 32.8 Hz, $J_{H\ H}$ = 8.1 Hz, 1H), 4.59 4.38 (m, 2H), 4.35 (s, 2H), 2.62 2.38 (m, 2H), 1.91 1.64 (m, 3H), 1.45 (s, 9H). ^{13}C NMR (75 MHz, $CDCl_3$): δ 154.8, 152.1 (d, $J_{C\ F}$ = 300 Hz), 140.5, 131.0, 129.5, 129.2, 128.7, 128.4, 126.8, 126.4, 120.9 (d, $J_{C\ F}$ = 3.1 Hz), 80.3, 58.9, 46.1, 36.2, 31.8, 28.5. The (*Z*)-isomer was not isolated.

*tert Butyl (S,E) (1 Fluoro 5 (methylthio) 1 (phenylsulfonyl)pent 1 en 3 yl)carbamate (**11**).* Synthesized following procedure B using 0.93 g phosphonate **5**, 0.75 g boc-Met-H, and 3.15 mL LHMDS (1 M in THF) in 20 mL THF. Column chromatography: Petroleum ether/EtOAc 3:1. (*E*)-isomer: Yield 0.88 g (75%). ^{1}H NMR (300 MHz, $CDCl_3$): δ 7.94 (d, J = 7.8 Hz, 2H), 7.70 (t, J = 7.3 Hz, 1H), 7.58 (t, J = 7.6 Hz, 2H), 6.21 (br d, $J_{H\ F}$ = 31.5 Hz, 1H), 4.74 (br s, 1H), 4.55 (br s, 1H), 2.57 2.40 (m, 2H), 2.07 (s, 3H), 2.00 1.78 (m, 2H), 1.37 (s, 9H). ^{13}C NMR (75 MHz, $CDCl_3$): δ 154.9, 154.7 (d, $J_{C\ F}$ = 300 Hz), 137.1, 134.7, 129.6, 128.8, 118.0 (d, $J_{C\ F}$ = 4.6 Hz), 80.4, 46.0 (d, $J_{C\ F}$ = 1.0 Hz), 33.8, 30.2, 28.3, 15.7. The (*Z*)-isomer was not further characterized.

*tert Butyl (R,E) (1 (Benzylthio) 4 fluoro 4 (phenylsulfonyl)but 3 en 2 yl)carbamate (**12**).* Synthesized following procedure B using 0.55 g phosphonate **5**, 0.55 g boc-L-Cys(Bn)-H, and 1.85 mL LHMDS (1 M in THF) in 10 mL THF. Column chromatography: Petroleum ether/EtOAc 3:1. (*E*)-isomer: yield 0.44 g (54%). ^{1}H NMR (300 MHz, $CDCl_3$): δ 8.00 7.92 (m, 3H), 7.75 7.53 (m, 5H), 7.30 7.27 (m, 3H), 6.23 (dd, $J_{H\ F}$ = 31.8 Hz, $J_{H\ H}$ = 8.5 Hz, 1H), 4.83 (s, 1H), 4.59 (s, 1H), 3.70 (s, 2H), 2.73 2.44 (m, 2H), 1.39 (s, 9H). ^{13}C NMR (75 MHz, $CDCl_3$): δ 156.9, 154.8, 137.5, 137.1, 135.0, 134.7, 129.7, 129.6, 129.2, 129.0, 128.9, 128.8, 127.5, 117.5, 80.5, 46.0, 36.7, 35.4, 28.4.

Peptide Chemistry. *Coupling Protocols. Procedure C.* The specified carboxylic acid (1.0 equiv) and HOBt (1.0 equiv) were dissolved in DCM (8 mL) and cooled to 0 °C. DIEA (3.0 equiv) was added slowly, and the mixture was stirred until all materials were solubilized. TBTU (1.0 equiv) was added in one portion and the mixture was stirred for 15 min at 0 °C. The specific amine (1.0 equiv) was dissolved in DCM and added dropwise to the reaction mixture. After stirring for 12 h at rt, DCM was removed in vacuo and the residue was dissolved in EtOAc. The organic phase was washed with water (5×), conc. $NaHCO_3$ (2×), and 1 M aq HCl (2×) and then dried with Na_2SO_4. Evaporation of the solvent gave the crude product, which was purified by column chromatography.

Procedure D. The specified carboxylic acid (1.0 equiv) and TBTU (1.0 equiv) were dissolved in DCM and cooled to 0 °C. DIEA (3.0 equiv) was added and the mixture was stirred for 15 min. The respective amine (1.0 equiv) was added in one portion. After stirring for 12 h at rt, DCM was removed in vacuo, and the residue was dissolved in EtOAc. The organic phase was washed with water (5×), conc. $NaHCO_3$ (2×), and 1 M aq HCl (2×) and then dried with Na_2SO_4. Evaporation of the solvent gave the crude product, which was purified by column chromatography.

Procedure E. The respective carboxylic acid (**IX** or **X**, 1.0 equiv) and HOBt (1.0 equiv) were dissolved in DMF (5 mL) and cooled to 0 °C. DIEA (3.0 equiv) was added and the mixture was stirred for 15 min. The respective amine (1.0 equiv) was added in one portion and the mixture was stirred for 12 h at rt. EtOAc was added and aqueous work-up was performed with 5% aq LiCl (5×), water (2×), and saturated aq $NaHCO_3$ (2×). After evaporation of the solvent, the residue was purified by column chromatography.

Removal of Boc Groups. Procedure F. Boc-protected compounds (**8** **10**) were dissolved in 4 M HCl/dioxane solution (5 10 mL). After stirring for 30 min at rt, dioxane was evaporated in vacuo and the residue was washed several times with diethyl ether. The precipitate was collected and dried under reduced pressure. The amines were obtained as hydrochloride salts and were sufficiently pure to be used in the next step without further purification.

Procedure G. Boc-protected compounds (**11** **12**) were dissolved in DCM (10 mL) and cooled to 0 °C. 1 mL TFA was added dropwise, and the resulting mixture was stirred for 1 h. After evaporation to dryness in high vacuum, the residue was washed with diethyl ether and collected by filtration. The amines were obtained as TFA salt and directly used for the next step.

*(S,E) 1 Fluoro 5 phenyl 1 (phenylsulfonyl)pent 1 en 3 amine Hydrochloride (**13**).* Prepared following procedure F using 0.60 g of compound **8** in 12 mL 4 M HCl/dioxane. Yield: 0.47 g (93%). ^{1}H NMR (300 MHz, DMSO-d_6): δ 8.65 (s, 3H), 8.03 (d, J = 7.8 Hz, 2H), 7.89 (t, J = 7.3 Hz, 1H), 7.77 (t, J = 7.6 Hz, 2H), 7.32 7.13 (m, 3H), 7.06 (d, J = 7.3 Hz, 2H), 6.54 (dd, $J_{H\ F}$ = 33 Hz, $J_{H\ H}$ = 9.8 Hz, 1H), 4.09 3.90 (m, 1H), 2.62 2.34 (m, 2H), 2.25 2.07 (m, 1H), 2.07 1.89 (m, 1H). ^{13}C NMR (75 MHz, DMSO-d_6): δ 155.2 (d, $J_{C\ F}$ = 301 Hz), 139.9, 135.9, 135.6, 130.2, 128.54, 128.45, 128.1, 126.2, 114.5 (d, $J_{C\ F}$ = 3.7 Hz), 45.0 (d, $J_{C\ F}$ = 2.7 Hz), 33.4 (d, $J_{C\ F}$ = 1.4 Hz), 30.5.

*Phenyl (S,E) 3 Amino 1 fluoro 5 phenylpent 1 ene 1 sulfonate Hydrochloride (**14**).* Prepared following procedure F using 0.3 g of compound **9** in 7 mL 4 M HCl/dioxane. Yield: 0.23 g (89%). ^{1}H NMR (300 MHz, DMSO-d_6): δ 8.72 (s, 3H), 7.56 7.47 (m, 2H), 7.47 7.37 (m, 3H), 7.31 (t, J = 7.2 Hz, 2H), 7.26 7.19 (m, 1H), 7.19 7.09 (m, 2H), 6.42 (dd, $J_{H\ F}$ = 32 Hz, $J_{H\ H}$ = 9.7 Hz, 1H), 4.15 (td, J = 9.2, 5.3 Hz, 1H), 2.48 2.32 (m, 2H), 2.19 2.01 (m, 1H), 2.00 1.81 (m, 1H). ^{13}C NMR (75 MHz, DMSO-d_6): δ 149.3 (d, $J_{C\ F}$ = 300 Hz), 148.6, 140.0, 130.6, 128.5, 128.4, 128.1, 126.3, 122.0, 118.4 (d, $J_{C\ F}$ = 3.2 Hz), 45.2 (d, $J_{C\ F}$ = 2.2 Hz), 40.4, 33.3, 30.4.

*Phenyl (S,Z) 3 Amino 1 fluoro 5 phenylpent 1 ene 1 sulfonate Hydrochloride (**14 (Z)**).* Prepared following procedure F using 0.2 g of compound **9**-(**Z**) in 7 mL 4 M HCl/dioxane. Yield: 0.16 g (93%). ^{1}H

https://doi.org/10.1021/acs.jmedchem.1c01002
J. Med. Chem. 2021, 64, 12322 12358

NMR (300 MHz, DMSO-d_6): δ 8.68 (s, 3H), 7.59 7.45 (m, 2H), 7.44 7.13 (m, 6H), 7.08 6.98 (m, 2H), 6.73 (dd, $J_{H\ F}$ = 21.2 Hz, $J_{H\ H}$ = 10.6 Hz, 1H), 4.27 (q, J = 7.8, 1H), 2.29 2.02 (m, 2H), 1.95 1.80 (m, 1H), 1.68 1.47 (m, 1H). ^{13}C NMR (75 MHz, DMSO-d_6): δ 148.3, 148.1 (d, $J_{C\ F}$ = 288 Hz), 140.1, 130.6, 128.7, 128.4, 128.0, 126.1, 122.1, 120.6 (d, J = 16 Hz), 45.9 (d, $J_{C\ F}$ = 6.7 Hz), 34.3, 30.2.

Phenyl (S,E) 3 Amino 5 phenylpent 1 ene 1 sulfonate Hydrochloride (14 (H)). Prepared following procedure F using 0.78 g of compound **9-(H)** in 14 mL 4 M HCl/dioxane. Yield: 0.34 g (51%). ^{1}H NMR (300 MHz, DMSO-d_6): δ 8.64 (s, 3H), 7.50 7.41 (m, 2H), 7.41 7.34 (m, 2H), 7.34 7.24 (m, 3H), 7.24 7.17 (m, 1H), 7.16 7.10 (m, 2H), 6.81 (dd, $J_{H\ H}$ = 15.3, 6.8 Hz, 1H), 4.15 3.95 (m, 1H), 2.61 2.38 (m, 2H), 2.10 1.84 (m, 2H). ^{13}C NMR (75 MHz, DMSO-d_6): δ 149.0, 145.3, 140.3, 130.1, 128.5, 128.2, 127.6, 127.6, 126.2, 122.6, 50.1, 33.3, 30.4.

(S,E) 1 (Benzylsulfonyl) 1 fluoro 5 phenylpent 1 en 3 amine Hydrochloride (15). Prepared following procedure F using 0.46 g of compound **10** in 10 mL 4 M HCl/dioxane. Yield: 0.37 g (95%). ^{1}H NMR (300 MHz, DMSO-d_6): δ 8.66 (s, 3H), 7.48 7.27 (m, 7H), 7.26 7.09 (m, 3H), 6.13 (dd, $J_{H\ F}$ = 33 Hz, $J_{H\ H}$ = 9.9 Hz, 1H), 4.87 (s, 2H), 4.04 (td, J = 9.3, 5.0 Hz, 1H), 2.39 (t, J = 8.1 Hz, 2H), 2.13 1.97 (m, 1H), 1.91 1.74 (m, 1H). ^{13}C NMR (75 MHz, DMSO-d_6): δ 154.1 (d, $J_{C\ F}$ = 304 Hz), 140.2, 131.2, 129.0, 128.7, 128.5, 128.2, 127.0, 126.2, 115.7 (d, $J_{C\ F}$ = 2.9 Hz), 57.6, 45.0 (d, $J_{C\ F}$ = 2.2 Hz), 33.5, 30.4.

(S,E) 1 Fluoro 5 (methylthio) 1 (phenylsulfonyl)pent 1 en 3 aminium 2,2,2 Trifluoroacetate (16). Prepared following procedure G with 0.88 g compound **11**. Yield: 0.60 g (65%). ^{1}H NMR (300 MHz, DMSO-d_6): δ 7.89 7.82 (m, 2H), 7.82 7.63 (m, 1H), 7.57 7.52 (m, 2H), 6.21 (d, $J_{H\ F}$ = 32 Hz, 1H), 4.46 (m, 1H), 2.69 2.41 (m, 2H), 2.06 (s, 3H), 2.05 1.75 (m, 2H).

(R,E) 1 (Benzylthio) 4 fluoro 4 (phenylsulfonyl)but 3 en 2 aminium 2,2,2 Trifluoroacetate (17). Prepared following procedure G with 0.44 g compound **12**. Yield: 0.37 g (81%). ^{1}H NMR (300 MHz, DMSO-d_6): δ 8.04 (s, 3H), 7.95 7.84 (m, 2H), 7.77 7.55 (m, 4H), 7.25 7.19 (m, 4H), 6.44 (dd, $J_{H\ F}$ = 30 Hz, $J_{H\ H}$ = 9.1 Hz, 1H), 4.20 4.01 (m, 1H), 3.71 (s, 2H), 2.91 2.62 (m, 2H). ^{13}C NMR (75 MHz, DMSO-d_6): δ 161.4, 160.8, 155.5, 136.6, 135.5, 135.0, 129.9, 129.7, 129.2, 129.1, 128.9, 127.9, 117.3, 113.5, 111.1, 77.2, 46.2, 36.2, 33.3.

tert Butyl ((S) 1 (((S,E) 1 Fluoro 5 phenyl 1 (phenylsulfonyl) pent 1 en 3 yl)amino) 1 oxo 3 phenylpropan 2 yl)carbamate (18). Synthesized following procedure C with 0.180 g compound **13**, 0.135 g boc-L-Phe-OH, 0.162 g TBTU, 0.078 g HOBt, and 0.265 mL DIEA. Purification by column chromatography (petroleum ether/EtOAc 3:1). Yield: 0.21 g (73%). ^{1}H NMR (300 MHz, $CDCl_3$): δ 8.00 7.89 (m, 2H), 7.79 7.68 (m, 1H), 7.67 7.55 (m, 2H), 7.39 7.12 (m, 8H), 7.10 7.00 (m, 2H), 6.00 (dd, $J_{H\ F}$ = 32 Hz, $J_{H\ H}$ = 8.5 Hz, 1H), 5.82 (d, J = 8.0 Hz, 1H), 4.91 (s, 1H), 4.69 (quint, J = 7.7 Hz, 1H), 4.20 (q, J = 7.5 Hz, 1H), 3.04 (dd, J = 13.7, 6.6 Hz, 1H), 2.95 (dd, J = 13.7, 7.6 Hz, 1H), 2.52 (t, J = 7.2 Hz, 2H), 1.96 1.75 (m, 2H), 1.40 (s, 9H). ^{13}C NMR (75 MHz, $CDCl_3$): δ 170.8, 155.6, 154.8 (d, $J_{C\ F}$ = 301 Hz), 140.4, 137.1, 136.6, 134.8, 129.7, 129.4, 129.0, 128.8, 128.7, 128.4, 127.3, 126.4, 117.3 (d, $J_{C\ F}$ = 4.7 Hz), 80.6, 56.2, 45.0, 38.4, 35.7, 31.8, 28.4.

Phenyl (S,E) 3 ((S) 2 ((tert Butoxycarbonyl)amino) 3 phenylpropanamido) 1 fluoro 5 phenylpent 1 Ene 1 sulfonate (19). Synthesized following procedure C with 0.160 g compound **14**, 0.114 g boc-Phe-OH, 0.138 g TBTU, 0.066 g HOBt, and 0.225 mL DIEA. Purification by column chromatography (petroleum ether/EtOAc 3:1). Yield: 0.20 g (78%). ^{1}H NMR (300 MHz, $CDCl_3$): δ 7.47 7.35 (m, 2H), 7.35 7.10 (m, 9H), 7.08 6.95 (m, 4H), 5.65 (d, J = 7.9 Hz, 1H), 5.60 (dd, $J_{H\ F}$ = 32 Hz, $J_{H\ H}$ = 8.3 Hz, 1H), 5.02 (d, J = 7.1 Hz, 1H), 4.68 (q, J = 7.4 Hz, 1H), 4.18 (dd, J = 8.6, 5.6 Hz, 1H), 3.04 (dd, J = 13.4, 6.2 Hz, 1H), 2.85 (dd, J = 13.4, 8.4 Hz, 1H), 2.55 2.35 (m, 2H), 1.83 1.60 (m, 2H), 1.41 (s, 9H). ^{13}C NMR (75 MHz, $CDCl_3$): δ 170.8, 155.8, 149.4, 149.0 (d, $J_{C\ F}$ = 297 Hz), 147.0, 140.1, 136.5, 130.2, 129.3, 129.0, 128.8, 128.4, 128.0, 127.4, 126.6, 122.5, 121.3 (d, $J_{C\ F}$ = 5.1 Hz), 80.6, 56.2, 44.8, 38.7, 35.3, 31.7, 28.4.

Phenyl (S,Z) 3 ((S) 2 ((tert Butoxycarbonyl)amino) 3 phenylpropanamido) 1 fluoro 5 phenylpent 1 ene 1 sulfonate (19 (Z)). Synthesized following procedure C with 0.128 g compound **14-(Z)**, 0.091 g boc-L-Phe-OH, 0.110 g TBTU, 0.053 g HOBt, and 0.204 mL DIEA. Purification by column chromatography (petroleum ether/EtOAc 3:1). Yield: 0.150 g (81%). ^{1}H NMR (300 MHz, $CDCl_3$): δ 7.46 7.08 (m, 13H), 6.97 (d, J = 6.8 Hz, 2H), 5.94 5.59 (m, 2H), 4.96 (s, 1H), 4.80 (q, J = 8.2 Hz, 1H), 4.25 4.11 (m, 1H), 3.14 2.87 (m, 2H), 2.44 2.17 (m, 2H), 1.82 1.61 (m, 1H), 1.53 1.42 (m, 1H), 1.41 (s, 9H). ^{13}C NMR (75 MHz, $CDCl_3$): δ 171.0, 155.6, 149.2, 148.0 (d, $J_{C\ F}$ = 289 Hz), 140.6, 136.7, 130.2, 129.5, 128.9, 128.6, 128.4, 128.1, 127.2, 126.3, 123.0, 123.0 (d, $J_{C\ F}$ = 12 Hz), 80.6, 56.1, 46.1 (d, $J_{C\ F}$ = 5.9 Hz), 38.5, 35.7, 31.8, 28.4.

tert Butyl ((S) 1 (((S,E) 1 (Benzylsulfonyl) 1 fluoro 5 phenylpent 1 en 3 yl)amino) 1 oxo 3 phenylpropan 2 yl)carbamate (20). Synthesized following procedure C with 0.230 g compound **15**, 0.165 g boc-L-Phe-OH, 0.200 g TBTU, 0.095 g HOBt, and 0.325 mL DIEA. Purification by column chromatography (petroleum ether/EtOAc 3:1). Yield: 0.30 g (85%). ^{1}H NMR (300 MHz, $CDCl_3$): δ 7.42 7.15 (m, 11H), 7.13 6.97 (m, 4H), 5.68 (d, J = 8.0 Hz, 1H), 5.53 (dd, $J_{H\ F}$ = 33 Hz, $J_{H\ H}$ = 8.9 Hz, 1H), 4.99 (br s, 1H), 4.68 (quint, J = 7.8 Hz, 1H), 4.35 (s, 2H), 4.18 (q, J = 7.9 Hz, 1H), 3.03 (dd, J = 13.5, 6.4 Hz, 1H), 2.91 (dd, J = 13.5, 8.0 Hz, 1H), 2.49 2.29 (m, 2H), 1.70 1.56 (m, 2H), 1.42 (s, 9H). ^{13}C NMR (75 MHz, $CDCl_3$): δ 170.6, 155.6, 152.3 (d, $J_{C\ F}$ = 301 Hz), 140.3, 136.6, 131.0, 129.5, 129.4, 129.2, 129.0, 128.7, 128.4, 127.3, 126.7, 126.5, 119.7 (d, $J_{C\ F}$ = 4.0 Hz), 80.6, 58.8, 56.2, 44.7 (d, $J_{C\ F}$ = 1.3 Hz), 38.6, 35.5 (d, $J_{C\ F}$ = 1.4 Hz), 31.7, 28.4.

tert Butyl ((S) 1 (((S,E) 1 Fluoro 5 phenyl 1 (phenylsulfonyl) pent 1 en 3 yl)amino) 1 oxo 3 (m tolyl)propan 2 yl)carbamate (21). Synthesized following procedure C with 0.220 g compound **13**, 0.173 g boc-L-Phe(3-Me)-OH, 0.198 g TBTU, 0.095 g HOBt, and 0.330 mL DIEA. Purification by column chromatography (petroleum ether/EtOAc 3:1). Yield: 0.28 g (77%). ^{1}H NMR (300 MHz, $CDCl_3$): δ 8.00 7.88 (m, 2H), 7.76 7.65 (m, 1H), 7.64 7.53 (m, 2H), 7.31 7.12 (m, 4H), 7.11 6.88 (m, 5H), 6.04 (dd, $J_{H\ F}$ = 32.1 Hz, $J_{H\ H}$ = 8.4 Hz, 1H), 5.93 (d, J = 8.0 Hz, 1H), 4.92 (s, 1H), 4.78 4.59 (m, 1H), 4.21 (q, J = 7.3 Hz, 1H), 3.01 (dd, J = 13.8, 6.6 Hz, 1H), 2.92 (dd, J = 13.8, 7.5 Hz, 1H), 2.58 2.46 (m, 2H), 2.31 (s, 3H), 1.93 1.77 (m, 2H), 1.41 (s, 9H). ^{13}C NMR (75 MHz, $CDCl_3$): δ 170.9, 155.62, 154.9 (d, $J_{C\ F}$ = 303 Hz), 140.4, 138.7, 137.1, 136.5, 134.8, 130.1, 129.7, 128.9, 128.8, 128.7, 128.4, 128.1, 126.4, 126.4, 117.4 (d, $J_{C\ F}$ = 3.6 Hz), 80.6, 56.2, 45.2, 38.2, 35.8, 31.8, 28.4, 21.5.

Phenyl (S,E) 3 ((S) 2 ((tert Butoxycarbonyl)amino) 3 (m tolyl) propanamido) 1 fluoro 5 phenylpent 1 ene 1 sulfonate (22). Synthesized following procedure C with 0.280 g compound **14**, 0.210 g boc-L-Phe(3-Me)-OH, 0.242 g TBTU, 0.115 g HOBt, and 0.40 mL DIEA. Purification by column chromatography (petroleum ether/EtOAc 3:1). Yield: 0.34 g (75%). ^{1}H NMR (300 MHz, $CDCl_3$): δ 7.40 (t, J = 7.3 Hz, 2H), 7.35 7.08 (m, 7H), 7.08 7.00 (m, 3H), 6.91 (s, 1H), 6.80 (d, J = 7.3 Hz, 1H), 5.78 (d, J = 7.7 Hz, 1H), 5.65 (dd, $J_{H\ F}$ = 31.4 Hz, $J_{H\ H}$ = 8.3 Hz, 1H), 5.04 (s, 1H), 4.70 (quint, J = 8.2, 7.0 Hz, 1H), 4.18 (quint, J = 8.7, 8.0 Hz, 1H), 3.01 (dd, J = 13.3, 6.1 Hz, 1H), 2.83 (dd, J = 13.3, 8.6 Hz, 1H), 2.55 2.37 (m, 2H), 2.28 (s, 3H), 1.81 1.65 (m, 2H), 1.42 (s, 9H). ^{13}C NMR (75 MHz, $CDCl_3$): δ 170.9, 155.6, 149.4, 149.0 (d, $J_{C\ F}$ = 297 Hz), 140.2, 138.7, 136.5, 130.2, 130.0, 128.9, 128.8, 128.4, 128.1, 128.0, 126.5, 126.4, 122.4, 121.3 (d, $J_{C\ F}$ = 4.9 Hz), 80.6, 56.2, 44.9 (d, $J_{C\ F}$ = 1.2 Hz), 38.5, 35.4 (d, $J_{C\ F}$ = 0.9 Hz), 31.7, 28.4, 21.4.

tert Butyl ((S) 1 (((S,E) 1 (Benzylsulfonyl) 1 fluoro 5 phenylpent 1 en 3 yl)amino) 1 oxo 3 (m tolyl)propan 2 yl)carbamate (23). Synthesized following procedure C with 0.230 g compound **15**, 0.174 g boc-L-Phe(3-Me)-OH, 0.200 g TBTU, 0.095 g HOBt, and 0.325 mL DIEA. Purification by column chromatography (petroleum ether/EtOAc 3:1). Yield: 0.28 g (69%). ^{1}H NMR (300 MHz, $CDCl_3$): δ 7.41 7.12 (m, 9H), 7.04 (d, J = 7.3 Hz, 3H), 6.94 (s, 1H), 6.85 (d, J = 7.3 Hz, 1H), 5.73 (d, J = 7.8 Hz, 1H), 5.56 (dd, $J_{H\ F}$ = 32.8 Hz, $J_{H\ H}$ = 8.8 Hz, 1H), 4.99 (s, 1H), 4.69 (quint, J = 8.3, 7.8 Hz, 1H), 4.34 (s, 2H), 4.18 (q, J = 8.7 Hz, 1H), 3.01 (dd, J = 13.6, 6.5 Hz, 1H), 2.87 (dd, J = 13.6, 7.9 Hz, 1H), 2.49 2.33 (m, 2H), 2.30 (s, 3H), 1.72 1.57 (m, 2H), 1.42 (s, 9H). ^{13}C NMR (75 MHz, $CDCl_3$): δ 170.7, 155.6, 152.3 (d, $J_{C\ F}$ = 301 Hz), 140.4, 138.7, 136.5, 131.1, 130.1, 129.5, 129.2, 128.9, 128.7, 128.4, 128.1, 126.7, 126.5, 119.8 (d, $J_{C\ F}$ = 4.2 Hz), 80.6, 58.8, 56.2, 44.8 (d, $J_{C\ F}$ = 1.3 Hz), 38.4, 35.6, 31.7, 28.4, 21.5.

https://doi.org/10.1021/acs.jmedchem.1c01002
J. Med. Chem. 2021, 64, 12322 12358

*tert Butyl ((S) 1 (((S,E) 1 Fluoro 5 phenyl 1 (phenylsulfonyl) pent 1 en 3 yl)amino) 1 oxo 3 (p tolyl)propan 2 yl)carbamate (**24**).* Synthesized following procedure C with 0.200 g compound **13**, 0.173 g boc-L-Phe(4-Me)-OH, 0.198 g TBTU, 0.095 g HOBt, and 0.30 mL DIEA. Purification by column chromatography (petroleum ether/EtOAc 3:1). Yield: 0.25 g (77%). ^{1}H NMR (300 MHz, $CDCl_3$): δ 7.94 (d, J = 7.8 Hz, 2H), 7.70 (t, J = 7.2 Hz, 1H), 7.59 (t, J = 7.6 Hz, 2H), 7.35 6.92 (m, 9H), 6.03 (dd, $J_{H\ F}$ = 32.0 Hz, $J_{H\ H}$ = 8.4 Hz, 1H), 5.89 (d, J = 8.0 Hz, 1H), 4.93 (s, 1H), 4.70 (quint, J = 7.4 Hz, 1H), 4.20 (q, J = 7.2 Hz, 1H), 3.01 (dd, J = 13.6, 6.4 Hz, 1H), 2.91 (dd, J = 13.6, 7.6 Hz, 1H), 2.52 (t, J = 7.5 Hz, 2H), 2.33 (s, 3H), 1.95 1.77 (m, 2H), 1.41 (s, 9H). ^{13}C NMR (75 MHz, $CDCl_3$): δ 170.9, 155.6, 154.8 (d, $J_{C\ F}$ = 301 Hz), 140.4, 137.2, 137.0, 134.7, 133.4, 129.70, 129.65, 129.3, 128.8, 128.7, 128.4, 126.4, 117.4 (d, $J_{C\ F}$ = 4.4 Hz), 80.5, 56.2, 45.0, 38.0, 35.8, 31.8, 28.4, 21.2.

*Phenyl (S,E) 3 ((S) 2 ((tert Butoxycarbonyl)amino) 3 (p tolyl) propanamido) 1 fluoro 5 phenylpent 1 ene 1 sulfonate (**25**).* Synthesized following procedure C with 0.292 g compound **14**, 0.220 g boc-L-Phe(4-Me)-OH, 0.252 g TBTU, 0.121 g HOBt, and 0.410 mL DIEA. Purification by column chromatography (petroleum ether/EtOAc 3:1). Yield: 0.39 g (83%). ^{1}H NMR (300 MHz, $CDCl_3$): δ 7.47 7.35 (m, 2H), 7.35 7.15 (m, 6H), 7.10 6.98 (m, 4H), 6.92 (d, J = 8.0 Hz, 2H), 5.75 (d, J = 7.9 Hz, 1H), 5.62 (dd, $J_{H\ F}$ = 31 Hz, $J_{H\ H}$ = 9.0 Hz, 1H), 5.05 (d, J = 7.8 Hz, 1H), 4.70 (quint, J = 7.7 Hz, 1H), 4.20 4.08 (m, 1H), 3.00 (dd, J = 13.5, 6.1 Hz, 1H), 2.81 (dd, J = 13.5, 8.3 Hz, 1H), 2.53 2.36 (m, 2H), 2.29 (s, 3H), 1.83 1.62 (m, 2H), 1.41 (s, 9H). ^{13}C NMR (75 MHz, $CDCl_3$): δ 170.9, 155.6, 149.4, 149.0 (d, $J_{C\ F}$ = 297 Hz), 140.2, 137.0, 133.3, 130.2, 129.7, 129.2, 128.8, 128.4, 128.0, 126.5, 122.4, 121.4, 121.3, 80.6, 56.3, 44.8 (d, $J_{C\ F}$ = 1.5 Hz), 38.3, 35.4, 31.7, 28.4, 21.1.

*Phenyl (S,E) 3 ((S) 2 ((tert Butoxycarbonyl)amino) 3 (p tolyl) propanamido) 5 phenylpent 1 ene 1 sulfonate (**25 (H)**).* Synthesized following procedure C with 0.34 g compound **14-(H)**, 0.28 g boc-L-Phe(4-Me)-OH, 0.32 g TBTU, 0.14 g HOBt, and 0.70 mL DIEA. Purification by column chromatography (cyclohexane/EtOAc 4:1). Yield: 0.24 g (42%). ^{1}H NMR (300 MHz, $CDCl_3$): δ 7.42 7.32 (m, 2H), 7.31 7.02 (m, 12H), 6.52 (dd, $J_{H\ H}$ = 15.2, 4.6 Hz, 1H), 5.92 (dd, $J_{H\ H}$ = 37.5, 11.8 Hz, 2H), 5.00 (s, 1H), 4.63 4.47 (m, 1H), 4.31 4.18 (q, 1H), 3.08 2.89 (m, 2H), 2.62 2.42 (m, 2H), 2.31 (s, 3H), 1.88 1.60 (m, 2H), 1.43 (s, 9H). ^{13}C NMR (75 MHz, $CDCl_3$): δ 171.1, 149.5, 149.1, 140.1, 137.3, 133.0, 129.8 (d, J = 3.6 Hz), 129.1 (d, J = 6.7 Hz), 128.6, 128.3, 127.3, 126.4, 124.4, 122.6, 56.5, 49.2, 35.1, 31.7, 28.3, 21.0. mp 93 95 °C.

*tert Butyl ((S) 1 (((S,E) 1 (Benzylsulfonyl) 1 fluoro 5 phenylpent 1 en 3 yl)amino) 1 oxo 3 (p tolyl)propan 2 yl)carbamate (**26**).* Synthesized following procedure C with 0.230 g compound **15**, 0.174 g boc-L-Phe(4-Me)-OH, 0.200 g TBTU, 0.095 g HOBt, and 0.325 mL DIEA. Purification by column chromatography (petroleum ether/EtOAc 3:1). Yield: 0.290 g (79%). ^{1}H NMR (300 MHz, $CDCl_3$): δ 7.43 7.14 (m, 8H), 7.12 6.99 (m, 4H), 6.96 (d, J = 7.4 Hz, 2H), 5.66 (d, J = 7.8 Hz, 1H), 5.54 (dd, $J_{H\ F}$ = 32.9 Hz, $J_{H\ H}$ = 8.7 Hz, 1H), 4.98 (s, 1H), 4.69 (quint, J = 8.3 Hz, 1H), 4.34 (s, 2H), 4.15 (q, J = 7.8, 7.4 Hz, 1H), 3.01 (dd, J = 13.6, 5.9 Hz, 1H), 2.85 (dd, J = 13.6, 8.0 Hz, 1H), 2.54 2.33 (m, 2H), 2.30 (s, 3H), 1.70 1.55 (m, 3H), 1.42 (s, 9H). ^{13}C NMR (75 MHz, $CDCl_3$): δ 170.7, 155.6, 152.3 (d, $J_{C\ F}$ = 301 Hz), 140.4, 137.0, 133.4, 131.0, 129.7, 129.5, 129.3, 129.2, 128.7, 128.4, 126.7, 126.5, 119.8 (d, $J_{C\ F}$ = 4.0 Hz), 80.5, 58.8, 56.2, 44.7 (d, $J_{C\ F}$ = 1.6 Hz), 38.1, 35.6, 31.7, 28.4, 21.2.

*(S) 1 (((S,E) 1 Fluoro 5 phenyl 1 (phenylsulfonyl)pent 1 en 3 yl)amino) 1 oxo 3 phenylpropan 2 aminium Chloride (**27**).* Synthesized by following procedure F with 0.21 g of compound **18** in 10 mL 4 M HCl/dioxane. Yield: 0.19 g (99%) The crude product was used without further purification and characterization for the next step.

*(S) 1 (((S,E) 1 Fluoro 1 (phenoxysulfonyl) 5 phenylpent 1 en 3 yl)amino) 1 oxo 3 phenylpropan 2 aminium Chloride (**28**).* Synthesized by following procedure F with 0.20 g of compound **19** in 8 mL 4 M HCl/dioxane. Yield: 0.18 g (99%). The crude product was used without further purification and characterization for the next step.

*(S) 1 (((S,Z) 1 Fluoro 1 (phenoxysulfonyl) 5 phenylpent 1 en 3 yl)amino) 1 oxo 3 phenylpropan 2 aminium Chloride (**28 (Z)**).* Synthesized by following procedure F with 0.15 g of compound **19-(Z)** in 8 mL 4 M HCl/dioxane. Yield: 0.13 g (99%). The crude product was used without further purification and characterization for the next step.

*(S) 1 (((S,E) 1 (Benzylsulfonyl) 1 fluoro 5 phenylpent 1 en 3 yl) amino) 1 oxo 3 phenylpropan 2 aminium Chloride (**29**).* Synthesized by following procedure F with 0.30 g of compound **20** in 10 mL 4 M HCl/dioxane. Yield: 0.26 g (99%). The crude product was used without further purification and characterization for the next step.

*(S) 1 (((S,E) 1 Fluoro 5 phenyl 1 (phenylsulfonyl)pent 1 en 3 yl)amino) 1 oxo 3 (m tolyl)propan 2 aminium Chloride (**30**).* Synthesized by following procedure F with 0.28 g of compound **21** in 8 mL 4 M HCl/dioxane. Yield: 0.25 g (99%). The crude product was used without further purification and characterization for the next step.

*(S) 1 (((S,E) 1 Fluoro 1 (phenoxysulfonyl) 5 phenylpent 1 en 3 yl)amino) 1 oxo 3 (m tolyl)propan 2 aminium Chloride (**31**).* Synthesized by following procedure F with 0.34 g of compound **22** in 10 mL 4 M HCl/dioxane. Yield: 0.30 g (99%). The crude product was used without further purification and characterization for the next step.

*(S) 1 (((S,E) 1 (Benzylsulfonyl) 1 fluoro 5 phenylpent 1 en 3 yl) amino) 1 oxo 3 (m tolyl)propan 2 aminium Chloride (**32**).* Synthesized by following procedure F with 0.28 g of compound **23** in 8 mL 4 M HCl/dioxane. Yield: 0.25 g (99%). The crude product was used without further purification and characterization for the next step.

*(S) 1 (((S,E) 1 Fluoro 5 phenyl 1 (phenylsulfonyl)pent 1 en 3 yl)amino) 1 oxo 3 (p tolyl)propan 2 aminium Chloride (**33**).* Synthesized by following procedure F with 0.25 g of compound **24** in 8 mL 4 M HCl/dioxane. Yield: 0.22 g (99%). The crude product was used without further purification and characterization for the next step.

*(S) 1 (((S,E) 1 Fluoro 1 (phenoxysulfonyl) 5 phenylpent 1 en 3 yl)amino) 1 oxo 3 (p tolyl)propan 2 aminium Chloride (**34**).* Synthesized by following procedure F with 0.39 g of compound **25** in 10 mL 4 M HCl/dioxane. Yield: 0.34 g (99%). The crude product was used without further purification and characterization for the next step.

*(S) 1 Oxo 1 (((S,E) 1 (phenoxysulfonyl) 5 phenylpent 1 en 3 yl) amino) 3 (p tolyl)propan 2 aminium Chloride (**34 (H)**).* Synthesized by following procedure F with 0.20 g of compound **25-(H)** in 4 mL 4 M HCl/dioxane. Yield: 0.15 g (89%), colorless solid. ^{1}H NMR (300 MHz, DMSO-d_6): δ 9.06 (d, J = 8.4 Hz, 1H), 8.57 (s, 3H), 7.48 7.38 (m, 2H), 7.37 7.21 (m, 5H), 7.20 6.97 (m, 7H), 6.58 (dd, J = 15.3, 4.4 Hz, 1H), 6.21 (dt, J = 15.3, 2.1 Hz, 1H), 4.46 (s, 1H), 4.17 (s, 1H), 3.17 2.94 (m, 2H), 2.63 2.50 (m, 2H), 2.23 (d, J = 2.7 Hz, 3H), 1.82 1.62 (m, 2H). ^{13}C NMR (75 MHz, DMSO-d_6): δ 167.8, 150.5, 149.1, 141.1, 136.4, 131.7, 130.0, 129.2 (d, J = 5.5 Hz), 128.3 (d, J = 6.1 Hz), 127.4, 125.9, 123.4, 122.6, 53.5, 49.2, 34.3, 31.1, 20.7.

*(S) 1 (((S,E) 1 (Benzylsulfonyl) 1 fluoro 5 phenylpent 1 en 3 yl) amino) 1 oxo 3 (p tolyl)propan 2 aminium Chloride (**35**).* Synthesized by following procedure F with 0.29 g of compound **26** in 10 mL 4 M HCl/dioxane. Yield: 0.26 g (99%). The crude product was used without further purification and characterization for the next step.

*Phenyl (S,E) 1 Fluoro 3 ((S) 2 (isonicotinamido) 3 phenylpropa namido) 5 phenylpent 1 ene 1 sulfonate (**2a**).* Synthesized by following procedure E with 0.14 g of compound **14**, 0.10 g compound **X**, 0.13 g TBTU, 0.062 HOBt, and 0.21 mL DIEA. Column chromatography: petroleum ether/EtOAc 1:3 to 0:1. Yield: 0.16 g (73%), colorless solid. mp 71 73 °C. ^{1}H NMR (300 MHz, $CDCl_3$): δ 8.70 (d, J = 5.9 Hz, 2H), 7.64 (d, J = 6.0 Hz, 2H), 7.51 (d, J = 7.6 Hz, 1H), 7.45 7.34 (m, 2H), 7.34 7.11 (m, 9H), 7.12 7.02 (m, 2H), 6.97 (d, J = 6.6 Hz, 2H), 6.22 (d, J = 7.6 Hz, 1H), 5.61 (dd, $J_{H\ F}$ = 31.0 Hz, $J_{H\ H}$ = 9.2 Hz, 1H), 4.80 4.62 (m, 2H), 3.22 (dd, J = 13.3, 6.2 Hz, 1H), 2.96 (dd, J = 13.3, 9.0 Hz, 1H), 2.52 2.27 (m, 2H), 1.82 1.55 (m, 2H). ^{13}C NMR (75 MHz, $CDCl_3$): δ 170.2, 164.8, 149.3, 149.2 (d, $J_{C\ F}$ = 297 Hz), 147.2, 142.1, 139.9, 136.0, 130.3, 129.3, 129.1, 128.8, 128.3, 128.1, 127.7, 126.6, 122.4, 121.8, 120.94 (d, $J_{C\ F}$ = 4.8 Hz), 55.7, 44.9 (d, $J_{C\ F}$ = 1.9 Hz), 38.9, 35.3, 31.7. mp 71 73 °C. LC MS (ESI, m/z): $[M + H]^+$ calcd for $C_{32}H_{30}FN_3O_5S$, 588.20; found, 588.3. Purity: 97%. $[\alpha]_D^{22}$ 10° (c 0.5, $CHCl_3$).

*Phenyl (S,Z) 1 Fluoro 3 ((S) 2 (isonicotinamido) 3 phenylpropa namido) 5 phenylpent 1 ene 1 sulfonate (**2a (Z)**).* Synthesized by following procedure E with 0.10 g of compound **14-(Z)**, 0.073 g compound **X**, 0.086 g TBTU, 0.041 g HOBt, and 0.14 mL DIEA. Column chromatography: petroleum ether/EtOAc 1:3. Yield: 0.12 g

https://doi.org/10.1021/acs.jmedchem.1c01002
J. Med. Chem. 2021, 64, 12322 12358

(79%), colorless solid. ^{1}H NMR (300 MHz, $CDCl_3$): δ 8.65 (d, J = 5.5 Hz, 2H), 7.85 (d, J = 7.4 Hz, 1H), 7.60 (d, J = 5.3 Hz, 2H), 7.44 7.07 (m, 14H), 6.98 6.83 (m, 2H), 6.38 (d, J = 7.2 Hz, 1H), 5.58 (dd, $J_{H\ F}$ = 20.5 Hz, $J_{H\ H}$ = 10.1 Hz, 1H), 4.96 (dt, J = 14.8, 6.6 Hz, 1H), 4.77 (q, J = 7.7 Hz, 1H), 3.24 (dd, J = 13.5, 6.6 Hz, 1H), 3.08 (dd, J = 13.4, 8.7 Hz, 1H), 2.37 2.22 (m, 1H), 2.20 2.08 (m, 1H), 1.69 1.52 (m, 1H), 1.43 1.32 (m, 1H). ^{13}C NMR (75 MHz, $CDCl_3$): δ 170.7, 164.9, 149.3, 149.1, 148.25 (d, $J_{C\ F}$ = 290 Hz), 141.9, 140.3, 136.4, 130.2, 129.5, 129.0, 128.6, 128.7, 128.2, 127.5, 126.4, 122.5 (d, $J_{C\ F}$ = 11.4 Hz), 122.3, 121.8, 55.8, 45.9 (d, $J_{C\ F}$ = 5.5 Hz), 38.6, 35.8 (d, $J_{C\ F}$ = 2.3 Hz), 31.6. mp 173 175 °C. LC MS (ESI, m/z): $[M + H]^+$ calcd for $C_{32}H_{30}FN_3O_5S$, 588.20; found, 588.3. Purity: 95%. $[\alpha]_D^{22}$ 13° (c 0.5, $CHCl_3$).

*Phenyl (S,E) 3 ((S) 2 (2,3 Dihydrobenzo[b][1,4]dioxine 6 carbox amido) 3 phenylpropanamido) 1 fluoro 5 phenylpent 1 ene 1 sulfonate (**2b**).* Synthesized by following procedure D with 0.10 g of compound **28**, 0.035 g 1,4-benzodioxane-6-carboxylic acid, 0.062 g TBTU, and 0.10 mL DIEA. Column chromatography: petroleum ether/EtOAc 2:1. Yield: 0.088 g (71%), colorless solid. ^{1}H NMR (300 MHz, $CDCl_3$): δ 7.46 7.35 (m, 2H), 7.35 7.10 (m, 11H), 7.04 (d, J = 6.5 Hz, 2H), 6.96 6.80 (m, 4H), 6.60 (d, J = 7.4 Hz, 1H), 5.60 (dd, $J_{H\ F}$ = 31.0 Hz, $J_{H\ H}$ = 9.0 Hz, 1H), 4.82 (q, J = 7.4 Hz, 1H), 4.67 (quint, J = 7.8 Hz, 1H), 4.34 4.19 (m, 4H), 3.17 (dd, J = 13.2, 6.2 Hz, 1H), 2.96 (dd, J = 13.2, 8.6 Hz, 1H), 2.45 2.26 (m, 2H), 1.72 1.52 (m, 2H). ^{13}C NMR (75 MHz, $CDCl_3$): δ 170.9, 167.0, 149.4, 149.0 (d, $J_{C\ F}$ = 297 Hz), 147.0, 143.6, 140.1, 136.3, 130.2, 129.4, 129.0, 128.6, 128.3, 128.0, 127.4, 126.4, 122.4, 121.4 (d, $J_{C\ F}$ = 4.4 Hz), 120.7, 117.5, 116.8, 64.7, 64.3, 55.2, 44.8 (d, $J_{C\ F}$ = 2.0 Hz), 38.9, 35.2 (d, $J_{C\ F}$ = 1.5 Hz), 31.6. mp 167 168 °C. LC MS (ESI, m/z): $[M + H]^+$ calcd for $C_{35}H_{33}FN_2O_7S$, 645.2; found, 645.3. Purity: 98%. $[\alpha]_D^{22}$ 12° (c 1, $CHCl_3$).

*Phenyl (S,E) 1 Fluoro 3 ((S) 2 (isonicotinamido) 3 (p tolyl) propanamido) 5 phenylpent 1 ene 1 sulfonate (**2d**).* Synthesized by following procedure D with 0.12 g of compound **34**, 0.028 g isonicotinic acid, 0.073 g TBTU, and 0.12 mL DIEA. Column chromatography: petroleum ether/EtOAc 1:3. Yield: 0.10 g (77%), colorless solid. ^{1}H NMR (300 MHz, $CDCl_3$): δ 8.69 (d, J = 3.5 Hz, 2H), 7.56 (d, J = 3.5 Hz, 2H), 7.44 7.36 (m, 3H), 7.36 7.12 (m, 7H), 7.06 (d, J = 7.7 Hz, 2H), 7.01 6.88 (m, 4H), 6.29 (d, J = 7.7 Hz, 1H), 5.62 (dd, $J_{H\ F}$ = 31.0 Hz, $J_{H\ H}$ = 9.1 Hz, 1H), 4.81 4.63 (m, 2H), 3.16 (dd, J = 13.4, 5.7 Hz, 1H), 2.92 (dd, J = 12.9, 9.6 Hz, 1H), 2.47 2.30 (m, 2H), 2.27 (s, 3H), 1.80 1.56 (m, 3H). ^{13}C NMR (75 MHz, $CDCl_3$): δ 170.3, 165.3, 150.4, 149.3, 149.2 (d, $J_{C\ F}$ = 297 Hz), 141.0, 139.9, 137.4, 132.8, 130.2, 129.8, 129.2, 128.8, 128.2, 128.1, 126.6, 122.4, 121.2, 120.9 (d, $J_{C\ F}$ = 5.2 Hz), 55.6, 44.8 (d, $J_{C\ F}$ = 1.6 Hz), 38.6, 35.4, 31.6, 21.1. mp 78 79 °C. LC MS (ESI, m/z): $[M + H]^+$ calcd for $C_{33}H_{32}FN_3O_5S$, 602.21; found, 602.3. Purity: 97%. $[\alpha]_D^{22}$ 8° (c 0.5, MeOH).

*Phenyl (S,E) 3 ((S) 2 (Isonicotinamido) 3 ((p tolyl) propanamido) 5 phenylpent 1 ene 1 sulfonate (**2d (H)**).* Synthesized by following procedure D with 0.21 g of compound **34-(H)**, 0.054 g isonicotinic acid, 0.014 g TBTU, and 0.28 mL DIEA. Column chromatography: cyclohexane/EtOAc 1:3. Yield: 0.080 g (35%), colorless solid. ^{1}H NMR (300 MHz, $CDCl_3$): δ 8.71 (d, J = 13.0 Hz, 2H), 7.65 (d, J = 21.2 Hz, 2H), 7.52 7.41 (m, 1H), 7.42 7.32 (m, 1H), 7.32 7.23 (m, 3H), 7.22 7.15 (m, 4H), 7.15 7.03 (m, 2H), 7.02 6.90 (m, 2H), 6.71 6.59 (m, 1H), 6.51 (dd, J = 15.2, 5.1 Hz, 1H), 6.32 (d, J = 7.7 Hz, 1H), 5.99 (dd, J = 15.2, 1.5 Hz, 1H), 4.92 4.73 (m, 1H), 4.53 (s, 1H), 3.29 3.13 (m, 1H), 3.07 (dd, J = 13.5, 8.9 Hz, 1H), 2.60 2.40 (m, 2H), 2.32 (s, 3H), 1.83 1.58 (m, 3H). ^{13}C NMR (75 MHz, $CDCl_3$): δ 170.5, 164.5, 149.4, 148.7, 139.9, 137.6, 132.7, 129.9, 129.1, 128.7, 128.3, 127.4, 126.5, 124.6, 122.5, 126.6, 55.9, 49.6, 35.1, 31.7, 21.1. mp 84 86 °C. LC MS (ESI, m/z): $[M + H]^+$ calcd for $C_{33}H_{33}N_3O_5S$, 584.21; found, 584.3. Purity: 98%. $[\alpha]_D^{22}$ 11° (c 0.5, MeOH).

*Phenyl (S,E) 3 ((S) 2 (2,3 Dihydrobenzo[b][1,4]dioxine 6 carbox amido) 3 (p tolyl)propan amido) 1 fluoro 5 phenylpent 1 ene 1 sulfonate (**2e**).* Synthesized by following procedure D with 0.100 g of compound **34**, 0.034 g 1,4-benzodioxane-6-carboxylic acid, 0.060 g TBTU, and 0.10 mL DIEA. Column chromatography: petroleum ether/EtOAc 2:1. Yield: 0.094 g (78%), colorless solid. ^{1}H NMR (300 MHz, $CDCl_3$): δ 7.46 7.35 (m, 2H), 7.34 7.23 (m, 5H), 7.23 7.12 (m, 4H), 7.03 (d, J = 7.9 Hz, 2H), 6.97 6.88 (m, 4H), 6.88 6.78 (m, 2H), 6.58 (d, J = 7.7 Hz, 1H), 5.61 (dd, $J_{H\ F}$ = 31.2 Hz, $J_{H\ H}$ = 9.1 Hz, 1H), 4.85 4.60 (m, 2H), 4.34 4.20 (m, 4H), 3.12 (dd, J = 13.3, 6.1 Hz, 1H), 2.91 (dd, J = 13.3, 8.6 Hz, 1H), 2.44 2.30 (m, 2H), 2.26 (s, 3H), 1.72 1.55 (m, 2H). ^{13}C NMR (75 MHz, $CDCl_3$): δ 170.9, 166.8, 149.4, 148.9 (d, $J_{C\ F}$ = 296 Hz), 147.1, 143.6, 140.1, 137.1, 133.2, 130.2, 129.6, 129.3, 128.6, 128.3, 128.0, 126.4, 122.4, 121.5 (d, $J_{C\ F}$ = 4.6 Hz), 120.6, 117.5, 116.8, 64.7, 64.3, 55.3, 44.7 (d, $J_{C\ F}$ = 1.7 Hz), 38.5, 35.3, 31.6, 21.1. mp 92 93 °C. LC MS (ESI, m/z): $[M + H]^+$ calcd for $C_{36}H_{35}FN_2O_7S$, 659.22; found, 659.3. Purity: 95%. $[\alpha]_D^{22}$ 26° (c 1, MeOH).

*Phenyl (S,E) 3 ((S) 2 (3,5 Difluorobenzamido) 3 (p tolyl) propanamido) 1 fluoro 5 phenylpent 1 ene 1 sulfonate (**2f**).* Synthesized by following procedure D with 0.10 g of compound **34**, 0.030 g 3,5-difluorobenzoic acid, 0.060 g TBTU, and 0.10 mL DIEA. Column chromatography: petroleum ether/EtOAc 3:1. Yield: 0.097 g (81%), colorless solid. ^{1}H NMR (300 MHz, $CDCl_3$): δ 7.46 7.10 (m, 12H), 7.04 (d, J = 7.8 Hz, 2H), 6.99 6.84 (m, 5H), 6.23 (d, J = 7.7 Hz, 1H), 5.58 (dd, $J_{H\ F}$ = 31.0 Hz, $J_{H\ H}$ = 9.2 Hz, 1H), 4.80 4.60 (m, 2H), 3.15 (dd, J = 13.3, 6.0 Hz, 1H), 2.91 (dd, J = 13.3, 9.1 Hz, 1H), 2.49 2.31 (m, 2H), 2.26 (s, 3H), 1.73 1.56 (m, 2H). ^{13}C NMR (75 MHz, $CDCl_3$): δ 170.6, 164.9 (t, $J_{C\ F}$ = 2.6 Hz), 163.0 (dd, $J_{C\ F}$ = 251, 12 Hz), 149.3, 149.2 (d, $J_{C\ F}$ = 297 Hz), 140.0, 137.4, 136.8 (t, $J_{C\ F}$ = 8.5 Hz), 132.9, 130.2, 129.8, 129.2, 128.7, 128.3, 128.1, 126.6, 122.4, 121.0 (d, J = 5.0 Hz), 110.5 (dd, $J_{C\ F}$ = 26.2, 8.8 Hz), 107.4 (t, $J_{C\ F}$ = 25.4 Hz), 55.8, 44.9 (d, $J_{C\ F}$ = 2.4 Hz), 38.5, 35.4 (d, $J_{C\ F}$ = 1.6 Hz), 31.7, 21.1. mp 175 177 °C. LC MS (ESI, m/z): $[M + H]^+$ calcd for $C_{34}H_{31}F_3N_2O_5S$, 637.20; found, 637.2. Purity: >99%. $[\alpha]_D^{22}$ 7° (c 0.5, $CHCl_3$).

*Phenyl (S,E) 1 Fluoro 3 ((S) 2 (isonicotinamido) 3 (m tolyl) propanamido) 5 phenylpent 1 ene 1 sulfonate (**2g**).* Synthesized by following procedure D with 0.11 g of compound **31**, 0.026 g isonicotinic acid, 0.067 g TBTU, and 0.11 mL DIEA. Column chromatography: petroleum ether/EtOAc 1:3. Yield: 0.096 g (77%), colorless solid. ^{1}H NMR (300 MHz, $CDCl_3$): δ 8.62 (d, J = 4.6 Hz, 2H), 7.49 (d, J = 4.0 Hz, 2H), 7.39 7.03 (m, 11H), 6.97 (d, J = 7.3 Hz, 1H), 6.94 6.81 (m, 3H), 6.74 (d, J = 7.3 Hz, 1H), 6.10 (d, J = 7.5 Hz, 1H), 5.57 (dd, $J_{H\ F}$ = 31.0 Hz, $J_{H\ H}$ = 9.1 Hz, 1H), 4.74 4.50 (m, 2H), 3.11 (dd, J = 13.1, 5.7 Hz, 1H), 2.88 2.78 (m, 1H), 2.39 2.21 (m, 2H), 2.17 (s, 3H), 1.72 1.49 (m, 2H). ^{13}C NMR (75 MHz, $CDCl_3$): δ 170.2, 165.3, 150.3, 149.33, 149.25 (d, $J_{C\ F}$ = 297 Hz), 147.3, 141.2, 139.9, 138.9, 136.0, 130.2, 130.0, 129.0, 128.8, 128.5, 128.2, 128.1, 126.6, 126.4, 122.4, 121.2, 120.9 (d, $J_{C\ F}$ = 5.0 Hz), 55.5, 45.0 (d, $J_{C\ F}$ = 2.0 Hz), 38.9, 35.4, 31.6, 21.4. mp 67 68 °C. LC MS (ESI, m/z): $[M + H]^+$ calcd for $C_{33}H_{32}FN_3O_5S$, 602.21; found, 602.3. Purity: >99%. $[\alpha]_D^{22}$ 8° (c 0.5, $CHCl_3$).

*Phenyl (S,E) 3 ((S) 2 (2,3 Dihydrobenzo[b][1,4]dioxine 6 carbox amido) 3 (m tolyl)propanamido) 1 fluoro 5 phenylpent 1 ene 1 sulfonate (**2h**).* Synthesized by following procedure D with 0.10 g of compound **31**, 0.034 g 1,4-benzodioxane-6-carboxylic acid, 0.060 g TBTU, and 0.10 mL DIEA. Column chromatography: petroleum ether/EtOAc 2:1. Yield: 0.088 g (72%), colorless solid. ^{1}H NMR (300 MHz, $CDCl_3$): δ 7.37 7.27 (m, 2H), 7.27 6.99 (m, 10H), 6.94 (d, J = 7.7 Hz, 1H), 6.91 6.80 (m, 3H), 6.80 6.70 (m, 3H), 6.52 (d, J = 7.7 Hz, 1H), 5.57 (dd, $J_{H\ F}$ = 31.1 Hz, $J_{H\ F}$ = 9.1 Hz, 1H), 4.73 (q, J = 7.9 Hz, 1H), 4.59 (quint, J = 7.6 Hz, 1H), 4.26 4.09 (m, 4H), 3.07 (dd, J = 13.4, 6.3 Hz, 1H), 2.85 (dd, J = 13.4, 8.5 Hz, 1H), 2.38 2.19 (m, 2H), 2.15 (s, 3H), 1.65 1.46 (m, 2H). ^{13}C NMR (75 MHz, $CDCl_3$): δ 170.9, 166.9, 149.4, 149.0 (d, $J_{C\ F}$ = 297 Hz), 147.1, 143.6, 140.1, 138.7, 136.3, 130.2, 130.1, 128.8, 128.6, 128.3, 128.2, 128.0, 126.8, 126.5, 126.4, 122.4, 121.4 (d, $J_{C\ F}$ = 3.6 Hz), 120.6, 117.5, 116.8, 64.7, 64.3, 55.2, 44.9 (d, $J_{C\ F}$ = 1.1 Hz), 38.8, 35.3, 31.6, 21.4. mp 126 128 °C. LC MS (ESI, m/z): $[M + H]^+$ calcd for $C_{36}H_{35}FN_2O_7S$, 659.22; found, 659.3. Purity: 98%. $[\alpha]_D^{22}$ 3° (c 0.5, MeOH).

*Phenyl (S,E) 3 ((S) 2 (3,5 Difluorobenzamido) 3 (m tolyl) propanamido) 1 fluoro 5 phenylpent 1 ene 1 sulfonate (**2i**).* Synthesized by following procedure D with 0.10 g of compound **31**, 0.030 g 3,5-difluorobenzoic acid, 0.060 g TBTU, and 0.10 mL DIEA. Column

https://doi.org/10.1021/acs.jmedchem.1c01002
J. Med. Chem. 2021, 64, 12322 12358

chromatography: petroleum ether/EtOAc 3:1. Yield: 0.075 g (62%), colorless solid. ^{1}H NMR (300 MHz, $CDCl_3$): δ 7.36 7.27 (m, 2H), 7.28 7.03 (m, 10H), 7.03 6.94 (m, 2H), 6.94 6.80 (m, 4H), 6.74 (d, J = 7.4 Hz, 1H), 5.82 (d, J = 7.7 Hz, 1H), 5.54 (dd, $J_{H\ F}$ = 30.9 Hz, $J_{H\ H}$ = 9.1 Hz, 1H), 4.68 4.52 (m, 2H), 3.10 (dd, J = 13.4, 6.0 Hz, 1H), 2.80 (dd, J = 13.3, 9.1 Hz, 1H), 2.41 2.21 (m, J = 7.2 Hz, 2H), 2.19 (s, 3H), 1.68 1.57 (m, 2H). ^{13}C NMR (75 MHz, $CDCl_3$): δ 170.3, 165.0 (t, $J_{C\ F}$ = 2.7 Hz), 163.0 (dd, $J_{C\ F}$ = 251, 12 Hz), 149.4, 149.3 (d, $J_{C\ F}$ = 298 Hz), 139.9, 139.0, 137.0, 136.9, 136.8, 136.1, 130.2, 130.0, 129.1, 128.8, 128.5, 128.3, 128.1, 126.6, 126.4, 122.4, 120.9 (d, $J_{C\ F}$ = 5.0 Hz), 110.5 (dd, $J_{C\ F}$ = 26, 8.7 Hz), 107.5 (t, $J_{C\ F}$ = 25 Hz), 55.6, 45.0 (d, $J_{C\ F}$ = 2.3 Hz), 38.8, 35.4, 31.6, 21.4. mp 129 130 °C. LC MS (ESI, m/z): $[M + H]^+$ calcd for $C_{34}H_{31}F_3N_2O_5S$, 637.20; found, 637.3. Purity: 96%. $[\alpha]_D^{22}$ 9° (c 0.5, MeOH).

*Phenyl (S,E) 3 ((S) 2 (((Benzyloxy)carbonyl)amino) 3 phenylpropanamido) 1 fluoro 5 phenylpent 1 ene 1 sulfonate (**2j**).* Synthesized by following procedure E with 0.090 g of compound **14**, 0.076 g Cbz-L-Phe-OH, 0.082 g TBTU, 0.039 g HOBt, and 0.13 mL DIEA. Column chromatography: petroleum ether/EtOAc 2:1. Yield: 0.12 g (78%), colorless solid. ^{1}H NMR (300 MHz, $CDCl_3$): δ 7.48 7.14 (m, 17H), 7.06 6.92 (m, 4H), 5.56 (dd, $J_{H\ F}$ = 31.1 Hz, $J_{H\ H}$ = 9.0 Hz, 2H), 5.32 (d, J = 5.7 Hz, 1H), 5.06 (s, 2H), 4.68 (quint, J = 7.5 Hz, 1H), 4.22 (d, J = 6.6 Hz, 1H), 3.07 (dd, J = 13.4, 6.0 Hz, 1H), 2.83 (dd, J = 13.4, 8.6 Hz, 1H), 2.52 2.30 (m, 2H), 1.80 1.64 (m, 2H). ^{13}C NMR (75 MHz, $CDCl_3$): δ 170.3, 156.4, 149.4, 149.0 (d, $J_{C\ F}$ = 297 Hz), 140.1, 136.2, 136.1, 130.2, 129.3, 129.1, 128.8, 128.7, 128.5, 128.3, 128.2, 128.0, 127.5, 126.6, 122.5, 121.1 (d, $J_{C\ F}$ = 4.6 Hz), 67.4, 56.6, 44.9 (d, $J_{C\ F}$ = 1.1 Hz), 38.9, 35.2, 31.7. mp 127 128 °C. LC MS (ESI, m/z): $[M + H]^+$ calcd for $C_{34}H_{33}FN_2O_6S$, 617.21; found, 617.4. Purity: >99%. $[\alpha]_D^{22}$ 17° (c 0.5, $CHCl_3$).

*Phenyl (S,E) 1 Fluoro 3 ((S) 2 (4 methylpiperazine 1 carboxamido) 3 phenylpropanamido) 5 phenylpent 1 ene 1 sulfonate (**2k**).* Synthesized by following procedure E with 0.11 g of compound **14**, 0.086 g compound **IX**, 0.095 g TBTU, and 0.155 mL DIEA. Column chromatography: DCM/MeOH 95:5. Yield: 0.096 g (59%), colorless solid. ^{1}H NMR (300 MHz, $CDCl_3$): δ 7.45 7.35 (m, 2H), 7.35 7.14 (m, 10H), 7.06 6.93 (m, 4H), 6.62 (d, J = 7.6 Hz, 1H), 5.62 (dd, $J_{H\ F}$ = 31.2 Hz, $J_{H\ H}$ = 9.1 Hz, 1H), 5.21 (d, J = 7.6 Hz, 1H), 4.66 (quint, J = 7.7 Hz, 1H), 4.45 (q, J = 7.9 Hz, 1H), 3.42 3.24 (m, 4H), 3.05 (dd, J = 13.4, 6.5 Hz, 1H), 2.88 (dd, J = 13.4, 8.4 Hz, 1H), 2.49 2.33 (m, 6H), 2.31 (s, 3H), 1.78 1.52 (m, 3H). ^{13}C NMR (75 MHz, $CDCl_3$): δ 171.8, 156.9, 149.4, 148.9 (d, $J_{C\ F}$ = 297 Hz), 140.2, 136.8, 130.2, 129.4, 128.9, 128.7, 128.4, 128.0, 127.3, 126.5, 122.4, 121.5 (d, $J_{C\ F}$ = 5.1 Hz), 56.1, 54.4, 45.9, 44.7, 43.6, 39.1, 35.4, 31.6. mp 109 110 °C. LC MS (ESI, m/z): $[M + H]^+$ calcd for $C_{32}H_{37}FN_4O_5S$, 608.26; found, 609.3. Purity: >99%. $[\alpha]_D^{22}$ 10° (c 0.5, $CHCl_3$).

*N ((S) 1 (((S,E) 1 (Benzylsulfonyl) 1 fluoro 5 phenylpent 1 en 3 yl)amino) 1 oxo 3 phenylpropan 2 yl)isonicotinamide (**3a**).* Synthesized by following procedure E with 0.11 g of compound **15**, 0.080 g compound **X**, 0.095 g TBTU, 0.045 g HOBt, and 0.155 mL DIEA. Column chromatography: pure EtOAc. Yield: 0.14 g (81%), colorless solid. ^{1}H NMR (300 MHz, DMSO-d_6): δ 8.97 (d, J = 7.9 Hz, 1H), 8.71 (d, J = 4.4 Hz, 2H), 8.35 (d, J = 7.8 Hz, 1H), 7.70 (d, J = 4.4 Hz, 2H), 7.44 7.08 (m, 15H), 5.81 (dd, $J_{H\ F}$ = 34.1 Hz, $J_{H\ H}$ = 8.8 Hz, 1H), 4.75 (s, 2H), 4.70 4.50 (m, 2H), 3.19 2.87 (m, 2H), 2.49 2.39 (m, 3H), 1.86 1.56 (m, 2H). ^{13}C NMR (75 MHz, DMSO): δ 170.4, 164.8, 151.4 (d, $J_{C\ F}$ = 298 Hz), 150.2, 140.9, 140.9, 137.9, 131.0, 129.1, 128.8, 128.6, 128.30, 128.29, 128.1, 127.5, 126.4, 125.9, 121.4, 120.4 (d, $J_{C\ F}$ = 3.8 Hz), 57.6, 55.0, 43.7 (d, $J_{C\ F}$ = 2.0 Hz), 37.0, 35.0, 30.9. mp 169 171 °C. LC MS (ESI, m/z): $[M + H]^+$ calcd for $C_{33}H_{32}FN_3O_4S$, 586.22; found, 586.4. Purity: 96%. $[\alpha]_D^{22}$ 9° (c 0.5, MeOH).

*N ((S) 1 (((S,E) 1 (Benzylsulfonyl) 1 fluoro 5 phenylpent 1 en 3 yl)amino) 1 oxo 3 phenylpropan 2 yl) 2,3 dihydrobenzo[b][1,4] dioxine 6 carboxamide (**3b**).* Synthesized by following procedure D with 0.100 g of compound **29**, 0.036 g 1,4-benzodioxane-6-carboxylic acid, 0.064 g TBTU, and 0.104 mL DIEA. Column chromatography: petroleum ether/EtOAc 2:1 to pure EtOAc. Yield: 0.096 g (75%), colorless solid. ^{1}H NMR (300 MHz, DMSO-d_6): δ 8.44 (d, J = 8.1 Hz, 1H), 8.24 (d, J = 8.0 Hz, 1H), 7.45 7.09 (m, 17H), 6.89 (d, J = 8.3 Hz, 1H), 5.82 (dd, $J_{H\ F}$ = 34.2 Hz, $J_{H\ H}$ = 9.0 Hz, 1H), 4.74 (s, 2H), 4.65 4.47 (m, 2H), 4.34 4.16 (m, 4H), 3.11 2.91 (m, 2H), 2.48 2.35 (m, 2H), 1.87 1.54 (m, 2H). ^{13}C NMR (75 MHz, DMSO-d_6): δ 171.0, 165.4, 151.3 (d, $J_{C\ F}$ = 297 Hz), 146.1, 142.8, 140.9, 138.2, 131.0, 129.1, 128.7, 128.6, 128.3, 128.1, 127.5, 127.0, 126.2, 125.9, 120.9, 120.5 (d, $J_{C\ F}$ = 3.9 Hz), 116.6, 116.5, 64.3, 64.0, 57.6, 55.0, 43.6 (d, $J_{C\ F}$ = 2.4 Hz), 36.9, 35.0, 30.9. mp 204 206 °C (decomposition). LC MS (ESI, m/z): $[M + H]^+$ calcd for $C_{36}H_{35}FN_3O_6S$, 643.23; found, 643.3. Purity: >99%. $[\alpha]_D^{22}$ 7° (c 0.5, $CHCl_3$/MeOH 1:1).

*N ((S) 1 (((S,E) 1 (Benzylsulfonyl) 1 fluoro 5 phenylpent 1 en 3 yl)amino) 1 oxo 3 phenylpropan 2 yl) 3,5 difluorobenzamide (**3c**).* Synthesized by following procedure D with 0.120 g of compound **29**, 0.037 g 3,5-difluorobenzoic acid, 0.075 g TBTU, and 0.12 mL DIEA. Column chromatography: petroleum ether/EtOAc 3:1. Yield: 0.094 g (65%), colorless solid. ^{1}H NMR (300 MHz, DMSO-d_6): δ 8.86 (d, J = 8.2 Hz, 1H), 8.35 (d, J = 7.9 Hz, 1H), 7.56 7.41 (m, 3H), 7.41 7.10 (m, 16H), 5.81 (dd, $J_{H\ F}$ = 34.2 Hz, $J_{H\ H}$ = 9.1 Hz, 1H), 4.75 (s, 2H), 4.69 4.51 (m, 2H), 3.09 (dd, J = 13.7, 5.1 Hz, 1H), 2.97 (dd, J = 13.7, 10.1 Hz, 1H), 2.49 2.40 (m, 2H), 1.86 1.57 (m, 2H). ^{13}C NMR (75 MHz, DMSO-d_6): δ 170.48, 163.7 (t, $J_{C\ F}$ = 2.8 Hz), 162.2 (dd, $J_{C\ F}$ = 251, 12 Hz), 151.4 (d, $J_{C\ F}$ = 298 Hz), 140.9, 137.9, 137.4 (t, $J_{C\ F}$ = 8.5 Hz), 137.3, 131.0, 129.1, 128.8, 128.6, 128.3, 128.1, 127.5, 126.4, 126.0, 120.4 (d, $J_{C\ F}$ = 4.1 Hz), 110.8 (dd, $J_{C\ F}$ = 27, 8.7 Hz), 106.9 (t, $J_{C\ F}$ = 26 Hz), 57.6, 55.2, 43.7 (d, $J_{C\ F}$ = 2.3 Hz), 37.0, 35.0, 30.9. mp 194 196 °C (decomposition). LC MS (ESI, m/z): $[M + H]^+$ calcd for $C_{34}H_{31}F_3N_2O_4S$, 621.2; found, 621.3. Purity: >99%. $[\alpha]_D^{22}$ 6° (c 0.5, $CHCl_3$).

*N ((S) 1 (((S,E) 1 (Benzylsulfonyl) 1 fluoro 5 phenylpent 1 en 3 yl)amino) 1 oxo 3 (p tolyl)propan 2 yl)isonicotinamide (**3d**).* Synthesized by following procedure D with 0.11 g of compound **35**, 0.026 g isonicotinic acid, 0.067 g TBTU, and 0.11 mL DIEA. Column chromatography: petroleum ether/EtOAc 1:3. Yield: 0.091 g (73%), colorless solid. ^{1}H NMR (300 MHz, $CDCl_3$): δ 8.69 (d, J = 6.0 Hz, 2H), 7.61 7.53 (m, 2H), 7.43 7.28 (m, 6H), 7.25 7.14 (m, 3H), 7.07 (d, J = 7.8 Hz, 2H), 7.01 6.88 (m, 4H), 6.19 (d, J = 7.9 Hz, 1H), 5.55 (dd, $J_{H\ F}$ = 32.6 Hz, $J_{H\ H}$ = 9.2 Hz, 1H), 4.76 4.59 (m, 2H), 4.36 (s, 2H), 3.14 (dd, J = 13.5, 6.0 Hz, 1H), 2.93 (dd, J = 13.4, 8.6 Hz, 1H), 2.44 2.19 (m, 5H), 1.75 1.50 (m, 2H). ^{13}C NMR (75 MHz, $CDCl_3$): δ 170.2, 165.1, 152.5 (d, $J_{C\ F}$ = 301 Hz), 141.3, 140.1, 137.3, 132.8, 131.0, 129.8, 129.5, 129.3, 129.2, 128.7, 128.3, 126.7, 126.5, 121.3, 119.4 (d, $J_{C\ F}$ = 4.3 Hz), 58.7, 55.6, 44.7 (d, $J_{C\ F}$ = 2.2 Hz), 38.4, 35.6 (d, $J_{C\ F}$ = 1.6 Hz), 31.6, 21.2. mp 181 183 °C. LC MS (ESI, m/z): $[M + H]^+$ calcd for $C_{34}H_{34}FN_3O_4S$, 600.24; found, 600.4. Purity: 95%. $[\alpha]_D^{22}$ 13° (c 0.5, MeOH).

*N ((S) 1 (((S,E) 1 (Benzylsulfonyl) 1 fluoro 5 phenylpent 1 en 3 yl)amino) 1 oxo 3 (p tolyl)propan 2 yl) 2,3 dihydrobenzo[b][1,4] dioxine 6 carboxamide (**3e**).* Synthesized by following procedure D with 0.110 g of compound **35**, 0.037 g 1,4-benzodioxane-6-carboxylic acid, 0.067 g TBTU, and 0.108 mL DIEA. Column chromatography: petroleum ether/EtOAc 1:1 to 0:1. Yield: 0.10 g (76%), colorless solid. ^{1}H NMR (300 MHz, DMSO-d_6): δ 8.41 (d, J = 8.0 Hz, 1H), 8.23 (d, J = 8.0 Hz, 1H), 7.43 7.23 (m, 9H), 7.23 7.11 (m, 5H), 7.04 (d, J = 7.9 Hz, 2H), 6.89 (d, J = 8.4 Hz, 1H), 5.81 (dd, $J_{H\ F}$ = 34.3 Hz, $J_{H\ H}$ = 9.1 Hz, 1H), 4.74 (s, 2H), 4.63 4.47 (m, 2H), 4.32 4.18 (m, 4H), 3.05 2.87 (m, 2H), 2.49 2.39 (m, 2H), 2.22 (s, 3H), 1.86 1.57 (m, 2H). ^{13}C NMR (75 MHz, DMSO-d_6): δ 171.0, 165.4, 151.3 (d, $J_{C\ F}$ = 297 Hz), 146.0, 142.8, 140.9, 135.14, 135.10, 131.0, 129.0, 128.8, 128.7, 128.6, 128.3, 127.5, 127.0, 125.9, 121.0, 120.5 (d, $J_{C\ F}$ = 3.7 Hz), 116.6, 116.5, 64.3, 64.0, 57.6, 55.1, 43.6 (d, $J_{C\ F}$ = 1.6 Hz), 36.6, 35.0, 30.9, 20.6. mp 193 195 °C. LC MS (ESI, m/z): $[M + H]^+$ calcd for $C_{37}H_37FN_2O_6S$, 657.25; found, 657.4. Purity: 97%. $[\alpha]_D^{22}$ 8° (c 0.5, $CHCl_3$/MeOH 1:1).

*N ((S) 1 (((S,E) 1 (Benzylsulfonyl) 1 fluoro 5 phenylpent 1 en 3 yl)amino) 1 oxo 3 (p tolyl)propan 2 yl) 3,5 difluorobenzamide (**3f**).* Synthesized by following procedure D with 0.12 g of compound **35**, 0.036 g 3,5-difluorobenzoic acid, 0.073 g TBTU, and 0.12 mL DIEA. Column chromatography: petroleum ether/EtOAc 3:1 to pure EtOAc. Yield: 0.12 g (81%), colorless solid. ^{1}H NMR (300 MHz, DMSO-d_6): δ 8.82 (d, J = 8.1 Hz, 1H), 8.32 (d, J = 8.0 Hz, 1H), 7.61 7.40 (m, 3H), 7.40 7.23 (m, 8H), 7.23 7.10 (m, 5H), 7.05 (d, J = 7.9

https://doi.org/10.1021/acs.jmedchem.1c01002
J. Med. Chem. 2021, 64, 12322 12358

Hz, 2H), 5.79 (dd, $J_{H\ F}$ = 33.9 Hz, $J_{H\ H}$ = 9.3 Hz, 1H), 4.75 (s, 2H), 4.65 4.48 (m, 2H), 3.02 (dd, J = 13.5, 5.1 Hz, 1H), 2.92 (dd, J = 13.6, 10.0 Hz, 1H), 2.48 2.39 (m, 1H), 2.22 (s, 3H), 1.83 1.56 (m, 2H). ^{13}C NMR (75 MHz, DMSO-d_6): δ 170.5, 163.86, 163.7 (t, $J_{C\ F}$ = 2.6 Hz), 162.1 (dd, $J_{C\ F}$ = 251, 12 Hz), 151.3 (d, $J_{C\ F}$ = 298 Hz), 140.9, 137.4 (t, $J_{C\ F}$ = 8.4 Hz), 135.3, 134.8, 131.0, 129.0, 128.7, 128.6, 128.3, 127.5, 126.0, 120.4 (d, $J_{C\ F}$ = 4.0 Hz), 110.8 (dd, $J_{C\ F}$ = 26, 8.4 Hz), 106.9 (t, $J_{C\ F}$ = 25 Hz), 57.6, 55.3, 43.7 (d, $J_{C\ F}$ = 1.5 Hz), 36.6, 35.0, 30.9, 20.6. mp 196 198 °C (decomposition). LC MS (ESI, m/z): [M + H]$^+$ calcd for $C_{35}H_{33}F_3N_2O_4S$, 635.22; found, 635.3. Purity: 95%. $[\alpha]_D^{22}$ 9° (c 0.5, MeOH/$CHCl_3$ 1:1).

*Phenyl (S,E) 1 Fluoro 3 ((S) 2 (isonicotinamido) 3 (m tolyl) propanamido) 5 phenylpent 1 ene 1 sulfonate (**3g**).* Synthesized by following procedure D with 0.11 g of compound **32**, 0.026 g isonicotinic acid, 0.067 g TBTU, and 0.11 mL DIEA. Column chromatography: petroleum ether/EtOAc 1:3. Yield: 0.086 g (69%), colorless solid. ^{1}H NMR (300 MHz, $CDCl_3$): δ 8.68 (d, J = 4.7 Hz, 2H), 7.56 (d, J = 5.7 Hz, 2H), 7.40 (d, J = 7.6 Hz, 1H), 7.37 7.28 (m, 5H), 7.25 7.11 (m, 4H), 7.04 (d, J = 7.6 Hz, 1H), 6.99 6.90 (m, 3H), 6.84 (d, J = 7.5 Hz, 1H), 6.24 (d, J = 7.8 Hz, 1H), 5.57 (dd, $J_{H\ F}$ = 32.5 Hz, $J_{H\ H}$ = 9.1 Hz, 1H), 4.78 4.58 (m, 2H), 4.36 (s, 2H), 3.15 (dd, J = 13.4, 6.2 Hz, 1H), 2.93 (dd, J = 13.4, 8.5 Hz, 1H), 2.43 2.26 (m, 2H), 2.24 (s, 3H), 1.74 1.48 (m, 2H). ^{13}C NMR (75 MHz, $CDCl_3$): δ 170.2, 165.2, 152.5 (d, $J_{C\ F}$ = 301 Hz), 150.3, 141.2, 140.1, 138.8, 136.0, 131.0, 130.0, 129.5, 129.2, 129.0, 128.7, 128.4, 128.3, 126.7, 126.5, 126.5, 121.2, 119.4 (d, $J_{C\ F}$ = 4.1 Hz), 58.7, 55.5, 44.8 (d, $J_{C\ F}$ = 2.3 Hz), 38.7, 35.6, 35.7, 31.6, 21.4. mp 81 82 °C. LC MS (ESI, m/z): [M + H]$^+$ calcd for $C_{34}H_{34}FN_3O_4S$, 600.24; found, 600.4. Purity: 95%. $[\alpha]_D^{22}$ 7° (c 0.5, MeOH).

*N ((S) 1 (((S,E) 1 (Benzylsulfonyl) 1 fluoro 5 phenylpent 1 en 3 yl)amino) 1 oxo 3 (m tolyl)propan 2 yl) 2,3 dihydrobenzo[b][1,4] dioxine 6 carboxamide (**3h**).* Synthesized by following procedure D with 0.11 g of compound **32**, 0.037 g 1,4-benzodioxane-6-carboxylic acid, 0.067 g TBTU and 0.11 mL DIEA. Column chromatography: petroleum ether/EtOAc 2:1 to 0:1. Yield: 0.094 g (69%), colorless solid. ^{1}H NMR (300 MHz, DMSO-d_6): δ 8.43 (d, J = 8.1 Hz, 1H), 8.25 (d, J = 8.0 Hz, 1H), 7.46 7.23 (m, 9H), 7.23 7.03 (m, 6H), 6.97 (d, J = 7.2 Hz, 1H), 6.90 (d, J = 8.3 Hz, 1H), 5.83 (dd, $J_{H\ F}$ = 34.2 Hz, $J_{H\ H}$ = 9.0 Hz, 1H), 4.74 (s, 2H), 4.64 4.49 (m, 2H), 4.39 4.17 (m, 4H), 3.08 2.86 (m, 2H), 2.49 2.38 (m, 2H), 2.23 (s, 3H), 1.87 1.55 (m, 2H). ^{13}C NMR (75 MHz, DMSO-d_6): δ 171.0, 165.5, 151.3 (d, $J_{C\ F}$ = 298 Hz), 146.1, 142.8, 140.9, 138.2, 137.0, 131.0, 129.8, 128.7, 128.6, 128.3, 127.9, 127.5, 127.1, 126.9, 126.2, 125.9, 120.9, 120.5 (d, $J_{C\ F}$ = 4.2 Hz), 116.6, 116.5, 64.3, 64.0, 57.6, 55.0, 43.6 (d, $J_{C\ F}$ = 0.9 Hz), 36.9, 35.1, 30.9, 21.0. mp 188 190 °C. LC MS (ESI, m/z): [M + H]$^+$ calcd for $C_{37}H_{37}FN_2O_6S$, 657.25; found, 657.4. Purity >99%. $[\alpha]_D^{22}$ 11° (c 0.5, $CHCl_3$).

*N ((S) 1 (((S,E) 1 (Benzylsulfonyl) 1 fluoro 5 phenylpent 1 en 3 yl)amino) 1 oxo 3 (m tolyl)propan 2 yl) 3,5 difluorobenzamide (**3i**).* Synthesized by following procedure D with 0.12 g of compound **32**, 0.036 g 3,5-difluorobenzoic acid, 0.073 g TBTU, and 0.12 mL DIEA. Column chromatography: petroleum ether/EtOAc 2:1. Yield: 0.11 g (77%), colorless solid. ^{1}H NMR (300 MHz, DMSO-d_6): δ 8.83 (d, J = 8.1 Hz, 1H), 8.33 (d, J = 7.8 Hz, 1H), 7.61 7.02 (m, 17H), 6.98 (d, J = 7.1 Hz, 1H), 5.81 (dd, $J_{H\ F}$ = 34.1 Hz, $J_{H\ H}$ = 9.0 Hz, 1H), 4.74 (s, 2H), 4.67 4.46 (m, 2H), 3.04 (dd, J = 13.5, 4.7 Hz, 1H), 2.93 (dd, J = 13.5, 4.7 Hz, 1H), 2.48 2.39 (m, 2H), 2.23 (s, 3H), 1.83 1.59 (m, 2H). ^{13}C NMR (75 MHz, DMSO-d_6): δ 170.5, 163.8 (t, $J_{C\ F}$ = 2.7 Hz), 162.1 (dd, $J_{C\ F}$ = 247 Hz, 13 Hz), 151.3 (d, $J_{C\ F}$ = 298 Hz), 140.9, 137.9, 137.5 (t, $J_{C\ F}$ = 8.5 Hz), 137.1, 131.0, 129.8, 128.8, 128.6, 128.3, 128.0, 127.5, 127.0, 126.2, 126.0, 120.42 (d, $J_{C\ F}$ = 3.5 Hz), 110.8 (dd, $J_{C\ F}$ = 25 Hz, 8.6 Hz), 106.8 (t, $J_{C\ F}$ = 26 Hz), 57.6, 55.2, 43.7 (d, $J_{C\ F}$ = 2.0 Hz), 36.9, 35.0, 30.9, 21.0. mp 176 178 °C. LC MS (ESI, m/z): [M + H]$^+$ calcd for $C_{35}H_{33}F_3N_2O_4S$, 635.22; found, 635.3. Purity >99%. $[\alpha]_D^{22}$ 6° (c 0.5, $CHCl_3$).

*N ((S) 1 (((S,E) 1 Fluoro 5 phenyl 1 (phenylsulfonyl)pent 1 en 3 yl)amino) 1 oxo 3 phenylpropan 2 yl)isonicotinamide (**4a**).*[11] Synthesized by following procedure E with 0.14 g of compound **13**, 0.107 g compound **X**, 0.13 g TBTU, 0.062 g HOBt, and 0.21 mL DIEA. Column chromatography: DCM/MeOH 19:1. Yield: 0.17 g (75%), colorless solid. ^{1}H NMR (300 MHz, $CDCl_3$): δ 8.71 (br, 2H), 7.95 (d, J = 7.5 Hz, 2H), 7.76 7.54 (m, 5H), 7.50 (d, J = 7.4 Hz, 1H), 7.40 7.08 (m, 8H), 6.99 (d, J = 6.4 Hz, 2H), 6.40 (d, J = 7.7 Hz, 1H), 6.03 (dd, $J_{H\ F}$ = 31.9 Hz, $J_{H\ H}$ = 8.8 Hz, 1H), 4.87 4.60 (m, 2H), 3.21 (dd, J = 13.5, 6.3 Hz, 1H), 3.08 (dd, J = 13.5, 8.2 Hz, 1H), 2.49 (t, J = 7.4 Hz, 2H), 1.96 1.68 (m, 2H). ^{13}C NMR (75 MHz, $CDCl_3$): δ 170.3, 164.9, 155.1 (d, $J_{C\ F}$ = 301 Hz), 149.4, 142.1, 140.2, 137.1, 136.2, 134.9, 129.7, 129.4, 129.1, 128.8, 128.7, 128.3, 127.7, 126.50, 121.7, 117.0 (d, $J_{C\ F}$ = 5.3 Hz), 55.6, 45.1, 38.8, 35.7 (d, $J_{C\ F}$ = 1.9 Hz), 31.8. mp 184 187 °C. LC MS (ESI, m/z): [M + H]$^+$ calcd for $C_{32}H_{30}FN_3O_4S$, 572.20; found, 572.4. Purity: 95%. $[\alpha]_D^{22}$ 11° (c 0.5, $CHCl_3$).

*N ((S) 1 (((S,E) 1 Fluoro 5 phenyl 1 (phenylsulfonyl)pent 1 en 3 yl)amino) 1 oxo 3 phenylpropan 2 yl) 2,3 dihydrobenzo[b][1,4] dioxine 6 carboxamide (**4b**).* Synthesized by following procedure D with 0.100 g of compound **27**, 0.036 g 1,4-benzodioxane-6-carboxylic acid, 0.064 g TBTU, and 0.104 mL DIEA. Column chromatography: petroleum ether/EtOAc 1:1. Yield: 0.084 g (67%), colorless solid. ^{1}H NMR (300 MHz, DMSO-d_6): δ 8.43 (d, J = 8.0 Hz, 1H), 8.35 (d, J = 7.8 Hz, 1H), 7.94 (dt, J = 7.3, 1.7 Hz, 2H), 7.85 (tt, J = 7.3, 1.2 Hz, 1H), 7.73 (tt, J = 6.7, 1.1 Hz, 2H), 7.43 7.06 (m, 12H), 6.89 (d, J = 8.3 Hz, 1H), 6.30 (dd, $J_{H\ F}$ = 34.0 Hz, $J_{H\ H}$ = 8.9 Hz, 1H), 4.68 4.47 (m, 2H), 4.33 4.18 (m, 4H), 3.10 2.90 (m, 2H), 2.59 2.50 (m, 2H), 1.96 1.73 (m, 2H). ^{13}C NMR (75 MHz, DMSO-d_6): δ 171.0, 165.4, 153.0 (d, $J_{C\ F}$ = 296 Hz), 146.1, 142.8, 140.8, 138.2, 136.6, 135.2, 130.1, 129.1, 128.27, 128.26, 128.1, 128.0, 127.0, 126.3, 125.9, 120.9, 119.2 (d, $J_{C\ F}$ = 4.8 Hz), 116.6, 116.5, 64.3, 64.0, 54.9, 43.8 (d, $J_{C\ F}$ = 1.6 Hz), 36.9, 35.0 (d, $J_{C\ F}$ = 2.3 Hz), 31.0. mp 187 189 °C. LC MS (ESI, m/z): [M + H]$^+$ calcd for $C_{35}H_{33}FN_2O_6S$, 629.2; found, 629.3. Purity >99%. $[\alpha]_D^{22}$ 3° (c 0.5, $CHCl_3$).

*3,5 Difluoro N ((S) 1 (((S,E) 1 fluoro 5 phenyl 1 (phenylsulfonyl)pent 1 en 3 yl)amino) 1 oxo 3 phenylpropan 2 yl)benzamide (**4c**).* Synthesized by following procedure D with 0.124 g of compound **27**, 0.039 g 3,5-difluorobenzoic acid, 0.079 g TBTU, and 0.125 mL DIEA. Column chromatography: petroleum ether/EtOAc 2:1. Yield: 0.12 g (81%), colorless solid. ^{1}H NMR (300 MHz, $CDCl_3$): δ 7.99 7.90 (m, 2H), 7.73 7.63 (m, 1H), 7.57 (t, J = 7.6 Hz, 2H), 7.37 7.09 (m, 12H), 7.00 6.91 (m, 2H), 6.87 (tt, J = 8.5, 2.3 Hz, 1H), 6.37 (d, J = 7.7 Hz, 1H), 5.96 (dd, $J_{H\ F}$ = 31.8 Hz, $J_{H\ H}$ = 8.9 Hz, 1H), 4.82 4.61 (m, 2H), 3.14 (dd, J = 13.5, 6.4 Hz, 1H), 3.03 (dd, J = 13.5, 8.2 Hz, 1H), 2.45 (t, J = 7.7 Hz, 2H), 1.88 1.72 (m, 2H). ^{13}C NMR (75 MHz, $CDCl_3$): δ 170.6, 165.0 (t, $J_{C\ F}$ = 2.8 Hz), 163.0 (dd, $J_{C\ F}$ = 251, 12 Hz), 155.2 (d, $J_{C\ F}$ = 301 Hz), 140.2, 137.1, 136.8 (t, $J_{C\ F}$ = 8.3 Hz), 136.2, 134.8, 129.7, 129.4, 129.1, 128.8, 128.7, 128.3, 127.6, 126.5, 116.9 (d, $J_{C\ F}$ = 5.1 Hz), 110.5 (dd, $J_{C\ F}$ = 27, 8.7 Hz), 107.4 (t, $J_{C\ F}$ = 25 Hz), 55.7, 45.1 (d, $J_{C\ F}$ = 1.5 Hz), 38.7, 35.7, 31.8. mp 90 92 °C. LC MS (ESI, m/z): [M + H]$^+$ calcd for $C_{33}H_{29}F_3N_2O_4S$, 607.2; found, 607.3. Purity: 95%. $[\alpha]_D^{22}$ 5° (c 0.5, MeOH).

*N ((S) 1 (((S,E) 1 Fluoro 5 phenyl 1 (phenylsulfonyl)pent 1 en 3 yl)amino) 1 oxo 3 (p tolyl)propan 2 yl)isonicotinamide (**4d**).* Synthesized by following procedure D with 0.10 g of compound **33**, 0.024 g isonicotinic acid, 0.063 g TBTU, and 0.10 mL DIEA. Column chromatography: pure EtOAc. Yield: 0.094 g (83%), colorless solid. ^{1}H NMR (300 MHz, $CDCl_3$): δ 8.69 (d, J = 3.8 Hz, 2H), 7.95 (d, J = 7.7 Hz, 2H), 7.70 (t, J = 7.3 Hz, 1H), 7.65 7.46 (m, 4H), 7.30 7.23 (m, 1H), 7.23 7.01 (m, 7H), 6.96 (d, J = 6.8 Hz, 2H), 6.32 (d, J = 7.8 Hz, 1H), 6.01 (dd, $J_{H\ F}$ = 31.9 Hz, $J_{H\ H}$ = 8.8 Hz, 1H), 4.84 4.60 (m, 2H), 3.15 (dd, J = 13.6, 5.7 Hz, 1H), 3.01 (dd, J = 13.4, 8.2 Hz, 1H), 2.46 (t, J = 7.6 Hz, 2H), 2.32 (s, 3H), 1.90 1.73 (m, 2H). ^{13}C NMR (75 MHz, $CDCl_3$): δ 170.3, 165.4, 155.12 (d, $J_{C\ F}$ = 301 Hz), 150.7, 140.8, 140.1, 137.4, 137.1, 134.8, 132.9, 129.8, 129.7, 129.3, 128.8, 128.7, 128.3, 126.5, 121.0, 116.9 (d, $J_{C\ F}$ = 4.8 Hz), 55.4, 45.0 (d, $J_{C\ F}$ = 1.7 Hz), 38.4, 35.8, 31.8, 21.2. mp 84 86 °C. LC MS (ESI, m/z): [M + H]$^+$ calcd for $C_{33}H_{32}FN_3O_4S$, 586.22; found, 586.4. Purity: 96%. $[\alpha]_D^{22}$ 12° (c 0.5, MeOH).

*N ((S) 1 (((S,E) 1 Fluoro 5 phenyl 1 (phenylsulfonyl)pent 1 en 3 yl)amino) 1 oxo 3 (p tolyl)propan 2 yl) 2,3 dihydrobenzo[b] [1,4]dioxine 6 carboxamide (**4e**).* Synthesized by following procedure D with 0.065 g of compound **33**, 0.023 g 1,4-benzodioxane-6-carboxylic acid, 0.041 g TBTU, and 0.066 mL DIEA. Column chromatography: petroleum ether/EtOAc 2:1 to 1:1. Yield: 0.057 g (70%), colorless

https://doi.org/10.1021/acs.jmedchem.1c01002
J. Med. Chem. 2021, 64, 12322 12358

solid. ^{1}H NMR (300 MHz, $CDCl_3$): δ 8.00 7.90 (m, 2H), 7.75 7.65 (m, 1H), 7.64 7.53 (m, 2H), 7.26 (s, 1H), 7.23 7.03 (m, 8H), 6.93 (dd, J = 7.8, 1.5 Hz, 2H), 6.85 (d, J = 8.4 Hz, 1H), 6.79 (d, J = 7.7 Hz, 1H), 6.70 (d, J = 7.9 Hz, 1H), 6.02 (dd, $J_{H\ F}$ = 32.0 Hz, $J_{H\ H}$ = 8.7 Hz, 1H), 4.83 (q, J = 7.5 Hz, 1H), 4.68 (quint, J = 7.7 Hz, 1H), 4.34 4.21 (m, 4H), 3.13 (dd, J = 13.6, 6.3 Hz, 1H), 3.02 (dd, J = 13.6, 7.8 Hz, 1H), 2.54 2.38 (m, 2H), 2.31 (s, 3H), 1.87 1.69 (m, 2H). ^{13}C NMR (75 MHz, $CDCl_3$): δ 170.8, 166.8, 154.8 (d, $J_{C\ F}$ = 300 Hz), 147.0, 143.6, 140.3, 137.3, 137.0, 134.7, 133.3, 129.7, 129.6, 129.3, 128.8, 128.6, 128.4, 126.9, 126.3, 120.6, 117.62 (d, $J_{C\ F}$ = 5.1 Hz), 117.5, 116.8, 64.7, 64.3, 55.1, 44.9 (d, $J_{C\ F}$ = 1.7 Hz), 38.3, 35.7, 31.8, 21.2. mp 95 97 °C. LC MS (ESI, m/z): $[M + H]^+$ calcd for $C_{36}H_{35}FN_2O_6S$, 643.23; found, 643.3. Purity: 96%. $[\alpha]_D^{22}$ 13° (c 1, $CHCl_3$).

3,5 Difluoro N ((S) 1 (((S,E) 1 fluoro 5 phenyl 1 (phenylsulfonyl)pent 1 en 3 yl)amino) 1 oxo 3 (p tolyl)propan 2 yl)benzamide (4f). Synthesized by following procedure D with 0.065 g of compound **33**, 0.020 g 3,5-difluorobenzoic acid, 0.041 g TBTU, and 0.066 mL DIEA. Column chromatography: petroleum ether/EtOAc 3:1. Yield: 0.059 g (73%), colorless solid. ^{1}H NMR (300 MHz, $CDCl_3$): δ 8.00 7.91 (m, 2H), 7.74 7.63 (m, 1H), 7.62 7.53 (m, 2H), 7.31 (d, J = 7.6 Hz, 1H), 7.25 7.09 (m, 7H), 7.05 (d, J = 8.0 Hz, 2H), 6.97 6.82 (m, 3H), 6.39 (d, J = 7.7 Hz, 1H), 5.98 (dd, $J_{H\ F}$ = 31.9 Hz, $J_{H\ H}$ = 8.8 Hz, 1H), 4.83 4.60 (m, 2H), 3.11 (dd, J = 13.5, 6.3 Hz, 1H), 2.99 (dd, J = 13.5, 8.2 Hz, 1H), 2.52 2.40 (m, 2H), 2.31 (s, 3H), 1.90 1.74 (m, 2H). ^{13}C NMR (75 MHz, $CDCl_3$): δ 170.7, 164.95 (t, $J_{C\ F}$ = 2.9 Hz), 163.02 (dd, $J_{C\ F}$ = 251, 12 Hz), 155.12 (d, $J_{C\ F}$ = 301 Hz), 140.2, 137.3, 137.2, 136.9 (t, $J_{C\ F}$ = 8.3 Hz), 134.8, 133.0, 129.8, 129.7, 129.3, 128.8, 128.7, 128.3, 126.5, 117.05 (d, $J_{C\ F}$ = 4.8 Hz), 110.50 (dd, $J_{C\ F}$ = 27, 9.4 Hz), 107.37 (t, $J_{C\ F}$ = 25 Hz), 55.6, 45.1 (d, $J_{C\ F}$ = 1.6 Hz), 38.3, 35.7 (d, $J_{C\ F}$ = 1.5 Hz), 31.8, 21.2. mp 174 176 °C. LC MS (ESI, m/z): $[M + H]^+$ calcd for $C_{34}H_{31}F_3N_2O_4S$, 621.21; found, 621.3. Purity: 95%. $[\alpha]_D^{22}$ 9° (c 0.5, MeOH).

N ((S) 1 (((S,E) 1 Fluoro 5 phenyl 1 (phenylsulfonyl)pent 1 en 3 yl)amino) 1 oxo 3 (m tolyl)propan 2 yl)isonicotinamide (4g). Synthesized by following procedure D with 0.10 g of compound **30**, 0.024 g isonicotinic acid, 0.063 g TBTU, and 0.10 mL DIEA. Column chromatography: pure EtOAc. Yield: 0.071 g (63%), colorless solid. ^{1}H NMR (300 MHz, $CDCl_3$): δ 8.69 (d, J = 5.2 Hz, 2H), 7.94 (d, J = 7.5 Hz, 2H), 7.74 7.65 (m, 1H), 7.63 7.48 (m, 4H), 7.34 7.11 (m, 6H), 7.11 6.88 (m, 5H), 6.31 (d, J = 7.8 Hz, 1H), 6.01 (dd, $J_{H\ F}$ = 31.9 Hz, $J_{H\ H}$ = 8.8 Hz, 1H), 4.84 4.59 (m, 2H), 3.16 (dd, J = 13.5, 6.2 Hz, 1H), 3.00 (dd, J = 13.5, 8.4 Hz, 1H), 2.45 (t, J = 7.5 Hz, 2H), 2.29 (s, 3H), 1.89 1.73 (m, 2H). ^{13}C NMR (75 MHz, $CDCl_3$): δ 170.3, 165.4, 155.10 (d, $J_{C\ F}$ = 301 Hz), 150.6, 140.9, 140.1, 138.8, 137.0, 136.0, 134.7, 130.1, 129.7, 129.0, 128.8, 128.7, 128.4, 128.3, 126.5, 126.4, 121.1, 116.9 (d, $J_{C\ F}$ = 5.2 Hz), 55.4, 45.1 (d, $J_{C\ F}$ = 1.9 Hz), 38.7, 35.8 (d, $J_{C\ F}$ = 1.4 Hz), 31.8, 21.5. mp 182 184 °C. LC MS (ESI, m/z): $[M + H]^+$ calcd for $C_{33}H_{32}FN_3O_4S$, 586.22; found, 586.4. Purity: 95%. $[\alpha]_D^{22}$ 3° (c 0.5, $CHCl_3$).

N ((S) 1 (((S,E) 1 Fluoro 5 phenyl 1 (phenylsulfonyl)pent 1 en 3 yl)amino) 1 oxo 3 (m tolyl)propan 2 yl) 2,3 dihydrobenzo[b] [1,4]dioxine 6 carboxamide (4h). Synthesized by following procedure D with 0.10 g of compound **30**, 0.035 g 1,4-benzodioxane-6-carboxylic acid, 0.063 g TBTU, and 0.10 mL DIEA. Column chromatography: petroleum ether/EtOAc 1:1. Yield: 0.10 g (84%), colorless solid. ^{1}H NMR (300 MHz, DMSO-d_6): δ 8.44 (d, J = 8.1 Hz, 1H), 8.38 (d, J = 7.8 Hz, 1H), 7.94 (dt, J = 7.3, 1.5 Hz, 2H), 7.89 7.80 (m, 1H), 7.80 7.68 (m, 2H), 7.42 7.30 (m, 2H), 7.29 7.02 (m, 8H), 6.98 (d, J = 6.9 Hz, 1H), 6.90 (d, J = 8.3 Hz, 1H), 6.31 (dd, $J_{H\ F}$ = 34.0 Hz, $J_{H\ H}$ = 8.9 Hz, 1H), 4.65 4.46 (m, 2H), 4.27 (d, J = 5.4 Hz, 4H), 3.08 2.84 (m, 2H), 2.61 2.50 (m, 2H), 2.25 (s, 3H), 1.96 1.72 (m, 2H). ^{13}C NMR (75 MHz, DMSO-d_6): δ 171.1, 165.5, 152.9 (d, $J_{C\ F}$ = 295 Hz), 146.1, 142.8, 140.8, 138.1, 137.0, 136.6, 135.2, 130.1, 129.8, 128.3, 128.3, 128.2, 127.9, 127.0, 126.9, 126.2, 125.9, 121.0, 119.3 (d, $J_{C\ F}$ = 4.3 Hz), 116.6, 116.5, 64.3, 64.0, 55.0, 43.8 (d, $J_{C\ F}$ = 1.5 Hz), 36.8, 35.4, 31.0, 21.0. mp 186 188 °C. LC MS (ESI, m/z): $[M + H]^+$ calcd for $C_{36}H_{35}FN_2O_6S$, 643.23; found, 643.3. Purity: >99%. $[\alpha]_D^{22}$ 11° (c 1, $CHCl_3$).

3,5 Difluoro N ((S) 1 (((S,E) 1 fluoro 5 phenyl 1 (phenylsulfonyl)pent 1 en 3 yl)amino) 1 oxo 3 (m tolyl)propan 2 yl)benzamide (4i). Synthesized by following procedure D with 0.10 g of compound **30**, 0.031 g 3,5-difluorobenzoic acid, 0.063 g TBTU, and 0.10 mL DIEA. Column chromatography: petroleum ether/EtOAc 2:1. Yield: 0.075 g (62%), colorless solid. ^{1}H NMR (300 MHz, $CDCl_3$): δ 7.95 (d, J = 7.5 Hz, 2H), 7.72 7.64 (m, 1H), 7.57 (t, J = 7.6 Hz, 2H), 7.29 7.23 (m, 1H), 7.25 6.81 (m, 13H), 6.38 (d, J = 7.7 Hz, 1H), 6.01 (dd, $J_{H\ F}$ = 31.8 Hz, $J_{H\ H}$ = 8.8 Hz, 1H), 4.81 4.60 (m, 2H), 3.12 (dd, J = 13.5, 6.5 Hz, 1H), 2.98 (dd, J = 13.5, 8.1 Hz, 1H), 2.45 (t, J = 7.7 Hz, 2H), 2.28 (s, 3H), 1.88 1.74 (m, 2H). ^{13}C NMR (75 MHz, $CDCl_3$): δ 170.6, 165.02 (t, $J_{C\ F}$ = 2.4 Hz), 162.99 (dd, $J_{C\ F}$ = 251, 12 Hz), 155.14 (d, $J_{C\ F}$ = 301 Hz), 140.2, 138.8, 137.1, 136.8 (t, $J_{C\ F}$ = 8.4 Hz), 136.2, 134.8, 130.1, 129.7, 129.0, 128.8, 128.7, 128.4, 128.3, 126.5, 117.0 (d, $J_{C\ F}$ = 4.9 Hz), 110.5 (dd, $J_{C\ F}$ = 26, 8.7 Hz), 107.4 (t, $J_{C\ F}$ = 25 Hz), 55.6, 45.2 (d, $J_{C\ F}$ = 1.6 Hz), 38.5, 35.7, 31.8, 21.4. mp 176 178 °C. LC MS (ESI, m/z): $[M + H]^+$ calcd for $C_{34}H_{31}F3N_2O_4S$, 621.21; found, 621.3. Purity >99%. $[\alpha]_D^{22}$ 5° (c 0.5, MeOH/$CHCl_3$ 1:1).

N ((S) 1 (((S,E) 1 Fluoro 5 (methylthio) 1 (phenylsulfonyl)pent 1 en 3 yl)amino) 1 oxo 3 phenylpropan 2 yl) 4 methylpiperazine 1 carboxamide (4j). Synthesized by following procedure E with 0.11 g of compound **16**, 0.089 g compound **IX**, 0.088 g TBTU, 0.042 g HOBt, and 0.14 mL DIEA. Column chromatography: DCM/MeOH 19:1. Yield: 0.11 g (73%), colorless solid. (300 MHz, CD_2Cl_2): δ 7.85 (dd, J = 7.3, 1.7 Hz, 2H), 7.71 7.59 (m, 1H), 7.59 7.47 (m, 2H), 7.25 7.13 (m, 3H), 7.12 7.01 (m, 3H), 5.99 (dd, $J_{H\ F}$ = 32.4 Hz, $J_{H\ H}$ = 8.8 Hz, 1H), 5.06 (d, J = 7.7 Hz, 1H), 4.76 4.59 (m, 1H), 4.41 (q, J = 7.2 Hz, 1H), 3.21 (q, J = 4.5 Hz, 4H), 3.02 2.79 (m, 2H), 2.31 2.25 (m, 2H), 2.22 (t, J = 5.1 Hz, 4H), 2.16 (s, 3H), 1.90 (s, 3H), 1.82 1.60 (m, 2H). (75 MHz, CD2Cl2): δ 172.3, 157.5, 155.0 (d, $J_{C\ F}$ = 298 Hz), 137.6, 137.2, 135.2, 130.1, 129.9, 129.1, 127.4, 118.2 (d, $J_{C\ F}$ = 4.9 Hz), 56.3, 55.1, 54.0, 46.4, 44.7 (d, $J_{C\ F}$ = 1.8 Hz), 44.3, 39.0, 33.8, 30.4, 15.7. mp 110 112 °C. HR-MS (ESI, m/z): $[M + Na]^+$ calcd for $C_{27}H_{35}FN_4O_4S_2$, 585.1981; found, 585.1973. $[\alpha]_D^{22}$ 12° (c 1, $CHCl_3$).

N ((S) 1 (((S,E) 1 Fluoro 5 (methylthio) 1 (phenylsulfonyl)pent 1 en 3 yl)amino) 1 oxo 3 phenylpropan 2 yl)isonicotinamide (4k). Synthesized by following procedure E with 0.11 g of compound **16**, 0.074 g compound **X**, 0.088 g TBTU, 0.042 g HOBt, and 0.14 mL DIEA. Column chromatography: DCM/MeOH 95:5. Yield: 0.098 g (66%), colorless solid. (300 MHz, CD_2Cl_2): δ 8.70 (d, J = 4.5 Hz, 2H), 7.94 (d, J = 7.5 Hz, 2H), 7.76 7.53 (m, 5H), 7.44 7.15 (m, 9H), 7.07 (d, J = 7.3 Hz, 1H), 6.26 (d, J = 7.8 Hz, 1H), 6.04 (dd, $J_{H\ F}$ = 32.2 Hz, $J_{H\ H}$ = 8.8 Hz, 1H), 4.92 4.55 (m, 2H), 3.23 3.00 (m, 2H), 2.44 2.24 (m, 2H), 2.05 1.91 (m, 3H), 1.88 1.74 (m, 2H). (75 MHz, CD2Cl2): δ 170.0, 165.2, 151.4, 150.6, 140.7, 139.4, 137.0, 136.2, 134.8, 129.6, 129.3, 128.9, 128.6, 127.3, 120.8, 55.1, 45.3, 38.3, 29.8, 15.2. mp 64 66 °C. HR-MS (ESI, m/z): $[M + Na]^+$ calcd for $C_{27}H_{28}FN_3O_4S_2$, 564.1403; found, 564.1411. $[\alpha]_D^{22}$ 21° (c 1, $CHCl_3$).

N ((S) 1 (((R,E) 1 (Benzylthio) 4 fluoro 4 (phenylsulfonyl)but 3 en 2 yl)amino) 1 oxo 3 phenylpropan 2 yl) 4 methylpiperazine 1 carboxamide (4l). Synthesized by following procedure E with 0.11 g of compound **17**, 0.077 g compound **IX**, 0.076 g TBTU, 0.036 g HOBt, and 0.13 mL DIEA. Column chromatography: DCM/MeOH 9:1. Yield: 0.093 g (63%). (300 MHz, $CDCl_3$): δ 8.02 7.91 (m, 2H), 7.79 7.67 (m, 1H), 7.67 7.54 (m, 2H), 7.43 7.09 (m, 10H), 6.81 (dd, J = 47.2, 7.8 Hz, 1H), 6.16 (dd, J = 43.5, 31.8, 8.6 Hz, 1H), 5.15 (dd, J = 14.7, 7.4 Hz, 1H), 4.93 4.75 (m, 1H), 4.52 (m, 1H), 3.64 (s, 2H), 3.54 3.30 (m, 4H), 3.18 2.99 (m, 2H), 2.67 2.47 (m, 2H), 2.50 2.38 (m, 4H), 2.36 (s, 3H). (75 MHz, $CDCl_3$): δ 171.7, 156.9, 137.4, 137.4, 137.0, 136.93, 136.90, 136.87, 134.8, 129.7, 129.5, 129.4, 129.0, 128.9, 128.85, 128.76, 127.5, 127.3, 127.2, 116.6, 116.57, 116.5, 77.2, 55.9, 55.88, 54.4, 54.4, 45.9, 45.8, 44.5, 44.3, 43.55, 38.8, 38.6, 36.5, 35.1, 35.0. mp 84 86 °C. HR-MS (ESI, m/z): $[M + Na]^+$ calcd for $C_{32}H_{37}FN_4O_4S_2$, 647.2138; found, 647.2152. $[\alpha]_D^{22}$ 13° (c 1, $CHCl_3$).

Synthesis of the Metabolites. tert Butyl 4 (((S) 1 (((S,E) 1 Fluoro 5 phenyl 1 (phenylsulfonyl)pent 1 en 3 yl)amino) 1 oxo 3 phenyl propan 2 yl)carbamoyl)piperazine 1 carboxylate (36). Compound **XIII** (0.31 g) was dissolved in DCM and cooled to 0 °C. 0.11 g HOBt, 0.26 g TBTU, and 0.42 mL DIEA were added and the mixture was stirred for 30 min. 0.24 g of compound **13** was added and the mixture was stirred for an additional 24 h at rt. The reaction was stopped with 7 equiv of water and the mixture was washed with a saturated solution of

https://doi.org/10.1021/acs.jmedchem.1c01002
J. Med. Chem. 2021, 64, 12322 12358

$NaHCO_3$ and brine, dried with Na_2SO_4, and the solvent was removed under reduced pressure. The crude product was purified by column chromatography (cyclohexane/EtOAc 1:1), resulting in a colorless oil (0.21 g, 45%). ^{1}H NMR (300 MHz, CDCl3): δ 7.97 7.88 (m, 2H), 7.74 7.65 (m, 1H), 7.63 7.53 (m, 2H, *H*-27), 7.35 7.11 (m, 8H), 7.02 (ddd, J = 7.8, 3.2, 1.5 Hz, 2H), 6.54 (d, J = 41.8 Hz, 1H), 5.99 (dd, J = 32.0, 8.7 Hz, 1H), 5.11 (d, J = 27.5 Hz, 1H), 4.71 4.56 (m, 1H), 4.47 (d, $J_{C\ F}$ = 10.3 Hz), 3.45 3.17 (m, 8H), 3.14 2.91 (m, 2H), 2.56 2.36 (m, 2H), 1.95 1.62 (m, 2H), 1.46 (s, 9H). ^{13}C NMR (75 MHz, CDCl3): δ 171.6, 157.0, 154.7, 140.4, 137.1 (d, J = 7.3 Hz), 136.8, 134.8, 129.7, 129.4, 128.9, 128.8, 128.7, 128.4, 127.3 (d, J = 5.1 Hz), 126.4, 117.4, 80.4, 56.1, 45.1, 43.7, 38.5, 35.8, 31.8, 28.5.

*(S) 4 ((1 Ethoxy 1 oxo 3 phenylpropan 2 yl)carbamoyl) 1 methylpiperazine 1 oxide (**28**).* Compound **IX** (1.3 g) was dissolved in DCM and cooled to 0 °C. 0.7 g of 3-chloroperbenzoic acid was added and the mixture was stirred for 16 h. Triphenylphosphine was added to stop the reaction. The solvent was removed under reduced pressure, giving the crude product as a colorless oil (0.82 g, 63%). ^{1}H NMR (300 MHz, methanol-d_4): δ 7.35 7.11 (m, 5H), 4.87 (t, J = 2.0 Hz, 4H), 4.49 (td, J = 5.9, 2.9 Hz, 1H), 4.22 4.03 (m, 2H), 3.47 3.40 (m, 1H), 3.23 2.87 (m, 4H), 2.39 (d, J = 2.9 Hz, 3H), 2.04 1.89 (m, 2H), 1.26 1.10 (m, 3H). ^{13}C NMR (75 MHz, methanol-d_4): δ 174.4, 159.3, 138.8, 130.2, 129.4, 127.8, 62.2, 57.0, 55.2, 45.6, 44.1, 38.5, 14.4.

*(S) 4 ((1 Carboxy 2 phenylethyl)carbamoyl) 1 methylpiperazine 1 oxide (**38**).* Compound **37** (0.65 g) was dissolved in THF and cooled to 0 °C, and 0.33 g of LiOH in water was added dropwise. The mixture was stirred for 3 h at room temperature. The product was isolated from the aqueous phase giving a colorless solid (0.31 g, 53%). ^{1}H NMR (300 MHz, DMSO-d_6): δ 11.49 (s, 1H), 7.39 6.82 (m, 5H), 4.15 3.96 (m, 1H), 3.96 3.67 (m, 1H), 3.16 2.68 (m, 8H), 2.50 (s, 2H), 2.33 (s, 3H). ^{13}C NMR (75 MHz, DMSO-d_6): δ 173.9, 157.1, 138.6, 129.3, 128.2, 126.4, 55.8, 51.9, 42.0, 40.8, 36.4.

*Ethyl Isonicotate (**39**).* Isonicotinic acid (2.46 g) was dissolved in 40 mL ethanol and 1 mL of concentrated H_2SO_4 was added dropwise. The mixture was refluxed for 24 h and the solvent was removed under reduced pressure. The residue was extracted with DCM and the combined extracts were washed with a saturated solution of $NaHCO_3$, resulting in a colorless oil (2.2 g, 73%). ^{1}H NMR (300 MHz, DMSO-d_6): δ 8.83 8.73 (m, 2H), 7.88 7.73 (m, 2H), 4.34 (q, J = 7.1 Hz, 2H), 1.32 (t, J = 7.1 Hz, 3H). ^{13}C NMR (75 MHz, DMSO-d_6): δ 164.8, 150.8, 137.2, 122.6, 61.7, 14.1.

*4 (Ethoxycarbonyl)pyridine 1 Oxide (**40**).* Compound **39** (1.51 g) was dissolved in DCM and cooled to 0 °C. 1.73 g of 3-chloroperbenzoic acid was added and the mixture was stirred for 16 h. Triphenylphosphine was added to stop the reaction. The solvent was removed under reduced pressure, giving the crude product that was further purified by column chromatography (cyclohexane/EtOAc 1:6), resulting in a colorless oil (0.24 g, 29%). ^{1}H NMR (300 MHz, DMSO-d_6): δ 8.43 8.19 (m, 2H), 7.97 7.77 (m, 2H), 4.31 (q, J = 7.1 Hz, 2H), 1.31 (t, J = 7.1 Hz, 3H). ^{13}C NMR (75 MHz, DMSO-d_6): δ 163.7, 139.9, 126.85, 125.7, 61.9, 14.5.

*4 Carboxypyridine 1 Oxide (**41**).* Compound **40** (0.20 g) was dissolved in THF and cooled to 0 °C. 0.20 g of LiOH was dissolved in water and added dropwise to the mixture, then stirred for 3 h at rt. The product was isolated from the aqueous phase giving a colorless solid (0.17 g, 100%). ^{1}H NMR (300 MHz, DMSO-d_6): δ 8.31 (d, J = 6.2 Hz, 2H), 7.82 (d, J = 6.2 Hz, 2H). ^{13}C NMR (75 MHz, DMSO-d_6): δ 165.00, 139.8, 127.5, 127.1.

*4 (((S) 1 (((S,E) 1 Fluoro 5 phenyl 1 (phenylsulfonyl)pent 1 en 3 yl)amino) 1 oxo 3 phenylpropan 2 yl)carbamoyl)piperazin 1 ium Chloride (**1a**).* A 4 M solution of HCl in dioxane (3 mL) was added to 0.208 g of compound **36**. The mixture was stirred for 12 h and the solvent was removed under reduced pressure. The residue was washed three times with diethyl ether in an ultrasonic bath and then lyophilized, resulting in a colorless solid (0.177 g, 93%). ^{1}H NMR (300 MHz, DMSO-d_6): δ 8.53 (s, 2H), 8.10 7.97 (m, 2H), 7.98 7.66 (m, 3H), 7.40 6.89 (m, 11H), 6.51 (dd, J = 32.7, 9.8 Hz, 1H), 4.58 4.40 (m, 1H), 4.33 3.93 (m, 1H), 3.61 3.44 (m, 8H), 3.09 2.83 (m, 4H), 2.34 1.78 (m, 2H). ^{13}C NMR (75 MHz, DMSO-d_6): δ 163.2, 157.2, 139.3, 136.6, 135.8, 132.6, 130.2, 129.1, 128.1, 126.1, 119.7, 117.8, 115.1, 57.2, 52.4, 46.0, 42.4, 42.4, 36.5, 35.2, 35.0, 33.3. mp 93 94 °C. LC MS (ESI, m/z): [M + H]$^+$ calcd for $C_{31}H_{35}FN_4O_4S$, 579.24; found, 579.3. Purity: 98%. $[\alpha]_D^{22}$ 10° (c 0.5, MeOH).

*4 (((S) 1 (((S,E) 1 Fluoro 5 phenyl 1 (phenylsulfonyl)pent 1 en 3 yl)amino) 1 oxo 3 phenylpropan 2 yl)carbamoyl) 1 methylpiperazine 1 oxide (**1b**).* Compound **38** (0.20 g) was dissolved in a 1:1 mixture of DCM/DMF and cooled to 0 °C. 0.05 g HOBt, 0.11 g TBTU, and 0.20 mL DIEA were added, and the mixture was stirred for 30 min until all components dissolved. 0.10 g of compound **13** were added, and the mixture was stirred for an additional 48 h at room temperature. The reaction was stopped by adding 7 equiv of water and the residue was extracted with EtOAc and washed with water (2×), $NaHCO_3$ (2×), 1 M HCl (2×), and brine (1×). The solvent was removed under reduced pressure and the crude product was purified by preparative HPLC and eluted with 70% water and 30% ACN, resulting in a colorless oil (0.04 g, 23%). ^{1}H NMR (300 MHz, DMSO-d_6): δ 10.13 (s, 1H), 8.43 7.45 (m, 10H), 7.33 7.03 (m, 5H), 6.33 6.26 (m, 1H), 5.81 (dd, J = 22.1, 10.2 Hz, 1H), 5.50 5.28 (m, 1H), 4.48 (q, J = 8.0 Hz, 1H), 4.36 4.20 (m, 2H), 3.71 3.12 (m, 8H), 2.50 (quint, J = 1.9 Hz, 3H), 2.06 (d, J = 43.8 Hz, 2H), 2.04 1.64 (m, 2H). ^{13}C NMR (300 MHz, DMSO-d_6): δ 172.0, 157.3, 142.4, 139.6, 136.9, 134.0, 129.8, 129.0, 128.9, 128.6, 128.2, 127.7, 126.0, 105.6, 60.2, 57.2, 50.4, 42.5, 36.9, 30.4. LC MS (ESI, m/z): [M + H]$^+$ calcd for $C_{32}H_{37}FN_4O_5S$, 609.25; found, 609.4. Purity: 99%. $[\alpha]_D^{22}$ 4° (c 0.5, MeOH).

*4 (((S) 1 Oxo 1 (((S,E) 1 (phenoxysulfonyl) 5 phenylpent 1 en 3 yl)amino) 3 (p tolyl)propan 2 yl)carbamoyl)pyridine 1 Oxide (**2I**).* Compound **41** (0.038 g) was dissolved in DCM and cooled to 0 °C. 0.036 g HOBt, 0.087 g TBTU, and 0.19 mL DIEA were added and the mixture was stirred for 30 min. Then, 0.14 g of compound **34-(H)** was added and the mixture was stirred for an additional 24 h at room temperature. The reaction was stopped by adding 7 equiv of water and the residue was extracted with DCM and washed with water (2×), $NaHCO_3$ (2×), 1 M HCl (2×), and brine (1×). The solvent was removed under reduced pressure and the product was further purified by column chromatography (EtOAc/MeOH 9:1), resulting in a colorless solid (0.021 g, 13%). ^{1}H NMR (300 MHz, DMSO-d_6): δ 9.11 8.90 (m, 1H), 8.51 8.39 (m, 1H), 8.36 8.20 (m, 2H), 7.91 7.78 (m, 2H), 7.52 7.38 (m, 2H), 7.37 7.29 (m, 2H), 7.27 7.18 (m, 6H), 7.15 7.00 (m, 4H), 6.68 (dt, J = 15.4, 4.0 Hz, 1H), 6.35 (dd, J = 15.4, 3.0 Hz, 1H), 4.72 (q, J = 10.1, 9.0 Hz, 1H), 4.41 (s, 1H), 3.13 2.92 (m, 2H), 2.66 2.46 (m, 2H), 2.22 (s, 3H), 1.27 1.09 (m, 2H). ^{13}C NMR (75 MHz, DMSO-d_6): δ 171.4, 163.6, 149.6, 141.4, 139.3, 136.0, 135.0, 130.4, 129.5, 129.3, 128.8 (d, J = 3.6 Hz), 127.9, 126.3, 125.5, 123.6, 123.0, 55.9, 49.4, 39.9 (m), 34.5, 31.6, 21.1. mp 112 114 °C. LC MS (ESI, m/z): [M + H]$^+$ calcd for $C_{33}H_{33}N_3O_6S$, 600.21; found, 600.3. Purity: 97%. $[\alpha]_D^{22}$ 6° (c 0.5, MeOH).

Enzyme Assays. *Fluorometric Assays.* Rhodesain was expressed as published previously.[34] The increase of fluorescence upon cleavage of the fluorogenic substrate Cbz-Phe-Arg-AMC (Bachem) by rhodesain, CatB, or CatL was monitored using a TECAN Infinite F200 Pro fluorimeter (δ excitation: 365 nm, δ emission: 460 nm). The enzymes were diluted from a stock solution (rhodesain: 4 mg/mL in 10 mM sodium citrate buffer, pH 5.5; CatB (human liver, Calbiochem): 0.532 mg/mL; CatL (human liver, Calbiochem): 0.266 mg/mL) with enzyme buffer (rhodesain: 50 mM sodium acetate pH 5.5, 5 mM EDTA, 200 mM NaCl and 2 mM DTT; CatB/CatL: 50 mM Tris HCl, 5 mM EDTA, 200 mM NaCl, 2 mM DTT, pH 6.5) and were incubated for 1 h at rt. Assays were performed in black, flat-bottom 96-well microtiter plates (Greiner bio-one) with a total volume of 200 μL at 37 °C. Inhibitors and the substrate were prepared as stock solutions in DMSO. Dilution series of inhibitors in DMSO with a minimum of seven different concentrations were prepared in duplicate at least. 180 μL assay buffer (rhodesain: 50 mM sodium acetate pH 5.5, 5 mM EDTA, 200 mM NaCl, and 0.005% Brij35; CatB/CatL: 50 mM Tris HCl, 5 mM EDTA, 200 mM NaCl, 0.005% Brij35, pH 6.5) was added to the 96-well plates, then 5 μL of the respective enzyme in enzyme buffer, followed by 10 μL DMSO with or without inhibitor and finally 5 μL substrate (final substrate concentrations for rhodesain 10 μM, for CatB 100 μM, and for CatL 6.5 μM). Fluorescence emission was monitored directly after addition of the substrate. The presented data

https://doi.org/10.1021/acs.jmedchem.1c01002
J. Med. Chem. 2021, 64, 12322 12358

are mean values of three independent measurements. Standard deviations are less than 10% unless otherwise depicted.

Screening of activity against the catalytically active subunits of the proteasome (commercially obtained from Enzo) and Dengue virus NS2/NS3 protease was performed with an inhibitor concentration of 11 μM in DMSO.[68] Human 20S proteasome (from human erythrocytes, 0.5 mg/mL) was diluted with enzyme buffer (for trypsin-like activity: 50 mM Tris HCl, 50 mM NaCl, 0.5 mM EDTA, pH 7.4; for α-chymotrypsin-/caspase-like activity: 50 mM Tris HCl, 25 mM KCl, 10 mM NaCl, 1 mM $MgCl_2$, 0.03% SDS, pH 7.5). Trypsin-like activity was measured with the fluorogenic substrate boc-Leu-Arg-Arg-AMC (Bachem), α-chymotrypsin-like activity with Succ-Leu-Leu-Val-Tyr-AMC (Bachem), and caspase-like activity with Cbz-Leu-Leu-Glu-AMC (Bachem). Measurements were conducted in in black, flat-bottom 96-well microtiter plates (Greiner bio-one) by successive addition of 180 μL enzyme buffer, 5 μL proteasome in enzyme buffer, 10 μL inhibitor (11 μM in DMSO) or 10 μL pure DMSO, and 5 μL of the respective substrate (final substrate concentrations for trypsin-like activity 85 μM, α-chymotrypsin-like activity 70 μM, and caspase-like activity 80 μM). Fluorescence emission was monitored directly after addition of the substrate. Dengue virus NS2B/NS3 protease was diluted from a stock solution (1 mg/mL) with enzyme buffer (50 mM Tris HCl, 1 mM Chaps, 20% glycerol).[68] Screening was performed with the substrate boc-Gly-Arg-Arg-AMC (Bachem) in black, flat-bottom 96-well microtiter plates (Greiner bio-one) by successive addition of 180 μL enzyme buffer, 5 μL Dengue protease in enzyme buffer, 10 μL inhibitor (11 μM in DMSO) or 10 μL pure DMSO, and 5 μL of the substrate (final substrate concentration 100 μM). Fluorescence emission was monitored directly after addition of the substrate.

The presented inhibition data for all enzymes are mean values of three independent measurements. Standard deviations are less than 10% unless otherwise depicted.

Calculations. The GraFit program (version 5.0.13, 2006, Erithacus Sofware Ltd., UK) was used for data analysis and non-linear regression.

For inhibitors showing time-independent inhibition (**2a-(Z)**, **2k**, **2j**, **3a** **3i**, and **4a** **4l**), the residual enzyme activity was plotted against the inhibitor concentration. IC_{50} values were obtained by non-linear regression using the equation

$$v_i = \frac{v_0}{1 + \left(\frac{[I]}{IC_{50}}\right)^S}$$

with v_0 = enzyme activity in the absence of inhibitor, v_i = enzyme activity in the presence of inhibitor, [I] = inhibitor concentration, and S = slope factor.

K_i values were obtained by correcting the IC_{50} values to zero substrate concentration using the Cheng Prusoff relationship[32]

$$K_i = \frac{IC_{50}}{1 + \frac{[S]}{K_M}}$$

Rhodesain: [S] = 10 μM, K_M = 0.8265 μM, CatL: [S] = 6.25 μM, K_M = 6.5 μM, CatB: [S] = 100 μM, and K_M = 150 μM.

Calculation for the inhibitors with slow, tight-binding properties (**2a** **2i**) is presented in the Results and Discussion section.

Dilution Assays. Rhodesain (5 μL from 4 mg/mL stock solution) in enzyme buffer (85 μL) was incubated for 30 min with inhibitors (10 μL in DMSO) at concentrations corresponding to 10-fold the IC_{50} value obtained from fluorometric enzyme assay to ensure complete inhibition. These mixtures (2 μL) were diluted 100-fold in assay buffer (198 μL) containing 5 μL substrate (400 μM) to give a final substrate concentration of 10 μM. Recovery of enzyme activity was measured immediately using a fluorescence readout. Rhodesain with DMSO and no inhibitor added was used as a reference while the irreversible inhibitor **K11777** was used as an irreversible control.

Dialysis Experiments. Dialysis experiments for rhodesain were performed in a custom-built dialysis chamber, allowing the parallel examination of five samples.[26] A 3.5 kDa MW cut-off dialysis tubing (Carl Roth, Zellutrans MWCO 3.5 kDa) was cut into half and placed in the instrument, separating a continuous flow of buffer from five cavities at the top of the instrument, where the samples (800 μL) were added. Therefore, 20 μL rhodesain in enzyme buffer was added to 740 μL assay buffer and 40 μL DMSO with or without inhibitor. Inhibitor concentrations of 10-fold the IC_{50} value were chosen in order to guarantee complete inhibition. After incubation for 30 min, the mixtures were transferred to the cavities in the instrument and dialyzed against a continuous flow of assay buffer containing 5% DMSO (300 mL/h). Samples (97.5 μL) were taken at different time points (10, 30, 60, and 120 min) and 2.5 μL of a substrate solution was added to give a final substrate concentration of 10 μM. Enzyme activity was determined by directly measuring the fluorescence emission. The results are given in fractional activity of uninhibited rhodesain used in the same experiment as positive control.

Docking Procedures. *Procedure for Non covalent Docking with FlexX/LeadIT (vs. 2.1.3).*[11] Non-covalent docking experiments were performed using the crystal structure of rhodesain with covalently bound inhibitor **K11777** (pdb entry 2p7u).[60] The binding site was defined as a 6.5 Å shell around **K11777**. Water molecules present in the crystal structure were omitted except HOH-512, which mediates hydrogen bonding between the inhibitor and the peptide backbone. Generation of 3D-coordinates and energy minimization of the ligands were accomplished with the Molecular Operating Environment (MOE2014.09) using the MMFF94x force field.[26] Docking calculations were executed with LeadIT version 2.1.3.[27] The results presented in Table 1 are those with the best HYDE score[69,70] selected from the 10 highest-priced solutions according to FlexX score (Table 7.1).

Procedure for Covalent Docking with DOCKTITE.[60] Covalent docking was performed with the DOCKTITE software implementation (version 1.2) for Molecular Operating Environment (MOE, 2014.09; Chemical Computing Group ULC, 1010 Sherbooke St. West, Suite #910, Montreal, QC, Canada, H3A 2R7, **2021**)[11,27] using the crystal structure of rhodesain with covalently bound inhibitor **K11777** (pdb entry 2p7u).[60] Energy minimization of the ligands was performed with MOE using the MMFF94x force field.[71] The different warheads were implemented into the DOCKTITE warhead filter file as described in the DOCKTITE manual. The standard DOCKTITE protocol was followed as described. The main pharmacophore docking step was performed without pharmacophore restriction for the nucleophilic sulfur of Cys25. The Amber12:EHT force field[72] was used for the pharmacophore docking step. Docking solutions were rescored with the MOE implemented scoring functions Affinity dG and additionally with the external empirical scoring function DSX.[73] The results shown in Table S1 are those with the best DSX scores.

Mass Spectrometry (MS). *ESI MS Analysis.* Lyophilized rhodesain was reconstituted at 4 mg/mL in 50 mM NaOAc, 200 mM NaCl, and 5 mM EDTA (pH 5.5). Prior to MS analysis, rhodesain was purified by weak anion exchange (WAX) chromatography using an *AKTA* protein purification system (GE Healthcare) equipped with a ProPac WAX-10G 4 × 50 mm guard and a ProPac WAX-10 4 × 250 mm analytical column (Thermo Fisher Scientific). 100 μL of rhodesain stock solution (4 mg/mL) was diluted in 20 mM imidazole, 1 mM DTT in water (pH 6.0) to a final volume of 1 mL, and separated running a gradient from 0 to 40% B in 40 min. Mobile phase A was 20 mM imidazole, 1 mM DTT in water (pH 6) and Solvent B 1 M NaCl, 20 mM imidazole, and 1 mM DTT in water (pH 6). Collected fractions were tested for activity.

For mass spectrometric analysis, the WAX fraction containing active rhodesain was further diluted in 50 mM NaOAc, 200 mM NaCl, 5 mM EDTA, and 5 mM DTT (pH 5.5) and incubated for 1 h at rt. After the addition of the inhibitors at a final concentration of 10 μM, samples were analyzed by LC MS using a nanoAcquity UPLC system (Waters Corporation) coupled to a nano-ESI-Q-TOF mass spectrometer (Synapt G2-S HDMS, Waters Corporation). Rhodesain without compound served as control. Protein drug complexes were loaded onto a 200 μm × 5 cm PepSwift Monolithic PS-DVB column from Dionex (Thermo Scientific) using direct injection mode. For LC separation, two mobile phases were used. Mobile phase A contained 0.1% formic acid (FA) and 3% DMSO in ultrapure water, whereas mobile phase B consisted of 0.1% FA and 3% DMSO in ACN. A gradient of 10 90% mobile phase B was run over 7 min at a flow rate of

https://doi.org/10.1021/acs.jmedchem.1c01002
J. Med. Chem. 2021, 64, 12322 12358

2000 nL/min. Column temperature was set to 45 °C. After separation, the column was rinsed with 90% of mobile phase B and re-equilibrated under initial conditions. All MS analyses were conducted in positive-mode ESI.

MALDI TOF MS Analysis. For this analysis, a recombinant rhodesain mutant expressed in *Pichia pastoris* was used as described in the enzyme assay section. The lyophilized protein was reconstituted in buffer A (pH 5.5, 50 mM NaOAc, 200 mM NaCl, 5 mM EDTA) at a concentration of 4 mg/mL (= 174 μM). This stock solution was diluted into buffer B (pH 5.5, 50 mM NaOAc, 200 mM NaCl, 5 mM EDTA, 5 mM DTT) to a final protein concentration of 1 or 10 μM and incubated for approximately 1 h, after which the compound of interest (4 mM stock in DMSO) was added at a final inhibitor concentration of 100 μM. Later, the analytes were desalted using Zeba Spin Desalting Columns (7 kDa MWCO, 0.5 mL; Thermo Fisher Scientific) in accordance with the manufacturer's instructions and afterward coprecipitated with a MALDI-matrix, utilizing two separate approaches: For the first method, a thin layer of sinapinic acid (saturated ethanolic solution) was prepared on the target, onto which, after film formation, a volumetric 3:1 mixture of matrix-solution to analyte solution was applied. For the second method, using a mixture of α-cyano-4-hydroxycinnamic acid and 2,5-dihydroxybenzoic acid,[40,44] the preparation of a basal matrix film was omitted and a volumetric 1:1 mixture of matrix-solution to analyte solution was prepared and applied to the target. After evaporation of the solvents (ca. 15 min), measurements were carried out on a rapifleX MALDI-TOF/TOF mass spectrometer (Bruker Daltonik GmbH, Bremen, Germany). The instrument is equipped with a scanning smartbeam 10 kHz Nd:YAG laser at a wavelength of 355 nm and a 10 bit 5 GHz digitizer. The acceleration voltage was set to 20 kV and the mass spectra were recorded in positive ion linear mode. Calibration was done with the Bruker protein calibration standard II in a mass range from 10 to 70 kDa. Samples were measured at a laser power of 100% (sinapinic acid) or 70% (matrix mixture), with random walk ionization across the sample spot. As control samples, rhodesain in buffer B with a DMSO concentration matching the samples, rhodesain incubated with a reportedly non-covalent inhibitor,[11] and a known covalent-irreversible inhibitor (**K11777**)[74] were used. Data analysis was performed using the open-source software mMass.[68]

QM/MM Computations. MD simulations were performed with the Amber program package (version 2018) in combination with the FF14SB force field. The unknown parameters for the ligand were calculated using GAFF.[75] The obtained enzymatic system was balanced with sodium ions. We added an octahedral water envelope of 10 Å consisting of TIP3P water molecules Figure S11).[76] All MD simulations were performed under periodic boundary conditions in three consecutive steps. In the first step, the cage of water molecules and then the whole system was minimized. In the next step, the system was heated in a controlled way from 0 to 300 K at 1 bar, using the SHAKE algorithm[77] employing the Langevin or Berendsen thermostat.[77,78] In the last step, the actual MD simulation with a duration of at least 10 ns was performed.

We used the subtractive QM/MM approach employing the electrostatic embedding scheme as implemented in the program package Gaussian (version 2016).[79] The QM part is specified in Figure S12. Please note that larger QM spaces did not lead to considerably changes (Table S4). For the QM part, we employed the ωB97XD functional in combination with the 6-31+G* basis sets.[80−82] The TAO-Toolkit was used.[83] For the intrinsic reaction coordinate (IRC) computations, the transition states were determined using the Berny-Algorithm.[84] All transition states were proved by frequency calculations.

The reaction paths were characterized by a two-step procedure. The covalent step of the inhibition mechanism first consists of the attack of the sulfur center of the thiolate group of Cys25 on the C_2 center of the alkene group. Additionally, a proton transfer from the protonated His152 moiety to the C_1 center occurs (Figure 1). Because it is unclear whether both steps proceed subsequently or simultaneously, we first computed two-dimensional scans selecting the distances $R(S_{Cys}\ C_2)$ and $R(H_{His}\ C_1)$ as main reaction parameters (Figure 14). By varying the main reaction parameters and optimizing all other internal coordinates for each pair of main coordinates, a minimum energy path (MEP) from the reactant to the product is obtained, which gives the first information about the shape of the reaction path. Starting from the barriers obtained in these scans, we performed intrinsic reaction coordinate (IRC) simulations. Due to the roughness of the computed PES, often more than one transition state was found for the two-dimensional surface. In such cases, we started IRC from each TS to ensure that they lead to similar reactants and products. This was indeed the case. One example is shown in Figures S8 and S10 in which computations started from slightly different TS but yielded comparable shapes for the reaction paths. The same holds for the second step of the reaction path given in Figure 16. For this frame, we found four TS whose IRCs all lead to very similar results.

Antitrypanosomal Activity and Cytotoxicity. Antitrypanosomal activity of **2a**, **2d**, **2e**, **3d**, **4d**, and **4e** against the *T. brucei brucei* BS449 cell line, a descendant of the Lister 427 strain,[85,86] was determined using the ATPlite assay as described previously.[56,57,87] **2a**, **2d**, **2e**, **3d**, **4d**, and **4e** were prepared as 5 mM stock solutions in DMSO and diluted in HMI-9 medium in multiple steps (1:3, then 1:10, and subsequently in ten 1:2 dilution steps using separate microplates). In white 96-well microplates (PerkinElmer), 10 μL of the final 101 dilutions were added to 90 μL of a cell suspension containing 2500 cells/mL, leading to final concentrations of each tested compound from 16.67 μM to 32.55 nM in the microplates. As a negative control, 0.3% DMSO was added to the cell suspension corresponding to the highest DMSO concentration added by compound application. Addition of 10% DMSO served as a positive control because all cells die at this concentration. The plates were prepared as triplicates and incubated for 24 and 48 h at 37 °C and 5% CO_2. After the respective incubation time, 50 μL ATPlite 1 step solution (PerkinElmer) was added to each well. The plate was shaken orbitally for 2 min and luminescence was measured at room temperature with an Infinite M200 PRO plate reader (Tecan Trading AG). The measured luminescence was plotted against the compound concentration to obtain a dose response curve. The EC_{50} values were determined using GraFit version 5.013 (Erithacus Software Ltd.).

Antitrypanosomal activity of the compounds **1**, **4a**, **4j**, and **4l** was determined as described previously using the Alamar Blue assay.[54,55] Cytotoxicities against the macrophage cell line J774.1 and HeLa cells were investigated according to previously described methods.[12,88]

In Vitro Metabolism Studies. Rat liver microsomes were purchased from Sigma-Aldrich and characterized for cytochrome P450, cytochrome B5, and the activity of CYP1A, CYP3A, CYP2C, and cytochrome *c* reductase. The assay was performed as published previously.[68]

First, NADPH was generated by incubating potassium phosphate buffer (395 μL, 100 mM, pH 7.4), $MgCl_2$ (25 μL, 80 mM), glucose-6-phosphate (25 μL, 100 mM), NADP disodium salt (25 μL, 20 mM), and glucose-6-dehydrogenase (25 μL, 100 IU/mL, Sigma-Aldrich) at 37 °C for 10 min. After addition of the microsomes (25 μL, 20 mg/mL) and incubation (10 min) at 37 °C, the inhibitors (1 μL, 5.21 mM in acetonitrile) were added to the mixture and the incubation continued at 37 °C for 60 min. Aliquots of 50 μL were taken at 0, 15, 30, 45, and 60 min and added to 100 μL of ice-cold acetonitrile to stop the reaction. The samples were centrifuged at 4 °C, 10,000*g* for 10 min. The supernatant was analyzed by LC MS/MS using an Agilent Poroshell 120 EC-C18 150 × 2.10 mm 4 μm column; mobile phase: compound **1** (35% acetonitrile, 55% H_2O, 10% of a 0.1% solution of formic acid in water) and compound **2d-(H)** (55% acetonitrile, 35% H_2O, 10% of a 0.1% solution of formic acid in water). Ion chromatograms were obtained using electronic filters for the ions of interest. Control incubations were performed with potassium phosphate buffer instead of microsomes. The LC MS chromatograms and their corresponding mass spectra were analyzed using MestReNova (v. 12.0.4).[89]

In Vivo Distribution Studies. *Animals and Treatments.* 60 male and female CD1 mice of 35 45 g body weight (56 62 days of age) were purchased from Charles River Laboratories, Sulzfeld, Germany. Five mice per cage were housed in a controlled room (22 °C, 50 65% humidity; day/night cycle of 12/12 h) with free access to water and the standard laboratory diet (Altromin, Germany). After 7 days of

https://doi.org/10.1021/acs.jmedchem.1c01002
J. Med. Chem. 2021, 64, 12322 12358

acclimatization, they were randomly divided into eight groups in which each group received four different testing compounds (**1**, **2d-(H)**) at a dose of 25 mg/kg by i.p. injection or oral gavage (p.o.). Compound **1** was diluted in 1% DMSO, while **2d-(H)** was diluted in 2% DMSO. The i.p. injection was given once only while the p.o. administrations were given for 4 days, twice daily (8 doses in total) at 9 and 18 o'clock. The dose of 25 mg/kg was chosen based on preliminary tests. 60 min after the administration of the testing compounds, blood was collected (about 0.2 mL) from the facial vein using a lancet (Goldenrod animal lancet). At the end of the experiment (3 h after the last drug administration), the animals were sacrificed by decapitation under isoflurane anesthesia. Trunk blood was collected, and the brain was removed and homogenized. Experiments were carried out according to the German Law for Animal Protection and were registered with Regierungsprasidium Darmstadt (FR/1021). All efforts were made to minimize animal numbers and animal suffering.

Microdialysis Experiments. Mice were anesthetized with isoflurane (induction dose 5%, maintenance dose 1.5% v/v in synthetic air) (Air Liquide, Dusseldorf, Germany) and placed in a stereotaxic frame (Stoelting, Chicago, IL, USA). A Y-shaped, concentric microdialysis probe with a molecular weight cutoff of 30 kDa and an exchange area of 2 mm was manufactured as described previously.[90] The probe was implanted in the hippocampus with the following coordinates from bregma: AP 2.0 mm; *L* +2.0 mm; DV 2.3 mm.[91] The mice were allowed to recover overnight. On the next day, the probes were perfused (rate: 2 μL/min) with artificial cerebrospinal fluid (aCSF; 147 mM NaCl, 4 mM KCl, 1.2 mM $CaCl_2$, and 1.2 mM $MgCl_2$) for 4 h and dialysates were collected every 20 min. After dialysates were collected for 1 h for equilibration, the test compound was given as described above. A blood sample was collected 1 h after administration of the test compound. At the end of the experiment (3 h after the last drug administration), the animals were sacrificed by decapitation under isoflurane anesthesia. Trunk blood was collected, and the brain was removed and homogenized.

Sample Preparation and LC MS Analysis. The blood was centrifuged at 4 °C, 1500*g* for 20 min and the plasma supernatant was extracted with acetonitrile and centrifuged again at 4 °C, 10,000*g* for 10 min. The supernatant was analyzed by LC MS using an Agilent Poroshell 120 EC-C18 150 × 2.10 mm 4 μm column; mobile phase: compound **1** (35% acetonitrile, 55% H_2O, 10% of a 0.1% solution of formic acid in water) and compound **2d-(H)** (55% acetonitrile, 35% H_2O, 10% of a 0.1% solution of formic acid in water). Ion chromatograms were obtained using electronic filters for the ions of interest. The LC MS chromatograms and their corresponding mass spectra were analyzed using MestReNova (v. 12.0.4).[89]

The brain tissue was homogenized using a mixture of acetonitrile/MilliQ-water (ratio 2:1, 2 mL per 300 mg brain) in a tissue grinder (Potter S, B. Braun, Melsungen, Germany) at 1,500 rpm and 15 strokes. Afterward, the homogenate was centrifuged at 4 °C, 10,000*g* for 10 min and the supernatant was lyophilized. The lyophilizate was extracted with 400 μL acetonitrile and this extract was analyzed via LC MS as described above. The fractions of the microdialysate were used without further processing. The AUC that was obtained from the extracted ion chromatograms was normalized to a volume of 500 μL for the plasma samples or a weight of 450 mg for the brain homogenates. The average AUC for every sample was calculated from experiments performed in triplicate.

■ ASSOCIATED CONTENT

● Supporting Information

The Supporting Information is available free of charge at https://pubs.acs.org/doi/10.1021/acs.jmedchem.1c01002.

Scores for non-covalent (FlexX) and covalent docking (DOCKTITE); MALDI-TOF MS spectra of complexes of rhodesain with different inhibitors and different matrix substances; ESI MS spectra of complexes of rhodesain with inhibitors (*Z*)-**2a** and **2j**; additional data for the QM/MM computations; and ESI MS spectra of the in vitro metabolism and in vivo distribution studies of **1** and **2d-(H)** (PDF)

HPLC traces of lead compounds and molecular formula strings (CSV)

■ AUTHOR INFORMATION

Corresponding Author

Tanja Schirmeister *Institute of Pharmaceutical and Biomedical Sciences (IPBS), Johannes Gutenberg University, 55128 Mainz, Germany*; Email: schirmei@uni-mainz.de

Authors

Sascha Jung *Institute of Pharmaceutical and Biomedical Sciences (IPBS), Johannes Gutenberg University, 55128 Mainz, Germany*; Present Address: Faculty of Chemistry and Chemical Biology, TU Dortmund, Otto-Hahn-Str. 6, 44227 Dortmund, Germany

Natalie Fuchs *Institute of Pharmaceutical and Biomedical Sciences (IPBS), Johannes Gutenberg University, 55128 Mainz, Germany*; orcid.org/0000-0001-6404-676X

Patrick Johe *Institute of Pharmaceutical and Biomedical Sciences (IPBS), Johannes Gutenberg University, 55128 Mainz, Germany*

Annika Wagner *Department of Chemistry, Biochemistry Section, Johannes Gutenberg University, 55128 Mainz, Germany*; Present Address: Institute of Organic Chemistry & Macromolecular Chemistry (IOMC), Friedrich Schiller University, Humboldtstraße 10, 07743 Jena, Germany; Cluster of Excellence "Balance of the Microverse", Friedrich-Schiller-University Jena, Germany.

Erika Diehl *Department of Chemistry, Biochemistry Section, Johannes Gutenberg University, 55128 Mainz, Germany*

Tri Yuliani *Institute for Pharmacology and Clinical Pharmacy, Goethe University, 60439 Frankfurt, Germany*; Present Address: Research Center for Chemistry, Indonesian Institute of Sciences (LIPI), Gd. 452 Kawasan PUSPIPTEK, Tangerang Selatan, Indonesia.

Collin Zimmer *Institute of Pharmaceutical and Biomedical Sciences (IPBS), Johannes Gutenberg University, 55128 Mainz, Germany*

Fabian Barthels *Institute of Pharmaceutical and Biomedical Sciences (IPBS), Johannes Gutenberg University, 55128 Mainz, Germany*

Robert A. Zimmermann *Institute of Pharmaceutical and Biomedical Sciences (IPBS), Johannes Gutenberg University, 55128 Mainz, Germany*

Philipp Klein *Department of Chemistry, Organic Chemistry Section, Johannes Gutenberg University, 55128 Mainz, Germany*

Waldemar Waigel *Department of Physical and Theoretical Chemistry, Julius-Maximilians-University, 97074 Würzburg, Germany*

Jessica Meyr *Department of Physical and Theoretical Chemistry, Julius-Maximilians-University, 97074 Würzburg, Germany*

Till Opatz *Department of Chemistry, Organic Chemistry Section, Johannes Gutenberg University, 55128 Mainz, Germany*; orcid.org/0000-0002-3266-4050

Stefan Tenzer *Institute for Immunology, University Medical Center, Johannes Gutenberg University, 55131 Mainz, Germany*; orcid.org/0000-0003-3034-0017

https://doi.org/10.1021/acs.jmedchem.1c01002
J. Med. Chem. 2021, 64, 12322 12358

Ute Distler *Institute for Immunology, University Medical Center, Johannes Gutenberg University, 55131 Mainz, Germany;* orcid.org/0000-0002-8031-6384
Hans-Joachim Räder *Max Planck Institute for Polymer Research, 55128 Mainz, Germany;* orcid.org/0000-0002-7292-4013
Christian Kersten *Institute of Pharmaceutical and Biomedical Sciences (IPBS), Johannes Gutenberg University, 55128 Mainz, Germany*
Bernd Engels *Department of Physical and Theoretical Chemistry, Julius-Maximilians-University, 97074 Würzburg, Germany;* orcid.org/0000-0003-3057-389X
Ute A. Hellmich *Department of Chemistry, Biochemistry Section, Johannes Gutenberg University, 55128 Mainz, Germany; Center for Biomolecular Magnetic Resonance (BMRZ), Goethe University, 60438 Frankfurt, Germany;* Present Address: Institute of Organic Chemistry & Macromolecular Chemistry (IOMC), Friedrich Schiller University, Humboldtstraße 10, 07743 Jena, Germany; Cluster of Excellence "Balance of the Microverse", Friedrich-Schiller-University Jena, Germany.
Jochen Klein *Institute for Pharmacology and Clinical Pharmacy, Goethe University, 60439 Frankfurt, Germany*

Complete contact information is available at: https://pubs.acs.org/10.1021/acs.jmedchem.1c01002

Author Contributions

‡‡S.J. and N.F. contributed equally.

Funding

Financial support by the Rhine-Main Universities fund (RMU-Initiativfonds Forschung) is gratefully acknowledged. Funded by the Deutsche Forschungsgemeinschaft (DFG, German Research Foundation) under Germany's Excellence Strategy EXC 2051 Project ID390713860.

Notes

The authors declare no competing financial interest.

■ ACKNOWLEDGMENTS

E.D. acknowledges a PhD fellowship from the Sibylle Kalkhof-Rose-Stiftung.

■ ABBREVIATIONS

AcOH, acetic acid; aCSF, artificial cerebrospinal fluid; ADME, absorption, distribution, metabolism, excretion; AMC, 7-amido-4-methylcoumaryl; aq, aqueous; Arg, arginine; Asp, aspartate; AUC, area under the curve; Bn, benzyl; boc, *tert*-butyl carbonate; CatB, cathepsin B; CatL, cathepsin L; Cbz, carbobenzoxy; chymotrps., chymotrypsin; cpd, compound; Cys, cysteine; CYP, cytochrome P450; DCM, dichloromethane; DCTB, *trans*-2-[3-(4-*tert*-butylphenyl)-2-methyl-2-propenylidene]malononitrile; DECP, diethyl chlorophosphate; DIEA, *N*,*N*-diisopropylethylamine; DHBD, 2,3-dihydrobenzo-[*b*][1,4]dioxine; DMF, dimethyl formamide; DMSO, dimethyl sulfoxide; DTT, dithiothreitol; EDC, 1-ethyl-3-(3-dimethylaminopropyl)carbodiimide; EDTA, ethylenediamine tetraacetic acid; EtOAc, ethyl acetate; ESI, electrospray ionization; Glu, glutamate; Gly, glycine; HAT, Human African *Trypanosomiasis*; HeLa cells, Henrietta Lacks cells; HOBt, hydroxybenzotriazole; HPhe, homophenylalanine; HPLC, high-pressure liquid chromatography; HWE, Horner Wadsworth Emmons; i.p., intraperitoneal; KHMDS, potassium bis-(trimethylsilyl)amide; LC, liquid chromatography; Leu, leucin; LHMDS, lithium bis(trimethylsilyl)amide; MALDI, matrix-assisted laser desorption/ionization; *m*CPBA, *meta*-chloroperbenzoic acid; Me, methyl; Met, methionine; MM, molecular mechanics; MOE, molecular operating environment; MS, mass spectrometry; MS-Cl, mesyl chloride; mp, melting point; NADPH, nicotinamide adenine dinucleotide phosphate (reduced form); *n*-BuLi, *n*-butyllithium; n.d., not determined; NHS, *N*-hydroxysuccinimide; NMR, nuclear magnetic resonance; NTD, neglected tropical disease; PDB, Protein Database; Ph, phenyl; Phe, phenylalanine; Pip, piperazine; ppm, parts per million; Pyr, pyridine; QM, quantum mechanics; RMSD, root-mean-square deviation; rt, room temperature; SAR, structure activity relationship; SPR, surface plasmon resonance; Succ, *N*-succinyl; *T. b. gambiense*, *Trypanosoma brucei gambiense*; *T. b. rhodesiense*, *Trypanosoma brucei rhodesiense*; TBTU, 2-(1*H*-benzotriazole-1-yl)-1,1,3,3-tetramethyluronium tetrafluoroborate; TEA, triethyl amine; TFA, trifluoroacetic acid; THF, tetrahydrofuran; TLC, thin layer chromatography; TOF, time of flight; Tris, tris(hydroxymethyl)aminomethane; Trp, tryptophan; Tyr, tyrosine; UV, ultraviolet; val, valine; VS, vinyl sulfone; X-ray, energetic high-frequency electromagnetic radiation

■ REFERENCES

(1) Malvy, D.; Chappuis, F. Sleeping Sickness. *Clin. Microbiol. Infect.* **2011**, *17*, 986 995.
(2) Brun, R.; Blum, J.; Chappuis, F.; Burri, C. Human African Trypanosomiasis. *Lancet* **2010**, *375*, 148 159.
(3) Priotto, G.; Kasparian, S.; Mutombo, W.; Ngouama, D.; Ghorashian, S.; Arnold, U.; Ghabri, S.; Baudin, E.; Buard, V.; Kazadi-Kyanza, S.; Ilunga, M.; Mutangala, W.; Pohlig, G.; Schmid, C.; Karunakara, U.; Torreele, E.; Kande, V. Nifurtimox-Eflornithine Combination Therapy for Second-Stage African Trypanosoma Brucei Gambiense Trypanosomiasis: A Multicentre, Randomised, Phase III, Non-Inferiority Trial. *Lancet* **2009**, *374*, 56 64.
(4) Mesu, V. K. B. K.; Kalonji, W. M.; Bardonneau, C.; Mordt, O. V.; Blesson, S.; Simon, F.; Delhomme, S.; Bernhard, S.; Kuziena, W.; Lubaki, J.-P. F.; Vuvu, S. L.; Ngima, P. N.; Mbembo, H. M.; Ilunga, M.; Bonama, A. K.; Heradi, J. A.; Solomo, J. L. L.; Mandula, G.; Badibabi, L. K.; Dama, F. R.; Lukula, P. K.; Tete, D. N.; Lumbala, C.; Scherrer, B.; Strub-Wourgaft, N.; Tarral, A. Oral Fexinidazole for Late-Stage African Trypanosoma Brucei Gambiense Trypanosomiasis: A Pivotal Multicentre, Randomised, Non-Inferiority Trial. *Lancet* **2018**, *391*, 144 154.
(5) Fairlamb, A. H. Chemotherapy of Human African Trypanosomiasis: Current and Future Prospects. *Trends Parasitol.* **2003**, *19*, 488 494.
(6) Steverding, D.; Sexton, D. W.; Wang, X.; Gehrke, S. S.; Wagner, G. K.; Caffrey, C. R. Trypanosoma Brucei: Chemical Evidence That Cathepsin L Is Essential for Survival and a Relevant Drug Target. *Int. J. Parasitol.* **2012**, *42*, 481 488.
(7) Nikolskaia, O. v.; de A Lima, A. P. C.; Kim, Y. v.; Lonsdale-Eccles, J. D.; Fukuma, T.; Scharfstein, J.; Grab, D. J. Blood-Brain Barrier Traversal by African Trypanosomes Requires Calcium Signaling Induced by Parasite Cysteine Protease. *J. Clin. Invest.* **2006**, *116*, 2739 2747.
(8) Scory, S.; Caffrey, C. R.; Stierhof, Y.-D.; Ruppel, A.; Steverding, D. Trypanosoma Brucei: Killing of Bloodstream Formsin Vitroandin Vivo by the Cysteine Proteinase Inhibitor Z-Phe-Ala-CHN2. *Exp. Parasitol.* **1999**, *91*, 327 333.
(9) Kerr, I. D.; Wu, P.; Marion-Tsukamaki, R.; Mackey, Z. B.; Brinen, L. S. Crystal Structures of TbCatB and Rhodesain, Potential Chemotherapeutic Targets and Major Cysteine Proteases of Trypanosoma Brucei. *PLoS Neglected Trop. Dis.* **2010**, *4*, No. e701.
(10) Johé, P.; Jaenicke, E.; Neuweiler, H.; Schirmeister, T.; Kersten, C.; Hellmich, U. A. Structure, Interdomain Dynamics and PH-Dependent Autoactivation of pro-Rhodesain, the Main Lysosomal

Cysteine Protease from African Trypanosomes. *J. Biol. Chem.* **2021**, *296*, 100565.
(11) Kerr, I. D.; Lee, J. H.; Farady, C. J.; Marion, R.; Rickert, M.; Sajid, M.; Pandey, K. C.; Caffrey, C. R.; Legac, J.; Hansell, E.; Mckerrow, J. H.; Craik, C. S.; Rosenthal, P. J.; Brinen, L. S. Vinyl Sulfones as Antiparasitic Agents and a Structural Basis for Drug Design. *J. Biol. Chem.* **2009**, *284*, 25697 25703.
(12) Schirmeister, T.; Kesselring, J.; Jung, S.; Schneider, T. H.; Weickert, A.; Becker, J.; Lee, W.; Bamberger, D.; Wich, P. R.; Distler, U.; Tenzer, S.; Johé, P.; Hellmich, U. A.; Engels, B. Quantum Chemical-Based Protocol for the Rational Design of Covalent Inhibitors. *J. Am. Chem. Soc.* **2016**, *138*, 8332 8335.
(13) Singh, J.; Petter, R. C.; Baillie, T. A.; Whitty, A. The Resurgence of Covalent Drugs. *Nat. Rev. Drug Discovery* **2011**, *10*, 307 317.
(14) Bauer, R. A. Covalent Inhibitors in Drug Discovery: From Accidental Discoveries to Avoided Liabilities and Designed Therapies. *Drug Discovery Today* **2015**, *20*, 1061 1073.
(15) Kalgutkar, A. S.; Dalvie, D. K. Drug Discovery for a New Generation of Covalent Drugs. *Expert Opin. Drug Discovery* **2012**, *7*, 561 581.
(16) Lammert, C.; Einarsson, S.; Saha, C.; Niklasson, A.; Bjornsson, E.; Chalasani, N. Relationship between Daily Dose of Oral Medications and Idiosyncratic Drug-Induced Liver Injury: Search for Signals. *Hepatology* **2008**, *47*, 2003 2009.
(17) Lee, C.-U.; Grossmann, T. N. Reversible Covalent Inhibition of a Protein Target. *Angew. Chem., Int. Ed.* **2012**, *51*, 8699 8700.
(18) Copeland, R. A.; Pompliano, D. L.; Meek, T. D. Drug-Target Residence Time and Its Implications for Lead Optimization. *Nat. Rev. Drug Discovery* **2006**, *5*, 730 739.
(19) Bradshaw, J. M.; McFarland, J. M.; Paavilainen, V. O.; Bisconte, A.; Tam, D.; Phan, V. T.; Romanov, S.; Finkle, D.; Shu, J.; Patel, V.; Ton, T.; Li, X.; Loughhead, D. G.; Nunn, P. A.; Karr, D. E.; Gerritsen, M. E.; Funk, J. O.; Owens, T. D.; Verner, E.; Brameld, K. A.; Hill, R. J.; Goldstein, D. M.; Taunton, J. Prolonged and Tunable Residence Time Using Reversible Covalent Kinase Inhibitors. *Nat. Chem. Biol.* **2015**, *11*, 525 531.
(20) Johe, P.; Jung, S.; Endres, E.; Kersten, C.; Zimmer, C.; Ye, W.; Sönnichsen, C.; Hellmich, U. A.; Sotriffer, C.; Schirmeister, T.; Neuweiler, H. Warhead Reactivity Limits the Speed of Inhibition of the Cysteine Protease Rhodesain. *ACS Chem. Biol.* **2021**, *16*, 661 670.
(21) Schechter, I.; Berger, A. On the Size of the Active Site in Proteases. I. Papain. *Biochem. Biophys. Res. Commun.* **1967**, *27*, 157 162.
(22) Jaishankar, P.; Hansell, E.; Zhao, D.-M.; Doyle, P. S.; McKerrow, J. H.; Renslo, A. R. Potency and Selectivity of P2/P3-Modified Inhibitors of Cysteine Proteases from Trypanosomes. *Bioorg. Med. Chem. Lett.* **2008**, *18*, 624 628.
(23) Schirmeister, T.; Schmitz, J.; Jung, S.; Schmenger, T.; Krauth-Siegel, R. L.; Gutschow, M. Evaluation of Dipeptide Nitriles as Inhibitors of Rhodesain, a Major Cysteine Protease of Trypanosoma Brucei. *Bioorg. Med. Chem. Lett.* **2017**, *27*, 45 50.
(24) Yang, P.-Y.; Wang, M.; Li, L.; Wu, H.; He, C. Y.; Yao, S. Q. Design, Synthesis and Biological Evaluation of Potent Azadipeptide Nitrile Inhibitors and Activity-Based Probes as Promising Anti-*Trypanosoma Brucei* Agents. *Chem. Eur. J.* **2012**, *18*, 6528 6541.
(25) Caffrey, C. R.; Hansell, E.; Lucas, K. D.; Brinen, L. S.; Alvarez Hernandez, A.; Cheng, J.; Gwaltney, S. L.; Roush, W. R.; Stierhof, Y.-D.; Bogyo, M.; Steverding, D.; McKerrow, J. H. Active Site Mapping, Biochemical Properties and Subcellular Localization of Rhodesain, the Major Cysteine Protease of Trypanosoma Brucei Rhodesiense. *Mol. Biochem. Parasitol.* **2001**, *118*, 61 73.
(26) *LeadIT/FlexX*; BioSolveIT GmbH: St. Augustin, Germany 2012.
(27) Scholz, C.; Knorr, S.; Hamacher, K.; Schmidt, B. DOCKTITE-A Highly Versatile Step-by-Step Workflow for Covalent Docking and Virtual Screening in the Molecular Operating Environment. *J. Chem. Inf. Model.* **2015**, *55*, 398 406.
(28) Ng, S. L.; Yang, P.-Y.; Chen, K. Y.-T.; Srinivasan, R.; Yao, S. Q. "Click" Synthesis of Small-Molecule Inhibitors Targeting Caspases. *Org. Biomol. Chem.* **2008**, *6*, 844 847.
(29) Sun, A. C.; McClain, E. J.; Beatty, J. W.; Stephenson, C. R. J. Visible Light-Mediated Decarboxylative Alkylation of Pharmaceutically Relevant Heterocycles. *Org. Lett.* **2018**, *20*, 3487 3490.
(30) Ehmke, V.; Winkler, E.; Banner, D. W.; Haap, W.; Schweizer, W. B.; Rottmann, M.; Kaiser, M.; Freymond, C.; Schirmeister, T.; Diederich, F. Optimization of Triazine Nitriles as Rhodesain Inhibitors: Structure-Activity Relationships, Bioisosteric Imidazopyridine Nitriles, and X-Ray Crystal Structure Analysis with Human Cathepsin L. *ChemMedChem* **2013**, *8*, 967 975.
(31) DIXON, M. The Determination of Enzyme Inhibitor Constants. *Biochem. J.* **1953**, *55*, 170 171.
(32) Yung-Chi, C.; Prusoff, W. H. Relationship between the Inhibition Constant (KI) and the Concentration of Inhibitor Which Causes 50 per Cent Inhibition (I50) of an Enzymatic Reaction. *Biochem. Pharmacol.* **1973**, *22*, 3099 3108.
(33) Purich, D. L. *Enzyme Kinetics, Catalysis and Control, A Reference of Theory and Best-Practice Methods*; Elsevier, 2010.
(34) Ludewig, S.; Kossner, M.; Schiller, M.; Baumann, K.; Schirmeister, T. Enzyme Kinetics and Hit Validation in Fluorimetric Protease Assays. *Curr. Top. Med. Chem.* **2010**, *10*, 368 382.
(35) Berman, H. M.; Westbrook, J.; Feng, Z.; Gilliland, G.; Bhat, T. N.; Weissig, H.; Shindyalov, I. N.; Bourne, P. E. The Protein Data Bank. *Nucleic Acids Res.* **2000**, *28*, 235 242.
(36) Hardegger, L. A.; Kuhn, B.; Spinnler, B.; Anselm, L.; Ecabert, R.; Stihle, M.; Gsell, B.; Thoma, R.; Diez, J.; Benz, J.; Plancher, J. M.; Hartmann, G.; Banner, D. W.; Haap, W.; Diederich, F. Systematic Investigation of Halogen Bonding in Protein-Ligand Interactions. *Angew. Chem., Int. Ed.* **2011**, *50*, 314 318.
(37) Mirković, B.; Renko, M.; Turk, S.; Sosič, I.; Jevnikar, Z.; Obermajer, N.; Turk, D.; Gobec, S.; Kos, J. Novel Mechanism of Cathepsin B Inhibition by Antibiotic Nitroxoline and Related Compounds. *ChemMedChem* **2011**, *6*, 1351 1356.
(38) Illy, C.; Quraishi, O.; Wang, J.; Purisima, E.; Vernet, T.; Mort, J. S. Role of the Occluding Loop in Cathepsin B Activity. *J. Biol. Chem.* **1997**, *272*, 1197 1202.
(39) Zehl, M.; Allmaier, G. n. Investigation of Sample Preparation and Instrumental Parameters in the Matrix-Assisted Laser Desorption/Ionization Time-of-Flight Mass Spectrometry of Noncovalent Peptide/Peptide Complexes. *Rapid Commun. Mass Spectrom.* **2003**, *17*, 1931 1940.
(40) Salih, B.; Zenobi, R. MALDI Mass Spectrometry of Dye - Peptide and Dye - Protein Complexes. *Anal. Chem.* **1998**, *70*, 1536 1543.
(41) Woods, A. S.; Huestis, M. A. A Study of Peptide-Peptide Interaction by Matrix-Assisted Laser Desorption/Ionization. *J. Am. Soc. Mass Spectrom.* **2001**, *12*, 88 96.
(42) Heck, A. J. R.; van den Heuvel, R. H. H. Investigation of Intact Protein Complexes by Mass Spectrometry. *Mass Spectrom. Rev.* **2004**, *23*, 368 389.
(43) Laugesen, S.; Roepstorff, P. Combination of Two Matrices Results in Improved Performance of MALDI MS for Peptide Mass Mapping and Protein Analysis. *J. Am. Soc. Mass Spectrom.* **2003**, *14*, 992 1002.
(44) Klein, P.; Johe, P.; Wagner, A.; Jung, S.; Kuhlborn, J.; Barthels, F.; Tenzer, S.; Distler, U.; Waigel, W.; Engels, B.; Hellmich, U. A.; Opatz, T.; Schirmeister, T. New Cysteine Protease Inhibitors: Electrophilic (Het)Arenes and Unexpected Prodrug Identification for the Trypanosoma Protease Rhodesain. *Molecules* **2020**, *25*, 1451.
(45) Whittal, R. M.; Li, L. High-Resolution Matrix-Assisted Laser Desorption/Ionization in a Linear Time-of-Flight Mass Spectrometer. *Anal. Chem.* **1995**, *67*, 1950 1954.
(46) Bahr, U.; Stahl-Zeng, J.; Gleitsmann, E.; Karas, M. Delayed Extraction Time-of-Flight MALDI Mass Spectrometry of Proteins above 25 000 Da. *J. Mass Spectrom.* **1997**, *32*, 1111 1116.
(47) Kollmeier, A. S.; de la Torre, X.; Muller, C.; Botrè, F.; Parr, M. K. In-Depth Gas Chromatography/Tandem Mass Spectrometry Fragmentation Analysis of Formestane and Evaluation of Mass Spectral Discrimination of Isomeric 3-Keto-4-Ene Hydroxy Steroids. *Rapid Commun. Mass Spectrom.* **2020**, *34*, No. e8937.

https://doi.org/10.1021/acs.jmedchem.1c01002
J. Med. Chem. 2021, 64, 12322 12358

(48) Mladenovic, M.; Ansorg, K.; Fink, R. F.; Thiel, W.; Schirmeister, T.; Engels, B. Atomistic Insights into the Inhibition of Cysteine Proteases: First QM/MM Calculations Clarifying the Stereoselectivity of Epoxide-Based Inhibitors. *J. Phys. Chem. B* **2008**, *112*, 11798 11808.
(49) Mladenovic, M.; Junold, K.; Fink, R. F.; Thiel, W.; Schirmeister, T.; Engels, B. Atomistic Insights into the Inhibition of Cysteine Proteases: First QM/MM Calculations Clarifying the Regiospecificity and the Inhibition Potency of Epoxide- and Aziridine-Based Inhibitors. *J. Phys. Chem. B* **2008**, *112*, 5458 5469.
(50) Vicik, R.; Busemann, M.; Gelhaus, C.; Stiefl, N.; Scheiber, J.; Schmitz, W.; Schulz, F.; Mladenovic, M.; Engels, B.; Leippe, M.; Baumann, K.; Schirmeister, T. Aziridide-Based Inhibitors of Cathepsin L: Synthesis, Inhibition Activity, and Docking Studies. *ChemMedChem* **2006**, *1*, 1126 1141.
(51) Muller, K.; Faeh, C.; Diederich, F. Fluorine in Pharmaceuticals: Looking beyond Intuition. *Science* **2007**, *317*, 1881 1886.
(52) Tosstorff, A.; Cole, J. C.; Taylor, R.; Harris, S. F.; Kuhn, B. Identification of Noncompetitive Protein-Ligand Interactions for Structural Optimization. *J. Chem. Inf. Model.* **2020**, *60*, 6595 6611.
(53) Maeda, S.; Harabuchi, Y.; Ono, Y.; Taketsugu, T.; Morokuma, K. Intrinsic Reaction Coordinate: Calculation, Bifurcation, and Automated Search. *Int. J. Quantum Chem.* **2015**, *115*, 258 269.
(54) Vicik, R.; Hoerr, V.; Glaser, M.; Schultheis, M.; Hansell, E.; McKerrow, J. H.; Holzgrabe, U.; Caffrey, C. R.; Ponte-Sucre, A.; Moll, H.; Stich, A.; Schirmeister, T. Aziridine-2,3-Dicarboxylate Inhibitors Targeting the Major Cysteine Protease of Trypanosoma Brucei as Lead Trypanocidal Agents. *Bioorg. Med. Chem. Lett.* **2006**, *16*, 2753 2757.
(55) Ettari, R.; Pinto, A.; Previti, S.; Tamborini, L.; Angelo, I. C.; la Pietra, V.; Marinelli, L.; Novellino, E.; Schirmeister, T.; Zappalà, M.; Grasso, S.; de Micheli, C.; Conti, P. Development of Novel Dipeptide-like Rhodesain Inhibitors Containing the 3-Bromoisoxazoline Warhead in a Constrained Conformation. *Bioorg. Med. Chem.* **2015**, *23*, 7053 7060.
(56) Wagner, A.; Le, T. A.; Brennich, M.; Klein, P.; Bader, N.; Diehl, E.; Paszek, D.; Weickhmann, A. K.; Dirdjaja, N.; Krauth-Siegel, R. L.; Engels, B.; Opatz, T.; Schindelin, H.; Hellmich, U. A. Inhibitor-Induced Dimerization of an Essential Oxidoreductase from African Trypanosomes. *Angew. Chem., Int. Ed.* **2019**, *58*, 3640 3644.
(57) Previti, S.; Ettari, R.; Cosconati, S.; Amendola, G.; Chouchene, K.; Wagner, A.; Hellmich, U. A.; Ulrich, K.; Krauth-Siegel, R. L.; Wich, P. R.; Schmid, I.; Schirmeister, T.; Gut, J.; Rosenthal, P. J.; Grasso, S.; Zappalà, M. Development of Novel Peptide-Based Michael Acceptors Targeting Rhodesain and Falcipain-2 for the Treatment of Neglected Tropical Diseases (NTDs). *J. Med. Chem.* **2017**, *60*, 6911 6923.
(58) Mellott, D. M.; Tseng, C.-T.; Drelich, A.; Fajtová, P.; Chenna, B. C.; Kostomiris, D. H.; Hsu, J.; Zhu, J.; Taylor, Z. W.; Kocurek, K. I.; Tat, V.; Katzfuss, A.; Li, L.; Giardini, M. A.; Skinner, D.; Hirata, K.; Yoon, M. C.; Beck, S.; Carlin, A. F.; Clark, A. E.; Beretta, L.; Maneval, D.; Hook, V.; Frueh, F.; Hurst, B. L.; Wang, H.; Raushel, F. M.; O'Donoghue, A. J.; de Siqueira-Neto, J. L.; Meek, T. D.; McKerrow, J. H. A Clinical-Stage Cysteine Protease Inhibitor Blocks SARS-CoV-2 Infection of Human and Monkey Cells. *ACS Chem. Biol.* **2021**, *16*, 642 650.
(59) Jacobsen, W.; Christians, U.; Benet, L. Z. In Vitro Evaluation of the Disposition of a Novel Cysteine Protease Inhibitor. *Drug Metab. Dispos.* **2000**, *28*, 1343 1351.
(60) *Molecular Operating Environment (MOE)|MOEsaic|PSILO*; Chemical Computing Group Inc.: Montreal, QC, Canada, 2014.
(61) Lei, X.; Jalla, A.; Abou Shama, M.; Stafford, J.; Cao, B. Chromatography-Free and Eco-Friendly Synthesis of Aryl Tosylates and Mesylates. *Synthesis* **2015**, *47*, 2578 2585.
(62) Stokes, B. J.; Liu, S.; Driver, T. G. Rh2(II)-Catalyzed Nitro-Group Migration Reactions: Selective Synthesis of 3-Nitroindoles from β-Nitro Styryl Azides. *J. Am. Chem. Soc.* **2011**, *133*, 4702 4705.
(63) Scheidt, K. A.; Roush, W. R.; McKerrow, J. H.; Selzer, P. M.; Hansell, E.; Rosenthal, P. J. Structure-Based Design, Synthesis and Evaluation of Conformationally Constrained Cysteine Protease Inhibitors. *Bioorg. Med. Chem.* **1998**, *6*, 2477 2494.
(64) Ivkovic, J.; Lembacher-Fadum, C.; Breinbauer, R. A Rapid and Efficient One-Pot Method for the Reduction of N-Protected α-Amino Acids to Chiral α-Amino Aldehydes Using CDI/DIBAL-H. *Org. Biomol. Chem.* **2015**, *13*, 10456 10460.
(65) White, J. D.; Xu, Q.; Lee, C.-S.; Valeriote, F. A. Total Synthesis and Biological Evaluation of (+)-Kalkitoxin, a Cytotoxic Metabolite of the Cyanobacterium Lyngbya Majuscula. *Org. Biomol. Chem.* **2004**, *2*, 2092 2102.
(66) Weissenborn, M. J.; Wehner, J. W.; Gray, C. J.; Šardzík, R.; Eyers, C. E.; Lindhorst, T. K.; Flitsch, S. L. Formation of Carbohydrate-Functionalised Polystyrene and Glass Slides and Their Analysis by MALDI-TOF MS. *Beilstein J. Org. Chem.* **2012**, *8*, 753 762.
(67) Andrei, D.; Wnuk, S. F. Synthesis of the Multisubstituted Halogenated Olefins via Cross-Coupling of Dihaloalkenes with Alkylzinc Bromides. *J. Org. Chem.* **2006**, *71*, 405 408.
(68) Millies, B.; von Hammerstein, F.; Gellert, A.; Hammerschmidt, S.; Barthels, F.; Göppel, U.; Immerheiser, M.; Elgner, F.; Jung, N.; Basic, M.; Kersten, C.; Kiefer, W.; Bodem, J.; Hildt, E.; Windbergs, M.; Hellmich, U. A.; Schirmeister, T. Proline-Based Allosteric Inhibitors of Zika and Dengue Virus NS2B/NS3 Proteases. *J. Med. Chem.* **2019**, *62*, 11359 11382.
(69) Schneider, N.; Lange, G.; Hindle, S.; Klein, R.; Rarey, M. A Consistent Description of HYdrogen Bond and DEhydration Energies in Protein-Ligand Complexes: Methods behind the HYDE Scoring Function. *J. Comput.-Aided Mol. Des.* **2013**, *27*, 15 29.
(70) Reulecke, I.; Lange, G.; Albrecht, J.; Klein, R.; Rarey, M. Towards an Integrated Description of Hydrogen Bonding and Dehydration: Decreasing False Positives in Virtual Screening with the HYDE Scoring Function. *ChemMedChem* **2008**, *3*, 885 897.
(71) Halgren, T. A. Merck Molecular Force Field. I. Basis, Form, Scope, Parameterization, and Performance of MMFF94. *J. Comput. Chem.* **1996**, *17*, 490 519.
(72) Maier, J. A.; Martinez, C.; Kasavajhala, K.; Wickstrom, L.; Hauser, K. E.; Simmerling, C. Ff14SB: Improving the Accuracy of Protein Side Chain and Backbone Parameters from Ff99SB. *J. Chem. Theory Comput.* **2015**, *11*, 3696 3713.
(73) Neudert, G.; Klebe, G. DSX: A Knowledge-Based Scoring Function for the Assessment of Protein-Ligand Complexes. *J. Chem. Inf. Model.* **2011**, *51*, 2731 2745.
(74) Marinas, M.; Sa, E.; Rojas, M. M.; Moalem, M.; Urbano, F. J.; Guillou, C.; Rallo, L. A Nuclear Magnetic Resonance (1 H and 13 C) and Isotope Ratio Mass Spectrometry (d 13 C , d 2 H and d 18 O) Study of Andalusian Olive Oils. *Rapid Commun. Mass Spectrom.* **2010**, *24*, 1457 1466.
(75) Wang, J.; Wolf, R. M.; Caldwell, J. W.; Kollman, P. A.; Case, D. A. Development and Testing of a General Amber Force Field. *J. Comput. Chem.* **2004**, *25*, 1157 1174.
(76) Jorgensen, W. L.; Chandrasekhar, J.; Madura, J. D.; Impey, R. W.; Klein, M. L. Comparison of Simple Potential Functions for Simulating Liquid Water. *J. Chem. Phys.* **1983**, *79*, 926 935.
(77) Ryckaert, J.-P.; Ciccotti, G.; Berendsen, H. J. C. Numerical Integration of the Cartesian Equations of Motion of a System with Constraints: Molecular Dynamics of n-Alkanes. *J. Comput. Phys.* **1977**, *23*, 327 341.
(78) Berendsen, H. J. C.; Postma, J. P. M.; van Gunsteren, W. F.; Dinola, A.; Haak, J. R. Molecular Dynamics with Coupling to an External Bath. *J. Chem. Phys.* **1984**, *81*, 3684 3690.
(79) Frisch, M. J.; Trucks, G. W.; Schlegel, H. B.; Scuseria, G. E.; Robb, M. A.; Cheeseman, J. R.; Scalmani, G.; Barone, V.; Petersson, G. A.; Nakatsuji, H.; Li, X.; Caricato, M.; Marenich, A. V.; Bloino, J.; Janesko, B. G.; Gomperts, R.; Mennucci, B.; Hratchian, H. P.; Ortiz, J. V.; Izmaylov, A. F.; Sonnenberg, J. L.; Ding, F.; Lipparini, F.; Egidi, F.; Goings, J.; Peng, B.; Petrone, A.; Henderson, T.; Ranasinghe, D.; Zakrzewski, V. G.; Gao, J.; Rega, N.; Zheng, G.; Liang, W.; Hada, M.; Ehara, M.; Fukuda, R.; Hasegawa, J.; Ishida, M.; Nakajima, T.; Honda, Y.; Kitao, O.; Nakai, H.; Vreven, T.; Throssell, K.; Montgomery, J. A., Jr.; Peralta, J. E.; Ogliaro, F.; Bearpark, M. J.; Heyd, J. J.; Brothers, E. N.; Kudin, K. N.; Staroverov, V. N.; Keith, T. A.; Kobayashi, R.; Normand, J.; Raghavachari, K.; Rendell, A. P.; Burant, J. C.; Iyengar, S. S.; Tomasi, J.; Cossi, M.; Millam, J. M.; Klene, M.; Adamo, C.; Cammi, R.; Ochterski, J. W.; Martin, R. L.; Morokuma, K.; Farkas, O.; Foresman, J.

https://doi.org/10.1021/acs.jmedchem.1c01002
J. Med. Chem. 2021, 64, 12322 12358

B.; Fox, D. J. *Gaussian 16*, Rev. C.01; Gaussian Inc., Wallingford, CT, 2016.
(80) Hariharan, P. C.; Pople, J. A. The Influence of Polarization Functions on Molecular Orbital Hydrogenation Energies. *Theor. Chim. Acta* **1973**, *28*, 213 222.
(81) Chai, J.-D.; Head-Gordon, M. Long-Range Corrected Hybrid Density Functionals with Damped Atom-Atom Dispersion Corrections. *Phys. Chem. Chem. Phys.* **2008**, *10*, 6615 6620.
(82) Ditchfield, R.; Hehre, W. J.; Pople, J. A. Self-Consistent Molecular-Orbital Methods. IX. An Extended Gaussian-Type Basis for Molecular-Orbital Studies of Organic Molecules. *J. Chem. Phys.* **1971**, *54*, 724.
(83) Tao, P.; Schlegel, H. B. A Toolkit to Assist ONIOM Calculations. *J. Comput. Chem.* **2010**, *31*, 2363 2369.
(84) Li, X.; Frisch, M. J. Energy-Represented Direct Inversion in the Iterative Subspace within a Hybrid Geometry Optimization Method. *J. Chem. Theory Comput.* **2006**, *2*, 835 839.
(85) Biebinger, S.; Elizabeth Wirtz, L.; Lorenz, P.; Christine Clayton, C. Vectors for Inducible Expression of Toxic Gene Products in Bloodstream and Procyclic Trypanosoma Brucei. *Mol. Biochem. Parasitol.* **1997**, *85*, 99 112.
(86) Cunningham, M. P.; Vickerman, K. Antigenic Analysis in the Trypanosoma Brucei Group, Using the Agglutination Reaction. *Trans. R. Soc. Trop. Med. Hyg.* **1962**, *56*, 48 59.
(87) Klein, P.; Barthels, F.; Johe, P.; Wagner, A.; Tenzer, S.; Distler, U.; Le, T. A.; Schmid, P.; Engel, V.; Engels, B.; Hellmich, U. A.; Opatz, T.; Schirmeister, T. Naphthoquinones as Covalent Reversible Inhibitors of Cysteine Proteases-Studies on Inhibition Mechanism and Kinetics. *Molecules* **2020**, *25*, 2064.
(88) Barthels, F.; Marincola, G.; Marciniak, T.; Konhäuser, M.; Hammerschmidt, S.; Bierlmeier, J.; Distler, U.; Wich, P. R.; Tenzer, S.; Schwarzer, D.; Ziebuhr, W.; Schirmeister, T. Asymmetric Disulfanylbenzamides as Irreversible and Selective Inhibitors of Staphylococcus Aureus Sortase A. *ChemMedChem* **2020**, *15* (10), 839 850.
(89) Mnova 12.0.4 Mestrelab. https://mestrelab.com/download_file/mnova-12-0-4/ (accessed May 3, 2021).
(90) Lietsche, J.; Gorka, J.; Hardt, S.; Karas, M.; Klein, J. Custom-Made Microdialysis Probe Design. *J. Visualized Exp.* **2015**, *2015*, 53048.
(91) Buttner-Ennever, J. *The Rat Brain in Stereotaxic Coordinates*, 3; Paxinos, G.; Watson, C.; Academic Press: San Diego, 1996; Journal of Anatomy 1997, Vol. *191* (2), pp 315 317.

https://doi.org/10.1021/acs.jmedchem.1c01002
J. Med. Chem. 2021, 64, 12322 12358

1.3 Perspectives

In this project, we were able to design new inhibitors for the parasitic cysteine protease rhodesain. Unlike previously published inhibitors,[176,198,231] the new compounds are covalent-reversible with lead compound **2d** as a slow-tight binder. This innovative characteristic provides a solution to the limitations associated with conventional covalent drugs, such as haptenization, off-target effects, and toxicity, while still preserving their benefits, such as longer residence times, reduced dosages, and increased efficiency.[246] Of particular significance, one of the optimized inhibitors (**2d-(H)**) has demonstrated the ability to cross the blood-brain barrier (BBB), offering a promising starting point for future optimizations in the fight against HAT.

To obtain more information on the pharmacokinetic properties, additional organs and tissues should be investigated. In particular, the liver would be interesting to gain more insights into the complete metabolism and possible first-pass effects. Analysis of CYP enzymes involved could predict potential drug-drug interactions. Prodrug strategies could also extend the compounds' half-life, especially if first-pass effects occur or to improve cell permeability.

Cell permeability is another major parameter to investigate. Caco-2 or PAMPA assays could provide valuable information on this matter, particularly on passive diffusion. However, several transporter mechanisms exist for CNS penetration when passive diffusion is not sufficient, such as carrier-mediated transport (e.g., GLUT1, LAT1, MCT1, CNT2).[88,263] By incorporating targeting structures for such carriers in P3, our inhibitors' BBB crossing could be improved. Another possibility would be a chemical drug delivery system (CDS) that links a biodegradable lipophilic targetor moiety (e.g., 1,4-dihydro-*N*-methylnicotinic acid) to the desired compound via hydroxyl groups.[264] This construct would be more lipophilic and thus, accumulate in brain tissue, where the targetor moiety would be oxidized to a cationic intermediate. The positive charge traps the construct inside the brain, where the active agent is slowly released by hydrolysis, followed by a readily removal of the targetor moiety via active processes. Since there are also many efflux transporters that could affect CNS penetration, it would be intruiging to see if some of our compounds are substrates for P-glycoprotein or other efflux pumps.

Finally, targeted delivery of our inhibitors to trypanosomes could further improve their efficacy, e.g., by coupling them to aptamers that bind to *T. brucei*'s membrane and are transported to the lysosome, where they could release the active agent.[265]

2 Dual Strategy to Design New Agents Targeting *Schistosoma mansoni*: Advancing Phenotypic and *Sm*CB1 Inhibitors for Improved Efficacy

2.1 Summary and Own Contribution

This project was part of an Open Lab Initiative with [redacted].

Schistosomiasis, also known as “snail fever”, is a parasitic disease caused by flatworms of the genus *Schistosoma,* e.g., *Schistosoma mansoni*. It is considered a neglected tropical disease, affecting more than 200 million people worldwide, mainly in sub-Saharan Africa, but also in parts of South America, the Caribbean, and Southeast Asia.[266] Schistosomiasis is a chronic illness that can lead to long-term health problems, including damage to the liver, spleen, and bladder, as well as increased susceptibility to other infections.[266,267] Praziquantel (**PZQ**) is currently the drug of choice to treat schistosomiasis. It is a safe and effective medication that targets Ca^{2+} channels, paralyzing the worms, which allows the body to expel them naturally.[268] However, there have been reports of reduced sensitivity to **PZQ** in some areas, which is concerning given the reliance on this drug in schistosomiasis treatment.[269] The emergence of drug-resistant *Schistosoma* strains highlights the need for continued research into new treatments and approaches to control the spread of the disease.[270]

The parasite’s major cysteine protease, *Schistosoma mansoni* cathepsin B1 (*Sm*CB1), is a promising target for new schistosomiasis treatments. Inhibitors of this enzyme have shown efficacy in preclinical studies and offer the potential to disrupt the parasite's ability to feed and grow, while minimizing the risk of resistance development due to the enzyme's essential function.[195,254]

In this project, we focused on finding new covalent *Sm*CB1 inhibitors based on the results of an in-house screening (enzyme inhibition and phenotypic assay). We then optimized the lead scaffolds towards better effectivity against the larvae, so called newly transformed schistosomula (NTS), and the adult worms, with emphasis on improving the physicochemical parameters. The workflow for this project is depicted in **Figure 20**.

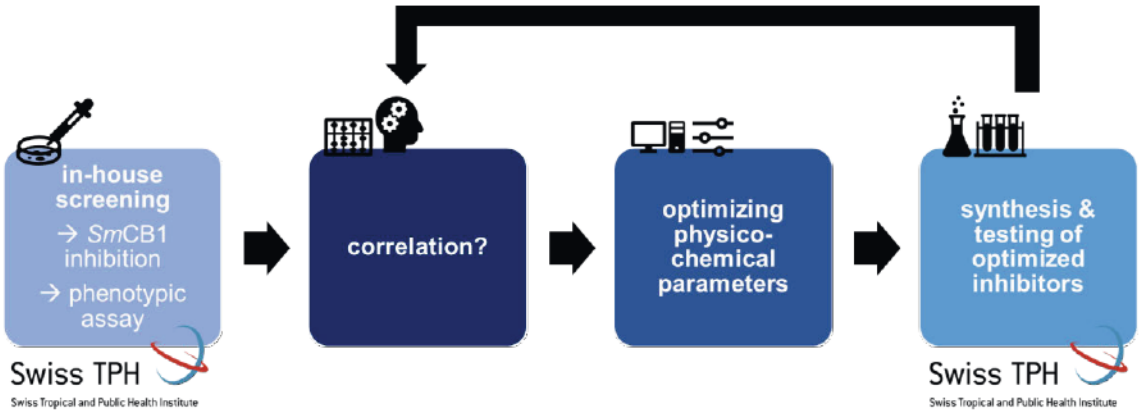

Figure 20. Workflow for project 2.

We evaluated the in-house screening data by correlation analysis and picked lead structures for a dual approach. Then, we optimized these leads, synthesized, and tested them in collaboration with the SWISS TROPICAL HEALTH INSTITUTE.

The results of the project are presented in the following preliminary manuscript, titled "Dual Strategy to Design New Agents Targeting *Schistosoma mansoni*: Advancing Phenotypic and *Sm*CB1 Inhibitors for Improved Efficacy" to be submitted for publication in *ACS Infectious Diseases* after inserting pending permeability data.

Own contribution: fluorometric assay establishment and K_m determination with [redacted], in-house screening for *Sm*CB1 inhibition with [redacted], correlation analysis, design and synthesis of optimized compounds **2a–q**, calculating physicochemical properties, testing optimized inhibitors **2a–q** against *Sm*CB1, writing main part of the manuscript, writing parts of the supporting information, preparing tables (2, 3), and figures (1, 2, 4–7, graphical abstract).

Contribution from others: *Sm*CB1 expression and purification, *Sm*CB1 activation protocol, phenotypic assays, design and synthesis of optimized compounds **1a–m**, testing compounds **1a–m**, writing parts of the manuscript and supporting information, preparing table 1 and figure 3.

2.2 Manuscript

Dual Strategy to Design New Agents Targeting *Schistosoma mansoni*: Advancing Phenotypic and *Sm*CB1 Inhibitors for Improved Efficacy

Natalie Fuchs,[1‡] [redacted],[1‡] [redacted],[1‡] [redacted],[1] [redacted],[1] [redacted],[1] [redacted],[1] [redacted],[2] [redacted],[1] and [redacted][1*]

[1] *Institute of Pharmaceutical and Biomedical Sciences, Johannes Gutenberg University Mainz, Staudingerweg 5, 55128 Mainz, Germany.*

[2] *Swiss Tropical and Public Health Institute, Kreuzstrasse 2, 4123 Allschwil, Switzerland.*

**All correspondence to Prof. Dr. Tanja Schirmeister, schirmei@uni-mainz.de.*

‡*N. F., R. A. Z., and M. S. contributed equally.*

ABSTRACT

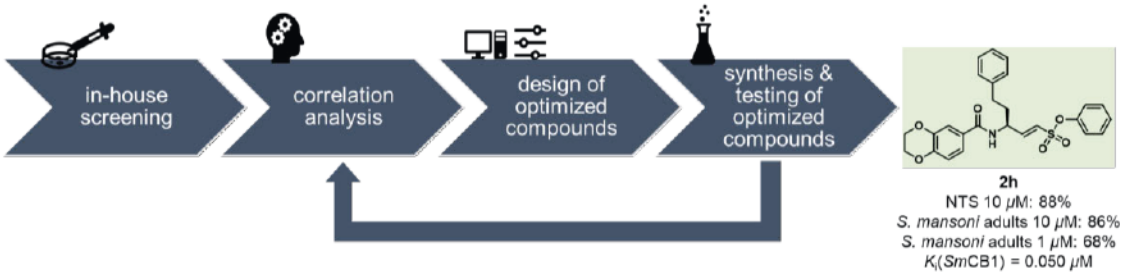

In this study, we have identified and optimized two lead structures from an in-house screening, with promising results against the parasitic flatworm *Schistosoma mansoni* and/or its target protease *S. mansoni* cathepsin B1 (*Sm*CB1). Our correlation analysis highlighted the significance of physicochemical properties for the compounds' efficacy, resulting in a dual approach to optimize the lead structures regarding both phenotypic effects and *Sm*CB1 inhibition. The optimized compounds from both approaches ("phenotypic" vs "*Sm*CB1" approach) demonstrated improved efficacy against *S. mansoni* adult worms, with **2h** from the "*Sm*CB1" approach emerging as the most potent compound. **2h** displayed nanomolar inhibition against *Sm*CB1 (K_i = 0.050 μM) while maintaining selectivity towards human off-target cathepsins, and

greatly improved efficacy towards *S. mansoni* adults (86% at 10 μM, 68% at 1 μM), demonstrating potential as a new therapeutic agent for schistosomiasis.

ABBREVIATIONS

ACN, acetonitrile; AMC, 7-amino-4-methylcoumarin; aq., aqueous; Boc, *tert*-butyl carbamoyl; CatB, human cathepsin B; CatL, human cathepsin L; CH, cyclohexane; cpd, compound; DCM, dichloromethane; DECP, diethyl chlorophosphate; DHBD, 2,3-dihydrobenzo[*b*][1,4]dioxine; DIPEA, *N,N*-diisopropylethylamine; DMF, dimethylformamide; DTT, dithiothreitol; EA, ethyl acetate; EDTA, ethylenediamine tetraacetic acid; eq., equivalent; ESI, electrospray ionization; HIC, hydrophobic interaction chromatography; HOBt, 1-hydroxybenzotriazole; hPhe, homophenylalanine; HWE, Horner-Wadsworth-Emmons; KHMDS, potassium bis(trimethylsilyl)amide; LHMDS, lithium bis(trimethylsilyl)amide; Me, methyl; MOE, Molecular Operating Environment; NTS, newly transformed schistosomula; ppm, parts per million; SI, selectivity index; *Sm*CB1, *Schistosoma mansoni* cathepsin B1; SD, standard deviation; TBTU, 2-(1*H*-benzotriazole-1-yl)-1,1,3,3-tetramethylaminium tetrafluoroborate; TEA, triethyl amine; THF, tetrahydrofuran; TPSA, topological polar surface area.

INTRODUCTION

Schistosomiasis is an acute or chronic infectious disease, that can be caused by different species of the genus Schistosoma, a family of human blood flukes. More than 140 million patients are affected by this disease worldwide, most of them in sub-Saharan Africa.[1,2] Of all five *Schistosoma* species that can cause schistosomiasis in humans, *Schistosoma mansoni* is the most widespread, throughout Africa, the Middle East and even the Americas.[3] Infections can lead to intestinal or hepatic forms of schistosomiasis.[4] During its life cycle, *S. mansoni* depends on two different hosts, freshwater snails of the genus *Biomphalaria* for asexual replication and a mammalian host for sexual replication.[3] Upon completing asexual replication the snails release cercariae into the freshwater. These infectious cercariae penetrate human skin exposed to contaminated water and start their sexual replication within the human body. Over the next 5–7 weeks, this larval stage, called schistosomula, develops into matured schistosomes until they begin to mate.[3] Female schistosomes are capable to produce hundreds of eggs daily.[5,6] Egg migration into the intestinal lumen, where

they are excreted with faeces, completes the sexual reproduction process. Once released into freshwater, the eggs will hatch and release ciliated miracidia, which can now infect the snail hosts to begin asexual replication.[5] Fecal excretion of eggs is not quantitative, meaning that a considerable number of eggs remain in the human body. An early study with hamsters as mammalian hosts found that only ~20% eggs were found in faeces, while ~80% of the eggs remained in the body.[6] After 1–2 weeks, the eggs will die, independent if they reach freshwater.[3] The hundreds of trapped, partially dead, eggs in the human body can induce severe inflammatory reactions that may cause the full picture of the schistosomiasis disease.[7,8]

Today, the only approved drug for the treatment of schistosomiasis is praziquantel (**PZQ**). Although praziquantel was introduced in the 1970s, very few cases of resistance have been reported.[9] Until recently, even attempts to induce a resistance against **PZQ** in the laboratory has failed.[10] With a reported cure rate of ~ 90%, **PZQ** remains a powerful tool to fight schistosomiasis. Despite the achieved success, the actual mechanism of action remained elusive until 2021, when PARK AND CO-WORKERS demonstrated that the transient receptor potential melastatin ion channel is the target of praziquantel.[11] However, to control or even eradicate this disease, it seems necessary to pursue further drug development to also treat those patients who have shown resistance to **PZQ**. By focusing on additional targets that are vital to the parasite, an improved treatment could be accomplished. Recent publications have shown that the cathepsin B-like protease of *S. mansoni* (*Sm*CB1) presents a promising target for small molecular inhibitors, since its inhibition is lethal to *S. mansoni.*[12–14] Previous studies also showed that suppression of *Sm*CB1 activity in early stage schistosomula had a long-term effect on their growth and development, underlining a certain vulnerability, arising from this target.[15]

To date, several *Sm*CB1 inhibitors have been reported. One well-known example is the pan-cathepsin inhibitor **K11777** (IC_{50} = 0.0021 μM, k_{2nd} = 8.8 · 10^4 $M^{-1}s^{-1}$), an irreversible vinylsulfone.[16] It has proven to be efficient against schistosomes in mice, reducing both worm numbers and egg production.[14] Based on the **K11777** scaffold, JÍLKOVÁ AND CO-WORKERS have developed the potent irreversible *Sm*CB1 inhibitors **WRR-391** (IC_{50} = 0.2 nM, k_{2nd} = 2.1 · 10^5 $M^{-1}s^{-1}$) and **WRR-286** (IC_{50} = 0.6 nM, k_{2nd} = 2.0 · 10^5 $M^{-1}s^{-1}$).[13,16] The compounds are effective against newly transformed schistosomula (NTS) at concentrations of 10 μM for both and 1 μM for **WRR-286** after 72 hours.[13] Additionally, they introduced azapeptide nitriles as covalent-reversible *Sm*CB1 inhibitors with high efficacy against NTS.[12] However, their efficacy against *S. mansoni* adults has not yet been published.

In order to discover new potential anti-schistosomal compounds, we developed a workflow (see Graphical Abstract) starting with an in-house screening including 76 compounds, that provided us with lead structures (for all structures and data see **Supporting Information**) for a dual optimization approach. We then performed a correlation analysis of the entire screening data to obtain optimization ideas. From these ideas, we designed new compounds using molecular docking approaches and input from literature. We synthesized several optimized structures and tested them on the target enzyme as well as in the phenotypic assay.

RESULTS AND DISCUSSION

In-house screening.

We initiated our search for lead structures with anti-schistosomal activity by screening our in-house library including 76 compounds in a phenotypic assay on newly transformed schistosomula (NTS) and *S. mansoni* adults.[17] This library consisted of several cysteine-targeting inhibitors decorated with different covalent warheads, such as (F-)vinylsulfon(at)es, nitriles, aldehydes, 4-oxoenoates, nitroalkenes, and acrylamides.[18–23] In addition, we evaluated all compounds for their inhibitory effect on *Sm*CB1 using a fluorometric enzyme assay to analyze potential correlations with the results of the phenotypic assay. We determined IC_{50} and K_i values for all compounds with *Sm*CB1 inhibition >50% at 20 μM. In the phenotypic assay, all substances were initially analyzed at 10 μM on NTS. If an efficacy of >70% dead was achieved, a second screening was performed at 1 μM on NTS and at 10 μM on *S. mansoni* adults. Lower concentrations of 1 μM and 0.1 μM were tested on adult worms when 70% efficacy was achieved in the respective previous screening. A table with all data from the in-house screening can be found in the **Supporting Information**. The procedure of the initial screenings is described in **Figure 1**.

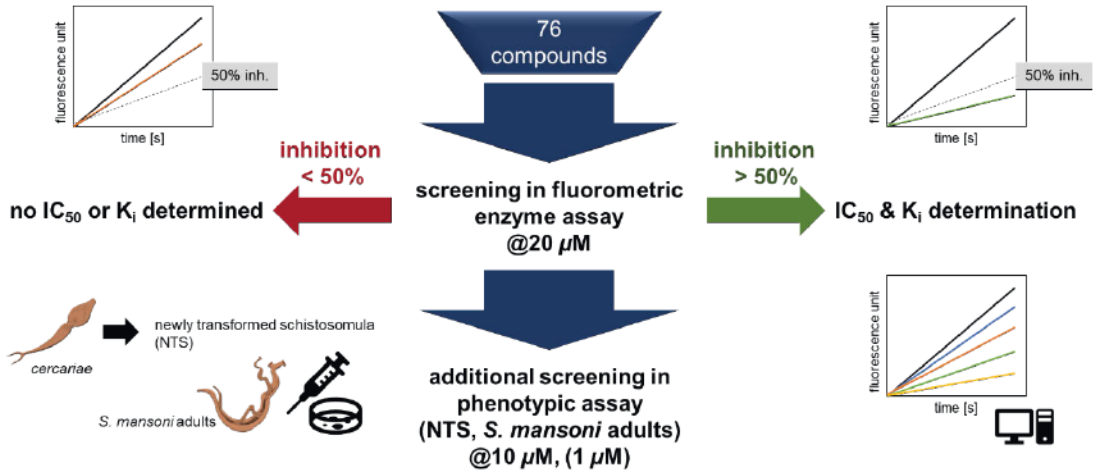

Figure 1. Workflow of the initial in-house screening. All compounds were screened for their *Sm*CB1 inhibition in a fluorometric enzyme assay as well as their efficacy in a phenotypic assay against NTS and adult worms.

The top three compounds (**KS309**, **SJ605**, **SJ606**) from the phenotypic screening against *S. mansoni* adults are shown in **Figure 2**. While two of them are vinylsulfonate-based inhibitors (**SJ605**, **SJ606**), originally developed for rhodesain,[19,20] the third is an 4-oxoenoate-based diastereomeric bortezomib congener (unpublished results). All three compounds are highly efficient against NTS at 10 µM (100% efficacy). Although **SJ605** and **SJ606** exhibit high *Sm*CB1 inhibition with K_i values in the low nanomolar range, only moderate efficacy against adult worms at 10 µM (55% for **SJ605**, 58% for **SJ606**) was achieved. In contrast, **KS309** shows weak inhibition of *Sm*CB1 (K_i >100 µM) but a strong effect on adult worms (76% at 10 µM, 29% at 1 µM) in the phenotypic assay, indicating that it addresses another target.

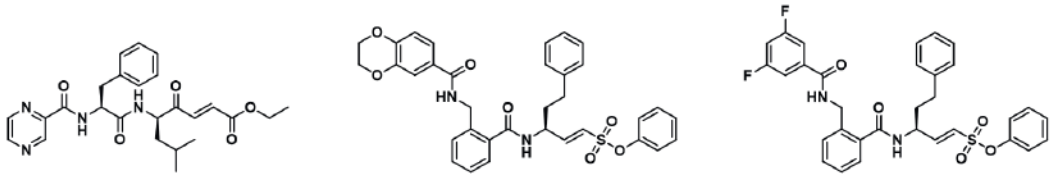

KS309
NTS 10 µM: 100%
S. mansoni adults 10 µM: 76%
K_i(*Sm*CB1) > 100 µM

SJ606
NTS 10 µM: 100%
S. mansoni adults 10 µM: 58%
K_i(*Sm*CB1) = 0.0034 µM

SJ605
NTS 10 µM: 100%
S. mansoni adults 10 µM: 55%
K_i(*Sm*CB1) = 0.0018 µM

Figure 2. Phentotypic screening of in-house library – top 3 compounds with screening results and K_i values.

Based on these findings, we pursued a dual strategy to increase the anti-schistosomal effect of both compound classes on adult *S. mansoni*. In order to maximize their effect, we focused primarily on improving their physicochemical properties, such as lipophilicity, since the substances have to pass two cell membranes to reach their

target site.[24] This resulted in two approaches, the "phenotypic" approach focusing on **KS309** derivatization and the "*Sm*CB1" approach including **SJ605**/**SJ606** derivatizations.

Chemistry.

The synthesis of compounds **1b–d**, and **1g**, **1i**, **1j** started from Boc-D-leucine (**Scheme 5** in the **Supporting Information**). Weinreb chemistry to generate the required aldehydes, phosphonate preparation followed by TBTU couplings, Boc group removals, and Horner-Wadsworth-Emmons reactions to form the *N*-methylated oxoenoate or vinylsulfonate were performed (detailed route in **Supporting Information**). The *N*-methylated oxoenoate **1a** (P2-*N*-Me-P1) was prepared analogously (**Scheme 6** in the **Supporting Information**).

The azapeptide **1k** was prepared starting from Cbz-L-phenylalanine which was brought to reaction with *tert*-butyl carbazate using TBTU coupling (**Scheme 7** in the **Supporting Information**). Cbz cleavage, TBTU couplings and Boc group removal led to a hydrazide that was alkylated in a two-step reductive amination (more details in **Supporting Information**). In the last step, reaction with ethyl fumaroyl chloride generated the final azapeptide **1k**. Propargyl and nitrile compounds **1e** and **1f** were prepared by the same synthetic pathway (**Scheme 8** in the **Supporting Information**).

The synthesis of the acrylamide decorated compound **1h** with inverted amide bonds was conducted starting from Boc-D-phenylalanine (**Scheme 9** in the **Supporting Information).** First, coupling with 2-aminopyrazine using COMU, followed by Boc deprotection led to an intermediate that was then reacted with Boc-L-leucine by TBTU coupling. After Boc group removal, the acrylamide function was introduced by reaction with acryloyl chloride yielding the final product **1h**.

The small molecule derivatives **1l** and **1m** were each prepared in a two-step synthesis (**Scheme 10** in the **Supporting Information**). Reaction of a Weinreb amide with vinylmagnesium bromide yielded an acryl derivative which was treated with ethyl acrylate using Hoveyda Grubbs II catalyst to give the final compound **1l**. The azapeptide analogue **1m** was prepared starting from a *tert*-butyl carbazate that was alkylated in a two-step reductive amination using isobutyraldehyde followed by treatment with Pd/C under hydrogen atmosphere. The resulting intermediate was then

reacted with ethyl fumaroyl chloride to yield the azapeptide analogue **1m** (detailed route in the **Supporting Information**).

The (F-)vinylsulfone- and -sulfonate-based inhibitors **2a–q** were synthesized as previously published. A schematic overview is shown in **Scheme 11** in the **Supporting Information.**[18,19,24]

Derivatization of KS309.

In our first approach, the "phenotypic approach", we investigated various changes in the structure of **KS309** (**Figure 3**). To increase lipophilicity, we reduced the number of hydrogen bond donors by methylating one of each of the amide bonds (**1a**, **1b**). Furthermore, the effect of replacing the polar pyrazinoyl moiety in P3 with more lipophilic Cbz (**1c**) and Boc (**1d**) groups was investigated as such modifications have also been shown to be effective in *Sm*CB1 inhibitor design.[12] Since 4-oxoenoates exhibit high reactivity, we tested alternative warheads such as propargylamide (**1e**), nitrile (**1f**), and vinylsulfonate (**1g**). To analyze the effect of inverted amide bonds, the acrylamide derivative **1h** was prepared. The precursors **1i** and **1j** of vinylsulfonate **1g** were also tested due to their higher lipophilicity. Synthesizing 4-oxoenoates and vinylsulfonates causes epimerization at P1. To avoid the separation of diastereomers at a later stage of the synthetic procedure, we prepared the P1 azapeptide derivative **1k** of **KS309**. In addition, small molecule derivatives (**1l**, **1m**) of **KS309** and **1k** were tested.

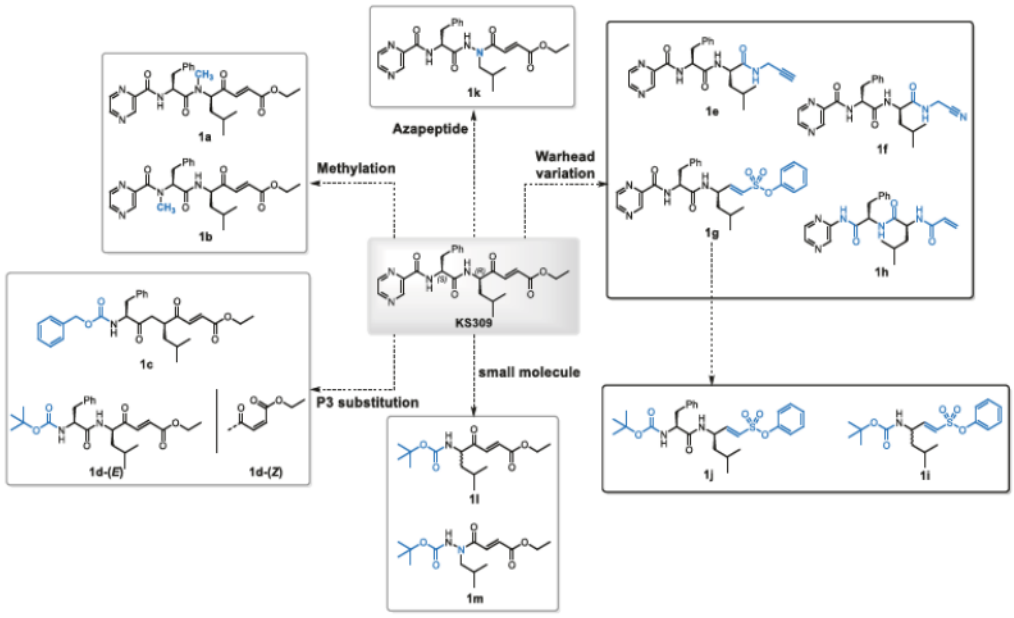

Figure 3. Derivatization of **KS309**.

The **KS309** derivatives were evaluated for their *Sm*CB1 inhibition as well as their efficacy on NTS and *S. mansoni* adults. The results are listed in **Table 1**. Additionally, calculated SlogP values and topological polar surface areas (TPSA) are given.

Regarding the results in **Table 1**, **1g**, **1i**, and **1j** showed higher efficacy on *S. mansoni* adults compared to **KS309** (93–100% vs 76% at 10 μM; 36–45% vs 29% at 1 μM). **1a**, **1b**, and **1d-(*E*)** caused slightly lower efficacy (61–65% at 10 μM), while all other compounds appeared to be distinctly less efficient (<60% at 10 μM). A correlation between the reduction in TPSA compared to **KS309** (<127 Å^2) and the increase in efficacy on adult worms could not be observed. Although **1i** and **1j** showed higher efficacy with TPSAs of 111 Å^2 and 82 Å^2, respectively, several compounds with TPSAs ranging from 82 Å^2 to 119 Å^2 (**1a–c**, **1d-(*E*)**, **1d-(*Z*)**, **1e** and **1h**) were less efficient.

Table 1. Physicochemical parameters and *in vitro* effects of **1a–m**.

Cpd	SlogP[a]	TPSA [Å^2]	*Sm*CB1 inhibition at 20 μM [%]	NTS effect [%]		*S. mansoni* adults effect [%]	
				at 10 μM	at 1 μM	at 10 μM	at 1 μM
KS309	2.04	127	58	100	23	76	29
1a	2.38	119	11	100	48	61	n. d.
1b	2.38	119	12	96	44	48	n. d.
1c	4.01	111	67	98	15	65	36
1d-(*E*)	3.34	111	42	100	78	61	n. d.
1d-(*Z*)	3.34	111	47	100	40	40	n. d.
1e	1.10	113	18	46	n. d.	n. d.	n. d.
1f	0.99	137	10	39	n. d.	n. d.	n. d.
1g	3.27	127	68	100	38	100	43
1h	1.86	113	9	48	n. d.	n. d.	n. d.
1i	3.85	82	9	98	27	93	36
1j	4.58	111	80	100	65	100	45
1k	1.45	131	17	50	33	47	n. d.
1l	2.61	82	7	100	14	58	n. d.
1m	2.03	85	3	61	32	34	n. d.

a: calculated using MOE 2019.01;[25]

On the other hand, a statistically significant correlation (described as correlation factor *r*) between SlogP value and efficacy on NTS at 10 μM could be observed (r = 0.84, p = 0.0001), suggesting that higher SlogP values result in higher efficacy (see **Table**

4, **Figure 2** in the **Supporting Information**). Compounds with SlogP values of ≥2.04 (**KS309**, **1a–c**, **1d-(*E*)**, **1d-(*Z*)**, **1g**, **1i**, **1j**, and **1l**) appeared to have an efficacy of at least 96%. For SlogP values ranging from 0.99 to 2.03, efficacy was only 39–61%. This correlation was also observed for *S. mansoni* adults at 10 μM (r = 0.69, p = 0.015). Overall, **1g** as well as its precursors **1i** and **1j** showed the highest efficacy in the compound series on both NTS and *S. mansoni* adults. Interestingly, **1g** and **1j** even exhibited stronger inhibition of *Sm*CB1 compared to **KS309** (68–80% vs 58% at 20 μM), albeit weak compared to the SJ600-series (**SJ605**/**SJ606**). Substituting the 4-oxoenoate warhead of **KS309** with a vinylsulfonate (**1g**) retained the same TPSA (127 Å^2) but increased the SlogP value (3.27 vs 2.04), which might have improved cell permeability. Furthermore, the vinylsulfonate might be less prone to off-target reactions compared to the highly reactive 4-oxoenoate substructure. Replacing the polar pyrazinoyl moiety of **1g** in P3 with a more lipophilic Boc group (**1j**) did not change efficacy, although it decreased the TPSA (111 Å^2 vs 127 Å^2) and increased the SlogP value (4.58 vs 3.27, **1g** and 2.04, **KS309**). In summary, the anti-schistosomal effect could be increased, however, the target of **KS309** derivatives remains unknown. Therefore, we did not further focus on the phenotypic approach by optimizing this series, but rather on the optimization of the **SJ605**/**SJ606** inhibitors as their effects appeared to correlate with *Sm*CB1 inhibition.

Correlations and hit optimizations.

Correlation analysis.

For correlations and optimization ideas, we started by calculating several important physicochemical parameters (logP, TPSA etc.) using MOE (see **Table 1** in **Supporting Information**).[25] We then performed a correlation analysis for each physicochemical parameter or the K_i values with the observed effects from phenotypic screening, including NTS (10 μM, 1 μM inhibitor) and *S. mansoni* adults (10 μM inhibitor). The resulting correlations are shown in **Table 2** in the Supporting Information with their respective p-values. Only p-values <0.05 are considered statistically significant.

There is a slight, but statistically significant, correlation between K_i values and the effect in the phenotypic screening against NTS at 1 μM (p = 0.025). The correlation factor (r) is negative (r = –0.43) implying that lower K_i values lead to a higher effect. The negative correlation for K_i and the effect on *S. mansoni* adults is not significant (p = 0.18). The adult worms seem to compensate the inhibition more effectively than

the NTS. It was reported earlier that several proteases are involved in the digestion of blood haemoglobin. One explanation for this observation could be that inhibition of *Sm*CB1 alone can be compensated by other proteases such as *S. mansoni* cathepsin D or cathepsin L. Since the expression levels of proteases fluctuate in different stages of development, adult worms may overcome inhibition of *Sm*CB1 more effectively than NTS.[15,26] Furthermore an additional second membrane has to be crossed in adult worms.[27] The positive correlation factor between SlogP and the effect against NTS (r = 0.44 at 1 μM) indicates that higher logP values are beneficial (p = 0.048, 0.021). TPSA and molecular flexibility (KierFlex) do not have a significant effect on the screening results.

Since two compounds from the SJ600s series (**SJ605**, **SJ606**) are among the top three, we decided to investigate a sub-set containing only these compounds (n = 16, results in **Table 3** in the **Supporting Information**). The compounds are known to be potent cysteine protease inhibitors with low cytotoxicity as reported by JUNG ET AL. (2022).[20] Again, there is a significant correlation (p = 0.005) between the K_i value for *Sm*CB1 and the effect against NTS at 10 μM inhibitor concentration (r = –0.67) like the correlation described above. The SlogP correlates with the effect against NTS at 10 μM (r = 0.66, p = 0.005) as well. Here, we have an additional correlation between the molecular flexibility (KierFlex) and the effect against NTS at 10 μM (r = –0.54, p = 0.032), suggesting that lower flexibility is advantageous. KIER's definition of flexibility is entirely structure-based upon molecular size, branching, cycles and number of heteroatoms.[28]

The significant correlations for the complete compound set and the SJ600 subgroup are shown in **Figure 4**, suggesting stronger correlations within the SJ600 subgroup as can also be drawn from the correlation factors (for example NTS 10 μM vs. K_i: all compounds r = −0.27 vs. SJ600s r = −0.67).

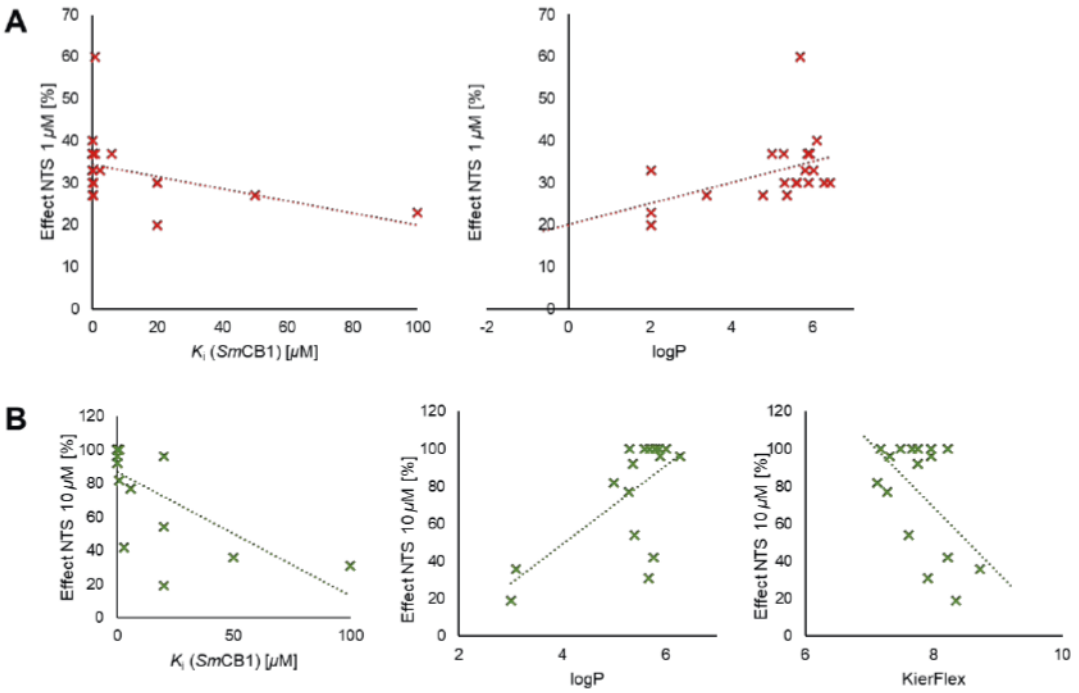

Figure 4. Correlations between K_i values or physicochemical parameters and the effect in the phenotypic screening. (**A**) All compounds (n = 76). Left: effect on NTS at 1 μM vs. K_i (*Sm*CB1) in μM in red (n = 27). Right: effect on NTS at 1 μM vs. logP in red (n = 27). (**B**) SJ600s (n = 16). Left: effect on NTS at 10 μM vs. K_i (*Sm*CB1) in μM in green (n = 16). Middle: effect on NTS at 10 μM vs. logP in green (n = 16). Right: effect on NTS at 10 μM vs. KierFlex in green (n = 16).

Inhibitor design.

The correlation analysis suggested that a higher rigidity results in a higher activity in the phenotypic assay (**Figure 4**, **Table 3** in the **Supporting Information**). Nevertheless, the *Sm*CB1 inhibition should not be compromised since it also correlates with the effect in NTS. **Figure 5** shows non-covalent docking poses (generated with LEADIT)[29] for lead structures **SJ605** (K_i = 1.8 nM) and **SJ606** (K_i = 3.4 nM) revealing that the most important interactions occur in the S1' and S1 subsites. Gly144 and Gly269 both interact with the amide group between P1 and P2, and Gln94 can form an H-bond with the sulfonyl-oxygen atom as well as Trp292. The residues in P2/P3 do not form essential interactions in the active site since the residues rather protrude from the binding site.

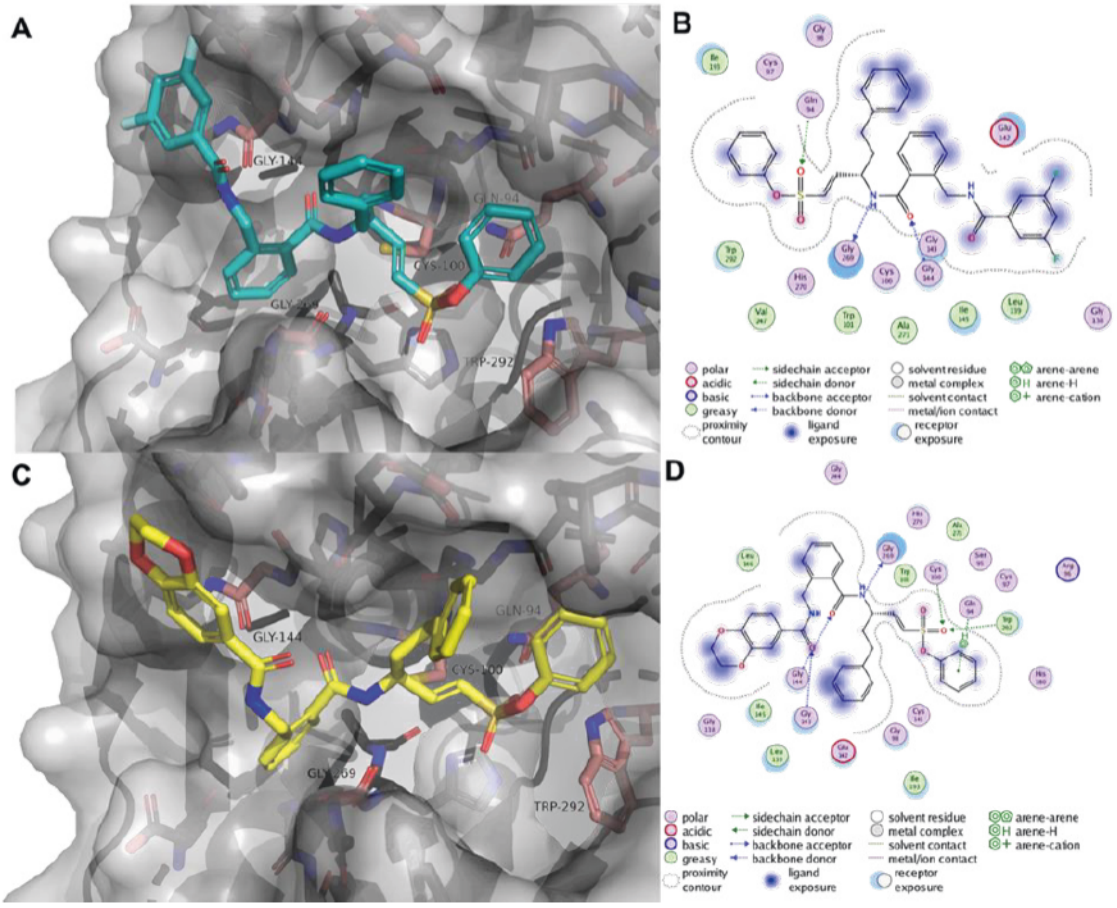

Figure 5. Non-covalent docking for lead compounds **SJ605** and **SJ606** with LEADIT.[29] Images generated using PYMOL.[30] Ligand interaction map generated with MOE.[25] PDB ID: 3s3r.[16] (**A**) Docking pose for **SJ605** (teal). Important interaction partner shown in salmon. Hyde score: – 34 kJ/mol. (**B**) Ligand interactions of **SJ605** with the *Sm*CB1 active site. (**C**) Docking pose for **SJ606** (yellow). Important interaction partners shown in salmon. Hyde score: –25 kJ/mol. (**D**) Ligand interactions of **SJ606** with the *Sm*CB1 active site.

Based on these interactions, we decided to modify P2/P3 while maintaining the P1' and P1 residues. To enhance rigidity, we chose various bi- or tricycles in P2, such as indole, 2,3-dihydrobenzo[*b*][1,4]dioxine (DHBD), and several others, resulting in compounds **2a–q** (**Figure 6**). We prepared corresponding irreversible vinylsulfones (**2b–f**) and -sulfonates (**2g–q**) as well as one compound with a reversible *α*-fluorovinylsulfone warhead (**2a**).

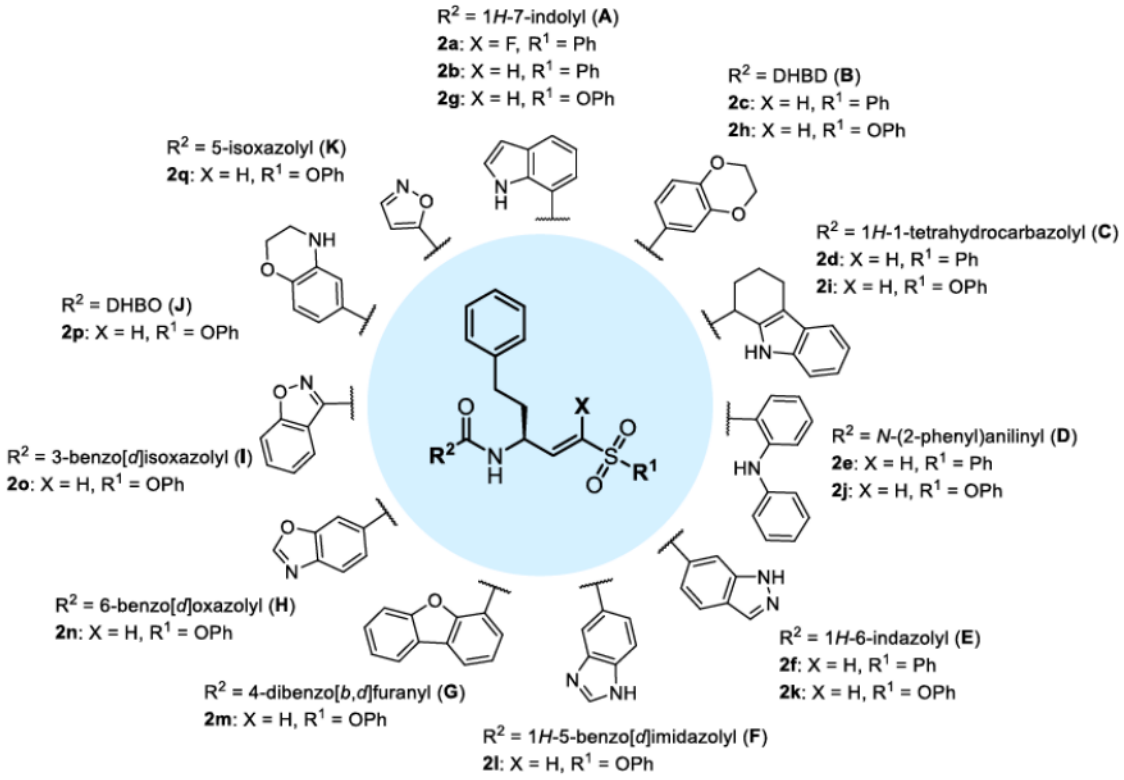

Figure 6. Optimized vinysulfon(at)e-based compounds **2a–q**.

*Sm*CB1 inhibition and structure-activity relationship.

Fluorometric enzyme assay.

We tested all compounds in a fluorometric enzyme assay to evaluate their inhibitory activity for *Sm*CB1 and their selectivity towards off-target cathepsins (procedures in **Supporting Information**). The results are shown in **Table 2**.

The vinylsulfone-based compounds are moderate *Sm*CB1 inhibitors with K_i values in the low micromolar range except for **2e** (K_i >100 μM). The covalent reaction occurs slowly (k_{inact} around 10^{-4} s^{-1}) and there is moderate selectivity towards cathepsins B and L. **2a**, an α-fluorovinylsulfone, is the only inhibitor in the series that reversibly inhibits the enzyme by a covalent-reversible Michael addition.[18,19] The K_i is in the same range as for the irreversible vinylsulfones with only little selectivity towards CatB and CatL.

Table 2. Inhibition data from fluorometric enzyme assay for (F-)vinylsulfon(at)es **2a–q**.

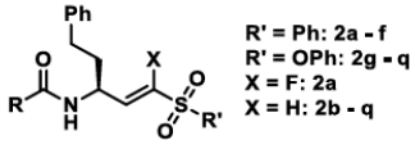

cpd	R	*Sm*CB1			CatB		CatL	
		K_i [μM]	k_{inact} [s^{-1}]	k_{2nd} [$M^{-1} s^{-1}$]	K_i [μM] or %inh @20 μM	SI	K_i [μM] or %inh @20 μM	SI
2a	A	5.8 ± 1.5	-	-	30%	> 3	45%	> 3
2b	A	4.7 ± 0.3	$1.1 \cdot 10^{-4}$	23	38%	> 4	n. i.	> 4
2c	B	6.7 ± 0.8	$2.3 \cdot 10^{-4}$	34	29%	> 3	24%	> 3
2d	C	2.2 ± 0.8	$1.6 \cdot 10^{-4}$	7.3	41%	> 9	41%	> 9
2e	D	> 100	n. d.	n. d.	28%	n. d.	30%	n. d.
2f	E	2.5 ± 0.6	$2.5 \cdot 10^{-4}$	10	22%	> 8	32%	> 8
2g	A	0.72 ± 0.005*	$1.8 \cdot 10^{-3}$	$2.5 \cdot 10^{3}$	n. i.	>28	43%	>28
2h	B	0.050 ± 0.003*	$7.0 \cdot 10^{-4}$	$1.4 \cdot 10^{4}$	29%	>400	37%	>400
2i	C	1.6 ± 0.36*	$3.0 \cdot 10^{-4}$	$1.9 \cdot 10^{2}$	31%	>13	28%	>13
2j	D	2.3 ± 1.0*	$5.0 \cdot 10^{-4}$	$2.2 \cdot 10^{2}$	20%	> 9	26%	>9
2k	E	0.83 ± 0.065*	$1.3 \cdot 10^{-3}$	$1.5 \cdot 10^{3}$	6.5 ± 1.0	7.8	0.54 ± 0.05	7.8
2l	F	0.078 ± 0.007*	$1.1 \cdot 10^{-3}$	$1.4 \cdot 10^{4}$	0.41 ± 0.06	5.3	4.8 ± 0.28	5.3
2m	G	> 100	n. d.	n. d.	n. i.	n. d.	20%	n. d.
2n	H	0.030 ± 0.020*	$2.4 \cdot 10^{-3}$	$8.0 \cdot 10^{4}$	1.0 ± 0.16	33	2.2 ± 0.19	73
2o	I	0.050 ± 0.030*	$1.8 \cdot 10^{-3}$	$3.6 \cdot 10^{4}$	48%	>400	0.37 ± 0.03	7.4
2p	J	0.41 ± 0.30*	$5.4 \cdot 10^{-3}$	$1.3 \cdot 10^{4}$	39%	>49	8.2 ± 2.1	20
2q	K	0.15 ± 0.040*	$2.8 \cdot 10^{-3}$	$1.8 \cdot 10^{4}$	0.26 ± 0.01	1.7	2.3 ± 0.23	15

n. d., not determined; n. i., no inhibition @20 μM inhibitor concentration; %inh @20 μM, mean inhibition in % from three independent measurements at 20 μM inhibitor concentration with SD <20%; SI, selectivity index. *time-dependent inhibition.

Table 2 also shows the inhibition data for vinylsulfonate-based compounds **2g–q**. Notably, their inhibitory potency has improved in all cases compared to the vinylsulfone counterparts, for example **2h** (K_i = 0.050 μM) vs **2c** (K_i = 6.7 μM). Since vinylsulfonates proved to be more potent *Sm*CB1 inhibitors, we designed and synthesized additional compounds (**2l–q**) and with these obtained K_i values mostly in the nanomolar range. The optimizations for **2l–q** were performed based on similar or even improved physicochemical properties compared to **2a–k** and their feasibility was tested in molecular docking studies.

Overall, **2h** (K_i = 0.050 μM, **Figure 6** in the **Supporting Information**), **2n** (K_i = 0.030 μM), and **2o** (K_i = 0.050 μM) are the top 3 compounds in terms of inhibitory potency. **2h** also has the highest selectivity in the series (>400-fold towards CatB and CatL) compared to the moderate selectivity of **2n** and **2o**. Notably, the k_{inact} values for most vinylsulfonates are higher than for the vinylsulfones, suggesting a faster covalent bond formation.

SAR discussion.

Docking scores and Hyde scores were generated using LEADIT and are shown in **Table 6** in the **Supporting Information**.[29] Since we maintained P1' and P1 compared to **SJ605** and **SJ606** (**Figure 7B**), we still observed interactions between Gly144 and Gly269 with the amide bond as well as an additional H-bond with Gly143 during non-covalent docking. Gln94 and Trp292 are also involved in H-bond formation with the sulfonyl group. The docking poses for top compound **2h** overlapping with **SJ606** or **2p** are shown in **Figure 7**. The poses for **2h** and **2p** are very similar (**Figure 7A**) as expected from Hyde scores (**2h**: –39 kJ/mol, **2p**: –37 kJ/mol). Nonetheless, there is a difference in *Sm*CB1 inhibition. **2h** is one of the most potent inhibitors in the series (K_i = 0.050 μM) whereas **2p** is only a moderate inhibitor (K_i = 0.41 μM). Their k_{2nd} values, on the other hand, are in the same range (10^4 $M^{-1}s^{-1}$) due to **2p**'s faster irreversible reaction compared to **2h** (see **Table 2**).

2i surprisingly shows a very weak inhibition of *Sm*CB1 (K_i >100 μM) which is not reflected in its Hyde score (–33 kJ/mol). Looking at the docking poses of both **2i** and **SJ606**, we noticed that the distance between the β-carbon of the vinylsulfonate double bond that undergoes the covalent reaction with the nucleophilic Cys100 is increased from 2.9 Å to 4.3 Å (**Figure 5** in the **Supporting Information**). Covalent reactions occur more readily at distances up to 3.5 Å which could explain the poor inhibitory activity.[31] The same may apply for **2m** (K_i >100 μM) for which a distance of

3.9 Å was found. The distances for compounds **2a–q** are listed in **Table 6** in the **Supporting Information**.

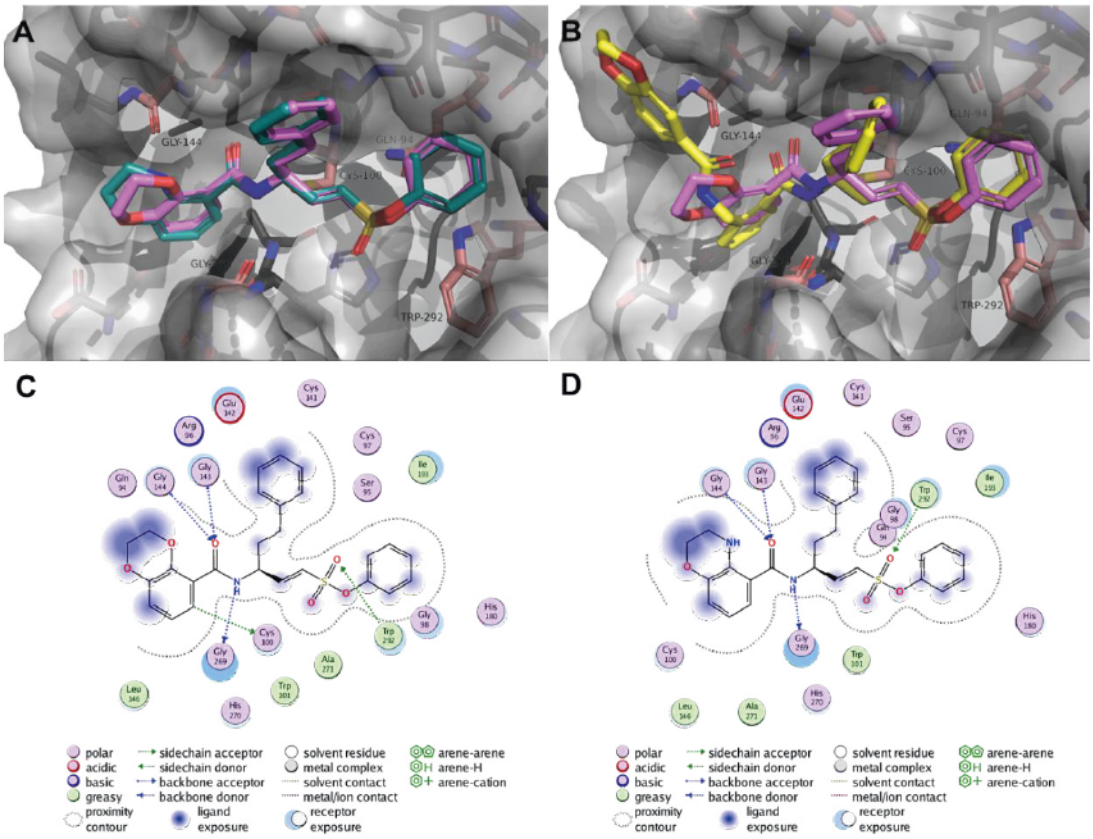

Figure 7. Molecular docking of **2h**, **2p** and initial lead **SJ606**. Non-covalent docking with LEADIT, images were generated with PYMOL, ligand interaction map generated with MOE.[25,30] PDB ID: 3s3r.[16] (**A**) Overlay of **2h** (violet) and **2p** (deepteal). Important actives site residues are shown in salmon. Both poses are very similar which is reflected by their Hyde scores (**2h**: –39 kJ/mol, **2p**: –37 kJ/mol).[32] (**B**) Overlay of **2h** (violet) and **SJ606** (yellow). Important residues in the binding site are shown in salmon. The binding poses are similar except for additional interactions of the DHBD moiety of **SJ606** with Ile145 and Gly118. (**C**) Ligand interactions for **2h**. (**D**) Ligand interactions for **2p**.

In vitro activity in phenotypic assay.

The results for the phenotypic assay of **2a–q** compared to leads **SJ605** and **SJ606** as well as the approved drug praziquantel (**PZQ**) are shown in **Table 3**. All compounds were tested against newly transformed schistosomula (NTS) and *S. mansoni* adults.

Compared to starting compounds **SJ605** and **SJ606**, several vinysulfonate-based inhibitors are more efficient against NTS and *S. mansoni* adults. Especially compounds **2h**, **2i**, **2k**, and **2p** are outstanding since they display a high efficacy (≥ 75%) against *S. mansoni* adults at 10 μM. **2h** has the highest efficacy in the series with 68% at 1 μM and 35% at 0.1 μM which is in a similar range as **PZQ**

(IC_{50} = 0.16 μM).[33] Notably, **2h** and **2p** (*S. mansoni* adults: 75% at 10 μM, 23% at 1 μM) share a high structural similarity, also with **SJ606**. This indicates that the DHBD/DHBO moiety is beneficial for phenotypic efficacy, particularly in *S. mansoni* adults.

Table 3. Physicochemical parameters and *in vitro* effects of **2a–q** compared to praziquantel (**PZQ**) and **SJ605**, **SJ606**.

cpd	R	SlogP[a]	TPSA [Å²][a]	Kier Flex[a,b]	NTS effect [%][c]		S. mansoni adults effect [%][c]		
					10 μM	1 μM	10 μM	1 μM	0.1 μM
SJ605	-	5.81	102	7.96	100 ± 0	33 ± 12	55 ± 4	-	-
SJ606	-	5.31	120	8.22	100 ± 0	30 ± 0	58 ± 5	-	-
2a	A	5.18	79	5.30	60 ± 1	38 ± 2	n. d.	-	-
2b	A	4.89	79	5.14	85 ± 1	40 ± 3	27 ± 2	-	-
2c	B	4.18	82	6.11	92 ± 0	27 ± 1	29 ± 0	-	-
2d	C	5.69	79	5.75	100 ± 0	48 ± 1	31 ± 2	-	-
2e	D	6.15	75	6.36	42 ± 4	27 ± 1	-	-	-
2f	E	4.28	92	5.09	75 ± 2	38 ± 4	47 ± 6	-	-
2g	A	4.82	88	5.59	100 ± 0	27 ± 1	63 ± 6	-	-
2h	B	4.11	91	6.59	88 ± 0	33 ± 0	86 ± 2	68 ± 0	35 ± 2
2i	C	5.63	88	6.19	100 ± 0	42 ± 2	86 ± 2	57 ± 0	-
2j	D	6.08	85	6.84	100 ± 0	35 ± 1	31 ± 2	-	-
2k	E	4.22	101	5.54	100 ± 0	33 ± 2	86 ± 2	36 ± 0	-
2l	F	4.22	101	5.54	100 ± 0	33 ± 2	63 ± 2	-	-
2m	G	6.04	82	6.24	100 ± 0	44 ± 4	71 ± 4	29 ± 4	-
2n	H	4.48	99	5.74	100 ± 0	48 ± 8	42 ± 4	-	-
2o	I	4.48	99	5.74	100 ± 0	40 ± 4	38 ± 8	-	-
2p	J	4.14	94	6.37	100 ± 0	58 ± 10	75 ± 0	23 ± 2	-
2q	K	3.33	99	5.83	100 ± 0	44 ± 4	40 ± 2	-	-
PZQ[d]	-	2.63	41	3.10	IC_{50}: 1.5 μg/mL[d] = 4.8 μM		IC_{50}: 0.05 μg/mL[d] = 0.16 μM		

a: calculated with MOE;[25] b: KIER's molecular flexibility index;[28] c: % dead after 72 hours; d: MEISTER ET AL.[33]

A correlation analysis suggests that lower K_i values result in a higher efficacy in NTS at 10 μM (r = –0.47, p = 0.048, **Table 5** in **Supporting Information**) as well as a slight

correlation between higher TPSA (ranging from 75 up to 110 Å^2) and higher efficacy (r = 0.55, p = 0.023, **Table 5** in **Supporting Information**).

Although the initial correlation analysis suggested that a higher lipophilicity could be beneficial, this is not the case for all optimized compounds. An example is **2e** with the highest SlogP in the series (6.15) but only limited potency (NTS: 42% at 10 μM, *S. mansoni* adults: n. d.). In contrast, **2k** is one of the top compounds (NTS: 100% at 10 μM, *S. mansoni* adults: 86% at 10 μM) with one of the lowest SlogP values (4.22). Flexibility also seems to have a smaller impact on efficacy than assumed. The top compounds' KierFlex values range from 5.54 to 6.59 whereas compounds with a higher rigidity, such as **2a** (5.09), **2b** (5.14), and **2f** (5.09) did not perform as well in the phenotypic assay.

In summary, several factors combine to influence phenotypic efficacy in schistosomes. Regardless, compound **2h** displays high potency and should be considered for further studies.

CONCLUSIONS AND PERSPECTIVES

Using an in-house screening with 76 compounds, we have identified two lead structures, **KS309** and the SJ600-scaffold (**SJ605**, **SJ606**), which showed promising results against *S. mansoni* adults and/or the target protease *Sm*CB1. **KS309** was most effective against *S. mansoni* adults at 10 μM but did not show relevant inhibition of the target protease *Sm*CB1 at 100 μM. **SJ605** and **SJ606**, on the other hand, were only moderately effective against *S. mansoni* at *10* μM but displayed strong *Sm*CB1 inhibition in the low nanomolar range. A correlation analysis revealed the importance of several physicochemical properties for the phenotypic efficacy, such as higher logP values or, in case of the **SJ600s**, more rigidity. Therefore, we started a dual approach to optimize the lead structures with regard to physicochemical properties. The "phenotypic approach" using **KS309** resulted in 14 derivatives with altered physicochemical properties yielding two optimized compounds (**1g**, **1j**). **1g** (*Sm*CB1 inhibition: 68% at 20 μM; *S. mansoni* adults: 100% at 10 μM, 43% at 1 μM) and **1j** (*Sm*CB1 inhibition: 80% at 20 μM; *S. mansoni* adults: 100% at 10 μM, 45% at 1 μM) emerged to be the most potent compounds in this series, although their main target remains unknown. The "*Sm*CB1 approach" using **SJ605** and **SJ606** as leads resulted in 17 derivatives with higher rigidity and lower TPSA including 7 optimized compounds in terms of efficacy (**2g**, **2h**, **2j–m**, **2p**). Several compounds displayed strong *Sm*CB1 inhibition in the nanomolar range with improved phenotypic efficacy compared to

SJ605 and **SJ606**. Vinysulfonates generally proved to be more effective than vinylsulfones. The most potent compound, **2h**, shows nanomolar inhibition of *Sm*CB1 while maintaining selectivity towards human off-target cathepsins (K_i = 50 nM, SI >400). The efficacy of **2h** towards *S. mansoni* adults improved enormously (86% at 10 μM, 68% at 1 μM and 35% at 0.1 μM), demonstrating efficacy in a similar range as found for the approved drug praziquantel (*S. mansoni* adults IC_{50} = 0.16 μM).

Further optimization of **2h** has the potential to yield even more potent compounds, offering a promising alternative to the currently available drug **PZQ**, which is facing rising resistance.[9] Next steps include metabolism studies and plasma stability tests to prevent problems that may arise in future *in vivo* studies. Finally, preclinical *in vivo* studies could give valuable insights into biodistribution, followed up by *in vivo* efficacy, e.g., with infected mice.

EXPERIMENTAL SECTION

All experimental procedures including analytical data can be found in the **Supporting Information**.

ACKNOWLEDGEMENTS

We would kindly like to acknowledge the support of [redacted], [redacted], and [redacted] (all from Johannes Gutenberg University, Mainz) during this project.

SUPPORTING INFORMATION

Parts of the **Supporting Information** are found within the thesis, especially those concerning compounds that were synthesized by myself as well as assays that I have performed (see chapter **2.3**). The complete **Supporting Information** including spectra can be found on the Appendix CD.

REFERENCES

(1) James, S. L.; Abate, D.; Abate, K. H.; Abay, S. M.; Abbafati, C.; Abbasi, N.; Abbastabar, H.; Vos, T.; Murray, C. J. L.; Al., E. Global, Regional, and National Incidence, Prevalence, and Years Lived with Disability for 354 Diseases and Injuries for 195 Countries and Territories, 1990–2017: A Systematic Analysis for the Global Burden of Disease Study 2017. *Lancet* **2018**, *392* (*10159*), 1789–1858.

(2) Hotez, P. J.; Alvarado, M.; Basáñez, M. G.; Bolliger, I.; Bourne, R.; Boussinesq, M.; Brooker, S. J.; Brown, A. S.; Buckle, G.; Budke, C. M.; Carabin, H.; Coffeng, L. E.; Fèvre, E. M.; Fürst, T.; Halasa, Y. A.; Jasrasaria, R.; Johns, N. E.; Keiser, J.; King, C. H.; Lozano, R.; Murdoch, M. E.; O'Hanlon, S.; Pion, S. D. S.; Pullan, R. L.; Ramaiah, K. D.; Roberts, T.; Shepard, D. S.; Smith, J. L.; Stolk, W. A.; Undurraga, E. A.; Utzinger, J.; Wang, M.; Murray, C. J. L.; Naghavi, M. The Global Burden of Disease Study 2010: Interpretation and Implications for the Neglected Tropical Diseases. *PLoS Negl. Trop. Dis.* **2014**, *8* (*7*).

(3) Colley, D. G.; Bustinduy, A. L.; Secor, W. E.; King, C. H. Human Schistosomiasis. *Lancet* **2014**, *383* (*9936*), 2253–2264.

(4) Gryseels, B.; Polman, K.; Clerinx, J.; Kestens, L. Human Schistosomiasis. *Lancet* **2006**, *368* (*9541*), 1106–1118.

(5) Fitzpatrick, J. M.; Johnston, D. A.; Williams, G. W.; Williams, D. J.; Freeman, T. C.; Dunne, D. W.; Hoffmann, K. F. An Oligonucleotide Microarray for Transcriptome Analysis of Schistosoma Mansoni and Its Application/Use to Investigate Gender-Associated Gene Expression. *Mol. Biochem. Parasitol.* **2005**, *141* (*1*), 1–13.

(6) Moore, D. V.; Sandground, J. H. The Relative Egg Producing Capacity of Schistosoma Mansoni and Schistosoma Japonicum. *Am. J. Trop. Med. Hyg.* **1956**, *5* (*5*), 831–840.

(7) Hams, E.; Aviello, G.; Fallon, P. G. The Schistosoma Granuloma: Friend or Foe? *Front. Immunol.* **2013**, *4* (*APR*), 89.

(8) Burke, M. L.; Jones, M. K.; Gobert, G. N.; Li, Y. S.; Ellis, M. K.; McManus, D. P. Immunopathogenesis of Human Schistosomiasis. *Parasite Immunol.* **2009**, *31* (*4*), 163–176.

(9) Wang, W.; Wang, L.; Liang, Y. S. Susceptibility or Resistance of Praziquantel in Human Schistosomiasis: A Review. *Parasitol. Res.* **2012**, *111* (*5*), 1871–1877.

(10) de Souza Dias, L. C.; Olivier, C. E. Failure at Inducing Resistance to Schistosomicidal Drugs in a Brazilian Human Strain of Schistosoma Mansoni. *Rev. do Inst. Med. Trop. São Paulo* **1986**, *28* (*5*), 352–357.

(11) Park, S. K.; Friedrich, L.; Yahya, N. A.; Rohr, C. M.; Chulkov, E. G.; Maillard, D.; Rippmann, F.; Spangenberg, T.; Marchant, J. S. Mechanism of Praziquantel Action at a Parasitic Flatworm Ion Channel. *Sci. Transl. Med.* **2021**, *13* (*625*).

(12) Jílková, A.; Horn, M.; Fanfrlík, J.; Küppers, J.; Pachl, P.; Řezáčová, P.; Lepšík, M.; Fajtová, P.; Rubešová, P.; Chanová, M.; Caffrey, C. R.; Gütschow, M.; Mareš, M. Azanitrile Inhibitors of the SmCB1 Protease Target Are Lethal to Schistosoma Mansoni: Structural and Mechanistic Insights into Chemotype Reactivity. *ACS Infect. Dis.* **2021**, *7* (*1*), 189–201.

(13) Jílková, A.; Rubešová, P.; Fanfrlík, J.; Fajtová, P.; Řezáčová, P.; Brynda, J.; Lepšík, M.; Mertlíková-Kaiserová, H.; Emal, C. D.; Renslo, A. R.; Roush, W. R.; Horn, M.; Caffrey, C. R.; Mareš, M. Druggable Hot Spots in the Schistosomiasis Cathepsin B1 Target Identified by Functional and Binding Mode Analysis of Potent Vinyl Sulfone Inhibitors. *ACS Infect. Dis*. **2021**, *7* (*5*), 1077–1088.

(14) Abdulla, M. H.; Lim, K. C.; Sajid, M.; McKerrow, J. H.; Caffrey, C. R. Schistosomiasis Mansoni: Novel Chemotherapy Using a Cysteine Protease Inhibitor. *PLoS Med.* **2007**, *4* (*1*), 0130–0138.

(15) Correnti, J. M.; Brindley, P. J.; Pearce, E. J. Long-Term Suppression of Cathepsin B Levels by RNA Interference Retards Schistosome Growth. *Mol. Biochem. Parasitol.* **2005**, *143* (*2*), 209–215.

(16) Jílková, A.; Řezáčová, P.; Lepšík, M.; Horn, M.; Váchová, J.; Fanfrlík, J.; Brynda, J.; McKerrow, J. H.; Caffrey, C. R.; Mareš, M. Structural Basis for Inhibition of Cathepsin B Drug Target from the Human Blood Fluke, Schistosoma Mansoni. *J. Biol. Chem*. **2011**, *286* (*41*), 35770–35781.

(17) Lombardo, F. C.; Pasche, V.; Panic, G.; Endriss, Y.; Keiser, J. Life Cycle Maintenance and Drug-Sensitivity Assays for Early Drug Discovery in Schistosoma Mansoni. *Nat. Protoc.* **2019**, *14* (*2*), 461–481.

(18) Schirmeister, T.; Kesselring, J.; Jung, S.; Schneider, T. H.; Weickert, A.; Becker, J.; Lee, W.; Bamberger, D.; Wich, P. R.; Distler, U.; Tenzer, S.; Johé, P.; Hellmich, U. A.; Engels, B. Quantum Chemical-Based Protocol for the Rational Design of Covalent Inhibitors. *J. Am. Chem. Soc.* **2016**, *138* (*27*), 8332–8335.

(19) Jung, S.; Fuchs, N.; Johe, P.; Wagner, A.; Diehl, E.; Yuliani, T.; Zimmer, C.; Barthels, F.; Zimmermann, R. A.; Klein, P.; Waigel, W.; Meyr, J.; Opatz, T.; Tenzer, S.; Distler, U.; Räder, H. J.; Kersten, C.; Engels, B.; Hellmich, U. A.; Klein, J.; Schirmeister, T. Fluorovinylsulfones and -Sulfonates as Potent Covalent Reversible Inhibitors of the Trypanosomal Cysteine Protease Rhodesain: Structure-Activity Relationship, Inhibition Mechanism, Metabolism, and in Vivo Studies. *J. Med. Chem.* **2021**, *64* (*16*), 12322–12358.

(20) Jung, S.; Fuchs, N.; Grathwol, C.; Hellmich, U. A.; Wagner, A.; Diehl, E.; Willmes, T.; Sotriffer, C.; Schirmeister, T. New Peptidomimetic Rhodesain Inhibitors with Improved Selectivity towards Human Cathepsins. *Eur. J. Med. Chem.* **2022**, *238*.

(21) Gauthier, J. Y.; Black, W. C.; Courchesne, I.; Cromlish, W.; Desmarais, S.; Houle, R.; Lamontagne, S.; Li, C. S.; Massé, F.; McKay, D. J.; Ouellet, M.; Robichaud, J.; Truchon, J. F.; Truong, V. L.; Wang, Q.; Percival, M. D. The Identification of Potent, Selective, and Bioavailable Cathepsin S Inhibitors. *Bioorganic Med. Chem. Lett.* **2007**, *17* (*17*), 4929–4933.

(22) Barthels, F.; Marincola, G.; Marciniak, T.; Konhäuser, M.; Hammerschmidt, S.; Bierlmeier, J.; Distler, U.; Wich, P. R.; Tenzer, S.; Schwarzer, D.; Ziebuhr, W.; Schirmeister, T. Asymmetric Disulfanylbenzamides as Irreversible and Selective Inhibitors of Staphylococcus Aureus Sortase A. *ChemMedChem* **2020**, *15* (*10*), 839–850.

(23) Barthels, F.; Meyr, J.; Hammerschmidt, S. J.; Marciniak, T.; Räder, H. J.; Ziebuhr, W.; Engels, B.; Schirmeister, T. 2-Sulfonylpyrimidines as Privileged Warheads for the Development of S. Aureus Sortase A Inhibitors. *Front. Mol. Biosci.* **2022**, *8*, 1284.

(24) Pearce, E. J.; MacDonald, A. S. The Immunobiology of Schistosomiasis. *Nat. Rev. Immunol.* **2002**, *2* (*7*), 499–511.

(25) Molecular Operating Environment (MOE). *Chemical Computing Group ULC*: 1010 Sherbrooke St. West, Suite #910, Montreal, QC, Canada, H3A 2R7 2020.

(26) Liu, S.; Cai, P.; Piao, X.; Hou, N.; Zhou, X.; Wu, C.; Wang, H.; Chen, Q. Expression Profile of the Schistosoma Japonicum Degradome Reveals Differential Protease Expression Patterns and Potential Anti-Schistosomal Intervention Targets. *PLOS Comput. Biol.* **2014**, *10* (*10*), e1003856.

(27) Furlong, S. T. Unique Roles for Lipids in Schistosoma Mansoni. *Parasitol. Today* **1991**, *7* (*2*), 59–62.

(28) Kier, L. B. An Index of Molecular Flexibility from Kappa Shape Attributes. *Quant. Struct. Relationships* **1989**, *8* (*3*), 221–224.

(29) LeadIT. *BioSolveIT* GmbH: Sankt Augustin, Germany 2017. www.biosolveit.de/LeadIT.

(30) Schrödinger, L.; DeLano, W. The PyMOL Molecular Graphics System. *Schrödinger*, LLC. 2020. http://www.pymol.org/pymol.

(33) Gehringer, M.; Laufer, S. A. Emerging and Re-Emerging Warheads for Targeted Covalent Inhibitors: Applications in Medicinal Chemistry and Chemical Biology. *J. Med. Chem.* **2019**, *62* (*12*), 5673–5724.

(34) Reulecke, I.; Lange, G.; Albrecht, J.; Klein, R.; Rarey, M. Towards an Integrated Description of Hydrogen Bonding and Dehydration: Decreasing False Positives in Virtual Screening with the HYDE Scoring Function. *ChemMedChem* **2008**, *3* (*6*), 885–897.

(35) Meister, I.; Ingram-Sieber, K.; Cowan, N.; Todd, M.; Robertson, M. N.; Meli, C.; Patra, M.; Gasser, G.; Keiser, J. Activity of Praziquantel Enantiomers and Main Metabolites against Schistosoma Mansoni. *Antimicrob. Agents Chemother.* **2014**, *58* (*9*), 5466–5472.

2.3 Supporting Information

General.

SOLVENTS AND REAGENTS.

All reagents and solvents were commercially purchased from MERCK KGAA (Darmstadt, Germany), VWR (Darmstadt, Germany), BLD PHARMATECH (Kaiserslautern, Germany), TCI GERMANY (Eschborn, Germany) or THERMO FISHER SCIENTIFIC (Schwerte, Germany). Unless otherwise stated, chemicals and solvents were used without further purification. For reaction control, thin layer chromatographies (TLC) were performed using TLC ready-to-use films "ALUGRAM XTRA SIL G/UV254" from MACHEREY-NAGEL (Düren, Germany) and subsequently detected using a UV lamp at λ = 254 nm or λ = 266 nm. For purification by column chromatography, silica gel (40–60 μm) from MACHEREY-NAGEL (Düren, Germany) was used. The applied solvents were adapted to the sample and are indicated individually.

INSTRUMENTS AND SOFTWARE.

Both ^{1}H and ^{13}C NMR spectra were recorded by means of a Bruker Fourier 300 nuclear magnetic resonance spectrometer. MestReNova (version 12.0, MestReLab Research) was used for evaluation. The chemical shift δ is given in ppm (parts per million) and the coupling constant J in Hz (Hertz). Multiplicities are given by s (singlet), d (doublet), dd (doublet from doublet) t (triplet), q (quintet), and m (multiplet). Either deuterated chloroform (δH = 7.26 ppm, δC = 77.2 ppm) or deuterated DMSO-d_6 (δH = 2.5 ppm, δC = 39.5 ppm) served as solvent and reference.

HPLC/ESI-MS analyses were performed for identification, reaction control, and purity measurements. An Agilent 1100 series system with an AGILENT R POROSHELL 120 EC-C18 RP column (150 mm x 2.1 mm, pore size: 4 μm) was used. Detection was performed at λ = 254 nm. Samples were dissolved in acetonitrile, acetonitrile/water, or methanol. Acetonitrile/water (+ 0.01% formic acid) in different ratios was used as flow agent. Molecular masses were calculated using PERKINELMER CHEMDRAW STANDARD software (version 12.0.02). Purity was determined using MESTRENOVA (version 12.0, MESTRELAB RESEARCH).

Purification of the final stages was achieved by high performance liquid chromatography using a VARIAN PREPSTAR 210 system and an AGILENT ZORBAX XDB column (21.2 x 150 mm, 5 μm). All final compounds have a purity of ≥95%.

For chiral compounds, the optical rotation was determined using a KRÜSS OPTRONIC P3000 polarimeter (Hamburg, Germany) at a wavelength of λ = 589 nm, a temperature of T = 20 °C, and a concentration of 10 mg/mL. Declared melting points were measured with glass capillaries closed on one side and an MPM-H3 melting point meter from SCHORPP DEVICE TECHNOLOGY (Überlingen, Germany).

Syntheses.

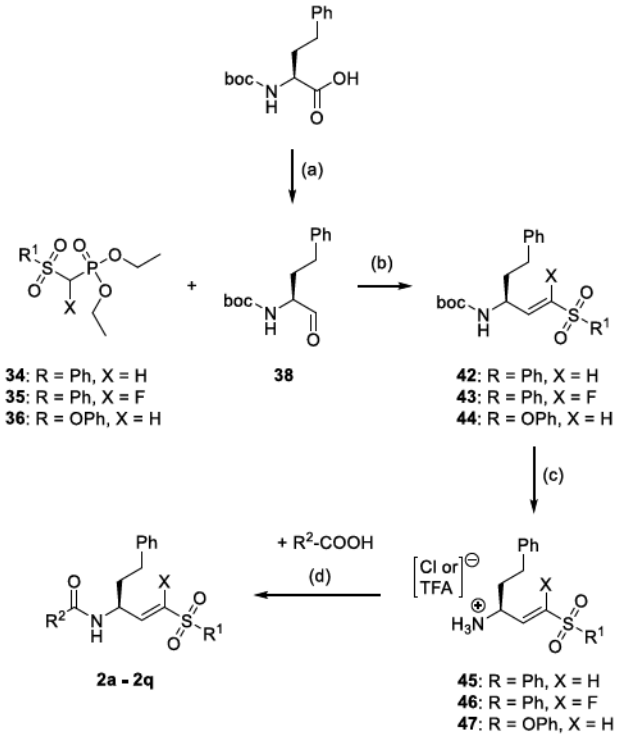

Scheme 3. Synthesis of (F-)vinylsulfon(at)es **2a–q**. Reagents and conditions: (a) 1. HOBt, TBTU, DIPEA, *N,O*-dimethyl hydroxylamine, DCM, 0 °C – rt, 12 – 24 h. 2. $LiAlH_4$, diethyl ether, 0 °C, 2 h, 86%. (b) LiHMDS or KHMDS, THF (dry), −78 °C, 3 – 4 h, 30 – 47%. (c) HCl or TFA, dioxane, rt, 2 – 12 h, 95 – 98%. (d) HOBt, TBTU, DIPEA, DCM or DCM/DMF, 0 °C – rt, 24 – 48 h, 10 – 50%.

GENERAL SYNTHETIC PROCEDURES.

Procedure A: TBTU coupling with amine hydrochlorides

To a 0 °C cold solution of the carboxylic acid (1.0 equiv.) in DCM and/or DMF, HOBt · H_2O (1.0 eq.) and 2,4,6-collidine (2.0 eq.) or DIPEA (3.5 eq.) were added. After stirring at 0 °C for 30 min, TBTU (1.0 eq.) was added. The solution was stirred for further 30 min at 0 °C, and the amine hydrochloride (1.0 or 1.1 eq.) was added. After stirring at rt overnight, the solvent was removed under reduced pressure. If DMF was used, it was removed by co-distillation with *n*-heptane (3x 150 mL) under reduced pressure. The residue was taken up in ethyl acetate and washed with saturated

$NaHCO_3$ solution (3x) and 1 M HCl (3x). The filtrate was concentrated under reduced pressure to yield the desired product. If necessary, further purification by column chromatography was conducted.

Procedure B: Horner-Wadsworth-Emmons reaction

The corresponding phosphonate (**34**–**36**, 1 eq.) was dissolved in dry THF and cooled to –80 °C. Then, LHMDS (1 M in THF, 1.4 eq.) was added over 20 min. The aldehyde (**38**, 0.95 eq.) was dissolved in THF and added to the solution. After stirring for 2 h, the mixture was warmed to rt. THF was removed under reduced pressure and the residue was extracted with EA (3x). The combined organic extracts were washed with water (3x) and brine (1x). The extract was dried over Na_2SO_4, and volatiles were removed under reduced pressure. After column chromatographic work-up (CH/EA 6:1–4:1), the products were obtained as colorless oils.

Procedure C: Boc deprotection

To a solution of the Boc-protected amine in DCM, TFA was added dropwise at 0 °C. The reaction was stirred overnight. Subsequently, all volatiles were removed under reduced pressure. The product was then lyophilized to remove TFA. Alternatively, 4 M HCl in dioxane was used at room temperature.

STARTING MATERIALS AND WARHEAD PREPARATION.

Diethyl((phenylsulfonyl)methyl)phosphonate (**34**)

To a solution of methylphenyl sulfone (1 eq., 20 mmol, 3.1 g) in dry THF, *n*-BuLi was added (2.5 eq., 2.5 M in hexane, 50 mmol, 18 mL) at 0 °C with stirring. After 30 min, diethyl chlorophosphate (1.1 eq., 17 mmol, 3.6 mL) was added dropwise. Stirring was continued for 1 h at 0 °C. Subsequently, 25 mL of a saturated NH_4Cl solution was added to terminate the reaction. Volatile components were removed under reduced pressure and the residue was extracted with EA (3x). The combined organic extracts were washed (3x) with brine and dried over Na_2SO_4. After purification by column chromatography (CH/EA 1:2), the product was obtained as a colorless solid (3.9 g, 13.5 mmol, 68%). ^{1}H NMR (300 MHz, $CDCl_3$) δ[ppm] = 7.99 (d, J = 1.3 Hz, 1H), 7.96 (d, J = 1.6 Hz), 7.69 – 7.62 (m, 1H), 7.60 – 7.52 (m, 2H), 4.19 – 4.08 (m, 4H), 3.75 (d, J = 16.9 Hz, 2H), 1.28 (td, J = 7.1, 0.6 Hz, 6H). ^{13}C NMR (75 MHz, $CDCl_3$) δ[ppm] = 139.9, 134.1, 129.1, 128.3, 63.4, 54.7, 52.9, 116.2. MP = 45 – 50 °C.

Phenyl (diethoxyphosphoryl)methansulfonate (**35**)

Phenyl methanesulfonate (1 eq., 30 mmol, 5.0 g) was dissolved in dry THF and cooled to –80 °C. KHMDS (1 M in THF, 1.4 eq., 41 mmol, 41 mL) was added slowly. The solution was stirred for 15 min. Then, diethyl chlorophosphate (1.1 eq., 32 mmol, 5.2 mL) was added slowly. Stirring was performed for one hour at –80 °C and then the reaction was stopped with acetic acid. After warming to rt, THF was removed at reduced pressure and the mixture was extracted with EA (3x). The combined organic extracts were washed with water (3x) and with brine, and dried over Na_2SO_4. The solvent was evaporated. After purification by column chromatography (cyclohexane/ethyl acetate 1:2), a yellow solid was obtained (1.9 g, 6.2 mmol, 21%). ^{1}H NMR (300 MHz, $CDCl_3$) δ[ppm] = 7.39 –7.31 (m, 2H), 7.31 – 7.26 (m, 3H), 4.29 – 4.11 (m, 4H), 3.76 (d, J = 17.2 Hz, 2H), 1.31 (td, J = 7.1, 0.7 Hz, 6H).

Diethyl (fluoro(phenylsulfonyl)methyl)phosphonate (**36**)

Phosphonate **34** (1 eq., 12 mmol, 3.5 g) was dissolved in dry THF and stirred at –80 °C. Then, LHMDS in THF (1 M in THF, 1.4 eq., 15 mmol, 15 mL) was added dropwise, and after 30 min, *Selectfluor* (1.5 eq., 17.9 mmol, 6.3 g) dissolved in 10 mL of DMF was added. After stirring for 3 h, the temperature was slowly warmed to 0 °C. 15 mL of saturated ammonium chloride solution was added to terminate the reaction. All volatiles were removed, and the residue was taken up in DCM and washed first with saturated $NaHCO_3$ (3x) and then with brine (3x). The solution was dried over Na_2SO_4, and solvents were removed under reduced pressure. After column chromatographic separation (CH/EA 1:2), a colorless solid (0.7 g, 2.5 mmol, 21%) was obtained. ^{1}H NMR (300 MHz, $CDCl_3$) δ[ppm] = 8.06 – 7.96 (m, 2H), 7.76 –7.68 (m, 1H), 7.65 – 7.55 (m, 2H), 5.38 (dd, J = 45.5, 6.6 Hz, 1H), 4.38 – 4.18 (m, 4H), 1.35 (tt, J = 7.1, 0.8 Hz, 6H). ^{13}C NMR (75 MHz, $CDCl_3$) δ[ppm] = 136.2, 134.1, 129.1, 128.3, 63.4, 54.7, 52.9, 116.2. MP = 61 – 65 °C (lit. 62 °C).[237]

(*S*)-*tert*-Butyl (1-(methoxy(methyl)amino)-1-oxo-4-phenylbutan-2-yl) carbamate (**37**)

Boc-L-homophenylalanine (1 eq., 12 mmol, 3.4 g) was dissolved in DCM and cooled to 0 °C. Then, TBTU (1.2 eq. 14 mmol, 4.5 g), HOBt (1.2 eq., 14 mmol, 1.9 g), and DIPEA (4.3 eq., 52 mmol, 8.8 mL) were added and the mixture was stirred for 15 min. *N*,*O*-dimethyl hydroxylamine (1.2 eq., 14 mmol, 1.4 g) was added and the reaction was stirred at rt for 18 h. Volatile components were removed at reduced pressure and the residue was taken up in EA. It was deacidified 4x with saturated $NaHCO_3$ and washed with brine. The extract was then dried over Na_2SO_4, all solvents were evaporated, and the crude product was used without further workup. ^{1}H NMR

(300 MHz, $CDCl_3$) δ[ppm] = 7.22 – 7.14 (m, 3H, H), 7.11 (dt, *J* = 7.9, 2.0 Hz, 3H), 4.60 (s, 1H), 3.08 (s, 3H), 2.74 (s, 3H), 2.59 (m, *J* = 13.9, 8.9, 5.6 Hz, 2H), 2.01 – 1.65 (m, 3H), 1.37 (s, 9H). ^{13}C NMR (75 MHz, $CDCl_3$) δ[ppm] = 173.2, 155.7, 141.3, 128.6, 128.5, 126.1, 79.7, 61.6, 50.2, 38.9, 34.7, 31.8, 28.5. $[\alpha]_{589}^{20} = -33°$ (c = 10 $\frac{mg}{mL}$, MeOH).

(*S*)-*tert*-Butyl (1-oxo-4-phenylbutan-2-yl)carbamate (**38**)

Weinreb amide **37** (1 eq., 11 mmol, 3.5 g) was dissolved in 15 mL dry THF and the mixture was cooled to 0 °C. $LiAlH_4$ (1.3 eq., 14 mmol, 0.54 g) was added in portions. The mixture was slowly warmed to RT and stirred overnight. The excess $LiAlH_4$ was destroyed using 0.33 M $KHSO_4$. THF was removed under reduced pressure. The residue was taken up in EA and washed with 3 M HCl, $NaHCO_3$, and brine. The organic phase was dried over Na_2SO_4, and the solvent was evaporated. The crude product remained as a colorless oil that solidified in the refrigerator (2.46 g, 9.3 mmol, 86%). ^{1}H NMR (300 MHz, $CDCl_3$) δ[ppm] = 9.54 (s, 1H), 7.36 – 7.07 (m, 5H), 4.12 (q, *J* = 7.2 Hz, 1H), 2.72 – 2.66 (m, 1H), 2,04 (s, 1H), 1.54 – 1.39 (m, 9H). ^{13}C NMR (75 MHz, $CDCl_3$) δ[ppm] = 199.5, 156.2, 140.3, 128.7, 125.9, 110.5, 60.4, 30.9, 28.3, 21.1. $[\alpha]_{589}^{20} = -15°$ (c = 10 $\frac{mg}{mL}$, MeOH).

Dibenzo[*b,d*]furan-4-carboxylic acid (**39**)

Dibenzofuran (1 eq. 12 mmol, 2.0 g) was dissolved in dry THF and cooled to –80 °C. Then, *n*-BuLi (1 eq., 12 mmol, 4.8 mL of a 2.5 M solution in THF) was added slowly with stirring, giving an orange-yellow precipitate. The mixture was slowly warmed to rt and stirred for 3 h. It was then cooled again to –80 °C and dry ice (CO_2(s)) was added in large excess. A colorless solid was formed. After stirring for 1 h, a 2 M NaOH solution was added. The aqueous phase was acidified to pH=5 with HCl. The product was extracted using EA and the extract was dried over Na_2SO_4. Subsequently, the product was processed by column chromatography (DCM/MeOH 95:1), obtaining a colorless solid (0.36 g, 1.7 mmol, 14%). ^{1}H NMR (300 MHz, DMSO-d_6) δ[ppm] = 13.31 (s, 1H), 8.40 (dd, *J* = 7.7, 1.4 Hz, 1H), 8.24 – 8.18 (m, 1H), 8.04 (dd, *J* = 7.7, 1.4 Hz, 1H), 7.79 (dt, *J* = 8.3, 0.8 Hz, 1H), 7.61 – 7.56 (m, 1H), 7.53 – 7.40 (m, 2H). ^{13}C NMR (75 MHz, DMSO-d_6) δ[ppm] = 165.4, 155.7, 154.1, 129.3, 28.2, 125.8, 125.3, 123.5, 122.9, 122.7, 121.3, 116.0, 111.8. MP = 210 – 214 °C (lit. 212 °C).[271]

Ethyl 3,4-dihydro-2*H*-benzo[*b*][1,4]oxazine-6-carboxylate (**40**)[272]

Ethyl 3-amino-4-hydroxybenzoic acid (1 eq., 5.5 mmol, 1.0 g) and K_2CO_3 (4 eq., 22 mmol, 3.0 g) were dissolved in 20 mL DMF. Then, 1,2-dibromoethane (4 eq.,

22 mmol, 1.9 mL) was added, followed by stirring at 70 °C for 14 h. After cooling to rt, the reaction mixture was diluted with 40 mL of 5% LiCl solution. It was extracted with DCM (3x), washed with water (1x), a saturated $NaHCO_3$ solution (2x), and brine (1x), then dried over $MgSO_4$. The solvent was removed under reduced pressure, and the product was purified by column chromatography (cyclohexane/ethyl acetate 1:3), obtaining a light red oil (0.59 g, 2.85 mmol, 52%). ^{1}H NMR (300 MHz, $CDCl_3$) *δ*[ppm] = 7.89 (s, 1H), 7.23 (d, *J* = 2.0 Hz, 1H), 4.25 (d, *J* = 2.4 Hz, 2H), 4.23 – 4.19 (m, 2H), 3.37 – 3.32 (m, 2H), 1.29 (td, *J* = 7.1, 4.2 Hz, 3H). ^{13}C NMR (75 MHz, $CDCl_3$) *δ*[ppm] = 166.6, 149.1, 133.3, 123.4, 120.9, 116.8, 116.4, 65.6, 60.6, 40.6, 14.4.

3,4-Dihydro-2*H*-benzo[*b*][1,4]oxazine-6-carboxylic acid (**41**)

Compound **40** (1 eq., 2.4 mmol, 0.50 g) was dissolved in THF and water. Subsequently, LiOH monohydrate (4 eq., 9.7 mmol, 0.41 g) was added dropwise and the mixture was stirred for 3 h. The product was precipitated at pH = 4–5 with 2 M HCl. The solid was aspirated, and the filtrate lyophilized, obtaining a brown solid (0.10 g, 0.57 mmol, 24%). ^{1}H NMR (300 MHz, $CDCl_3$) *δ*[ppm] = 12.14 (s, 1H), 7.08 – 6.81 (m, 2H), 5.75 (s, 1H), 4.25 – 3.84 (m, 2H), 3.03 (s, 2H). ^{13}C NMR (75 MHz, $CDCl_3$) *δ*[ppm] = 167.9, 149.3, 147.4, 139.2, 135.1, 116.2, 116.1, 65.5. MP = 131 °C.

(*S,E*)-*tert*-Butyl (5-phenyl-1-(phenylsulfonyl)pent-1-en-3-yl)carbamate (**42**)

Synthesized using phosphonate **34** (1 eq., 6.0 mmol, 1.76 g) and aldehyde **38** (0.95 eq., 5.7 mmol, 1.50 g) according to procedure B, resulting in a colorless oil (1.1 g, 2.8 mmol, 47%). ^{1}H NMR (300 MHz, $CDCl_3$) *δ*[ppm] = 7.96 – 7.83 (m, 2H), 7.71 – 7.47 (m, 3H), 7.34 – 7.11 (m, 5H), 6.91 (dd, *J* = 15.0, 5.1 Hz, 1H), 6.44 (dd, *J* = 15.0, 1.6 Hz, 1H), 4.58 (d, *J* = 8.7 Hz, 1H), 2.74 – 2.62 (m, 2H), 2.00 – 1.77 (m, 2H), 1.54 – 1.31 (m, 9H). ^{13}C NMR (75 MHz, $CDCl_3$) *δ*[ppm] = 205.1, 171.1, 152.9, 145.2, 140.4, 133.9, 129.4, 128.6, 128.4, 128.0, 126.3, 60.4, 44.3, 35.2, 29.6, 28.2. $[\alpha]_{589}^{20} = -38°$ (c = 10 $\frac{\mathbf{mg}}{\mathbf{mL}}$, MeOH).

(*S,E*)-Phenyl 3-((*tert*-butoxycarbonyl)amino)-5-phenylpent-1-ene-1-sulfonate (**43**)

Synthesized using phosphonate **35** (1 eq., 6.0 mmol, 1.85 g) and aldehyde **38** (0.95 eq., 5.7 mmol, 1.5 g) according to procedure B, resulting in a colorless oil (0.75 g, 1.8 mmol, 30%). ^{1}H NMR (300 MHz, $CDCl_3$) *δ*[ppm] = 7.48 – 7.34 (m, 2H), 7.35 – 7.01 (m, 6H), 6.75 (dd, *J* = 15.1, 5.1 Hz, 1H), 6.47 (dd, *J* = 15.1, 1.6 Hz, 1H), 4.32 (s, 1H), 2.79 – 2.54 (m, 2H), 1.84 – 1.79 (m, 2H), 1.52 – 1.24 (m, 9H). ^{13}C NMR (75 MHz, $CDCl_3$) *δ*[ppm] = 154.8, 149.5, 140.1, 129.8, 128.7, 128.4, 128.3, 127.3, 126.4, 124.3, 122.5, 35.5, 29.4, 29.3, 28.3. $[\alpha]_{589}^{20} = -5°$ (c = 10 $\frac{\mathbf{mg}}{\mathbf{mL}}$, MeOH).

(*S,E*)-*tert*-Butyl (1-fluoro-5-phenyl-1-(phenylsulfonyl)pent-1-en-3-yl)carbamate (**44**)

Synthesized using phosphonate **36** (1 eq., 4.0 mmol, 1.2 g) and aldehyde **38** (0.95 eq., 3.8 mmol, 1.0 g) according to procedure B, resulting in a colorless oil (0.65 g, 1.6 mmol, 39%). ^{1}H NMR (300 MHz, $CDCl_3$) *δ*[ppm] = 8.12 (s, 2H), 7.77 – 7.55 (m, 3H), 7.41 – 7.18 (m, 4H), 5.86 (dd, *J* = 21.2, 10.0 Hz, 1H), 5.32 (t, *J* = 8.3 Hz, 1H), 2.93 – 2.66 (m, 2H), 2.12 – 1.88 (m, 1H), 1.50 (s, 9H). ^{13}C NMR (75 MHz, $CDCl_3$) *δ*[ppm] = 207.0, 154.9, 140.9, 137.6, 134.6, 129.3, 129.0, 128.5, 128.4, 126.1, 121.3, 46.4, 37.2, 32.2, 28.4. $[\alpha]_{589}^{20} = -97°$ (c = 10 $\frac{\mathbf{mg}}{\mathbf{mL}}$, MeOH).

(*S,E*)-5-Phenyl-1-(phenylsulfonyl)pent-1-en-3-amine (**45**)

Synthesized using vinysulfone **42** (1 eq., 2.8 mmol, 1.1 g) according to procedure C, giving a colorless oil (0.83 g, 2.7 mmol, 98%). ^{1}H NMR (300 MHz, DMSO-*d*$_6$) *δ*[ppm] = 8.39 (s, 3H), 7.95 – 7.85 (m, 2H), 7.80 – 7.73 (m, 1H), 7.72 – 7.64 (m, 2H), 7.31 – 7.23 (m, 2H), 7.23 – 7.13 (m, 3H), 7.13 – 7.08 (m, 1H), 6.88 (dd, *J* = 15.3, 7.0 Hz, 1H), 4.00 (d, *J* = 7.3 Hz, 1H), 2.75 (dt, *J* = 14.8, 7.2 Hz, 1H), 2.54 (d, *J* = 8.2 Hz, 1H), 2.08 – 1.82 (m, 2H). ^{13}C NMR (75 MHz, DMSO-*d*$_6$) *δ*[ppm] = 141.3, 140.7, 134.0, 134.6, 134.4, 130.2, 129.0, 128.60, 127.8, 126.7, 50.6, 34.0, 31.0. $[\alpha]_{589}^{20} = -33°$ (c = 10 $\frac{\mathbf{mg}}{\mathbf{mL}}$, MeOH).

(*S,E*)-Phenyl 3-amino-5-phenylpent-1-ene-1-sulfonate (**46**)

Synthesized using vinylsulfonate **43** (1 eq., 1.8 mmol, 0.75 g) according to procedure C, giving a colorless oil (0.56 g, 1.8 mmol, 98%). ^{1}H NMR (300 MHz, DMSO-*d*$_6$) *δ*[ppm] = 7.96 – 7.83 (m, 2H), 7.44 – 7.07 (m, 6H), 7.05 – 7.01 (m, 2H), 6.96 (dt, *J* = 7.5, 2.5 Hz, 1H), 6.75 (dd, *J* = 15.5, 7.5 Hz, 2H), 6.69 – 6.63 (m, 1H), 3.08 – 2.94 (m, 1H), 1.59 (m, 2H), 0.91 – 0.78 (m, 2H). ^{13}C NMR (75 MHz, DMSO-*d*$_6$)*δ* [ppm] = 157.8, 157.3, 129.8, 128.8, 126.3, 119.2, 115.7, 52.3, 23.4, 14.4.$[\alpha]_{589}^{20} = -41°$ (c = 10 $\frac{\mathbf{mg}}{\mathbf{mL}}$, MeOH).

(*S,E*)-1-Fluoro-5-phenyl-1-(phenylsulfonyl)pent-1-en-3-amine (**47**)

Synthesized using fluorovinysulfone **44** (1 eq., 1.6 mmol, 0.65 g) according to procedure C, giving a colorless oil (0.49 g, 1.5 mmol, 95%). ^{1}H NMR (300 MHz, DMSO-*d*$_6$) *δ*[ppm] = 8.70 (s, 3H), 8.02 (dd, *J* = 7.3, 1.7 Hz, 2H), 7.96 – 7.66 (m, 3H), 7.35 – 7.11 (m, 3H), 7.10 – 7.03 (m, 2H), 6.55 (dd, $J_{H\text{-}F}$ = 32.6 Hz, $J_{H\text{-}H}$ = 9.8 Hz, 1H), 4.01 (qd, *J* = 8.6, 7.9, 3.4 Hz, 1H) 2.55 – 2.45 (m, 2H), 2.26 – 1.91 (m, 2H). ^{13}C NMR (75 MHz, DMSO-*d*$_6$) *δ*[ppm] = 157.2, 153.2, 139.9, 135.9, 135.6, 130.2, 128.5, 128.5, 128.1, 126.2, 114.6, 45.3, 33.4, 30.5. $[\alpha]_{589}^{20} = -37°$ (c = 10 $\frac{\mathbf{mg}}{\mathbf{mL}}$, MeOH).

FINAL COMPOUNDS.

(*S,E*)-*N*-(1-Fluoro-5-phenyl-1-(phenylsulfonyl)pent-1-en-3-yl)-1*H*-indole-7-carboxamide (**2a**)

Synthesized according to procedure A using fluorovinylsulfone **47** (1 eq., 1 mmol, 0.34 g) and 1*H*-indole-7-carboxylic acid (1.2 eq., 1.2 mmol, 0.16 g). The product was obtained as a colorless solid (0.01 g, 0.02 mmol, 2%). ^{1}H NMR (300 MHz, $CDCl_3$) δ[ppm] = 10.19 (s, 1H), 7.97 (dd, *J* = 7.3, 1.8 Hz, 2H), 7.82 (d, J = 7.6 Hz, 1H), 7.76 – 7.66 (m, 1H), 7.58 (dd, *J* = 8.5, 7.0 Hz, 2H), 7.31 (dt, *J* = 6.6, 1.5 Hz, 2H), 7.26 – 7.21 (m, 2H), 7.20 – 7.11 (m, 3H), 7.08 (t, *J* = 7.6 Hz, 1H), 6.58 (dd, $J_{H\text{-}F}$ = 32.0 Hz, $J_{H\text{-}H}$ = 8.2 Hz, 1H), 6.47 – 6.28 (m, 1H), 5.08 (p, *J* = 7.6 Hz, 1H), 2.76 (t, *J* = 7.6 Hz, 2H), 2.18 – 2.14 (m, 2H). ^{13}C NMR (75 MHz, $CDCl_3$) δ[ppm] = 167.2, 156.9, 140.3, 136.9, 135.4, 134.6, 129.6, 129.5, 128.8, 128.7, 128.4, 126.4, 125.7, 125.3, 118.9, 118.6, 117.7, 117.6, 115.0, 102.1, 45.3, 35.8, 32.0. $[\alpha]_{589}^{20} = -8°$ (c = 10 $\frac{\mathbf{mg}}{\mathbf{mL}}$, MeOH). MP = 61 °C. LC-MS: [M+H$^+$] calc. 463.5, found 463.1. Purity: 98% (HPLC, 254 nm, ACN/H_2O 65/35, 0.01% HCOOH, t_R = 1.28 min).

(*S,E*)-*N*-(5-Phenyl-1-(phenylsulfonyl)pent-1-en-3-yl)-1*H*-indole-7-carboxamide (**2b**)

Synthesized according to procedure A using vinylsulfone **45** (1 eq., 0.71 mmol, 0.24 g) and 1*H*-indole-7-carboxylic acid (1.2 eq., 0.85 mmol, 0.14 g). The product was obtained as a colorless solid (0.15 g, 0.30 mmol, 42%). ^{1}H NMR (300 MHz, $CDCl_3$) δ[ppm] = 10.07 (s, 1H), 7.80 – 7.73 (m, 2H), 7.70 (dt, *J* = 7.7, 0.9 Hz, 1H), 7.54 – 7.46 (m, 1H), 7.46– 7.36 (m, 2H), 7.22 – 7.17 (m, 2H), 7.17 – 7.10 (m, 2H), 7.08 – 7.02 (m, 3H), 7.01 – 6.96 (m, 1H), 6.96 – 6.91 (m, 1H), 6.46 (dd, *J* = 3.2, 2.2 Hz, 1H), 6.40 (dd, *J* = 15.1, 1.7 Hz, 1H), 4.99 – 4.90 (m, 1H), 2.66 (hept, *J* = 7.4 Hz, 2H), 2.05 – 2.00 (m, 2H). ^{13}C NMR (75 MHz, $CDCl_3$) δ[ppm] = 167.3, 146.1, 140.4, 134.0, 135.0, 133.6, 130.9, 129.6, 129.4, 128.8, 128.4, 127.7, 126.5, 125.7, 125.3, 119.0, 118.6, 114.9, 102.1, 49.4, 35.4, 32.1. $[\alpha]_{589}^{20} = -20°$ (c = 10 $\frac{\mathbf{mg}}{\mathbf{mL}}$, MeOH). MP = 65 °C. LC-MS: [M+H$^+$] calc. 445.6, found 445.4. Purity: 98% (HPLC, 254 nm, ACN/H_2O 55/45, 0.01% HCOOH, t_R = 3.86 min).

(*S,E*)-*N*-(5-Phenyl-1-(phenylsulfonyl)pent-1-en-3-yl)-2,3-dihydrobenzo[*b*][1,4]dioxine-5-carboxamide (**2c**)

Synthesized according to procedure A using vinylsulfone **45** (1 eq., 0.71 mmol, 0.24 g) and 2,3-dihydrobenzo[*b*][1,4]dioxine-5-carboxylic acid (1.2 eq., 0.85 mmol, 0.15 g). The product was obtained as a colorless solid (0.12 g, 0.30 mmol, 42%). ^{1}H NMR (300 MHz, $CDCl_3$) δ[ppm] = 7.77 (dd, *J* = 7.2, 1.9 Hz, 2H), 7.58 – 7.46 (m, 2H), 7.43

(dd, *J* = 8.3, 6.6 Hz, 2H), 7.18 (dd, *J* = 7.9, 6.4 Hz, 2H), 7.13 – 7.09 (m, 1H), 7.08 – 7.03 (m, 2H), 6.99 – 6.93 (m, 1H), 6.93 – 6.89 (m, 1H), 6.84 (t, *J* = 7.9 Hz, 1H), 6.41 (dd, *J* = 15.1, 1.8 Hz, 1H), 4.99 – 4.78 (m, 1H), 4.29 – 4.25 (m, 4H), 2.73 – 2.53 (m, 2H), 2.03 – 1.77 (m, 2H). ^{13}C NMR (75 MHz, $CDCl_3$) *δ*[ppm] = 164.5, 146.3, 143.7, 142.0, 140.5, 140.1, 133.5, 130.7, 129.4, 128.6, 128.3, 127.7, 126.3, 124.2, 121.5, 121.5, 121.2, 65.1, 63.5, 49.5, 36.0, 32.1. $[\alpha]_{589}^{20} = -39°$ (c = 10 $\frac{\mathrm{mg}}{\mathrm{mL}}$, MeOH). MP = 63 °C. LC-MS: [M+H$^+$] calc. 464.6, found 464.4. Purity: 100% (HPLC, 254 nm, ACN/H_2O 55/45, 0.01% HCOOH, t_R = 2.50 min).

N-((*S*,*E*)-5-Phenyl-1-(phenylsulfonyl)pent-1-en-3-yl)-2,3,4,9-tetrahydro-1*H*-carbazol-1-carboxamide (**2d**)

Synthesized according to procedure A using vinylsulfone **45** (1 eq., 0.74 mmol, 0.25 g) and 2,3,4,9-tetrahydro-1*H*-carbazole-1-carboxylic acid (1.2 eq., 0.88 mmol, 0.19 g). The product was obtained as a colorless solid (0.09 g, 0.20 mmol, 27%). ^{1}H NMR (300 MHz, $CDCl_3$) *δ*[ppm] = 8.75 (s, 1H), 7.76 – 7.66 (m, 2H), 7.55 – 7.46 (m, 1H), 7.41 (tt, *J* = 8.5, 5.2 Hz, 3H), 7.22 (dd, *J* = 8.0, 3.9 Hz, 1H), 7.17 – 7.08 (m, 3H), 7.08 – 7.01 (m, 2H), 6.96 (td, *J* = 8.6, 7.7, 1.6 Hz, 2H), 6.76 (dt, *J* = 15.1, 5.6 Hz, 1H), 6.36 – 6.22 (m, 1H), 5.60 (d, *J* = 8.7 Hz, 1H), 4.68 (d, *J* = 6.5 Hz, 1H), 3.66 (q, *J* = 7.2, 6.5 Hz, 1H), 2.65 (dd, *J* = 13.3, 6.6 Hz, 2H), 2.51 (q, *J* = 9.6, 7.0 Hz, 2H), 2.07 –1.65 (m, 6H). ^{13}C NMR (75 MHz, $CDCl_3$) *δ*[ppm] = 173.2, 145.4, 140.7, 140.2, 136.4, 133.6, 131.1, 130.7, 129.4, 128.7, 128.5, 128.3, 127.6, 122.3, 119.5, 118.4, 112.7, 111.3, 49.8, 42.2, 35.3, 32.1, 27.7, 20.7. $[\alpha]_{589}^{20} = -18°$ (c = 10 $\frac{\mathrm{mg}}{\mathrm{mL}}$, MeOH). MP = 78 °C. LC-MS: [M+H$^+$] calc. 500.1, found 500.5. Purity: 96% (HPLC, 254 nm, ACN/H_2O 70/30, 0.01% HCOOH, t_R = 1.29 min).

(*S*,*E*)-*N*-(5-Phenyl-1-(phenylsulfonyl)pent-1-en-3-yl)-2-(phenylamino)benzamide (**2e**)

Synthesized according to procedure A using vinylsulfone **45** (1 eq., 0.80 mmol, 0.27 g) and 2-(phenylamino)benzoic acid (1.2 eq., 0.96 mmol, 0.20 g). The product was obtained as a colorless solid (0.18 g, 0.40 mmol, 50%). ^{1}H NMR (300 MHz, $CDCl_3$) *δ*[ppm] = 7.90 – 7.81 (m, 2H), 7.61 – 7.53 (m, 1H), 7.48 (dd, *J* = 8.2, 6.6 Hz, 2H), 7.38 – 7.27 (m, 7H), 7.26 (s, 1H), 7.24 (d, *J* = 2.1 Hz, 1H), 7.18 (dt, *J* = 8.4, 1.5 Hz, 4H), 7.11 – 7.05 (m, 1H), 6.76 – 6.73 (m, 1H), 6.50 (td, *J* = 15.6, 15.1, 1.6 Hz, 1H), 6.38 (d, *J* = 8.2 Hz, 1H), 4.91 (p, *J* = 6.7 Hz, 1H), 2.90 – 2.63 (m, 2H), 2.20 – 1.98 (m, 2H). ^{13}C NMR (75 MHz, $CDCl_3$) *δ*[ppm] = 168.8, 145.7, 141.2, 140.3, 139.9, 133.5, 132.7, 131.0, 129.3, 128.8, 128.4, 127.6, 127.5, 126.5, 122.9, 121.1, 118.2, 117.2, 115.8, 49.6, 35.3, 32.1. $[\alpha]_{589}^{20} = -46°$ (c = 10 $\frac{\mathrm{mg}}{\mathrm{mL}}$, MeOH). MP = 59 °C. LC-MS: [M+H$^+$] calc.

497.6, found 497.3. Purity: 100% (HPLC, 254 nm, ACN/H_2O 65/35, 0.01% HCOOH, t_R = 1.99 min).

(*S,E*)-*N*-(5-Phenyl-1-(phenylsulfonyl)pent-1-en-3-yl)-1*H*-indazol-6-carboxamide (**2f**)

Synthesized according to procedure A using vinylsulfone **45** (1 eq., 0.74 mmol, 0.25 g) and 1*H*-indazole-6-carboxylic acid (1.2 eq., 0.88 mmol, 0.14 g). The product was obtained as a colorless solid (0.20 g, 0.20 mmol, 27%). ^{1}H NMR (300 MHz, $CDCl_3$) δ[ppm] = 8.06 (s, 1H), 7.96 (s, 1H), 7.80 (d, *J* = 7.6 Hz, 2H), 7.70 – 7.49 (m, 2H), 7.49 – 7.31 (m, 3H), 7.19 (p, *J* = 6.8 Hz, 3H), 7.13 – 6.98 (m, 3H), 6.58 (d, *J* = 15.0 Hz, 1H), 4.96 (p, *J* = 7.1, 6.6 Hz, 1H), 2.70 (hept, *J* = 6.9 Hz, 2H), 2.04 (q, *J* = 7.7 Hz, 2H). ^{13}C NMR (75 MHz, $CDCl_3$) δ[ppm] = 167.4, 146.2, 140.5, 139.7, 133.7, 132.6, 130.8, 129.4, 128.7, 128.4, 127.6, 126.3, 120.0, 110.1, 50.2, 35.3, 32.1. $[\alpha]_{589}^{20} = -20°$ (c = 10 $\frac{mg}{mL}$, MeOH). MP = 85 °C. LC-MS: [M+H$^+$] calc. 445.5, found 445.9. Purity: 100% (HPLC, 254 nm, ACN/H_2O 65/35, 0.01% HCOOH, t_R = 1.24 min).

(*S,E*)-Phenyl 3-(1*H*-indol-7-carboxamido)-5-phenylpent-1-ene-1-sulfonate (**2g**)

Synthesized according to procedure A using vinylsulfonate **46** (1 eq., 0.74 mmol, 0.27 g) and 1*H*-indole-7-carboxylic acid (1.2 eq., 0.88 mmol, 0.14 g). The product was obtained as a colorless solid (0.10 g, 0.20 mmol, 27%). ^{1}H NMR (300 MHz, $CDCl_3$) δ[ppm] = 10.33 (s, 1H), 7.90 (d, *J* = 7.2 Hz, 1H), 7.36 – 7.33 (m, 6H), 7.31 – 7.19 (m, 6H), 7.18 – 7.08 (m, 2H), 6.89 (dd, *J* = 15.2, 8.4 Hz, 1H), 6.67 (q, *J* = 2.3 Hz, 1H), 6.63 – 6.53 (m, 1H), 6.43 (d, *J* = 7.9 Hz, 1H), 4.96 (dq, *J* = 13.7, 6.8, 6.4 Hz, 1H), 2.78 (hept, *J* = 7.3 Hz, 2H), 2.11 (q, *J* = 7.7 Hz, 2H). ^{13}C NMR (75 MHz, $CDCl_3$) δ[ppm] = 167.4, 149.6, 149.4, 140.2, 135.4, 129.8, 129.7, 128.9, 128.4, 127.3, 126.6, 125.8, 125.5, 124.8, 122.5, 119.1, 118.7, 114.8, 102.2, 49.8, 34.7, 32.0. $[\alpha]_{589}^{20} = -17°$ (c = 10 $\frac{mg}{mL}$, MeOH). MP = 62 °C. LC-MS: [M+H$^+$] calc. 460.5, found 460.9. Purity: 100% (HPLC, 254 nm, ACN/H_2O 55/45, 0.01% HCOOH, t_R = 2.37 min).

(*S,E*)-Phenyl 3-(2,3-dihydrobenzo[*b*][1,4]dioxin-5-carboxamido)-5-phenylpent-1-en-1-sulfonate (**2h**)

Synthesized according to procedure A using vinylsulfonate **46** (1 eq., 0.71 mmol, 0.26 g) and 2,3-dihydrobenzo[*b*][1,4]dioxine-5-carboxylic acid (1.2 eq., 0.85 mmol, 0.15 g). The product was obtained as a colorless solid (0.10 g, 0.20 mmol, 28%). ^{1}H NMR (300 MHz, $CDCl_3$) δ[ppm] = 7.65 (dd, *J* = 7.7, 1.9 Hz, 1H), 7.48 (d, *J* = 7.8 Hz, 1H), 7.28 – 7.17 (m, 4H), 7.17 – 7.11 (m, 4H), 7.09 – 7.02 (m, 2H), 6.98 (dd, *J* = 8.0, 1.9 Hz, 1H), 6.91 (t, *J* = 7.9 Hz, 1H), 6.72 (dd, *J* = 15.1, 5.2 Hz, 1H), 6.46 (dd, *J* = 15.1, 1.5 Hz, 1H), 4.90 – 4.71 (m, 1H), 4.37 – 4.17 (m, 4H), 2.62 (dd, *J* = 14.1,

9.1 Hz, 2H), 2.03 –1.78 (m, 3H). ^{13}C NMR (75 MHz, $CDCl_3$) δ[ppm] = 164.5, 149.7, 149.5, 143.7, 142.3, 140.2, 129.8, 128.7, 128.3, 127.3, 126.4, 124.6, 124.2, 122.7, 121.7, 121.3, 65.2, 63.5, 49.8, 35.4, 32.1. $[\alpha]_{589}^{20} = -41°$ (c = 10 $\frac{\text{mg}}{\text{mL}}$, MeOH). MP = 64 °C. LC-MS: [M+H$^+$] calc. 479.5, found 479.9. Purity: 100% (HPLC, 254 nm, ACN/H_2O 55/45, 0.01% HCOOH, t_R = 1.76 min).

(*S,E*)-Phenyl 5-phenyl-3-(2,3,4,9-tetrahydro-1*H*-carbazol-1-carboxamido)pent-1-en-1-sulfonate (**2i**)

Synthesized according to procedure A using vinylsulfonate **46** (1 eq., 0.77 mmol, 0.28 g) and 2,3,4,9-tetrahydro-1*H*-carbazole-1-carboxylic acid (1.2 eq., 0.92 mmol, 0.20 g). The product was obtained as a colorless solid (0.06 g, 0.10 mmol, 13%). ^{1}H NMR (300 MHz, $CDCl_3$) δ[ppm] = 8.52 (s, 1H), 7.92 (s, 1H), 7.43 (td, *J* = 6.7, 6.0, 1.3 Hz, 1H), 7.32 – 6.99 (m, 11H), 6.94 (td, *J* = 8.5, 7.7, 1.6 Hz, 1H), 6.57 (dd, *J* = 15.1, 9.7 Hz, 1H), 6.31 – 6.28 (m, 1H), 4.67 – 4.52 (m, 1H), 3.61 (dt, *J* = 23.3, 5.8 Hz, 1H), 2.67 (h, *J* = 6.8, 6.1 Hz, 2H), 2.54 – 2.34 (m, 2H), 2.09 –1.92 (m, 2H), 1.81 (dq, *J* = 12.1, 5.6 Hz, 2H), 1.68 – 1.64 (m, 2H). ^{13}C NMR (75 MHz, $CDCl_3$) δ[ppm] = 173.2, 149.4, 149.0, 140.4, 139.9, 136.4, 129.8, 128.7, 128.2, 127.3, 127.2, 126.5, 124.6, 122.5, 122.4, 119.7, 118.5, 112.9, 111.3, 49.5, 41.9, 35.0, 32.3, 27.8, 21.1, 20.7. $[\alpha]_{589}^{20} = -47°$ (c = 10 $\frac{\text{mg}}{\text{mL}}$, MeOH). MP = 60 °C. LC-MS: [M+H$^+$] calc. 515.6, found 515.1. Purity: 99% (HPLC, 254 nm, ACN/H_2O 55/45, 0.01% HCOOH, t_R = 3.35 min).

(*S,E*)-Phenyl 5-phenyl-3-(2-(phenylamino)benzamido)pent-1-en-1-sulfonate (**2j**)

Synthesized according to procedure A using vinylsulfonate **46** (1 eq., 0.71 mmol, 0.26 g) and 2-(phenylamino)benzoic acid (1.2 eq., 0.86 mmol, 0.18 g). The product was obtained as a colorless solid (0.13 g, 0.25 mmol, 35%). ^{1}H NMR (300 MHz, $CDCl_3$) δ[ppm] = 7.32 – 6.98 (m, 18H), 6.96 (t, *J* = 7.3 Hz, 1H), 6.74 – 6.60 (m, 1H), 6.39 (d, *J* = 15.1 Hz, 1H), 6.12 (d, *J* = 7.7 Hz, 1H), 4.71 (p, *J* = 6.7 Hz, 1H), 2.61 (hept, *J* = 7.3 Hz, 2H), 1.93 (p, *J* = 6.8 Hz, 2H). ^{13}C NMR (75 MHz, $CDCl_3$) δ[ppm] = 168.7, 149.4, 149.3, 145.9, 141.2, 140.1, 132.9, 129.8, 129.4, 128.9, 128.4, 127.5, 127.3, 126.6, 124.9, 123.0, 122.5, 121.2, 118.1, 116.8, 115.9, 49.8, 34.8, 32.0. $[\alpha]_{589}^{20} = -42°$ (c = 10 $\frac{\text{mg}}{\text{mL}}$, MeOH). MP = 61 °C. LC-MS: [M+H$^+$] calc. 512.2, found 512.1. Purity: 99% (HPLC, 254 nm, ACN/H_2O 65/35, 0.01% HCOOH, t_R = 2.30 min).

(*S,E*)-Phenyl 3-(1*H*-indazol-6-carboxamido)-5-phenylpent-1-en-1-sulfonate (**2k**)

Synthesized according to procedure A using vinylsulfonate **46** (1 eq., 0.69 mmol, 0.25 g) and 1*H*-indazole-6-carboxylic acid (1.2 eq., 0.83 mmol, 0.13 g). The product

was obtained as a colorless solid (0.04 g, 0.09 mmol, 13%). ^{1}H NMR (300 MHz, $CDCl_3$) δ[ppm] = 7.81 (s, 1H), 7.61 (d, J = 8.5 Hz, 1H), 7.26 (s, 1H), 7.21 – 7.14 (m, 4H), 7.11 (t, J = 7.5 Hz, 5H), 7.03 (d, J = 7.3 Hz, 2H), 6.74 (dd, J = 15.1, 5.4 Hz, 1H), 6.49 (d, J = 15.1 Hz, 1H), 4.80 (t, J = 6.8 Hz, 1H), 2.59 (hept, J = 7.0 Hz, 2H), 1.93 (q, J = 7.3 Hz, 2H). ^{13}C NMR (75 MHz, $CDCl_3$) δ[ppm] = 167.4, 149.5, 149.3, 145.2, 140.2, 129.8, 128.8, 128.3, 127.4, 126.5,125.0, 124.8, 123.2, 122.5, 50.5, 34.7, 32.0. $[\alpha]_{589}^{20} = -8°$ (c = 10 $\frac{\text{mg}}{\text{mL}}$, MeOH). MP = 79 °C. LC-MS: [M+H$^+$] calc. 462.5, found 462.4. Purity: 99% (HPLC, 254 nm, ACN/H_2O 65/35, 0.01% HCOOH, t_R = 1.00 min).

(*S,E*)-Phenyl 3-(1*H*-benzo[*d*]imidazol-5-carboxamido)-5-phenylpent-1-en-1-sulfonate (**2l**)

Synthesized according to procedure A using vinylsulfonate **46** (1 eq., 0.66 mmol, 0.24 g) and 1*H*-benzo[*d*]imidazole-5-carboxylic acid (1.2 eq., 0.79 mmol, 0.13 g). The product was obtained as a colorless solid (0.09 g, 0.19 mmol, 29%). ^{1}H NMR (300 MHz, $CDCl_3$) δ[ppm] = 9.59 (s, 1H), 8.08 (d, J = 32.4 Hz, 1H), 7.80 – 7.55 (m, 1H), 7.56 – 7.40 (m, 1H), 7.38 – 7.22 (m, 1H), 7.11 – 6.94 (m, 8H), 6.89 (d, J = 7.4 Hz, 3H), 6.72 (dd, J = 15.2, 5.5 Hz, 1H), 6.50 (d, J = 14.9 Hz, 1H), 4.69 (d, J = 8.7 Hz, 1H), 2.46 (qt, J = 14.8, 8.8, 8.2 Hz, 2H), 1.85 (d, J = 29.3 Hz, 2H). ^{13}C NMR (75 MHz, $CDCl_3$) δ[ppm] = 168.0, 162.0, 150.2, 149.2, 144.7, 140.2, 136.3, 129.8, 128.6, 128.3, 127.4, 126.3, 124.4, 122.4, 115.3, 50.4, 34.7, 32.1. $[\alpha]_{589}^{20} = -45°$ (c = 10 $\frac{\text{mg}}{\text{mL}}$, MeOH). MP = 89 °C. LC-MS: [M+H$^+$] calc. 462.5, found 462.4. Purity: 95% (HPLC, 254 nm, ACN/H_2O 65/35, 0.01% HCOOH, t_R = 0.70 min).

(*S,E*)-Phenyl-5-phenyl-3-(9*H*-xanthen-4-carboxamido)pent-1-en-1-sulfonate (**2m**)

Synthesized according to procedure A using vinylsulfonate **46** (1 eq., 0.85 mmol, 0.30 g) and benzo[*d*]oxazole-6-carboxylic acid (1.2 eq., 1.0 mmol, 0.22 g). The product was obtained as a colorless solid (0.11 g, 0.22 mmol, 25%). ^{1}H NMR (300 MHz, DMSO-d_6) δ[ppm] = 8.78 – 8.75 (d, 1H), 8.38 – 8.31 (m, 1H), 8.23 – 8.21 (d, J = 7.6 Hz, 2H), 7.87 – 7.82 (dt, J = 7.5, 1.4 Hz, 2H), 7.68 – 7.66 (d, 1H), 7.61 – 7.44 (m, 4H), 7.39 – 7.36 (m, 2H), 7.31 – 7.28 (dd, J = 7.7, 1.8 Hz, 6H), 6.95 – 6.89 (dd, J = 15.2, 5.1 Hz, 2H), 4.86 – 4.80 (m, 1H), 3.33 – 3.27 (d, J = 1.4 Hz, 2H), 2.73 – 2.65 (tt, J = 9.5, 4.2 Hz, 2H), 2.07 – 1.93 (m, 2H). ^{13}C NMR (75 MHz, $CDCl_3$) δ[ppm] = 164.5, 155.9, 152.9, 151.8, 149.6, 141.5, 130.4, 128.9, 128.8, 128.6, 127.9, 127.7, 126.4, 125.0, 124.0, 123.6, 121.9, 120.6, 50.2, 34.7, 32.1. $[\alpha]_{589}^{20} = -28°$ (c = 10 $\frac{\text{mg}}{\text{mL}}$, MeOH). MP = 57 – 60 °C. LC-MS: [M+H$^+$] calc. 512.5, found 512.1. Purity: 100% (HPLC, 254 nm, ACN/H_2O 65/35, 0.01% HCOOH, t_R = 3.65 min).

Phenyl (*S,E*)-3-(benzo[*d*]oxazole-6-carboxamido)-5-phenylpent-1-ene-1-sulfonate (**2n**)

Synthesized according to procedure A using vinylsulfonate **46** (1 eq., 0.43 mmol, 0.15 g) and carboxylic acid **6** (1.2 eq., 0.51 mmol, 0.08 g). The product was obtained as a colorless solid (0.08 g, 0.16 mmol, 39%). ^{1}H NMR (300 MHz, DMSO-d_6) δ[ppm] = 10.07 (s, 1H, *H*-12), 9.52 (s, 1H), 8.65 (s, 1H), 8.54 – 8.49 (d, 1H), 8.29 (s, 1H), 7.14 – 7.08 (m, 2H), 7.02 – 6.99 (m, 3H), 6.93 – 6.90 (d, J = 7.1 Hz, 1H), 6.61 – 6.50 (dd, J = 15.2, 1.3 Hz, 1H), 4.46 – 4.32 (m, 1H), 3.11 (s, 5H), 2.23 – 2.10 (m, 1H), 1.67 – 1.55 (m, 1H). ^{13}C NMR (75 MHz, DMSO-d_6) δ[ppm] = 166.2, 156.7, 151.8, 151.6, 149.6, 146.6, 142.6, 141.5, 132.2, 130.4, 128.8, 128.3, 128.7, 127.9, 126.4, 123.0, 111.1, 50.4, 34.5, 32.1. $[\alpha]_{589}^{20} = -5°$ (c = 10 $\frac{\mathbf{mg}}{\mathbf{mL}}$, MeOH). MP = 64 – 67 °C. LC-MS: [M+H$^+$] calc. 463.1, found 463.0. Purity: 97% (HPLC, 254 nm, ACN/H_2O 50/50, 0.01% HCOOH, t_R = 3.29 min).

Phenyl (*S,E*)-3-(benzo[*d*]isoxazole-3-carboxamido)-5-phenylpent-1-ene-1-sulfonate (**2o**)

Synthesized according to procedure A using vinylsulfonate **46** (1 eq., 0.45 mmol, 0.16 g) and benzo[*d*]isoxazole-3-carboxylic acid (1.2 eq., 0.54 mmol, 0.09 g). The product was obtained as a colorless solid (0.04 g, 0.05 mmol, 10%). ^{1}H NMR (300 MHz, DMSO-d_6) δ[ppm] = 9.17 – 9.12 (d, J = 8.5 Hz, 1H), 7.89 – 7.76 (d, J = 10.2 Hz, 1H), 7.65 – 7.59 (d, J = 8.6 Hz, 2H), 7.51 – 7.44 (t, 2H), 7.29 – 7.18 (t, 2H), 7.13 – 7.08 (m, 2H), 7.04 – 7.00 (m, 3H), 6.92 – 6.86 (m 2H), 6.78 – 6.66 (dd, J = 15.2, 1.3 Hz, 1H), 6.61 – 6.56 (dd, J = 15.7, 5.0 Hz, 1H), 4.53 – 4.44 (m, 1H), 2.25 – 2.19 (d, J = 1.9 Hz, 1H), 1.71 – 1.67 (m, 1H), 1.17 (s, 1H). ^{13}C NMR (75 MHz, DMSO-d_6) δ[ppm] = 163.7, 159.1, 152.5, 150.7, 141.3, 131.5, 130.4, 128.8, 127.9, 126.4, 125.6, 110.5, 49.8, 34.3, 32.1. $[\alpha]_{589}^{20} = -13°$ (c = 10 $\frac{\mathbf{mg}}{\mathbf{mL}}$, MeOH). MP = 75 – 77 °C. LC-MS: [M+H$^+$] calc. 463.1, found 463.0. Purity: 100% (HPLC, 254 nm, ACN/H_2O 55/45, 0.01% HCOOH, t_R = 1.43 min).

(*S,E*)-Phenyl-3-(3,4-dihydro-2*H*-benzo[*b*][1,4]oxazin-7-carboxamido)-5-phenylpent-1-en-1-sulfonate (**2p**)

Synthesized according to procedure A using vinylsulfonate **46** (1 eq., 0.85 mmol, 0.30 g) and carboxylic acid **8** (1.2 eq., 1.0 mmol, 0.18 g). The product was obtained as a colorless solid (0.04 g, 0.09 mmol, 12%). ^{1}H NMR (300 MHz, DMSO-d_6) δ[ppm] = 8.39 – 8.34 (d, 1H), 7.40 – 7.35 (d, J = 8.1 Hz, 1H), 7.33 (s, 3H), 7.31 – 7.27 (m, 4H), 7.21 – 7.16 (m, 4H), 6.83 – 6.70 (dd, J = 12.1, 1.1 Hz, 2H), 5.07 (s, 1H), 4.18 –

4.09 (m, 2H), 3.33 – 3.22 (m, 2H), 1.91 – 1.86 (q, *J* = 7.7 Hz, 2H), 1.25 (s, 1H). ^{13}C NMR (75 MHz, DMSO-d_6) δ[ppm] = 166.9, 152.0, 149.6, 141.5, 130.4, 129.0, 128.9, 128.8, 128.7, 126.4, 124.1, 123.0, 117.0, 115.9, 115.0, 49.9, 34.6, 32.1. $[\alpha]_{589}^{20} = -10°$ (c = 10 $\frac{\text{mg}}{\text{mL}}$, MeOH). MP = 52 – 55 °C. LC-MS: [M+H$^+$] calc. 479.6, found 479.3. Purity: 96% (HPLC, 254 nm, ACN/H_2O 55/45, 0.01% HCOOH, t_R = 2.13 min).

(*S,E*)-Phenyl-3-(isoxazole-5-carboxamido)-5-phenylpent-1-en-1-sulfonate (**2q**)

Synthesized according to procedure A using vinylsulfonate **46** (1 eq., 0.34 mmol, 0.12 g) and isoxazole-5-carboxylic acid (1.2 eq., 0.41 mmol, 0.05 g). The product was obtained as a colorless solid (0.03 g, 0.07 mmol, 18%). ^{1}H NMR (300 MHz, DMSO-d_6) δ[ppm] = 8.94 – 8.91 (d, *J* = 8.2 Hz, 1H), 8.53 – 8.51 (d, *J* = 1.9 Hz, 1H), 7.24 – 7.06 (m, 2H), 7.12 – 6.99 (m, 3H), 7.02 (s, 1H), 7.00 (s, 1H), 6.99 – 6.86 (m, 4H), 6.75 – 6.66 (dd, *J* = 15.2, 1.4 Hz, 1H), 6.55 – 6.47 (dd, *J* = 15.2, 5.6 Hz, 1H), 4.43 – 4.39 (p, *J* = 7.4 Hz, 1H), 2.36 – 2.30 (td, *J* = 15.7, 8.1, 1H), 1.13 (s, 1H). ^{13}C NMR (75 MHz, DMSO-d_6) δ[ppm] = 162.8, 155.9, 152.2, 150.6, 149.5, 141.2, 130.4, 128.8, 127.9, 123.0, 106.9, 49.8, 34.2, 32.0. $[\alpha]_{589}^{20} = -8°$ (c = 10 $\frac{\text{mg}}{\text{mL}}$, MeOH). MP = 130 – 132 °C. LC-MS: [M+H$^+$] calc. 413.5, found 413.1. Purity: 99% (HPLC, 254 nm, ACN/H_2O gradient, 0.01% HCOOH, t_R = 6.08 min).

Fluorometric enzyme assays.

*Sm*CB1 AUTO-ACTIVATION.

Inactive zymogen of *Sm*CB1 was activated by auto-activation as described in literature.[273] Zymogen was diluted to a final concentration of 2 μM in activation buffer (100 mM sodium acetate pH 5.0, 2.5 mM DTT, 1 mM EDTA, 0.1% PEG 6000), dextran sulfate 500 kDa was added to a final concentration of 10 mg/L to induce autocleavage of *Sm*CB1. Cleavage was performed at 37 °C for 6 h.

*Sm*CB1 ASSAY PROCEDURE.

The assay was modified after JÍLKOVÁ ET AL.[195] Assay buffer (100 mM sodium citrate, 2.5 mM DTT, 1 mM EDTA, 0.1% PEG 6000, pH 6.0) was incubated with 1 nM activated *Sm*CB1 at 37 °C for 10 min. Afterwards, inhibitor in DMSO or DMSO (negative control) was added followed by 20 μM of the substrate *Z*-Phe-Arg-AMC (BACHEM, Basel, Switzerland). The mixture was measured at 37 °C for 10 min (screening) or 30 min (IC_{50}, K_i) on a TECAN SPARK (ẟ excitation: 365 nm, ẟ emission: 460 nm; TECAN GROUP, Männedorf, Switzerland) plate reader using black GREINER

BIO-ONE CHIMNEY 96 well microtiter plates (GREINER BIO-ONE GMBH, Frickenhausen, Germany). Inhibitor screening concentrations started at 50 μM, followed by 20 μM, 1 μM, 200 nM, and 50 nM. IC_{50} or K_i values were determined for compounds with >50% inhibition at 20 μM.

K_m DETERMINATION.

The assay was performed as described above using various substrate concentrations (1.25 – 100 μM). GRAFIT (version 5.0.13, 2006, ERITHRACUS SOFTWARE LTD., UK) was used for data analysis and non-linear regression.[274] The K_m value was calculated as described by Michaelis-Menten:

$$v_0 = \frac{v_{max} \cdot [S]}{K_m + [S]}$$

v_0 = initial velocity; v_{max} = maximal velocity; [S] = substrate concentration.

IC_{50} AND K_i CALCULATIONS.

We used GRAFIT (version 5.0.13, 2006, ERITHRACUS SOFTWARE LTD., UK) for data analysis and non-linear regression.[274] For compounds without a time-dependent mode of inhibition ((fluorinated) vinylsulfones vs *Sm*CB1, CatB, CatL; vinylsulfonates vs CatB, CatL), we plotted residual enzyme activity in % against the inhibitor concentration in μM, obtaining IC_{50} values by non-linear regression:

$$v_i = \frac{v_o}{1 + (\frac{[I]}{IC_{50}})^S}$$

v_0 = enzyme activity without inhibitor; v_i = enzyme activity in presence of inhibitor; [I] = inhibitor concentration; S = slope factor.

K_i values were calculated with the CHENG-PRUSOFF equation to correct IC_{50} values to zero substrate concentration:[238]

$$K_i = \frac{IC_{50}}{1 + \frac{[S]}{K_m}}$$

*Sm*CB1: [S] = 20 μM, K_m = 4.3 μM.
CatB: [S] = 100 μM, K_m = 150 μM. CatL: [S] = 6.25 μM, K_m = 6.5 μM.

For compounds with a time-dependent mode of inhibition (vinylsulfonates vs *Sm*CB1), the K_i values were calculated as previously published for irreversible binders.[275]

$$E + I \underset{k_2}{\overset{k_1}{\rightleftharpoons}} [E\text{---}I] \xrightarrow[k_i]{} E\text{-}I$$

E = enzyme; I = inhibitor, k = reaction constant;
[E---I] = non-covalent enzyme-inhibitor complex; E—I = covalent enzyme-inhibitor complex.

Pseudo-first order rate constants k_{obs} were determined for individual inhibitor concentrations according to a continuous method by TIAN and TSOU, monitoring the formation in the presence of inhibitor as a function of time and fitted to the following equation:[275]

$$[P]_t = [P]_\infty \cdot \left(1 - e^{-k_{obs} \cdot t}\right) + off$$

$[P]_t$ = product concentration at time t; $[P]_\infty$ = product concentration at infinite time; off = offset value.

Followed by plotting the k_{obs} values against the inhibitor concentrations [I] and fitting to a hyperbolic equation:

$$k_{obs} = \frac{k_i \cdot [I]}{K_i^{app} + [I]}$$

The resulting dissociation constant of the initial enzyme-inhibitor complex K_i^{app} was then corrected to zero substrate concentration with the CHENG-PRUSOFF relationship, giving the K_i value.[238] The first-order rate constant k_i was further used to calculate second-order rate constants (k_{2nd}).

$$k_{2nd} = \frac{k_i}{K_i}$$

Selectivity towards human cathepsins.

Cathepsin B (CatB, SIGMA-ALDRICH, Darmstadt, Germany) and cathepsin L (CatL, SIGMA-ALDRICH, Darmstadt, Germany) were incubated in enzyme buffer (50 mM Tris-HCl, 5 mM EDTA, 200 mM NaCl, 2 mM DTT, pH 6.5) at room temperature for 20 – 30 min. Assay buffer (50 mM Tris-HCl, 5 mM EDTA, 200 mM NaCl, 0.005% Brij35, pH 6.5) was mixed with cathepsin B or L in enzyme buffer, then inhibitor in DMSO or DMSO (negative control) was added, followed by 100 μM (CatB) or 6.25 μM (CatL) substrate *Z*-Phe-Arg-AMC (BACHEM, Basel, Switzerland). Measurements were performed on a TECAN SPARK (δ excitation: 365 nm, δ emission: 460 nm; TECAN GROUP, Männedorf, Switzerland) plate reader on black GREINER BIO-ONE CHIMNEY 96 well microtiter plates (GREINER BIO-ONE GMBH, Frickenhausen, Germany). Inhibitor

screening concentrations started at 20 μM, followed by 1 μM, 200 nM, and 50 nM. K_i values were determined for inhibitors with >50% inhibition at 20 μM.

Correlation analysis.

The correlation analysis was conducted via MICROSOFT EXCEL (version 2301), giving correlation factors (r). To determine p-values, the t-value was calculated first.

$$t = \frac{r \cdot \sqrt{n-2}}{\sqrt{1-r^2}}$$

n = number of compounds; r = correlation factor.

The p-value should remain <0.05 and was then calculated in MICROSOFT EXCEL (version 2301):

$$T.VERT.2S(ABS(x); variance)$$

ABS(x) = $|r|$; variance = n − 2.

Molecular docking.

Non-covalent approach.

The protein crystal structure of *Sm*CB1 with reference ligand **K11777** (3s3r) was loaded into PYMOL and water molecules were removed.[195,276] Molecular modeling was performed using MOE (version 2019.01) with energy minimizing using an MMFF94x force field.[187,277] Docking calculations were performed using LEADIT (version 2.3.2) from BIOSOLVEIT GMBH and scores were determined using a FlexX and Hyde algorithm.[278,279] The binding site was defined in a 6.5 Å radius around the reference ligand.

Redocking of ligand **K11777** resulted in a pose with an RMSD of 1.26 Å (see **Figure S1**). FlexX and Hyde scores are shown in **Table S1**.

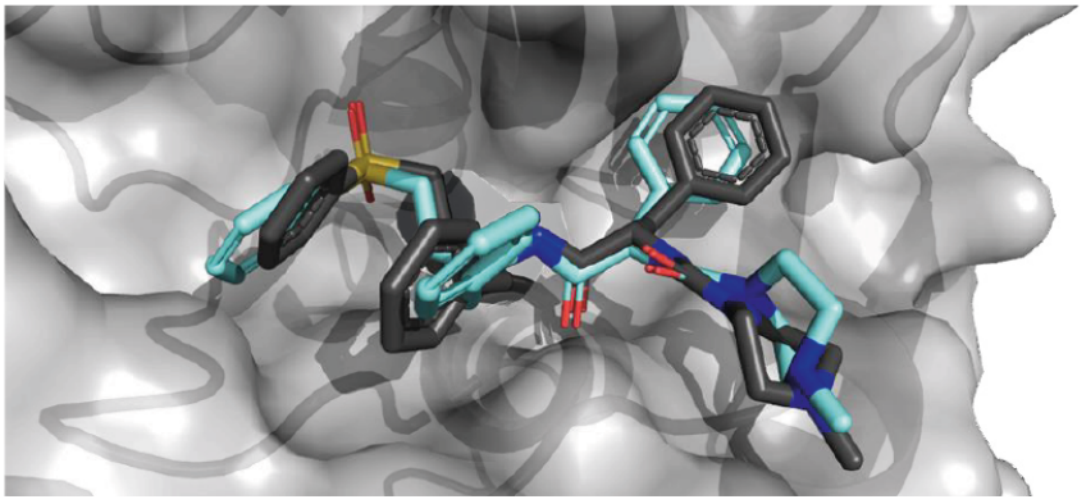

Figure S1. Redocking of **K11777**. PDB 3s3r.[195] Original ligand from crystal structure in dark grey, redocked ligand in cyan. Image created with PYMOL.[276]

Table S1. Non-covalent docking scores.

cpd	FlexX score [kJ/mol]	Hyde score [kJ/mol]	distance warhead-Cys [Å]
SJ605	−24.8	−34	3.2
SJ606	−23.9	−25	2.9
2a	−24.4	−28	3.5
2b	−23.7	−29	3.5
2c	−25.5	−43	3.7
2d	−22.6	−31	3.6
2e	−24.8	−33	3.2
2f	−26.6	−24	3.7
2g	−22.7	−35	3.5
2h	−25.3	−39	3.4
2i	−22.8	−33	4.3
2j	−25.9	−38	3.6
2k	−27.5	−16	3.4
2l	−26.2	−25	3.4
2m	−26.7	−36	3.9
2n	−23.0	−34	3.5
2o	−25.2	−43	3.5
2p	−22.0	−37	3.5
2q	−17.7	−41	3.4

2.4 Perspectives

We have successfully improved our lead structures from the in-house screening, particularly the vinylsulfonate-based compounds. **2h** emerged as the most potent compound in the series with inhibition in the nanomolar range (K_i = 50 nM) and the highest efficacy in *S. mansoni* adults (86% at 10 μM, 68% at 1 μM, 35% at 0.1 μM). Its efficacy is in a similar range to that of praziquantel (IC_{50} = 0.16 μM), the only approved drug to treat schistosomiasis.

Although **2h** is already more than 400-fold selective towards CatB and CatL, warhead modifications, like introducing a fluorine, to result in covalent reversible inhibitors can further diminish the potential for off-target effects. Since the inhibition potency is still in the micromolar range for covalent reversible F-vinylsulfone **2a**, the peptidomimetic scaffold could be combined with the α-fluorovinylsulfonate warhead. If the inhibitory potency is still not sufficient, further scaffold optimizations to improve the active site interactions should be performed.

Other next steps include pharmacokinetic evaluations. Permeability assays are inevitable, e.g., parallel artificial membrane permeation assay (PAMPA) or Caco-2 assays. As a preliminary test before animal experiments, *in vitro* metabolism studies with microsomes could already give some hints about biotransformation processes and metabolic stability. Then, *in vivo* studies with healthy animals could provide essential knowledge on biodistribution and metabolism, important parts of ADME. With the acquired data, further structural optimizations could be performed.

Further preclinical studies involve *in vivo* studies with infected animals, to find out more about the compounds' efficacy. Depending on the *in vivo* performance, targeted delivery systems could be developed to improve efficacy. The outer surface of schistosomes is enclosed with the so-called tegument where several receptors are found.[280,281] Based on these schistosome-specific proteins, the surface of nanocarriers could be functionalized for targeting. An example for such proteins would be tetraspanins that can interact with extacellular proteins and glycans.[280] Nanocarriers could have additional beneficial effects on compound stability, solubility and reduce off-target effects.

3 New subnanomolar cathepsin S inhibitors with high selectivity: Optimizing covalent-reversible α-fluorovinylsulfones and -sulfonates as potential immunomodulators in cancer

3.1 Summary and Own Contribution

This project was part of the subproject Q5 ("*Targeting and immunomodulator structures and their coupling to therapeutic nanosystems for oncological application*") in the CRC1066 ("*Nanodimensional polymer therapeutics for tumor therapy*").

During the last decades, targeting the immune system in cancer therapy has become a valid strategy. Several checkpoint inhibitors, mainly monoclonal antibodies, are approved for various cancers, e.g., ipilimumab or pembrolizumab.[282,283] Discovering new targets in the immune system and developing potential drugs for them is of utmost importance to overcome arising resistances to current therapies.[282,283] Covalent protease inhibitors have recently gained interest for tumor immunotherapy.[284] A primary example for a potential target is the human cysteine protease cathepsin S (CatS) that is overexpressed in various cancers and involved in tumor progression.[166] This involves not only extracellular matrix (ECM) degradation to support angiogenesis, but also the suppression of cytotoxic CD8+ T cells that can attack tumor cells. CatS is crucial for antigen processing in antigen-presenting cells (APC) and favors MHC-II expression, and thus, CD4+ T cells, also including Treg cells.[151–154] Recent studies have shown that CatS knock-down can improve the CD8+ immune response towards tumors.[164,167]

To date, monoclonal antibodies are the main players in immune therapy, but they are associated with several disadvantages, such as poor pharmacokinetic profiles, immune-related side effects, ineffective tumor penetration, and high costs.[285] Our objective was to develop small molecule immunomodulators that inhibit CatS and shift the immune response towards cytotoxic CD8+ T cells. For that purpose, we focused on in-house cathepsin inhibitors from project **1** and optimized them for CatS in terms of potency and selectivity towards cathepsins B and L, following the workflow in **Figure 21**.

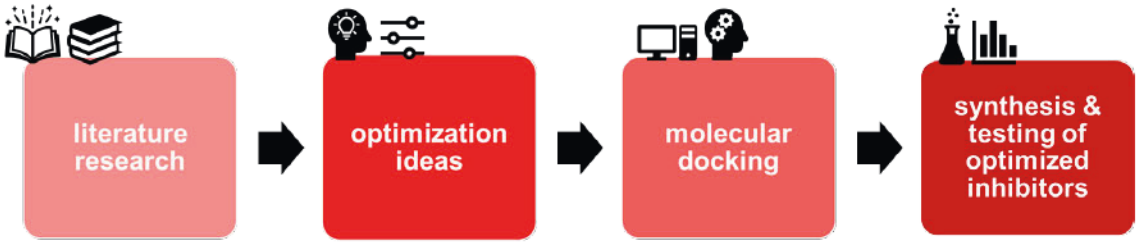

Figure 21. Workflow for project 3.

Ideas from literature research that were verified by molecular docking resulted in optimized inhibitors that we have synthesized and tested in a fluorometric enzyme assay for CatS, CatB and CatL. The resulting compounds are highly active against CatS and selective towards off-target cathepsins.

The results of the project are presented in the following manuscript, titled "New subnanomolar cathepsin S inhibitors with high selectivity: Optimizing covalent-reversible α-fluorovinylsulfones and -sulfonates as potential immunomodulators in cancer" that was submitted to *ChemMedChem* in March 2023.

Own contribution: design and synthesis of optimized compounds **2a–6b**, fluorometric enzyme assay establishment, K_m determination, testing of compounds in enzyme assays, selectivity assays for cathepsins B and L, writing main part of the manuscript, writing main part of the supporting information, preparing tables (1, 2), schemes (1–4), and figures (1–6).

Contribution from others: design and synthesis of initial lead compounds **1a** and **1b**, synthesis of **6c**, molecular docking, cell viability assays on MDA-MB-231 and dendritic cells.

Supporting Information is available on the Appendix CD.

3.2 Manuscript

WILEY-VCH

RESEARCH ARTICLE

New subnanomolar cathepsin S inhibitors with high selectivity: Optimizing covalent-reversible α-fluorovinylsulfones and -sulfonates as potential immunomodulators in cancer

Natalie Fuchs,[a]‡ Mergim Meta,[a]‡ Bellinda Lantzberg,[b] Matthias Bros,[c] Seah Ling Kuan,[b] Tanja Weil,[b] and Tanja Schirmeister*[a]

[a] Institute of Pharmaceutical and Biomedical Sciences (IPBS) Johannes Gutenberg University Mainz
Staudingerweg 5, DE-55128 Mainz

[b] Max Planck Institute for Polymer Research
Ackermannweg 10, DE-55128 Mainz

[c] Department of Dermatology, University Medical Center Mainz,
Langenbeckstr. 1, DE-55131 Mainz

‡ N. F. and M. M. contributed equally.
* All correspondence to Prof. Dr. Tanja Schirmeister, schirmei@uni-mainz.de.

Supporting information for this article is given via a link at the end of the document.

Abstract The cysteine protease cathepsin S (CatS) is overexpressed in many tumors. It is known to be involved in tumor progression as well as antigen processing in antigen-presenting cells (APC). Recent evidence suggests that silencing CatS improves the anti-tumor immune response in several cancers. Therefore, CatS is an interesting target to modulate the immune response in these diseases. Here, we present a series of covalent-reversible CatS inhibitors based on the α-fluorovinylsulfone and -sulfonate warheads. We optimized the lead structures **1a** and **1b** by molecular docking approaches, resulting in 22 final compounds which were evaluated in fluorometric enzyme assays for CatS inhibition and for selectivity towards the off-targets CatB and CatL. The most potent inhibitor in the series, 6c, has subnanomolar affinity (K_i = 0.08 nM) and more than 100,000-fold selectivity towards cathepsins B and L. These new reversible and non-cytotoxic inhibitors could serve as interesting leads to develop new immunomodulators in cancer therapy.

Introduction

Cysteine cathepsins are ubiquitous papain-like proteases, in mammalians mainly located in the lysosome, involved in extracellular matrix degradation and intracellular protein processing.[1] They have various func ions in cells and, above all, share a high structural similarity.[2] However, cathepsin S (CatS) differs from other cysteine ca hepsins in its stability at neutral pH and its limited tissue distribu ion (mainly in antigen-presenting cells, e.g. macrophages).[3,4] CatS is known to be overexpressed in many tumors (e.g., follicular lymphoma, breast, gastric, colon, pancrea ic cancer).[5–8] To date, various mechanisms how CatS is involved in tumor progression are known. For example, CatS is known to turn over extracellular matrix proteins and to drive tumor angiogenesis.[7,9] Additionally, RIESE AND CO-WORKERS showed that CatS regulates antigen processing and presentation in an igen-presenting cells (APC).[10–15] With his important role in immune cells, cathepsin S intervenes in the body's immune response also to tumors. It shifts MHC-II expression to MHC-I, resulting in a favored activation of CD4+ T cells (e.g., regulatory T cells) over cytotoxic CD8+ T cells.[5,6,16] JAKOŠ AND CO-WORKERS and WILK NSON AND CO-WORKERS also stated that CatS polarizes APCs from M1 to M2 phenotype that is associated with tumor progression, supporting he proliferation of myeloid-derived suppressor cells (MDSC) and tumor-associated macrophages.[9,16] This shift results in a suppressed T cell-induced immune response.[17–19] Data from murine models also indicates that CatS inhibition reduces the overall T cell immunity in healthy mice but enhances the CD8+ T cell immunity in mice with cancer.[20] Cytotoxic CD8+ T cells can attack tumor cells and hus lead to tumor volume reduction.[20] Experiments with small-interfering RNA (siRNA) targeting CatS mRNA and hus, reducing CatS expression, resulted in tumor volume and invasion reduction as well as increased apoptosis and attenuated angiogenesis.[21,22] BURDEN AND CO-WORKERS used inhibitory CatS antibodies and observed an increased effect of chemotherapeutics plus a significant tumor growth limitation.[23,24] Furthermore, CatS overexpression occurs in follicular lymphoma including the expression of an overactive mutant (Y132D) with enhanced auto-activation.[5] Knocking down the protease leads to an improved immune response towards lymphoma cells.[6] Overall, CatS is an interesting new target to enhance anti-tumor immunogenicity and thus, stop tumor growth, especially in case of resistances to current tumor immunotherapies.[6,10,25,26] **Figure 1** summarizes the mentioned effects of CatS in the tumor microenvironment (TME). CatS is a papain-like protease expressed as an inactive zymogen.[27,28] After cleaving off the propeptide, the mature enzyme consists of 217 residues and a cataly ic dyad (Cys25, His164) in the active site.[3,4,29] Despite the high structural similarity to other human cathepsins, there are various residues in the S1' to S3 subsites that differ and can be addressed to gain selectivity.[4,29] The first selective CatS inhibitors were published in the early 2000s based on a publication by PAULY ET AL. that described the binding site and especially the differences towards other cysteine cathepsins.[1,29] The S2 subsite contains a flexible Phe211 residue that can flip and open up to Phe70 from the S3 site, creating space for bulkier residues in S2. Fur hermore, it allows ligand π-stacking with these Phe residues.[1,30]

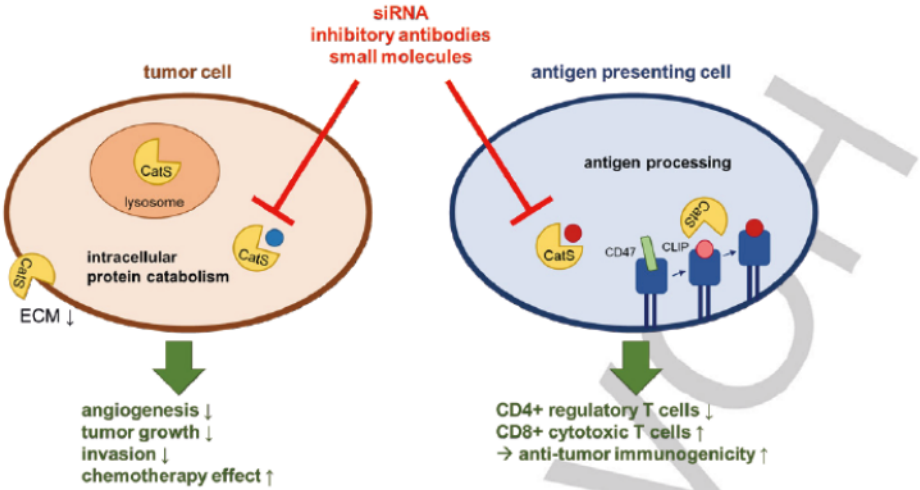

Figure 1. Cathepsin S inhibition affects tumor cells and antigen presenting cells (APC). CLIP = Class II-associated invariant chain peptide.

During the last 20 years, many cathepsin S inhibitors have been developed, including non-covalent as well as covalent ones (e. g. vinylsulfones, nitriles, aldehydes).[1,30-38] One nitrile-based inhibitor has already been tested *in vivo*. The compound led to significant reduction of tumor volume in murine models.[39]

Here, we focus on developing new selective cathepsin S inhibitors based on he structure of the well-known pan-cathepsin inhibitor **K11777**. This compound wi h an electrophilic vinylsulfone warhead is known to be a covalent irreversible ca hepsin inhibitor (**Figure 2**). The ac ive site cysteine undergoes a Michael-type addition and cannot dissociate from the inhibitor after the covalent bond formation. Since irreversible inhibition has several drawbacks, e.g., off-target effects, toxicity, haptenization,[40-42] we have recen ly developed modified **K11777** deriva ives by introducing a fluorine atom at the α-position of the vinylsulfone double bond. The generated *α*-fluorovinylsulfone (**1a**) undergoes a reversible Michael-type addition with hiols (**Figure 2**).[43] With this reversibility we maintain the benefits of covalent inhibition, e.g., longer residence times, higher potency, thus possible dosage reduction, and a lower pharmacokinetic sensitivity, without the drawbacks of irreversible inhibition mentioned above.[44-46]

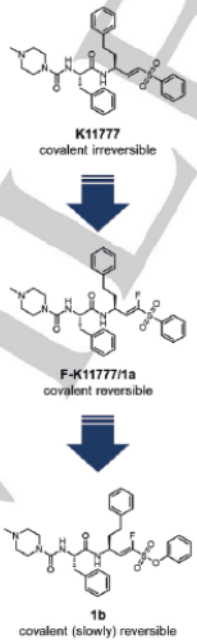

Figure 2. Reversible K11777 derivatives as lead structures for CatS inhibitor development.

Our most recent findings suggest that modifying the warhead from an α-fluorovinylsulfone (**1a**) to an α-fluorovinylsulfonate (**1b**) results in slowly reversible cathepsin inhibitors, further prolonging the target residence time (**Figure 2**).[47]

Since covalent-reversible inhibition has many benefits, we chose previously described fluorinated derivatives from SCHIRMEISTER ET AL. and JUNG, FUCHS ET AL. as initial starting structures (**1a**, **1b**) for the development of new CatS inhibitors.[43,47] Results of molecular docking studies combined with literature-known motifs resulted in 22 new compounds (**Figure 3**) that were tested in fluorometric enzyme assays against cathepsins S, B, and L. We evaluated their potency and selectivity profiles in a structure-activity relationship study backed up by molecular docking results. Finally, their cytotoxicities against the breast cancer cell line MDA-MB-231 and murine bone marrow-derived dendritic cells were tested in cell viability assays.

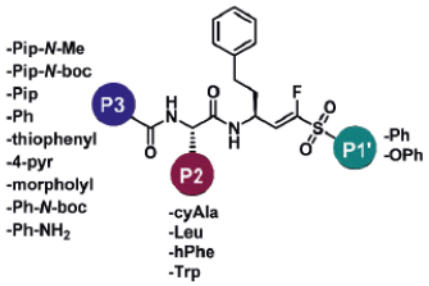

Figure 3. SAR variations for compounds **1a** (P1'= Ph) and **1b** (P1' = OPh).

Results and Discussion

Starting from lead structures **1a** and **1b**,[43,47] we prepared 22 new compounds (**2a** – **6c**, **Scheme 1**).

The compounds differ in their P2 and P3 positions (**Scheme 1**). They contain morpholine (**2c**, **3c**, **6c**), piperazine (Pip, **2b**, **3b**), *N*-boc-piperazine (Pip-*N*-boc, **2a**, **3a**), pyridine (**2d**, **3d**, **4a** – **5d**), thiophene (**2e**, **3e**) or aniline (Ph-NH_2, **6b**) in the P3 position and hPhe (**4c**, **5c**), cyAla (**4a**, **5a**, **6a** – **c**), Leu (**4b**, **5b**) and Trp (**4d**, **5d**; all with (*S*)-configured stereo center) in the P2 position. These latter residues were previously described to improve the binding affinity in CatS inhibitors.[34] For the covalently reacting warhead functionality, we prepared α-fluorovinylsulfones and the corresponding α-fluorovinylsulfonates occupying the P1´position.

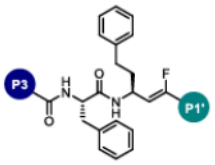

2a: P1' = SO_2Ph, P3 = Pip-*N*-boc
2b: P1' = SO_2Ph, P3 = Pip
2c: P1' = SO_2Ph, P3 = morpholyl
2d: P1' = SO_2Ph, P3 = 4-pyridyl
2e: P1' = SO_2Ph, P3 = 3-thiophenyl
3a: P1' = SO_3Ph, P3 = Pip-*N*-boc
3b: P1' = SO_3Ph, P3 = Pip
3c: P1' = SO_3Ph, P3 = morpholyl
3d: P1' = SO_3Ph, P3 = 4-pyridyl
3e: P1' = SO_3Ph, P3 = 3-thiophenyl
3f: P1' = SO_3Ph, P3 = phenyl

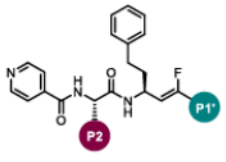

4a: P1' = SO_2Ph, P2 = cyAla
4b: P1' = SO_2Ph, P2 = Leu
4c: P1' = SO_2Ph, P2 = hPhe
4d: P1' = SO_2Ph, P2 = Trp
5a: P1' = SO_3Ph, P2 = cyAla
5b: P1' = SO_3Ph, P2 = Leu
5c: P1' = SO_3Ph, P2 = hPhe
5d: P1' = SO_3Ph, P2 = Trp

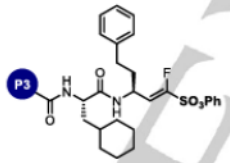

6a: P3 = Ph-*N*-boc
6b: P3 = Ph-NH_2
6c: P3 = morpholyl

Scheme 1. Optimized cathepsin S inhibitors with variations in P1', P2 and P3.

Chemistry.

The synthesis route allowed many combinations of the two warhead variations with various dipeptides, resulting in the final inhibitors **1a** – **6c**.

Warhead preparation.

To prepare the warhead, we first synthesized fluorinated phosphonates **11** and **12** (**Scheme 2**) as previously published.[47] To synthesize aldehyde **14**, we prepared the Weinreb amide **13** of boc-homophenyl alanine which was subsequently reduced to **14** using $LiAlH_4$ (**Scheme 2**). Aldehyde **14** and phosphonates **11** or **12** then reacted in a Horner-Wadsworth-Emmons olefination, providing fluorovinylsulfone **15** and fluorovinylsulfonate **16**. Boc-deprotection with HCl in dioxane resulted in **17**/**18** (**Scheme 2**).

Dipeptide synthesis.

For ester-protected dipeptides **19**, **21**, **23** and **41**, we prepared isocyanates which then reacted with piperazine derivatives or morpholine. We synthesized the other ester-protected dipeptides using standard amide coupling reactions. The cleavage of the ester moieties by hydrolysis under basic conditions gave access to the final dipeptides **20** – **42** (**Scheme 3**).

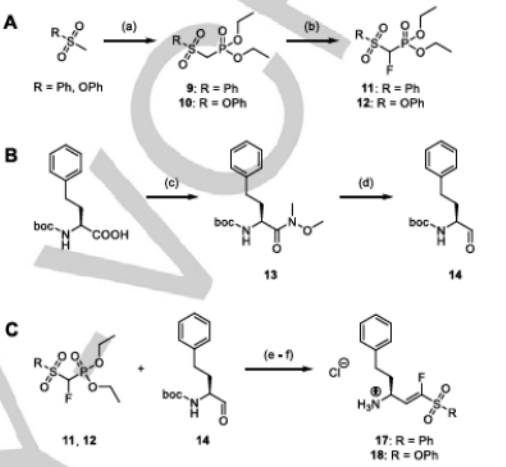

Scheme 2. (**A**) Phosphonate preparation (**9** – **12**). (a) KHMDS/*n*-BuLi, DECP; THF; –78/0 °C; 3 h; 43 – 82%. (b) LHMDS, Selectfluor; THF/DMF; –78 °C – 0 °C; 4 h; 45 – 46%. (**B**) Aldehyde preparation (**13** – **14**). (c) *N,O*-dimethyl hydroxylamine, HOBt, TBTU, DIPEA; DCM; 0 °C – rt; 12 h; 100%. (d) $LiAlH_4$; diethyl ether; 0 °C; 2 h; 99%. (**C**) HWE olefination (**15** – **16**) and boc deprotection (**17** – **18**). (e) LHMDS; THF; –78 °C; 4 h; 46 – 59%. (f) 4 M HCl; dioxane; rt; 2 h; 88 – 95%.

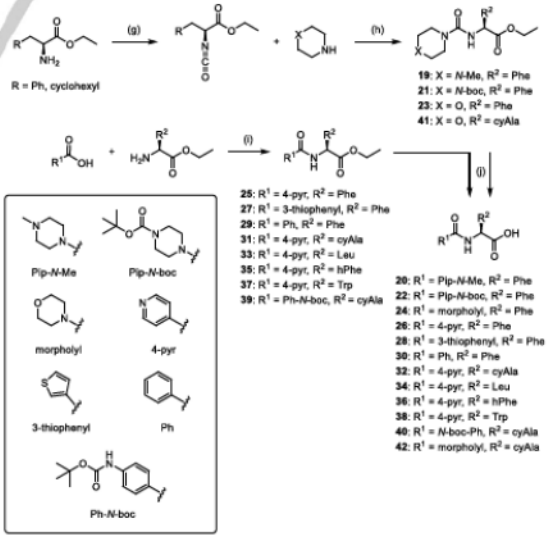

Scheme 3. Synthesis of dipeptides **20** – **42**. (g) Triphosgene, $NaHCO_3$; DCM/toluene; 0 °C; 3 h; 64%. (h) DIPEA; THF; 0 °C – rt; 12 – 24 h; 84 – 100%. (i) HOBt, TBTU, DIPEA; DCM; 0 °C – rt; 12 – 24 h; 67 – 100%. (j) LiOH x 1 H_2O; THF/H_2O; rt; 12 – 24 h; 44 – 100%.

Amide couplings.

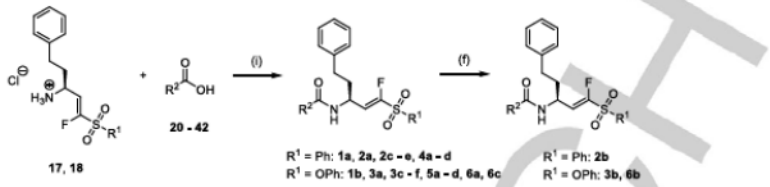

Scheme 4. Amide coupling reactions of warheads and dipeptides resulting in the final inhibitors **1a** – **6c**. (i) HOBt, TBTU or HATU, D PEA; DCM or DCM/DMF; 0 °C – rt; 12 – 24 h; 11 – 65%. (f) 4 M HCl; dioxane; rt; 2 h; 74 – 96%.

Warheads **17** or **18** were coupled wi h dipeptides **20** – **42** in standard amide coupling reactions (**Scheme 4**). The resulting inhibitors **1a** – **6c** were purified by HPLC (> 95% purity in all cases).

Fluorometric enzyme assays.

The synthesized compounds' inhibitory activities against CatS and he off-targets CatB and CatL were tested using well-known fluorometric enzyme assays (**Table 1**).[48] The inhibitors were initially screened at different concentrations (20 μM, 1 μM) followed by IC_{50}/K_i value determination if >50% inhibition @20 μM. For more information regarding assay procedures and calculations of inhibition constants see chapter **Fluorometric enzyme assay** in the **Experimental section**.

We started by varying the P3 position of lead compounds **1a** and **1b** (**Figure 3**) and prepared two compound sets, namely the corresponding fluorovinylsulfones/-sulfonates (**2a** – **6c**), and evaluated their inhibitory activities and selectivities (**Table 1**). We generally observed all α-fluorovinylsulfonates (**3a** – **3f** & **5a** – **5c**) to be more potent cathepsin S inhibitors than the corresponding α-fluorovinylsulfones (**2a** – **2e** & **4a** – **4d**) which already improves their selectivity towards CatB and CatL (**Table 1**).

Table 1. Enzyme assay results for compounds **2a** – **6c** compared to **1a** and **1b**.

cpd	P1'	P2	P3	K_i CatS [μM]	K_i CatB [μM]	SI CatB/CatS	K_i CatL [μM]	SI CatL/CatS
1a	Ph	Phe	Pip-*N*-Me	1.2 ± 0.28	0.47[a]	0 39	0.023[a]	0 02
1b	OPh	Phe	Pip-*N*-Me	0.010 ± 0.002*	0.26 ± 0.038	26	0.024 ± 0.003	2.4
2a	Ph	Phe	Pip-*N*-boc	0.14 ± 0.056	> 12	> 86	> 10	> 71
2b	Ph	Phe	Pip	1.3 ± 0.37	0.66 ± 0.084	0 51	0.79 ± 0.21	0 61
2c	Ph	Phe	morpholyl	0.040 ± 0.004	0.37 ± 0.096	9 3	0.18 ± 0.043	4 5
2d	Ph	Phe	4-pyridyl	0.10 ± 0.012	3.1[a]	31	0.11[a]	1.1
2e	Ph	Phe	3-thiophenyl	0.057 ± 0.008	1.1 ± 0.38	19	0.56 ± 0.097	9 8
3a	OPh	Phe	Pip-*N*-boc	0.0085 ± 0 0045*	> 12	> 1,400	> 10	> 1,100
3b	OPh	Phe	Pip	0.0057 ± 0 0023*	0.84 ± 0.20	147	0.087 ± 0.010	15
3c	OPh	Phe	morpholyl	0.0009 ± 0 0005*	1.2 ± 0.20	1,333	0.30 ± 0.014	333
3d	OPh	Phe	4-pyridyl	0.0008 ± 0 0004*	1.7[b]	85	0.26[b]	13
3e	OPh	Phe	3-thiophenyl	0.011 ± 0.0039*	4.0 ± 0.98	363	0.97 ± 0.059	88
3f	OPh	Phe	Ph	0.0073 ± 0 0018*	> 12	> 1,600	0.19 ± 0.16	26
4a	Ph	cyAla	4-pyridyl	0.0059 ± 0 0008	> 15	> 2,500	> 10	> 1,700
4b	Ph	Leu	4-pyridyl	0.11 ± 0.011	> 12	> 110	0.56 ± 0.11	5.1
4c	Ph	hPhe	4-pyridyl	0.17 ± 0.0033	> 15	> 88	> 10	> 59
4d	Ph	Trp	4-pyridyl	0.32 ± 0.043	> 12	> 38	2.3 ± 0.61	7 2

5a	OPh	cyAla	4-pyridyl	0.0079 ± 0 0038*	> 15	> 1,900	> 10	> 1,300
5b	OPh	Leu	4-pyridyl	0.035 ± 0.012*	> 12	> 340	> 10	> 290
5c	OPh	hPhe	4-pyridyl	0.24 ± 0.11*	> 12	> 50	> 10	> 42
5d	OPh	Trp	4-pyridyl	0.018 ± 0.0023*	1.7 ± 0.17	94	0.66 ± 0.076	37
6a	OPh	cyAla	Ph-*N*-boc	0.0059 ± 0 0018*	> 12	> 2,000	> 10	> 1,700
6b	OPh	cyAla	Ph-NH_2	0.0090 ± 0 0017*	> 12	> 1,330	> 10	> 1,100
6c	OPh	cyAla	morpholyl	0.00008 ± 0 00003*	> 12	> 150,000	> 10	> 125,000

[a]: see SCHIRMEISTER ET AL.[43] [b]: see JUNG, FUCHS ET AL.[47] *time-dependent inhibition.

We noted a good inhibition for compound **2c** (K_i = 40 nM), but a low selectivity (only 9 3-fold vs. CatB and 4.5-fold vs. CatL). The corresponding fluorovinylsulfonate **3c** has a 40-fold increased inhibitory activity (K_i = 0.9 nM), also resulting in higher selectivity towards other cathepsins (1,333-fold vs. CatB, 333-fold vs. CatL).

Next, we altered the P2 position while maintaining a 4-pyridyl residue in P3 that has proven to be beneficial for CatS inhibition and selectivity.[35] Here, we also prepared corresponding α-fluorovinylsulfones/-sulfonates (**4a** – **5d**) and determined their inhibitory activities and selectivity profiles (**Table 1**). The cyclohexylalanine residue in P2 seems to be the most favorable, with K_i values in the low nanomolar range (5.9 – 7.9 nM) for both warheads (**4a**, **5a**, see **Table 1**). The resulting selectivity towards CatB and CatL is >1,000-fold for bo h compounds and enzymes. Leucin in P2 combined with an α-fluorovinylsulfonate (**5b**) also shows good CatS inhibition (K_i = 35 nM) and high selectivity. However, homophenylalanine and tryptophane are not suitable as they lack affinity and selectivity compared to the most favorable compounds.

Based on the results from these first optimizations, we prepared three additional compounds (**6a** – **6c**) wi h cyclohexylalanine in P2 and modifications in P3. For future attachments of our inhibitors onto nanodelivery systems via various linkers, we chose to introduce an amino-substituted phenyl ring in the P3 position (**6b**). We also tested the *N*-boc protected intermediate **6a**. Since we had found the morpholyl substituted compounds **2c**, **3c** to be very potent, with K_i values of 0.9 nM (**3c**) and 40 nM (**2c**) respectively, we prepared a final inhibitor combining the favorable cyclohexylalanine residue in P2 with the morpholyl moiety in P3 (**6c**).The results shown in **Table 1** reveal that all three moieties are suitable for the P3 position with K_i values in he low nanomolar or even subnanomolar range and high selectivities towards cathepsins B and L. Compound **6c** with a K_i value around 80 pM and more than 100,000-fold selectivity towards the other two cathepsins is the most potent and selective inhibitor of the series.

Generally, the progress curves for α-fluorovinylsulfones are linear, indicating that the inhibition is not time-dependent (**Figure 4**). For the α-fluorovinylsulfonates, we observed time-dependent inhibition (**Figure 5Fehler! Verweisquelle konnte nicht gefunden werden.**) wi h biphasic binding behavior as we have reported previously for α-fluorovinylsulfonate inhibitors of the cysteine protease rhodesain.[47] Thus, we also determined further inhibition constants, such as k_3, k_4 and K_i* (dissociation constant of final covalent complex) using the slow-binding equation for these compounds (**1b**, **3a** – **f**, **5a** – **6c, Table 2**).[50]

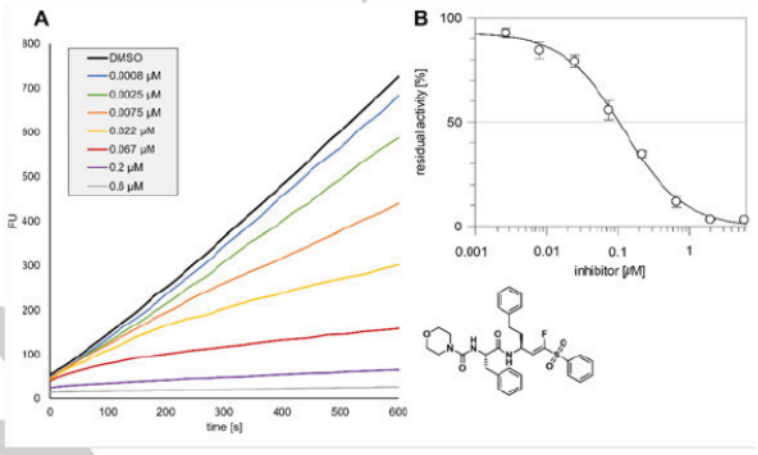

Figure 4. Assay results for **4a** (bottom right). (**A**) Fluorescence-time plot for **4a** vs. CatS with different inhibitor concentrations [μM] showing linear progress curves. (**B**) Residual enzyme activity [%] vs. inhibitor concentration [μM] for IC_{50} calculation. K_i value was calculated using the Cheng-Prusoff equation.[49]

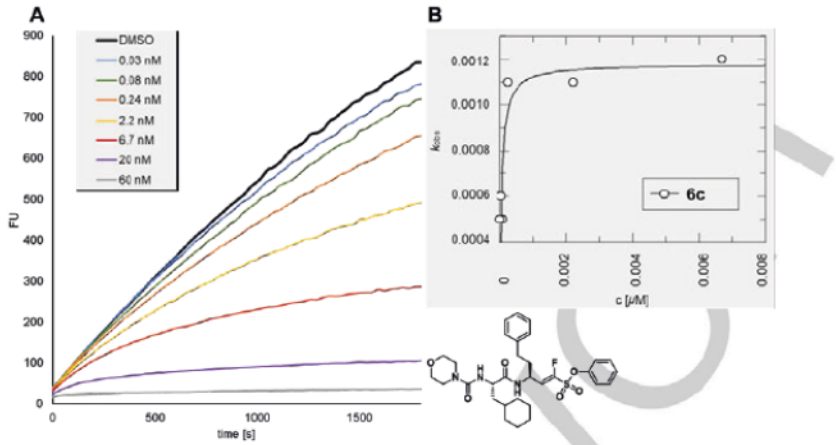

Figure 5. Assay results for **6c** (bottom right). (**A**) Fluorescence-time plot for **6c** vs. CatS with different inhibitor concentrations [nM] showing a biphasic behavior, thus a time-dependent inhibition mode. (B) k_{obs} [s^{-1}] vs. inhibitor concentration [μM] for K_i calculation with the slow-binding equation.[50]

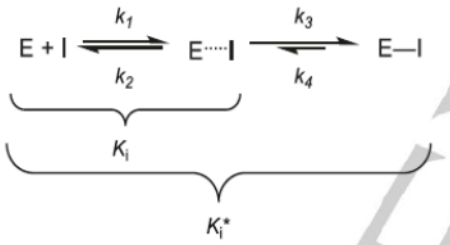

We found the rate constant of the dissociation of he final complex (k_4) to be significan ly lower han he associa ion rate constant (k_3) for all time-dependent compounds (**Table 2**), suggesting tight-binding behavior. The dissocia ion constants of the final covalent complexes (K_i^*) are in the low nanomolar to subnanomolar range proving the very tight binding of the inhibitors.

Dilution assay.

With dilution assays, we proved that the inhibitors are reversible as expected from our previous experiences with such compounds.[47] For the experiments, two compounds (F-vinylsulfonate **3c**, F-vinylsulfone **4a**) were incubated with cathepsin S, followed by 100-fold dilution with substrate-containing assay buffer. In case of reversible inhibition, the enzyme activity should recover. Furthermore, we used the pan-cathepsin inhibitor **K11777** as an irreversible control.[51]

Table 2. Inhibition data and kinetic constants for time-dependent CatS inhibitors.

cpd	P2	P3	K_i [μM]	k_3 [s^{-1}]	k_4 [s^{-1}]	K_i^* [μM]
1b	Phe	Pip-*N*-Me	0.010 ± 0.002	0 0015	0.0002	0 0012
3a	Phe	Pip-*N*-boc	0.0085 ± 0 0045	0 0024	0.0004	0 0012
3b	Phe	Pip	0.0057 ± 0 0023	0 0020	0.0004	0 0010
3c	Phe	Morpholyl	0.0009 ± 0 0005	0 0021	0.0003	0 00011
3d	Phe	4-pyridyl	0.0008 ± 0 0004	0 0012	0.0004	0 00020
3e	Phe	3-thiophenyl	0.011 ± 0.0039	0 0016	0.0002	0 0012
3f	Phe	Ph	0.0073 ± 0 0018	0 0018	0.0003	0 0010
5a	cyAla	4-pyridyl	0.0079 ± 0 0038	0 0015	0.0003	0 0013
5b	Leu	4-pyridyl	0.035 ± 0.012	0 0016	0.0003	0 0055
5c	hPhe	4-pyridyl	0.24 ± 0.11	0 0017	0.0002	0 025

5d	Trp	4-pyridyl	0.018 ± 0.0023	0 0022	0.0002	0 0015
6a	cyAla	Ph-*N*-boc	0.0059 ± 0 0018	0 0019	0.0002	0 00056
6c	cyAla	Ph-NH_2	0.0090 ± 0 0017	0 0007	0.0001	0 00038
6c	cyAla	morpholyl	0.00008 ± 0 00003	0 0009	0.0003	0 00002

k_3, k_4 and K_i* calculated with the slow-binding equation.[50]

Figure 6 shows that the α-fluorovinylsulfones and -sulfonates are dissocia ing from the enzyme, proving hat their covalent reaction is reversible. This is also supported by previous findings from JUNG, FUCHS ET AL. and SCHIRMEISTER ET AL..[43,47] **K11777**, on he other hand, forms an irreversible covalent bond and cannot dissociate from he active site.[519]

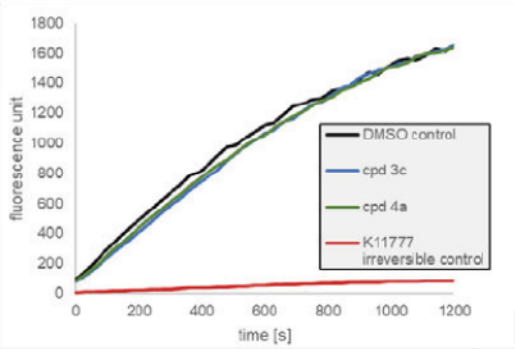

Figure 6. Dilution assay. DMSO as control (black) and **K11777** as irreversible control (red). Incubation of CatS with compounds **3c** (F-vinylsulfonate, blue) and **4a** (F-vinylsulfone, green) followed by 100-fold dilution results in an enzyme activity recovery.

SAR discussion.

Comparing the K_i values of he lead compounds F-vinylsulfone **1a** (K_i = 1.2 μM) and F-vinylsulfonate **1b** (K_i = 0.010 μM) with P3 substituted inhibitors **2a**–**2e** and **3a**–**3f** shows significantly enhanced affinity towards the target enzyme CatS in all cases except for piperidyl substituted vinylsulfone **2b** (K_i = 1.3 μM) and 3-thiophenyl substituted vinylsulfonate **3e** (K_i = 0.011 μM). The non-covalent docking results show scores in the same range or even higher compared to the leads **1a** & **1b**. For compound **3f** the predicted score for the stability of the covalent complex is even higher compared to the lead compounds (see **Table B**, **Supporting information**). Additionally, the selec ivities for CatS increased significantly towards CatB for all P3 modified compounds (**2a**–**3f**) by up to 220-fold for inhibitor **2a** vs **1a**. The selectivity towards CatL also improved in all cases (**2a**–**3f**) from 0.02-fold for **1a** to >71-fold for **2a** (vinylsulfones) and from 2.4-fold for **1b** to >1,100-fold for **3a** (vinylsulfonates). Overall, he vinylsulfonate warhead resulted in more potent inhibitors as exemplified for compounds **2b** vs **3b**. Superposition of the non-covalent docking poses of both compounds revealed that he additional oxygen atom in **3b** leads to a different orientation of he phenyl ring inside the S1´-subpocket of the active site, where additional face to edge and face to face π-stacking interactions with Trp186 and His164 are possible, possibly leading to tighter binding of **3b** compared to **2b** (**Figure 7**).

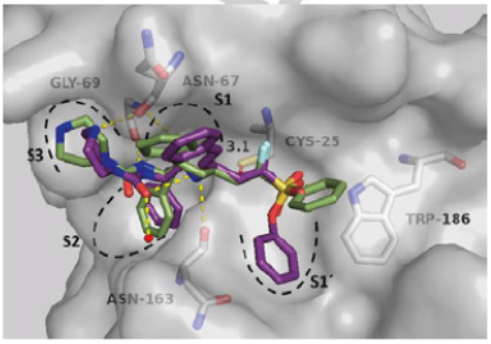

Figure 7. Superposition of the non-covalent docking poses of **2b** (smudge green carbon atoms) and **3b** (purple carbon atoms) inside the active site of CatS (pdb: 1NPZ). Polar interactions between **3b** and the enzyme are depicted as yellow dashed lines. The distance between the electrophilic C-atom of inhibitor **3b** and Cys25 is shown as red dashed line with the measured distance in Å.

Replacing phenylalanine in P2 with four different amino acids while maintaining the 4-pyridyl substituent in P3 lead to he result that the cyAla-residue is best suited to address the S2 pocket of the enzyme wi h both warheads. This is highlighted by the increase in potency for the vinylsulfone-based inhibitor **4a** (K_i = 0.006 μM) compared to **2d** (K_i = 0.10 μM) and a better selectivity towards both off-targets (>2,500-fold vs CatB and >1,700-fold vs CatL). For the vinylsulfonate-based inhibitor series, the same exchange resulted in a potency drop of about 10-fold (**3d** vs **5a**) but a big jump in selectivity (>1,900-fold vs CatL and >1300-fold vs CatL) for inhibitor **5a**. This might be due to the sp^3-hybridiza ion of the carbon atoms of the cyAla substituent, which better fills the S2 subpocket and presumably generates new non-polar interactions wi h the subpocket atoms compared to the sp^2-hybridized planar phenyl ring (**Figure 8**).

Combining the cyAla motif in P2 with morpholine in P3 and the vinylsulfonate warhead yielded the most potent inhibitor **6c**, with a K_i-value in the picomolar range and excellent selectivities over CatB (> 150,000) and CatL (> 125,000). Superposition of the non-covalent docking pose of **6c** with the covalent enzyme-inhibitor complex shows that all polar interac ions between the non-covalently bond inhibitor and the enzyme should still be intact after the covalent bond forma ion (**Figure 9**). Compound **6c** also has one of the highest scores for the stability of the covalent enzyme inhibitor complex (Affinity ΔG, MOE-score = 6.0 kcal/mol) as well as the second highest HYDE-score of all inhibitors with 50 kJ/mol (**Table B**, **Supporting information**).

The incorporation of an amine functionality in the P3 site for compound **6b** (K_i = 9 nM) and its boc-protected intermediate **6a** (K_i = 6 nM) did not deteriorate the affinity or the selectivity for the

target enzyme (**Table 1**). Therefore, **6b** can be used in future studies with nanodelivery systems.

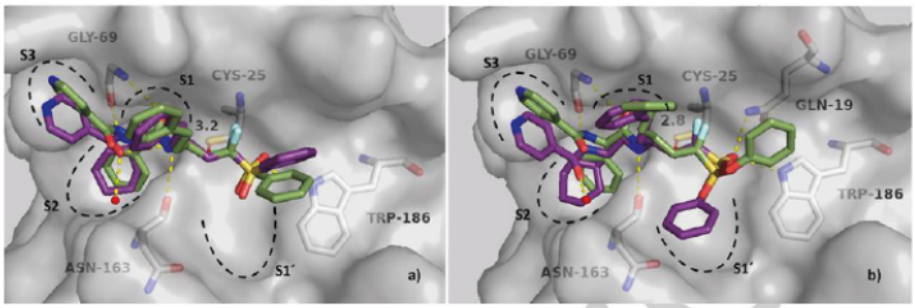

Figure 8. Predicted binding modes and non-covalent interactions (yellow dashed lines) of different inhibitors inside the CatS binding pocket (pdb: 1NPZ). (**A**) Superposition of the non-covalent docking poses of **2d** (smudge green carbon atoms) & **4a** (purple carbon-atoms). (**B**) Superposition of the non-covalent docking poses **3d** (smudge green carbon atoms) & **5a** (purple carbon-atoms).

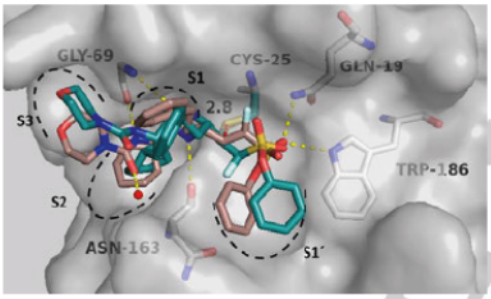

Figure 9. Superposition of the non-covalent docking pose of **6c** (darksalmon carbon atoms) and the covalent docking pose of **6c** (teal carbon atoms) inside the active site of CatS (pdb: 1NPZ). Polar interactions between the non-covalent pose of **6c** and the enzyme are depicted as yellow dashed lines. The distance between the electrophilic C-atom of **6c** and Cys-25 is shown as red dashed line with the measured distance in Å.

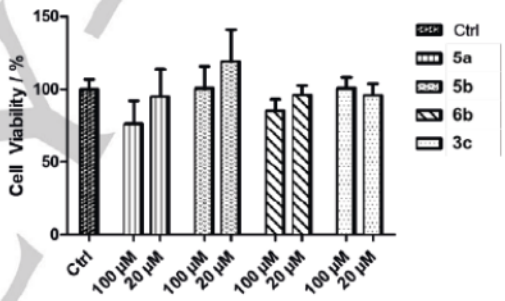

Figure 10. Cell viability of compounds **5a**, **5b**, **6b** and **3c**-treated MDA-MB-231 cells determined by CELLTITER-GLO Luminescent Cell Viability Assay. Cells were treated for 24 h with each compound at two different concentrations, 100 μM or 20 μM, respectively. Significant cytotoxic effect was observed for MDA-MB-231 cells treated with **5a** and **6b** at 100 μM. All experiments were performed in quadruplicates and data are shown as mean ± SD from three independent experiments.

Cell viability.

Selected compounds were tested in a CELLTITER-GLO Luminescent Cell Viability assay to assess their cytotoxicity. We used MDA-MB-231 cells which are breast cancer cells hat compensate the inhibition of CatS and other ca hepsins. Therefore, only unspecific cytotoxic effects, that are not related to CatS inhibi ion, are detected.[52]We did not observe significant cytotoxicity (**Figure 10**) after 24 h treatment at concentra ions >1,000-fold higher (20 μM) than the compounds' K_i values in he low nanomolar range. Only compounds **5a** and **6b** exhibited low cytotoxic effects at the highest concentra ion applied (100 μM), which was >10,000-fold the compounds' K_i values. In conclusion, the exemplarily selected compounds do not affect cell viability of MDA-MB-231 cells at their biologically active concentrations.

In addi ion, the cytotoxic effect of several compounds was also tested on single cell level using murine DC. The various compounds (1 μM) were applied alone or followed by administration of the DC activator lipopolysaccharide (100 ng/mL) required to achieve robust T cell stimulatory activity. Neither compound exerted major cytotoxic activity on $CD11c^+$ DC at concentrations about 1,000-fold higher than their K_i values as assessed using membrane impermeable fixable viability dye, which binds to amines of cytoplasmic proteins of dead cells with a porous cell membrane (**Figure 11**).

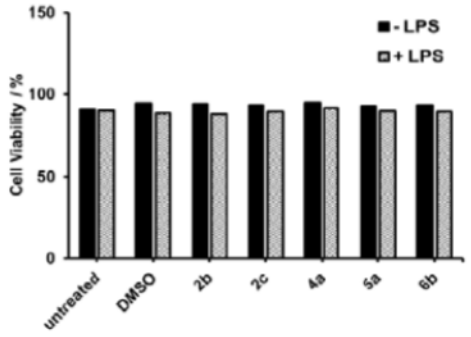

Figure 11. Cell viability of compounds **2b**, **2c**, **4a**, **5a**, and **6b**-treated murine CD11c⁺ DC. Cells were treated for 24 h with each compound at 1 μM concentration. No significant cytotoxic effects were observed.

Conclusion

Here, we have demonstrated hat α-fluorovinylsulfones and -sulfonates are potent covalent-reversible cathepsin S inhibitors. Both warheads are well suitable for the target enzyme, with he α-fluorovinylsulfonates being more effective. Starting from the **K11777** scaffold, we replaced residues in the P2 and P3 positions, resulting in highly selective compounds that barely affect off-target cathepsins. In he P3 position, we observed a morpholyl (**3c**) or 4-pyridyl (**3d**) residue to be most suitable with K_i values in the subnanomolar range and moderate selec ivity. In the P2 posi ion, we found that cyAla (**4a**, **5a**) increased the selectivity immensely with K_i values in the low nanomolar range for he on-target CatS. Combining the best-performing residues of P2 and P3 to form a morpholyl-cyAla-hPhe-F-vinylsulfonate-Ph motif (**6c**) proved to be most effective with subnanomolar affinity (K_i = 0.08 nM, K_i* = 0 02 nM) and exceptional selectivity towards cathepsins B and L (>150,000/125,000-fold). The time-dependent inhibition enables slow-tight binding, thus prolonging target residence times.

Therefore, compound **6c** will be an excellent candidate for further op imizations regarding new small molecule immunomodulators in cancer therapy, where already resistances to existing immunotherapies are known.[26] Cell viability experiments using a non-CatS sensitive cancer cell line and murine derived dendritic cells both did not show cytotoxic effects for all tested inhibitors at relevant concentra ions (>1,000-fold K_i). The next steps include immunoassays with macrophages or dendritic cells to evaluate the potential of our CatS inhibitors, e.g., for immune cell polarization. This could involve markers like MHC-I and MHC-II expression as well as functional assays for T cell activation.

Moreover, development of inhibitor-nanocarrier constructs is possible with these compounds. By attaching ca hepsin S inhibitors to nanocarriers, their efficacy could be further enhanced through specific targeting, e. g., to dendritic cells or other APC.[25] Compound **6b** with a free amino moiety (K_i = 9 nM, SI > 1,000) allows he attachment of various functionali ies, such as linkers or nanodelivery systems.

Experimental Section

General.

All reagents and solvents were purchased from SIGMA-ALDRICH, ALFA AESAR, ACROS, TCI, BLD PHARMATECH, CARBOLUTION or CARL ROTH in analytical or HPLC grade quality. Chemicals were used without further purification, whereas solvents were distilled and desiccated by standard methods if necessary. ^{1}H and ^{13}C spectra were recorded on a Bruker Fourier 300 device using DMSO-d_6 or $CDCl_3$ as solvents. Chemical shifts δ are given in parts per million (ppm) using residual proton peaks of the solvent as internal standard (^{1}H/^{13}C: DMSO 2.50/39 52 ppm; $CHCl_3$ 7 26/77.16 ppm). The compound purity was determined via HPLC-MS at λ = 254 nm using an Agilent 1100 series HPLC with an AGILENT POROSHELL 120 EC-C_{18} column (150 x 2.10 mm, 4 μm) coupled with an Agilent 1100 series LC/MSD Trap with electron spray ionization (ESI) in positive mode. All compounds tested in enzymatic assays are ≥95% pure by HPLC analysis. The mobile phase consisted of a variable mixture of ACN and H_2O with 0.01% formic acid. For purification we used a VARIAN PREPSTAR system (model 218) with a MZ-AQUA PERFECT C_{18} column (250 x 20 mm, 7 μm) by MZ-ANALYSENTECHNIK. Column chromatography was performed with silica gel (0 040 – 0.063 mm) and all reactions were monitored by thin-layer chromatography using MACHEREY-NAGEL ALUGRAM Xtra S L G/UV254 silica gel 60 plates for detection at λ = 254 nm. Melting points were determined in open capillaries with a SCHORPP Device Technology MPM-H3 instrument. Optical rotation $[\alpha]_D^{22}$ was measured on a KRÜSS P3000 polarimeter (c = 10 mg/mL in MeOH) at 22 °C.

Syntheses.

General procedures.

Procedure A (HWE olefination).

The respective phosphonate (1.0 eq) was dissolved in dry THF and cooled to –78 °C. Then, 1 M KHMDS or LHMDS in THF (1.3 eq) was added dropwise and stirred for 30 min, followed by addition of boc-L-homophenylalaninal (**14**, 1.1 eq). The mixture was stirred for 3 – 5 h at –78 °C and stopped by adding water. The solvent was evaporated under reduced pressure and the residue was extracted with EA (3x), washed with water (2x), sat. aq. $NaHCO_3$ (2x), and brine (2x), then dried over Na_2SO_4. Purification by column chromatography.

Procedure B (amide couplings).

The carboxylic acid (1.2 eq) was dissolved in DCM or a mixture of DCM/DMF, and cooled to 0 °C. Then, HOBt (1 2 eq), TBTU (1.2 eq), and D PEA (3.5 eq) were added, and the mixture was stirred for 20 min until all components dissolved. The respective amine (1.0 eq) was added, and the mixture was stirred for an additional 12 – 24 h, then stopped by adding water. The mixture was extracted with DCM (2x) and the combined organic extracts were washed with water (2x), sat. aq. $NaHCO_3$ (2x), and brine (2x).

After drying the crude product over Na_2SO_4, it was purified by column chromatography.

Procedure C (boc deprotection).

HCl (4 M) in dioxane was added dropwise to the boc-protected amine (1.0 eq) until all components dissolve. The mixture was stirred for 2 – 12 h and the product was precipitated with diethyl ether and lyophilized afterwards.

Procedure D (alkaline hydrolysis).

The ester (1.0 eq) was dissolved in THF. LiOH monohydrate (4.0 eq) was dissolved in water and added to the reaction dropwise. The mixture was stirred for 12 – 24 h, then the solvent was removed under reduced pressure. The pH of the aqueous phase was adjusted with $KHSO_4$ to 5, giving the products as solids that were further lyophilized.

Starting material preparation.

Ethyl (*S*)-2-isocyanato-3-phenylpropanoate **(7)**

Phenylalanine ethyl ester (1 0 eq, 10 mmol, 2.2 g) was dissolved in DCM and an sat. aq. $NaHCO_3$ solution and cooled to 0 °C. Triphosgene (0.33 eq, 3.3 mmol, 0.99 g) was added and the mixture was stirred for 1 h. The mixture was extracted with DCM (2x) and the combined organic extracts were washed with sat. aq. $NaHCO_3$ (2x), and brine (2x), then dried over Na_2SO_4 and concentrated under reduced pressure, resulting in the crude product that was used without further purification (1.4 g, 6.4 mmol, 64%). ^{1}H NMR (300 MHz, $CDCl_3$) δ[ppm] = 7.35 – 7.03 (m, 5H), 4.73 – 4.51 (m, 1H), 4.30 – 4.07 (m, 2H), 3.16 – 2 91 (m, 2H), 1.32 – 1.09 (m, 3H). ^{13}C NMR (75 MHz, $CDCl_3$) δ[ppm] = 170.7, 135.7, 129 5, 128.7, 127.5, 62.7, 58.7, 40.1, 14 2. $[\alpha]_D^{22}$ = –9°.

Ethyl (*S*)-2-amino-3-cyclohexylpropanoate **(8)**

(*S*)-2-Amino-3-cyclohexylpropanoic acid (1.0 eq, 10 mmol, 1.7 g) was dissolved in EtOH and $SOCl_2$ (1.1 eq, 11 mmol, 0.8 mL) was added dropwise. The mixture was stirred under reflux for 12 h and the reaction was stopped with sat. aq. $NaHCO_3$. The solvent was evaporated under reduced pressure and the residue was extracted with EA, giving the crude product that was used without further purification (1.4 g, 7.0 mmol, 68%). ^{1}H NMR (300 MHz, $CDCl_3$) δ[ppm] = 4.20 – 4.01 (m, 2H), 4 00 – 3.83 (m, 2H, NH_2), 3.75 (tt, *J* = 9.3, 7.0 Hz, 1H), 1.90 (t, *J* = 7 0 Hz, 2H), 1 65 – 1 31 (m, 11H), 1.24 (t, *J* = 8 0 Hz, 3H). ^{13}C NMR (75 MHz, $CDCl_3$) δ[ppm] = 173.1, 60.5, 54.7, 36.9, 33.4, 33.0, 26 2, 25.5, 13.9. $[\alpha]_D^{22}$ = –25°.

Phosphonate preparation.

Diethyl ((phenylsulfonyl)methyl)phosphonate **(9)**

Phenyl methylsulfone (1.0 eq, 15 mmol, 2 2 g) was dissolved in dry THF and cooled to 0 °C. After dropwise addition of 2.5 M *n*-BuLi in hexanes (2.5 eq, 37.5 mmol, 15 mL), the mixture was stirred for 30 min. Then, DECP (1.1 eq, 16.5 mmol, 2.71 mL) was added and the mixture was stirred for 3 h. The reaction was stopped with acetid acid, and the solvent was evaporated under reduced pressure. The residue was extracted with EA (3x) and the combined extracts were washed with water (2x), and brine (2x), then dried over Na_2SO_4. The crude product was purified using column chromatography (CH EA 1 3 – 100% EA), resulting in a yellow oil (3.6 g, 12.3 mmol, 82%). ^{1}H NMR (300 MHz, DMSO-d_6) δ[ppm] = 8 00 – 7.90 (m, 2H), 7.79 – 7.54 (m, 3H), 4.44 (d, *J* = 17 0 Hz, 2H), 4.06 – 3.88 (m, 4H), 1 21 – 1.04 (m, 6H). ^{13}C NMR (75 MHz, DMSO-d_6) δ[ppm] = 140 5, 133.8, 129 0, 127.8, 62.3, 52 3, 50.6, 16.0.

Phenyl (diethoxyphosphoryl)methanesulfonate **(10)**

Phenyl methanesulfonate (1.0 eq, 67 mmol, 11 54 g) was dissolved in dry THF and cooled to –78 °C. Then, 1 M KHMDS (1 3 eq, 88 mmol, 88 mL) was added dropwise and the mixture was stirred for 30 min. Afterwards, DECP (1.1 eq, 74 mmol, 12.2 mL) was added and the mixture was stirred for 3 h and stopped by adding sat. aq. NH_4Cl. The solvent was evaporated under reduced pressure and the residue was extracted with EA (3x). The combined extracts were washed with water (2x), and brine (2x), then dried over Na_2SO_4. The crude product was purified by column chromatography (CH:EA 1 2 – 100% EA), resulting in a colorless oil (9 0 g, 29 mmol, 43%). ^{1}H NMR (300 MHz, DMSO-d_6) δ[ppm] = 7 55 – 7.44 (m, 2H), 7.42 – 7.31 (m, 3H), 4.63 (d, *J* = 17.4 Hz, 2H), 4.24 – 4 05 (m, 4H), 1.25 (t, *J* = 7.0 Hz, 6H). ^{13}C NMR (75 MHz, DMSO-d_6) δ[ppm] = 148 9, 130.2, 127.5, 122 3, 62.9, 47.7, 45.9, 16.1.

Diethyl (fluoro(phenylsulfonyl)methyl)phosphonate **(11)**

9 (1 0 eq, 18 mmol, 5.4 g) was dissolved in dry THF and cooled to –78 °C. Then, 1 M LHMDS in THF (1.3 eq, 24 mmol, 24 mL) was added dropwise and the mixture was stirred for 30 min. Afterwards, *Selectfluor* (1 5 eq, 27 mmol, 9 6 g) was dissolved in DMF and added to the mixture. It was stirred for 4 h at 0 °C and stopped by adding sat. aq. NH_4Cl. The solvent was evaporated under reduced pressure and the residue was extracted with DCM (3x). The combined extracts were washed with water (2x), sat. aq. $NaHCO_3$ (2x), and brine (2x), then dried over Na_2SO_4. The crude product was purified by column chromatography (CH:EA 2:1 – 1:2), resulting in a colorless solid (2 5 g, 8.0 mmol, 45%). ^{1}H NMR (300 MHz, DMSO-d_6) δ[ppm] = 8.00 – 7 92 (m, 2H), 7.88 – 7.76 (m, 1H), 7.77 – 7.65 (m, 2H), 6.62 (dd, *J* = 42.8, 6.8 Hz, 1H), 4.27 – 4.02 (m, 4H), 1.30 – 1.16 (m, 6H). ^{13}C NMR (75 MHz, DMSO-d_6) δ[ppm] = 136.2, 135.2, 129.5, 129.3, 64.3, 64.1, 16.1. MP = 67 – 69 °C.

Phenyl (diethoxyphosphoryl)fluoromethanesulfonate **(12)**

10 (1.0 eq, 28 mmol, 8.9 g) was dissolved in dry THF and cooled to –78 °C. Then, 1 M LHMDS in THF (1 3 eq, 37 mmol, 37 mL) was added dropwise and the mixture was stirred for 30 min. Afterwards, *Selectfluor* (1.5 eq, 42 5 mmol, 15.0 g) was dissolved in DMF and added to the mixture. t was allowed to warm to 0 °C, stirred for 4 h, and stopped by adding sat. aq. NH_4Cl. The solvent was evaporated under reduced pressure and the residue was extracted with DCM (3x). The combined extracts were washed with water (2x), sat. aq. $NaHCO_3$ (2x), and brine (2x), then dried over Na_2SO_4. The crude product was purified by column chromatography (CH EA 2:1 – 1 2), resulting in a colorless oil (4.4 g, 13.3 mmol, 46%). ^{1}H NMR (300 MHz, $CDCl_3$) δ[ppm] = 7.40 – 7.19 (m, 2H), 7 22 – 7.02 (m, 3H), 5.66 (dd, J = 45 2, 7.2 Hz, 1H), 4 37 – 4.18 (m, 1H), 4.18 – 4.02 (m, 4H), 1.41 – 1.14 (m, 6H). ^{13}C NMR (75 MHz, $CDCl_3$) δ[ppm] = 129.6, 127.8, 124.8, 122.0, 119 9, 64 5, 15 9.

Aldehyde preparation.

tert-Butyl (*S*)-(1-(methoxy(methyl)amino)-1-oxo-4-phenylbutan-2-yl)carbamate **(13)**

Boc-L-homophenylalanine (1.2 eq, 18 mmol, 5.0 g) was dissolved in DCM and cooled to 0 °C. Then, HOBt (1.2 eq, 18 mmol, 2.4 g), TBTU (1 2 eq, 18 mmol, 5 8 g), and DIPEA (3 5 eq, 52.5 mmol, 9.2 mL) were added and the mixture was stirred for 20 min until all components were dissolved. *N,O*-Dimethyl hydroxylamine (1.0 eq, 15 mmol, 1.5 g) was added and the mixture was stirred for an additional 12 – 24 h, then stopped by adding water. The mixture was extracted with DCM (2x) and the combined organic extracts were washed with water (2x), sat. aq. $NaHCO_3$ (2x), and brine (2x). After drying the crude product over Na_2SO_4, it was purified by column chromatography (CH:EA 2:1 – 1:4), giving the product as a colorless oil (4.8 g, 15 mmol, 100%). ^{1}H NMR (300 MHz, DMSO-d_6) δ[ppm] = 6.77 – 6.65 (m, 2H), 6.66 – 6.51 (m, 3H), 3.82 – 3 65 (m, 1H), 2 99 (s, 3H), 2.76 (s, 3H), 2.22 – 2.03 (m, 1H), 2.01 – 1 87 (m, 2H), 1.23 (q, J = 7 0, 6.4 Hz, 2H), 0 91 – 0.78 (m, 9H). ^{13}C NMR (75 MHz, DMSO-d_6) δ[ppm] = 155.6, 141.1, 128.4, 128 2, 125.8, 77.9, 60.9, 50.09, 40.4, 40.1, 39.8, 39.5, 39.2, 39 0, 38.7, 32 3, 31 6, 28 2, 26 3. $[\alpha]_D^{22}$ = –40°.

tert-Butyl (*S*)-(1-oxo-4-phenylbutan-2-yl)carbamate **(14)**

13 (1.0 eq, 15 mmol, 5.2 g) was dissolved in dry diethyl ether and cooled to 0 °C. $LiAlH_4$ (1 3 eq, 19.5 mmol, 0.74 g) was added in portions and the mixture was stirred for 2 h. Afterwards, the reaction was stopped with 0.33 M $KHSO_4$ and the mixture was extracted with diethyl ether (2x). The combined extracts were washed with water (2x), 1 M HCl (2x), sat. aq. $NaHCO_3$ (2x), and brine (2x). The product was dried over Na_2SO_4, resulting in a colorless oil that solidified upon standing (3.9 g, 14.7 mmol, 99%). ^{1}H NMR (300 MHz, $CDCl_3$) δ[ppm] = 9 55 (s, 1H), 7.46 – 7.00 (m, 5H), 5.07 (s, 1H), 4 37 – 4.09 (m, 1H), 2.71 (t, J = 7.5 Hz, 2H), 2 37 – 2 01 (m, 2H), 1.56 – 1.28 (m, 9H). ^{13}C NMR (75 MHz, $CDCl_3$) δ[ppm] = 199.7, 128.8, 128.6, 126.5, 77.6, 77.2, 76.7, 66 0, 31 6, 31.1, 28.4, 15.4. $[\alpha]_D^{22}$ = –28°.

Warhead preparation.

tert-Butyl (*S,E*)-(1-fluoro-5-phenyl-1-(phenylsulfonyl)pent-1-en-3-yl)carbamate **(15)**

15 was prepared according to procedure A using 1 M LHMDS (2.6 mmol, 2 6 mL), phosphonate **11** (2.0 mmol, 0.60 g), and aldehyde 14 (2.2 mmol, 0 58 g). Purification by column chromatography (CH:EA 6:1 – 4:1) resulted in a colorless oil (0 50 g, 1 2 mmol, 59%). ^{1}H NMR (300 MHz, $CDCl_3$) δ[ppm] = 8.10 (s, 2H), 7.77 – 7 51 (m, 3H), 7.40 – 7.19 (m, 5H), 5.85 (dd, $J_{H\text{-}F}$ = 21.3 Hz, $J_{H\text{-}H}$ = 10.1 Hz, 1H), 5.38 – 5.22 (m, 1H), 4.81 – 4 68 (m, 1H), 2.80 (ddd, J = 16.9, 10.2, 6.0 Hz, 2H), 2.13 – 1.80 (m, 2H), 1.47 (s, 9H). ^{13}C NMR (75 MHz, $CDCl_3$) δ[ppm] = 149.8 (d, $J_{C\text{-}F}$ = 299 Hz), 140 8, 137 6, 134.5, 129.4, 128 9, 128.6, 128.4, 126 2, 121.0 (d, $J_{C\text{-}F}$ = 4.2 Hz), 77.0, 46.1 (d, $J_{C\text{-}F}$ = 2 2 Hz), 32 0, 31 0, 28.3. $[\alpha]_D^{22}$ = –10°.

Phenyl (*S,E*)-3-((*tert*-butoxycarbonyl)amino)-1-fluoro-5-phenylpent-1-ene-1-sulfonate **(16)**

16 was prepared according to procedure A using phosphonate **12** (4.0 mmol, 1.3 g). Purification by column chromatography (CH:EA 5:1 – 3:1) resulted in a colorless oil (0.80 g, 1.8 mmol, 46%). ^{1}H NMR (300 MHz, $CDCl_3$) δ[ppm] = 7.46 – 7.32 (m, 2H), 7.32 – 7.15 (m, 6H), 7.10 (d, J = 7.0 Hz, 2H), 5.91 (dd, $J_{H\text{-}F}$ = 31 3 Hz, $J_{H\text{-}H}$ = 8.6 Hz, 1H), 4.68 – 4.27 (m, 2H), 2.66 – 2.43 (m, 2H), 1.97 – 1.66 (m, 2H), 1.43 (s, 9H). ^{13}C NMR (75 MHz, $CDCl_3$) δ[ppm] = 154 8, 150.8, 148.9 (d, $J_{C\text{-}F}$ = 296 Hz), 140 2, 130 2, 128 8, 128.4, 128.0, 126.5, 122.4 (d, $J_{C\text{-}F}$ = 4.1 Hz), 122.3, 80.4, 46.3 (d, $J_{C\text{-}F}$ = 2.1 Hz), 35 9, 31 9, 28.4. $[\alpha]_D^{22}$ = –15°.

(*S,E*)-1-Fluoro-5-phenyl-1-(phenylsulfonyl)pent-1-en-3-aminium chloride **(17)**

17 was prepared according to procedure C using **15** (1.2 mmol, 0.50 g), resulting in a colorless solid (0.39 g, 1.1 mmol, 95%). ^{1}H NMR (300 MHz, DMSO-d_6) δ[ppm] = 8.71 (s, 3H), 8.02 (dd, J = 7.3, 1.7 Hz, 2H), 7 97 – 7.82 (m, 1H), 7.76 (dd, J = 8.4, 7.0 Hz, 2H), 7.28 – 7.10 (m, 3H), 7.11 – 7.02 (m, 2H), 6.55 (dd, $J_{H\text{-}F}$ = 32.6 Hz, $J_{H\text{-}H}$ = 9.8 Hz, 1H), 4 07 – 3.94 (m, 1H), 2 57 – 2 39 (m, 2H), 2 26 – 1 95 (m, 2H). ^{13}C NMR (75 MHz, DMSO-d_6) δ[ppm] = 154.6 (d, $J_{C\text{-}F}$ = 298 Hz), 140.3, 136.4, 136.1, 130.7, 130.2, 129.0, 128.9, 128.6, 126.7, 115 0 (d, $J_{C\text{-}F}$ = 3 5 Hz), 45 5 (d, $J_{C\text{-}F}$ = 2.6 Hz), 33.9 (d, $J_{C\text{-}F}$ = 1.3 Hz), 31 0. $[\alpha]_D^{22}$ = –15°. MP = 130 – 132 °C.

Phenyl (*S,E*)-3-amino-1-fluoro-5-phenylpent-1-ene-1-sulfonate hydrochloride **(18)**

18 was prepared according to procedure C using **16** (1.7 mmol, 0.73 g), resulting in a colorless solid (0.55 g, 1 5 mmol, 88%). ^{1}H NMR (300 MHz, DMSO-d_6) δ[ppm] = 8.77 (s, 3H), 7.59 – 7.50 (m, 2H), 7.49 – 7.39 (m, 3H), 7 36 (t, J = 7.2 Hz, 2H), 7 28 – 7 21 (m, 1H), 7.21 – 7.11 (m, 2H), 6.45 (dd, $J_{H\text{-}F}$ = 32 Hz, $J_{H\text{-}H}$ = 9.7 Hz, 1H), 4.15 (td, J = 9 2, 5.3 Hz, 1H), 2.52 – 2.36 (m, 2H), 2 22 – 2 03 (m, 1H), 2.02 – 1.85 (m, 1H). ^{13}C NMR (75 MHz, DMSO-d_6) δ[ppm] = 149.7 (d, $J_{C\text{-}F}$ = 300 Hz), 149.0, 140.4, 130.9, 129 3,

129.2, 128.9, 126.4, 122 3, 118 6 (d, J_{C-F} = 3.2 Hz), 45.5 (d, J_{C-F} = 2 2 Hz), 40 5, 33 6, 30 5. $[\alpha]_D^{22}$ = –13°. MP = 141 – 143 °C.

Dipeptide preparation.

Ethyl (4-methylpiperazine-1-carbonyl)-l-phenylalaninate **(19)**

Compound 7 (1.0 eq, 8 5 mmol, 1.9 g) was dissolved in THF and cooled to 0 °C. Then, *N*-methyl piperazine (1.1 eq, 9.3 mmol, 1.0 mL) was added dropwise. After 12 h, THF was removed under reduced pressure and the residue was extracted with EA (3x). The combined organic extracts were washed with water (2x), sat. aq. $NaHCO_3$ (2x), and brine (2x). The organic layer was dried with Na_2SO_4 and evaporated. Purification by column chromatography (DCM:MeOH 19:1) resulted in a colorless solid (2.4 g, 7.4 mmol, 87%). ^{1}H NMR (300 MHz, DMSO-d_6) δ[ppm] = 7 35 – 7.09 (m, 5H), 6.79 (d, *J*=7 9 Hz, 1H, NH), 4.23 (ddd, *J*=8.9, 7.8, 6.5 Hz, 1H), 4 01 (qd, *J*=7.1, 1.7 Hz, 2H), 3.24 (q, *J*=4 5 Hz, 4H), 3.04 – 2 83 (m, 2H), 2 20 – 2.15 (m, 4H), 2.13 (s, 3H), 1.09 (t, *J*=7.1 Hz, 3H). ^{13}C NMR (75 MHz, DMSO-d_6) δ[ppm] = 173.0, 157 2, 138.0, 129 3, 128.3, 126.5, 60.3, 55.7, 54.4, 45 8, 43 5, 36 8, 14.1. $[\alpha]_D^{22}$ = –18°. MP = 97 – 99 °C.

(4-Methylpiperazine-1-carbonyl)-L-phenylalanine **(20)**

20 was prepared according to procedure D using **19** (7.4 mmol, 2.4 g), resulting in a colorless solid (1.8 g, 6.3 mmol, 85%). ^{1}H NMR (300 MHz, DMSO-d_6) δ[ppm] = 7 33 – 7.05 (m, 5H), 6 68 (d, *J* = 7.9 Hz, 1H), 4.28 – 4.09 (m, 1H), 3.50 – 3.16 (m, 4H), 2.98 (m, 2H), 2.46 – 2.30 (m, 4H), 2 25 (s, 3H). ^{13}C NMR (75 MHz, DMSO-d_6) δ[ppm] = 174.6, 157.1, 139.0, 129.4, 128.0, 126.1, 56 0, 53.1, 44.8, 42.7, 39.5, 36.9. $[\alpha]_D^{22}$ = –17°. MP = 121 – 123 °C.

tert-Butyl (*S*)-4-((1-ethoxy-1-oxo-3-phenylpropan-2-yl)carbamoyl)piperazine-1-carboxylate **(21)**

1-Boc piperazine (1.1 eq, 1.3 mmol, 0 24 g) was dissolved in THF. Compound 7 (1.0 eq, 1.2 mmol, 0.27 g) was added dropwise, and the mixture was stirred for 18 h at room temperature. Then, the solvent was evaporated, and the residue was extracted with EA (3x). The combined organic extracts were washed with water (2x), sat. aq. $NaHCO_3$ (2x), and brine. The crude product was dried with Na_2SO_4, and the solvent was evaporated under reduced pressure. Purification by column chromatography (DCM:MeOH 49:1) gave the product as a colorless oil (0.41 g, 1.0 mmol, 84%). ^{1}H NMR (300 MHz, $CDCl_3$) δ[ppm] = 7.33 – 7.18 (m, 3H), 7.11 (dd, *J* = 7.7, 1.8 Hz, 2H), 4.89 (d, *J* = 7 5 Hz, 1H, NH), 4.76 (q, *J* = 6.1 Hz, 1H), 4.17 (q, *J* = 7.1 Hz, 2H), 3.48 – 3.23 (m, 8H), 3 09 (dd, *J* = 13.1, 5.8 Hz), 1.85 (s, 1H), 1.46 (s, 9H), 1 24 (td, *J* = 7.1, 1.0 Hz, 3H). ^{13}C NMR (75 MHz, $CDCl_3$) δ[ppm] = 172.7, 156.6, 154.7, 136.3, 129.5, 128.6, 127.2, 80.3, 61.6, 54.5, 53.6, 43.6, 38.5, 28.5, 14.3. $[\alpha]_D^{22}$ = –24°.

(4-(*tert*-Butoxycarbonyl)piperazine-1-carbonyl)-l-phenylalanine **(22)**

22 was prepared according to procedure D using **21** (0 94 mmol, 0.38 g), resulting in a colorless solid (0.27 g, 0.71 mmol, 76%). ^{1}H NMR (300 MHz, $CDCl_3$) δ[ppm] = 8.79 (s, 1H, OH), 7 33 – 7.22 (m, 3H), 7.20 – 7.14 (m, 2H), 5 07 (d, *J* = 7.1 Hz, 1H, NH), 4 65 (q, *J* = 6.4 Hz, 1H), 3.42 – 3.21 (m, 8H), 3.21 – 3 04 (m, 2H), 1.45 (s, 9H). ^{13}C NMR (75 MHz, $CDCl_3$) δ[ppm] = 174.7, 157.5, 154.8, 136.4, 129.5, 128.8, 127 3, 80 6, 55.0, 43.7, 37.4, 28.5. $[\alpha]_D^{22}$ = –23°. MP = 82 – 84 °C.

Ethyl (morpholine-4-carbonyl)-L-phenylalaninate **(23)**

Compound 7 (1.0 eq, 4.5 mmol, 1 0 g) was dissolved in THF and cooled to 0 °C. Then, DIPEA (2.5 eq, 11 mmol, 2.0 mL) and morpholine (1.4 eq, 6.4 mmol, 0.55 mL) were added dropwise. After 12 h, THF was removed under reduced pressure and the residue was extracted with EA (3x). The combined organic extracts were washed with water (2x), sat. aq. $NaHCO_3$ (2x), and brine (2x). The organic layer was dried with Na_2SO_4 and evaporated, giving a colorless oil (1.3 g, 4.5 mmol, 100%). ^{1}H NMR (300 MHz, $CDCl_3$) δ[ppm] = 7 38 – 7.16 (m, 5H), 7.12 (d, *J* = 11.7 Hz, 1H, NH), 4 69 (dt, *J* = 11.7, 7.0 Hz, 1H), 4.27 – 3 98 (m, 2H), 3.64 (td, *J* = 7.1, 1.3 Hz, 4H), 3.38 (dt, *J* = 10.6, 7.1 Hz, 4H), 2 97 (ddt, *J* = 7.0, 2.6, 0.9 Hz, 2H), 1.22 (t, *J* = 8.0 Hz, 3H). ^{13}C NMR (75 MHz, $CDCl_3$) δ[ppm] = 172.1, 157 3, 136.8, 129.2, 128.6, 127.2, 66.0, 61.7, 55.2, 46.7, 37.6, 14.1. $[\alpha]_D^{22}$ = –19°.

(Morpholine-4-carbonyl)-L-phenylalanine **(24)**

24 was prepared according to procedure D using **23** (4 5 mmol, 1.3 g), resulting in a colorless oil (0.71 g, 2.7 mmol, 59%). ^{1}H NMR (300 MHz, $CDCl_3$) δ[ppm] = 7.77 (d, *J* = 11.9 Hz, 1H), 7.31 – 7.11 (m, 5H), 4.48 (dt, *J* = 11.9, 7.0 Hz, 1H), 3 64 (td, *J* = 7.1, 1.7 Hz, 4H), 3.30 (dt, *J* = 8 8, 7.1 Hz, 4H), 3 03 (dq, *J* = 7 0, 1 0 Hz, 2H). ^{13}C NMR (75 MHz, $CDCl_3$) δ[ppm] = 174.8, 157.6, 137 0, 130.1, 128.7, 126.9, 66.0, 56.2, 46 5, 37 5. $[\alpha]_D^{22}$ = –12°.

(*S*)-Ethyl-2-(isonicotinamido)-3-phenylpropanoate **(25)**

25 was prepared according to procedure B using L-phenylalanine ethyl ester hydrochloride (14 mmol, 3 0 g) and isonicotinic acid (15 mmol, 1 9 g). Purification by column chromatography (CH EA 1:4) gave a colorless oil (3.3 g, 12 mmol, 84%). ^{1}H NMR (300 MHz, DMSO-d_6) δ[ppm] = 9.18 (d, *J* = 7 9 Hz, 1H, NH), 8.76 – 8.68 (m, 2H), 7.72 – 7.64 (m, 2H), 7.33 – 7.15 (m, 5H), 4.69 (ddd, *J* = 10.1, 7.8, 5 2 Hz, 1H), 3.65 (s, 3H), 3.20 (dd, *J* = 13.7, 5.3 Hz, 1H), 3.08 (dd, *J* = 13.7, 10.2 Hz, 1H). ^{13}C NMR (75 MHz, DMSO-d_6) δ[ppm] = 171.8, 164.9, 150.3, 140.5, 137.5, 129.1, 128.3, 126 6, 121 3, 54.3, 52.1, 36 2. $[\alpha]_D^{22}$ = –37°.

(*S*)-2-(Isonicotinamido)-3-phenylpropanoic acid **(26)**

26 was prepared according to procedure D using **25** (7 8 mmol, 2.2 g), resulting in a colorless solid (1.4 g, 5.0 mmol, 65%). ^{1}H NMR (300 MHz, DMSO-d_6) δ[ppm] = 12 87 (s, 1H, OH), 9.04 (d, *J* = 8.2 Hz, 1H, NH), 8.76

– 8 66 (m, 2H), 7.74 – 7.62 (m, 2H), 7 36 – 7.22 (m, 4H), 7.22 – 7.13 (m, 1H), 4.64 (ddd, *J* = 10.7, 8.1, 4.4 Hz, 1H), 3 22 (dd, *J* = 13 8, 4.5 Hz, 1H), 3.05 (dd, *J* = 13.8, 10.7 Hz, 1H). ^{13}C NMR (75 MHz, DMSO-d_6) δ[ppm] = 172.8, 164.8, 150.3, 140.8, 138.0, 129.1, 128.3, 126.5, 121.3, 54 3, 36 2. $[\alpha]_D^{22}$ = –35°. MP = 166 – 168 °C.

Ethyl (thiophene-3-carbonyl)-L-phenylalaninate **(27)**

27 was prepared according to procedure B using L-phenylalanine ethyl ester hydrochloride (20 mmol, 4.5 g) and thiophene-3-carboxylic acid (20 mmol, 1.9 g), resulting in a colorless oil (5.5 g, 19 mmol, 95%). ^{1}H NMR (300 MHz, $CDCl_3$) δ[ppm] = 8 06 (d, *J* = 11.9 Hz, 1H, NH), 7 98 (dd, *J* = 2.7, 1.6 Hz, 1H), 7.73 – 7.49 (m, 2H), 7 34 – 7.07 (m, 5H), 4.85 (dt, *J* = 11.9, 7 0 Hz, 1H), 4 31 – 3 95 (m, 2H), 3.16 – 2 89 (m, 2H), 1 34 – 1.11 (m, 3H). ^{13}C NMR (75 MHz, $CDCl_3$) δ[ppm] = 171 8, 162.9, 136 8, 134.4, 130.2, 129.9, 129 2, 128.6, 127.2, 125.9, 61.6, 53.9, 37.7, 14.1. $[\alpha]_D^{22}$ = –25°.

(Thiophene-3-carbonyl)- L-phenylalanine **(28)**

28 was prepared according to procedure D using **27** (15 mmol, 4.4 g), resulting in a colorless solid (4 0 g, 15 mmol, 100%). ^{1}H NMR (300 MHz, $CDCl_3$) δ[ppm] = 9.60 (s, 1H, OH), 8.22 (d, *J* = 12.1 Hz, 1H, NH), 7.95 (dd, *J* = 2 8, 1.6 Hz, 1H), 7.76 (dd, *J* = 7.5, 1.5 Hz, 1H), 7.60 (dd, *J* = 7.4, 2.8 Hz, 1H), 7 38 – 7.16 (m, 5H), 4 66 (dt, *J* = 12.1, 7.0 Hz, 1H), 3.35 – 3 04 (m, 2H). ^{13}C NMR (75 MHz, $CDCl_3$) δ[ppm] = 173 8, 163.0, 137.4, 134.6, 130.5, 130.1, 130 0, 128.7, 127.0, 125.4, 54 9, 37.5. $[\alpha]_D^{22}$ = –20°. MP = 95 – 97 °C.

Ethyl benzoyl-L-phenylalaninate **(29)**

29 was prepared according to procedure B using L-phenylalanine ethyl ester hydrochloride (22 mmol, 5.0 g) and benzoic acid (26 mmol, 3 2 g), resulting in a colorless solid (5 2 g, 18 mmol, 80%). ^{1}H NMR (300 MHz, $CDCl_3$) δ[ppm] = 8.04 (d, *J* = 11.9 Hz, 1H, NH), 7.80 – 7.70 (m, 2H), 7 65 – 7.49 (m, 1H), 7.41 – 7.33 (m, 2H), 7.31 – 7.14 (m, 5H), 4.88 (dt, *J* = 11.9, 7.0 Hz, 1H), 4.32 – 3.93 (m, 2H), 3.17 – 2 90 (m, 2H), 1 26 (t, *J* = 8.0 Hz, 3H). ^{13}C NMR (75 MHz, $CDCl_3$) δ[ppm] = 171 8, 167.1, 136.8, 133.8, 131.8, 129.3, 128.9, 128.6, 127.4, 127.2, 61.5, 54 2, 37.80, 14 3. $[\alpha]_D^{22}$ = –28°. MP = 115 – 117 °C.

Benzoyl-L-phenylalanine **(30)**

30 was prepared according to procedure D using **29** (6.4 mmol, 1 9 g), resulting in a colorless solid (1.6 g, 5 8 mmol, 91%). ^{1}H NMR (300 MHz, $CDCl_3$) δ[ppm] = 9 55 (s, 1H, OH), 8.29 (d, *J* = 11.9 Hz, 1H, NH), 7.83 – 7.60 (m, 3H), 7.51 – 7.42 (m, 1H), 7 38 – 7.35 (m, 3H), 7.34 – 7.15 (m, 7H), 4.67 (dt, *J* = 12.1, 7.0 Hz, 1H), 3.31 – 3 07 (m, 3H). ^{13}C NMR (75 MHz, $CDCl_3$) δ[ppm] = 174 8, 167 0, 137.4, 134.2, 131.7, 130.1, 128.7, 128.7, 127.4, 126.9, 54.8, 37.5. $[\alpha]_D^{22}$ = –20°. MP = 148 – 150 °C.

Ethyl (*S*)-3-cyclohexyl-2-(isonicotinamido)propanoate **(31)**

31 was prepared according to procedure B using **8** (6.5 mmol, 1.3 g) and isonicotinic acid (7.8 mmol, 0 96 g). Purification by column chromatography (CH:EA 1:1 – 100% EA) resulted in a colorless oil (1 8 g, 5 9 mmol, 93%). ^{1}H NMR (300 MHz, $CDCl_3$) δ[ppm] = 8.71 – 8.53 (m, 2H), 7 65 – 7.46 (m, 2H), 7.05 (d, *J* = 8.2 Hz, 1H, NH), 4.77 (ddd, *J* = 9.0, 8.1, 5.4 Hz, 1H), 4 24 – 4.08 (m, 2H), 1.96 (s, 2H), 1.82 – 1.49 (m, 10H), 1.46 – 1.27 (m, 1H), 1.27 – 1.11 (m, 3H). ^{13}C NMR (75 MHz, $CDCl_3$) δ[ppm] = 174.2, 165.3, 150.5, 141.1, 121.1, 61.4, 51.8, 34.4, 33.5, 32.7, 26.4, 26.2, 26.1, 14.2. $[\alpha]_D^{22}$ = –29°.

(*S*)-3-Cyclohexyl-2-(isonicotinamido)propanoic acid **(32)**

32 was prepared according to procedure D using **31** (5 9 mmol, 1.8 g), resulting in a colorless solid (0.80 g, 2 9 mmol, 49%). ^{1}H NMR (300 MHz, DMSO-d_6) δ[ppm] = 8 89 (d, *J* = 7.9 Hz, 1H, *NH*), 8.78 – 8.57 (m, 2H), 7.97 – 7.61 (m, 2H), 4.47 (ddd, *J* = 10.4, 7 8, 4.7 Hz, 1H), 1.82 – 1.49 (m, 6H), 1 51 – 1.25 (m, 1H), 1 25 – 0 98 (m, 3H), 1 00 – 0.77 (m, 3H). ^{13}C NMR (75 MHz, DMSO-d_6) δ[ppm] = 173.9, 165.0, 150.3, 140.9, 121.4, 50 3, 37.9, 33.8, 33.2, 31.5, 26.0, 25.7, 25.6. $[\alpha]_D^{22}$ = –35°. MP = 115 – 117 °C.

Ethyl isonicotinoyl-L-leucinate **(33)**

33 was prepared according to procedure B using L-leucin ethyl ester hydrochloride (6.0 mmol, 1.2 g) and isonicotinic acid (7.2 mmol, 0.9 g), resulting in a yellow oil (1 6 g, 6 0 mmol, 100%). ^{1}H NMR (300 MHz, DMSO-d_6) δ[ppm] = 8 84 (d, *J* = 7.7 Hz, 1H), 8 65 – 8.49 (m, 2H), 7.69 – 7 51 (m, 2H), 4.45 – 4.17 (m, 1H), 3.93 (q, *J* = 7 2 Hz, 2H), 1.69 – 1.37 (m, 2H), 1.21 (dt, *J* = 11.8, 6.8 Hz, 1H), 1.00 (t, *J* = 7.1 Hz, 3H), 0.81 – 0.56 (m, 6H). ^{13}C NMR (75 MHz, DMSO-d_6) δ[ppm] = 172 6, 165 6, 150.7, 141.2, 121 8, 61.0, 51.6, 39 6, 24.9, 23 2, 21 6, 14 5. $[\alpha]_D^{22}$ = –28°.

Isonicotinoyl- L-leucine **(34)**

34 was prepared according to procedure D using **33** (6 0 mmol, 1.6 g), resulting in a yellow solid (1 3 g, 5.4 mmol, 90%). ^{1}H NMR (300 MHz, DMSO-d_6) δ[ppm] = 9.43 (d, *J* = 7.7 Hz, 1H, *NH*), 9.08 – 8.77 (m, 2H), 8 32 – 8.10 (m, 2H), 4.43 (ddd, *J* = 11.1, 7.7, 4.2 Hz, 1H), 1.99 – 1.72 (m, 1H), 1.72 – 1.43 (m, 2H), 1.00 – 0 66 (m, 6H). ^{13}C NMR (75 MHz, DMSO-d_6) δ[ppm] = 173 8, 164.1, 146.2, 145.6, 124.2, 39 9, 51.8, 25 0, 23.4, 21.6. $[\alpha]_D^{22}$ = –14°. MP = 122 – 124 °C.

Ethyl (*S*)-2-(isonicotinamido)-4-phenylbutanoate **(35)**

35 was prepared according to procedure B using L-homophenylalanine ethyl ester hydrochloride (6.0 mmol, 1 5 g) and isonicotinic acid (7 2 mmol, 0 89 g), resulting in a yellow solid (1.2 g, 3.8 mmol, 67%). ^{1}H NMR (300 MHz, DMSO-d_6) δ[ppm] = 8.99 – 8.81 (m, 1H, *NH*), 8.66 – 8.47 (m, 2H), 7 62 (dt, *J* = 4.5, 1 8 Hz, 2H), 7.17 – 6.89 (m, 5H), 4.20 (qd, *J* = 7.4, 1.7 Hz,

1H), 4 00 – 3 85 (m, 2H), 2.61 – 2.50 (m, 2H), 1.98 – 1.84 (m, 2H), 0 99 (td, *J* = 7.1, 1.7 Hz, 3H). ^{13}C NMR (75 MHz, DMSO-d_6) δ[ppm] = 172.2, 165.8, 150.7, 141 3, 141.2, 128.9, 128.8, 126.5, 121.9, 61.1, 52 8, 32.7, 32.1, 14 5. $[\alpha]_D^{22}$ = –30°. MP = 101 – 103 °C.

(*S*)-2-(Isonicotinamido)-4-phenylbutanoic acid **(36)**

36 was prepared according to procedure D using **35** (3.8 mmol, 1 2 g), resulting in a yellow solid (0.6 g, 2.1 mmol, 56%). ^{1}H NMR (300 MHz, DMSO-d_6) δ[ppm] = 12.72 (s, 1H, *OH*), 9 01 (d, *J* = 7.7 Hz, 1H, *NH*), 8.75 (q, *J* = 2.2 Hz, 2H), 7.81 (q, *J* = 2.3 Hz, 2H), 7.46 – 7.03 (m, 5H), 4.34 (q, *J* = 7.6, 7.1 Hz, 1H), 2.92 – 2 51 (m, 2H), 2.23 – 1.94 (m, 2H). ^{13}C NMR (75 MHz, DMSO-d_6) δ[ppm] = 173.8, 165.7, 150.7, 141.4, 128.9, 128.8, 126.4, 121.9, 52.7, 32.7, 32.2. $[\alpha]_D^{22}$ = –31°. MP = 133 – 135 °C.

Ethyl isonicotinoyl- L-tryptophanate **(37)**

37 was prepared according to procedure B using L-tryptophane ethyl ester hydrochloride (6.0 mmol, 1.6 g) and isonicotinic acid (7 2 mmol, 0.89 g), resulting in a yellow oil (2.0 g, 6.0 mmol, 100%). ^{1}H NMR (300 MHz, $CDCl_3$) δ[ppm] = 8.70 – 8.60 (m, 2H), 8.54 (s, 1H, *NH*), 7.55 – 7.49 (m, 1H), 7.49 – 7.42 (m, 2H), 7.35 (dt, *J* = 8.2, 1 0 Hz, 1H), 7.22 – 7 02 (m, 2H), 7.00 (d, *J* = 2.4 Hz, 1H), 6 82 (d, *J* = 7.7 Hz, 1H), 5.10 (dt, *J* = 7.7, 5 3 Hz, 1H), 4.19 (qd, *J* = 7.2, 4.2 Hz, 2H), 3 54 – 3.35 (m, 2H), 1 26 (t, *J* = 7.1 Hz, 3H). ^{13}C NMR (75 MHz, $CDCl_3$) δ[ppm] = 171.7, 165.1, 150.5, 141.2, 136.3, 127.8, 123.0, 122 5, 121.1, 119.9, 118.6, 111.6, 109.8, 61.9, 53 9, 27.6, 14 2. $[\alpha]_D^{22}$ = –14°.

Isonicotinoyl- L-tryptophan **(38)**

38 was prepared according to procedure D using **37** (6.0 mmol, 2 0 g), resulting in an orange solid (0.81 g, 2.6 mmol, 44%). ^{1}H NMR (300 MHz, DMSO-d_6) δ[ppm] = 10 93 (d, *J* = 2.4 Hz, 1H, *OH*), 9.00 (d, *J* = 7 9 Hz, 1H, *NH*), 8 82 – 8.54 (m, 2H), 7.78 – 7.69 (m, 2H), 7.59 (d, *J* = 7.8 Hz, 1H), 7.32 (d, *J* = 8 0 Hz, 1H), 7.22 (d, *J* = 2.3 Hz, 1H), 7.10 – 6 91 (m, 2H), 4 66 (ddd, *J* = 9.5, 7.8, 4.5 Hz, 1H), 3.45 – 3.12 (m, 2H). ^{13}C NMR (75 MHz, DMSO-d_6) δ[ppm] = 173 3, 164 8, 150 2, 141 0, 136.1, 127.2, 123.7, 121.4, 120.9, 118.3, 118.2, 111.5, 110.4, 54.2, 26.7. $[\alpha]_D^{22}$ = –10°. MP = 150 – 152 °C.

Ethyl (*S*)-2-(4-((*tert*-butoxycarbonyl)amino)benzamido)-3-cyclohexylpropanoate **(39)**

39 was prepared according to procedure B using *N*-boc-4-amino benzoic acid (7 5 mmol, 1.5 g), resulting in a colorless solid (3.1 g, 7 5 mmol, 100%). ^{1}H NMR (300 MHz, $CDCl_3$) δ[ppm] = 7.97 – 7.85 (m, 1H), 7 62 – 7.38 (m, 4H), 6.38 (d, *J* = 8.2 Hz, 1H), 4.61 (td, *J* = 8.5, 5 6 Hz, 1H), 3.99 (qd, *J* = 7.1, 1 9 Hz, 2H), 2.58 (s, 1H), 1.66 – 1.52 (m, 2H), 1.33 – 0.89 (m, 18H), 0.92 – 0.49 (m, 3H). ^{13}C NMR (75 MHz, $CDCl_3$) δ[ppm] = 173.5, 166.7, 152.6, 142.0, 132 3, 128 3, 128.1, 117.8, 81 0, 61.4, 50.7, 34.4, 33 5, 32.8, 28.4, 28 3, 26.4, 26 2, 26.1, 14.2. $[\alpha]_D^{22}$ = –12°. MP = 87 – 89 °C.

(*S*)-2-(4-((*tert*-Butoxycarbonyl)amino)benzamido)-3-cyclohexylpropanoic acid **(40)**

40 was prepared according to procedure D using **39** (7 5 mmol, 3.1 g), resulting in a colorless solid (2.7 g, 6.9 mmol, 92%). ^{1}H NMR (300 MHz, DMSO-d_6) δ[ppm] = 9.47 (d, *J* = 32.7 Hz, 1H), 8.18 (d, *J* = 7 9 Hz, 1H), 7.78 – 7.49 (m, 2H), 7.46 – 7.19 (m, 2H), 4.45 – 4.11 (m, 1H), 3 54 – 3.07 (m, 2H), 2.37 – 2.08 (m, 1H), 1.64 – 1.29 (m, 10H), 1.40 – 1 21 (m, 9 H). ^{13}C NMR (75 MHz, DMSO) δ[ppm] = 174.9, 167.5, 153.0, 144.2, 130 8, 124 5, 117.7, 117.5, 80.1, 50.6, 34.3, 33.7, 31.9, 28.5, 28.5, 26.5, 25 6. $[\alpha]_D^{22}$ = –11°. MP = 104 – 106 °C.

(4-Morpholine-1-carbonyl)-L -cyclohexylalanine methylester **(41)**

L-Cyclohexylalanine methylester hydrochloride (1 0 eq, 2.48 mmol, 0 55 g) was dissolved in DCM and a sat. aq. $NaHCO_3$ (40 mL) solution and cooled to 0 °C. Triphosgene (0.33 eq, 0.83 mmol, 0.25 g) was added and the mixture was stirred for 30 min. The mixture was extracted with DCM (2x 40 mL) and the combined organic extracts were washed with sat. aq. $NaHCO_3$ (2x 30 mL), and brine (2x 30 mL), then dried over Na_2SO_4 and concentrated under reduced pressure, resulting in a crude product that was dissolved in THF (30 mL) and cooled to 0 °C. Morpholine (1.0 eq, 2.5 mmol, 0.22 g) was added and the mixture stirred for 1 h. The solvent was removed under reduced pressure. Water and ethyl acetate were added to the crude residue, which was then extracted with ethyl acetate (3x 25 mL), washed with brine (2x 20 mL), dried over Na_2SO_4, and concentrated under reduced pressure to yield a colorless oil (0.75 g, 2.5 mmol, 98%). ^{1}H NMR (300 MHz, $CDCl_3$) δ[ppm] = 4.96 – 4.83 (m, 1H), 4 58 – 4.40 (m, 1H), 4 09 (q, J = 7.1 Hz, 1H), 3.70 (s, 3H), 3.69 – 3.61 (m, 4H), 3.41 – 3.28 (m, 4H), 2.01 (s, 1H), 1.76 (d, *J* = 12.8 Hz, 1H), 1.70 – 1.55 (m, 6H), 1 53 – 1.43 (m, 1H), 1.38 – 1.28 (m, 1H), 1 28 – 1.10 (m, 4H), 1.02 – 0.75 (m, 2H). ^{13}C NMR (75 MHz, $CDCl_3$) δ[ppm] = 175.1, 157.4, 66.5, 52.3, 51.6, 44.1, 40.4, 34 2, 33.6, 32.7, 26.4, 26.2, 26.1, 21.1, 14 3. $[\alpha]_D^{22}$ = +16°. MP = 105 – 106 °C.

(4-Morpholine-1-carbonyl)-L -cyclohexylalanine **(42)**

42 was prepared according to procedure D using **41** (1.0 eq, 0.7 g, 2.4 mmol), resulting in a colorless solid (0.65 g, 2 3 mmol, 97%).^{1}H NMR (300 MHz, $CDCl_3$) δ[ppm] = 9 37 (s, 1H), 5.27 – 5.07 (m, 1H), 4.41 (s, 1H), 3.75 – 3 55 (m, 4H), 3.46 – 3.28 (m, 4H), 1.83 – 1.47 (m, 6H), 1.44 – 1.30 (m, 1H), 1 26 – 1 04 (m, 4H), 1 04 – 0.79 (m, 2H). ^{13}C NMR (75 MHz, $CDCl_3$) δ[ppm] = 176.9, 158.1, 66.5, 51.9, 44.2, 39.6, 34.3, 33.6, 32.6, 26.6, 26 2, 26.1. 176.9, 158.1, 66.5, 51.9, 44 2, 39.6, 34.3, 33 6, 32.6, 26.5, 26.2, 26.1. $[\alpha]_D^{22}$ = +20°. MP = 96 – 97 °C.

Inhibitor preparation.

N-((*S*)-1-(((*S,E*)-1-Fluoro-5-phenyl-1-(phenylsulfonyl)pent-1-en-3-yl)amino)-1-oxo-3-phenylpropan-2-yl)-4-methylpiperazine-1-carboxamide **(1a)**

1a was published previously and provided in form of a colorless solid. For experimental date see SCHIRMEISTER ET AL.[43]

Phenyl (*S,E*)-1-fluoro-3-((*S*)-2-(4-methylpiperazine-1-carboxamido)-3-phenylpropanamido)-5-phenylpent-1-ene-1-sulfonate **(1b)**

1b was published previously and provided in form of a colorless solid. For experimental date see JUNG, FUCHS ET AL.[47]

tert-Butyl 4-(((*S*)-1-(((*S,E*)-1-fluoro-5-phenyl-1-(phenylsulfonyl)pent-1-en-3-yl)amino)-1-oxo-3-phenylpropan-2-yl)carbamoyl)piperazine-1-carboxylate **(2a)**

2a was prepared as published previously[46] according to procedure B using **17** (0.70 mmol, 0.25 g) and **22** (0.84 mmol, 0.30 g). Purification via HPLC resulted in a colorless solid (0.15 g, 0 22 mmol, 32%). ^{1}H NMR (300 MHz, DMSO-d_6) δ[ppm] = 8.24 (d, J = 7.7 Hz, 1H), 7 98 – 7.90 (m, 2H), 7.89 – 7.77 (m, 1H), 7.79 – 7 67 (m, 2H), 7.31 – 7.12 (m, 8H), 7.13 – 7 05 (m, 2H), 6.66 (d, J = 8.2 Hz, 1H), 6.26 (dd, $J_{H\text{-}F}$ = 33 9 Hz, $J_{H\text{-}H}$ = 8.9 Hz, 1H), 4.51 (t, J = 7.8 Hz, 1H), 4.28 (td, J = 8.8, 5.6 Hz, 1H), 3 23 (dd, J = 9.5, 5.4 Hz, 8H), 2.99 – 2.70 (m, 2H), 1 99 – 1 64 (m, 2H), 1 39 (s, 9H). ^{13}C NMR (75 MHz, DMSO-d_6) δ[ppm] = 172.4, 157.4, 154.3, 141.3, 138.8, 137.1, 135.7, 130.6, 129.7, 128.8, 128.7, 128.6, 128.4, 126.6, 126.4, 119.8, 79 5, 56.4, 44.2, 43 8, 37.8, 35 5, 31.5, 28.5. $[\alpha]_D^{22}$ = –16°. MP = 87 – 89 °C. ESI-MS: [M+H$^+$] calc. 679.2, found 679.1. Purity: 99%.

4-(((*S*)-1-(((*S,E*)-1-Fluoro-5-phenyl-1-(phenylsulfonyl)pent-1-en-3-yl)amino)-1-oxo-3-phenylpropan-2-yl)carbamoyl)piperazin-1-ium chloride **(2b)**

2b was published previously and provided in form of a colorless solid. For experimental date see JUNG, FUCHS ET AL.[47]

N-((*S*)-1-(((*S,E*)-1-Fluoro-5-phenyl-1-(phenylsulfonyl)pent-1-en-3-yl)amino)-1-oxo-3-phenylpropan-2-yl)morpholine-4-carboxamide **(2c)**

2c was prepared according to procedure B using **17** (0.70 mmol, 0.25 g) and **24** (0.84 mmol, 0 23 g). Purification via HPLC resulted in a colorless solid (0.15 g, 0 26 mmol, 37%). ^{1}H NMR (300 MHz, DMSO-d_6) δ[ppm] = 8.25 (d, J = 7.7 Hz, 1H), 8.00 – 7.90 (m, 2H), 7 89 – 7.79 (m, 1H), 7.78 – 7.66 (m, 2H), 7.30 – 7.13 (m, 8H), 7.15 – 7.05 (m, 2H), 6.62 (d, J = 8.1 Hz, 1H), 6 26 (dd, $J_{H\text{-}F}$ = 33 9 Hz, $J_{H\text{-}H}$ = 8.9 Hz, 1H), 4 61 – 4.42 (m, 1H), 4 36 – 4.16 (m, 1H), 3.57 – 3 39 (m, 4H), 3.29 – 3.13 (m, 4H), 2.98 – 2.72 (m, 2H), 2.58 – 2 38 (m, J = 2 8, 2.4 Hz, 2H), 1 99 – 1.64 (m, 2H). ^{13}C NMR (75 MHz, DMSO-d_6) δ[ppm] = 172.8, 158.1, 155 8, 141.7, 139.2, 137.5, 136.0, 130.9, 130.1, 129.1, 129.0, 128.8, 127.0, 126.8, 120.1, 66.7, 56 8, 44.8, 44.6, 41 2, 38.1, 35 8, 31.8. $[\alpha]_D^{22}$ = –10°. MP = 95 – 97 °C. ESI-MS: [M+H$^+$] calc. 580 2, found 580 0. Purity: 100%.

N-((*S*)-1-(((*S,E*)-1-Fluoro-5-phenyl-1-(phenylsulfonyl)pent-1-en-3-yl)amino)-1-oxo-3-phenylpropan-2-yl)isonicotinamide **(2d)**

2d was published previously and provided in form of a colorless solid. For experimental date see JUNG, FUCHS ET AL.[47]

N-((*S*)-1-(((*S,E*)-1-Fluoro-5-phenyl-1-(phenylsulfonyl)pent-1-en-3-yl)amino)-1-oxo-3-phenylpropan-2-yl)thiophene-3-carboxamide **(2e)**

2e was prepared according to procedure B using **17** (0.70 mmol, 0.25 g) and **28** (0.84 mmol, 0.23 g). Purification via HPLC resulted in a colorless solid (0.090 g, 0.16 mmol, 22%). ^{1}H NMR (300 MHz, DMSO-d_6) δ[ppm] = 8 51 – 8 37 (m, 2H), 8.17 (ddd, J = 6 5, 3.0, 1.3 Hz, 1H), 7 99 – 7 85 (m, 2H), 7.87 – 7.76 (m, 1H), 7.77 – 7.60 (m, 2H), 7.59 – 7.44 (m, 2H), 7.36 – 7 00 (m, 10H), 6.32 (ddd, $J_{H\text{-}F}$ = 33.7 Hz, 24.5 Hz, $J_{H\text{-}H}$=9.0 Hz, 1H), 4.77 – 4.36 (m, 2H), 3.14 – 2.82 (m, 2H), 2.45 – 2.31 (m, 2H), 2 01 – 1.64 (m, 2H). ^{13}C NMR (75 MHz, DMSO-d_6) δ[ppm] = 171 5, 162.4, 141 2, 138.5, 137.7, 137.0, 135.7, 130.6, 130.5, 129.6, 128.7, 128.6, 128.6, 127.5, 127 0, 126 8, 126.4, 119.6, 55.2, 44.4, 37 8, 31 5. $[\alpha]_D^{22}$ = –21°. MP = 136 – 138 °C. ESI-MS: [M+H$^+$] calc. 577 2, found 577.2. Purity: 100%.

tert-Butyl 4-(((S)-1-(((*S,E*)-1-fluoro-1-(phenoxysulfonyl)-5-phenylpent-1-en-3-yl)amino)-1-oxo-3-phenylpropan-2-yl)carbamoyl)piperazine-1-carboxylate **(3a)**

3a was prepared according to procedure B using **18** (0.67 mmol, 0.25 g) and **22** (0.81 mmol, 0.29 g). Purification via HPLC resulted in a colorless solid (0.18 g, 0.26 mmol, 43%). ^{1}H NMR (300 MHz, DMSO-d_6) δ[ppm] = 8.17 (d, J = 7 6 Hz, 1H, *NH*), 7 54 – 7.44 (m, 2H), 7.43 – 7.35 (m, 1H), 7 34 – 7.10 (m, 12H), 6 68 (d, J = 8.2 Hz, 1H, *NH*), 6.03 (dd, $J_{H\text{-}F}$ = 33.3 Hz, $J_{H\text{-}H}$ = 9 0 Hz, 1H), 4.56 (q, J = 7 8 Hz, 1H), 4.28 (td, J = 8 8, 5.9 Hz, 1H), 3.28 – 3.08 (m, 8H), 2.99 – 2.70 (m, 2H), 2.51 – 2.37 (m, 2H), 1.90 – 1.65 (m, 2H), 1.39 (s, 9H). ^{13}C NMR (75 MHz, DMSO-d_6) δ[ppm] = 172.6, 157.5, 154.3, 149 2, 141.2, 138.7, 130 9, 129.7, 128 8, 128.7, 128.4, 126.6, 126.4, 124 0, 122 5, 79.5, 56.4, 44 3, 43.8, 37.8, 34 9, 31.3, 28.5. $[\alpha]_D^{22}$ = –18°. MP = 107 – 109 °C. ESI-MS: [M+H$^+$] calc. 639 2, found 639.1. Purity: 99%.

4-(((*S*)-1-(((*S,E*)-1-Fluoro-1-(phenoxysulfonyl)-5-phenylpent-1-en-3-yl)amino)-1-oxo-3-phenylpropan-2-yl)carbamoyl)piperazin-1-ium chloride **(3b)**

3b was prepared according to procedure C using **3a** (0.23 mmol, 0.16 g). Purification via HPLC resulted in a colorless solid (0.14 g, 0.22 mmol, 96%). ^{1}H NMR (300 MHz, DMSO-d_6) δ[ppm] = 9.29 (s, 2H), 8.40 (d, J = 7.4 Hz, 1H), 7.53 – 7.43 (m, 2H), 7.42 – 7.35 (m, 1H), 7.34 – 7.12 (m, 12H), 7.06 – 6.96 (m, 1H), 6 03 (dd, $J_{H\text{-}F}$ = 33.3 Hz, $J_{H\text{-}H}$ = 9.0 Hz, 1H), 4.65 – 4.46 (m, 1H), 4.37 – 4.17 (m, 1H), 3 62 – 3.44 (m, 4H), 3.12 – 2.76 (m, 4H),

2.50 – 2 35 (m, 2H), 1.91 – 1 63 (m, 2H). ^{13}C NMR (75 MHz, DMSO-d_6) δ[ppm] = 172.5, 157.2, 149.2, 145.4, 141.3, 138.7, 130.9, 129.7, 128.8, 128.7, 128.5, 126.7, 126.4, 124.0, 122.4, 56.7, 44 5, 42.9, 41.1, 37 9, 34.9, 31.4. $[\alpha]_D^{22}$ = –16°. MP = 125 – 127 °C. ESI-MS: [M+H$^+$] calc. 595.2, found 595.1. Purity: 98%.

Phenyl (*S,E*)-1-fluoro-3-((*S*)-2-(morpholine-4-carboxamido)-3-phenylpropanamido)-5-phenylpent-1-ene-1-sulfonate **(3c)**

3c was prepared according to procedure B using **18** (0.40 mmol, 0.15 g) and **24** (0.48 mmol, 0.13 g). Purification via HPLC resulted in a colorless solid (0.14 g, 0 24 mmol, 59%). ^{1}H NMR (300 MHz, DMSO-d_6) δ[ppm] = 8.18 (d, *J* = 7.6 Hz, 1H, *NH*), 7.54 – 7.43 (m, 3H), 7.43 – 7 35 (m, 2H), 7 36 – 7.10 (m, 10H), 6.64 (d, *J* = 8.2 Hz, 1H, *NH*), 6.03 (dd, $J_{H\text{-}F}$ = 33.3 Hz, $J_{H\text{-}H}$ =9 0 Hz, 1H), 4 58 (p, *J* = 7.7 Hz, 1H), 4.29 (td, *J* = 8.7, 5.9 Hz, 1H), 3.54 – 3.40 (m, 4H), 3.31 – 3.13 (m, 4H), 2.97 – 2.76 (m, 2H), 2.55 – 2.38 (m, 2H), 1.88 – 1.65 (m, 2H). ^{13}C NMR (75 MHz, DMSO-d_6) δ[ppm] = 172 6, 157.7, 149 3, 149 2, 145.4, 141.2, 138.7, 130.9, 129.7, 128.8, 128.7, 128.4, 126.6, 126.4, 124.0, 122.5, 122.4, 66.3, 56.4, 44.4, 40.8, 37.8, 34.9, 31.3. $[\alpha]_D^{22}$ = –12°. ESI-MS: [M+H$^+$] calc. 596.2, found 596.1. Purity: 97%.

Phenyl (*S,E*)-1-fluoro-3-((*S*)-2-(isonicotinamido)-3-phenylpropanamido)-5-phenylpent-1-ene-1-sulfonate **(3d)**

3d was published previously and provided in form of a colorless solid. For experimental date see JUNG, FUCHS ET AL.[47]

Phenyl (*S,E*)-1-fluoro-5-phenyl-3-((*S*)-3-phenyl-2-(thiophene-3-carboxamido)propanamido)pent-1-ene-1-sulfonate **(3e)**

3e was prepared according to procedure B using **18** (0.40 mmol, 0.15 g) and **28** (0.48 mmol, 0.13 g). Purification via HPLC resulted in a colorless solid (0.14 g, 0 24 mmol, 59%). ^{1}H NMR (300 MHz, DMSO-d_6) δ[ppm] = 8.53 – 8.39 (m, 2H), 8 34 (d, *J* = 7.6 Hz, 1H), 8.19 (ddd, *J* = 11.6, 2.9, 1.3 Hz, 1H), 7.61 – 7.43 (m, 2H), 7.45 – 7.34 (m, 1H), 7.35 – 7.17 (m, 10H), 7.19 – 7.10 (m, 3H), 6.10 (dd, $J_{H\text{-}F}$ = 33.3 Hz, $J_{H\text{-}H}$ = 9.1 Hz, 1H), 4.81 – 4.46 (m, 2H), 3.13 – 2 86 (m, 2H), 2.47 – 2 32 (m, 2H), 1.99 – 1 60 (m, 2H). ^{13}C NMR (75 MHz, DMSO-d_6) δ[ppm] = 171.7, 171.6, 162.4, 162.2, 149.1, 141.2, 141.2, 138.4, 137.7, 130.9, 130.8, 129.6, 129.6, 128.8, 128.7, 128.6, 128.5, 127 5, 127.1, 126.8, 126.4, 123.9, 122.5, 55.0, 40.8, 39.2, 38.1, 26 8. $[\alpha]_D^{22}$ = –20°. MP = 119 – 121 °C. ESI-MS: [M+H$^+$] calc. 593.2, found 593 2. Purity: 99%.

Phenyl (*S,E*)-3-((*S*)-2-benzamido-3-phenylpropanamido)-1-fluoro-5-phenylpent-1-ene-1-sulfonate **(3f)**

3f was prepared according to procedure B using **18** (0.40 mmol, 0.15 g) and **30** (0.48 mmol, 0.13 g). Purification via HPLC resulted in a colorless solid (0.025 g, 0 043 mmol, 11%). ^{1}H NMR (300 MHz, DMSO-d_6) δ[ppm] = 8.68 – 8.57 (m, 1H, *NH*), 8.47 – 8.29 (m, 1H, *NH*), 7 90 – 7.76 (m, 2H), 7.60 – 7.04 (m, 20H), 6.25 (dd, $J_{H\text{-}F}$ = 15.4 Hz, $J_{H\text{-}H}$ = 9.2 Hz, 1H), 5 00 – 4.75 (m, 1H), 4.78 – 4.47 (m, 1H), 3.16 – 2.93 (m, 2H), 2.61 – 2 36 (m, 2H), 1.94 – 1.67 (m, 2H). ^{13}C NMR (75 MHz, DMSO-d_6) δ[ppm] = 171.7, 166.7, 149.2, 141 2, 138.5, 134.4, 134.3, 132.1, 131.8, 130 9, 130.8, 130.8, 129.6, 129.6, 128.8, 128.8, 128.7, 128.7, 128.6, 127.9, 127.9, 127.8, 126.8, 126.4, 123.9, 122.5, 55.4, 45.1, 39.2, 31.7, 31.4. $[\alpha]_D^{22}$ = –15°.
MP = 150 – 152 °C. ESI-MS: [M+H$^+$] calc. 587.2, found 587.0. Purity: 96%.

N-((*S*)-3-Cyclohexyl-1-(((*S,E*)-1-fluoro-5-phenyl-1-(phenylsulfonyl)pent-1-en-3-yl)amino)-1-oxopropan-2-yl)isonicotinamide **(4a)**

4a was prepared according to procedure B using **17** (0.32 mmol, 0.11 g) and **32** (0.39 mmol, 0.11 g), resulting in a colorless solid (0.052 g, 0 090 mmol, 28%) after purification via HPLC. ^{1}H NMR (300 MHz, DMSO-d_6) δ[ppm] = 8 85 – 8 66 (m, 2H), 8.42 (d, *J* = 7 8 Hz, 1H), 7.96 – 7 87 (m, 2H), 7 85 – 7.76 (m, 3H), 7.73 – 7.61 (m, 2H), 7 35 – 7.04 (m, 5H), 6 35 (dd, $J_{H\text{-}F}$ = 33 2 Hz, $J_{H\text{-}H}$ = 8 9 Hz, 1H), 4.52 (dt, *J* = 15.1, 7.9 Hz, 2H), 2 97 – 2.83 (m, 2H), 1 98 – 1.77 (m, 2H), 1.77 – 1.49 (m, 8H), 1.43 – 1.20 (m, 3H), 1.12 (d, *J* = 7 9 Hz, 2H). ^{13}C NMR (75 MHz, DMSO-d_6) δ[ppm] = 172.1, 165.3, 150.6, 141.4, 141.3, 137.0, 135.6, 130.5, 128.7, 128.6, 126.4, 122 0, 52.0, 40.8, 34 2, 33.5, 31.6, 26.5, 26.2, 26.1. $[\alpha]_D^{22}$ = –15°. MP = 108 – 110 °C. ESI-MS: [M+H$^+$] calc. 578 2, found 578.2. Purity: 95%.

N-((*S*)-1-(((*S,E*)-1-Fluoro-5-phenyl-1-(phenylsulfonyl)pent-1-en-3-yl)amino)-4-methyl-1-oxopentan-2-yl)isonicotinamide **(4b)**

4b was prepared according to procedure B using **17** (0.32 mmol, 0.11 g) and **34** (0.39 mmol, 0.090 g), resulting in a colorless solid (0.045 g, 0 083 mmol, 26%) after purification via HPLC. ^{1}H NMR (300 MHz, DMSO-d_6) δ[ppm] = 8.80 – 8 58 (m, 2H), 8.06 – 7.81 (m, 2H), 7 87 – 7.66 (m, 3H), 7.69 – 7.47 (m, 3H), 7 33 – 7.20 (m, 3H), 7.24 – 7.07 (m, 1H), 6.12 (d, *J* = 10.4 Hz, 1H), 5.86 (dd, $J_{H\text{-}F}$ = 32.5 Hz, $J_{H\text{-}H}$ = 8.1 Hz, 1H), 4.70 – 4.54 (m, 1H), 4.43 – 4.11 (m, 1H), 2 84 – 2.40 (m, 2H), 2.17 – 1.76 (m, 2H), 1.73 – 1.48 (m, 2H), 1 53 – 1.32 (m, 1H), 1.05 – 0.64 (m, 6H). ^{13}C NMR (75 MHz, DMSO-d_6) δ[ppm] = 173.0, 166.9, 150.6, 142.4, 141 9, 140.8, 140.4, 137.9, 133.5, 129.4, 128.5, 127.8, 126.1, 122.0, 121.8, 121.1, 53.0, 47.1, 40 8, 35.9, 32.6, 24 6, 22.3. $[\alpha]_D^{22}$ = –13°. MP = 90 – 92 °C. ESI-MS: [M+H$^+$] calc. 538 2, found 538 0. Purity: 99%.

N-((*S*)-1-(((*S,E*)-1-Fluoro-5-phenyl-1-(phenylsulfonyl)pent-1-en-3-yl)amino)-1-oxo-4-phenylbutan-2-yl)isonicotinamide **(4c)**

4c was prepared according to procedure B using **17** (0.28 mmol, 0.10 g) and **36** (0 34 mmol, 0.10 g), resulting in a colorless solid (0.043 g, 0 073 mmol, 26%) after purification via HPLC. ^{1}H NMR (300 MHz, DMSO-d_6) δ[ppm] = 8.96 – 8.50 (m, 2H), 8.40 (d, *J* = 7 9 Hz, 1H), 7 96 – 7.41 (m, 6H), 7.41 – 6.69 (m, 11H), 6 39 (dd, $J_{H\text{-}F}$ = 34 0 Hz, $J_{H\text{-}H}$ = 8.9 Hz, 1H), 4 69 – 4.12 (m, 2H), 3.59 – 3.07 (m, 2H), 2.77 – 2.50 (m, 2H), 2.14 – 1.70 (m, 2H). ^{13}C NMR (75 MHz, DMSO-d_6) δ[ppm] = 171.9, 166 0, 151.1, 142.1, 136.1, 131.0, 129.2, 126.8, 122 5, 120.0, 106.9, 70 3,

44 8, 34.0, 32.8, 30.1. $[\alpha]_D^{22}$ = –19°. MP = 85 – 87 °C. ESI-MS: [M+H⁺] calc. 586.2, found 586.2. Purity: 95%.

N-((*S*)-1-(((*S,E*)-1-Fluoro-5-phenyl-1-(phenylsulfonyl)pent-1-en-3-yl)amino)-3-(1H-indol-3-yl)-1-oxopropan-2-yl)isonicotinamide **(4d)**

4d was prepared according to procedure B using **17** (0 28 mmol, 0.10 g) and **38** (0.34 mmol, 0.11 g), resulting in a colorless solid (0 054 g, 0.088 mmol, 31%) after purification via HPLC. ^{1}H NMR (300 MHz, $CDCl_3$) δ[ppm] = 10.73 (t, *J* = 3.4 Hz, 1H), 8.89 – 8.73 (m, 1H), 8.73 – 8.55 (m, 2H), 8 51 – 8 32 (m, 1H), 8.01 – 7.47 (m, 8H), 7.32 – 6.80 (m, 9H), 6 31 (ddd, $J_{H\text{-}F}$ = 33.8 Hz, $J_{H\text{-}F}$ = 8.9, 4.7 Hz, 1H), 4.73 – 4.56 (m, 1H), 4.50 (q, *J* = 8.1 Hz, 1H), 3.22 – 2 99 (m, 2H), 2 85 – 2.38 (m, 2H), 2.05 – 1.52 (m, 2H). ^{13}C NMR (75 MHz, $CDCl_3$) δ[ppm] = 172.0, 168.6, 150.9, 141.6, 139.4, 138.6, 137.3, 133.6, 129.6, 128.4, 128.2, 127.6, 126.0, 123.9, 123.0, 122.8, 121.6, 121.2, 119.1, 118.8, 117.8, 116.8, 113.1, 110.1, 54.7, 47 0, 37.4, 32.4, 28.4. $[\alpha]_D^{22}$ = –21°. MP = 101 – 103 °C. ESI-MS: [M+H⁺] calc. 611.2, found 611 2. Purity: 96%.

Phenyl (*S,E*)-3-((*S*)-3-cyclohexyl-2-(isonicotinamido)propanamido)-1-fluoro-5-phenylpent-1-ene-1-sulfonate **(5a)**

5a was prepared according to procedure B using **18** (0.27 mmol, 0.10 g) and **32** (0 32 mmol, 0.088 g), resulting in a colorless solid (0.038 g, 0.064 mmol, 24%) after purification via HPLC. ^{1}H NMR (300 MHz, DMSO-d_6) δ[ppm] = 8.89 – 8.71 (m, 2H), 8.44 (m, 1H), 7.96 – 7.87 (m, 2H), 7.87 – 7.79 (m, 3H), 7.77 – 7.66 (m, 2H), 7.41 – 7 09 (m, 5H), 6.40 (dd, $J_{H\text{-}F}$ = 33.1 Hz, $J_{H\text{-}H}$ = 9 0 Hz, 1H), 4 58 (dt, *J* = 15.2, 7.9 Hz, 2H), 2.99 – 2 88 (m, 2H), 2.00 – 1 80 (m, 2H), 1.78 – 1.48 (m, 8H), 1.48 – 1 25 (m, 3H), 1.16 (d, *J* = 7.9 Hz, 2H). ^{13}C NMR (75 MHz, DMSO-d_6) δ[ppm] = 172.2, 165.5, 150.9, 141.5, 141.4, 137.2, 135.9, 130.6, 128.9, 128.8, 126.7, 122.5, 52.4, 41.2, 34.6, 33.9, 32.0, 26.6, 26.3, 26.0. $[\alpha]_D^{22}$ = –12°. MP = 123 – 125 °C. ESI-MS: [M+H⁺] calc. 594.2, found 594.2. Purity: 99%.

Phenyl (*S,E*)-1-fluoro-3-((*S*)-2-(isonicotinamido)-4-methylpentanamido)-5-phenylpent-1-ene-1-sulfonate **(5b)**

5b was prepared according to procedure B using **18** (0.25 mmol, 0.093 g) and **34** (0 30 mmol, 0 071 g), resulting in a colorless solid (0.031 g, 0.056 mmol, 22%) after purification via HPLC. ^{1}H NMR (300 MHz, $CDCl_3$) δ[ppm] = 8 81 (d, *J* = 8.4 Hz, 1H), 8.73 (s, 2H), 8.36 (dd, *J* = 14 8, 8.0 Hz, 1H), 7 80 (d, *J* = 7 5 Hz, 2H), 7 54 – 7.36 (m, 2H), 7.35 – 7.08 (m, 7H), 7.01 (d, *J* = 7.5 Hz, 1H), 6.15 (dd, $J_{H\text{-}F}$ = 32.4 Hz, $J_{H\text{-}H}$ = 8.8 Hz, 1H), 4.89 (s, 1H), 4.69 – 4.31 (m, 1H), 1 67 (s, 2H), 1.10 – 0.58 (m, 11H). ^{13}C NMR (75 MHz, $CDCl_3$) δ[ppm] = 173 0, 166.9, 150.6, 147.8, 147.7, 141.9, 140.8, 136.8, 134.8, 131.2, 131.1, 129.3, 128.5, 126.8, 126.1, 122.4, 121.1, 53.0, 47.1, 40.8, 35 9, 32 6, 24.6, 22.3. $[\alpha]_D^{22}$ = –20°. MP = 76 – 78 °C. ESI-MS: [M+H⁺] calc. 554.2, found 554.0. Purity: 99%.

Phenyl (*S,E*)-1-fluoro-3-((*S*)-2-(isonicotinamido)-4-phenylbutanamido)-5-phenylpent-1-ene-1-sulfonate **(5c)**

5c was prepared according to procedure B using **18** (0.40 mmol, 0.15 g) and **36** (0.48 mmol, 0.18 g), resulting in a colorless solid (0.060 g, 0.10 mmol, 25%) after purification via HPLC. ^{1}H NMR (300 MHz, $CDCl_3$) δ[ppm] = 9.02 (dd, *J* = 7.6, 5.4 Hz, 1H), 8.88 (t, *J* = 5 3 Hz, 2H), 8.53 (d, *J* = 7 9 Hz, 1H), 8 09 – 7.82 (m, 5H), 7.86 – 7 66 (m, 2H), 7.51 – 7.09 (m, 10H), 6.51 (ddd, $J_{H\text{-}F}$ = 33 9 Hz, $J_{H\text{-}F}$ = 8.9, 5.1 Hz, 1H), 4 83 – 4.34 (m, 2H), 2 86 – 2.68 (m, 4H), 2.33 – 1 81 (m, 4H). ^{13}C NMR (75 MHz, $CDCl_3$) δ[ppm] = 172.2, 166.3, 151.6, 142 2, 136 5, 131.4, 129 5, 127 0, 122 9, 120.4, 107.3, 70.4, 44.9, 34.3, 32.8, 30 3. $[\alpha]_D^{22}$ = –15°. MP = 96 – 98 °C. ESI-MS: [M+H⁺] calc. 602 2, found 602 2. Purity: 99%.

Phenyl (*S,E*)-3-((*S*)-3-(1H-indol-3-yl)-2-(isonicotinamido)propanamido)-1-fluoro-5-phenylpent-1-ene-1-sulfonate **(5d)**

5d was prepared according to procedure B using **18** (0.54 mmol, 0.20 g) and **38** (0 65 mmol, 0.20 g), resulting in a colorless solid (0.071 g, 0.11 mmol, 20%) after purification via HPLC. ^{1}H NMR (300 MHz, $CDCl_3$) δ[ppm] = 10.68 – 10.33 (m, 1H), 8.75 – 8.52 (m, 1H), 8 50 – 8.35 (m, 2H), 8 22 (d, *J* = 8.5 Hz, 1H), 7.79 – 7 51 (m, 4H), 7.52 – 7.36 (m, 5H), 7 09 – 6 67 (m, 9H), 6.12 (dd, $J_{H\text{-}F}$ = 33.9 Hz, $J_{H\text{-}H}$ = 8.9 Hz, 1H), 4 60 – 4.14 (m, 2H), 3 00 – 2.80 (m, 2H), 2 67 – 2.39 (m, 2H), 1 80 – 1.39 (m, 2H). ^{13}C NMR (75 MHz, $CDCl_3$) δ[ppm] = 172.0, 168 6, 150.9, 149.4, 141 6, 138.6, 137.3, 133.0, 132.9, 129.8, 128.4, 127.6, 127.3, 126.0, 123.9, 122.1, 121.6, 121.2, 119.1, 117.8, 117.0, 115.0, 113.1, 110.1, 54.7, 47.1, 47.0, 37.4, 32.4, 28.4. $[\alpha]_D^{22}$ = –22°. MP = 114 – 116 °C. ESI-MS: [M+H⁺] calc. 627 2, found 627.1. Purity: 96%.

Phenyl (*S,E*)-3-((*S*)-2-(4-((*tert*-butoxycarbonyl)amino)benzamido)-3-cyclohexylpropanamido)-1-fluoro-5-phenylpent-1-ene-1-sulfonate **(6a)**

6a was prepared according to procedure B using **18** (0.54 mmol, 0.20 g) and **40** (0.65 mmol, 0 25 g), resulting in a colorless solid (0.25 g, 0 35 mmol, 65%) after purification via HPLC. ^{1}H NMR (300 MHz, DMSO-d_6) δ[ppm] = 9.60 (d, *J* = 2.6 Hz, 1H), 8.40 – 8.10 (m, 2H), 7.94 – 7.70 (m, 2H), 7 61 – 7.34 (m, 4H), 7.35 – 7.05 (m, 6H), 7.00 (d, *J* = 7.2 Hz, 2H), 6.15 (dd, $J_{H\text{-}F}$ = 33 2 Hz, $J_{H\text{-}H}$ =9 0 Hz, 1H), 4.95 – 4.81 (m, 1H), 4 66 – 4 38 (m, 1H), 2 61 – 2 32 (m, 2H), 1.85 – 1.52 (m, 8H), 1.48 (s, 9H), 1 28 – 1.02 (m, 3H), 1.04 – 0.73 (m, 2H). ^{13}C NMR (75 MHz, DMSO-d_6) δ[ppm] = 166.3, 153.1, 142.9, 141.2, 130.9, 128.9, 128 8, 128.7, 127 8, 122.4, 117.5, 79.9, 34.3, 32.4, 31.5, 28.5, 26.5, 26.1. $[\alpha]_D^{22}$ = –15°. MP = 118 – 120 °C. ESI-MS: [M+Na⁺] calc. 730.2, found 730.2. Purity: 97%.

4-(((*S*)-3-Cyclohexyl-1-(((*S,E*)-1-fluoro-1-(phenoxysulfonyl)-5-phenylpent-1-en-3-yl)amino)-1-oxopropan-2-yl)carbamoyl)benzenaminium chloride **(6b)**

6b was prepared according to procedure C using **6a** (0.35 mmol, 0.25 g). Purification via HPLC resulted in a colorless solid (0.17 g, 0.26 mmol, 74%). ^{1}H NMR (300 MHz, DMSO-d_6) δ[ppm] = 8.56 – 8.19 (m, 4H), 8.06 – 7.72 (m, 2H), 7.61 – 7.07 (m, 10H), 7 07 – 6.90 (m, 2H), 6.45 (dd, *J* = 21.8, 10.0 Hz, 1H), 6.14 (dd, $J_{H\text{-}F}$ = 33.3 Hz, $J_{H\text{-}H}$ =9.1 Hz, 1H), 5 06 – 4.72 (m, 1H), 4.66 – 4.35 (m, 1H), 2.63 – 2.34 (m, 2H), 2.34 – 2.09 (m, 2H),

1.98 – 1.43 (m, 6H), 1.45 – 0.99 (m, 3H), 1.04 – 0.73 (m, 2H). ^{13}C NMR (75 MHz, DMSO-d_6) δ[ppm] = 172.7, 166.0, 149.2, 141.2, 130.9, 129.6, 128.8, 128.7, 126.4, 122.4, 120.1, 66.8, 34 3, 33.59, 32.4, 31.5, 26 5, 26.2, 26.1. $[\alpha]_D^{22}$ = –9°. MP = 130 – 132 °C. ESI-MS: [M+H$^+$] calc. 607 3, found 607.2. Purity: 95%.

Phenyl (*S,E*)-3-((*S*)-3-cyclohexyl-2-(morpholine-4-carboxamido)propanamido)-1-fluoro-5-phenylpent-1-ene-1-sulfonate **(6c)**

6c was prepared according to procedure B using **18** (0.08 mmol, 0.030 g) and **42** (0.08 mmol, 23 mg), resulting in a colorless solid (5.5 mg, 0.009 mmol, 9%) after purification via HPLC. ^{1}H NMR (600 MHz, DMSO-d_6) δ[ppm] = 8 32 (s, 1H), 8.15 (d, *J* = 7.7 Hz, 1H), 7.52 – 7.37 (m, 3H), 7.33 – 7.11 (m, 5H), 6.51 (d, *J* = 7.9 Hz, 1H), 6.11 (dd, *J* = 33.3, 9.0 Hz, 1H), 4.61 – 4.52 (m, 1H), 4.17 – 4.08 (m, 1H), 3.60 – 3.46 (m, 4H), 3.33 – 3 22 (m, 4H), 1.88 – 1.71 (m, 2H), 1.71 – 1 55 (m, 4H), 1.53 – 1 36 (m, 3H), 1 30 – 1.21 (m, 2H), 1.19 – 1 06 (m, 4H), 0.95 – 0.75 (m, 3H). ^{13}C NMR (151 MHz, DMSO-d_6) δ[ppm] = 173 2, 157 5, 148.7, 147.8, 145.9, 140.9, 130.5, 126.0, 123.6, 122.0, 79.2, 66 0, 52.0, 44.1, 43.78, 34 5, 33.7, 33 2, 32.0, 30.9, 26.1, 25.8, 25.7. $[\alpha]_D^{22}$ = –2°. MP = 116 – 117 °C. ESI-MS: [M+Na$^+$] calc. 601.3, found 601.2. Purity: 95%.

Molecular docking.

Since the inhibitors were designed to react covalently with cysteine-25 of CatS, two different docking approaches were followed. First, a conventional non-covalent docking was performed, to estimate affinity and geometry of the pre-organized enzyme-inhibitor complex, secondly a covalent docking was used to determine the final covalent enzyme-inhibitor complex. In both docking setups a crystallographic reference ligand was used for validation via redocking (**Table A**, **Supporting information**). Molecular docking experiments were performed using the following crystal structure freely available in the protein data bank (PDB):[53] Cathepsin S covalently bound to *N*-2-(morpholin-4-ylcarbonyl)-*N*-[(3*S*)-1-phenyl-5-(phenylsulfonyl)pentan-3-yl]-l-leucinamide (C1P), PDB entry 1NPZ.[29] For both docking approaches, chain A of the dimer of 1NPZ was extracted via PyMOL 2.5.2.[54] All ligands were energetically minimized prior docking with Molecular operating environment (MOE Version 2020.09)[55] using the MMF94x force field.[56] For visual presentation of the top binding poses, PyMOL 2 5 2 was used.[54]

Docking approach A: non-covalent docking with LeadIT.

The non-covalent docking was performed with LeadIT 2 3 2.[57] The receptors were prepared in MOE with the protonate3D functionality and the covalent bond between the co-crystallized ligand and the corresponding protease was untethered via the Builder tool in MOE. For the receptor the binding site was defined as a 6.5 Å shell around the bound reference ligand. Water molecules that form at least three hydrogen bonds with the receptor and ligand were kept as part of the binding site. The docking was performed under default settings using the enthalpy-entropy hybrid approach with 2,000 solutions per iteration and fragmentation. Only the top pose of the initial docking was kept and re-scored using the HYDE scoring function.[57] For the docking, pharmacophore constraints needed to be included to obtain reasonable binding modes. The nitrogen atoms of the peptide backbone were therefore defined as H-bond donors with a 1 Å sphere radius.

Docking approach B: covalent docking with MOE.

Covalent docking was performed with MOE. The receptor was prepared using the 3D protonation tool inside MOE. For the covalent reaction of the different warheads, the already existing template reactions were used. Initial 30 poses from the triangle match placement with London ΔG scoring were re-scored using the Affinity ΔG scoring function and induced fit refinement implemented in MOE. 10 Poses were kept and visually inspected for binding geometry the interactions matching between the docked inhibitor pose and co-crystallized ligand with the enzyme. The poses best matching inspected interaction patterns are further discussed.

Fluorometric enzyme assay.

Cathepsin S.

Assay procedure.

The assay was modified after BRÖMME ET AL.[48] The fluorescence increase upon cleavage of the fluorogenic substrate *Z*-Val-Val-Arg-AMC by Cathepsin S (CatS) was monitored by a TECAN SPARK fluorimeter (δ excitation: 365 nm, δ emission: 460 nm; TECAN GROUP, Switzerland). CatS (recombinant from *E. coli*, SIGMA-ALDRICH, Germany) was incubated with enzyme buffer (35 mM potassium phosphate, 35 mM sodium acetate, 2 mM DTT, 2 mM EDTA, pH 6.5) at room temperature for 20 – 30 min. Assay buffer (50 mM KH_2PO_4, 50 mM K_2HPO_4, 2.5 mM DTT, 2.5 mM EDTA, pH 6 5) was mixed with 1 – 5 nM CatS in enzyme buffer, followed by inhibitor in DMSO or DMSO (negative control), and 10 μM substrate *Z*-Val-Val-Arg-AMC (BACHEM, Switzerland). Black, flat-bottom 96-well microtiter plates (GREINER BIO-ONE, Germany) were used. Inhibitor screening concentrations started at 20 μM, followed by 1 μM, 200 nM, and 50 nM.

K_M determination.

The assay was performed as described above using different substrate concentrations (3.125 μM, 6 25 μM, 12.5 μM, 25 μM, 50 μM). GRAFIT (version 5 0.13, 2006, ERITHRACUS SOFTWARE LTD., UK)[58] was used for data analysis and non-linear regression. The K_M value was calculated as described by Michaelis-Menten (K_M = 34 μM):

$$v_0 = \frac{v_{max} \cdot [S]}{K_M + [S]}$$

v_0 = initial velocity; v_{max} = maximal velocity; [S] = substrate concentration.

IC_{50} and K_i calculations.

GRAFIT (version 5.0.13, 2006, ERITHRACUS SOFTWARE LTD., UK) was used for data analysis and non-linear regression.[58]

For compounds without a time-dependent mode of inhibition (fluorinated vinylsulfones as inhibitors of CatS, CatB, CatL; fluorinated vinylsulfonates as inhibitors of CatB, CatL), the residual enzyme activity in % was plotted against the inhibitor concentration in μM. Then, IC_{50} values were obtained by non-linear regression:

$$v_i = \frac{v_0}{1 + (\frac{[I]}{IC_{50}})^S}$$

v_0 = enzyme activity without inhibitor; v_i = enzyme activity in presence of inhibitor; [I] = inhibitor concentration; S = slope factor.

K_i values were calculated by using the Cheng-Prusoff equation to correct the IC_{50} values to zero substrate concentration:[49]

$$K_i = \frac{IC_{50}}{1 + \frac{[S]}{K_M}}$$

CatS: [S] = 10 μM, K_M = 34 μM. CatB: [S] = 100 μM, K_M = 150 μM. CatL: [S] = 6 25 μM, K_M = 6.5 μM.

For compounds with a time-dependent mode of inhibition (fluorinated vinylsulfonates as inhibitors of CatS), the K_i values were calculated as published previously for slow, tight binders.[47]

$$E + I \underset{k_2}{\overset{k_1}{\rightleftharpoons}} E\cdots I \underset{k_4}{\overset{k_3}{\rightleftharpoons}} E{-}I$$

E = enzyme; I = inhibitor, k = reaction constant; E···I = non-covalent enzyme-inhibitor complex; E—I = covalent enzyme-inhibitor complex.

The initial (v_i) and steady-state (v_s) velocities in inhibitor presence and the pseudo-first order rate constants k_{obs} were determined for different inhibitor concentrations. The progress curves were fitted to the slow-binding equation (*off* = offset):[50]

$$[P] = v_s \cdot t + \frac{v_i - v_s}{k_{obs}} \cdot [1 - \exp(-k_{obs} \cdot t)] + off$$

Then, the k_{obs} values were plotted against the inhibitor concentrations [I] with the following equation:

$$k_{obs} = k_4 + (\frac{k_3 \cdot [I]}{K_i^{app} + [I]})$$

The resulting dissociation constant of the initial enzyme-inhibitor complex K_i^{app} was then corrected to zero substrate concentration using the Cheng-Prusoff relationship, giving the K_i value.[49]

Dilution assay.

Dilution assays were performed for selected compounds as published previously.[47] CatS (0.5 μM) in enzyme buffer (90 μL) was incubated for with inhibitors (10 μL in DMSO) for 30 min in concentrations corresponding to tenfold the IC_{50} value obtained from the fluorometric enzyme assay ensuring complete inhibition. These mixtures (2 μL) were diluted 100-fold in assay buffer (198 μL) containing 5 μL substrate (400 μM) to give a final substrate concentration of 10 μM. Recovery of enzyme activity was measured immediately by fluorescence readout. CatS with DMSO and no inhibitor added was used as a reference while the irreversible inhibitor **K11777** was used as an irreversible control.[51]

Selectivity towards CatL and CatB.[43,47]

Cathepsin B (CatB, SIGMA-ALDRICH, Germany) and cathepsin L (CatL, SIGMA-ALDRICH, Germany) were incubated in enzyme buffer (50 mM Tris-HCl, 5 mM EDTA, 200 mM NaCl, 2 mM DTT, pH 6.5) at room temperature for 20 – 30 min. Assay buffer (50 mM Tris-HCl, 5 mM EDTA, 200 mM NaCl, 0 005% Brij35, pH 6.5) was mixed with CatB or CatL in enzyme buffer, then inhibitor in DMSO or DMSO (negative control) was added, followed by 100 μM (CatB) or 6.25 μM (CatL) substrate *Z*-Phe-Arg-AMC (BACHEM, Switzerland). The enzyme activity was monitored by a TECAN SPARK (TECAN GROUP, Switzerland) fluorescence reader using black GREINER flat-bottom 96-well microtiter plates (GREINER BIO-ONE GmbH, Germany). Inhibitor screening concentrations started at 20 μM, followed by 1 μM, and 200 nM if the percentual inhibition exceeded 50% for the previous inhibitor concentration. IC_{50} values were determined for inhibitors with >50% inhibition at 20 μM.

Cytotoxicity.

Cell Culture.

The human cell line MDA-MB-231 from adenocarcinomic breast tissue was cultured at 37 °C and 5% CO_2 in DULBECCO'S MODIFIED EAGLE'S Medium

(DMEM, 4.5 g/L D-Glucose, L-Glutamine; Gibco by THERMOFISHER SCIENTIFIC, Germany), supplemented with 10% FBS (SIGMA-ALDRICH, Germany) and 1% Penicillin/Streptomycin (INVITROGEN, Germany). Cells were cultured in a T75 culture flask and passaged two to three times per week using TrypLE™ Express (Gibco by THERMOFISHER SCIENTIFIC, Germany).

Murine bone marrow derived from C7BL/6 mice was seeded (2x10 cells/mL) in untreated 12 well plates (Gibco by THERMOFISHER SCIENTIFIC, Germany) using ISCOVE's Modified Dulbecco's Medium, supplement with 5% FBS, 2 mM L-glutamine, 100 IU/mL penicillin, 100 µg/mL streptomycin and 50 µM β-mercaptoethanol (all components from SIGMA-ALDRICH, Germany) and 10 ng/mL GM-CSF (M LTENYI BIOTEC, Germany). Media was replenished on days 3 and 6 of culture.

Cell Viability Assay.

MDA-MB-231 cells were seeded at a density of 2,500 cells/well in a white half area 96-well plate (GREINER BIO-ONE, Germany) and incubated at 37 °C. 24 h after seeding, the medium was removed and cells were treated with 50 µL of either 100 µM or 20 µM solution of compounds **5a**, **5b**, **6b** and **3c** in fresh culture medium (0.1% DMSO) or culture medium (0.1% DMSO) only. For each condition, quadruplicates were performed. Cells were incubated for 24 h. After the treatment, CELLTITER-GLO® Assay solution (50 µL) was added to each well, and the plate was placed on an orbital shaker for 2 minutes and subsequently incubated 10 minutes at room temperature. Luminescence readout was performed with a PROMEGA GLOMAX®-Multi Detection System using the manufacturer's protocol.

DC cytotoxicity

On day 7 of DC culture, compounds (1 µM) and lipopolysaccharide (100 ng/mL) was applied as indicated. On the following day, samples were harvested, washed with buffer (PBS, 2% FBS, 2mM EDTA) and preincubated with Fc receptor blocking rat-anti-mouse antibody (clone 2.4G2; THERMOFISHER SCIENTIFIC, Germany) to prevent unspecific antibody binding. Then, samples were incubated with phycoerythrin-labeled rat-anti-mouse CD11c antibody (clone N418; THERMOFISHER SCIENTIFIC, Germany) to delineate $CD11c^+$ DC, washed with PBS and incubated with allophycocyanin-eFluor780 tandem conjugate labeled fixable viability dye to detect dead cells within the $CD11c^+$ DC fraction. Fluorescence intensities were measured using an ATTUNE NXT Flow Cytometer and were analyzed using ATTUNE NXT software (both from THERMOFISHER SCIENTIFIC, Germany).

Abbreviations

ACN, acetonitrile; AMC, 7-amino-4-methylcoumarin; APC, an igen-presenting cell; boc, tert-butyl carbamoyl; CatB, cathepsin B; CatL, ca hepsin L; CatS, cathepsin S; CH, cyclohexane; cpd, compound; cyAla, cyclohexylalanine; DC, dendritic cell; DCM, dichloromethane; DECP, diethyl chlorophosphate; DIPEA, *N,N*-diisopropylethylamine; DMF, dimethylformamide; EA, ethyl acetate; HOBt, 1-hydroxybenzotriazole; hPhe, homophenylalanine; HWE, Horner-Wadsworth-Emmons; KHMDS, potassium bis(trimethylsilyl)amide; LHMDS, lithium bis(trimethylsilyl)amide; Me, methyl; Pip; piperazine; SAR, structure-activity relationship; SI, selectivity index; TBTU, 2-(1*H*-benzotriazole-1-yl)-1,1,3,3-tetramethylaminium tetrafluoroborate; THF, tetrahydrofuran, Z/Cbz; benzyloxycarbonyl.

Supporting information

The supporting information includes molecular docking score tables, enzyme assay plots, and characterization data (LC-MS, NMR) and is available free of charge.

Acknowledgements

We want to acknowledge Ann-Katrin Fuchs, Albin Lahu, and Anna Riede (all Johannes Gutenberg University Mainz) for their support in his project as well as all other co-workers in the Q5 subproject of the CRC1066 (JGU Mainz, MPIP Mainz).

Conflict of interest

The authors state that there is no conflict of interest for his publication.

Funding

Financial support by the DFG (Deutsche Forschungsgemeinschaft) in the framework of the CRC 1066 (Nanodimensional Polymeric Therapeutics for Tumor Therapy), project Q5 (Targeting and Immunomodulator Structures and their Coupling to Therapeutic Nanosystems for Oncological Application) is gratefully acknowledged.

Keywords: cathepsins • inhibitors • molecular docking • structure-activity relationship • tumor microenvironment

(1) Leroy, V.; Thurairatnam, S. *Exp. Opin. Therap. Patents* **2005**, 14 (3), 301–311.
(2) Otto, H. H.; Schirmeister, T. *Chem. Rev.* **1997**, *97* (1), 133–171.
(3) Kirschke H., Wiederanders B., Brömme D., Rinne, A. Cathepsin S from Bovine Spleen. *Biochem. J.* **1989**, *264*, 467–473.
(4) Shi, G. P.; Webb, A. C.; Foster, K. E.; Knoll, J. H. M.; Lemere, C. A.; Munger, J. S.; Chapman, H. A. *J. Biol. Chem.* **1994**, *269* (*15*), 11530–11536.
(5) Bararia, D.; Hildebrand, J. A.; Stolz, S.; Haebe, S.; Alig, S.; Trevisani, C. P.; Osorio-Barrios, F.; Bartoschek, M. D.; Mentz, M.; Pastore, A.; Gaitzsch, E.; Heide, M.; Jurinovic, V.; Rautter, K.; Gunawardana, J.; Sabdia, M. B.; Szczepanowski, M.; Richter, J.; Klapper, W.; Louissaint, A.; Ludwig, C.; Bultmann, S.; Leonhardt, H.; Eustermann, S.; Hopfner, K. P.; Hiddemann, W.; von Bergwelt-Baildon, M.; Steidl, C.; Kridel, R.; Tobin, J. W. D.; Gandhi, M. K.; Weinstock, D. M.; Schmidt-Supprian, M.; Sárosi,

M. B.; Rudelius, M.; Passerini, V.; Mautner, J.; Weigert, O. *Cell Rep.* **2020**, *31* (5).
(6) Dheilly, E.; Battistello, E.; Katanayeva, N.; Sungalee, S.; Michaux, J.; Duns, G.; Wehrle, S.; Sordet-Dessimoz, J.; Mina, M.; Racle, J.; Farinha, P.; Coukos, G.; Gfeller, D.; Mottok, A.; Kridel, R.; Correia, B. E.; Steidl, C.; Bassani-Sternberg, M.; Ciriello, G.; Zoete, V.; Oricchio, E. *Cancer Cell* **2020**, *37* (5), 674-689.e12.
(7) McDowell, S. H.; Gallaher, S. A.; Burden, R. E.; Scott, C. J. *Biochim. Biophys. Acta - Mol. Cell Res.* **2020**, *1867* (*10*), 118781.
(8) Da Costa, A. C.; Santa-Cruz, F.; Mattos, L. A. R.; Aquino, M. A. R.; Martins, C. R.; Ferraz, Á. A. B.; Figueiredo, J. L. *Mol. Clin. Oncol.* **2020**, *12* (*2*), 99–103.
(9) Wilkinson, R. D. A.; Williams, R.; Scott, C. J.; Burden, R. E. *Biol. Chem.* **2015**, *396* (*8*), 867–882.
(10) Riese, R. J.; Mitchell, R. N.; Villadangos, J. A.; Shi, G. P.; Palmer, J. T.; Karp, E. R.; De Sanctis, G. T.; Ploegh, H. L.; Chapman, H. A. *J. Clin. Invest.* **1998**, *101* (*11*), 2351–2363.
(11) Villadangos, J. A.; Riese, R. J.; Peters, C.; Chapman, H. A.; Ploegh, H. L.. *J. Exp. Med.* **1997**, *186* (*4*), 549–560.
(12) Riese, R. J.; Wolf, P. R.; Brömme, D.; Natkin, L. R.; Villadangos, J. A.; Ploegh, H. L.; Chapman, H. A. *Immunity* **1996**, *4* (*4*), 357–366.
(13) Guo-Ping, S.; Villadangos, J. A.; Dranoff, G.; Small, C.; Lijuan, G.; Haley, K. J.; Riese, R.; Ploegh, H. L.; Chapman, H. A.. *Immunity* **1999**, *10* (*2*), 197–206.
(14) Beers, C.; Burich, A.; Kleijmeer, M. J.; Griffith, J. M.; Wong, P.; Rudensky, A. Y. *J. Immunol.* **2005**, *174* (*3*), 1205–1212.
(15) Hsing, L. C.; Rudensky, A. Y. *Immunol. Rev.* **2005**, *207*, 229–241.
(16) Jakoš, T.; Pišlar, A.; Jewett, A.; Kos, J. *Front. Immunol.* **2019**, *10* (*AUG*).
(17) Farhood, B.; Najafi, M.; Mortezaee, K *J. Cell. Physiol.* **2019**, *234* (*6*), 8509–8521.
(18) Quaranta, V.; Schmid, M. C. *Cells* **2019**, *8* (*7*), 747.
(19) Fu, C.; Jiang, A. *Front. Immunol.* **2018**, *9*, 3059.
(20) Yan, X.; Wu, C.; Chen, T.; Santos, M. M.; Liu, C. L.; Yang, C.; Zhang, L.; Ren, J.; Liao, S.; Guo, H.; Sukhova, G. K.; Shi, G. P. *Mol. Immunol.* **2017**, *82*, 66–74.
(21) Liu, W. L.; Liu, D.; Cheng, K.; Liu, Y. J.; Xing, S.; Chi, P. D.; Liu, X. H.; Xue, N.; Lai, Y. Z.; Guo, L.; Zhang, G. *Oncotarget* **2016**, *7* (*19*), 28124.
(22) Yixuan, Y.; Kiat, L. S.; Yee, C. L.; Huiyin, L.; Yunhao, C.; Kuan, C. P.; Hassan, A.; Ting, W. T.; Manuel, S. T.; Guan, Y. K.; Pin, L. Y. *J. Proteome Res.* **2010**, *9* (*9*), 4767–4778.
(23) Burden, R. E.; Gormley, J. A.; Kuehn, D.; Ward, C.; Kwok, H. F.; Gazdoiu, M.; McClurg, A.; Jaquin, T. J.; Johnston, J. A.; Scott, C. J.; Olwill, S. A. *Biochimie* **2012**, *94* (*2*), 487–493.
(24) Burden, R. E.; Gormley, J. A.; Jaquin, T. J.; Small, D. M.; Quinn, D. J.; Hegarty, S. M.; Ward, C.; Walker, B.; Johnston, J. A.; Olwill, S. A.; Scott, C. *J. Clin. Cancer Res.* **2009**, *15* (*19*), 6042–6051.
(25) Fuchs, N.; Meta, M.; Schuppan, D.; Nuhn, L.; Schirmeister, T. *Cells* **2020**, *9* (*9*), 2021.
(26) Bai, R.; Chen, N.; Li, L.; Du, N.; Bai, L.; Lv, Z.; Tian, H.; Cui, J. *Front. Oncol.* **2020**, *10*, 1290.
(27) Somoza, J. R.; Zhan, H.; Bowman, K. K.; Yu, L.; Mortara, K. D.; Palmer, J. T.; Clark, J. M.; McGrath, M. E. *Biochemistry* **2000**, *39* (*41*), 12543–12551.
(28) Kopitar, G.; Dolinar, M.; Štrukelj, B.; Pungerčar, J.; Turk, V. *Eur. J. Biochem.* **1996**, *236* (*2*), 558–562.
(29) Pauly, T. A.; Sulea, T.; Ammirati, M.; Sivaraman, J.; Danley, D. E.; Griffor, M. C.; Kamath, A. V.; Wang, I. K.; Laird, E. R.; Seddon, A. P.; Ménard, R.; Cygler, M.; Rath, V. L. *Biochemistry* **2003**, *42* (*11*), 3203–3213.
(30) Gauthier, J. Y.; Black, W. C.; Courchesne, I.; Cromlish, W.; Desmarais, S.; Houle, R.; Lamontagne, S.; Li, C. S.; Massé, F.; McKay, D. J.; Ouellet, M.; Robichaud, J.; Truchon, J. F.; Truong, V. L.; Wang, Q.; Percival, M. D. *Bioorganic Med. Chem. Lett.* **2007**, *17* (*17*), 4929–4933.
(31) Tully, D. C.; Liu, H.; Chatterjee, A. K.; Alper, P. B.; Epple, R.; Williams, J. A.; Roberts, M. J.; Woodmansee, D. H.; Masick, B. T.; Tumanut, C.; Li, J.; Spraggon, G.; Hornsby, M.; Chang, J.; Tuntland, T.; Hollenbeck, T.; Gordon, P.; Harris, J. L.; Karanewsky, D. S. *Bioorganic Med. Chem. Lett.* **2006**, *16* (*19*), 5112–5117.
(32) Cai, J.; Robinson, J.; Belshaw, S.; Everett, K.; Fradera, X.; Van Zeeland, M.; Van Berkom, L.; Van Rijnsbergen, P.; Popplestone, L.; Baugh, M.; Dempster, M.; Bruin, J.; Hamilton, W.; Kinghorn, E.; Westwood, P.; Kerr, J.; Rankovic, Z.; Arbuckle, W.; Bennett, D. J.; Jones, P. S.; Long, C.; Martin, I.; Uitdehaag, J. C. M.; Meulemans, T. *Bioorganic Med. Chem. Lett.* **2010**, *20* (*23*), 6890–6894.
(33) Jadhav, P. K.; Schiffler, M. A.; Gavardinas, K.; Kim, E. J.; Matthews, D. P.; Staszak, M. A.; Coffey, D. S.; Shaw, B. W.; Cassidy, K. C.; Brier, R. A.; Zhang, Y.; Christie, R. M.; Matter, W. F.; Qing, K.; Durbin, J. D.; Wang, Y.; Deng, G. G. *ACS Med. Chem. Lett.* **2014**, *5* (*10*), 1138–1142.
(34) Ahmad, S.; Siddiqi, M. I. *J. Mol. Model.* **2017**, *23* (*3*), 92.
(35) Ward, Y. D.; Thomson, D. S.; Frye, L. L.; Cywin, C. L.; Morwick, T.; Emmanuel, M. J.; Zindell, R.; McNeil, D.; Bekkali, Y.; Giradot, M.; Hrapchak, M.; DeTuri, M.; Crane, K.; White, D.; Pav, S.; Wang, Y.; Hao, M. H.; Grygon, C. A.; Labadia, M. E.; Freeman, D. M.; Davidson, W.; Hopkins, J. L.; Brown, M. L.; Spero, D. M. *J. Med. Chem.* **2002**, *45* (*25*), 5471–5482.
(36) Lee-Dutra, A.; Wiener, D. K.; Sun, S. Cathepsin S Inhibitors: 2004 – 2010. *Exp. Opin. Therap. Patents* **2011**, 21 (3), 311–337.
(37) J. M. Wiener, J.; Sun, S.; L. Thurmond, R. *Curr. Top. Med. Chem.* **2010**, *10* (*7*), 717–732.
(38) Hilpert, H.; Mauser, H.; Humm, R.; Anselm, L.; Kuehne, H.; Hartmann, G.; Gruener, S.; Banner, D. W.; Benz, J.; Gsell, B.; Kuglstatter, A.; Stihle, M.; Thoma, R.; Sanchez, R. A.; Iding, H.; Wirz, B.; Haap, W. *J. Med. Chem.* **2013**, *56* (*23*), 9789–9801.
(39) Wilkinson, R. D. A.; Young, A.; Burden, R. E.; Williams, R.; Scott, C. J. *Mol. Cancer.* **2016**, *15* (*1*), 1–11.
(409) Bauer, R. A. *Drug Discov. Today* **2015**, *20* (*9*), 1061–1073.
(41) Kalgutkar, A. S.; Dalvie, D. K. *Expert Opin. Drug Discov.* **2012**, *7* (*7*), 561–581.
(42) Lammert, C.; Einarsson, S.; Saha, C.; Niklasson, A.; Bjornsson, E.; Chalasani, N. *Hepatology* **2008**, *47* (*6*), 2003–2009.
(43) Schirmeister, T.; Kesselring, J.; Jung, S.; Schneider, T. H.; Weickert, A.; Becker, J.; Lee, W.; Bamberger, D.; Wich, P. R.; Distler, U.; Tenzer, S.; Johé, P.; Hellmich, U. A.; Engels, B. *J. Am. Chem. Soc.* **2016**, *138* (*27*), 8332–8335.
(44) Lee, C. U.; Grossmann, T. N. *Angew. Chemie - Int. Ed.* **2012**, *51* (*35*), 8699–8700.
(45) Copeland, R. A.; Pompliano, D. L.; Meek, T. D. *Nat. Rev. Drug Discov.* **2006**, *5* (*9*), 730–739.
(46) Bradshaw, J. M.; McFarland, J. M.; Paavilainen, V. O.; Bisconte, A.; Tam, D.; Phan, V. T.; Romanov, S.; Finkle, D.; Shu, J.; Patel, V.; Ton, T.; Li, X.; Loughhead, D. G.; Nunn, P. A.; Karr, D. E.; Gerritsen, M. E.; Funk, J. O.; Owens, T. D.; Verner, E.; Brameld, K. A.; Hill, R. J.; Goldstein, D. M.; Taunton, J. *Nat. Chem. Biol.* **2015**, *11* (*7*), 525–531.
(47) Jung, S.; Fuchs, N.; Johe, P.; Wagner, A.; Diehl, E.; Yuliani, T.; Zimmer, C.; Barthels, F.; Zimmermann, R. A.; Klein, P.; Waigel, W.; Meyr, J.; Opatz, T.; Tenzer, S.; Distler, U.; Räder, H. J.; Kersten, C.; Engels, B.; Hellmich, U. A.; Klein, J.; Schirmeister, T. *J. Med. Chem.* **2021**, *64* (*16*), 12322–12358.
(48) Brömme, D. *Curr. Protoc. Protein Sci.* **2000**, *21* (*1*), 21.2.1-21.2.14.
(49) Cheng, Y.-C.; Prusoff, W. H. *Biochem. Pharmacol.* **1973**, *22* (*23*), 3099–3108.
(50) Purich, D. L. Enzyme Kinetics, Catalysis and Control, A Reference of Theory and Best-Practice Methods; *Elsevier*, **2010**.
(51) Kerr, I. D.; Lee, J. H.; Farady, C. J.; Marion, R.; Rickert, M.; Sajid, M.; Pandey, K. C.; Caffrey, C. R.; Legac, J.; Hansell, E.; Mckerrow, J. H.; Craik, C. S.; Rosenthal, P. J.; Brinen, L. S. *J. Biol. Chem.* **2009**, *284* (*38*), 25697–25703.
(52) Wilder, C.L., Walton, C., Watson, V., Stewart, F A A., Johnson, J., Peyton, S.R., Payne, C K., Odero-Marah, V., and Platt, M.O. *Int. J. Biochem. Cell Biol.* **2016**, *79*, 199–208.
(53) Berman, H. M.; Westbrook, J.; Feng, Z.; Gilliland, G.; Bhat, T. N.; Weissig, H.; Shindyalov, I. N.; Bourne, P. E. *Nucleic Acids Res.* **2000**, *28* (*1*), 235–242.
(54) Schrödinger, L.; DeLano, ; W. The PyMOL Molecular Graphics System. Schrödinger, LLC. **2020**. http://www pymol.org/pymol.
(55) Molecular Operating Environment (MOE). Chemical Computing Group ULC: 1010 Sherbrooke St. West, Suite #910, Montreal, QC, Canada, H3A 2R7 **2020**.
(56) Halgren, T. A. *J. Comput. Chem.* **1999**, *20* (*7*).

(57) LeadIT. BioSolveIT GmbH: Sankt Augustin, Germany **2017**. www.biosolveit de/LeadIT.
(58) Reulecke, I.; Lange, G.; Albrecht, J.; Klein, R.; Rarey, M. *ChemMedChem* **2008**, *3* (6), 885–897.
(59) GraFit. Erithracus Software Ltd.: UK **2006**.

Entry for the Table of Contents

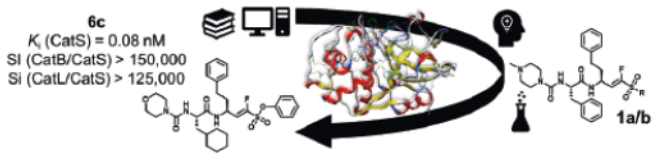

Here, we present a series of covalent-reversible CatS inhibitors based on the α-fluorovinylsulfone and -sulfonate warhead, which were op imized by molecular docking and evaluated for selectivity towards off-targets CatB and CatL. The most potent inhibitor, **6c**, has subnanomolar affinity and selectivity towards cathepsins B and L, making it a promising lead for developing new immunomodulators in cancer therapy.

3.3 Perspectives

The presented research on covalent reversible CatS inhibitors based on α-fluorovinylsulfones and -sulfonates provides a promising approach to modulate the immune response in cancers by targeting the overexpressed cysteine protease CatS. We have optimized the lead structures of the inhibitors and evaluated their selectivity and potency towards the off-targets CatB and CatL. The most potent inhibitor in the series, **6c**, has subnanomolar affinity and high selectivity towards cathepsins B and L without cytotoxic effects at relevant concentrations. These results provide a strategy to improve the anti-tumor immune response by inhibiting CatS and may lead to the development of new cancer immunotherapies with improved efficacy and reduced side effects.

The next steps would involve further studies to validate the inhibitors' effectiveness to modulate the immune response in cancers. Cell-based assays using immune cells (e.g., macrophages, dendritic cells) and cancer cells could provide more insights into their biological activity. The expression levels of MHC-I and MHC-II upon CatS inhibition could be determined by treating dendritic cells, also enabling additional functional assays for T cell activation. In case of positive results, further steps would include testing the inhibitors in animal models of cancer to evaluate their pharmacokinetic and pharmacodynamic properties, toxicity, and efficacy in reducing tumor growth and improving the anti-tumor immune response. Additionally, further optimization of the lead structures may be required to enhance their potency, selectivity, and pharmacokinetic properties for clinical use. To be discussed in project **4** is the coupling of the inhibitors to nanocarriers, potentially improving targeting and, thus, efficacy.

Overall, the next steps would involve a combination of cell-based and animal studies to further develop and validate the potential of the CatS inhibitors as new immunomodulators in cancer therapy.

4 Improving the Efficiency of Cathepsin S Inhibitors by Nanocarrier-Mediated Delivery

4.1 Introduction and Objectives

This project was part of the Q5 subproject (*"Targeting and immunomodulator structures and their coupling to therapeutic nanosystems for oncological application"*; [redacted], [redacted], and [redacted] group) in the CRC1066 (*"Nanodimensional polymer therapeutics for tumor therapy"*).

The use of nanocarriers for targeted drug delivery to immune cells is an innovative approach that has the potential to transform the field of medicine. Although pharmacodynamic target optimization is crucial, the *in vivo* effectiveness of small molecular drugs, such as some of the new CatS inhibitors discussed earlier, may be hindered by physicochemical parameters.[286] Poor solubility and reduced bioavailability can prevent them from entering *in vivo* testing. However, the variety of a nanocarrier's properties offers a unique advantage to modify a drug's pharmacokinetic profile and deliver it directly to its target site.[286] By preventing premature release from the carrier or unwanted early metabolic degradation of the drug, nanocarrier systems can improve the overall drug performance *in vivo* while reducing unwanted off-target effects. Nanocarriers can be engineered to respond to specific stimuli, allowing for precise and timely drug release at the site of the disease, e.g., lysosomal release of cathepsin inhibitors. This level of specificity and control can improve the efficacy of drugs, reduce the number of required doses, and enhance patient outcomes with an increased therapeutic window.[286,287] With the continued nanotechnology development, targeted drug delivery via nanocarriers is set to transform medicine by enabling personalized treatments for various diseases, including cancer, autoimmune disorders, and infectious diseases.[165,288–291]

As already discussed in project **3** (*"New subnanomolar cathepsin S inhibitors with high selectivity: Optimizing covalent-reversible α-fluorovinylsulfones and -sulfonates as potential immunomodulators in cancer"*), CatS inhibition in immune cells can improve the CD8+ immune response against cancer cells. Since CatS is expressed in many cells besides the immune cells, targeted delivery to immune cells can enhance the inhibitors' efficacy.[149] Nanocarrier attachment is an elegant way to improve cell-specific delivery and thus, efficacy. Therefore, the Q5 subproject aims at combining potent CatS inhibitors as immunomodulators with nanocarriers that are

decorated with carbohydrate sequences to target dendritic cells (**Figure 22**), where the cargo can be released in the lysosome to inhibit CatS.

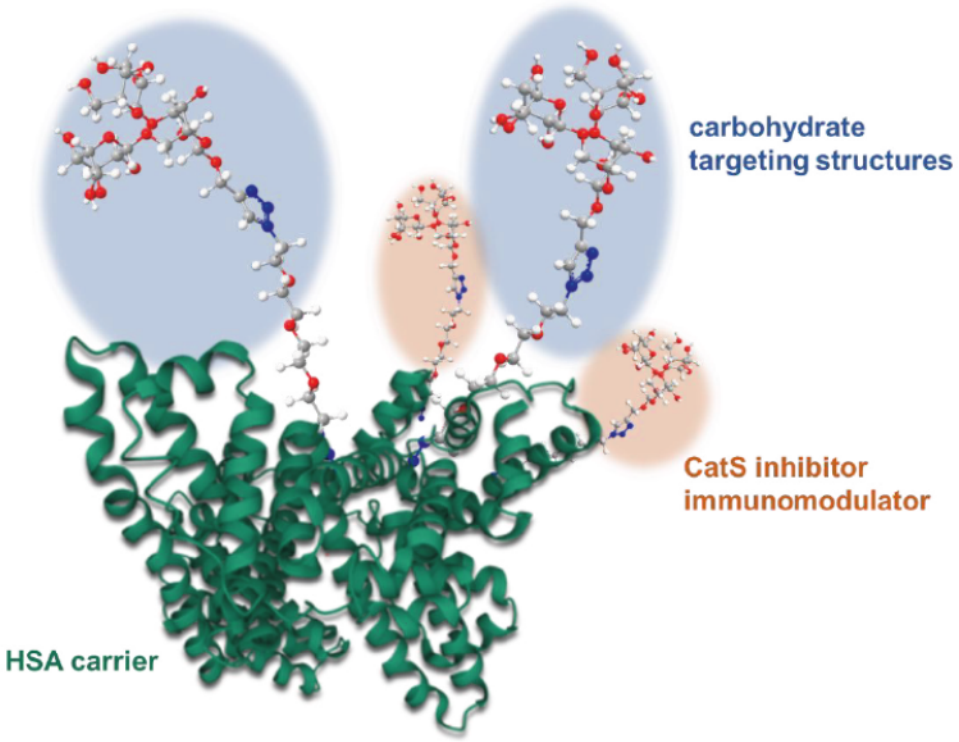

Figure 22. Schematic overview of the desired construct for the Q5 subproject. Human serum albumin (HSA) is used as a nanocarrier ([redacted] group) with carbohydrate targeting structures ([redacted] group) and our CatS inhibitors ([redacted]) attached to the surface via linkers. Figure modified after an original draft by [redacted].

Based on the results from the SAR study (project **3**), we designed linker-functionalized CatS inhibitors for nanocarrier attachment and lysosomal release. The project workflow is depicted in **Figure 23**.

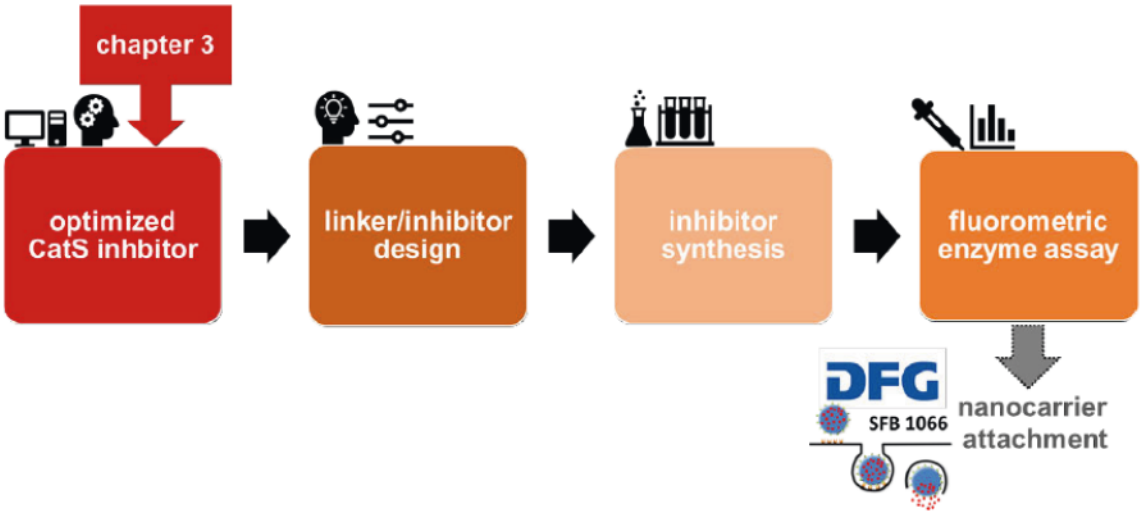

Figure 23. Workflow for project 4 (part of CRC1066 Q5).

4.2 Results and Discussion

4.2.1 Inhibitor Design

In order to achieve potent and selective CatS inhibition, we functionalized well-suited inhibitors from the SAR study in project **3** (*"New subnanomolar cathepsin S inhibitors with high selectivity: Optimizing covalent-reversible α-fluorovinylsulfones and -sulfonates as potential immunomodulators in cancer"*) with a linker for nanocarrier attachment. For my part of the project, I used the highly potent compound **2** (= **6b** in chapter **3,** K_i = 3 nM, SI >1,000) with a free amino moiety to attach linker structures via amide couplings. The linker should be cleavable at lysosomal pH (4–5) and not have a major effect on the enzyme inhibition. Linker attachment in the inhibitor's P3 position was found suitable in molecular docking studies since other CatS binding sites might be too narrow and the bulky S2 site is important for affinity and selectivity.[197,292]

Scheme 4 shows several literature-known responsive linkers that are cleaved at acidic pH.[293–295] As a first approach that will be discussed in this chapter, we decided to use a hydrazone linker since the pH optimum for its cleavage should be around 5, depending on the attached residues.[296]

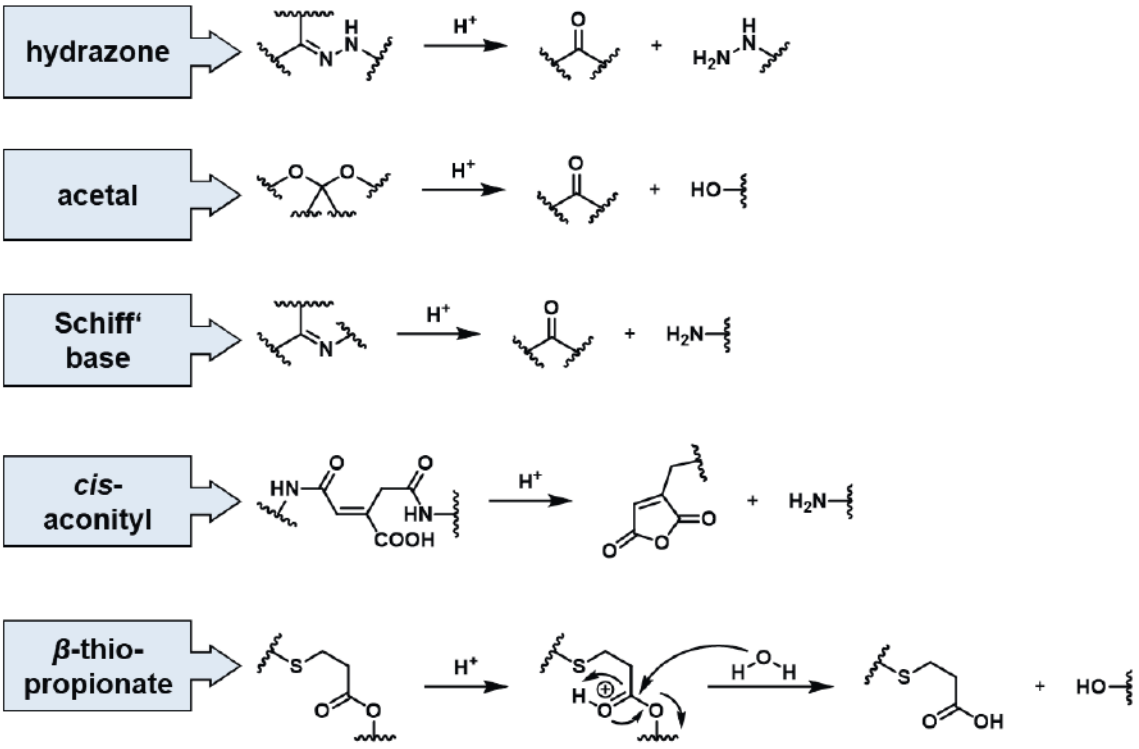

Scheme 4. pH-responsive linkers and their cleavage products.[293]

The hydrazone formation requires a keto- or aldehyde moiety. Therefore, I introduced this functionality at the N-terminal linker (compound **3**). In addition to the pH-sensitive hydrazone linker, I also prepared an inhibitor with a pH-stable linker (compound **4**). All inhibitors of interest are displayed in **Scheme 5**.

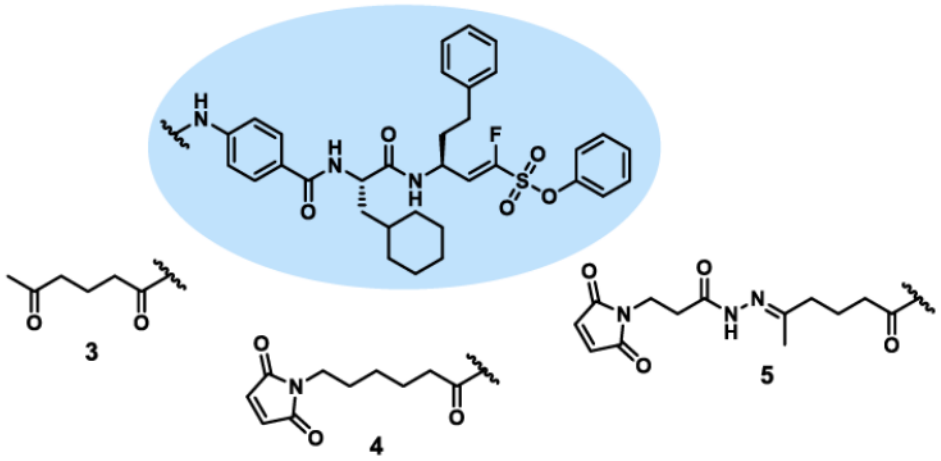

Scheme 5. Final compounds **3–5**. Compound **3** serves as a precursor of **5** and is also released upon linker cleavage at acidic pH. Compound **4** serves as a uncleavable control. Compound **5** with a pH-responsive hydrazone linker.

The α-fluorovinylsulfonate warhead has proven suitable since it resulted in slowly reversible tight binders as described in chapter **3**. Previous studies have also revealed that vinylsulfones and -sulfonates are not reactive towards endogenous thiol-containing nucleophiles, such as glutathione, which would be beneficial for future cell-based assays or *in vivo* studies.[232]

4.2.2 Synthesis and Purification

The fluorovinylsulfonate warhead **X** was prepared in a Horner-Wadsworth-Emmons reaction as previously published (details see **Experimental Section**).[242] Dipeptide **VI** was synthesized by amide coupling of ester **IV** with *N*-boc-4-amino benzoic acid to **V**, followed by alkaline hydrolysis (**Scheme 6**).

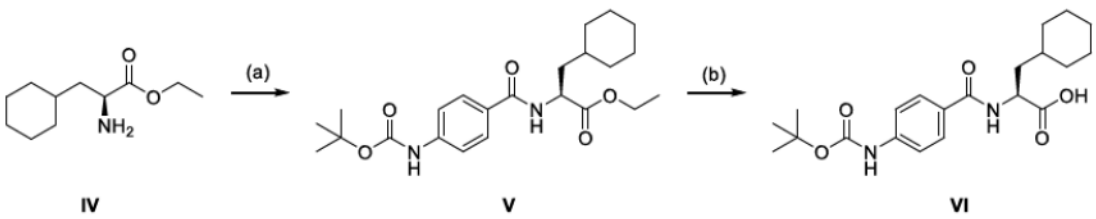

Scheme 6. Synthesis route of dipeptide **VI** starting with **IV**. (a) *N*-boc-4-amino benzoic acid, HOBt, TBTU, DIPEA, DCM, 0 °C – rt, 12 h, 100%. (b) LiOH monohydrate, THF/H_2O, rt, 12 h, 92%.

The linker-functionalized inhibitors **3–5** were prepared as shown in **Scheme 7**. TBTU coupling of warhead **X** and dipeptide **VI** resulted in compound **1** that was already part of the SAR study in project **3** *("New subnanomolar cathepsin S inhibitors with high selectivity: Optimizing covalent-reversible α-fluorovinylsulfones and -sulfonates as potential immunomodulators in cancer"*) as well as compound **2** after boc-group removal. In a next step, amide couplings of **2** with linker moieties (4-acetylbutyric acid or 6-maleimidohexanoic acid) using HOBt, HATU, and collidine gave access to **3** and **4**. Compound **3** was then converted to **5** in a hydrazone formation with 3-(2,5-dioxo-2,5-dihydro-1*H*-pyrrol-1-yl)propanehydrazide in methanol (with 0.1% TFA).

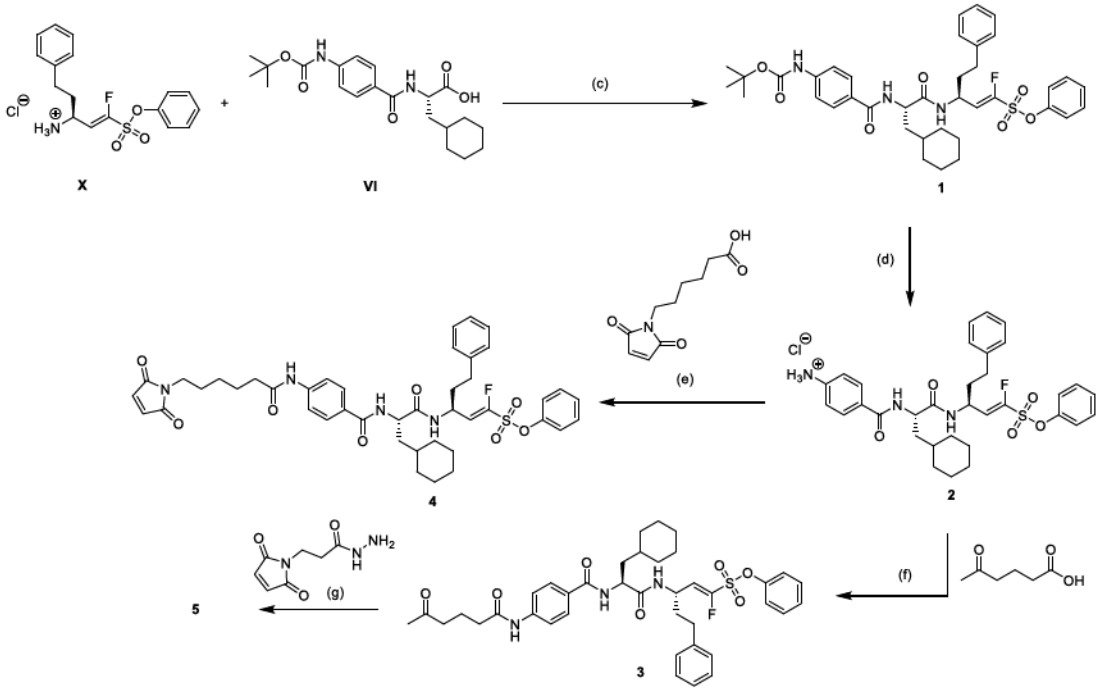

Scheme 7. Synthesis route of final compounds **3–5**. (c) HOBt, TBTU, DIPEA, DCM, 0 °C – rt, 24 h, 65%. (d) HCl, dioxane, rt, 6 h, 74%. (e) 6-maleimidohexanoic acid, HOBt, HATU, collidine, DCM/DMF, 0 °C – rt, 48 h, 23%. (f) 4-acetylbutyric acid, HOBt, HATU, collidine, DCM/DMF, 0 °C – rt, 48 h, 34%. (g) 3-(2,5-dioxo-2,5-dihydro-1*H*-pyrrol-1-yl)propanehydrazide, THF, methanol, rt, 12 h, 38%.

The reaction course of the hydrazone formation was monitored using HPLC-MS (**Figure 24**). Since it is an equilibrium reaction, there was no complete turnover from **3** to **5** as shown in the HPLC chromatogram at λ = 254 nm (**Figure 24A**). Nevertheless, the subsequent purification via preparative HPLC gave access to **5** with 99% purity.

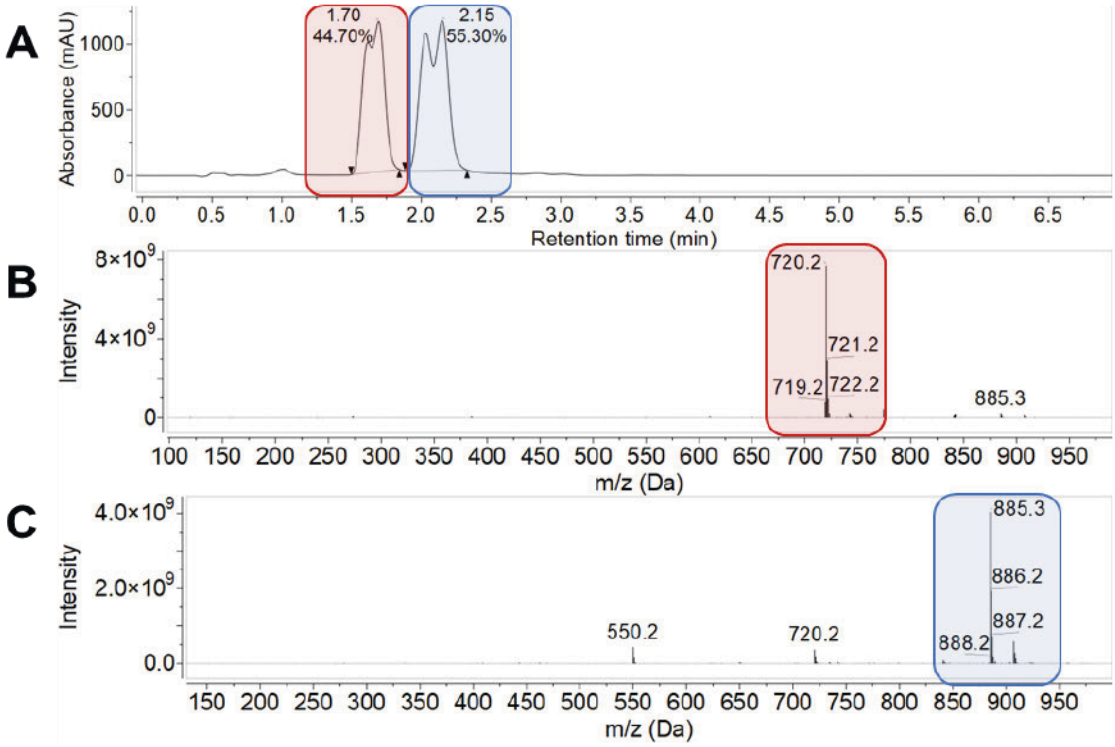

Figure 24. LC-MS reaction control for hydrazone formation of **5** after 3 h; 45% H_2O, 55% ACN, 0.01% HCOOH on an AGILENT Poroshell 120 EC-C_{18} 150 x 2.10 mm, 4 μm column. (**A**) HPLC chromatogram @254 nm, retention times: 1.70 min (peak 1, framed in red, educt **3**) and 2.15 min (peak 2, framed in blue, product **5**). (**B**) ESI-MS spectrum in positive mode for peak 1. m/z $[M+H^+]$ = 720.2 for compound **3**. (**C**) ESI-MS spectrum in positive mode for peak 2. m/z $[M+H^+]$ = 885.3 for compound **5**. Purification via HPLC.

4.2.3 Fluorometric Enzyme Assay

The functionalized inhibitors **3–5** were then evaluated in fluorometric enzyme assays for their CatS inhibition and selectivity towards off-target cathepsins (**Table 2**). Their biphasic progress curves indicate a time-dependent mode of inhibition (exemplified for **3**, **Figure 25**). Since α-fluorovinylsulfonates are known to be time-dependent, covalent reversible inhibitors, additional inhibition constants were determined (**Table 2**).[242]

Table 2. Inhibition data for compounds **3–5** (all time-dependent).[236]

		3	**4**	**5**
CatS	K_i [μM]	0.0005 ± 0.0001	0.0003 ± 0.0001	0.0009 ± 0.0004
	k_3 [s^{-1}]	$1.4 \cdot 10^{-3}$	$1.2 \cdot 10^{-3}$	$1.1 \cdot 10^{-3}$
	k_4 [s^{-1}]	$6.0 \cdot 10^{-4}$	$6.0 \cdot 10^{-4}$	$3.0 \cdot 10^{-4}$
	K_i^* [μM]	0.00014	0.00010	0.00019
CatB	K_i [μM]	>12	>12	>12
	SI CatB/CatS	>24,000	>40,000	>20,000
CatL	K_i [μM]	>10	>10	>10
	SI CatL/CatS	>20,000	>33,000	>16,000

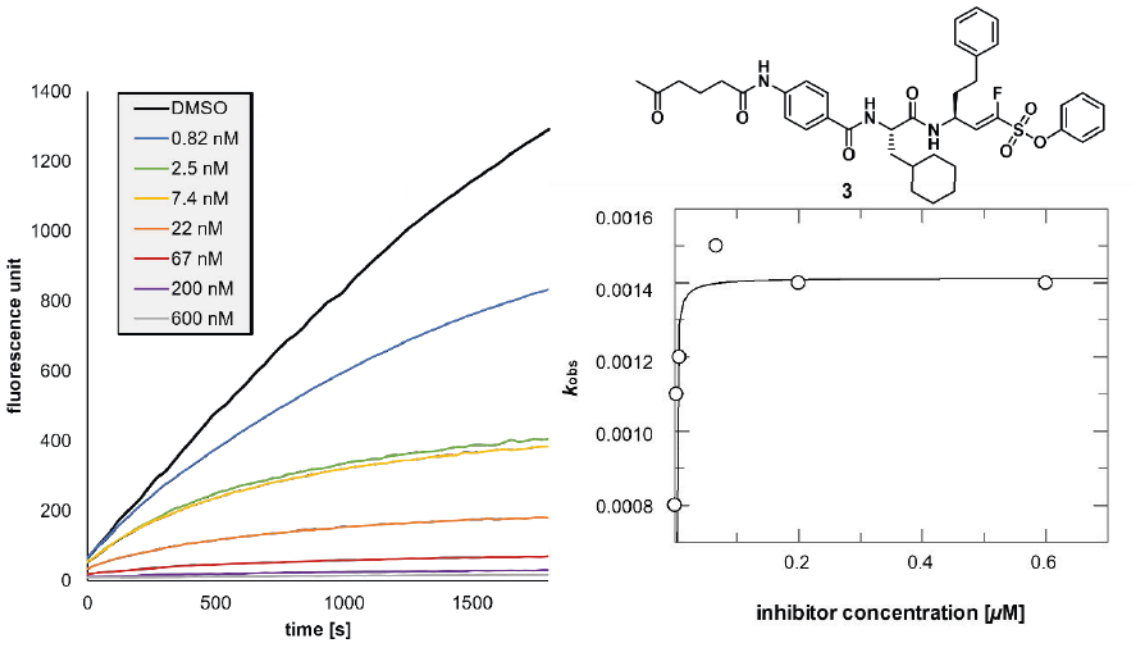

Figure 25. Inhibition data for compound **3** (top right). Biphasic progress curves (left) indicate time-dependent inhibition, k_{obs} vs. inhibitor concentration plot (bottom right) was used for K_i determination.

The inhibition constants K_i and K_i^* are in the subnanomolar range for all tested inhibitors, reflecting their high inhibitory potency. However, the compounds remain highly selective towards CatB and CatL with more than 16,000-fold selectivity.

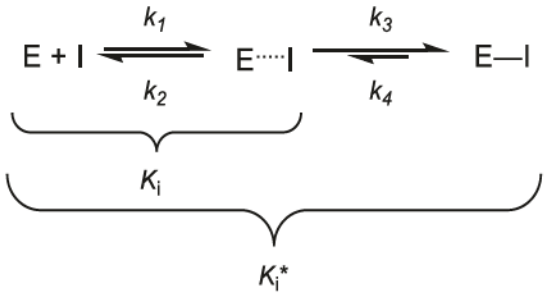

E = enzyme; I = inhibitor, k = rate constant;

E I = non-covalent enzyme-inhibitor complex; E—I = covalent enzyme-inhibitor complex.

In addition, the rate constant for the formation of the covalent enzyme-inhibitor complex k_3 is at least twice as high as k_4, suggesting tight binding that results in a slower dissociation of this complex. Since the functionalized inhibitors did not lose their inhibitory activity, they are great candidates for the future attachment to nanocarriers.

4.3 Conclusions and Perspectives

I have successfully functionalized compound **2** (K_i = 3 nM, SI >1,100), derived from a previous SAR study, to enable nanocarrier attachment. Compound **4,** with a non-cleavable linker, and compound **5**, with a pH sensitive linker, both exhibit potent inhibition of CatS with K_i and K_i* values in the subnanomolar range, while maintaining selectivity towards CatB and CatL (SI >16,000). Compound **3**, the cleavage product of **5** that is supposed to be released in the lysosome, demonstrates subnanomolar inhibition (K_i = 0.5 nM) and high selectivity (SI >20,000). These promising results indicate that further investigation and linkage to nanoscale delivery systems should be performed.

To better understand the kinetics of linker cleavage at acidic pH, an HPLC assay could be developed. By pre-incubating the compound at various pH values and then analyzing the samples via HPLC, valuable insights into cleavage kinetics and pH optimum could be obtained. It would also be essential to evaluate the biological activity of the inhibitor-carrier construct compared to the plain inhibitor, using techniques such as enzyme assays or immunoassays. Immunoassays with macrophages or dendritic cells could help to investigate the inhibitors' effect on immune cell polarization and T cell stimulation.

While the synthesized compounds provide a good starting point for first evaluations, future studies should explore alternative linkers to optimize inhibitor release. In addition to the HPLC cleavage assay, a cell-based cleavage assay would be a good enhancement, as metabolic enzymes, etc. could interfere with the inhibitor release. In order to already gain insights into metabolism, preceding microsomal stability assays could be performed. To facilitate imaging in cell-based or even *in vivo* assays, a fluorophore or radioactive marker would be necessary. Fluorescent or radioactive labeling allows a variety of detection methods. Here, the CatS inhibitor could serve as a therapeutic agent whereas a radioactive label, possibly ^{18}F for the α-fluorovinylsulfonates, could serve as a diagnostic tool for imaging. Alternatively, a modified linker with an option to attach a fluorescent or radioactive probe could be explored.

4.4 Experimental Section

4.4.1 General

All reagents and solvents were of analytical grade quality and purchased from SIGMA-ALDRICH, ALFA AESAR, ACROS, BLD PHARMATECH, FISHER SCIENTIFIC, CHEMPUR or TCI. Chemicals were used without further purification. Solvents were purified by distillation and desiccated by standard methods if necessary. ^{1}H and ^{13}C NMR spectra were recorded on a BRUKER Fourier 300 spectrometer using DMSO-d_6, $CDCl_3$ or CD_2Cl_2 as solvents. Chemical shifts δ are given in parts per million (ppm) using residual proton peaks of the solvent as internal standard (^{1}H / ^{13}C: DMSO: 2.50 / 39.52 ppm, $CHCl_3$: 7.26 / 77.16 ppm, CH_2Cl_2: 5.32 / 54.00 ppm). The purity of the compounds was determined via HPLC-MS (λ = 254 nm, 210 nm). LC chromatograms were obtained from an LC-MS system consisting of an *Agilent* 1100 series HPLC system with an AGILENT Poroshell 120 EC-C_{18} 150 x 2.10 mm, 4 μm column. The mobile phase consisted of acetonitrile, H_2O, and 0.01% formic acid in water. Mass spectra were detected by an AGILENT 1100 series LC/MSD Trap with electron spray ionization (ESI) in positive mode. Purification with a preparative HPLC system was performed by a VARIAN PrepStar system (model 218) with an AGILENT Zorbax XDB-C18 21.2 x 150 mm, 5 μm column, detected at 254 and 210 nm. Column chromatography was performed with silica gel (0.06 – 0.02 mm or 0.040 – 0.063 mm) obtained from CARL ROTH. All reactions were monitored by thin-layer chromatography using MACHEREY-NAGEL ALUGRAM Xtra SIL G/UV254 silica gel 60 plates for detection at 254 nm. Melting points were determined in open capillaries using a STUART SMP10-instrument. Optical rotation $[\alpha]_D^{22}$ was measured on an P3000 polarimeter from KRÜSS at 22 °C and are reported in $cm^3\ g^{-1}\ dm^{-1}$.

4.4.2 Syntheses

General procedures

Procedure A: Horner-Wadsworth-Emmons reaction.

A solution of the phosphonate (1.0 eq) in dry THF was cooled to –78 °C. Then, KHMDS or LHMDS (1.0 M in THF) was added dropwise, and the mixture was stirred for 30 – 60 min. Afterwards, a solution of the aldehyde (1.2 eq) in dry THF was added in portions and the reaction mixture was stirred for 3 – 4 h and then quenched by adding 7.0 eq of water. The solvent was removed under reduced pressure and the residue was extracted with EA or DCM (3x). The organic phase was washed with water (2x), saturated aq. $NaHCO_3$ (2x) and brine (1x) and dried with Na_2SO_4. Afterwards, the organic solvent was removed under reduced pressure and the crude product was purified by column chromatography.

Procedure B: Amide coupling with TBTU.

The carboxylic acid (1.2 eq), HOBt (1.2 eq), and TBTU (1.2 eq) were dissolved in DCM and cooled to 0 °C. Then, DIPEA (3.5 eq) was added dropwise, and the mixture was stirred for approx. 20 min until all components dissolved. The amine (1.0 eq) was added in portions and the reaction was stirred for at least 12 h at room temperature. The mixture was quenched by adding water and the aqueous phase was extracted with DCM. Then, the organic phase was washed with water (2x), saturated aq. $NaHCO_3$ (2x), and brine. After drying it over Na_2SO_4, the organic solvent was evaporated under reduced pressure and purified via column chromatography or HPLC.

Procedure C: Amide coupling with HATU.

The carboxylic acid (1.2 eq), HOBt (1.2 eq), and HATU (1.2 eq) were dissolved in DCM or DCM/DMF and cooled to 0 °C. Then, collidine (2.0 eq) was added dropwise, and the mixture was stirred for approx. 20 min until all components dissolved. The amine (1.0 eq) was added in portions and the reaction was stirred for at least 12 h at room temperature. The mixture was quenched by adding water and the aqueous phase was extracted with DCM. Then, the organic phase was washed with water (2x), saturated aq. $NaHCO_3$ (2x), and brine. After drying it over Na_2SO_4, the organic solvent was evaporated under reduced pressure and purified via column chromatography or HPLC.

Procedure D: Alkaline ester hydrolysis.

The compound (1.0 eq) was dissolved in THF. LiOH monohydrate (4.0 eq) was dissolved in water and added dropwise. Then, the mixture was stirred for at least 6 h at room temperature followed by evaporating THF under reduced pressure. The pH value of the aqueous residue was adjusted to 4–5 by adding 1 M HCl, resulting in the product precipitating as a solid.

Procedure E: Boc group removal.

A solution of 4 M HCl in dioxane was added to the boc-protected compound (1.0 eq) until complete dissolution and stirred for at least 30 min at room temperature. The residual solvent was either evaporated under reduced pressure and the crude product was lyophilized and used without further purification or the product was precipitated with diethyl ether or *n*-pentane.

Starting material synthesis

Phenyl methanesulfonate (**I**)

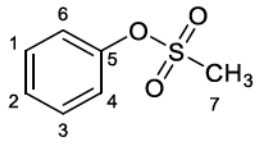

M = 172.20 g/mol

Phenol (1.0 eq, 50 mmol, 4.71 g) was dissolved in EA and cooled to 0 °C. TEA (2.0 eq, 100 mmol, 13.7 mL) was added dropwise as well as mesyl chloride (1.3 eq, 65 mmol, 5.10 mL), allowing the mixture to warm to room temperature and stir for 1 h. Then, the reaction mixture was extracted with EA (2x) and the organic phase was washed with water (3x) and brine (1x), and dried with Na_2SO_4. The organic solvent was removed under reduced pressure and the crude product was purified by column chromatography (CH:EA 4:1 – 2:1), giving a colorless solid (8.18 g, 95%).

^{1}H NMR (300 MHz, DMSO-d_6) δ [ppm] = 7.44 – 7.33 (m, 2H, *H-4, H-6*), 7.30 – 7.19 (m, 3H, *H-1, H-2, H-3*), 3.09 (s, 3H, *H-7*).

^{13}C NMR (75 MHz, DMSO-d_6) δ [ppm] = 149.7 (*C-5*), 129.9 (*C-1, C-3*), 127.1 (*C-2*), 122.0 (*C-4, C-6*), 37.1 (*C-7*).

F_p = 65 ± 2 °C.

tert-Butyl (*S*)-(1-(methoxy(methyl)amino)-1-oxo-4-phenylbutan-2-yl)carbamate (**II**)

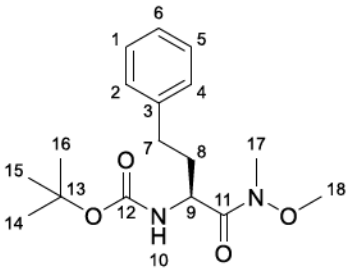

M = 322.41 g/mol

N-boc-L-homophenylalanine (1.0 eq, 20 mmol, 5.59 g) was dissolved in DCM and cooled to 0 °C. Then, TBTU (1.2 eq, 24 mmol, 7.71 g), HOBt (1.2 eq, 24 mmol, 3.24 g), and DIPEA (3.5 eq, 70 mmol, 12.2 mL) were added and the mixture was stirred for 20 – 30 min until all components dissolved. *N,O*-dimethyl hydroxylamine (1.2 eq, 24 mmol, 2.34 g) was added in portions and the mixture was stirred for at least 12 h at room temperature. The reaction was stopped by adding water and the aqueous phase was extracted with DCM (2x). The combined organic extracts were washed with saturated aq. $NaHCO_3$ (2x), and brine (1x), then dried with Na_2SO_4. After removal of the solvent at reduced pressure, the crude product, a colorless oil (6.13 g, 95%), was used without further purification.

^{1}H NMR (300 MHz, DMSO-d_6) δ [ppm] = 7.31 – 7.21 (m, 2H, *H-1, H-5*), 7.17 (t, J=7.0 Hz, 3H, *H-2, H-4, H-6*), 6.57 (s, 1H, *N-H*), 4.31 (q, *J* = 7.4 Hz, 1H, *H-9*), 3.55 (s, 3H, *H-18*), 3.06 (s, 3H, *H-17*), 2.83 – 2.51 (m, 2H, *H-7*), 1.87 – 1.72 (m, 2H, *H-8*), 1.39 (s, 9H, *H-14 – H-16*).

^{13}C NMR (75 MHz, DMSO-d_6) δ [ppm] = 173.9 (*C-11*), 155.6 (*C-12*), 142.1 (*C-3*), 128.4 (*C-6*), 128.2 (*C-1, C-5*), 125.8 (*C-2, C-4*), 77.9 (*C-13*), 60.9 (*C-18*), 50.1 (*C-9*), 32.3 (*C-17*), 31.6 (*C-8*), 31.5 (*C-7*), 28.2 (*C-14 – C-16*).

$\boldsymbol{\alpha_{22}^{D}}$ = –40° (c = 1 g/100 mL in MeOH).

tert-Butyl (*S*)-(1-oxo-4-phenylbutan-2-yl)carbamate (**III**)

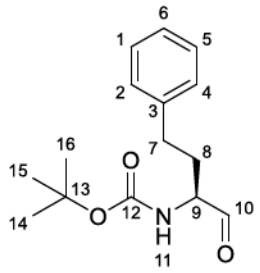

M = 263.34 g/mol

Compound **II** (1.0 eq, 15 mmol, 5.20 g) was dissolved in dry diethyl ether and cooled to 0 °C. $LiAlH_4$ (1.3 eq, 19.5 mmol, 0.74 g) was added portionwise and the mixture was stirred for 2 h. Afterwards, the reaction was stopped with 0.33 M $KHSO_4$ and then extracted with diethyl ether (2x). The combined extracts were washed with water (2x), 1 M HCl (2x), sat. aq. $NaHCO_3$ (2x), and brine (2x). The product was dried over Na_2SO_4, resulting in a colorless oil (3.90 g, 99%) that solidified upon standing.

^{1}H NMR (300 MHz, DMSO-d_6) δ [ppm] = 9.55 (s, 1H, *H-10*), 7.46 – 7.00 (m, 5H, *H-1, H-2*, *H-4 – H6*), 5.07 (s, 1H, *N-H*), 4.37 – 4.09 (m, 1H, *H-9*), 2.71 (t, *J* = 7.5 Hz, 2H, *H-7*), 2.37 – 2.01 (m, 2H, *H-8*), 1.56 – 1.28 (m, 9H, *H-14 – H-16*).

^{13}C NMR (75 MHz, DMSO-d_6) δ [ppm] = 199.7 (*C-10*), 159.8 (*C-12*), 140.2 (*C-3*), 128.8 (*C-1*, *C-5*), 128.6 (*C-2*, *C-4*), 126.5 (*C-6*), 76.7 (*C-13*), 66.0 (*C-9*), 31.6 (*C-7*), 31.1 (*C-8*), 28.4 (*C14 – C16*).

$\boldsymbol{\alpha_{22}^{D}}$ = –28° (c = 1 g/100 mL in MeOH).

Ethyl (*S*)-2-amino-3-cyclohexylpropanoate (**IV**)

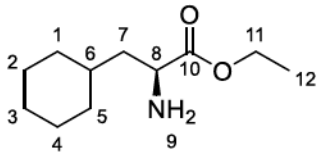

M = 199.29 g/mol

(*S*)-2-Amino-3-cyclohexylpropanoic acid (1.0 eq, 10 mmol, 1.70 g) was dissolved in EtOH. Then, $SOCl_2$ (1.1 eq, 11 mmol, 0.80 mL) was added dropwise. The mixture was stirred under reflux for 12 h and the reaction was stopped with sat. aq. $NaHCO_3$. The solvent was evaporated under reduced pressure and the residue was extracted with EA, giving the crude product as a colorless oil (1.40 g, 68%) that was used without further purification.

^{1}H NMR (300 MHz, DMSO-d_6) δ [ppm] = 4.20 – 4.01 (m, 2H- *H-7*), 4.00 – 3.83 (m, 2H, NH_2), 3.75 (tt, *J* = 9.3, 7.0 Hz, 1H, *H-8*), 1.90 (t, *J* = 7.0 Hz, 2H, *H-11*), 1.65 – 1.31 (m, 11H, *H-1* – *H-6*), 1.24 (t, *J* = 8.0 Hz, 3H, *H-12*).

^{13}C NMR (75 MHz, DMSO-d_6) δ [ppm] = 173.1 (*C-10*), 60.5 (*C-11*), 54.7 (*C-8*), 36.9 (*C-7*), 33.4 (*C-1, C-5*), 33.0 (C-6), 26.2 (*C-3*), 25.5 (*C-2, C-4*), 13.9 (*C-12*).

$\boldsymbol{\alpha_{22}^{D}}$ = –25° (c = 1 g/100 mL in MeOH).

Ethyl (*S*)-2-(4-((*tert*-butoxycarbonyl)amino)benzamido)-3-cyclohexylpropanoate (**V**)

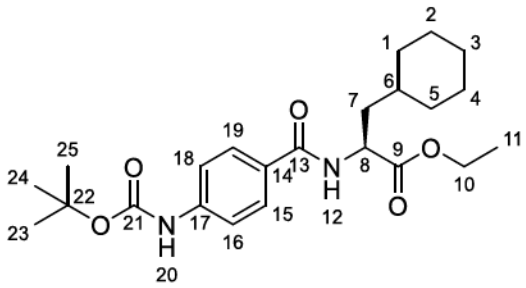

M = 418.53 g/mol

Compound **V** was synthesized according to **Procedure B** using *N*-boc-4-amino benzoic acid (1.2 eq, 7.5 mmol, 1.50 g) and **IV** (1.0 eq, 6.25 mmol, 1.25 g). The crude product, a colorless solid (3.10 g, 100%), was used without further purification.

^{1}H NMR (300 MHz, DMSO-d_6) δ [ppm] = 7.97 – 7.85 (m, 1H, *N-H*), 7.62 – 7.38 (m, 4H, *H-15, H-16, H-18, H-19*), 6.38 (d, *J* = 8.2 Hz, 1H, *N-H*), 4.61 (td, *J* = 8.5, 5.6 Hz, 1H, *H-8*), 3.99 (qd, *J* = 7.1, 1.9 Hz, 2H, *H-10*), 2.58 (s, 1H, *H-6*), 1.66 – 1.52 (m, 2H, *H-7*), 1.33 – 0.89 (m, 18H, *H-1* – *H-5*, *H-23* – *H-25*), 0.92 – 0.49 (m, 3H).

^{13}C NMR (75 MHz, DMSO-d_6) δ [ppm] = 173.5 (*C-9*), 166.7 (*C-13*), 152.6 (*C-21*), 142.0 (*C-17*), 132.3 (*C-14*), 128.3 (*C-16*), 128.1 (*C-18*), 117.8 (*C-15*, *C-19*), 81.0 (*C-22*), 61.4 (*C-10*), 50.7 (*C-8*), 34.4 (*C-7*), 33.5 (*C-1*, *C-5*), 32.8 (*C-6*), 28.4 (*C-23* – *C-25*), 26.4 (*C-3*), 26.2 (*C-2*), 26.1 (*C-1*), 14.2 (*C-11*).

α_{22}^{D} = –12° (c = 1 g/100 mL in MeOH). $\mathbf{F_p}$ = 88 ± 2 °C.

(*S*)-2-(4-((*tert*-Butoxycarbonyl)amino)benzamido)-3-cyclohexylpropanoic acid (**VI**)

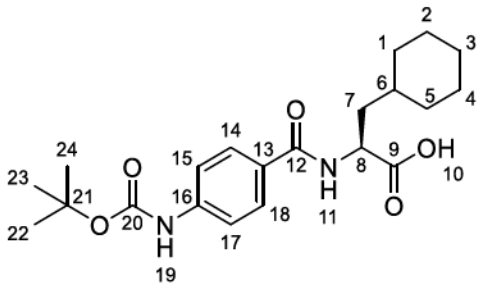

M = 390.48 g/mol

Compound **VI** was prepared according to **Procedure D** with compound **V** (1.0 eq, 7.5 mmol, 3.10 g) and LiOH monohydrate (4.0 eq, 30 mmol, 1.26 g). The final product was crystallized at pH 4, giving a colorless solid (2.70 g, 92%).

^{1}H NMR (300 MHz, DMSO-d_6) δ [ppm] = 9.47 (d, *J* = 32.7 Hz, 1H, *O-H*), 8.18 (d, *J* = 7.9 Hz, 1H, *N-H*), 7.78 – 7.49 (m, 2H, *H-14, H-18*), 7.46 – 7.19 (m, 2H, *H-15, H-17*), 4.45 – 4.11 (m, 1H, *H-8*), 3.54 – 3.07 (m, 2H, *H-7*), 2.37 – 2.08 (m, 1H, *H-6*), 1.64 – 1.29 (m, 10H, *H-1 – H-5*), 1.40 – 1.21 (m, 9 H, *H-22 – H-24*).

^{13}C NMR (75 MHz, DMSO-d_6) δ [ppm] = 174.9 (*C-9*), 167.5 (*C-12*), 153.0 (*C-20*), 144.2 (*C-16*), 130.8 (*C-13*), 124.5 (*C-15, C-17*), 117.7 (*C-14*), 117.5 (*C-18*), 80.1 (*C-21*), 50.6 (*C-8*), 34.3 (*C-7*), 33.7 (*C-1, C-5*), 31.9 (*C-6*), 28.5 (*C-22 – C-24*), 26.5 (*C-2, C-4*), 25.6 (*C-3*).

α_{22}^{D} = –11° (c = 1 g/100 mL in MeOH). $\mathbf{F_p}$ = 105 ± 2 °C.

Phosphonate synthesis

Phenyl (diethoxyphosphoryl)methanesulfonate (**VII**)

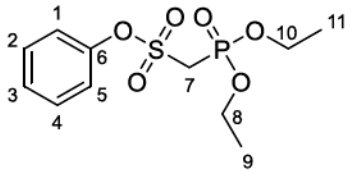

M = 308.28 g/mol

Compound **I** (1.0 eq, 35 mmol, 6.0 g) was dissolved in dry THF under argon atmosphere and cooled to –78 °C. Then, a 1.0 M solution of KHMDS (1.3 eq, 45.5 mmol, 45.5 mL) in THF was added dropwise and the mixture was stirred for 30 – 60 min followed by the addition of diethyl chlorophosphate (DECP, 1.1 eq, 38.5 mmol, 6.30 mL). The reaction mixture was stirred for an additional 2 h and then quenched with saturated aq. NH_4Cl. The solvent was removed under reduced pressure and the residue was extracted with EA and washed with water (2x), and brine (1x), dried with Na_2SO_4. The organic solvent was evaporated under reduced pressure giving the crude product that was purified by column chromatography (CH:EA 1:2 – 100% EA), resulting in a colorless oil (5.5 g, 51%).

^{1}H NMR (300 MHz, DMSO-d_6) δ [ppm] = 7.50 (ddt, J = 8.8, 6.3, 1.6 Hz, 2H, *H-1, H-5*), 7.43 – 7.33 (m, 3H, *H-2 – H-4*), 4.63 (d, J = 17.4 Hz, 2H, *H-7*), 4.25 – 4.03 (m, 4H, *H-8, H-10*), 1.26 (t, J = 7.0 Hz, 6H, *H-9, H-11*).

^{13}C NMR (75 MHz, DMSO-d_6) δ [ppm] = 148.9 (*C-3*), 130.2 (*C-2, C-4*), 127.5 (*C-1, C-5*), 122.3 (*C-6*), 63.0 (d, J = 6.1 Hz, *C-8, C-10*), 46.8 (d, J = 133.8 Hz, *C-7*), 16.1 (d, J = 6.2 Hz, *C-9, C-11*).

Phenyl (diethoxyphosphoryl)fluoromethanesulfonate (**VIII**)

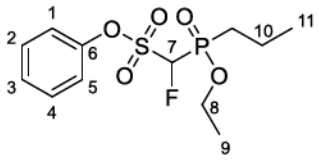

M = 326.28 g/mol

Compound **VII** (1.0 eq, 10 mmol, 3.10 g) was dissolved in dry THF under argon atmosphere and cooled to –78 °C followed by the addition of KHMDS (1.0 M in THF, 1.3 eq, 13 mmol, 13.0 mL). The mixture was stirred for 30 – 60 min and then SELECTFLUOR (1.5 eq, 15 mmol, 5.30 g) dissolved in DMF were added in portions. Afterwards, the reaction mixture was stirred for an additional 3 h at –78 °C and then allowed to warm to 0 °C, stirring for 1 h. The reaction was stopped by adding saturated aq. NH_4Cl and the solvent was removed under reduced pressure. The residue was extracted with DCM and the organic phase was washed with water (2x), saturated aq. $NaHCO_3$ (2x) and brine (1x), dried with Na_2SO_4. Next, the solvent was evaporated under reduced pressure resulting in the crude product that was purified by column chromatography (CH:EA 2:1 – 1:2), giving a colorless oil (1.41 g, 29%).

^{1}H NMR (300 MHz, $CDCl_3$) δ [ppm] = 7.40 – 7.19 (m, 2H, *H-1*, *H-5*), 7.22 – 7.02 (m, 3H, *H-2* – *H-4*), 4.63 (d, *J* = 17.4 Hz, 1H, *H-7*), 4.18 – 4.02 (m, 4H, *H-8, H-10*), 1.41 – 1.14 (m, 6H, *H-9, H-11*).

^{13}C NMR (75 MHz, $CDCl_3$) δ [ppm] = 151.2 (*C-6*), 129.6 (*C-2, C-4*), 127.8 (*C-1*), 124.8 (*C-5*), 122.0 (*C-3*), 119.9 (*C-7*), 64.5 (*C-8, C-10*), 15.9 (*C-9, C-11*).

Horner-Wadsworth-Emmons reactions

Phenyl (*S*,*E*)-3-((*tert*-butoxycarbonyl)amino)-1-fluoro-5-phenylpent-1-ene-1-sulfonate **(IX)**

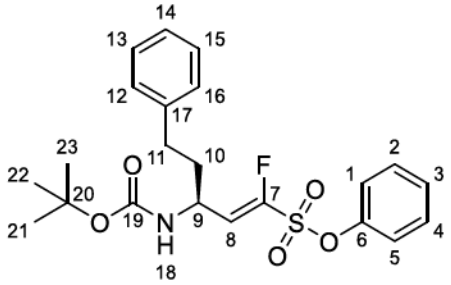

M = 435.51 g/mol

Fluorovinylsulfonate **IX** was preprared according to **Procedure A** using phosphonate **VIII** (1.0 eq, 4.0 mmol, 1.3 g) and aldehyde **III** (1.1 eq, 4.4 mmol, 1.16 g). The crude product was purified by column chromatography (CH:EA 6:1 – 4:1), giving the final product as a colorless oil (0.80 g, 46%).

^{1}H NMR (300 MHz, $CDCl_3$) δ [ppm] = 7.46 – 7.32 (m, 2H, *H-2, H-4*), 7.32 – 7.15 (m, 6H, *H-12* – *H-16*, *H-3*), 7.10 (d, J = 7.0 Hz, 2H, *H-1, H-5*), 5.91 (dd, $J_{H\text{-}F}$ = 31.3 Hz, $J_{H\text{-}H}$ = 8.6 Hz, 1H, *H-8*), 4.68 – 4.27 (m, 2H, *H-9, N-H*), 2.66 – 2.43 (m, 2H, *H-11*), 1.97 – 1.66 (m, 2H, *H-10*), 1.43 (s, 9H, *H-21* – *H-23*).

^{13}C NMR (75 MHz, $CDCl_3$) δ [ppm] = 154.8 (*C-19*), 150.8 (*C-6*), 148.9 (d, $J_{C\text{-}F}$ = 296 Hz, *C-7*), 140.2 (*C-17*), 130.2 (*C-13, C-15*), 128.8 (*C-12*), 128.4 (*C-16*), 128.0 (*C-14*), 126.5 (*C-1, C-5*), 122.4 (d, $J_{C\text{-}F}$ = 4.1 Hz, *C-8*), 122.3 (*C-3*), 80.4 (*C-20*), 46.3 (d, $J_{C\text{-}F}$ = 2.1 Hz, *C-9*), 35.9 (*C-10*), 31.9 (*C-11*), 28.4 (*C-21* – *C-23*).

α_{22}^{D} = –15° (c = 1 g/100 mL in MeOH).

Phenyl (*S*,*E*)-3-amino-1-fluoro-5-phenylpent-1-ene-1-sulfonate hydrochloride (**X**)

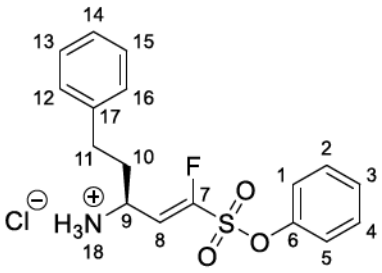

M = 371.85 g/mol

Fluorovinylsulfonate **X** was synthesized according to **Procedure E** with compound **IX** (1.0 eq, 1.7 mmol, 0.73 g). The crude product was precipitated with *n*-pentane and then lyophilized, resulting in colorless solid (0.55 g, 88%).

^{1}H NMR (300 MHz, DMSO-d_6) δ [ppm] = 8.77 (s, 3H, NH_3), 7.59 – 7.50 (m, 2H, *H-2, H-4*), 7.49 – 7.39 (m, 3H, *H-13 – H-15*), 7.36 (t, J = 7.2 Hz, 2H, *H-1, H-5*), 7.28 – 7.21 (m, 1H, *H-3*), 7.21 – 7.11 (m, 2H, *H-12, H-16*), 6.45 (dd, $J_{H\text{-}F}$ = 32.0 Hz, $J_{H\text{-}H}$ = 9.7 Hz, 1H, *H-8*), 4.15 (td, J = 9.2, 5.3 Hz, 1H, *H-9*), 2.52 – 2.36 (m, 2H, *H-11*), 2.22 – 1.85 (m, 2H, *H-10*).

^{13}C NMR (75 MHz, DMSO-d_6) δ [ppm] = 149.7 (d, $J_{C\text{-}F}$ = 300 Hz, *C-7*), 149.0 (*C-17*), 140.4 (*C-6*), 130.9 (*C-2, C-4*), 129.3 (*C-13*), 129.2 (*C-15*), 128.9 (*C-12, C-16*), 126.4 (*C-14*), 122.3 (*C-3*), 118.6 (d, $J_{C\text{-}F}$ = 3.2 Hz, *C-8*), 45.5 (d, $J_{C\text{-}F}$ = 2.2 Hz, *C-9*), 33.6 (*C-10*), 30.5 (*C-11*).

$\boldsymbol{\alpha_{22}^{D}}$ = –13° (c = 1 g/100 mL in MeOH). $\mathbf{F_p}$ = 142 ± 2 °C.

Amide couplings

Phenyl (*S*,*E*)-3-((*S*)-2-(4-((*tert*-butoxycarbonyl)amino)benzamido)-3-cyclohexyl-propanamido)-1-fluoro-5-phenylpent-1-ene-1-sulfonate (**1**)

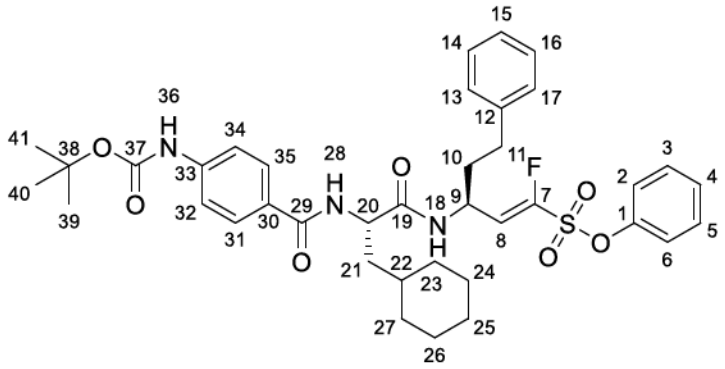

M = 707.86 g/mol

Compound **1** was prepared according to **Procedure B** using **X** (1.0 eq, 0.54 mmol, 0.20 g) and **VI** (1.2 eq, 0.65 mmol, 0.25 g). The crude product was purified via HPLC, giving a colorless solid (0.25 g, 65%).

^{1}H NMR (300 MHz, DMSO-d_6) δ [ppm] = 9.60 (d, J = 2.6 Hz, 1H, *N-H*), 8.40 – 8.10 (m, 2H, *N-H*), 7.94 – 7.70 (m, 2H, *H-32, H-34*), 7.61 – 7.34 (m, 4H, *H-31, H-35, H-3, H-5*), 7.35 – 7.05 (m, 5H, *H-13 – H-17*), 7.00 (d, J = 7.2 Hz, 2H, *H-2, H-4*), 6.15 (dd, $J_{H\text{-}F}$ = 33.2 Hz, $J_{H\text{-}H}$ = 9.0 Hz, 1H, *H-8*), 4.95 – 4.81 (m, 1H, *H-20*), 4.66 – 4.38 (m, 1H, *H-9*), 2.61 – 2.32 (m, 2H, *H-11*), 1.85 – 1.52 (m, 8H, *H-24 – H-27*), 1.48 (s, 9H, *H-39 – H-41*), 1.28 – 1.02 (m, 3H, *H-22, H-23*), 1.04 – 0.73 (m, 2H, *H-21*).

^{13}C NMR (75 MHz, DMSO-d_6) δ [ppm] = 166.3 (*C-29*), 153.1 (*C-1, C-37*), 142.9 (*C-12*), 141.2 (*C-33*), 130.9 (*C-3, C-5, C-30*), 128.9 (*C-32, C-34*), 128.8 (*C-13, C-17*), 128.6 (*C-15*), 127.8 (*C-2, C-6*), 122.4 (*C-4*), 117.5 (*C-8*), 79.9 (*C-38*), 42.0 (*C-9*), 34.3 (*C-21, C-10*), 32.4 (*C-23, C-27*), 31.5 (*C-22),* 28.5 (*C-39 – C-41*), 26.5 (*C-24, C-26*), 26.1 (*C-25*).

α_{22}^{D} = –15° (c = 1 g/100 mL in MeOH). **F_p** = 119 ± 2 °C. **Purity**: 97% (ESI-MS: [M+H$^+$] calc. 730.2, found 730.2).

4-(((*S*)-3-Cyclohexyl-1-(((*S*,*E*)-1-fluoro-1-(phenoxysulfonyl)-5-phenylpent-1-en-3-yl)amino)-1-oxopropan-2-yl)carbamoyl)benzenaminium chloride (**2**)

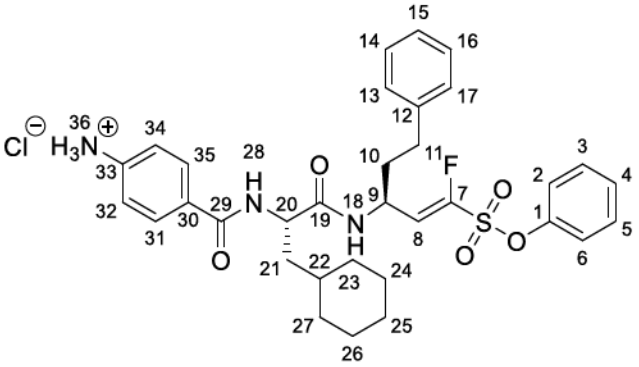

M = 644.20 g/mol

Compound **2** was synthesized according to **Procedure E** using **1** (1.0 eq, 0.35 mmol, 0.25 g). The crude product was purified using via HPLC and lyophilization, resulting in a colorless solid (0.17 g, 74%).

^{1}H NMR (300 MHz, DMSO-d_6) δ [ppm] = 8.56 – 8.19 (m, 3H, *N-H*), 8.06 – 7.72 (m, 2H, *H-32, H-34*), 7.61 – 7.07 (m, 10H, *H-3 – H-5, H-13 – H-17, H-31, H-35*), 7.07 – 6.90 (m, 2H, *H-2, H-6*), 6.45 (dd, J = 21.8, 10.0 Hz, 1H, *N-H*), 6.14 (dd, $J_{H\text{-}F}$ = 33.3 Hz, $J_{H\text{-}H}$ =9.1 Hz, 1H, *H-8*), 5.06 – 4.72 (m, 1H, *H-20*), 4.66 – 4.35 (m, 1H, *H-9*), 2.63 – 2.34 (m, 2H, *H-11*), 2.34 – 2.09 (m, 2H, *H-12*), 1.98 – 1.43 (m, 8H, *H-24 – H-27*), 1.45 – 0.99 (m, 3H, *H-22, H-23*), 1.04 – 0.73 (m, 2H, *H-21*).

^{13}C NMR (75 MHz, DMSO-d_6) δ [ppm] = 172.7 (*C-19*), 166.0 (*C-29*), 149.2 (*C-1*), 141.2 (*C-7, C-12*), 130.9 (*C-30*), 129.6 (*C-3, C-5*), 128.8 (*C-14, C-16*), 128.7 (*C-31, C-35*), 126.4 (*C-15*), 122.4 (*C-2, C-6*), 120.1 (*C-4, C-32, C-34, C-8*), 66.8 (*C-20*), 42.1 (*C-9*), 34.3 (*C-21, C-10*), 33.6 (*C-23, C-27*), 32.4 (*C-11*), 31.5 (*C-22*), 26.5 (*C-24*), 26.2 (*C-25*), 26.1 (*C-26*).

$\boldsymbol{\alpha}_{22}^{D}$ = –9° (c = 1 g/100 mL in MeOH). **F_p** = 131 ± 2 °C. **Purity**: 95% (ESI-MS: [M+H$^+$] calc. 607.3, found 607.2).

Phenyl (*S*,*E*)-3-((*S*)-3-cyclohexyl-2-(4-(5-oxohexanamido)benzamido)propanamido)-1-fluoro-5-phenylpent-1-ene-1-sulfonate (**3**)

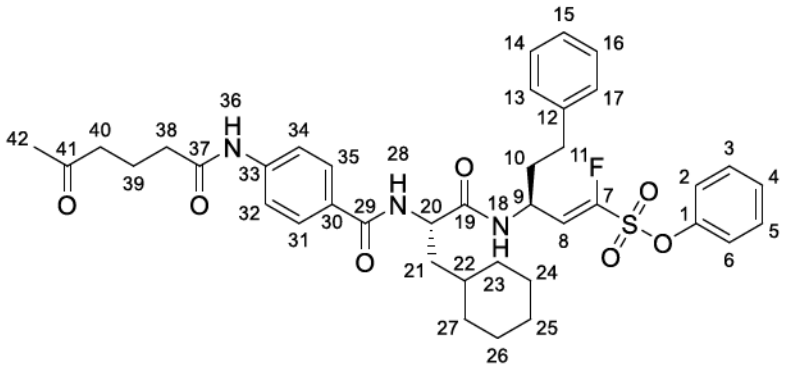

M = 719.87 g/mol

Compound **3** was prepared according to **Procedure C** using **2** (1.0 eq, 0.67 mmol, 0.40 g) and 4-acetylbutyric acid (1.2 eq, 0.80 mmol, 0.11 g). The crude product was purified by HPLC, resulting in a colorless solid (0.16 g, 34%).

^{1}H NMR (300 MHz, DMSO-d_6) δ [ppm] = 10.10 (s, 1H, *N-H*), 8.57 – 8.05 (m, 2H, *N-H*), 7.88 (ddd, *J* = 9.3, 6.1, 3.1 Hz, 2H, *H-32, H-34*), 7.67 (dt, *J* = 8.9, 2.3 Hz, 2H, *H-31, H-35*), 7.57 – 7.34 (m, 2H, *H-13, H-17*), 7.36 – 7.22 (m, 3H, *H-14 – H-16*), 7.21 – 7.10 (m, 2H, *H-3, H-5*), 7.01 (d, *J* = 7.4 Hz, 2H, *H-2, H-6*), 6.84 (m, 1H, *H-4*), 6.16 (ddd, $J_{H\text{-}F}$ = 33.3 Hz, $J_{H\text{-}H}$ = 9.1 Hz, 5.7 Hz, 1H, *H-8*), 4.69 – 4.54 (m, 1H, *H-20*), 4.54 – 4.40 (m, 1H, *H-9*), 2.52 (m, 2H, *H-11*), 2.34 (t, *J* = 7.4 Hz, 4H, *H-38, H-40*), 2.09 (s, 3H, *H-42*), 1.99 – 1.45 (m, 7H, *H-10, H-21, H-39, H-22*), 1.47 – 0.79 (m, 10H, *H-23 – H-27*).

^{13}C NMR (75 MHz, DMSO-d_6) δ [ppm] = 208.6 (*C-41*), 171.7 (*C-19, C-37*), 149.2 (*C-1, C-29*), 141.2 (*C-8, C-12, C-33*), 130.9 (*C-3, C-5, C-30*), 128.8 (*C-13, C-17*), 128.7 (*C-15*), 122.4 (*C-2, C-6, C-32, C-34*), 118.6 (*C-8, C-31, C-35*), 42.4 (*C-40*), 39.2 (*C-38*), 35.9 (*C-23, C-27*), 34.3 (*C-22*), 32.4 (*C-42*), 31.5 (*C-11*), 30.2 (*C-25*), 26.5 (*C-24*), 26.2 (*C-26*), 19.5 (*C-39*).

α_{22}^{D} = –14° (c = 1 g/100 mL in MeOH). **F_p** = 155 ± 2 °C. **Purity**: 99% (ESI-MS: [M+H$^+$] calc. 720.3, found 720.2).

Phenyl (*S*,*E*)-3-((*S*)-3-cyclohexyl-2-(4-(6-(2,5-dioxo-2,5-dihydro-1*H*-pyrrol-1-yl)-hexanamido)benzamido)propanamido)-1-fluoro-5-phenylpent-1-ene-1-sulfonate (**4**)

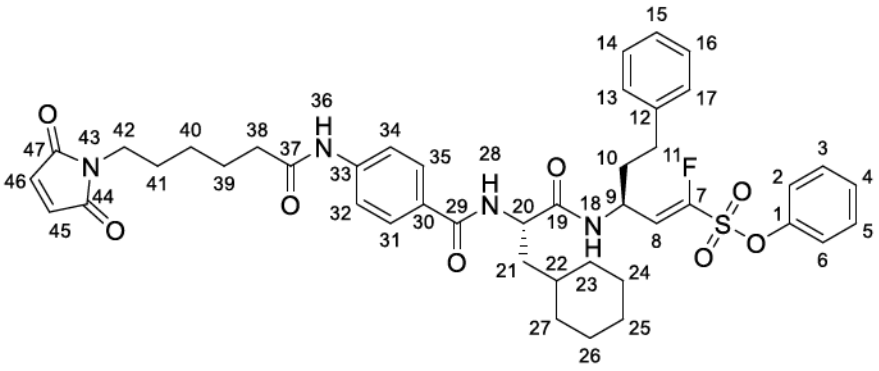

M = 800.94 g/mol

Compound **4** was prepared according to **Procedure C** using **2** (1.0 eq, 0.26 mmol, 0.17 g) and 6-maleimidohexanoic acid (1.2 eq, 0.31 mmol, 0.065 g). The crude product was purified by HPLC, giving a colorless solid (0.045 g, 23%).

^{1}H NMR (300 MHz, DMSO-d_6) δ [ppm] = 10.06 (s, 1H, *N-H*), 8.57 – 7.99 (m, 2H, *N-H*), 7.86 (ddt, *J* = 9.3, 6.9, 1.9 Hz, 2H, *H-45, H-46*), 7.65 (dt, *J* = 8.4, 1.9 Hz, 2H, *H-32, H-34*), 7.56 – 7.35 (m, 2H, *H-31, H-35*), 7.34 – 7.20 (m, 5H, *H-13* – *H-17*), 7.15 (tt, *J* = 8.1, 2.0 Hz, 2H, *H-3, H-5*), 6.98 (d, *J* = 1.7 Hz, 3H, *H-2, H-4, H-6*), 6.15 (dtd, $J_{H\text{-}F}$ = 33.2 Hz, $J_{H\text{-}H}$ = 9.1 Hz, 1H, *H-8*), 4.89 (s, 1H, H-20), 4.71 – 4.29 (m, 3H, *H-9*, *H-42*), 2.53 (m, 2H, H-*11*), 2.31 (t, *J* = 7.4 Hz, 2H, *H-38*), 1.95 – 1.68 (m, 4H, *H-10, H-21*), 1.43 – 0.50 (m, 17H, *H-22* – *H-27, H-39* – *H-41*).

^{13}C NMR (75 MHz, DMSO-d_6) δ [ppm] = 171.9 (*C-37*), 171.5 (*C-44, C-47*), 166.3 (*C-29*), 149.1 (*C-1*), 141.2 (*C-7, C-12, C-33*), 134.9 (*C-45, C-46*), 130.9 (*C-3, C-5*), 128.9 (*C-30*), 128.8 (*C-13*), 128.7 (*C-17*), 126.4 (C-*15, C-4*), 122.4 (*C-2, C-6, C-31, C-35*), 118.5 (*C-8*), 40.8 (*C-20*), 39.7 (*C-9*), 37.4 (*C-21*), 36.7 (*C-38*), 34.3 (*C-10*), 33.6 (*C-23, C-27*), 32.4 (*C-11*), 31.5 (*C-41*), 28.2 (*C-40*), 26.5 (*C-25*), 26.3 (*C-24*), 26.1 (*C-26*), 24.9 (*C-39*).

$\boldsymbol{\alpha}_{22}^{D}$ = –11° (c = 1 g/100 mL in MeOH). **F_p** = 150 ± 2 °C. **Purity**: 98% (ESI-MS: [M+H$^+$] calc. 801.3, found 801.2).

Phenyl (*S*,*E*)-3-((*S*)-3-cyclohexyl-2-(4-((*E*)-5-(2-(3-(2,5-dioxo-2,5-dihydro-1*H*-pyrrol-1-yl)propanoyl)hydrazono)hexanamido)benzamido)propanamido)-1-fluoro-5-phenylpent-1-ene-1-sulfonate (**5**)

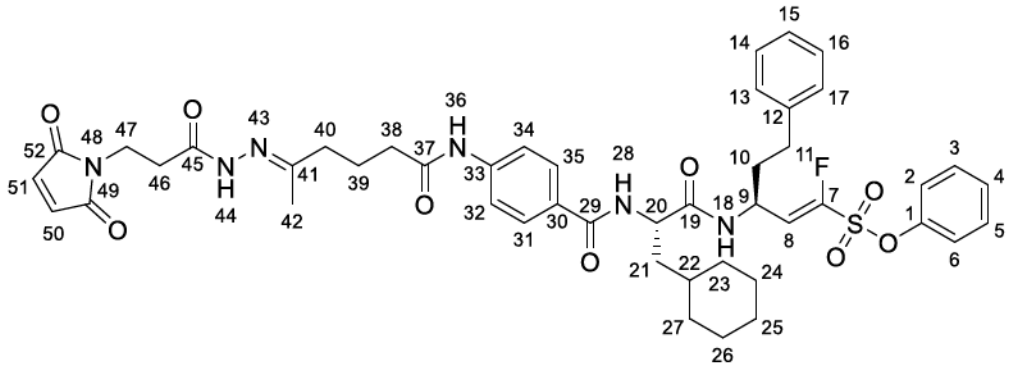

M = 885.02 g/mol

Compound **3** (1.0 eq, 0.083 mmol, 0.060 g) was dissolved in MeOH at room temperature, then adding 0.1% TFA. 3-(2,5-dioxo-2,5-dihydro-1*H*-pyrrol-1-yl)propanehydrazide (1.1 eq, 0.092 mmol, 0.020 g) was dissolved in MeOH and added dropwise. After 12 h, MeOH was removed under reduced pressure and the residue was purified via HPLC, resulting in a colorless solid (0.028 g, 38%).

^{1}H-NMR (300 MHz, DMSO-d_6) δ [ppm] = 10.10 (s, 2H, *N-H*), 8.42 – 8.10 (m, 2H, *N-H*), 7.95 – 7.80 (m, 2H, *H-50, H-51*), 7.67 (dt, J = 9.0, 2.4 Hz, 4H, *H-31, H-32, H-34, H-35*), 7.56 – 7.35 (m, 3H, *H-3, H-5, H-15*), 7.35 – 7.09 (m, 6H, *H-2, H-6, H-13, H-14, H-16, H-17*), 7.01 (d, J = 7.4 Hz, 1H, *H-4*), 6.16 (ddd, $J_{H\text{-}F}$ = 33.2 Hz, $J_{H\text{-}H}$ = 9.0 Hz, 5.7 Hz, 1H, *H-8*), 4.90 (m, 2H, *H-47*), 4.55 (dt, J = 24.9, 10.2 Hz, 2H, *H-9, H-20*), 2.51 – 2.39 (m, 4H, *H-11, H-46*), 2.34 (t, J = 7.4 Hz, 2H, *H-38*), 2.09 (s, 3H, *H-42*), 1.96 – 1.46 (m, 7H, *H-10, H-21, H-22, H-39*), 1.46 – 0.69 (m, 10H, *H-23 – H-27*).

^{13}C NMR (75 MHz, DMSO-d_6) δ [ppm] = 172.8 (*C-37*), 172.7 (*C-19*), 171.7 (*C-49, C-52*), 166.3 (*C-45*), 166.2 (*C-29*), 149.2 (*C-41*), 148.9 (*C-1*), 142.5 (*C-12*), 141.2 (*C-33*), 130.9 (*C-8*), 130.8 (*C-50, C-51*), 128.9 (*C-4, C-6*), 128.8 (*C-31, C-35*), 128.7 (*C-13, C-17*), 128.5 (*C-4, C-14, C-16*), 126.4 (*C-15*), 122.4 (*C-2, C-6, C-30*), 118.6 (*C-32, C-34, C-7*), 51.7 (*C-9*), 42.4 (*C-20*), 39.5 (*C-10*), 39.2 (*C-21*), 35.9 (*C-38*), 34.3 (*C-40, C-46*), 33.6 (*C-11, C-25*), 32.4 (*C-24, C-26*), 31.5 (*C-23, C-27*), 30.2 (*C-22*), 26.5 (*C-47*), 26.3 (*C-39*), 19.5 (*C-42*).

α_{22}^{D} = –12° (c = 1 g/100 mL in MeOH). **F_p** = 160 ± 2 °C. **Purity**: 99% (ESI-MS: [M+H$^+$] calc. 885.4, found 885.3).

4.4.3 *Fluorometric enzyme assays*

Cathepsin S

The assay was modified after BRÖMME ET AL.[297] Cathepsin S (CatS, recombinant from *E. coli*, SIGMA-ALDRICH, Darmstadt, Germany) was incubated in enzyme buffer (35 mM potassium phosphate, 35 mM sodium acetate, 2 mM DTT, 2 mM EDTA, pH 6.5) at room temperature for 20 – 30 min. Assay buffer (50 mM KH_2PO_4, 50 mM K_2HPO_4, 2.5 mM DTT, 2.5 mM EDTA, pH 6.5) was mixed with 1 – 5 nM CatS in enzyme buffer, followed by inhibitor in DMSO or DMSO (negative control), and 10 μM substrate *Z*-Val-Val-Arg-AMC (BACHEM, Basel, Switzerland). The fluorescence increase upon cleavage of *Z*-Val-Val-Arg-AMC was monitored by a TECAN SPARK fluorimeter (δ excitation: 365 nm, δ emission: 460 nm; TECAN GROUP, Männedorf, Switzerland). Black, flat-bottom 96-well chimney microtiter plates (GREINER BIO-ONE, Frickenhausen, Germany) were used. Inhibitor screening concentrations started at 20 μM, followed by 1 μM, 200 nM, and 50 nM. Inhibition constants were determined for compounds with >50% inhibition at 20 μM.

IC_{50} and K_i calculations.

GRAFIT (version 5.0.13, 2006, ERITHRACUS Software Ltd., UK) was used for data analysis and non-linear regression.

The K_i values were calculated as published previously for slow, tight binders.[236]

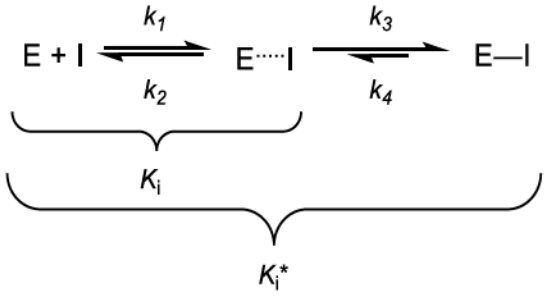

E = enzyme; I = inhibitor, *k* = reaction constant;
E I = non-covalent enzyme-inhibitor complex; E—I = covalent enzyme-inhibitor complex.

The initial (v_i) and steady-state (v_s) velocities in inhibitor presence and the pseudo-first order rate constants k_{obs} were determined for different inhibitor concentrations. The biphasic progress curves were fitted to the slow-binding equation (*off* = offset):[236]

$$\textbf{(I)} \qquad [\mathbf{P}] = \mathbf{v_s} \cdot \mathbf{t} + \frac{\mathbf{v_i} - \mathbf{v_s}}{\boldsymbol{k_{obs}}} \cdot [\mathbf{1} - \mathbf{exp}(-\boldsymbol{k_{obs}} \cdot \mathbf{t})] + \mathbf{off}$$

Then, the k_{obs} values were plotted against the inhibitor concentrations [I] using the following equation:

$$\textbf{(II)} \qquad k_{obs} = k_4 + \left(\frac{k_3 \cdot [I]}{K_i^{app} + [I]}\right)$$

The resulting dissociation constant of the initial enzyme-inhibitor complex K_i^{app} was then corrected to zero substrate concentration using the CHENG-PRUSOFF relationship (**III**), giving the K_i value:[238]

$$\textbf{(III)} \qquad K_i = \frac{IC_{50} \text{ or } K_i^{app}}{1 + \frac{[S]}{K_M}}$$

Further constants such as k_3, k_4, and K_i^* could be determined from the slow binding equation (**I**) and the k_{obs} vs [I] plot (**II**) using the following equation (**IV**):[236]

$$\textbf{(IV)} \qquad K_i^* = \frac{K_i}{\left(1 + \frac{k_3}{k_4}\right)}$$

Selectivity towards other human cathepsins

Human cathepsin B (CatB, SIGMA-ALDRICH, Darmstadt, Germany) and human cathepsin L (CatL, SIGMA-ALDRICH, Darmstadt, Germany) were incubated in enzyme buffer (50 mM Tris-HCl, 5 mM EDTA, 200 mM NaCl, 2 mM DTT, pH 6.5) at room temperature for 20 – 30 min. Assay buffer (50 mM Tris-HCl, 5 mM EDTA, 200 mM NaCl, 0.005% Brij35, pH 6.5) was mixed with CatB or CatL in enzyme buffer, then inhibitor in DMSO or DMSO (negative control) was added, followed by 100 μM (CatB) or 6.25 μM (CatL) substrate *Z*-Phe-Arg-AMC (BACHEM, Basel, Switzerland). The enzyme activity was monitored by a TECAN SPARK (TECAN GROUP, Männedorf, Switzerland) fluorescence reader using black GREINER flat-bottom 96-well chimney microtiter plates (GREINER BIO-ONE GmbH, Frickenhausen, Germany). Inhibitor screening concentrations started at 20 μM, followed by 1 μM, 200 nM, and 50 nM. Inhibition constants were determined for inhibitors with >50% inhibition at 20 μM.

Overall Conclusion and Perspectives

When it comes to developing effective drugs, there are few things more important than understanding how to modify their structures to achieve desired outcomes. The projects presented in this dissertation demonstrate a deep understanding of this principle, with a focus on covalent cysteine protease inhibitors. In my research, I have uncovered new ways to not only enhance the affinity of these inhibitors for their target proteases, but also to increase their selectivity and improve their pharmacokinetic properties.

One of the most exciting aspects is the potential to develop highly targeted and personalized treatments for a wide range of diseases, e.g., parasitic, or cancerous. By understanding how to fine-tune the structure of covalent cysteine protease inhibitors for certain targets and/or applications, we can create potential drugs that are tailored to specific patient populations, with fewer off-target effects and a higher chance of success. At the same time, the projects presented in this dissertation also offer valuable insights into some fundamental principles of drug design and development, particularly regarding ADME evaluation (**Figure 26**).

Leverage from computer-aided methods resulted in improved inhibitor properties ranging from potency over selectivity profiles to enhanced phenotypic efficacy. In particular, molecular docking approaches were helpful to design new potent and selective compounds (e.g., project **2** and **3**). Combining docking studies with optimized fluorometric enzyme assays was crucial for SAR studies and selectivity profiles (e.g., project **2** and **3**). *In silico* prediction of physicochemical parameters followed by a correlation analysis supported the identification of important structural modifications for improved efficacy in phenotypic assays (project **2**). Most recently, artificial intelligence (AI)-based tools, such as the language model CHATGPT, have gained immense popularity.[298] As AI systems are currently emerging in many fields (e.g., ALPHAFOLD2 to predict protein folds), computational tools for drug development and property prediction have the potential to be of even greater use in the field of medicinal chemistry in the next years.[299–301]

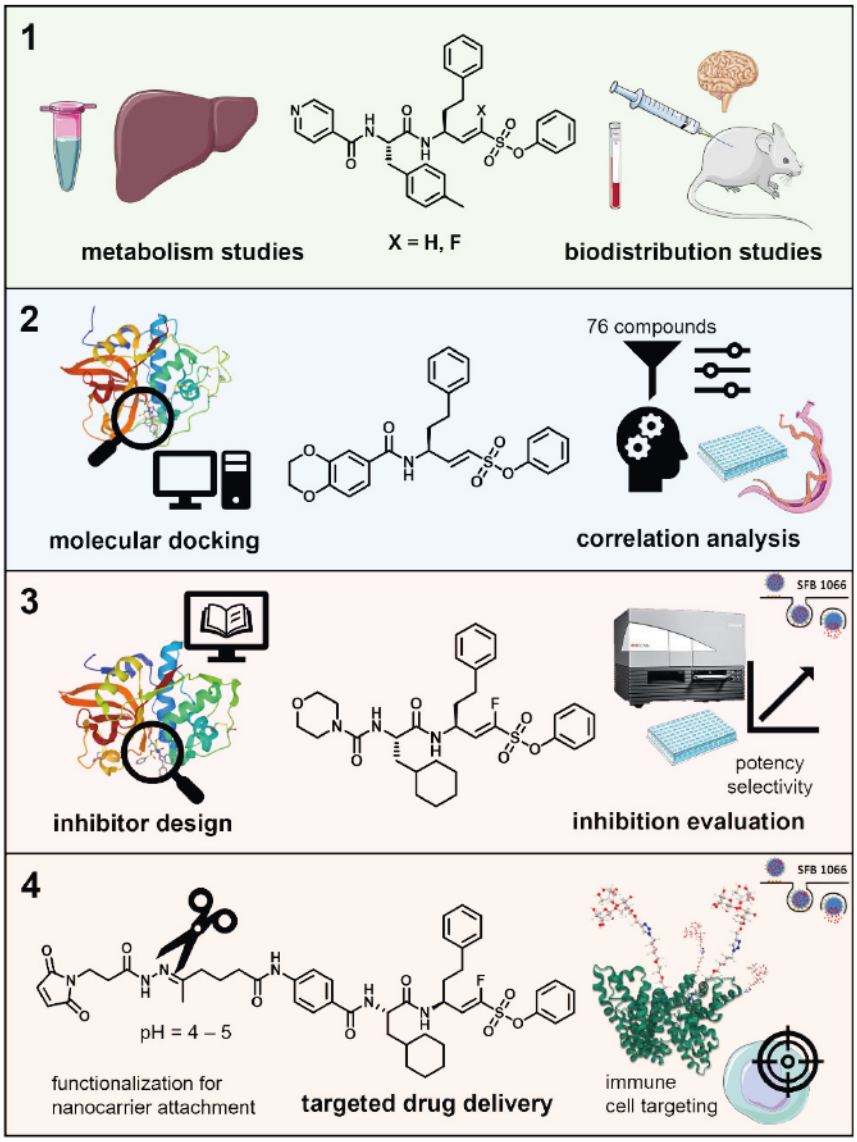

Figure 26. Schematic overview of projects **1–4** with their lead compounds and the used drug design principles. The figure was partly generated using SERVIER MEDICAL ART, provided by SERVIER, licensed under a Creative Commons Attribution 3.0 unported license.

Additionally, the combination of *in vitro* and *in vivo* studies has offered useful insights into our compounds' metabolism and biodistribution, essential parameters for the delivery to disease relevant tissues (project **1**). Further investigations into metabolism could be obtained by deepening experiments including the use of isolated CYP enzymes to gain more knowledge about the involved metabolizing enzymes. The sample preparation protocol for tissue extraction that I have established in our group can be adapted to future projects involving tissue samples.

Another principle that has been integral to my dissertation is the use of nanocarriers for targeted delivery which includes modifying our inhibitors (project **4**). The functionalized inhibitors that we have developed for nanocarrier attachment are a strong foundation for further investigations, not only coupling to nanocarriers but also

radioactive labeling or immobilization for various biophysical applications (e.g., surface plasmon resonance assays, switchSENSE). Future projects would particularly benefit from labeling compounds with a radioactive or fluorescent probe to investigate cell or tissue distribution to monitor targeting.

Overall, the presented work contributes to the field of drug development of cysteine protease inhibitors. While focusing on structural modifications of covalent cysteine protease inhibitors, I have provided valuable insights into how to create more effective and targeted potential drugs with regards to pharmacokinetic properties and selectivity profiles.

List of Figures

List of Schemes

List of Tables

References

(1) Lipinski, C. A.; Lombardo, F.; Dominy, B. W.; Feeney, P. J. Experimental and Computational Approaches to Estimate Solubility and Permeability in Drug Discovery and Development Settings. *Adv. Drug Deliv. Rev.* **2001**, *46* (1–3), 3–26. https://doi.org/10.1016/S0169-409X(00)00129-0.

(2) Lipinski, C. A. Lead- and Drug-like Compounds: The Rule-of-Five Revolution. *Drug Discov. Today. Technol.* **2004**, *1* (4), 337–341. https://doi.org/10.1016/J.DDTEC.2004.11.007.

(3) Waring, M. J. Defining Optimum Lipophilicity and Molecular Weight Ranges for Drug Candidates—Molecular Weight Dependent Lower Log D Limits Based on Permeability. *Bioorg. Med. Chem. Lett.* **2009**, *19* (10), 2844–2851. https://doi.org/10.1016/J.BMCL.2009.03.109.

(4) Raevsky, O. A. Physicochemical Descriptors in Property-Based Drug Design. *Mini-Reviews Med. Chem.* **2012**, *4* (10), 1041–1052. https://doi.org/10.2174/1389557043402964.

(5) Jacek, K.; Hanna, P.; Anna, M.; Beata, D.; K., B. M. The Log P Parameter as a Molecular Descriptor in the Computer-Aided Drug Design – an Overview. *CMST* **2012**, *18* (2), 81–88. https://doi.org/10.12921/CMST.2012.18.02.81-88.

(6) Veber, D. F.; Johnson, S. R.; Cheng, H. Y.; Smith, B. R.; Ward, K. W.; Kopple, K. D. Molecular Properties That Influence the Oral Bioavailability of Drug Candidates. *J. Med. Chem.* **2002**, *45* (12), 2615–2623. https://doi.org/10.1021/JM020017N/SUPPL_FILE/JM020017N_S.PDF.

(7) Kuhn, B.; Mohr, P.; Stahl, M. Intramolecular Hydrogen Bonding in Medicinal Chemistry. *J. Med. Chem.* **2010**, *53* (6), 2601–2611. https://doi.org/10.1021/JM100087S/SUPPL_FILE/JM100087S_SI_001.PDF.

(8) Kubinyi, H. Hydrogen Bonding: The Last Mystery in Drug Design? *Pharmacokinet. Optim. Drug Res.* **2007**, 513–524. https://doi.org/10.1002/9783906390437.CH28.

(9) Doak, B. C.; Kihlberg, J. Drug Discovery beyond the Rule of 5 - Opportunities and Challenges. *Expert Opin. Drug Discov.* **2016**, *12* (2), 115–119. https://doi.org/10.1080/17460441.2017.1264385.

(10) Lu, J. J.; Crimin, K.; Goodwin, J. T.; Crivori, P.; Orrenius, C.; Xing, L.; Tandler, P. J.; Vidmar, T. J.; Amore, B. M.; Wilson, A. G. E.; Stouten, P. F. W.; Burton, P. S. Influence of Molecular Flexibility and Polar Surface Area Metrics on Oral Bioavailability in the Rat. *J. Med. Chem.* **2004**, *47* (24), 6104–6107. https://doi.org/10.1021/JM0306529/SUPPL_FILE/JM0306529_S.PDF.

(11) Agarwal, N.; Bajpai, A.; Gupta, S. P. A Quantitative Structure-Activity Relationship and Molecular Modeling Study on a Series of Heteroaryl- and Heterocyclyl-Substituted Imidazo[1,2-a]Pyridine Derivatives Acting as Acid Pump Antagonists. *Biochem. Res. Int.* **2013**, *2013*. https://doi.org/10.1155/2013/141469.

(12) Kim, S.; Chen, J.; Cheng, T. PubChem 2023 Update. *Nucleic Acids Res.* **2023**, *51* (D1), D1373–D1380.

(13) Rowland, M.; Tozer, T. N.; Derendorf, H.; Hochhaus, G. Clinical Pharmacokinetics and Pharmacodynamics. **2011**.

(14) Wagner, J. G. History of Pharmacokinetics. *Pharmacol. Ther.* **1981**, *12* (3), 537–562. https://doi.org/10.1016/0163-7258(81)90097-8.

(15) Gibaldi, M.; Levy, G. Pharmacokinetics in Clinical Practice: I. Concepts. *J. Am. Med. Assoc.* **1976**, *235* (17), 1864–1867. https://doi.org/10.1001/jama.1976.03260430034020.

(16) Notari, R. E. Pharmacokinetics Molecular Modification: Implications in Drug Design Evaluation. *J. Pharm. Sci.* **1973**, *62* (6), 865–881. https://doi.org/10.1002/JPS.2600620602.

(17) Seydel, J. K.; Schaper, K. J. Quantitative Structure-Pharmacokinetic Relationships and Drug Design.

Pharmacol. Ther. **1981**, *15* (2), 131–182. https://doi.org/10.1016/0163-7258(81)90040-1.

(18) Hop, C. E. C. A. Role of ADME Studies in Selecting Drug Candidates: Dependence of ADME Parameters on Physicochemical Properties. *Encycl. Drug Metab. Interact.* **2012**, 1–43. https://doi.org/10.1002/9780470921920.EDM049.

(19) Sietsema, W. K. The Absolute Oral Bioavailability of Selected Drugs. *Int. J. Clin. Pharmacol. Ther. Toxicol.* **1989**, *27* (4), 179–211.

(20) Thomas, V. H.; Bhattachar, S.; Hitchingham, L.; Zocharski, P.; Naath, M.; Surendran, N.; Stoner, C. L.; El-Kattan, A. The Road Map to Oral Bioavailability: An Industrial Perspective. *Expert Opin. Drug Metab. Toxicol.* **2006**, *2* (4), 591–608. https://doi.org/10.1517/17425255.2.4.591.

(21) Matsson, P.; Doak, B. C.; Over, B.; Kihlberg, J. Cell Permeability beyond the Rule of 5. *Adv. Drug Deliv. Rev.* **2016**, *101*, 42–61. https://doi.org/10.1016/J.ADDR.2016.03.013.

(22) Matsson, P.; Kihlberg, J. How Big Is Too Big for Cell Permeability? *J. Med. Chem.* **2017**, *60* (5), 1662–1664. https://doi.org/10.1021/ACS.JMEDCHEM.7B00237/ASSET/IMAGES/LARGE/JM-2017-00237V_0002.JPEG.

(23) A bers, R. W. Biochemical Aspects of Active Transport. *Annu Rev. Biochem.* **1967**, *37*, 727–756.

(24) Van Asperen, J.; Mayer, U.; Van Tellingen, O.; Beijnen, J. H. The Functional Role of P-Glycoprotein in the Blood-Brain Barrier. *J. Pharm. Sci.* **2009**, *86* (8), 881–884. https://doi.org/10.1021/JS9701364.

(25) Tatsuta, T.; Naito, M.; Oh-hara, T.; Sugawara, I.; Tsuruo, T. Functional Involvement of P-Glycoprotein in Blood-Brain Barrier. *J. Biol. Chem.* **1992**, *267* (28), 20383–20391. https://doi.org/10.1016/S0021-9258(19)88713-6.

(26) Sadeque, A. J. M.; Wandel, C.; He, H.; Shah, S.; Wood, A. J. J. Increased Drug Delivery to the Brain by P-Glycoprotein Inhibition. *Clin. Pharmacol. Ther.* **2000**, *68* (3), 231–237. https://doi.org/10.1067/MCP.2000.109156.

(27) Schinkel, A. H. P-Glycoprotein, a Gatekeeper in the Blood–Brain Barrier. *Adv. Drug Deliv. Rev.* **1999**, *36* (2–3), 179–194. https://doi.org/10.1016/S0169-409X(98)00085-4.

(28) Bohnert, T.; Gan, L. S. Plasma Protein Binding: From Discovery to Development. *J. Pharm. Sci.* **2013**, *102* (9), 2953–2994. https://doi.org/10.1002/JPS.23614.

(29) Trainor, G. L. The Importance of Plasma Protein Binding in Drug Discovery. *Expert Opin. Drug Discov.* **2007**, *2* (1), 51–64. https://doi.org/10.1517/17460441.2.1.51.

(30) Howard, M. L.; Hill, J. J.; Galluppi, G. R.; McLean, M. A. Plasma Protein Binding in Drug Discovery and Development. *Comb. Chem. High Throughput Screen.* **2010**, *13* (2), 170–187. https://doi.org/10.2174/138620710790596745.

(31) Perucca, E. Plasma Protein Binding of Phenytoin in Health and Disease: Relevance to Therapeutic Drug Monitoring. *Ther. Drug Monit.* **1980**, *2* (4), 331–344. https://doi.org/10.1097/00007691-198010000-00005.

(32) Di, L. An Update on the Importance of Plasma Protein Binding in Drug Discovery and Development. *Expert Opin. Drug Discov.* **2021**, *16* (12), 1453–1465. https://doi.org/10.1080/17460441.2021.1961741.

(33) Gibaldi, M.; Levy, G.; McNamara, P. J. Effect of Plasma Protein and Tissue Binding on the Biologic Half-Life of Drugs. *Clin. Pharmacol. Ther.* **1978**, *24* (1), 1–4. https://doi.org/10.1002/CPT19782411.

(34) Kontermann, R. E. Strategies for Extended Serum Half-Life of Protein Therapeutics. *Curr. Opin. Biotechnol.* **2011**, *22* (6), 868–876. https://doi.org/10.1016/J.COPBIO.2011.06.012.

(35) Toutain, P. L.; Bousquet-Mélou, A. Volumes of Distribution. *J. Vet. Pharmacol. Ther.* **2004**, *27* (6), 441–453. https://doi.org/10.1111/J.1365-2885.2004.00602.X.

(36) Jostrand, T. S. Volume and Distribution of Blood and Their Significance in Regulating the Circulation.

(37) Smith, D. A.; Beaumont, K.; Maurer, T. S.; Di, L. Volume of Distribution in Drug Design. *J. Med. Chem.* **2015**, *58* (15), 5691–5698. https://doi.org/10.1021/ACS.JMEDCHEM.5B00201/ASSET/IMAGES/MEDIUM/JM-2015-002019_0004.GIF.

(38) Rodgers, T.; Rowland, M. Mechanistic Approaches to Volume of Distr bution Predictions: Understanding the Processes. *Pharm. Res.* **2007**, *24* (5), 918–933. https://doi.org/10.1007/S11095-006-9210-3/FIGURES/9.

(39) Lewis, D. F. V.; Jacobs, M. N.; Dickins, M. Compound Lipophilicity for Substrate Binding to Human P450s in Drug Metabolism. *Drug Discov. Today* **2004**, *9* (12), 530–537. https://doi.org/10.1016/S1359-6446(04)03115-0.

(40) Lewis, D. F. V. Structural Characteristics of Human P450s Involved in Drug Metabolism: QSARs and Lipophilicity Profiles. *Toxicology* **2000**, *144* (1–3), 197–203. https://doi.org/10.1016/S0300-483X(99)00207-3.

(41) Kwan, K. C. Oral Bioavailability and First-Pass Effects. *Drug Metab. Dispos.* **1997**, *25* (12).

(42) G baldi, M.; Boyes, R. N.; Feldman, S. Influence of First-Pass Effect on Availability of Drugs on Oral Administration. *J. Pharm. Sci.* **1971**, *60* (9), 1338–1340. https://doi.org/10.1002/JPS.2600600909.

(43) Doherty, M. M.; Pang, & K. S.; Doherty', M. M.; Pang',', K. S. First-Pass Effect: Significance of the Intestine for Absorption and Metabolism. *Drug Chem. Toxicol.* **2008**, *20* (4), 329–344. https://doi.org/10.3109/01480549709003891.

(44) Taft, D. R. Drug Excretion. *Pharmacol. Princ. Pract.* **2009**, 175–199. https://doi.org/10.1016/B978-0-12-369521-5.00009-9.

(45) Ito, S.; Lee, A. Drug Excretion into Breast Mi k—Overview. *Adv. Drug Deliv. Rev.* **2003**, *55* (5), 617–627. https://doi.org/10.1016/S0169-409X(03)00034-6.

(46) Gründemann, D.; Gorboulev, V.; Gambaryan, S.; Veyhl, M.; Koepsell, H. Drug Excretion Mediated by a New Prototype of Polyspecific Transporter. *Nature* **1994**, *372* (6506), 549–552. https://doi.org/10.1038/372549a0.

(47) van Montfoort, J. E.; Hagenbuch, B.; Groothuis, G. M. M.; Koepsell, H.; Meier, P. J.; Me jer, D. K. F. Drug Uptake Systems in Liver and Kidney. *Curr. Drug Metab.* **2005**, *4* (3), 185–211. https://doi.org/10.2174/1389200033489460.

(48) Dowling, R. H. The Enterohepatic Circulation. *Gastroenterology* **1972**, *62* (1), 122–140. https://doi.org/10.1016/S0016-5085(72)80018-0.

(49) Roberts, M. S.; Magnusson, B. M.; Burczynski, F. J.; Weiss, M. Enterohepatic Circulation. *Clin. Pharmacokinet. 2002 4110* **2012**, *41* (10), 751–790. https://doi.org/10.2165/00003088-200241100-00005.

(50) Caldwell, J. H.; Bush, C. A.; Greenberger, N. J. Interruption of the Enterohepatic Circulation of Digitoxin by Cholestyramine: II. Effect on Metabolic Disposition of Tritium-Labeled Digitoxin and Cardiac Systolic Intervals in Man. *J. Clin. Invest.* **1971**, *50* (12), 2638–2644. https://doi.org/10.1172/JCI106764.

(51) Weiner, I. M. Excretion of Drugs by the Kidney. *Concepts Biochem. Pharmacol.* **1971**, 328–353. https://doi.org/10.1007/978-3-642-65052-9_18.

(52) Fleck, C.; Braunlich, H. Factors Determining the Relationship between Renal and Hepatic Excretion of Xenobiotics. *Arzneimittelforschung.* **1990**, *40* (8), 942–946.

(53) Abbott, N. J.; Rönnbäck, L.; Hansson, E. Astrocyte-Endothelial Interactions at the Blood-Brain Barrier. *Nat. Rev. Neurosci.* **2006**, *7* (1), 41–53. https://doi.org/10.1038/NRN1824.

(54) Abbott, N. J.; Patabendige, A. A. K.; Dolman, D. E. M.; Yusof, S. R.; Begley, D. J. Structure and Function of the Blood-Brain Barrier. *Neurobiol. Dis.* **2010**, *37* (1), 13–25. https://doi.org/10.1016/J.NBD.2009.07.030.

(55) Abbott, N. J. Blood–Brain Barrier Structure and Function and the Challenges for CNS Drug Delivery. *J. Inherit. Metab. Dis. 2013 363* **2013**, *36* (3), 437–449. https://doi.org/10.1007/S10545-013-9608-0.

(56) Tajes, M.; Ramos-Fernández, E.; Weng-Jiang, X.; Bosch-Morató, M.; Guivernau, B.; Eraso-Pichot, A.; Salvador, B.; Fernàndez-Busquets, X.; Roquer, J.; Muñoz, F. J. The Blood-Brain Barrier: Structure, Function and Therapeutic Approaches to Cross It. *Mol. Membr. Biol.* **2014**, *31* (5), 152–167. https://doi.org/10.3109/09687688.2014.937468.

(57) Serlin, Y.; Shelef, I.; Knyazer, B.; Friedman, A. Anatomy and Physiology of the Blood-Brain Barrier. *Semin. Cell Dev. Biol.* **2015**, *38*, 2–6. https://doi.org/10.1016/J.SEMCDB.2015.01.002.

(58) Coomber, B. L.; Stewart, P. A. Morphometric Analysis of CNS Microvascular Endothelium. *Microvasc. Res.* **1985**, *30* (1), 99–115. https://doi.org/10.1016/0026-2862(85)90042-1.

(59) Van Itallie, C. M.; Anderson, J. M. Claudins and Epithelial Paracellular Transport. *Annu. Rev. Physiol.* **2006**, *68*, 403–429. https://doi.org/10.1146/ANNUREV.PHYSIOL.68.040104.131404.

(60) Abbott, N. J.; Friedman, A. Overview and Introduction: The Blood–Brain Barrier in Health and Disease. *Epilepsia* **2012**, *53*, 1–6. https://doi.org/10.1111/J.1528-1167.2012.03696.X.

(61) Peppiatt, C. M.; Howarth, C.; Mobbs, P.; Attwell, D. Bidirectional Control of CNS Capillary Diameter by Pericytes. *Nature* **2006**, *443* (7112), 700–704. https://doi.org/10.1038/nature05193.

(62) Berthiaume, A. A.; Grant, R. I.; McDowell, K. P.; Underly, R. G.; Hartmann, D. A.; Levy, M.; Bhat, N. R.; Shih, A. Y. Dynamic Remodeling of Pericytes In Vivo Maintains Capillary Coverage in the Adult Mouse Brain. *Cell Rep.* **2018**, *22* (1), 8–16. https://doi.org/10.1016/J.CELREP.2017.12.016.

(63) Wong, A. D.; Ye, M.; Levy, A. F.; Rothstein, J. D.; Bergles, D. E.; Searson, P. C. The Blood-Brain Barrier: An Engineering Perspective. *Front. Neuroeng.* **2013**, *6* (JUL). https://doi.org/10.3389/FNENG.2013.00007.

(64) Rodríguez-Arellano, J. J.; Parpura, V.; Zorec, R.; Verkhratsky, A. Astrocytes in Physiological Aging and Alzheimer's Disease. *Neuroscience* **2016**, *323*, 170–182. https://doi.org/10.1016/J.NEUROSCIENCE.2015.01.007.

(65) Williams, K.; Alvarez, X.; Lackner, A. A. Central Nervous System Perivascular Cells Are Immunoregulatory Cells That Connect the CNS with the Peripheral Immune System. *Glia* **2001**, *36* (2), 156–164. https://doi.org/10.1002/GLIA.1105.

(66) Streit, W. J.; Conde, J. R.; Fendrick, S. E.; Flanary, B. E.; Mariani, C. L. Role of Microglia in the Central Nervous System's Immune Response. *Neurol. Res.* **2005**, *27* (7), 685–691. https://doi.org/10.1179/016164105X49463A.

(67) Wu, C.; Ivars, F.; Anderson, P.; Hallmann, R.; Vestweber, D.; Nilsson, P.; Robenek, H.; Tryggvason, K.; Song, J.; Korpos, E.; Loser, K.; Beissert, S.; Georges-Labouesse, E.; Sorokin, L. M. Endothelial Basement Membrane Laminin Alpha5 Selectively Inhibits T Lymphocyte Extravasation into the Brain. *Nat. Med.* **2009**, *15* (5), 519–527. https://doi.org/10.1038/NM.1957.

(68) Sorokin, L. The Impact of the Extracellular Matrix on Inflammation. *Nat. Rev. Immunol.* **2010**, *10* (10), 712–723. https://doi.org/10.1038/NRI2852.

(69) Sharif, Y.; Jumah, F.; Coplan, L.; Krosser, A.; Sharif, K.; Tubbs, R. S. Blood Brain Barrier: A Review of Its

Anatomy and Physiology in Health and Disease. *Clin. Anat.* **2018**, *31* (6), 812–823. https://doi.org/10.1002/CA.23083.

(70) Xiao, M.; Xiao, Z. J.; Yang, B.; Lan, Z.; Fang, F. Blood-Brain Barrier: More Contributor to Disruption of Central Nervous System Homeostasis Than Victim in Neurological Disorders. *Front. Neurosci.* **2020**, *14*, 764. https://doi.org/10.3389/FNINS.2020.00764/BIBTEX.

(71) Löscher, W.; Potschka, H. Blood-Brain Barrier Active Efflux Transporters: ATP-Binding Cassette Gene Family. *NeuroRx* **2005**, *2* (1), 86–98. https://doi.org/10.1602/NEURORX.2.1.86.

(72) Mittapalli, R. K.; Manda, V. K.; Adkins, C. E.; Geldenhuys, W. J.; Lockman, P. R. Exploiting Nutrient Transporters at the Blood-Brain Barrier to Improve Brain Distribution of Small Molecules. *Ther. Deliv.* **2010**, *1* (6), 775–784. https://doi.org/10.4155/TDE.10.76.

(73) Cornford, E. M.; Hyman, S.; Swartz, B. E. The Human Brain GLUT1 Glucose Transporter: Ultrastructural Localization to the Blood-Brain Barrier Endothelia. *J. Cereb. Blood Flow Metab.* **1994**, *14* (1), 106–112. https://doi.org/10.1038/JCBFM.1994.15.

(74) Ha, S.; Hochman, J.; Sheridan, R. Mini Review on Molecular Modeling of P-Glycoprotein (Pgp). *Curr. Top. Med. Chem.* **2007**, *7* (15), 1525–1529. https://doi.org/10.2174/156802607782194806.

(75) Schinkel, A. H.; Mol, C. A. A. M.; Wagenaar, E.; van Deemter, L.; Smit, J. J. M.; Borst, P. Multidrug Resistance and the Role of P-Glycoprotein Knockout Mice. *Eur. J. Cancer* **1995**, *31A* (7–8), 1295–1298. https://doi.org/10.1016/0959-8049(95)00130-B.

(76) Schinkel, A. H.; Smit, J. J. M.; van Tellingen, O.; Beijnen, J. H.; Wagenaar, E.; van Deemter, L.; Mol, C. A. A. M.; van der Valk, M. A.; Robanus-Maandag, E. C.; te Riele, H. P. J.; Berns, A. J. M.; Borst, P. Disruption of the Mouse Mdr1a P-Glycoprotein Gene Leads to a Deficiency in the Blood-Brain Barrier and to Increased Sensitivity to Drugs. *Cell* **1994**, *77* (4), 491–502. https://doi.org/10.1016/0092-8674(94)90212-7.

(77) Hamilton, N. B. Pericyte-Mediated Regulation of Capillary Diameter: A Component of Neurovascular Coupling in Health and Disease. *Front. Neuroenergetics* **2010**, *2*, 5. https://doi.org/10.3389/FNENE.2010.00005/BIBTEX.

(78) Hall, C. N.; Reynell, C.; Gesslein, B.; Hamilton, N. B.; Mishra, A.; Sutherland, B. A.; Oâ Farrell, F. M.; Buchan, A. M.; Lauritzen, M.; Attwell, D. Capillary Pericytes Regulate Cerebral Blood Flow in Health and Disease. *Nature* **2014**, *508* (7494), 55–60. https://doi.org/10.1038/NATURE13165.

(79) Lindahl, P.; Johansson, B. R.; Levéen, P.; Betsholtz, C. Pericyte Loss and Microaneurysm Formation in PDGF-B-Deficient Mice. *Science* **1997**, *277* (5323), 242–245. https://doi.org/10.1126/SCIENCE.277.5323.242.

(80) Armulik, A.; Genové, G.; Mäe, M.; Nisancioglu, M. H.; Wallgard, E.; Niaudet, C.; He, L.; Norlin, J.; Lindblom, P.; Strittmatter, K.; Johansson, B. R.; Betsholtz, C. Pericytes Regulate the Blood-Brain Barrier. *Nature* **2010**, *468* (7323), 557–561. https://doi.org/10.1038/NATURE09522.

(81) Bell, R. D.; Winkler, E. A.; Sagare, A. P.; Singh, I.; LaRue, B.; Deane, R.; Zlokovic, B. V. Pericytes Control Key Neurovascular Functions and Neuronal Phenotype in the Adult Brain and during Brain Aging. *Neuron* **2010**, *68* (3), 409–427. https://doi.org/10.1016/J.NEURON.2010.09.043.

(82) Prat, A.; Biernacki, K.; Wosik, K.; Antel, J. P. Glial Cell Influence on the Human Blood-Brain Barrier. *Glia* **2001**, *36* (2), 145–155. https://doi.org/10.1002/GLIA.1104.

(83) Wosik, K.; Cayrol, R.; Dodelet-Devillers, A.; Berthelet, F.; Bernard, M.; Moumdjian, R.; Bouthillier, A.; Reudelhuber, T. L.; Prat, A. Angiotensin II Controls Occludin Function and Is Required for Blood Brain Barrier Maintenance: Relevance to Multiple Sclerosis. *J. Neurosci.* **2007**, *27* (34), 9032–9042.

https://doi.org/10.1523/JNEUROSCI.2088-07.2007.

(84) Bell, R. D.; Winkler, E. A.; Singh, I.; Sagare, A. P.; Deane, R.; Wu, Z.; Holtzman, D. M.; Betsholtz, C.; Armulik, A.; Sallstrom, J.; Berk, B. C.; Zlokovic, B. V. Apolipoprotein E Controls Cerebrovascular Integrity via Cyclophilin A. *Nature* **2012**, *485* (7399), 512–516. https://doi.org/10.1038/NATURE11087.

(85) Tait, M. J.; Saadoun, S.; Bell, B. A.; Papadopoulos, M. C. Water Movements in the Brain: Role of Aquaporins. *Trends Neurosci.* **2008**, *31* (1), 37–43. https://doi.org/10.1016/J.TINS.2007.11.003.

(86) Wolburg, H.; Wolburg-Buchholz, K.; Fallier-Becker, P.; Noell, S.; Mack, A. F. Structure and Functions of Aquaporin-4-Based Orthogonal Arrays of Particles. *Int. Rev. Cell Mol. Biol.* **2011**, *287*, 1–41. https://doi.org/10.1016/B978-0-12-386043-9.00001-3.

(87) Pardridge, W. M. Alzheimer's Disease Drug Development and the Problem of the Blood-Brain Barrier. *Alzheimers. Dement.* **2009**, *5* (5), 427. https://doi.org/10.1016/J.JALZ.2009.06.003.

(88) Pardridge, W. M. The Blood-Brain Barrier: Bottleneck in Brain Drug Development. *NeuroRx* **2005**, *2* (1), 3. https://doi.org/10.1602/NEURORX.2.1.3.

(89) Wade, L. A.; Katzman, R. Synthetic Amino Acids and the Nature of L-DOPA Transport at the Blood-Brain Barrier. *J. Neurochem.* **1975**, *25* (6), 837–842. https://doi.org/10.1111/J.1471-4159.1975.TB04415.X.

(90) Mealey, K. L. Therapeutic Implications of the MDR-1 Gene. *J. Vet. Pharmacol. Ther.* **2004**, *27* (5), 257–264. https://doi.org/10.1111/J.1365-2885.2004.00607.X.

(91) Fromm, M. F. P-Glycoprotein: A Defense Mechanism Limiting Oral Bioavailability and CNS Accumulation of Drugs. *Int. J. Clin. Pharmacol. Ther.* **2000**, *38* (2), 69–74. https://doi.org/10.5414/CPP38069.

(92) Niemegeers, C. J. E.; Lenaerts, F. M.; Janssen, P. A. J. Loperamide (R 18 553), a Novel Type of Antidiarrheal Agent. Part 1: In Vivo Oral Pharmacology and Acute Toxicity. Comparison with Morphine, Codeine, Diphenoxylate and Difenoxine. *Arzneimittelforschung.* **1974**, *24* (10), 1633–1636.

(93) Brown, B. A.; Kantesaria, P.; Mcdevitt, L. M. Fingolimod: A Novel Immunosuppressant for Multiple Sclerosis. *AnnPharmacother* **2007**, *41*, 1660–1668. https://doi.org/10.1345/aph.1.

(94) Brunkhorst, R.; Vutukuri, R.; Pfeilschifter, W. Fingolimod for the Treatment of Neurological Diseases—State of Play and Future Perspectives3. *Front. Cell. Neurosci.* **2014**, *8*, 283. https://doi.org/10.3389/FNCEL.2014.00283/BIBTEX.

(95) Zhang, Z.; Tang, W. Drug Metabolism in Drug Discovery and Development. *Acta Pharm. Sin. B* **2018**, *8* (5), 721–732. https://doi.org/10.1016/J.APSB.2018.04.003.

(96) Kumar, G. N.; Surapaneni, S. Role of Drug Metabolism in Drug Discovery and Development. *Med. Res. Rev.* **2001**, *21* (5), 397–411. https://doi.org/10.1002/MED.1016.

(97) Sevior, D. K.; Pelkonen, O.; Ahokas, J. T. Hepatocytes: The Powerhouse of Biotransformation. *Int. J. Biochem. Cell Biol.* **2012**, *44* (2), 257–261. https://doi.org/10.1016/J.BIOCEL.2011.11.011.

(98) Meyer, U. A.; Zanger, U. M. Molecular Mechanisms of Genetic Polymorphisms of Drug Metabolism. *Annu. Rev. Pharmacol. Toxicol.* **2003**, *37*, 269–296. https://doi.org/10.1146/ANNUREV.PHARMTOX.37.1.269.

(99) Nebert, D. W.; Russell, D. W. Clinical Importance of the Cytochromes P450. *Lancet* **2002**, *360* (9340), 1155–1162. https://doi.org/10.1016/S0140-6736(02)11203-7.

(100) De Montellano, P. R. O. *Cytochrome P450: Structure, Mechanism, and Biochemistry: Third Edition*; Springer US, 2005. https://doi.org/10.1007/B139087/COVER.

(101) Price Evans, D. A. N-Acetyltransferase. *Pharmacol. Ther.* **1989**, *42* (2), 157–234.

https://doi.org/10.1016/0163-7258(89)90036-3.

(102) Fukami, T.; Yokoi, T. The Emerging Role of Human Esterases. *Drug Metab. Pharmacokinet.* **2012**, *27* (5), 466–477. https://doi.org/10.2133/DMPK.DMPK-12-RV-042.

(103) Miner, D. J.; Kissinger, P. T. Evidence for the Involvement of N-Acetyl-p-Quinoneimine in Acetaminophen Metabolism. *Biochem. Pharmacol.* **1979**, *28* (22), 3285–3290. https://doi.org/10.1016/0006-2952(79)90123-0.

(104) Moldéus, P. Paracetamol Metabolism and Toxicity in Isolated Hepatocytes from Rat and Mouse. *Biochem. Pharmacol.* **1978**, *27* (24), 2859–2863. https://doi.org/10.1016/0006-2952(78)90201-0.

(105) Jancova, P.; Anzenbacher, P.; Anzenbacherova, E. Phase II Drug Metabolizing Enzymes. **2010**, *154* (2), 103–116.

(106) G baldi, M.; Levy, G. Pharmacokinetics in Clinical Practice: I. Concepts. *JAMA* **1976**, *235* (17), 1864–1867. https://doi.org/10.1001/JAMA.1976.03260430034020.

(107) Tukey, R. H.; Strassburg, C. P. Human UDP-Glucuronosyltransferases: Metabolism, Expression, and Disease. *Annu. Rev. Pharmacol. Toxicol.* **2000**, *40*, 581–616. https://doi.org/10.1146/ANNUREV.PHARMTOX.40.1.581.

(108) CD, K.; GR, R.; MD, G.; TR, T. UDP-Glucuronosyltransferases. *Curr. Drug Metab.* **2000**, *1* (2), 629–633. https://doi.org/10.2174/1389200003339171.

(109) Habuchi, O. Diversity and Functions of Glycosaminoglycan Sulfotransferases. *Biochim. Biophys. Acta* **2000**, *1474* (2), 115–127. https://doi.org/10.1016/S0304-4165(00)00016-7.

(110) Strott, C. A. Sulfonation and Molecular Action. *Endocr. Rev.* **2002**, *23* (5), 703–732. https://doi.org/10.1210/ER.2001-0040.

(111) Sheehan, D.; Meade, G.; Foley, V. M.; Dowd, C. A. Structure, Function and Evolution of Glutathione Transferases: Implications for Classification of Non-Mammalian Members of an Ancient Enzyme Superfamily. *Biochem. J.* **2001**, *360* (Pt 1), 1–16. https://doi.org/10.1042/0264-6021:3600001.

(112) Soboll, S.; Grundel, S.; Harris, J.; Kolb-Bachofen, V.; Ketterer, B.; Sies, H. The Content of Glutathione and Glutathione S-Transferases and the Glutathione Peroxidase Activity in Rat Liver Nuclei Determined by a Non-Aqueous Technique of Cell Fractionation. *Biochem. J.* **1995**, *311* (Pt 3), 889. https://doi.org/10.1042/BJ3110889.

(113) Hayes, J. D.; Flanagan, J. U.; Jowsey, I. R. Glutathione Transferases. *Annu. Rev. Pharmacol. Toxicol.* **2005**, *45*, 51–88. https://doi.org/10.1146/ANNUREV.PHARMTOX.45.120403.095857.

(114) Prescott, L. Kinetics and Metabolism of Paracetamol and Phenacetin. *Br. J. Clin. Pharmacol.* **1980**, *10* (S2), 291S-298S. https://doi.org/10.1111/J.1365-2125.1980.TB01812.X.

(115) Athersuch, T. J.; Antoine, D. J.; Boobis, A. R.; Coen, M.; Daly, A. K.; Possamai, L.; Nicholson, J. K.; Wilson, I. D. Paracetamol Metabolism, Hepatotoxicity, Biomarkers and Therapeutic Interventions: A Perspective. *Toxicol. Res. (Camb).* **2018**, *7* (3), 347–357. https://doi.org/10.1039/C7TX00340D.

(116) Jollow, D. J.; Thorgeirsson, S. S.; Potter, W. Z.; Hashimoto, M.; Mitchell, J. R. Acetaminophen-Induced Hepatic Necrosis. *Pharmacology* **1974**, *12* (4–5), 251–271. https://doi.org/10.1159/000136547.

(117) Xu, C.; Li, C. Y. T.; Kong, A. N. T. Induction of Phase I, II and III Drug Metabolism/Transport by Xenobiotics. *Arch. Pharmacal Res. 2005 283* **2005**, *28* (3), 249–268. https://doi.org/10.1007/BF02977789.

(118) Bond, J. S.; Butler, P. E. INTR.A.CELLULAR PROTEASES. **1987**.

(119) Barrett, A. J. Proteases. *Curr. Protoc. Protein Sci.* **2000**, *21* (1), 21.1.1-21.1.12. https://doi.org/10.1002/0471140864.PS2101S21.

(120) Ordóñez, G. R.; Puente, X. S.; Quesada, V.; López-Otín, C. Proteolytic Systems: Constructing Degradomes. *Methods Mol. Biol.* **2009**, *539*, 33–47. https://doi.org/10.1007/978-1-60327-003-8_2.

(121) Turk, B. Targeting Proteases: Successes, Failures and Future Prospects. *Nat. Rev. Drug Discov.* **2006**, *5* (9), 785–799. https://doi.org/10.1038/NRD2092.

(122) López-Otín, C.; Bond, J. S. Proteases: Multifunctional Enzymes in Life and Disease. *J. Biol. Chem.* **2008**, *283* (45), 30433–30437. https://doi.org/10.1074/JBC.R800035200.

(123) López-Otín, C.; Overall, C. M. Protease Degradomics: A New Challenge for Proteomics. *Nat. Rev. Mol. Cell Biol.* **2002**, *3* (7), 509–519. https://doi.org/10.1038/NRM858.

(124) Visscher, M.; De Henau, S.; Wildschut, M. H. E.; van Es, R. M.; Dhondt, I.; Michels, H.; Kemmeren, P.; Nollen, E. A.; Braeckman, B. P.; Burgering, B. M. T.; Vos, H. R.; Dansen, T. B. Proteome-Wide Changes in Protein Turnover Rates in C. Elegans Models of Longevity and Age-Related Disease. *Cell Rep.* **2016**, *16* (11), 3041–3051. https://doi.org/10.1016/J.CELREP.2016.08.025.

(125) Toyama, B. H.; Hetzer, M. W. Protein Homeostasis: Live Long, Won't Prosper. *Nat. Rev. Mol. Cell Biol.* **2013**, *14* (1), 55–61. https://doi.org/10.1038/NRM3496.

(126) Bonnans, C.; Chou, J.; Werb, Z. Remodelling the Extracellular Matrix in Development and Disease. *Nat. Rev. Mol. Cell Biol.* **2014**, *15* (12), 786–801. https://doi.org/10.1038/nrm3904.

(127) Boonen, S.; Rosenberg, E.; Claessens, F.; Vanderschueren, D.; Papapoulos, S. Inhibition of Cathepsin K for Treatment of Osteoporosis. *Curr. Osteoporos. Rep.* **2012**, *10* (1), 73–79. https://doi.org/10.1007/S11914-011-0085-9.

(128) Otto, H. H.; Schirmeister, T. Cysteine Proteases and Their Inhibitors. *Chem. Rev.* **1997**, *97* (1), 133–171. https://doi.org/10.1021/CR950025U/ASSET/IMAGES/LARGE/CR950025UF00023.JPEG.

(129) Mckerrow, J. H.; Sun, E.; Rosenthal, P. J.; Bouvier, J. The Proteases and Pathogenicity of Parasitic Protozoa. *Annu. Rev. Microbiol* **1993**, *47*, 821–853.

(130) Wellink, J.; Van Kammen, A. Proteases Involved in the Processing of Viral Polyproteins Brief Review. *Arch Virol* **1988**, *98*, 1–26.

(131) Culp, E.; Wright, G. D. Bacterial Proteases, Untapped Antimicrobial Drug Targets. *J. Antibiot. (Tokyo).* **2016**, *70* (4), 366–377. https://doi.org/10.1038/ja.2016.138.

(132) Schomburg, D.; Schomburg, I. Enzyme Databases. *Methods Mol. Biol.* **2010**, *609*, 113–128. https://doi.org/10.1007/978-1-60327-241-4_7.

(133) Rawlings, N. D.; Waller, M.; Barrett, A. J.; Bateman, A. MEROPS: The Database of Proteolytic Enzymes, Their Substrates and Inhibitors. *Nucleic Acids Res.* **2014**, *42* (Database issue), D503. https://doi.org/10.1093/NAR/GKT953.

(134) Rawlings, N. D.; Barrett, A. J. Evolutionary Families of Peptidases. *Biochem. J.* **1993**, *290* (Pt 1), 205. https://doi.org/10.1042/BJ2900205.

(135) Jadhav, P. K.; Schiffler, M. A.; Gavardinas, K.; Kim, E. J.; Matthews, D. P.; Staszak, M. A.; Coffey, D. S.; Shaw, B. W.; Cassidy, K. C.; Brier, R. A.; Zhang, Y.; Christie, R. M.; Matter, W. F.; Qing, K.; Durbin, J. D.; Wang, Y.; Deng, G. G. Discovery of Cathepsin S Inhibitor LY3000328 for the Treatment of Abdominal Aortic Aneurysm. *ACS Med. Chem. Lett.* **2014**, *5* (10), 1138–1142. https://doi.org/10.1021/ml500283g.

(136) Kim, M. J.; Yamamoto, D.; Matsumoto, K.; Inoue, M.; Ishida, T.; Mizuno, H.; Sumiya, S.; Kitamura, K. Crystal

Structure of Papain-E64-c Complex. Binding Diversity of E64-c to Papain S2 and S3 Subsites. *Biochem. J.* **1992**, *287* (3), 797–803. https://doi.org/10.1042/BJ2870797.

(137) Schechter, I.; Berger, A. On the Size of the Active Site in Proteases. I. Papain. *Biochem. Biophys. Res. Commun.* **1967**, *27* (2), 157–162. https://doi.org/10.1016/S0006-291X(67)80055-X.

(138) Hughes, A. L. Evolution of Cysteine Proteinases in Eukaryotes. *Mol. Phylogenet. Evol.* **1994**, *3* (4), 310–321. https://doi.org/10.1006/MPEV.1994.1038.

(139) Wei, D.; Huang, X.; Liu, J.; Tang, M.; Zhan, C. G. Reaction Pathway and Free Energy Profile for Papain-Catalyzed Hydrolysis of N-Acetyl-Phe-Gly 4-Nitroanilide. *Biochemistry* **2013**, *52* (30), 5145–5154. https://doi.org/10.1021/BI400629R/ASSET/IMAGES/LARGE/BI-2013-00629R_0005.JPEG.

(140) Vernet, T.; Tessier, D. C.; Chatellier, J.; Plouffe, C.; Tak Sing Lee; Thomas, D. Y.; Storer, A. C.; Menard, R. Structural and Functional Roles of Asparagine 175 in the Cysteine Protease Papain. *J. Biol. Chem.* **1995**, *270* (28), 16645–16652. https://doi.org/10.1074/JBC.270.28.16645.

(141) Lewis, S. D.; Johnson, F. A.; Shafer, J. A. Potentiometric Determination of Ionizations at the Active Site of Papain. *Biochemistry* **1976**, *15* (23), 5009–5017. https://doi.org/10.1021/BI00668A010.

(142) Lewis, S. D.; Johnson, F. A.; Shafer, J. A. Effect of Cysteine-25 on the Ionization of Histidine-159 in Papain as Determined by Proton Nuclear Magnetic Resonance Spectroscopy. Evidence for a His-159--Cys-25 Ion Pair and Its Possible Role in Catalysis. *Biochemistry* **1981**, *20* (1), 48–51. https://doi.org/10.1021/BI00504A009.

(143) Brocklehurst, K. Specific Covalent Modification of Thiols: Applications in the Study of Enzymes and Other Biomolecules. *Int. J. Biochem.* **1979**, *10* (4), 259–274. https://doi.org/10.1016/0020-711X(79)90088-0.

(144) Harrison, M. J.; Burton, N. A.; Hillier, I. H. Catalytic Mechanism of the Enzyme Papain: Predictions with a Hybrid Quantum Mechanical/Molecular Mechanical Potential. *J. Am. Chem. Soc.* **1997**, *119* (50), 12285–12291. https://doi.org/10.1021/JA9711472/ASSET/IMAGES/LARGE/JA9711472F00007.JPEG.

(145) Mladenovic, M.; Ansorg, K.; Fink, R. F.; Thiel, W.; Schirmeister, T.; Engels, B. Atomistic Insights into the Inhibition of Cysteine Proteases: First QM/MM Calculations Clarifying the Stereoselectivity of Epoxide-Based Inhibitors. *J. Phys. Chem. B* **2008**, *112* (37), 11798–11808. https://doi.org/10.1021/jp803895f.

(146) Hol, W. G. J.; Van Du jnen, P. T.; Berendsen, H. J. C. The Alpha-Helix Dipole and the Properties of Proteins. *Nature* **1978**, *273* (5662), 443–446. https://doi.org/10.1038/273443A0.

(147) Nägler, D. K.; Ménard, R. Family C1 Cysteine Proteases: Biological Diversity or Redundancy? *Biol. Chem.* **2003**, *384* (6), 837–843. https://doi.org/10.1515/BC.2003.094/MACHINEREADABLECITATION/RIS.

(148) Mohamed, M. M.; Sloane, B. F. Cysteine Cathepsins: Multifunctional Enzymes in Cancer. *Nat. Rev. Cancer* **2006**, *6* (10), 764–775. https://doi.org/10.1038/NRC1949.

(149) Prunk, M.; Kos, J. Nanoparticle Based Delivery of Protease Inhibitors to Cancer Cells. *Curr. Med. Chem.* **2016**, *24* (42). https://doi.org/10.2174/0929867323666160922162811.

(150) Saftig, P.; Hunziker, E.; Wehmeyer, O.; Jones, S.; Boyde, A.; Rommerskirch, W.; Moritz, J. D.; Schu, P.; Von Figura, K. Impaired Osteoclastic Bone Resorption Leads to Osteopetrosis in Cathepsin-K-Deficient Mice. *Proc. Natl. Acad. Sci. U. S. A.* **1998**, *95* (23), 13453–13458. https://doi.org/10.1073/PNAS.95.23.13453.

(151) Riese, R. J.; Wolf, P. R.; Brömme, D.; Natkin, L. R.; Villadangos, J. A.; Ploegh, H. L.; Chapman, H. A. Essential Role for Cathepsin S in MHC Class II-Associated Invariant Chain Processing and Peptide Loading. *Immunity* **1996**, *4* (4), 357–366. https://doi.org/10.1016/S1074-7613(00)80249-6.

(152) Riese, R. J.; Mitchell, R. N.; Villadangos, J. A.; Shi, G. P.; Palmer, J. T.; Karp, E. R.; De Sanctis, G. T.;

Ploegh, H. L.; Chapman, H. A. Cathepsin S Activity Regulates Antigen Presentation and Immunity. *J. Clin. Invest.* **1998**, *101* (11), 2351–2363. https://doi.org/10.1172/JCI1158.

(153) Guo-Ping, S.; Villadangos, J. A.; Dranoff, G.; Small, C.; L juan, G.; Haley, K. J.; Riese, R.; Ploegh, H. L.; Chapman, H. A. Cathepsin S Required for Normal MHC Class II Peptide Loading and Germinal Center Development. *Immunity* **1999**, *10* (2), 197–206. https://doi.org/10.1016/s1074-7613(00)80020-5.

(154) Villadangos, J. A.; Riese, R. J.; Peters, C.; Chapman, H. A.; Ploegh, H. L. Degradation of Mouse Invariant Chain: Roles of Cathepsins S and D and the Influence of Major Histocompatibility Complex Polymorphism. *J. Exp. Med.* **1997**, *186* (4), 549–560. https://doi.org/10.1084/jem.186.4.549.

(155) Gauthier, J. Y.; Black, W. C.; Courchesne, I.; Cromlish, W.; Desmarais, S.; Houle, R.; Lamontagne, S.; Li, C. S.; Massé, F.; McKay, D. J.; Ouellet, M.; Robichaud, J.; Truchon, J. F.; Truong, V. L.; Wang, Q.; Percival, M. D. The Identification of Potent, Selective, and Bioavailable Cathepsin S Inhibitors. *Bioorganic Med. Chem. Lett.* **2007**, *17* (17), 4929–4933. https://doi.org/10.1016/j.bmcl.2007.06.023.

(156) Brömme, D.; Lecaille, F. Cathepsin K Inh bitors for Osteoporosis and Potential Off-Target Effects. *Expert Opin. Investig. Drugs* **2009**, *18* (5), 585–600. https://doi.org/10.1517/13543780902832661.

(157) Weitoft, T.; Larsson, A.; Manivel, V. A.; Lysholm, J.; Knight, A.; Rönnelid, J. Cathepsin S and Cathepsin L in Serum and Synovial Fluid in Rheumatoid Arthritis with and without Autoantibodies. *Rheumatology (Oxford).* **2015**, *54* (10), 1923–1928. https://doi.org/10.1093/RHEUMATOLOGY/KEU486.

(158) Sudhan, D. R.; Siemann, D. W. Cathepsin L Targeting in Cancer Treatment. *Pharmacol. Ther.* **2015**, *155*, 105. https://doi.org/10.1016/J.PHARMTHERA.2015.08.007.

(159) Mason, S. D.; Joyce, J. A. Proteolytic Networks in Cancer. *Trends Cell Biol.* **2011**, *21* (4), 228–237. https://doi.org/10.1016/J.TCB.2010.12.002.

(160) Olson, O. C.; Joyce, J. A. Cysteine Cathepsin Proteases: Regulators of Cancer Progression and Therapeutic Response. *Nat. Rev. Cancer* **2015**, *15* (12), 712–729. https://doi.org/10.1038/NRC4027.

(161) Dennhöfer, R.; Kurschat, P.; Zigrino, P.; Klose, A.; Bosserhoff, A.; Van Mu jen, G.; Krieg, T.; Mauch, C.; Hunzelmann, N. Invasion of Melanoma Cells into Dermal Connective Tissue in Vitro: Evidence for an Important Role of Cysteine Proteases. *Int. J. cancer* **2003**, *106* (3), 316–323. https://doi.org/10.1002/IJC.11255.

(162) Kos, J.; Mitrović, A.; Mirković, B. The Current Stage of Cathepsin B Inhibitors as Potential Anticancer Agents. *Future Med. Chem.* **2014**, *6* (11), 1355–1371. https://doi.org/10.4155/FMC.14.73.

(163) Gora, J.; Latajka, R. Involvement of Cysteine Proteases in Cancer. *Curr. Med. Chem.* **2015**, *22* (8), 944–957. https://doi.org/10.2174/0929867321666141106115624.

(164) Bararia, D.; Hildebrand, J. A.; Stolz, S.; Haebe, S.; Alig, S.; Trevisani, C. P.; Osorio-Barrios, F.; Bartoschek, M. D.; Mentz, M.; Pastore, A.; Gaitzsch, E.; Heide, M.; Jurinovic, V.; Rautter, K.; Gunawardana, J.; Sabdia, M. B.; Szczepanowski, M.; Richter, J.; Klapper, W.; Louissaint, A.; Ludwig, C.; Bultmann, S.; Leonhardt, H.; Eustermann, S.; Hopfner, K. P.; Hiddemann, W.; von Bergwelt-Baildon, M.; Steidl, C.; Kridel, R.; Tobin, J. W. D.; Gandhi, M. K.; Weinstock, D. M.; Schmidt-Supprian, M.; Sárosi, M. B.; Rudelius, M.; Passerini, V.; Mautner, J.; Weigert, O. Cathepsin S Alterations Induce a Tumor-Promoting Immune Microenvironment in Follicular Lymphoma. *Cell Rep.* **2020**, *31* (5), 107522. https://doi.org/10.1016/J.CELREP.2020.107522.

(165) Fuchs, N.; Meta, M.; Schuppan, D.; Nuhn, L.; Schirmeister, T. Novel Opportunities for Cathepsin S Inh bitors in Cancer Immunotherapy by Nanocarrier-Mediated Delivery. *Cells* **2020**, *9* (9), 2021.

(166) Wi kinson, R. D. A.; Williams, R.; Scott, C. J.; Burden, R. E. Cathepsin S: Therapeutic, Diagnostic, and Prognostic Potential. *Biol. Chem.* **2015**, *396* (8), 867–882. https://doi.org/10.1515/HSZ-2015-0114/PDF.

(167) Dheilly, E.; Battistello, E.; Katanayeva, N.; Sungalee, S.; Michaux, J.; Duns, G.; Wehrle, S.; Sordet-Dessimoz, J.; Mina, M.; Racle, J.; Farinha, P.; Coukos, G.; Gfeller, D.; Mottok, A.; Kridel, R.; Correia, B. E.; Steidl, C.; Bassani-Sternberg, M.; Ciriello, G.; Zoete, V.; Oricchio, E. Cathepsin S Regulates Antigen Processing and T Cell Activity in Non-Hodgkin Lymphoma. *Cancer Cell* **2020**, *37* (5), 674-689.e12. https://doi.org/10.1016/j.ccell.2020.03.016.

(168) McDowell, S. H.; Gallaher, S. A.; Burden, R. E.; Scott, C. J. Leading the Invasion: The Role of Cathepsin S in the Tumour Microenvironment. *Biochim. Biophys. Acta - Mol. Cell Res.* **2020**, *1867* (10), 118781. https://doi.org/10.1016/J.BBAMCR.2020.118781.

(169) Farhood, B.; Najafi, M.; Mortezaee, K. CD8+ Cytotoxic T Lymphocytes in Cancer Immunotherapy: A Review. *J. Cell. Physiol.* **2019**, *234* (6), 8509–8521. https://doi.org/10.1002/JCP.27782.

(170) Quaranta, V.; Schmid, M. C. Macrophage-Mediated Subversion of Anti-Tumour Immunity. *Cells* **2019**, *8* (7). https://doi.org/10.3390/CELLS8070747.

(171) Jakoš, T.; Pišlar, A.; Jewett, A.; Kos, J. Cysteine Cathepsins in Tumor-Associated Immune Cells. *Front. Immunol.* **2019**, *10* (AUG). https://doi.org/10.3389/FIMMU.2019.02037.

(172) Hsing, L. C.; Rudensky, A. Y. The Lysosomal Cysteine Proteases in MHC Class II Antigen Presentation. *Immunol. Rev.* **2005**, *207*, 229–241. https://doi.org/10.1111/J.0105-2896.2005.00310.X.

(173) Fu, C.; Jiang, A. Dendritic Cells and CD8 T Cell Immunity in Tumor Microenvironment. *Front. Immunol.* **2018**, *9*. https://doi.org/10.3389/fimmu.2018.03059.

(174) Yan, X.; Wu, C.; Chen, T.; Santos, M. M.; Liu, C. L.; Yang, C.; Zhang, L.; Ren, J.; Liao, S.; Guo, H.; Sukhova, G. K.; Shi, G. P. Cathepsin S Inh bition Changes Regulatory T-Cell Activity in Regulating Bladder Cancer and Immune Cell Proliferation and Apoptosis. *Mol. Immunol.* **2017**, *82*, 66–74. https://doi.org/10.1016/j.molimm.2016.12.018.

(175) Hardegger, L. A.; Kuhn, B.; Spinnler, B.; Anselm, L.; Ecabert, R.; Stihle, M.; Gsell, B.; Thoma, R.; Diez, J.; Benz, J.; Plancher, J. M.; Hartmann, G.; Banner, D. W.; Haap, W.; Diederich, F. Systematic Investigation of Halogen Bonding in Protein-Ligand Interactions. *Angew. Chemie - Int. Ed.* **2011**, *50* (1), 314–318. https://doi.org/10.1002/anie.201006781.

(176) Kerr, I. D.; Lee, J. H.; Farady, C. J.; Marion, R.; Rickert, M.; Sajid, M.; Pandey, K.; Caffrey, C. R.; Legac, J.; Hansell, E.; McKerrow, J. H.; Craik, C. S.; Rosenthal, P. J.; Brinen, L. S. Vinyl Sulfones as Antiparasitic Agents and a Structural Basis for Drug Design. *J. Biol. Chem.* **2009**, *284* (38), 25697–25703. https://doi.org/10.1074/JBC.M109.014340.

(177) Wiederanders, B.; Kaulmann, G.; Schilling, K. Functions of Propeptide Parts in Cysteine Proteases. *Curr. Protein Pept. Sci.* **2003**, *4* (5), 309–326. https://doi.org/10.2174/1389203033487081.

(178) Wiederanders, B. The Function of Propeptide Domains of Cysteine Proteinases. *Adv. Exp. Med. Biol.* **2000**, *477*, 261–270. https://doi.org/10.1007/0-306-46826-3_28.

(179) Yadati, T.; Houben, T.; Bitorina, A.; Shiri-Sverdlov, R. The Ins and Outs of Cathepsins: Physiological Function and Role in Disease Management. *Cells* **2020**, *9* (7). https://doi.org/10.3390/CELLS9071679.

(180) Schilling, K.; Pietschmann, S.; Fehn, M.; Wenz, I.; Wiederanders, B. Folding Incompetence of Cathepsin L-like Cysteine Proteases May Be Compensated by the Highly Conserved, Domain-Building N-Terminal Extension of the Proregion. *Biol. Chem.* **2001**, *382* (5), 859–865. https://doi.org/10.1515/BC.2001.105.

(181) Nissler, K.; Kreusch, S.; Rommerskirch, W.; Strubel, W.; Weber, E.; Wiederanders, B. Sorting of Non-Glycosylated Human Procathepsin S in Mammalian Cells. *Biol. Chem.* **1998**, *379* (2), 219–224. https://doi.org/10.1515/BCHM.1998.379.2.219.

(182) Chapman, R. L.; Kane, S. E.; Erickson, A. H. Abnormal Glycosylation of Procathepsin L Due to N-Terminal Point Mutations Correlates with Failure to Sort to Lysosomes. *J. Biol. Chem.* **1997**, *272* (13), 8808–8816. https://doi.org/10.1074/JBC.272.13.8808.

(183) Johé, P.; Jaenicke, E.; Neuweiler, H.; Schirmeister, T.; Kersten, C.; Hellmich, U. A. Structure, Interdomain Dynamics and PH-Dependent Autoactivation of pro-Rhodesain, the Main Lysosomal Cysteine Protease from African Trypanosomes. *J. Biol. Chem.* **2021**, 100565. https://doi.org/10.1016/j.jbc.2021.100565.

(184) Ménard, R.; Carmona, E.; Takebe, S.; Dufour, É.; Plouffe, C.; Mason, P.; Mort, J. S. Autocatalytic Processing of Recombinant Human Procathepsin L. Contribution of Both Intermolecular and Unimolecular Events in the Processing of Procathepsin L in Vitro. *J. Biol. Chem.* **1998**, *273* (8), 4478–4484. https://doi.org/10.1074/JBC.273.8.4478.

(185) Cygler, M.; Sivaraman, J.; Grochulski, P.; Coulombe, R.; Storer, A. C.; Mort, J. S. Structure of Rat Procathepsin B: Model for Inh bition of Cysteine Protease Activity by the Proregion. *Structure* **1996**, *4* (4), 405–416. https://doi.org/10.1016/S0969-2126(96)00046-9.

(186) Coulombe, R.; Grochulski, P.; Sivaraman, J.; Ménard, R.; Mort, J. S.; Cygler, M. Structure of Human Procathepsin L Reveals the Molecular Basis of Inh bition by the Prosegment. *EMBO J.* **1996**, *15* (20), 5492. https://doi.org/10.1002/j.1460-2075.1996.tb00934.x.

(187) Molecular Operating Environment (MOE). Chemical Computing Group ULC: 1010 Sherbrooke St. West, Suite #910, Montreal, QC, Canada, H3A 2R7 2020.

(188) Carugo, O. How Root-Mean-Square Distance (r.m.s.d.) Values Depend on the Resolution of Protein Structures That Are Compared. *J. Appl. Crystallogr.* **2003**, *36* (1), 125–128. https://doi.org/10.1107/S0021889802020502.

(189) Yusuf, D.; Davis, A. M.; Kleywegt, G. J.; Schmitt, S. An Alternative Method for the Evaluation of Docking Performance: RSR vs RMSD. *J. Chem. Inf. Model.* **2008**, *48* (7), 1411–1422. https://doi.org/10.1021/CI800084X/SUPPL_FILE/CI800084X-FILE004.ZIP.

(190) Kerr, I. D.; Lee, J. H.; Farady, C. J.; Marion, R.; Rickert, M.; Sajid, M.; Pandey, K. C.; Caffrey, C. R.; Legac, J.; Hansell, E.; Mckerrow, J. H.; Cra k, C. S.; Rosenthal, P. J.; Brinen, L. S. Vinyl Sulfones as Antiparasitic Agents and a Structural Basis for Drug Design. *J. Biol. Chem.* **2009**, *284* (38), 25697–25703. https://doi.org/10.1074/jbc.M109.014340.

(191) Hardegger, L. A.; Kuhn, B.; Spinnler, B.; Anselm, L.; Ecabert, R.; Stihle, M.; Gsell, B.; Thoma, R.; Diez, J.; Benz, J.; Plancher, J. M.; Hartmann, G.; Isshiki, Y.; Morikami, K.; Shimma, N.; Haap, W.; Banner, D. W.; Diederich, F. Halogen Bonding at the Active Sites of Human Cathepsin L and MEK1 Kinase: Efficient Interactions in Different Environments. *ChemMedChem* **2011**, *6* (11), 2048–2054. https://doi.org/10.1002/CMDC.201100353.

(192) Illy, C.; Quraishi, O.; Wang, J.; Purisima, E.; Vernet, T.; Mort, J. S. Role of the Occluding Loop in Cathepsin B Activity. *J. Biol. Chem.* **1997**, *272* (2), 1197–1202. https://doi.org/10.1074/jbc.272.2.1197.

(193) Quraishi, O.; Nägler, D. K.; Fox, T.; Sivaraman, J.; Cygler, M.; Mort, J. S.; Storer, A. C. The Occluding Loop in Cathepsin B Defines the PH Dependence of Inhibition by Its Propeptide. *Biochemistry* **1999**, *38* (16), 5017–5023. https://doi.org/10.1021/BI981950O.

(194) Cathers, B. E.; Barrett, C.; Palmer, J. T.; Rydzewski, R. M. PH Dependence of Inhibitors Targeting the Occluding Loop of Cathepsin B. *Bioorg. Chem.* **2002**, *30* (4), 264–275. https://doi.org/10.1016/S0045-2068(02)00009-3.

(195) Jílková, A.; Řezáčová, P.; Lepšík, M.; Horn, M.; Váchová, J.; Fanfrlík, J.; Brynda, J.; McKerrow, J. H.; Caffrey, C. R.; Mareš, M. Structural Basis for Inhibition of Cathepsin B Drug Target from the Human Blood Fluke,

Schistosoma Mansoni. *J. Biol. Chem.* **2011**, *286* (41), 35770–35781. https://doi.org/10.1074/JBC.M111.271304.

(196) Greenspan, P. D.; Clark, K. L.; Tommasi, R. A.; Cowen, S. D.; McQuire, L. W.; Farley, D. L.; Van Duzer, J. H.; Goldberg, R. L.; Zhou, H.; Du, Z.; Fitt, J. J.; Coppa, D. E.; Fang, Z.; Macchia, W.; Zhu, L.; Capparelli, M. P.; Goldstein, R.; Wigg, A. M.; Doughty, J. R.; Bohacek, R. S.; Knap, A. K. Identification of Dipeptidyl Nitriles as Potent and Selective Inhibitors of Cathepsin B through Structure-Based Drug Design. *J. Med. Chem.* **2001**, *44* (26), 4524–4534. https://doi.org/10.1021/JM010206Q.

(197) Pauly, T. A.; Sulea, T.; Ammirati, M.; Sivaraman, J.; Danley, D. E.; Griffor, M. C.; Kamath, A. V.; Wang, I. K.; Laird, E. R.; Seddon, A. P.; Ménard, R.; Cygler, M.; Rath, V. L. Specificity Determinants of Human Cathepsin S Revealed by Crystal Structures of Complexes. *Biochemistry* **2003**, *42* (11), 3203–3213. https://doi.org/10.1021/b 027308i.

(198) Brömme, D.; Klaus, J. L.; Okamoto, K.; Rasnick, D.; Palmer, J. T. Peptidyl Vinyl Sulphones : A New Class of Potent and Selective Cysteine Protease Inhibitors S 2 P 2 Specificity of Human Cathepsin O2 in Comparison with Cathepsins S and L. *Biochem. J* **1996**, *315*, 85–89.

(199) Bauer, R. A. Covalent Inhibitors in Drug Discovery: From Accidental Discoveries to Avoided Liabilities and Designed Therapies. *Drug Discov. Today* **2015**, *20* (9), 1061–1073. https://doi.org/10.1016/j.drudis.2015.05.005.

(200) Savi, P.; Pereillo, J. M.; Uzabiaga, M. F.; Comba bert, J.; Picard, C.; Maffrand, J. P.; Pascal, M.; Herbert, J. M. Identification and Biological Activity of the Active Metabolite of Clopidogrel. *Thromb. Haemost.* **2000**, *84* (5), 891–896. https://doi.org/10.1055/S-0037-1614133/ID/JR4133-10.

(201) Herbert, J. M.; Savi, P. P2Y12, a New Platelet ADP Receptor, Target of Clopidogrel. *Semin. Vasc. Med.* **2003**, *3* (2), 113–121. https://doi.org/10.1055/s-2003-40669.

(202) Wright, P. M.; Seiple, I. B.; Myers, A. G. The Evolving Role of Chemical Synthesis in Ant bacterial Drug Discovery. *Angew. Chem. Int. Ed. Engl.* **2014**, *53* (34), 8840–8869. https://doi.org/10.1002/ANIE.201310843.

(203) Miller, J. A. The Metabolism of Xenobiotics to Reactive Electrophiles in Chemical Carcinogenesis and Mutagenesis: A Collaboration with Elizabeth Cavert Miller and Our Associates. *Drug Metab. Rev.* **2008**, *30* (4), 645–674. https://doi.org/10.3109/03602539808996326.

(204) Boike, L.; Henning, N. J.; Nomura, D. K. Advances in Covalent Drug Discovery. *Nat. Rev. Drug Discov. 2022 2112* **2022**, *21* (12), 881–898. https://doi.org/10.1038/s41573-022-00542-z.

(205) Bjij, I.; Olotu, F. A.; Agoni, C.; Adeniji, E.; Khan, S.; El Rashedy, A.; Cherqaoui, D.; Soliman, M. E. S. Covalent Inhibition in Drug Discovery: Filling the Void in Literature. *Curr. Top. Med. Chem.* **2018**, *18* (13), 1135–1145. https://doi.org/10.2174/1568026618666180731161438.

(206) Krishnan, S.; Miller, R. M.; Tian, B.; Mullins, R. D.; Jacobson, M. P.; Taunton, J. Design of Revers ble, Cysteine-Targeted Michael Acceptors Guided by Kinetic and Computational Analysis. *J. Am. Chem. Soc.* **2014**, *136* (36), 12624–12630. https://doi.org/10.1021/JA505194W/SUPPL_FILE/JA505194W_SI_002.PDB.

(207) Gehringer, M.; Laufer, S. A. Emerging and Re-Emerging Warheads for Targeted Covalent Inhibitors: Applications in Medicinal Chemistry and Chemical Biology. *J. Med. Chem.* **2019**, *62* (12), 5673–5724. https://doi.org/10.1021/ACS.JMEDCHEM.8B01153/ASSET/IMAGES/LARGE/JM-2018-011539_0038.JPEG.

(208) Baillie, T. A. Targeted Covalent Inhibitors for Drug Design. *Angew. Chemie Int. Ed.* **2016**, *55* (43), 13408–13421. https://doi.org/10.1002/ANIE.201601091.

(209) Lonsdale, R.; Ward, R. A. Structure-Based Design of Targeted Covalent Inhibitors. *Chem. Soc. Rev.* **2018**, *47* (11), 3816–3830. https://doi.org/10.1039/C7CS00220C.

(210) Guterman, L. Covalent Drugs from Long-Lived Ties. *Chem. Eng. News* **2012**, *89* (36), 19–26. https://doi.org/10.1021/CEN-V089N036.P019.

(211) Kisselev, A. F.; Van Der Linden, W. A.; Overkleeft, H. S. Proteasome Inhibitors: An Expanding Army Attacking a Unique Target. *Chem. Biol.* **2012**, *19* (1), 99–115. https://doi.org/10.1016/J.CHEMBIOL.2012.01.003.

(212) Njoroge, F. G.; Chen, K. X.; Shih, N. Y.; Piwinski, J. J. Challenges in Modern Drug Discovery: A Case Study of Boceprevir, an HCV Protease Inhibitor for the Treatment of Hepatitis C Virus Infection. *Acc. Chem. Res.* **2008**, *41* (1), 50–59. https://doi.org/10.1021/AR700109K.

(213) Joyce, R. P.; Hu, V. W.; Wang, J. The History, Mechanism, and Perspectives of Nirmatrelvir (PF-07321332): An Orally Bioavailable Main Protease Inhibitor Used in Combination with Ritonavir to Reduce COVID-19-Related Hospitalizations. *Med. Chem. Res.* **2022**, *31* (10), 1637. https://doi.org/10.1007/S00044-022-02951-6.

(214) Lamb, Y. N. Nirmatrelvir Plus Ritonavir: First Approval. *Drugs* **2022**, *82* (5), 585. https://doi.org/10.1007/S40265-022-01692-5.

(215) Barnett, A. DPP-4 Inhibitors and Their Potential Role in the Management of Type 2 Diabetes. *Int. J. Clin. Pract.* **2006**, *60* (11), 1454–1470. https://doi.org/10.1111/J.1742-1241.2006.01178.X.

(216) Minkovsky, N.; Berezov, A. BIBW-2992, a Dual Receptor Tyrosine Kinase Inhibitor for the Treatment of Solid Tumors. *Curr. Opin. Investig. Drugs* **2008**, *9* (12), 1336–1346.

(217) Yap, T. A.; Vidal, L.; Adam, J.; Stephens, P.; Spicer, J.; Shaw, H.; Ang, J.; Temple, G.; Bell, S.; Shahidi, M.; Uttenreuther-Fischer, M.; Stopfer, P.; Futreal, A.; Calvert, H.; De Bono, J. S.; Plummer, R. Phase I Trial of the Irreversible EGFR and HER2 Kinase Inhibitor BIBW 2992 in Patients with Advanced Solid Tumors. *J. Clin. Oncol.* **2010**, *28* (25), 3965–3972. https://doi.org/10.1200/JCO.2009.26.7278.

(218) Thurmond, R. L.; Beavers, M. P.; Cai, H.; Meduna, S. P.; Gustin, D. J.; Sun, S.; Almond, H. J.; Karlsson, L.; Edwards, J. P. Nonpeptidic, Noncovalent Inhibitors of the Cysteine Protease Cathepsin S. *J. Med. Chem.* **2004**, *47* (20), 4799–4801. https://doi.org/10.1021/JM0496133.

(219) Löser, R.; Abbenante, G.; Madala, P. K.; Halili, M.; Le, G. T.; Fairlie, D. P. Noncovalent Tripeptidyl Benzyl- and Cyclohexyl-Amine Inhibitors of the Cysteine Protease Caspase-1. *J. Med. Chem.* **2010**, *53* (6), 2651–2655. https://doi.org/10.1021/JM901790W.

(220) Klein, P.; Johe, P.; Wagner, A.; Jung, S.; Kühlborn, J.; Barthels, F.; Tenzer, S.; Distler, U.; Waigel, W.; Engels, B.; Hellmich, U. A.; Opatz, T.; Schirmeister, T. New Cysteine Protease Inh bitors: Electrophilic (Het)Arenes and Unexpected Prodrug Identification for the Trypanosoma Protease Rhodesain. *Molecules* **2020**, *25* (6), 1451. https://doi.org/10.3390/molecules25061451.

(221) Moon, J. B.; Coleman, R. S.; Hanzlik, R. P. Reversible Covalent Inhibition of Papain by a Peptide Nitrile. 13C NMR Evidence for a Thioimidate Ester Adduct. *J. Am. Chem. Soc.* **1986**, *108* (6), 1350–1351.

(222) Hanzl k, R. P.; Zygmunt, J.; Moon, J. B. Revers ble Covalent Binding of Peptide Nitriles to Papain. *Biochim. Biophys. Acta* **1990**, *1035* (1), 62–70. https://doi.org/10.1016/0304-4165(90)90174-U.

(223) Owen, D. R.; Allerton, C. M. N.; Anderson, A. S.; Aschenbrenner, L.; Avery, M.; Berritt, S.; Boras, B.; Cardin, R. D.; Carlo, A.; Coffman, K. J.; Dantonio, A.; Di, L.; Eng, H.; Ferre, R. A.; Gajiwala, K. S.; Gibson, S. A.; Greasley, S. E.; Hurst, B. L.; Kadar, E. P.; Kalgutkar, A. S.; Lee, J. C.; Lee, J.; Liu, W.; Mason, S. W.; Noell, S.; Novak, J. J.; Obach, R. S.; Ogilvie, K.; Patel, N. C.; Pettersson, M.; Rai, D. K.; Reese, M. R.; Sammons,

M. F.; Sathish, J. G.; Singh, R. S. P.; Steppan, C. M.; Stewart, A. E.; Tuttle, J. B.; Updyke, L.; Verhoest, P. R.; Wei, L.; Yang, Q.; Zhu, Y. An Oral SARS-CoV-2 Mpro Inh bitor Clinical Candidate for the Treatment of COVID-19. *Science (80-.).* **2021**, *374* (6575), 1586–1593. https://doi.org/10.1126/SCIENCE.ABL4784/SUPPL_FILE/SCIENCE.ABL4784_MDAR_REPRODUCIBILITY_CHECKLIST.PDF.

(224) Rock, B. M.; Hengel, S. M.; Rock, D. A.; Wienkers, L. C.; Kunze, K. L. Characterization of Ritonavir-Mediated Inactivation of Cytochrome P450 3A4. *Mol. Pharmacol.* **2014**, *86* (6), 665–674. https://doi.org/10.1124/MOL.114.094862.

(225) Hughes, T. E.; Mone, M. D.; Russell, M. E.; Weldon, S. C.; Villhauer, E. B. NVP-DPP728 (1-[[[2-[(5-Cyanopyridin-2-Yl)Amino]Ethy]Amino]Acetyl]-2-Cyano-(S)- Pyrrolidine), a Slow-Binding Inhibitor of Dipeptidyl Peptidase IV. *Biochemistry* **1999**, *38* (36), 11597–11603. https://doi.org/10.1021/BI990852F.

(226) Li, J.; Wilk, E.; Wilk, S. Aminoacylpyrrolidine-2-Nitriles: Potent and Stable Inhibitors of Dipeptidyl-Peptidase IV (CD 26). *Arch. Biochem. Biophys.* **1995**, *323* (1), 148–154. https://doi.org/10.1006/ABBI.1995.0020.

(227) Kania, D. S.; Gonzalvo, J. D.; Weber, Z. A. Saxagliptin: A Clinical Review in the Treatment of Type 2 Diabetes Mellitus. *Clin. Ther.* **2011**, *33* (8), 1005–1022. https://doi.org/10.1016/J.CLINTHERA.2011.06.016.

(228) Hanzlik, R. P.; Thompson, S. A. Vinylogous Amino Acid Esters: A New Class Of Inactivators For Thiol Proteases. *J. Med. Chem.* **1984**, *27* (6), 711–712. https://doi.org/10.1021/JM00372A001/ASSET/JM00372A001.FP.PNG_V03.

(229) Thompson, S. A.; Hanzlik, R. P.; Andrews, P. R. Carboxyl-Modified Amino Acids and Peptides as Protease Inhibitors. *J. Med. Chem.* **1986**, *29* (1), 104–111. https://doi.org/10.1021/JM00151A018.

(230) Liu, S.; Hanzl k, R. P. Structure-Activity Relationships for Inhibition of Papain by Peptide Michael Acceptors. *J. Med. Chem.* **1992**, *35* (6), 1067–1075. https://doi.org/10.1021/JM00084A012.

(231) Palmer, J. T.; Rasnick, D.; Klaus, J. L.; Brömme, D. Vinyl Sulfones as Mechanism-Based Cysteine Protease Inhibitors. *J. Med. Chem.* **1995**, *38* (17), 3193–3196. https://doi.org/10.1021/JM00017A002.

(232) Santos, M.; Moreira, R. Michael Acceptors as Cysteine Protease Inhibitors. *Mini Rev. Med. Chem.* **2007**, *7* (10), 1040–1050. https://doi.org/10.2174/138955707782110105.

(233) Bradshaw, J. M.; McFarland, J. M.; Paavilainen, V. O.; Bisconte, A.; Tam, D.; Phan, V. T.; Romanov, S.; Finkle, D.; Shu, J.; Patel, V.; Ton, T.; Li, X.; Loughhead, D. G.; Nunn, P. A.; Karr, D. E.; Gerritsen, M. E.; Funk, J. O.; Owens, T. D.; Verner, E.; Brameld, K. A.; Hill, R. J.; Goldstein, D. M.; Taunton, J. Prolonged and Tunable Residence Time Using Reversible Covalent Kinase Inh bitors. *Nat. Chem. Biol.* **2015**, *11* (7), 525–531. https://doi.org/10.1038/nchembio.1817.

(234) Patel, H.; Ahmad, I.; Jadhav, H.; Pawara, R.; Lokwani, D.; Surana, S. Investigating the Impact of Different Acrylamide (Electrophilic Warhead) on Osimertin b's Pharmacological Spectrum by Molecular Mechanic and Quantum Mechanic Approach. *Comb. Chem. High Throughput Screen.* **2020**, *25* (1), 149–166. https://doi.org/10.2174/1386207323666201204125524.

(235) Brogi, S.; Ibba, R.; Rossi, S.; Butini, S.; Calderone, V.; Gemma, S.; Campiani, G. Covalent Revers ble Inhibitors of Cysteine Proteases Containing the Nitrile Warhead: Recent Advancement in the Field of Viral and Parasitic Diseases. *Molecules* **2022**, *27* (8), 2561. https://doi.org/10.3390/MOLECULES27082561.

(236) Purich, D. L. *Enzyme Kinetics, Catalysis and Control, A Reference of Theory and Best-Practice Methods*; Elsevier, 2010.

(237) Schirmeister, T.; Kesselring, J.; Jung, S.; Schneider, T. H.; Weickert, A.; Becker, J.; Lee, W.; Bamberger, D.; Wich, P. R.; Distler, U.; Tenzer, S.; Johé, P.; Hellmich, U. A.; Engels, B. Quantum Chemical-Based Protocol

for the Rational Design of Covalent Inhibitors. *J. Am. Chem. Soc.* **2016**, *138* (27), 8332–8335. https://doi.org/10.1021/JACS.6B03052.

(238) Yung-Chi, C.; Prusoff, W. H. Relationship between the Inhibition Constant (KI) and the Concentration of Inhibitor Which Causes 50 per Cent Inhibition (I50) of an Enzymatic Reaction. *Biochem. Pharmacol.* **1973**, *22* (23), 3099–3108. https://doi.org/10.1016/0006-2952(73)90196-2.

(239) Johnson, K. A.; Goody, R. S. The Original Michaelis Constant: Translation of the 1913 Michaelis-Menten Paper. *Biochemistry* **2011**, *50* (39), 8264–8269. https://doi.org/10.1021/BI201284U/SUPPL_FILE/BI201284U_SI_001.PDF.

(240) Copeland, R. A. *Evaluation of Enzyme Inhibitors in Drug Discovery: A Guide for Medicinal Chemists and Pharmacologists, 2nd Edition*; Wiley-VCH Verlag: Hoboken, New Jersey, USA, 2013.

(241) Ludewig, S.; Kossner, M.; Schiller, M.; Baumann, K.; Schirmeister, T. Enzyme Kinetics and Hit Validation in Fluorimetric Protease Assays. *Curr. Top. Med. Chem.* **2010**, *10* (3), 368–382. https://doi.org/10.2174/156802610790725498.

(242) Jung, S.; Fuchs, N.; Johe, P.; Wagner, A.; Diehl, E.; Yuliani, T.; Zimmer, C.; Barthels, F.; Zimmermann, R. A.; Klein, P.; Waigel, W.; Meyr, J.; Opatz, T.; Tenzer, S.; Distler, U.; Räder, H. J.; Kersten, C.; Engels, B.; Hellmich, U. A.; Klein, J.; Schirmeister, T. Fluorovinylsulfones and -Sulfonates as Potent Covalent Revers ble Inhibitors of the Trypanosomal Cysteine Protease Rhodesain: Structure-Activity Relationship, Inhibition Mechanism, Metabolism, and in Vivo Studies. *J. Med. Chem.* **2021**, *64* (16), 12322–12358. https://doi.org/10.1021/ACS.JMEDCHEM.1C01002/SUPPL_FILE/JM1C01002_SI_002.CSV.

(243) Lammert, C.; Einarsson, S.; Saha, C.; Niklasson, A.; Bjornsson, E.; Chalasani, N. Relationship between Daily Dose of Oral Medications and Idiosyncratic Drug-Induced Liver Injury: Search for Signals. *Hepatology* **2008**, *47* (6), 2003–2009. https://doi.org/10.1002/hep.22272.

(244) Kalgutkar, A. S.; Dalvie, D. K. Drug Discovery for a New Generation of Covalent Drugs. *Expert Opin. Drug Discov.* **2012**, *7* (7), 561–581. https://doi.org/10.1517/17460441.2012.688744.

(245) Baillie, T. A. Targeted Covalent Inhibitors for Drug Design. *Angew. Chemie Int. Ed.* **2016**, *55* (43), 13408–13421. https://doi.org/10.1002/ANIE.201601091.

(246) Copeland, R. A.; Pompliano, D. L.; Meek, T. D. Drug-Target Residence Time and Its Implications for Lead Optimization. *Nat. Rev. Drug Discov.* **2006**, *5* (9), 730–739. https://doi.org/10.1038/nrd2082.

(247) Lee, C. U.; Grossmann, T. N. Reversible Covalent Inhibition of a Protein Target. *Angew. Chemie - Int. Ed.* **2012**, *51* (35), 8699–8700. https://doi.org/10.1002/anie.201203341.

(248) Ettari, R.; Tamborini, L.; Angelo, I. C.; Micale, N.; Pinto, A.; De Micheli, C.; Conti, P. Inh bition of Rhodesain as a Novel Therapeutic Modality for Human African Trypanosomiasis. *J. Med. Chem.* **2013**, *56* (14), 5637–5658. https://doi.org/10.1021/JM301424D.

(249) Mckerrow, J. H.; Doyle, P. S.; Engel, J. C.; Podust, L. M.; Robertson, S. A.; Ferreira, R.; Saxton, T.; Arkin, M.; Kerr, I. D.; Brinen, L. S.; Cra k, C. S. Two Approaches to Discovering and Developing New Drugs for Chagas Disease. *Mem. Inst. Oswaldo Cruz* **2009**, *104* (1), 263–269. https://doi.org/10.1590/S0074-02762009000900034.

(250) Clayton, J. Chagas Disease: Pushing through the Pipeline. *Nature* **2010**, *465* (7301). https://doi.org/10.1038/NATURE09224.

(251) Jílková, A.; Rubešová, P.; Fanfrlík, J.; Fajtová, P.; Řezáčová, P.; Brynda, J.; Lepšík, M.; Mertlíková-Kaiserová, H.; Emal, C. D.; Renslo, A. R.; Roush, W. R.; Horn, M.; Caffrey, C. R.; Mareš, M. Druggable Hot Spots in the Schistosomiasis Cathepsin B1 Target Identified by Functional and Binding Mode Analysis of

Potent Vinyl Sulfone Inhibitors. *ACS Infect. Dis.* **2021**, *7* (5), 1077–1088. https://doi.org/10.1021/ACSINFECDIS.0C00501/ASSET/IMAGES/LARGE/ID0C00501_0004.JPEG.

(252) Mellott, D. M.; Tseng, C. Te; Drelich, A.; Fajtová, P.; Chenna, B. C.; Kostomiris, D. H.; Hsu, J.; Zhu, J.; Taylor, Z. W.; Kocurek, K. I.; Tat, V.; Katzfuss, A.; Li, L.; Giardini, M. A.; Skinner, D.; Hirata, K.; Yoon, M. C.; Beck, S.; Carlin, A. F.; Clark, A. E.; Beretta, L.; Maneval, D.; Hook, V.; Frueh, F.; Hurst, B. L.; Wang, H.; Raushel, F. M.; O'Donoghue, A. J.; De Siqueira-Neto, J. L.; Meek, T. D.; McKerrow, J. H. A Clinical-Stage Cysteine Protease Inhibitor Blocks SARS-CoV-2 Infection of Human and Monkey Cells. *ACS Chem. Biol.* **2021**, *16* (4), 642–650. https://doi.org/10.1021/ACSCHEMBIO.0C00875/SUPPL_FILE/CB0C00875_SI_001.PDF.

(253) Chen, Y. T.; Brinen, L. S.; Kerr, I. D.; Hansell, E.; Doyle, P. S.; McKerrow, J. H.; Roush, W. R. In Vitro and In Vivo Studies of the Trypanocidal Properties of WRR-483 against Trypanosoma Cruzi. *PLoS Negl. Trop. Dis.* **2010**, *4* (9), e825. https://doi.org/10.1371/JOURNAL.PNTD.0000825.

(254) Abdulla, M. H.; Lim, K. C.; Sajid, M.; McKerrow, J. H.; Caffrey, C. R. Schistosomiasis Mansoni: Novel Chemotherapy Using a Cysteine Protease Inh bitor. *PLoS Med.* **2007**, *4* (1), 0130–0138. https://doi.org/10.1371/JOURNAL.PMED.0040014.

(255) Jung, S. Rational Design, Synthesis and Evaluation of Covalent Rhodesain Inhibitors, 2018.

(256) Kesselring, J. Rationales Design, Synthese Und Testung Kovalent- Reversibler Cysteinproteaseinhibitoren, 2017.

(257) Malvy, D.; Chappuis, F. Sleeping Sickness. *Clin. Microbiol. Infect.* **2011**, *17* (7), 986–995. https://doi.org/10.1111/j.1469-0691.2011.03536.x.

(258) Brun, R.; Blum, J.; Chappuis, F.; Burri, C. Human African Trypanosomiasis. *Lancet* **2010**, *375* (9709), 148–159.

(259) Nikolskaia, O. V.; Lima, A. P. C. D. A.; Kim, Y. V.; Lonsdale-Eccles, J. D.; Fukuma, T.; Scharfstein, J.; Grab, D. J. Blood-Brain Barrier Traversal by African Trypanosomes Requires Calcium Signaling Induced by Parasite Cysteine Protease. *J. Clin. Invest.* **2006**, *116* (10), 2739–2747. https://doi.org/10.1172/JCI27798.

(260) Fairlamb, A. H. Chemotherapy of Human African Trypanosomiasis: Current and Future Prospects. *Trends Parasitol.* **2003**, *19* (11), 488–494. https://doi.org/10.1016/j.pt.2003.09.002.

(261) D, S.; DW, S.; X, W.; SS, G.; GK, W.; CR, C. Trypanosoma Brucei: Chemical Evidence That Cathepsin L Is Essential for Survival and a Relevant Drug Target. *Int. J. Parasitol.* **2012**, *42* (5), 481–488. https://doi.org/10.1016/J.IJPARA.2012.03.009.

(262) Scory, S.; Caffrey, C. R.; Stierhof, Y.-D.; Ruppel, A.; Steverding, D. Trypanosoma Brucei: Killing of Bloodstream Formsin Vitroandin Vivoby the Cysteine Proteinase Inh bitor Z-Phe-Ala-CHN2. *Exp. Parasitol.* **1999**, *91* (4), 327–333. https://doi.org/10.1006/expr.1998.4381.

(263) Pardridge, W. M. Blood-Brain Barrier Genomics and the Use of Endogenous Transporters to Cause Drug Penetration into the Brain Biologic Drug Development for the CNS View Project Blood-Brain Barrier Genomics and the Use of Endogenous Transporters to Cause Drug Penetration I. *Curr. Opin. Drug Discov. Dev.* **2003**, *6* (5), 683–691.

(264) Rautio, J.; Laine, K.; Gynther, M.; Savolainen, J. Prodrug Approaches for CNS Delivery. *AAPS J.* **2008**, *10* (1), 92. https://doi.org/10.1208/S12248-008-9009-8.

(265) Homann, M.; Göringer, H. U. Uptake and Intracellular Transport of RNA Aptamers in African Trypanosomes Suggest Therapeutic "Piggy-Back" Approach. *Bioorganic Med. Chem.* **2001**, *9* (10), 2571–2580. https://doi.org/10.1016/S0968-0896(01)00032-3.

(266) Colley, D. G.; Bustinduy, A. L.; Secor, W. E.; King, C. H. Human Schistosomiasis. *Lancet (London, England)*

2014, *383* (9936), 2253–2264. https://doi.org/10.1016/S0140-6736(13)61949-2.

(267) Burke, M. L.; Jones, M. K.; Gobert, G. N.; Li, Y. S.; Ellis, M. K.; McManus, D. P. Immunopathogenesis of Human Schistosomiasis. *Parasite Immunol.* **2009**, *31* (4), 163–176. https://doi.org/10.1111/J.1365-3024.2009.01098.X.

(268) Park, S. K.; Friedrich, L.; Yahya, N. A.; Rohr, C. M.; Chu kov, E. G.; Maillard, D.; Rippmann, F.; Spangenberg, T.; Marchant, J. S. Mechanism of Praziquantel Action at a Parasitic Flatworm Ion Channel. *Sci. Transl. Med.* **2021**, *13* (625). https://doi.org/10.1126/SCITRANSLMED.ABJ5832.

(269) Wang, W.; Wang, L.; Liang, Y. S. Susceptibility or Resistance of Praziquantel in Human Schistosomiasis: A Review. *Parasitol. Res.* **2012**, *111* (5), 1871–1877. https://doi.org/10.1007/S00436-012-3151-Z/TABLES/1.

(270) Spangenberg, T. Alternatives to Praziquantel for the Prevention and Control of Schistosomiasis. *ACS Infect. Dis.* **2021**, *7* (5), 939–942. https://doi.org/10.1021/ACSINFECDIS.0C00542/ASSET/IMAGES/LARGE/ID0C00542_0002.JPEG.

(271) Tye, H.; Eldred, C.; Wills, M. Design, Synthesis and Preliminary Studies on a Novel Class of Chiral Receptor for the Recognition of Amino Acid Derivatives1. *J. Chem. Soc. Perkin Trans. 1* **1998**, No. 3, 457–466. https://doi.org/10.1039/A706843C.

(272) Spencer, J. A.; Baldwin, I. R.; Barton, N.; Chung, C. W.; Convery, M. A.; Edwards, C. D.; Jamieson, C.; Mallett, D. N.; Rowedder, J. E.; Rowland, P.; Thomas, D. A.; Hardy, C. J. Design and Development of a Macrocyclic Series Targeting Phosphoinositide 3-Kinase δ. *ACS Med. Chem. Lett.* **2020**, *11* (7), 1386–1391. https://doi.org/10.1021/ACSMEDCHEMLETT.0C00061/ASSET/IMAGES/LARGE/ML0C00061_0004.JPEG.

(273) Jílková, A.; Horn, M.; Řezáčová, P.; Marešová, L.; Fajtová, P.; Brynda, J.; Vondrášek, J.; McKerrow, J. H.; Caffrey, C. R.; Mareš, M. Activation Route of the Schistosoma Mansoni Cathepsin B1 Drug Target: Structural Map with a Glycosaminoglycan Switch. *Structure* **2014**, *22* (12), 1786–1798. https://doi.org/10.1016/J.STR.2014.09.015.

(274) GraFit. Erithracus Software Ltd.: UK 2006.

(275) Tian, W.; Tsou, C. Determination of the Rate Constant of Enzyme Modification by Measuring the Substrate Reaction in the Presence of the Modifier. *Biochemistry* **1982**, *21* (5), 1028–1032. https://doi.org/10.1021/BI00534A031.

(276) Schrödinger, L.; DeLano, ; W. The PyMOL Molecular Graphics System. Schrödinger, LLC. 2020. http://www.pymol.org/pymol.

(277) Halgren, T. A. MMFF VI. MMFF94s Option for Energy Minimization Studies. *J. Comput. Chem.* **1999**, *20* (7). https://doi.org/10.1002/(SICI)1096-987X(199905)20:7.

(278) LeadIT. BioSolveIT GmbH: Sankt Augustin, Germany 2017. www.biosolveit.de/LeadIT.

(279) Reulecke, I.; Lange, G.; Albrecht, J.; Klein, R.; Rarey, M. Towards an Integrated Description of Hydrogen Bonding and Dehydration: Decreasing False Positives in Virtual Screening with the HYDE Scoring Function. *ChemMedChem* **2008**, *3* (6), 885–897. https://doi.org/10.1002/CMDC.200700319.

(280) Mulvenna, J.; Moertel, L.; Jones, M. K.; Nawaratna, S.; Lovas, E. M.; Gobert, G. N.; Colgrave, M.; Jones, A.; Loukas, A.; McManus, D. P. Exposed Proteins of the Schistosoma Japonicum Tegument. *Int. J. Parasitol.* **2010**, *40* (5), 543–554. https://doi.org/10.1016/J.IJPARA.2009.10.002.

(281) Adekiya, T. A.; Kondiah, P. P. D.; Choonara, Y. E.; Kumar, P.; Pillay, V. A Review of Nanotechnology for Targeted Anti-Schistosomal Therapy. *Front. Bioeng. Biotechnol.* **2020**, *8*, 32. https://doi.org/10.3389/FBIOE.2020.00032/BIBTEX.

(282) O'Donnell, J. S.; Long, G. V.; Scolyer, R. A.; Teng, M. W. L.; Smyth, M. J. Resistance to PD1/PDL1 Checkpoint Inhibition. *Cancer Treat. Rev.* **2017**, *52*, 71–81. https://doi.org/10.1016/J.CTRV.2016.11.007.

(283) Jenkins, R. W.; Barbie, D. A.; Flaherty, K. T. Mechanisms of Resistance to Immune Checkpoint Inhibitors. *Br. J. Cancer* **2018**, *118* (1), 9–16. https://doi.org/10.1038/bjc.2017.434.

(284) Kim, H. R.; Tagirasa, R.; Yoo, E. Covalent Small Molecule Immunomodulators Targeting the Protease Active Site. *J. Med. Chem.* **2021**, *64* (9), 5291–5322. https://doi.org/10.1021/ACS.JMEDCHEM.1C00172/ASSET/IMAGES/LARGE/JM1C00172_0013.JPEG.

(285) Hansel, T. T.; Kropshofer, H.; Singer, T.; Mitchell, J. A.; George, A. J. T. The Safety and Side Effects of Monoclonal Antibodies. *Nat. Rev. Drug Discov.* **2010**, *9* (4), 325–338. https://doi.org/10.1038/NRD3003.

(286) Farokhzad, O. C.; Langer, R. Impact of Nanotechnology on Drug Delivery. *ACS Nano* **2009**, *3* (1), 16–20. https://doi.org/10.1021/NN900002M.

(287) McNeil, S. E. Nanoparticle Therapeutics: A Personal Perspective. *Wiley Interdiscip. Rev. Nanomedicine Nanobiotechnology* **2009**, *1* (3), 264–271. https://doi.org/10.1002/wnan.6.

(288) Jain, K. K. Nanotechnology-Based Drug Delivery for Cancer. *Technol. Cancer Res. Treat.* **2005**, *4* (4), 407–416. https://doi.org/10.1177/153303460500400408.

(289) Tran, T. H.; Mattheolabakis, G.; Aldawsari, H.; Amiji, M. Exosomes as Nanocarriers for Immunotherapy of Cancer and Inflammatory Diseases. *Clin. Immunol.* **2015**, *160* (1), 46–58. https://doi.org/10.1016/J.CLIM.2015.03.021.

(290) Walvekar, P.; Gannimani, R.; Govender, T. Combination Drug Therapy via Nanocarriers against Infectious Diseases. *Eur. J. Pharm. Sci.* **2019**, *127*, 121–141. https://doi.org/10.1016/J.EJPS.2018.10.017.

(291) Singh, V.; Eljaaly, K.; Md, S.; Alhakamy, N. A.; Kesharwani, P. Tr block Copolymeric Drug Delivery as an Emerging Nanocarrier for Treatment of Infectious Diseases. *J. Drug Deliv. Sci. Technol.* **2022**, *75*, 103691. https://doi.org/10.1016/J.JDDST.2022.103691.

(292) Wi kinson, R. D. A.; Young, A.; Burden, R. E.; Williams, R.; Scott, C. J. A Bioavailable Cathepsin S Nitrile Inhibitor Abrogates Tumor Development. *Mol. Cancer* **2016**, *15* (1), 1–11. https://doi.org/10.1186/S12943-016-0513-7/FIGURES/5.

(293) Pang, X.; Jiang, Y.; Xiao, Q.; Leung, A. W.; Hua, H.; Xu, C. PH-Responsive Polymer–Drug Conjugates: Design and Progress. *J. Control. Release* **2016**, *222*, 116–129. https://doi.org/10.1016/J.JCONREL.2015.12.024.

(294) Xin, Y.; Yuan, J. Schiff's Base as a Stimuli-Responsive Linker in Polymer Chemistry. *Polym. Chem.* **2012**, *3* (11), 3045–3055. https://doi.org/10.1039/C2PY20290E.

(295) Lv, S.; Tang, Z.; Zhang, D.; Song, W.; Li, M.; Lin, J.; Liu, H.; Chen, X. Well-Defined Polymer-Drug Conjugate Engineered with Redox and PH-Sensitive Release Mechanism for Efficient Delivery of Paclitaxel. *J. Control. Release* **2014**, *194*, 220–227. https://doi.org/10.1016/J.JCONREL.2014.09.009.

(296) Sonawane, S. J.; Kalhapure, R. S.; Govender, T. Hydrazone Linkages in PH Responsive Drug Delivery Systems. *Eur. J. Pharm. Sci.* **2017**, *99*, 45–65. https://doi.org/10.1016/J.EJPS.2016.12.011.

(297) Brömme, D. Papain-like Cysteine Proteases. *Curr. Protoc. Protein Sci.* **2000**, *21* (1), 21.2.1-21.2.14. https://doi.org/10.1002/0471140864.PS2102S21.

(298) Biswas, S. S. Role of Chat GPT in Public Health. *Ann. Biomed. Eng. 2023* **2023**, *1*, 1–2. https://doi.org/10.1007/S10439-023-03172-7.

(299) Bajorath, J. State-of-the-Art of Artificial Intelligence in Medicinal Chemistry. *Futur. Sci.* **2021**, *7* (6), 702–

2056. https://doi.org/10.2144/FSOA-2021-0030.

(300) Struble, T. J.; Alvarez, J. C.; Brown, S. P.; Chytil, M.; Cisar, J.; Desjarlais, R. L.; Engkvist, O.; Frank, S. A.; Greve, D. R.; Griffin, D. J.; Hou, X.; Johannes, J. W.; Kreatsoulas, C.; Lahue, B.; Mathea, M.; Mogk, G.; Nicolaou, C. A.; Palmer, A. D.; Price, D. J.; Robinson, R. I.; Salentin, S.; Xing, L.; Jaakkola, T.; Green, W. H.; Barzilay, R.; Coley, C. W.; Jensen, K. F. Current and Future Roles of Artificial Intelligence in Medicinal Chemistry Synthesis. *J. Med. Chem.* **2020**, *63* (16), 8667–8682. https://doi.org/10.1021/ACS.JMEDCHEM.9B02120/SUPPL_FILE/JM9B02120_SI_001.PDF.

(301) Skolnick, J.; Gao, M.; Zhou, H.; Singh, S. AlphaFold 2: Why It Works and Its Implications for Understanding the Relationships of Protein Sequence, Structure, and Function. *J. Chem. Inf. Model.* **2021**, *61* (10), 4827–4831. https://doi.org/10.1021/ACS.JCIM.1C01114/ASSET/IMAGES/LARGE/CI1C01114_0001.JPEG.